MEDICAL RADIOLOGY

Diagnostic Imaging

A. L. Baert
K. Sartor

Magnetic Resonance Imaging in Ischemic Stroke

R. von Kummer
T. Back
Editors

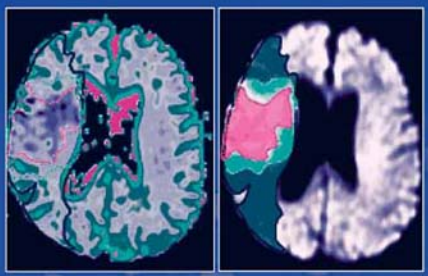

Springer

MEDICAL RADIOLOGY
Diagnostic Imaging

Rüdiger von Kummer and Tobias Back (Eds.)

Magnetic Resonance Imaging in Ischemic Stroke

With Contributions by

H. Ay · T. Back · S. M. Davis · J. M. Ferro · M. Fiorelli · G. Gahn · A. Gass · S. Gottschalk
S. Heiland · J. Helenius · M. G. Hennerici · M. Hoehn · T. Krishnamoorthy
H. Lanfermann · K. O. Lövblad · M. Mull · T. Neumann-Haefelin · M. W. Parsons
D. Petersen · U. Pilatus · J. Röther · K. Szabo · T. Tatlisumak · A. Thron · R. von Kummer
S. Wegener

Foreword by
K. Sartor

With 175 Figures in 327 Separate Illustrations, 50 in Color and 20 Tables

Springer

Rüdiger von Kummer, MD
Department of Neuroradiology
University of Technology Dresden
Fetscherstr. 74
01307 Dresden
Germany

Tobias Back, MD
Department of Neurology
University Hospital Mannheim
Ruprecht-Karls University Heidelberg
Theodor-Kutzer-Ufer 1–3
68167 Mannheim
Germany

Medical Radiology · Diagnostic Imaging and Radiation Oncology
Series Editors: A. L. Baert · L. W. Brady · H.-P. Heilmann · M. Molls · K. Sartor

Continuation of Handbuch der medizinischen Radiologie
Encyclopedia of Medical Radiology

Library of Congress Control Number: 2004115318

ISBN 3-540-00861-6 Springer Berlin Heidelberg New York
ISBN 978-3-540-00861-3 Springer Berlin Heidelberg New York

Springer is part of Springer Science+Business Media

http//www.springeronline.com

Printed in Germany

Medical Editor: Dr. Ute Heilmann, Heidelberg
Desk Editor: Ursula N. Davis, Heidelberg
Production Editor: Kurt Teichmann, Mauer
Cover-Design and Typesetting: Verlagsservice Teichmann, Mauer

Printed on acid-free paper – 21/3151xq – 5 4 3 2 1 0

Für *Hella* und *Clarisse*

Foreword

When MR imaging was added to the noninvasive diagnostic tools of radiology some 20 years ago, CT did not immediately lose its significance as the method for obtaining structural information on the brain in stroke. In fact, although MR imaging was soon found to have superior contrast resolution and to be essentially free of artifacts below the tentorium, the first large-scale treatment studies of acute stroke – in some of which Rüdiger von Kummer, one of the editors of this book, played a major role – were based on CT not MR. This was largely because CT had already reached an advanced technical stage, while MR imaging was more or less still in its infancy. With further improvement in hardware and software, including the advent of clinical imagers with higher field strengths, MR imaging did gain in importance, but its breakthrough in stroke imaging came only with the development of functional methods that allowed the study of cerebral pathophysiology, including perfusion. At the same time the technical evolution continued of several other non-structural MR methods considered in various ways useful in stroke: MR angiography, MR spectroscopy and functional (BOLD) MR imaging. All of these methods were soon studied by researchers from many countries as to their value for understanding, diagnosing, treating, and possibly preventing stroke. One method in particular, diffusion-weighted MR imaging, became rapidly accepted by (neuro)radiologists and neurologists alike, as it was soon recognized as being highly sensitive in visualizing even tiny areas of severe ischemia almost immediately after the offending event. Since then, the interest in fathoming the potential of functional MR (imaging) methods in ischemic stroke in particular and in neurovascular diseases in general has not waned.

Now, why this book? Because! Because it is not just a(nother) book on MR imaging in stroke but a lucid as well as comprehensive treatise on a complicated topic that succeeds in correlating major aspects of stroke – pathophysiology, clinical syndromes, structural and functional diagnostic MR findings, treatment and monitoring of therapeutic effects. Both editors have a long history of active, enthusiastic involvement in laboratory as well as clinical research on stroke; both are neurologists by training, with many years of clinical experience; and both have had additional training in neuroradiology, the field that one of them eventually chose for good.

The idea of "a book on stroke" was conceived at Heidelberg many years back. Fortunately, this idea never led to anything: had the book been written then, it would have been obsolete at the time of publication. The present book, which contains all the dramatic advances in MR stroke imaging that have occurred in recent years plus pertinent information on spinal stroke, is not likely to have this fate. Rather, it will soon be found on many desks and bookshelves, because clinicians and scientists interested in stroke will quickly recognize its eminent qualities: well designed, well written, and highly instructive.

Rüdiger von Kummer and Tobias Back, together with their 23 expert co-authors, have done a marvelous job in creating a timely book on stroke of great substance.

Heidelberg

Klaus Sartor

Preface

It is a part of the adventure of science
to try to find a limitation in all directions
and to stretch the human imagination
as far as possible everywhere.

Richard P. Feynman

Cerebrovascular diseases have an enormous and increasing impact on societies: they rank among the leading causes of death, are often associated with chronic handicap, and cause high costs for primary treatment, rehabilitation and chronic care. The advent of treatment options such as reperfusion therapies and, to a lesser degree, neuroprotective strategies on the one hand, and growing means to enhance rehabilitation and functional plasticity on the other hand, urges physicians to diagnose stroke subtypes as early and precisely as possible. The localization, extent and pathology of lesions should be recognized and followed up by imaging methods in order to develop and direct therapeutic approaches, detect complications, and start prevention.

Modern MR imaging and spectroscopy has provided new insights into the pathophysiology of stroke and offers a wide range of available technologies that have not by far been explored to their limits. Animal experiments have contributed considerably to our current understanding of the underlying mechanisms of cerebral ischemia. Diffusion-weighted MR imaging provides the best sensitivity for detection of patterns of ischemic lesions in acute stroke patients. Although it is still too early to assess the true potential of MR methods for stroke, nevertheless an attempt has to be made to demonstrate the diagnostic and scientific capabilities of MR imaging in ischemic stroke and related disorders. This is the purpose of our book.

When starting this project, it became clear that close correlations should be drawn between pathology, clinical picture and imaging findings. This book competes with a variety of publications, but differs from all of them in that it brings together what modern medical teaching offers to students: a comprehensive presentation of pathological features of cerebrovascular disease, an up-to-date clinical description of stroke syndromes, and the footprints of clinically relevant stroke syndromes in MR imaging modalities. For example, the reader who comes across a case of symptomatic carotid stenosis with ipsilateral MCA stroke can choose to consult Chap. 15 on occlusive carotid disease, but alternatively may be interested in reading about vascular pathology (Chap. 5) or disturbed brain perfusion (Chap. 6). Finally, he/she may be inclined to find out more about the therapeutic impact of imaging findings as presented in Chap. 3.

The dual concept of presenting MR imaging of stroke pathology and MR correlates of stroke syndromes has led to the division of this volume into two parts (Parts 2 and 3), preceded by Part 1 with introductory chapters on clinically relevant syndromes and information on the clinical and therapeutic efficacy of MR imaging. We hope that readers will find it intriguing to use the book and will always feel free to inform us about ways to improve this work

Dresden — Rüdiger von Kummer
Mannheim — Tobias Back

Contents

Part 1:
Clinical Presentation and Impact of Imaging

1 Stroke Syndromes

Georg Gahn

CONTENTS

1.1 Introduction

The major focus of this book is the evolving new technologies that help understand the underlying pathophysiological mechanisms of cerebral ischemia. Nevertheless, the anatomically based classification of stroke syndromes originally elaborated by C.M. Fisher still has a huge impact on the care of stroke patients. This chapter will give the reader a short overview of the most important stroke syndromes in the clinical setting. "Stroke" is defined as a sudden, non-convulsive focal neurological deficit. The terms apoplexy originating from the Greek "αποπλεξία" and "insult" from the Latin "insultus" describe the same phenomenon and can be used synonymously. The term "neurovascular syndrome" may be a better term since a stroke is not unusually a slow progressing process rather than a "stroke" (Kennedy and Buchan 2004). The neurological deficit reflects both the location and size of the ischemia or the hemorrhage, but may very well be due to an intracranial mass effect, a residuum after an epileptic seizure, a migraine attack, or an encephalitis. Combinations of neurological deficits are numerous, both in the hemispheres and in the brainstem (see as well chapter 14).

G. Gahn, MD
Department of Neurology, University of Technology Dresden, Fetscherstrasse 74, 01307 Dresden, Germany

1.2 Mechanisms of Ischemia

Focal cerebral ischemia differs from global ischemia. In global ischemia irreversible neuronal damage occurs after 4–8 min at normal body temperature (Hochachka et al. 1996). In focal cerebral ischemia collateral vessels almost always provide some degree of residual blood flow, which may be insufficient to preserve neuronal survival (Coyle and Heistad 1991). Location of arterial occlusion affects the impairment of cerebral function: Obstruction below the circle of Willis often permits collateral flow through the anterior or the posterior communicating arteries. Vertebral artery obstruction can be bypassed through small deep cervical arteries which are residuals from the embryonic rete mirabilis in the posterior circulation. In obstructions of the cervical internal carotid artery, which derives from a branchial arch and not from a rete mirabilis, limited collateral flow can be provided through external carotid artery branches such as the periorbital or the ethmoidal arteries. Collateral flow mainly derives from the arteries of the circle of Willis.

Additional factors influence the extent of the final infarction. The speed of obstruction may allow collateral arteries to develop, if it occurs gradually (Busch et al. 2003), whereas complete sudden blockade of a major artery by an embolus leaves only some minutes to activate sufficient collateral flow. Hypoxia, hyperglycemia, acidosis, fever, hypotonia, and normal or abnormal variants in vascular anatomy my contribute to the resulting infarction (Hossmann 1999). Basically, the loss of oxygen and

glucose supply results in the collapse of cellular energy production with subsequent changes in cellular metabolism, degradation of cell membranes, and finally necrosis.

The margins of the infarction are usually hyperemic due to activated meningeal collaterals. The ischemic tissue swells rapidly because of increased intracellular and intercellular water content. During ischemia, the arteries first dilate to increase blood supply to the oligemic tissue, but will subsequently constrict due to ischemic damage. Reperfusion may then lead to hyperemia due to impaired autoregulative capacity of the damaged arteries. In prolonged ischemia sludging and endothelial damage will prevent reperfusion (Markus 2004).

1.2.1 Territorial Infarcts

1.2.1.1 Large Vessel Occlusive Disease of the Anterior Circulation

In 1951 C. Miller Fisher described the clinical findings associated with occlusion of the internal carotid artery (ICA) (Fisher 1951). In his report he first called attention to warning episodes preceding cerebral ischemia and called them "transient ischemic attack" (TIA). The major cause for occlusive disease of the ICA is atherosclerotic narrowing at the bifurcation of the common carotid artery (CCA) extending into the external and internal carotid arteries. Often atherosclerotic disease of the ICA is accompanied by atherosclerotic disease of the coronary and peripheral arteries (de Groot et al. 2004). Atherosclerotic plaques gradually narrow the vascular lumen. Ulceration of the plaque and hemorrhage into the plaque cause clotting of thrombocytes to the vessel wall and finally embolization to more distal arteries in the brain (Hennerici 2004). Progressive narrowing of the arterial lumen may also cause hemodynamic impairment of the cerebral territory supplied by the diseased artery if collateral flow through the arteries of the circle of Willis is not sufficient.

An important warning sign for occlusive ICA disease is an episode of transient monocular visual disturbance also called "amaurosis fugax" or "ocular TIA" (Wray 1993). Patients often describe this phenomenon as a dimming, darkening, obscuration or a curtain from above or from the side, which resolves after seconds or a few minutes. These attacks are caused by a decrease in blood flow through the ophthalmic artery, distally to a hemodynamically relevant ICA obstruction. Alternatively small emboli, the so-called Hollenhorst plaques, may occlude retinal branches (Hollenhorst 1958).

Hemispheric TIAs display a variety of transient focal neurological deficits (Ferro 2004). Stereotyped TIAs point either to a hemodynamic rather than an embolic mechanism of cerebral ischemia or to an imminent lacunar infarction, the so-called capsular warning syndrome (see Sect. 1.2.2). Permanent ischemia with infarction within the MCA territory usually leads to weakness of the contralateral limbs more pronounced in the face and the arm than in the leg (Ferro 2004). Concomitant or isolated sensory symptoms are usually loss of position and pinprick sense and stereoagnosis. Neglect of the contralateral space and an attentional hemianopia are often prominent in larger hemispheric strokes which are then also accompanied by conjugate eye deviation towards the side of the brain lesion. Weakness mainly affecting the leg often occurs in anterior cerebral artery (ACA) territory stroke because of the representative area of the "homunculus" at the vertex (Bogousslavsky and Regli 1990). Left sided lesions are often accompanied by an aphasia (Kertesz 1993). Depending on the lesion location a more motor (frontal) or sensory (posterior) type of aphasia will occur (Pedersen et al. 2004).

1.2.1.1.1 Middle Cerebral Artery Occlusion

In Caucasians, the vast majority of MCA occlusions are of embolic origin with emboli arising from a carotid stenosis, the aortic arch or the heart (Heinsius et al. 1998) or from the venous side in case of a patent foramen ovale. In black or Asian patients a higher prevalence of intracranial occlusive disease is found with subsequent thrombotic arterial occlusion or stenosis (Feldmann et al. 1990).

Acute occlusion of the upper MCA trunk may lead to infarction in the frontal and superior parietal lobes. Hemiplegia, more pronounced in the face and arm, hemisensory loss, conjugate eye deviation and neglect to the contralateral side of space, especially to visual stimuli, will be the symptoms (Ferro 2004). Right sided lesions usually cause more severe visual neglect than left sided lesions (Karnath et al. 2002). Left sided lesions will also cause a motor aphasia in right handed patients (Kertesz 1993). Right sided lesions will also cause anosognosia more often than left sided lesions (Beis et al. 2004).

In inferior MCA trunk occlusion infarctions of the lateral surface of the temporal lobe and the inferior parietal lobe may occur (Olsen 1991; Ringelstein et al. 1992). Motor or sensory deficits may not be severe, but visual field deficit and sensory aphasia in left sided infarctions and constructional apraxia in right sided lesions occur (Geschwind 1975; Spinazzola et al. 2003). Right temporal lesions cause agitation and confusion resembling an organic psychosis (Ferro 2001).

Deep infarctions in the MCA territory result from proximal MCA occlusion with blockage or hypoperfusion of the lenticulostriate arteries causing striatocapsular infarcts (Russmann et al. 2003). The basal ganglia have poor collateral supply, but leptomeningeal collaterals may prevent extension of infarction to the cortex (Ringelstein et al. 1992). Striatocapsular infarcts cause dense hemiplegia and less pronounced sensory deficits if the posterior capsule is spared (Donnan et al. 1991). Left sided infarcts may cause a temporary mutism or dysarthria (Urban et al. 2001). Right sided lesions cause neglect to the contralateral side (Karnath et al. 2002).

Complete occlusion of the MCA trunk with infarction of the entire MCA territory is a potentially devastating situation with severe paralysis, hemisensory loss, attentional hemianopia, conjugate eye deviation, and global aphasia in left sided lesions (Hacke et al. 1996). Because of its high mortality this type of ischemic stroke has been called "malignant" MCA infarction (Fig. 1.1). The diagnosis of complete MCA territory infarction based on clinical judgment is unspecific and often requires neuroimaging studies (Berrouschot et al. 1998).

1.2.1.1.2 Anterior Cerebral Artery

The ACA supplies the head of the caudate nucleus, the anterior part of the internal capsule, the anterior perforated substance and the paramedian frontal lobe above the corpus callosum through the recurrent artery of Heubner (Ghika et al. 1990). Infarction of the paramedian frontal lobe causes weakness of foot, leg and shoulder and represents a typical pattern of neurological symptoms (Bogousslavsky and Regli 1990). Also apraxia of the left arm ("anterior disconnection syndrome") may be a typical sign (Geschwind 1965). Transcortical motor and sensory aphasia, urinary incontinence in bilateral lesions occur. Abulia is seen in both unilateral and bilateral frontal lobe infarctions, sometimes of fluctuating intensity. The "alien hand sign" is also found in frontal lobe infarctions and may be another form of disconnection syndrome (Geschwind et al. 1995). Occasionally both ACA territories are supplied by only one ACA in a unilateral hypoplastic or aplastic A1 segment. Infarction of both ACA territories will

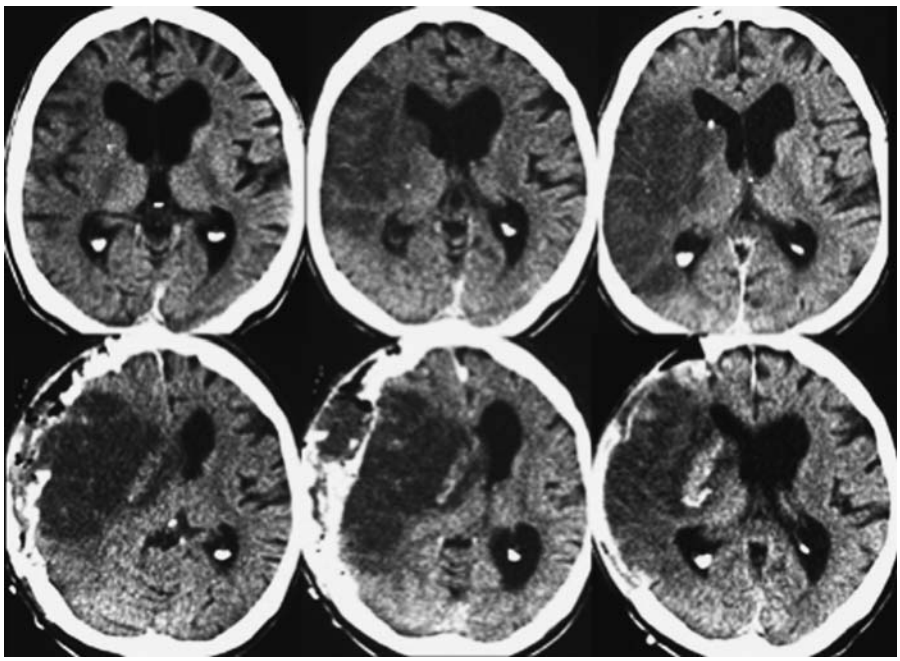

Fig. 1.1. *Upper row*, computed tomography of a patient with malignant right middle cerebral artery infarction on day one after onset of symptoms. *Lower row*, on day two massive edema with midline shift in spite of hemicraniectomy

cause a sudden onset of abulia, paraparesis, apathy, and incontinence, which may be misinterpreted as sudden onset of dementia (Ferro 2001). Infarction of the head of the caudate and the anterior internal capsule by occlusion of the Heubner artery will cause slight motor weakness, dysarthria, behavioral changes such as abulia or restlessness and hyperactivity. Cognitive and behavioral changes in these patients resemble the clinical signs found in patients with medial thalamic lesions (Bogousslavsky 1994).

1.2.1.1.3
Anterior Choroidal Artery

Blockade of the anterior choroidal artery may cause infarction of the lateral geniculate body causing hemianopia with preserved central vision and a prominent sensory loss with hemiparesis (Bruno et al. 1989).

1.2.1.2
Large Vessel Occlusive Disease of the Posterior Circulation

1.2.1.2.1
Obstruction of the Subclavian Artery

In severe occlusive disease of the subclavian artery (SCA) blood supply of the arm is mainly provided by reversed flow through the vertebral artery (VA) arising behind the obstruction. The so-called subclavian-steal syndrome consists of ischemic symptoms in the arm, especially after exercise, such as pain or numbness or coolness (Reivich et al. 1961). Consequently a diminished or delayed pulse in the radial artery or decreased blood pressure on the side of SCA stenosis can be palpated. Rarely neurological symptoms such as spells of dizziness may be brought about by exercise of the arm. Even more rare are ischemic brainstem strokes in subclavian-steal syndrome (Bornstein and Norris 1986).

1.2.1.2.2
Obstruction of the Vertebral Arteries

The origin of the VA at the SCA is the most common location of atherosclerotic VA disease. Dizziness, accompanied by other brainstem symptoms, such as diplopia, dysarthria, motor or sensory symptoms, suggest embolism towards the brainstem. Also hemianopia may occur due to VA embolism when the emboli travel through the basilar artery into the posterior cerebral arteries (PCA). The pathophysiology of proximal VA obstruction is not well understood, since the VA is rarely operated on and therefore specimens as in carotid endarterectomy are rare (Caplan 1993). The mechanical situation in VA is very different form the ICA since it leaves the SCA at a 90° angle, whereas the ICA takes off the CCA at an almost 180° angle (Brandt et al. 2000).

VA obstruction causes hemodynamic problems in approximately one third of patients with posterior circulation ischemia (Caplan et al. 2004). Asymmetrical caliber of the two VAs is normal. In the neck multiple nuchal and muscular branches provide a network for potential collateral pathways, that can be activated in VA obstruction.

Intracranial atherosclerotic VA obstruction is mainly located at the origin of the posterior inferior cerebellar artery (PICA) and less frequent at the site of dura penetration. Consequently the most frequent clinical syndrome in VA occlusive disease is the dorsolateral medullary syndrome ("Wallenberg's" syndrome) consisting of dizziness, retroorbital pain, facial numbness, dissociated sensory deficit, weakness, hoarseness, dysphagia and vomiting, nystagmus, Horner's syndrome and failure of autonomic respiration (Vuilleumier et al. 1995).

With involvement of the cerebellar hemisphere supplied by the PICA, subsequent edema may cause obstruction of the 4th ventricle, hydrocephalus or compression of the medulla oblongata. Clinically, involvement of the entire cerebellar hemisphere can not be distinguished from partial cerebellar infarction (Amarenco and Hauw 1990). Therefore patients with neurological symptoms suggesting infarction within the PICA territory require neuroimaging studies and close clinical monitoring.

In blockade of the anterior spinal artery, ischemia of the medial medulla may occur with contralateral hemiparesis, ipsilateral tongue weakness and contralateral loss of posterior column sensation (Ho and Meyer 1981).

Isolated cerebellar infarction without involvement of the medulla is often difficult to identify, since gait ataxia, vomiting and dizziness may not be accompanied by typical brainstem symptoms (Barth et al. 1994). Cerebellar edema may compress the medulla and the pons leading to conjugate eye deviation to the side opposite the lesion without contralateral hemiparesis. This sign is probably pathognomonic for severe cerebellar mass effect and requires immediate intervention.

1.2.1.2.3 Basilar Artery Obstruction

Basilar artery (BA) occlusive disease is a highly life-threatening condition first described by Kubik and Adams (1946). Atherosclerotic changes are mostly located at the origin of the BA, sometimes extending from the VAs. Often these patients experience brainstem TIAs such as diplopia, dizziness, weakness of both legs, or occipital headaches (von Campe et al. 2003). Obstruction of the BA often interrupts blood supply of the basis of the pons by the superior cerebellar arteries (SCA). Pseudobulbar paralysis by interruption of descending tracts to the bulbar nuclei is often seen. The spinothalamic tract and the cerebellar hemispheres are often spared from infarction. Disturbance of eye movements occur because of infarction of the lateral gaze centers in the paramedian pontine tegmentum, e.g. the medial longitudinal fasciculus (internuclear ophthalmoplegia), the parapontine reticular formation (PPRF), which generates lateral gazes, or the combination of both, resulting in the so called "one and a half-syndrome" (Mehler 1989; Voetsch et al. 2004).

Infarction of the medial pontine tegmentum will cause coma and is a poor prognostic sign (Fisher 1977; Kataoka et al. 1997).

In most patients with BA thrombosis, obstruction is limited to the mid portion of the basilar artery (Fig. 1.2) (Voetsch et al. 2004). Embolic occlusion rather than thrombotic occlusion mainly blocks the distal part of the BA when it divides into the PCAs. The distal BA supplies the midbrain and the diencephalon by small perforating arteries. Signs of dysfunction in the rostral brainstem are a variety of pupillary abnormalities (e.g. anisocoria, afferent pupillary deficit) (Martin et al. 1998; Mehler 1989). Vertical gaze palsy or skew deviation also point to the midbrain causing the "Top of the basilar" syndrome (Caplan 1980). Memory loss may occur in thalamic infarction as well as agitation, hallucinations mimicking frontal lobe disorders (Biller et al. 1985; Ghika-Schmid and Bogousslavsky 2000). The triad of hypersomnia, supranuclear vertical-gaze defect, and amnesia (the so-called "paramedian diencephalic syndrome") is typically due to bilateral paramedian thalamic strokes in the territory of the anterior thalamic/subthalamic (or thalamoperforating) arteries ("*en ailes de papillon*") (Meissner et al. 1987).

1.2.1.2.4 Posterior Cerebral Artery (PCA)

Historically, the French neurologist Charles Foix in 1923 first described the syndrome of infarction in the PCA territory as a thalamocapsular deficit (Foix and Masson 1923). The PCAs arise from the BA, but about 30% of patients have a hypo- or aplastic P1 segment with the PCA nourished by the ICA through the posterior communicating artery (Margolis et al. 1971).

Headache in patients with PCA disease is often retro-orbital or above the eye reflecting innervation of the upper surface of the tentorium by the first division of the trigeminal nerve (Brandt et

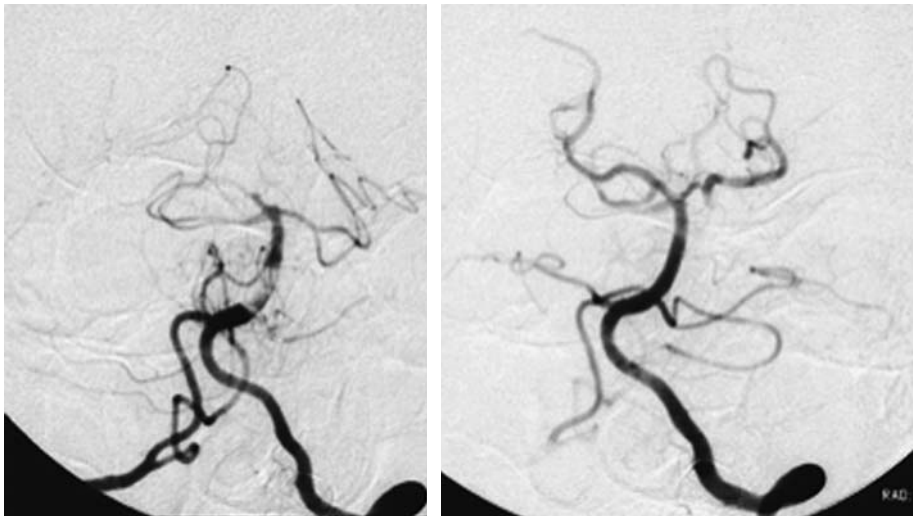

Fig. 1.2. Digital subtraction angiography of a patient with basilar artery thrombosis before (*left*) and after (*right*) thrombolytic therapy. (Courtesy of Prof. von Kummer)

al. 2000; Ferro et al. 1995). Infarction in the PCA territory usually causes visual symptoms such as homonymous hemianopia or quadrantanopia and sensory deficits but seldom paralysis. Patients with hemianopia due to infarction of the striate cortex are fully aware of their deficit. In contrast patients with infarction in the parietal lobe within the MCA territory have visual neglect and are unaware of their deficit (Ferber and Karnath 2001). Proximal PCA-occlusion may simulate MCA-infarction because of thalamic involvement (Chambers et al. 1991). Optokinetic nystagmus is normal in patients with hemianopia but reduced towards the side of the visual defect in those with visual neglect (Morrow and Sharpe 1993).

Some neuropsychological syndromes can be present in PCA infarction (Ferro 2001):

Alexia without agraphia in left occipital lobe infarction and the splenium of the corpus callosum. Transfer of read words from the functional right visual cortex to the left sided language center is impossible due to interruption of the splenium. Transfer of primary language information for writing or speech is not impaired.

Transcortical sensory aphasia appears in patients with left PCA infarctions and displays difficulties in naming objects but no problems in repeating without understanding. Gerstmann's syndrome with infarction of the angular gyrus consists of inability for right-left differentiation, finger anomia, constructional apraxia, agraphia and acalculia. In associative visual agnosia after left PCA infarctions visual but not tactile recognition of objects is impaired. Prosopagnosia is a problem with recognizing faces and occurs in right PCA infarctions. Cortical blindness occurs in bilateral PCA infarctions; however, pupillary reflexes are preserved (also see Chap. 14).

1.2.2 Lacunar Infarction

Cerebral microangiopathy accounts for 20%–30 % of all ischemic strokes and is mainly due to long lasting arterial hypertension. Narrowing of arterioles is caused by so called lipohyalinosis, a process collecting hyaline substances in the media of the small cerebral arteries (Fisher 1965c). These small arteries typically supply exclusively small territories of less than 1 or 2 cm in diameter. With progression of arterial narrowing blood flow towards the nourished territory diminishes until oligemia or ischemia occur. Eventually thrombotic mechanisms may contribute to the blockade of the artery at this point. Finally a small infarction, called a "lacune", will occur. Especially in the basilar artery atheromatous changes in the arterial wall may occlude the origins of the small penetrating arteries or be the origin of an expanding thrombosis adherent to the arterial wall ("microatheroma") (Fisher and Caplan 1971). Usually this will cause blockade of several perforating arteries and subsequent small deep infarcts in contrast to lacunar infarcts which result from single perforating artery disease. An animal model to study cerebral microangiopathy in a standardized matter is presently not available (Caplan 1993). Conversely we rely on clinical and imaging data in humans to understand this disease.

Lacunar infarcts are typically located in the basal ganglia, the deep white matter and in the brainstem (Fisher 1965a, 1998). Depending on their location and their size circumscribed neurological symptoms will occur. C. Miller Fisher described the four classical lacunar syndromes:

- Pure motor stroke (Fisher and Curry 1964)
- Pure sensory stroke (Fisher 1965b)
- Ataxic hemiparesis (Fisher 1978)
- Dysarthria-clumsy-hand-syndrome (Fisher 1967; Fisher and Curry 1964)

All these syndromes are a consequence of small lacunes interrupting pathways in the white matter. Lacunar strokes almost never cause cortical symptoms such as aphasia or apraxia. Depending again on the location of the infarctions, patients may present with combined symptoms sometimes with preceding stereotyped TIAs. Lacunes within the internal capsule may cause dense hemiplegia, but never combined with impaired consciousness or conjugate eye deviation as in territorial infarcts with mass effect. At presentation, symptoms may be subtle or mild and may fluctuate or progress. This is probably related to the hemodynamic aspect in the pathogenesis of the disease. Many patients experience progression of the neurological deficits during the first 24 h after onset of ischemic symptoms, the so-called capsular warning syndrome (Donnan et al. 1993; Staaf et al. 2004). Often these patients wake up in the morning with neurological deficits which occurred sometimes during sleep and with comparatively low blood pressure (Chaturvedi et al. 1999). In contrast embolic strokes tend to occur after getting up, when activation of the cardiovascular system provokes plaque disruption or increased cardiac contractility. Notably, recent MRI studies

showed no differences in stroke subtypes between waking strokes and strokes occurring during sleep (Donnan et al. 1993; Fink et al. 2002). Lacunar syndromes do not specifically help to localize the infarct to a certain territory in the brain and are not highly specific for the diagnosis of a "lacune" (Baumgartner et al. 2003; Gan et al. 1997).

1.2.3 Borderzone Infarction

Borderzone infarcts develop at the junction between different arterial territories (Adams et al. 1966). Pathophysiologically two different classes of borderzone infarcts can be identified: infarction between two arterial territories with a connecting arteriolar collateral network, so-called watershed infarcts, and infarcts between two arterial territories without arteriolar collaterals, so-called end-zone infarcts (Bogousslavsky and Moulin 1995). This classification is based on the anatomic distribution of the cerebral vascular supply consisting of two main systems: first, superficial arteries surround the brain parenchyma with an anastomotic network and send off perforating centripetal branches that do not anastomose (Moody et al. 1990). Second, deep branches originating from the major arterial branches penetrating the brain without anastomoses. Clinically relevant borderzones are the anterior borderzone between the MCA and the ACA and the posterior borderzone between the MCA and the PCA. They represent watershed areas and cause mainly cortical infarction. The subcortical borderzones between the deep and the superficial perforators represent end-zone areas and cause subcortical infarctions (Read et al. 1998). In the posterior circulation both watershed and end-zone areas exist between the PICA and the SCA territories. The penetrating branches of the basilar artery are a potential source of end-zone infarctions comparable to the lenticulostriate arteries (Bogousslavsky and Moulin 1995).

The underlying mechanism of borderzone infarcts is the low flow situation (Ringelstein et al. 1983) in the most distal fields supplied by the cerebral circulation ("last meadows") (also see Chap. 15). Hemodynamic impairment will consequently first cause ischemia in these areas. Typical clinical situations are a prolonged drop in systemic blood pressure, e.g. during cardiac surgery causing bilateral borderzone infarcts or severe occlusive disease of the internal carotid artery (Bladin and Chambers 1994). This may only lead to unilateral borderzone infarction in the case of poor collateral supply through the circle of Willis (Powers 1991).

Clinically stereotyped TIAs or the opticocerebral symptom with simultaneous amaurosis and contralateral hemiparesis due to critically low blood supply through an occluded or almost occluded ICA herald a pending borderzone ischemia (Tsiskaridze et al. 2001). Rarely so-called limb shaking TIAs may point to a hemodynamic ischemia in ICA occlusive disease (Baquis et al. 1985).

1.3 Particular Etiological Stroke Syndromes

1.3.1 Cardioembolic Stroke

Thromboembolic stroke mainly derives from cardiac thrombus formation (Schneider et al. 2004). Less frequently the source is intra-arterial, from the distal end of a thrombus within the lumen of an obstructed carotid or vertebral artery or from an atheromatous plaque in the cervical arteries or in the aortic arch. The cardiac embolus usually arises in the anterior circulation through the internal carotid artery up into the middle cerebral artery. At a site of sudden lumen reduction either at the origin of the middle cerebral artery or more distally at the bifurcation into the middle cerebral artery branches, it gets stuck and blocks the lumen of the artery (Caplan 1993). Embolic infarction often turns into hemorrhagic transformation. Most often the middle cerebral artery, especially its inferior branch, is the site of embolic obstruction (Bogousslavsky et al. 1989). The embolic material may remain arrested and plug the artery solidly. It also may break into fragments and spread into smaller branches more peripherally. The phenomenon of a clot first lodging in the internal carotid artery, producing profound symptoms of hemispheric ischemia, and then migrating distally to a MCA pial branch has been called the "spectacular shrinking deficit" (Minematsu et al. 1992). The dramatic initial deficit diminishes to a minor deficit corresponding to the terminal branch artery.

At total of 75% of cardiac emboli reach the brain. Non-valvular atrial fibrillation with thrombus formation within the left atrial appendix or the left atrium is the most common reason for cardiac emboli (Ferro 2003). Cardio-embolic infarcts within the MCA territory carry a high risk for hemorrhagic transformation after reperfusion. Hemor-

rhagic transformation is a natural consequence of cerebral infarction, occurring in up to 65% of stroke patients and in up to 90% of patients with cardioembolic stroke within the first week after symptom onset (Molina et al. 2001). Hemorrhagic transformation does not impair neurological outcome after embolic stroke (Fiorelli et al. 1999). It may even suggest favorable outcome indicating early reperfusion of the blocked MCA (Molina et al. 2002).

Paradoxical embolism can occur in a patent foramen ovale with a right to left shunt. Embolic material arising from the pelvic or leg veins or elsewhere in the venous system may bypass the pulmonary system and reach the cerebral arteries (Braun et al. 2004).

1.3.2 Dissection

Spontaneous dissection of the internal carotid or the vertebral artery is an important cause of ischemic stroke in young adults (Fig. 1.3). In the late 1970s Fisher et al. (1978) and Mokri et al. (1979) described dissections of carotid and vertebral arteries as detected by modern diagnostic techniques rather than by post-mortem examination. This may occur after both major or trivial traumatic head or neck injury (Schievink 2001). Many patients have preceding warning symptoms: the typical patient with carotid artery dissection presents with pain on one side of the head, face, or neck accompanied by a partial Horner's syndrome and followed hours or days later by cerebral or retinal ischemia (Schievink 2001). Final infarction may arise mostly due to embolic and seldom due to hemodynamic mechanism (Benninger et al. 2004). In carotid artery dissection, Horner's syndrome develops in less than half of patients as well as vagal, hypoglossal or accessorial nerve palsy. The underlying mechanism could be nerve compression, stretching or occlusion of small nourishing branches within an arterial wall by the intramural hematoma (Mokri et al. 1996). The pathogenesis of dissection remains obscure except in patients with obvious collagen tissue disease such as fibromuscular dysplasia. Other types of connective tissue alterations may also be associated with cervical artery dissections (Hausser et al. 2004). The site of dissection in adults is mainly the internal carotid artery at its distal extracranial course above the carotid bulb. In children the site of dissection is predominately intracranially (Fullerton et al. 2001). The risk for recurrent dissections is very low (Touze et al. 2003).

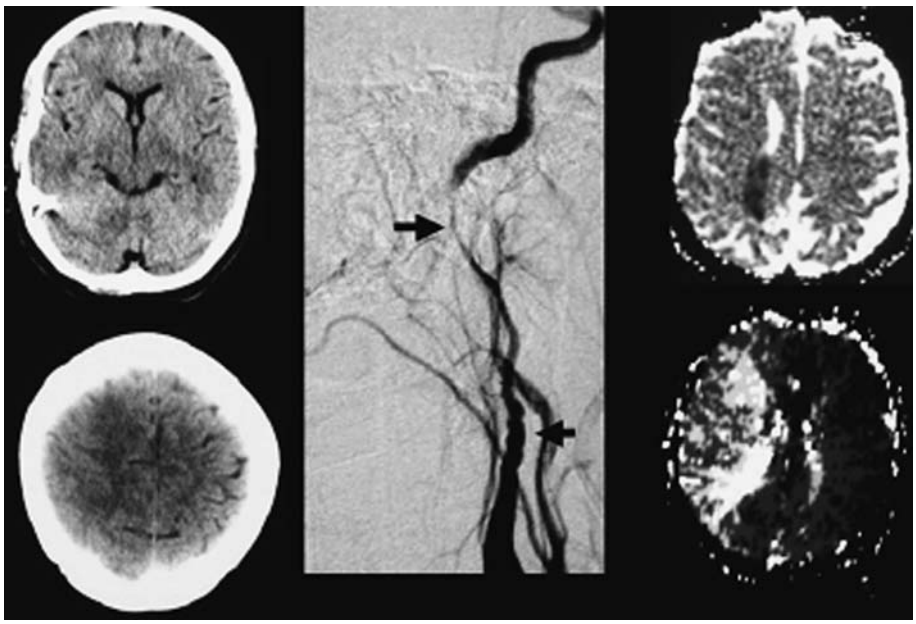

Fig. 1.3. Computed tomography (*left*), digital subtraction angiography (DSA, *middle*) and MRI (*right*) of a patient with internal carotid artery dissection. Note diffuse swelling of the frontal-parietal cortex on CT on day three after onset of symptoms. At this time point the patient suffered from a severe left hemiparesis. DSA shows classical "string sign" of cervical artery dissection with continuous narrowing of arterial lumen. MRI: ADC map (*upper images*) on day three after onset of symptoms shows small area of ischemia (*dark*). Time-to-peak parameter image (*lower images*) shows delayed contrast inflow to the entire right MCA territory. The patient underwent stent protected dilatation of the arterial stenosis 6 days after symptom onset and recovered almost completely from the severe hemiparesis. (Courtesy of Prof. von Kummer)

1.3.3 Cerebral Venous Thrombosis

Thrombosis of the cerebral veins or sinuses may develop secondary to infections of the ear or the paranasal sinuses, to coagulation disorders or spontaneously (Bousser et al. 1985) (also see Chap. 18). Occlusion of the cerebral venous system may cause venous infarction stroke. The clinical signs are often unspecific and may be mainly caused by an obscure increase in intracranial pressure (Higgins et al. 2004). Fluctuating or permanent focal neurological deficits combined with headache and confusion may lead to the correct diagnosis. Chemosis and proptosis with cranial nerve III, IV and VI, and the ophthalmic division of 5th cranial nerve palsy are characteristic signs for thrombosis of the anterior cavernous sinus. Seizures and hemiparesis, predominantly of the leg, are suggestive of the sagittal sinus (Fig. 1.4). Involvement of the caudal cranial nerves indicate thrombosis of the posterior part of the cavernous sinus or the inferior petrous sinus. Bilateral thalamic infarction should raise the question of straight sinus thrombosis (Herrmann et al. 2004).

1.3.4 Migraine

Classical migraine with typical visual symptoms preceding unilateral headache are seldom a differential diagnosis with ischemic stroke. Increased awareness of patients of ischemic symptoms and rapid presentation to emergency rooms with immediate initiation of thrombolytic therapy may challenge the physician to identify an ongoing migraine attack with spreading depression mimicking cerebral ischemia. Accompanying vegetative symptoms are unspecific. Familiar hemiplegic migraine is a rare and even more challenging disorder due to its dramatic course in young patients (Ducros et al. 2001). The association between migraine and stroke is a dilemma for neurologists. Migraine is associated with an increased stroke risk and it is considered an independent risk factor for ischemic stroke in a particular subgroup of patients. The pathogenesis is not known, but several studies report some common biochemical mechanisms between the two diseases. A classification of migraine-related stroke that encompasses the full spectrum of the possible relationship between migraine and stroke has been proposed. It includes three main entities: coexisting stroke and migraine, stroke with clinical features of migraine, and migraine-induced stroke. The concept of migraine-induced stroke is well represented by migrainous infarction; it is described in the revised classification of the International Headache Society (IHS), and it represents the strongest demonstration of the relationship between ischemic stroke and migraine (Fig. 1.5). An interesting common condition in stroke and migraine is a patent foramen ovale which could play a pathogenetic role in both disorders. The association between migraine and cervical artery dissection is reported in recent studies. Migraine is more frequent in patients with cervical artery dissection (Tzourio et al. 2002). This supports the hypothesis that an underlying arterial wall disease could be a predisposing condition for migraine.

Basilar artery or vertebrobasilar migraine is not an uncommon type of migraine. Often young woman

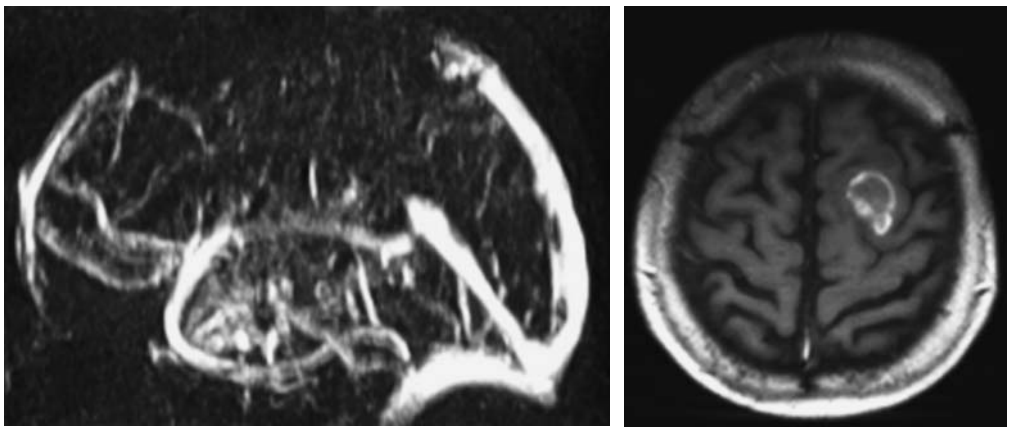

Fig. 1.4. Patient with cerebral venous thrombosis. Venous MRA demonstrates occlusion of the sagittal sinus. MRI shows an intracranial hemorrhage, the typical complication of cerebral venous thrombosis. (Courtesy of Prof. von Kummer)

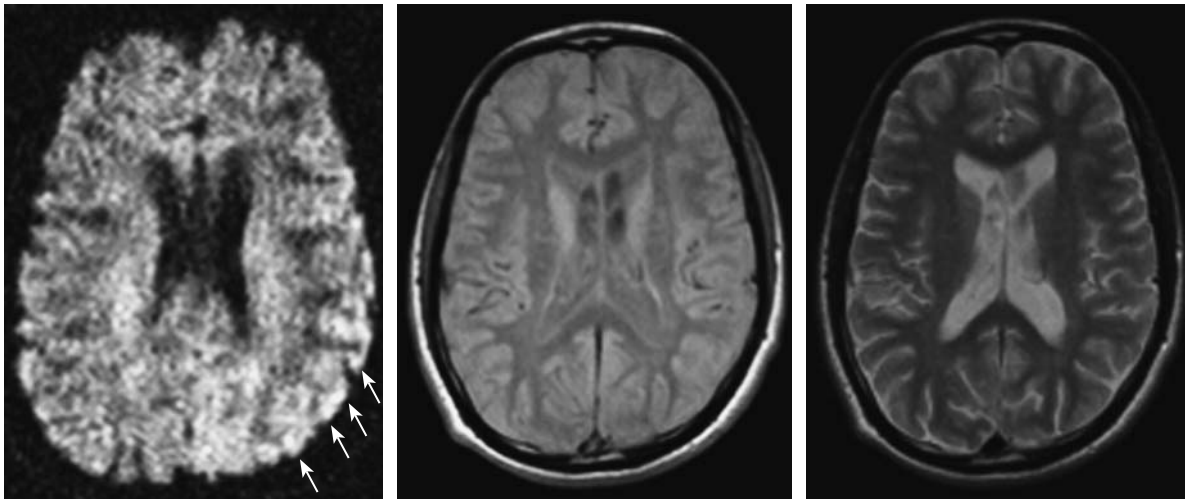

Fig. 1.5. Patient with hemiplegic migraine. *Left*, diffusion weighted MRI during migraine attack with severe right hemiparesis. Note the slight diffusion changes in the left temporal cortex suggesting ischemia. *Middle and right*, follow-up MRI (proton-density- and T2-weighted) 1 year after migraine attack show no structural changes in the left temporal cortex. Clinically the patient recovered completely. (Courtesy of Prof. von Kummer)

experience visual disturbance similar to those in typical migraine but involving both visual fields. These symptoms may be accompanied by vertigo, ataxia, dysarthria, and sensory disturbances in both arms or legs bilaterally (Evans and Linder 2002).

1.3.5 Coma

In animals, destruction of the ascending reticular activating system (ARAS) induces a state of coma (Moruzzi and Magoun 1949). In men the ARAS is located in the paramedian tegmentum of the dorsal pons and the midbrain extending as a complex polysynaptic system from the upper half of the pons through the midbrain to the dorsal part of the hypothalamus and to the thalamic reticular formation (Vincent 2000).

In close vicinity of the ARAS the medial longitudinal fasciculus (MLF) and the oculomotor and trochlear nuclei are situated. Combined coma and oculomotor disturbances points to a brainstem lesion (Parvizi and Damasio 2003). Other clinical symptoms like respiratory pattern, pupillary reflex, and position or movement patterns of the limbs may help localize the site of the lesion.

Abnormal respiratory breathing patterns are of limited practical value, since a comatose patient due to cerebrovascular disease often requires immediate airway protection and mechanical ventilation. Urgent diagnostic imaging will provide the appropriate diagnostic information (Brazis et al. 1990). "Cheyne-Stokes respiration" consists of brief periods of hyperventilation regularly combined with short episodes of apnea. During hyperventilation periods the patients may become more alert. The cause of Cheyne-Stokes respiration can be a large bilateral cortical lesion, bilateral thalamic lesions, as well as metabolic disturbances in uremia, anoxia, heart failure (Cherniack and Longobardo 1973). "Hyperventilation" may occur in midbrain or pontine lesions and is often accompanied by severe respiratory distress. It can also be found in brainstem tumors leading to local pH lowering because of their high metabolism and thereby providing a breathing stimulus to the medullary respiratory center (Plum 1972). A lesion in the lateral tegmentum of the lower pons may cause a "apneustic breathing" with long inspiratory pauses (Plum and Alvord 1964). Low pontine and medullary lesions may cause "cluster breathing" with irregular breathing sequences. "Ataxic breathing" displays completely irregular breathing patterns, often seen in terminally ill patients with impairment of the dorsomedial respiratory centers (Brazis et al. 1990).

The pupillary light reflex may help differentiating metabolic cause from structural brainstem lesion in comatose patients (Tokuda et al. 2003). The light reflex is very resistant to metabolic dysfunction. An abnormal light reflex, especially when unilateral, points to a midbrain lesion. Bilateral diencephalic lesions or metabolic coma may cause bilateral small pupils well reacting to light ("diencephalic pupils").

Midbrain lesions abolish the light reflex when located in the tectum or the pretectum and thereby disrupting the posterior commissure. Hippus and the ciliospinal reflex may be preserved. Tegmental lesions damaging the oculomotor nuclei may cause an irregular shape of the pupils, anisocoria and loss of light reflex. Tegmental lesions in the pons cause miosis by disruption of the descending sympathetic fibers (pinpoint pupils, minimally reacting to light). Lateral pontine or medullary lesions cause Horner's syndrome (Brazis et al. 1990).

1.3.6 Eye Movement Abnormalities

In comatose patients evaluation of the oculomotor system relies on evaluation and observation of involuntary eye movements. The oculocephalic and the oculovestibular reflexes disappear in deep coma.

"Periodic alternating gaze" (Ping-Pong gaze) with alternating eye movements from one extreme of horizontal gaze to the other lasting from 2 to 5 s indicate bilateral cerebral damage with preserved brainstem but may also occur in brainstem hemorrhage (Masucci et al. 1981).

"Repetitive divergence" consists of slow divergence of the eyes followed by rapid return to mid position. This rare phenomenon may be observed in metabolic coma (Noda et al. 1987).

Nystagmoid jerking of one eye may occur in mid- to lower pontine lesions (Plum and Posner 1980). Ocular bobbing consists of sudden bilateral downward movement of both eyes followed by slow return to mid position. Pontine and cerebellar lesions as well as metabolic and encephalitic disorders may cause ocular bobbing. Inverse ocular bobbing ("ocular dipping") may occur in hypoxic encephalopathy (Stark et al. 1984).

Conjugate gaze palsy or forced eye deviation may point to hemispheric lesions when looking towards the side of the lesion (Tijssen et al. 1991) and will point to a brainstem lesion when looking away from the side of lesion. Damage to the MLF will cause disconjugated gazes, e.g. failure of adduction of the eye on the side of lesion or, as in damage of the PPRF and the MLF preservation of only abduction of the contralateral eye (Wall and Wray 1983).

Abnormalities of vertical gazes may occur in both unilateral and bilateral midbrain and diencephalic lesions and can be evaluated by the doll's eye maneuver or alternatively by irrigation of warm water in both ears causing upward deviation or bilateral cold water causing downward deviation (Bogousslavsky et al. 1994; Hommel and Bogousslavsky 1991).

"Skew deviation" may be seen by various brainstem lesions and in increased intracranial pressure as well as in hepatic coma. Skew deviations are ipsiversive (ipsilateral eye undermost) with caudal pontomedullary lesions and contraversive (contralateral eye lowermost) with rostral pontomesencephalic lesions. They are associated with concomitant ocular torsion and tilts of the subjective visual vertical toward the undermost eye (Brandt and Dieterich 1993).

"Decorticate rigidity" may occur unilaterally with hemispheric and diencephalic lesions contralateral to the lesion. It consists of adduction of the arm, flexion in the elbow, and pronation and flexion of the wrist. "Decerebrate rigidity" displays extension and pronation of the arms and forced plantar flexion of the feet. It occurs in upper pontine and midbrain destruction. Extension of the arms and weak flexion of the legs suggest tegmental pontine damage (Bogousslavsky et al. 1994; Brazis et al. 1990).

1.4 Summary

We gave a short overview of the most important stroke syndromes in the clinical setting. Knowledge of these syndromes helps to understand the complex pathophysiology of cerebral ischemia. Combination of clinical findings with the data from the new and evolving imaging techniques certainly facilitates and improves care for stroke patients.

References

Adams JH, Brierley JB, Connor RC et al (1966) The effects of systemic hypotension upon the human brain. Clinical and neuropathological observations in 11 cases. Brain 89:235–268

Amarenco P, Hauw JJ (1990) Cerebellar infarction in the territory of the anterior and inferior cerebellar artery. A clinicopathological study of 20 cases. Brain 113:139–155

Baquis GD, Pessin MS, Scott RM (1985) Limb shaking – a carotid TIA. Stroke 16:444–448

Barth A, Bogousslavsky J, Regli F (1994) Infarcts in the territory of the lateral branch of the posterior inferior cerebellar artery. J Neurol Neurosurg Psychiatry 57:1073–1076

Baumgartner RW, Sidler C, Mosso M et al (2003) Ischemic lacunar stroke in patients with and without potential mechanism other than small-artery disease. Stroke 34:653–659

Beis JM, Keller C, Morin N et al (2004) Right spatial neglect after left hemisphere stroke: qualitative and quantitative study. Neurology 63:1600–1605
Benninger DH, Georgiadis D, Kremer C et al (2004) Mechanism of ischemic infarct in spontaneous carotid dissection. Stroke 35:482–485
Berrouschot J, Barthel H, von Kummer R et al (1998) 99m technetium-ethyl-cysteinate-dimer single-photon emission CT can predict fatal ischemic brain edema. Stroke 29:2556–2562
Biller J, Sand JJ, Corbett JJ et al (1985) Syndrome of the paramedian thalamic arteries: clinical and neuroimaging correlation. J Clin Neuroophthalmol 5:217–223
Bladin CF, Chambers BR (1994) Frequency and pathogenesis of hemodynamic stroke. Stroke 25:2179–2182
Bogousslavsky J (1994) Frontal stroke syndromes. Eur Neurol 34:306–315
Bogousslavsky, Moulin T (1995) Borderzone Infarcts. In: Bogousslavsky J, Caplan LR (eds) Stroke syndromes, 1st edn. Cambridge University Press, Cambridge, pp 358–365
Bogousslavsky J, Regli F (1990) Anterior cerebral artery territory infarction in the Lausanne Stroke Registry. Clinical and etiologic patterns. Arch Neurol 47:144–150
Bogousslavsky J, van Melle G, Regli F (1989) Middle cerebral artery pial territory infarcts: a study of the Lausanne Stroke Registry. Ann Neurol 25:555–560
Bogousslavsky J, Maeder P, Regli F et al (1994) Pure midbrain infarction: clinical syndromes, MRI, and etiologic patterns. Neurology 44:2032–2040
Bornstein NM, Norris JW (1986) Subclavian steal: a harmless haemodynamic phenomenon? Lancet 2:303–305
Bousser MG, Chiras J, Bories J et al (1985) Cerebral venous thrombosis-a review of 38 cases. Stroke 16:199–213
Brandt T, Dieterich M (1993) Skew deviation with ocular torsion: a vestibular brainstem sign of topographic diagnostic value. Ann Neurol 33:528–534
Brandt T, Steinke W, Thie A et al (2000) Posterior cerebral artery territory infarcts: clinical features, infarct topography, causes and outcome 1. Cerebrovasc Dis 10:170–182
Braun M, Gliech V, Boscheri A et al (2004) Transcatheter closure of patent foramen ovale (PFO) in patients with paradoxical embolism. Periprocedural safety and mid-term follow-up results of three different device occluder systems. Eur Heart J 25:424–430
Brazis PW, Masdeu JC, Biller J (1990) Localization in clinical neurology, 3rd edn. Little Brown, Boston
Bruno A, Graff-Radford NR, Biller J et al (1989) Anterior choroidal artery territory infarction: a small vessel disease. Stroke 20:616–619
Busch HJ, Buschmann IR, Mies G et al (2003) Arteriogenesis in hypoperfused rat brain. J Cereb Blood Flow Metab 23:621–628
Caplan LR (1980) "Top of the basilar" syndrome. Neurology 30:72–79
Caplan LR (1993) Stroke. A clinical approach, 2nd edn. Butterworth-Heinemann, Newton
Caplan LR, Wityk RJ, Glass TA et al (2004) New England Medical Center Posterior Circulation registry. Ann Neurol 56:389–398
Chambers BR, Brooder RJ, Donnan GA (1991) Proximal posterior cerebral artery occlusion simulating middle cerebral artery occlusion. Neurology 41:385–390
Chaturvedi S, Adams HP Jr, Woolson RF (1999) Circadian variation in ischemic stroke subtypes. Stroke 30:1792–1795
Cherniack NS, Longobardo GS (1973) Cheyne-stokes breathing. An instability in physiologic control. N Engl J Med 288:952–957
Coyle P, Heistad DD (1991) Development of collaterals in the cerebral circulation. Blood Vessels 28:183–189
De Groot E, Hovingh GK, Wiegman A et al (2004) Measurement of arterial wall thickness as a surrogate marker for atherosclerosis. Circulation 109:III33–III38
Donnan GA, Bladin PF, Berkovic SF et al (1991) The stroke syndrome of striatocapsular infarction. Brain 114:51–70
Donnan GA, O'Malley HM, Quang L et al (1993) The capsular warning syndrome: pathogenesis and clinical features. Neurology 43:957–962
Ducros A, Denier C, Joutel A et al (2001) The clinical spectrum of familial hemiplegic migraine associated with mutations in a neuronal calcium channel. N Engl J Med 345:17–24
Evans RW, Linder SL (2002) Management of basilar migraine. Headache 42:383–384
Feldmann E, Daneault N, Kwan E et al (1990) Chinese-white differences in the distribution of occlusive cerebrovascular disease. Neurology 40:1541–1545
Ferber S, Karnath HO (2001) Size perception in hemianopia and neglect. Brain 124:527–536
Ferro JM (2001) Hyperacute cognitive stroke syndromes. J Neurol 248:841–849
Ferro JM (2003) Cardioembolic stroke: an update. Lancet Neurol 2:177–188
Ferro JM (2004) Patterns of ischaemic cerebral diseases. J Neurol 251:1–10
Ferro JM, Melo TP, Oliveira V et al (1995) A multivariate study of headache associated with ischemic stroke. Headache 35:315–319
Fink JN, Kumar S, Horkan C et al (2002) The stroke patient who woke up: clinical and radiological features, including diffusion and perfusion MRI. Stroke 33:988–993
Fiorelli M, Bastianello S, von Kummer R et al (1999) Hemorrhagic transformation within 36 hours of a cerebral infarct: relationships with early clinical deterioration and 3-month outcome in the European Cooperative Acute Stroke Study I (ECASS I). Stroke 30:2280–2284
Fisher CM (1951) Occlusion of the internal carotid artery. Arch Neurol Psychiatry 65:346–377
Fisher CM (1965a) Lacunes: small, deep cerebral infarcts. Neurology 15:774–784
Fisher CM (1965b) Pure sensory stroke involving face, arm, and leg. Neurology 15:76–80
Fisher CM (1965c) The vascular lesion in lacunae. Trans Am Neurol Assoc 90:243-5:243–245
Fisher CM (1967) A lacunar stroke. The dysarthria-clumsy hand syndrome. Neurology 17:614–617
Fisher CM (1977) Bilateral occlusion of basilar artery branches. J Neurol Neurosurg Psychiatry 40:1182–1189
Fisher CM (1978) Ataxic hemiparesis. A pathologic study. Arch Neurol 35:126–128
Fisher CM (1998) Lacunes: small, deep cerebral infarcts. 1965. Neurology 50:841
Fisher CM, Caplan LR (1971) Basilar artery branch occlusion: a cause of pontine infarction. Neurology 21:900–905
Fisher CM, Curry HB (1964) Pure motor hemiplegia. Trans Am Neurol Assoc 89:94-7:94–97

Fisher CM, Ojemann RG, Roberson GH (1978) Spontaneous dissection of cervico-cerebral arteries. Can J Neurol Sci 5:9–19
Foix C, Masson A (1923) Le syndrome de l'atère cérebrale postérieur. Presse méd 31:261–365
Fullerton HJ, Johnston SC, Smith WS (2001) Arterial dissection and stroke in children. Neurology 57:1155–1160
Gan R, Sacco RL, Kargman DE et al (1997) Testing the validity of the lacunar hypothesis: the Northern Manhattan Stroke Study experience. Neurology 48:1204–1211
Geschwind N (1965) Disconnexion syndromes in animals and man. II. Brain 88:585–644
Geschwind N (1975) The apraxias: neural mechanisms of disorders of learned movement. Am Sci 63:188–195
Geschwind DH, Iacoboni M, Mega MS et al (1995) Alien hand syndrome: interhemispheric motor disconnection due to a lesion in the midbody of the corpus callosum. Neurology 45:802–808
Ghika JA, Bogousslavsky J, Regli F (1990) Deep perforators from the carotid system. Template of the vascular territories. Arch Neurol 47:1097–1100
Ghika-Schmid F, Bogousslavsky J (2000) The acute behavioral syndrome of anterior thalamic infarction: a prospective study of 12 cases. Ann Neurol 48:220–227
Hacke W, Schwab S, Horn M et al (1996) 'Malignant' middle cerebral artery territory infarction: clinical course and prognostic signs. Arch Neurol 53:309–315
Hausser I, Muller U, Engelter S et al (2004) Different types of connective tissue alterations associated with cervical artery dissections. Acta Neuropathol (Berl) 107:509–514
Heinsius T, Bogousslavsky J, van Melle G (1998) Large infarcts in the middle cerebral artery territory. Etiology and outcome patterns. Neurology 50:341–350
Hennerici MG (2004) The unstable plaque. Cerebrovasc Dis 17 [Suppl 3]:17–22
Herrmann KA, Sporer B, Yousry TA (2004) Thrombosis of the internal cerebral vein associated with transient unilateral thalamic edema: a case report and review of the literature. AJNR Am J Neuroradiol 25:1351–1355
Higgins JNP, Gillard JH, Owler BK et al (2004) MR venography in idiopathic intracranial hypertension: unappreciated and misunderstood. J Neurol Neurosurg Psychiatry 75:621–625
Ho KL, Meyer KR (1981) The medial medullary syndrome. Arch Neurol 38:385–387
Hochachka PW, Buck LT, Doll CJ et al (1996) Unifying theory of hypoxia tolerance: molecular/metabolic defense and rescue mechanisms for surviving oxygen lack. Proc Natl Acad Sci USA 93:9493–9498
Hollenhorst RW (1958) Ocular manifestations of insufficiency or thrombosis of the internal carotid artery. Trans Am Ophthalmol Soc 56:474–506
Hommel M, Bogousslavsky J (1991) The spectrum of vertical gaze palsy following unilateral brainstem stroke. Neurology 41:1229–1234
Hossmann KA (1999) The hypoxic brain. Insights from ischemia research. Adv Exp Med Biol 474:155–169
Karnath HO, Himmelbach M, Rorden C (2002) The subcortical anatomy of human spatial neglect: putamen, caudate nucleus and pulvinar. Brain 125:350–360
Kataoka S, Hori A, Shirakawa T et al (1997) Paramedian pontine infarction. Neurological/topographical correlation. Stroke 28:809–815
Kennedy J, Buchan AM (2004) Acute neurovascular syndromes: hurry up, please, it's time. Stroke 35:360–362
Kertesz A (1993) Clinical forms of aphasia. Acta Neurochir Suppl (Wien) 56:52–58
Kubik C, Adams R (1946) Occlusion of the basilar artery – a clinical and pathological study. Brain 69:73–121
Margolis MT, Newton TH, Hoyt WF (1971) Cortical branches of the posterior cerebral artery. Anatomic-radiologic correlation. Neuroradiology 2:127–135
Markus HS (2004) Cerebral perfusion and stroke. J Neurol Neurosurg Psychiatry 75:353–361
Martin PJ, Chang HM, Wityk R et al (1998) Midbrain infarction: associations and aetiologies in the New England Medical Center Posterior Circulation Registry. J Neurol Neurosurg Psychiatry 64:392–395
Masucci EF, Fabara JA, Saini N et al (1981) Periodic alternating ping-pong gaze. Ann.Ophthalmol 13:1123–1127
Mehler MF (1989) The rostral basilar artery syndrome: diagnosis, etiology, prognosis. Neurology 39:9–16
Meissner I, Sapir S, Kokmen E et al (1987) The paramedian diencephalic syndrome: a dynamic phenomenon. Stroke 18:380–385
Minematsu K, Yamaguchi T, Omae T (1992) 'Spectacular shrinking deficit': rapid recovery from a major hemispheric syndrome by migration of an embolus. Neurology 42:157–162
Mokri B, Sundt TM Jr, Houser OW (1979) Spontaneous internal carotid dissection, hemicrania, and Horner's syndrome. Arch Neurol 36:677–680
Mokri B, Silbert PL, Schievink WI et al (1996) Cranial nerve palsy in spontaneous dissection of the extracranial internal carotid artery. Neurology 46:356–359
Molina CA, Montaner J, Abilleira S et al (2001) Timing of Spontaneous Recanalization and Risk of Hemorrhagic Transformation in Acute Cardioembolic Stroke. Stroke 32:1079–1084
Molina CA, Alvarez-Sabin J, Montaner J et al (2002) Thrombolysis-related hemorrhagic infarction: a marker of early reperfusion, reduced infarct size, and improved outcome in patients with proximal middle cerebral artery occlusion. Stroke 33:1551–1556
Moody DM, Bell MA, Challa VR (1990) Features of the cerebral vascular pattern that predict vulnerability to perfusion or oxygenation deficiency: an anatomic study. AJNR Am J Neuroradiol 11:431–439
Morrow MJ, Sharpe JA (1993) Retinotopic and directional deficits of smooth pursuit initiation after posterior cerebral hemispheric lesions. Neurology 43:595–603
Moruzzi G, Magoun HW (1949) Brain stem reticular formation and activation of the EEG. Electroencephalogr Clin Neurophysiol 1:455
Noda S, Ide K, Umezaki H et al (1987) Repetitive divergence. Ann Neurol 21:109–110
Olsen TS (1991) Outcome following occlusion of the middle cerebral artery. Acta Neurol Scand 83:254–258
Parvizi J, Damasio AR (2003) Neuroanatomical correlates of brainstem coma. Brain 126:1524–1536
Pedersen PM, Vinter K, Olsen TS (2004) Aphasia after stroke: type, severity and prognosis. The Copenhagen aphasia study. Cerebrovasc Dis 17:35–43
Plum F (1972) Hyperpnea, hyperventilation, and brain dysfunction. Ann Intern Med 76:328
Plum F, Alvord EC (1964) Apneustic breathing in man. Arch Neurol 10:101–112

Plum F, Posner JB (1980) The diagnosis of stupor and coma, 3rd edn. Davis, Philadelphia
Powers WJ (1991) Cerebral hemodynamics in ischemic cerebrovascular disease. Ann Neurol 29:231–240
Read SJ, Pettigrew L, Schimmel L et al (1998) White matter medullary infarcts: acute subcortical infarction in the centrum ovale. Cerebrovasc Dis 8:289–295
Reivich M, Holling HE, Roberts B et al (1961) Reversal of blood flow through the vertebral artery and its effect on cerebral circulation. N Engl J Med 265:878–885
Ringelstein EB, Zeumer H, Angelou D (1983) The pathogenesis of strokes from internal carotid artery occlusion. Diagnostic and therapeutical implications. Stroke 14:867–875
Ringelstein EB, Biniek R, Weiller C et al (1992) Type and extent of hemispheric brain infarctions and clinical outcome in early and delayed middle cerebral artery recanalization. Neurology 42:289–298
Russmann H, Vingerhoets F, Ghika J et al (2003) Acute infarction limited to the lenticular nucleus: clinical, etiologic, and topographic features. Arch.Neurol 60:351–355
Schievink WI (2001) Spontaneous dissection of the carotid and vertebral arteries. N Engl J Med 344:898–906
Schneider AT, Kissela B, Woo D et al (2004) Ischemic stroke subtypes: a population-based study of incidence rates among blacks and whites. Stroke 35:1552–1556
Spinazzola L, Cubelli R, Della SS (2003) Impairments of trunk movements following left or right hemisphere lesions: dissociation between apraxic errors and postural instability. Brain 126:2656–2666
Staaf G, Geijer B, Lindgren A et al (2004) Diffusion-weighted MRI findings in patients with capsular warning syndrome. Cerebrovasc Dis 17:1–8
Stark SR, Masucci EF, Kurtzke JF (1984) Ocular dipping. Neurology 34:391–393
Tijssen CC, van Gisbergen JA, Schulte BP (1991) Conjugate eye deviation: side, site, and size of the hemispheric lesion. Neurology 41:846–850
Tokuda Y, Nakazato N, Stein GH (2003) Pupillary evaluation for differential diagnosis of coma. Postgrad Med J 79:49–51
Touze E, Gauvrit JY, Moulin T et al (2003) Risk of stroke and recurrent dissection after a cervical artery dissection: a multicenter study. Neurology 61:1347–1351
Tsiskaridze A, Devuyst G, de Freitas GR et al (2001) Stroke with internal carotid artery stenosis. Arch Neurol 58:605–609
Tzourio C, Benslamia L, Guillon B et al (2002) Migraine and the risk of cervical artery dissection: a case-control study. Neurology 59:435–437
Urban PP, Wicht S, Vukurevic G et al (2001) Dysarthria in acute ischemic stroke: lesion topography, clinicoradiologic correlation, and etiology. Neurology 56:1021–1027
Vincent SR (2000) The ascending reticular activating system-from aminergic neurons to nitric oxide. J Chem Neuroanat 18:23–30
Voetsch B, DeWitt LD, Pessin MS et al (2004) Basilar artery occlusive disease in the New England Medical Center Posterior Circulation Registry. Arch Neurol 61:496–504
Von Campe G, Regli F, Bogousslavsky J (2003) Heralding manifestations of basilar artery occlusion with lethal or severe stroke. J Neurol Neurosurg Psychiatry 74:1621–1626
Vuilleumier P, Bogousslavsky J, Regli F (1995) Infarction of the lower brainstem. Clinical, aetiological and MRI-topographical correlations. Brain 118:1013–1025
Wall M, Wray SH (1983) The one-and-a-half syndrome-a unilateral disorder of the pontine tegmentum: a study of 20 cases and review of the literature. Neurology 33:971–980
Wray SH (1993) The management of acute visual failure. J Neurol Neurosurg Psychiatry 56:234–240

2 Clinical Efficacy of MRI in Stroke

Rüdiger von Kummer

CONTENTS

2.1 Introduction

It is well established that computed tomography (CT) identifies patients with acute cerebral ischemia among stroke syndrome patients and thus enables effective thrombolytic therapy (The ATLANTIS, ECASS, and NINDS rt-PA Study Group Investigators 2004). It is a matter of debate, however, whether information provided by imaging other than the exclusion of hemorrhage, e.g. the assessment of ischemic edema, arterial pathology, or perfusion deficit, can really improve the clinical outcome of acute ischemic stroke patients and can thus reduce health costs (Powers 2000; Powers and Zivin 1998; Hacke and Warach 2000) Moreover, new imaging technology like magnetic resonance imaging (MRI) offers new insights into acute stroke pathology that may result in improved treatment for more patients. This book will provide arguments for the question of whether MRI should be implemented in acute stroke management or not. This chapter will outline the theoretical background needed to understand under which conditions vascular and brain pathology depicted by MRI will be clinically effective. Subsequent chapters will describe the stroke pathology depicted by MRI in more detail and discuss its impact on stroke treatment and clinical outcome.

R. von Kummer, MD
Department of Neuroradiology, University of Technology Dresden, Fetscherstrasse 74, 01307 Dresden, Germany

2.2 Hierarchy of Efficacy Levels for Diagnostic Imaging

In theory, MRI can be clinically effective in acute stroke patients on six different levels (Fryback and Thornbury 1991; Kent and Larson 1992; Sunshine and Applegate 2004) (Table 2.1): (1) MRI will reduce health care costs, if it enables treatment that prevents disability and death in stroke victims. (2) MRI will improve the clinical outcome of stroke patients if it can identify patients who will benefit from an effective treatment, e.g. thrombolysis, and exclude others who will not benefit. (3) To identify patients who will benefit from a specific treatment, MRI must provide relevant information for the choice of treatment not available from other sources. (4) This could include MRI sequences that make it possible to exclude brain hemorrhage and other diseases that mimic ischemic stroke, and assess ischemic edema, perfusion disturbance, mass effect, arterial wall pathology, and obstruction. (5) The MRI sequence should be sensitive and specific for stroke pathology early after symptom onset. (6) This requires that the MRI sequence is technically capable of reliably detecting the relevant stroke pathology and can be feasibly performed in acute stroke patients.

It is important to bear in mind that diagnostic imaging is only clinically effective if an effective treatment is available, and the information provided by imaging identifies conditions where such treatment is beneficial. The clinical efficacy at any level in this hierarchy is a precondition for the efficacy of a higher level, but is not sufficient to guarantee improved clinical outcome. For example, the capac-

Table 2.1. Hierarchy of clinical efficacy for MRI in acute stroke

Level	Measures to quantify clinical efficacy
1. Societal value	Cost per hospital stay, proportion of patients going back to work, cost per gained quality-adjusted life years
2. Clinical outcome	Mortality and disability
3. Impact on treatment	Increase in the proportion of patients identified by MRI that benefit from treatment
4. Diagnostic impact	Increase in the proportion of patients with a specific stroke pathology identified by MRI
5. Diagnostic accuracy	Sensitivity, specificity, and prospective values of MRI for a specific stroke pathology compared to a reference standard, assessment of validity
6. Technical capacity, feasibility	Interobserver agreement in assessing a specific stroke pathology on MRI, proportion of patients who can tolerate examination with MRI

ity of T2*-weighted (T2*w) sequences in detecting hemosiderin deposits within brain parenchyma may identify patients with amyloid angiopathy, but does not mean that stroke treatment can be improved with the knowledge of this finding. This finding would have an impact on treatment only if it can be shown that patients with such hemosiderin deposits may be harmed by thrombolysis. Moreover, it is impossible to assess the clinical efficacy of MRI for ischemic stroke patients in general. The different levels of clinical efficacy can be determined only with regard to specific brain pathology as depicted by MRI like arterial disease, perfusion deficit, vascular contrast enhancement, disturbed water diffusion, increase in brain tissue water content, and brain hemorrhage.

2.2.1 Feasibility and Technical Capacity of Stroke MRI

Feasibility and technical capacity of MRI represent the basic condition for its clinical effectiveness in acute stroke. MRI is suitable as a first line investigation for all acute stroke patients in clinical routine if it can be applied in all patients with suspected stroke, with only a few exceptions.

The availability of scanning equipment and trained personal, specific contraindications, patient claustrophobia, and the safety of the sometimes very ill or uncooperative stroke patients limit the feasibility of stroke MRI during the scan. To determine the true feasibility of MRI requires a prospective study in all patients presenting with suspected stroke. Singer et al. (2004) found that only 80% of 144 stroke patients recruited "at the hospital door" could be examined with MRI. Others reported even smaller numbers between 54% and 62% of the patients in whom MRI was feasible (Barber et al. 2005; Hand et al. 2005; Schramm et al. 2004). According to Barber et al. (2005) and Hand et al. (2005), feasibility was impaired by contraindications in about 10% of patients and medical instability in 23% and 28% of patients, respectively. In both studies, the MRI scanner was unavailable for about 20% of patients. Moreover, Hand et al.(2005) reported that 11 of 61 patients (18%) scanned became hypoxic in the MRI scanner and 20% were non-compliant during the scan. Even if 100% availability of MRI is assumed for stroke centers in the near future, it would appear that 20%–30% of acute stroke patients cannot tolerate this examination or take risks when being scanned. This numbers may be reduced with new scanner technology with larger bores or smaller magnets allowing better control of patients. Nevertheless, at the moment patient safety should be seriously taken into account, and oxygen saturation should be monitored in severely ill patients during MRI. For patients with severe stroke, CT should be considered as a useful alternative.

Technical capacity of stroke MRI is its capability to reproducibly display recognizable images that demonstrate specific stroke pathology with good intra- and interobserver reliability (Powers 2000). It is conventionally measured by the agreement among observers after definition of the pathology that is sought. Cohen's kappa is widely accepted as a measure of chance adjusted agreement that is sometimes difficult to interpret, however (Feinstein and Cicchetti 1990).

What is the specific stroke pathology that should be recognized as increasing the chances of stroke treatment being beneficial? So far, reperfusion strategies have only been shown to be beneficial in acute stroke (Hacke et al. 1995, 2005; The National Institute of Neurological Disorders and Stroke rt-PA Stroke Study Group 1995; Furlan et al. 1999), whereas neuroprotective drugs failed to show any effect. The rationale of a reperfusion strategy like thrombolysis is the recanalization of an occluded brain-supplying artery in order to

restore blood flow into ischemic brain tissue that is not yet irreversibly injured and can regain function. Consequently, imaging modalities that can reliably exclude brain hemorrhage or assess arterial occlusion, cerebral perfusion deficit, or ischemic tissue damage may identify patients who will benefit from thrombolysis.

Kidwell et al. (2004) have shown that MRI can detect primary brain hemorrhage as reliably as CT in acute stroke patients, but that it is superior to CT in detecting old hemorrhages within brain parenchyma (see Chap. 10). The reliability of MRI in detecting arterial disease and cerebral perfusion deficits is discussed in Chaps. 5 and 6 in detail. The detection of ischemic damage early after arterial occlusion is difficult even under experimental conditions with the possibility to study ischemic brain tissue under the microscope (Garcia et al. 1995). Severely ischemic brain tissue with blood flow below the threshold of structural integrity takes up water, however, immediately after arterial occlusion (Schuier and Hossmann 1980; Todd et al. 1986). CT can detect and measure the change in brain tissue water content and thus identify the volume of irreversibly injured brain tissue (Dzialowski et al. 2004; von Kummer et al. 2001). The signal of spin echo MRI sequences is relatively insensitive for brain tissue water content and cannot be used to define ischemic damage early on. As discussed by Back and Neumann-Haefelin in Chaps. 3 and 7, diffusion weighted imaging (DWI) also does not directly show the volume of brain tissue that cannot recover from ischemia. The apparent diffusion coefficient (ADC) declines at cerebral blood flow (CBF) values of 0.35–0.45 ml/g/min in animal studies and at 0.15–0.24 ml/g/min in humans, at the CBF threshold where the extracellular fluid space shrinks due to ischemic cell swelling (Kohno et al. 1995; Lin et al. 2003; The National Institute of Neurological Disorders and Stroke rt-PA Stroke Study Group et al. 1995; Schuier and Hossmann 1980; Wang et al. 2000). That means that brain tissue volume with increased signal on DWI and associated decreased ADC may include both brain tissue that is irreversibly injured and tissue that can recover if CBF is restored. It appears as if MRI has the technical capacity to exclude brain hemorrhage and to assess arterial pathology and perfusion deficits, but cannot reliably define ischemic brain damage within the first hours after stroke onset. Prediction of ischemic damage may be possible by combining the information of DWI and PI in a multimodal approach (Chap. 8).

2.2.2 Diagnostic Accuracy

In-vivo neuroimaging bears an inherent problem: The assessment of validity and diagnostic accuracy requires a reference that is accepted as gold standard, but is hardly achievable. Digital subtracted angiography is the accepted gold standard for MR angiography (MRA) in assessing arterial obstructions (Chap. 5), but is inferior to MRI in detecting arterial wall pathology like mural hematoma. Positron emission tomography was used to validate MR perfusion imaging (PI) (Chap. 6). However, for the most important findings in acute stroke, intracranial hemorrhage and ischemic edema, a reference standard is not available in most cases. When studying the sensitivity of MRI for intracranial hemorrhage, MRI can be compared with CT (Kidwell et al. 2004), the number of true positive patients remains unclear, however, because CT may miss the same bleedings as MRI, and surgery or autopsy is fortunately not performed in most of these patients. The same is true for acute ischemic edema: The sensitivity and specificity of brain imaging can be evaluated under experimental conditions only (Dzialowski et al. 2004). If one accepts that ischemic necrosis is represented by a well demarcated, hypoattenuating arterial territory on CT or a brain tissue volume with increased signal on T2w sequences on follow-up images, one could use this as a reference and assess the positive and negative predictive values of acute CT or MRI findings for the development of brain infarction. Again, this approach suffers from the same methodical problem: The sensitivity and specificity of CT and MRI findings for subacute or old brain infarctions are not yet assessed. It is evident that MRI shows more than CT does (Chaps. 7–10); it is not clear, however, what MRI fails to detect.

2.2.3 Diagnostic Impact

The diagnostic impact of stroke MRI can be measured by the percentage of patients in whom the diagnosis made without MRI is altered when the information from MRI is received (Albers et al. 2000). In acute hemorrhagic stroke, MRI does not increase the frequency of this diagnosis, if all patients were examined with CT, but MRI may clarify the cause of brain hemorrhage if gradient echo sequences are applied and detect, for example, signs of amyloid angiopathy or cavernous hemangioma.

MR angiography and PI do not add much to the diagnostic information that can be provided by CT angiography and CT PI. DWI is highly sensitive for ischemic brain tissue even above the CBF level of the penumbra and indicates brain tissue at high risk if not already irreversibly injured, whereas hypoattenuation on CT depicts ischemic edema and tissue damage with high specificity within the first 6 h of stroke onset (von Kummer et al. 2001). The pattern of areas with high signal on DWI may thus enable assessment of the affected brain territory and the cause of stroke early on (Chaps. 13–16).

2.2.4 Therapeutic Impact

The therapeutic impact of stroke MRI is measured by the percentage of patients in whom MRI changes treatment planned without MRI. As shown in Chap. 3, the MRI finding of extended brain perfusion deficit, but relatively small tissue volume with impaired water diffusion (perfusion-diffusion mismatch) may allow the treatment beyond currently accepted time windows. Parsons et al. (2002) showed a beneficial outcome after thrombolysis in patients with perfusion-diffusion mismatch within 6 h of stroke onset, but did not compare the effect of recombinant tissue plasminogen activator (rt-PA) with placebo treatment. It is evident – though without scientific proof – that reperfusion strategies are clinically effective only if a perfusion deficit is present. It was shown with CT-PI, that stroke patients without cerebral perfusion disturbance did not develop brain infarctions (Schramm et al. 2004). It is debatable whether PI is required in all stroke patients or whether the image of arterial obstruction or the clinical syndrome is sufficient to justify reperfusion strategies after brain hemorrhage and other stroke mimics have been excluded. With a view to the high sensitivity of DWI for even relatively mild degrees of brain ischemia, the risk of ischemic damage appears minimal in patients with small "DWI lesions". It is still unclear, however, which extent of "DWI lesion" is associated with a reduced chance to benefit from thrombolysis.

2.2.5 Impact on Patients' Clinical Outcome

The Desmoteplase in Acute Ischemic Stroke Trial (DIAS) was based on MRI and included patients with perfusion-diffusion mismatch up to 9 h after symptom onset (Hacke et al. 2005). Part 1 of this study was terminated prematurely because of high rates of symptomatic brain hemorrhages in patients treated with desmoteplase. The upper limit of the "DWI lesion" at baseline was reduced from two thirds to one third of the middle cerebral artery territory. This adjustment of the protocol did not reduce the incidence of brain hemorrhages. The rate of symptomatic hemorrhages was considerably reduced after lowering the dose of desmoteplase in 57 patients (part 2). Part 2 of this study showed a beneficial effect of desmoteplase on reperfusion and on clinical outcome. Patients without perfusion-diffusion mismatch were not studied. Consequently, the impact of MRI findings on patients' clinical outcome remains unclear. The study shows, however, that beneficial treatment can be achieved based on MRI imaging alone.

2.2.6 Impact on Health Care Costs

Although MRI is promising in that it provides specific information which could improve treatment in ischemic stroke, there is no scientific proof that it actually does improve patients' clinical outcome. Consequently, based on current knowledge, the recommendation to base acute stroke management solely on MRI means a big investment without a guaranteed return in the form of reduced health care costs.

2.3 Summary

MRI has the specific capability to detect brain areas with ischemic cell swelling and to identify deposits of hemoglobin degradation products within brain parenchyma. It can easily be combined with angiography and PI and thus assess important aspects of acute stroke pathology. MRI has the disadvantage that not all patients with suspected stroke can tolerate the examination. It will be discussed in the following chapters whether the diagnostic information provided by MRI has an impact on acute stroke treatment and can improve patients' clinical outcome compared to patients being examined with CT.

References

Albers G, Lansberg M, Norbash A, Tong D, O'Brien M, Woolfenden A, Marks M, Moseley M (2000) Yield of diffusion-weighted MRI for detection of potentially relevant findings in stroke patients. Neurology 54:1562–1567

Barber P, Hill M, Eliasziw M, Demchuk A, Warwick Pexman J, Hudon M, Tomanek A, Frayne R, Buchan A (2005) Neuroimaging of the brain in acute ischemic stroke: a comparison of computed tomography and magnetic resonance diffusion weighted imaging. J Neurol Neurosurg Psychiatry (in press)

Dzialowski I, Weber J, Doerfler A, Forsting M, von Kummer R. (2004) Brain tissue water uptake after middle cerebral artery occlusion assessed with CT. J Neuroimaging 14:42–48

Feinstein AR, Cicchetti DV (1990) High agreement but low kappa I. The problems of two paradoxes. J Clin Epidemiol 43:543–549

Fryback D, Thornbury J (1991) The efficacy of diagnostic imaging. Med Decis Making 11:88–94

Furlan A, Higashida R, Wechsler L, Gent M, Rowley H, Kase C, Pessin M, Ahuja A, Callahan F, Clark W, Silver F, Rivera F (1999) Intra-arterial Prourokinase for acute ischemic stroke. JAMA 282:2003–2011

Garcia J, Liu K-F, Ho K-L (1995) Neuronal necrosis after middle cerebral artery occlusion in Wistar rats progresses at different time intervals in the caudoputamen and the cortex. Stroke 26:636–643

Hacke E, Warach S (2000) Diffusion-weighted MRI as an evolving standard of care in acute stroke. Neurology 54:1548–1549

Hacke W, Kaste M, Fieschi C, Toni D, Lesaffre E, von Kummer R, Boysen G, Bluhmki E, Höxter G, Mahagne M, Hennerici M (1995) Intravenous thrombolysis with recombinant tissue plasminogen activator for acute hemispheric stroke. The European Cooperative Acute Stroke Study (ECASS). JAMA 274:1017–1025

Hacke W, Albers G, Al-Rawi Y, Bogousslavsky J, Davalos A, Eliasziew M, Fischer M, Furlan A, Kaste M, Lees K, Soehngen M, Warach S (2005) The desmoteplase in acute ischemic stroke trial (DIAS). A phase II MRI-based 9-hour window acute stroke thrombolysis trial with intravenous desmoteplase. Stroke 36:66–73

Hand P, Wardlaw J, Rowat A, Haisma J, Lindley R, Dennis M (2005) MR brain imaging in patients with acute stroke - feasibility and patient-related difficulties. J Neurol Neurosurg Psychiatry (in press)

Kent D, Larson E (1992) Disease, level of impact, and quality of research methods; three dimensions of clinical efficacy assessment applied to magnetic resonance imaging. Invest Radiol 27:245–254

Kidwell C, Chalela J, Saver J, Starkman S, Hill M, Demchuk A, Butman J, Patronas N, Alger J, Latour L, Luby M, Baird A, Leary M, Tremwel M, Ovbiagele B, Fredieu A, Suzuki S, Villablanca P, Davis S, Dunn B, Todd J, Ezzeddine M, Haymore J, Lynch J, Davis L, Warach S (2004) Comparison of MRI and CT for detection of acute intracerebral hemorrhage. JAMA 292:1823–1830

Kohno K, Back T, Hoehn-Berlage M, Hossmann K (1995) Relationship between diffusion-weighted magnetic resonance images, cerebral blood flow and energy status in experimental brain infarction. Magn Reson Imgang 13:65–71

Lin W, Lee J, Lee Y, Vo K, Pilgram T, Hsu C (2003) Temporal relationship between apparent diffusion coefficient and absolute measurements of cerebral blood flow in acute stroke patients. Stroke 34:64–70

Parsons M, Barber A, Chalk J, Darby D, Rose S, Desmond P, Gerraty R, Tress B, Wright P, Donnan G, Davis S (2002) Diffusion- and perfusion-weighted MRI response to thrombolysis in stroke. Ann Neurol 51:28–37

Powers W (2000) Testing a test. A report card for DWI in acute stroke. Neurology 54:1549–1551

Powers W, Zivin J (1998) Magnetic resonance imaging in acute stroke. Not ready for prime time. Neurology 50:842–843

Schramm P, Schellinger P, Klotz E, Kallenberg K, Fiebach J, Külkens S, Heiland S, Knauth M, Sartor K (2004) Comparison of perfusion CT and CTA source images with PWI and DWI in patients with acute stroke < 6 h. Stroke 35:1562–1568

Schuier FJ, Hossmann KA (1980) Experimental brain infarcts in cats II. Ischemic brain edema. Stroke 11:593–601

Singer O, Sitzer M, du Mesnil de Rochemont R, Neumann-Haefelin T (2004) Practical limitations of acute stroke MRI due to patient-related problems. Neurology 62:1848–1849

Sunshine J, Applegate K (2004) Technology assessment for radiologists. Radiology 230:309–314

The ATLANTIS, ECASS, and NINDS rt-PA Study Group Investigators (2004) Association of outcome with early stroke treatment: pooled analysis of ATLANTIS, ECASS, and NINDS rt-PA stroke trials. Lancet 363:768–774

The National Institute of Neurological Disorders and Stroke rt-PA Stroke Study Group (1995) Tissue plasminogen activator for acute ischemic stroke. N Engl J Med 333:1581–1587

Todd N, Picozzi P, Crockard A, Ross Russel R (1986) Duration of ischemia influences the development and resolution of ischemic brain edema. Stroke 17:466–471

Von Kummer R, Bourquain H, Bastianello S, Bozzao L, Manelfe C, Meier D, Hacke W (2001) Early prediction of irreversible brain damage after ischemic stroke by computed tomography. Radiology 219:95–100

Wang Y, Hu W, Perez-Trepichio A, Ng T, Furlan A, Majors A, Jones S (2000) Brain tissue sodium is a ticking clock telling time after arterial occlusion in rat focal cerebral ischemia. Stroke 31:1386–1392

3 Therapeutic Impact of MRI in Acute Stroke

Mark W. Parsons and Stephen M. Davis

CONTENTS

A decade ago, Warach et al. (1995) suggested that echoplanar MR techniques for imaging of acute stroke patients would come to be viewed as analogous to the introduction of electrocardiography for the diagnosis of myocardial infarction, in that it would become an essential emergency diagnostic test for guiding the development and application of acute therapeutic intervention (Warach et al. 1995). Currently, echoplanar MRI is being used to guide acute stroke therapy in many centres throughout the world, and most stroke physicians now regard echoplanar MRI as having supplanted non-contrast CT scanning as the emergency imaging 'workhorse' for acute stroke (Hacke and Warach 2000). With a number of trials now in progress using MRI to guide and assess acute treatments for stroke, Warach's prediction may yet come to fruition (Warach et al. 1995) (Table 3.1).

M. W. Parsons, B.Med. PhD, FRACP
Department of Neurology, John Hunter Hospital, University of Newcastle, New Lambton, NSW 2305, Australia
S. M. Davis, MBBS, MD, FRACP
Royal Melbourne Hospital, University of Melbourne, Parkville, Melbourne Vic 3050, Australia

The central premise of acute stroke therapy is to salvage hypoperfused but still viable tissue (the ischaemic penumbra) from progressing to infarction. When a major cerebral artery is occluded, there is a core of brain tissue in the centre of the vessel's territory that dies rapidly. Surrounding this infarct core is a larger area of brain that is hypoperfused but does not rapidly infarct due to collateral blood flow (the ischaemic penumbra) (Astrup et al. 1981; Ginsberg and Pulsinelli 1994; Hossmann et al. 1977). The hypoperfused region may also contain tissue with milder reductions in blood flow that is at lesser risk of infarction (benign oligaemia) (Astrup et al. 1981; Ginsberg and Pulsinelli 1994; Hossmann et al. 1977). The fate of penumbral tissue is dependent upon reperfusion of the ischaemic region. If the artery remains occluded, most of the ischaemic penumbra progressively becomes incorporated into the infarct core. Early reperfusion (spontaneous or thrombolytic-assisted) can salvage the ischaemic penumbra from progression to infarction. Additionally, effective neuroprotective treatments, including drug therapy and manipulation of physiologic variables, may preserve the penumbra until reperfusion occurs (Davis and Donnan 2002; Fisher and Brott 2003).

The positive National Institute of Neurological Disorders and Stroke trial of tissue plasminogen activator (tPA) for stroke in 1995 heralded the start of the thrombolytic era for stroke (National Institute of Neurological Disorders and Stroke rt-PA Stroke Study Group 1995). This trial showed that tPA, if given within 3 h of stroke onset, increased independent survival by 30%, with a 12% absolute increase in the number of patients with no, or minimal disability. Other large trials testing thrombolysis within 6 h of stroke onset have been less positive (Hacke et al. 1995, 1998). As a consequence thrombolysis is not a universally accepted routine treatment for stroke and remains the subject of intense debate and research. Despite this, stroke thrombolysis has the potential to dramatically improve the outcome of many patients with severe

Table 3.1. Stroke trials underway using MRI

Trial name	Validation of perfusion-diffusion mismatch	Use of MRI as Selection tool	Use of MRI as a Surrogate Outcome/ Proof of concept
Thrombolytic trials			
Echoplanar Imaging Thrombolysis Evaluation Trial (EPITHET)	Yes	No	Yes
DWI evolution for understanding stroke aetiology (DEFUSE)	Yes	No	No
Stroke evaluation for late endovascular cerebral thrombolysis with MR (SELECT MR)	No	Yes	Yes
Desmoteplase in acute stroke (DIAS/DEDAS)	No	Yes	Yes
MR and recanalization of stroke clots using embolectomy (MR RESCUE)	Yes	Yes	Yes
Combination approach to lysis using eptifibatide and rt-PA (CLEAR)	No	No	Yes
Neuroprotective trials			
Glucose Reduction and Cerebral Events (GRACE)	No	No	Yes
AMPA receptor antagonist treatment in ischaemic stroke (Artist-MRI)	No	No	Yes
Magnetic Resonance Intravenous Magnesium Efficacy in Stroke (MR IMAGES)	No	No	Yes

stroke. Furthermore, the available data suggest that treatment is promising for a far greater range of patients than the current restricted approvals, particularly those 3–6 h after stroke onset (Donnan et al. 2003; Wardlaw 2001).

Current thrombolysis guidelines are based on a rigid time clock (< 3 h) without any imaging of the ischaemic penumbra. This time window is quite restrictive and very few stroke patients receive thrombolytic treatment worldwide. Extension of the therapeutic window beyond 3 h could substantially increase the number of patients able to receive thrombolysis. However, for this to occur with improved outcomes better selection criteria based on identification of the ischaemic penumbra using rapid and accessible neuroimaging techniques are required (Baron et al. 1995; Davis and Donnan 2004). Although there are many definitions of the ischaemic penumbra, the most practical for stroke clinicians is tissue that is at risk of infarction but still salvageable and that is the target of acute stroke therapy (Astrup et al. 1981; Ginsberg and Pulsinelli 1994; Hossmann 1994). Therefore, to select patients for acute stroke treatment, neuroimaging must distinguish penumbral tissue from the ischaemic core and benign oligaemic tissue.

The presence and extent of the ischaemic penumbra is time-dependent. However, stroke is a heterogeneous disorder, and survival of the penumbra can vary from less than 3 h to well beyond 48 h from patient to patient (Darby et al. 1999; Read et al. 2000). Penumbral survival is dependent upon many factors, such as location of vessel occlusion, state of collateral blood supply, extent of grey versus white matter ischaemia, and physiologic variables such as blood glucose, body temperature and blood pressure (Davis and Donnan 2004). Approximately 90%–100% of patients with supratentorial large artery occlusion have penumbral tissue at 3 h after stroke onset (which likely explains the strongly positive sub-3 h tPA data) (Darby et al. 1999; Read et al. 2000). By 6 h, 75%–80% of patients still have penumbral tissue (Darby et al. 1999; Read et al. 2000). This is a substantial number, although a significant minority of patients in the 3- to 6-h window are unlikely to benefit from thrombolysis if the standard clinical and non-contrast CT criteria are applied (and may explain the less convincing 3- to 6-h tPA trial results to date) (Hacke et al. 1995, 1998). Indeed, it was recently demonstrated that the size of the infarct core varied dramatically between patients in the first 6 h after middle cerebral artery (MCA) occlusion, and was the strongest predictor of outcome (Jovin et al. 2003).

Thus, a 'tissue clock' where the extent of both irreversible (core) and reversible ischaemia (penumbra) is determined, rather than a rigid time window, would seem the ideal guide to patient selection for thrombolysis. A practical and accessible method of imaging the penumbra could also have a major impact on the institution of other new acute stroke therapies (Davis and Donnan 2002). Neuroprotective drugs have shown great promise in animal stroke models, but have failed many times to translate into positive human studies. These negative results may at least partly relate to the fact that no method of penumbral imaging has been used to select patients

for treatment, despite the penumbra being the target for these drugs (Davis and Donnan 2002).

Combining diffusion-weighted and perfusion MRI with MR angiography (MRA) (multimodal echoplanar MRI) has revolutionised the evaluation of patients with acute stroke and appears as the best technique currently available to guide acute therapy. Diffusion-weighted MRI (DWI) delineates ischemic brain tissue within minutes, and perfusion MRI (PI) defines the area of cerebral hypoperfusion. PI and DWI have higher sensitivities for ischaemic change in the crucial first hours following symptom onset than conventional MRI or CT. This is the window when acute stroke therapies are likely to be of most benefit. Furthermore, the loci and patterns of PI and DWI lesions enable inferences to be made about stroke pathophysiology, and likely lesion evolution and outcome at times when conventional imaging is normal or any ischaemic changes are subtle. In particular, the difference in volume between a larger PI lesion compared to the DWI lesion may outline the extent of ischaemic tissue at risk of infarction. Such 'perfusion-diffusion mismatch' is a simple and practical approach to define the ischaemic penumbra (Fig. 3.1). Other, more complicated (and perhaps less widely applicable) MRI models of the ischaemic penumbra have also been proposed (Kidwell et al. 2003).

3.1 MR Perfusion-Diffusion Mismatch: An Approach to Identifying the Ischaemic Penumbra

There is now a significant body of clinical data indicating that early DWI lesion volumes not only correlate well with final infarct size, but also with clinical outcome (Baird et al. 1997, 2000; Barber et al. 1998a; Lovblad et al. 1997; Saunders et al. 1995; Tong et al. 1998; Warach et al. 1996). Serial diffusion-weighted imaging has revealed progressive enlargement of the DWI lesion if the acute PI lesion is greater than the acute DWI lesion with a reduction of a perfusion-diffusion mismatch over time. Others have observed a rather constant extent of these lesions (Fiehler 2004). The eventual DWI lesion volume correlates closely with final T2-weighted lesion volume and neurologic outcome (Baird et al. 1997; Barber et al. 1998a; Tong et al. 1998; Warach et al. 1996).

Perfusion imaging (PI) is complementary to DWI in acute stroke assessment. In animal models, PI lesions are visible immediately after vessel occlusion and resolve rapidly after successful thrombolysis or reperfusion (Muller et al. 1995; Yenari et al. 1997). In stroke patients, serial PI studies can document

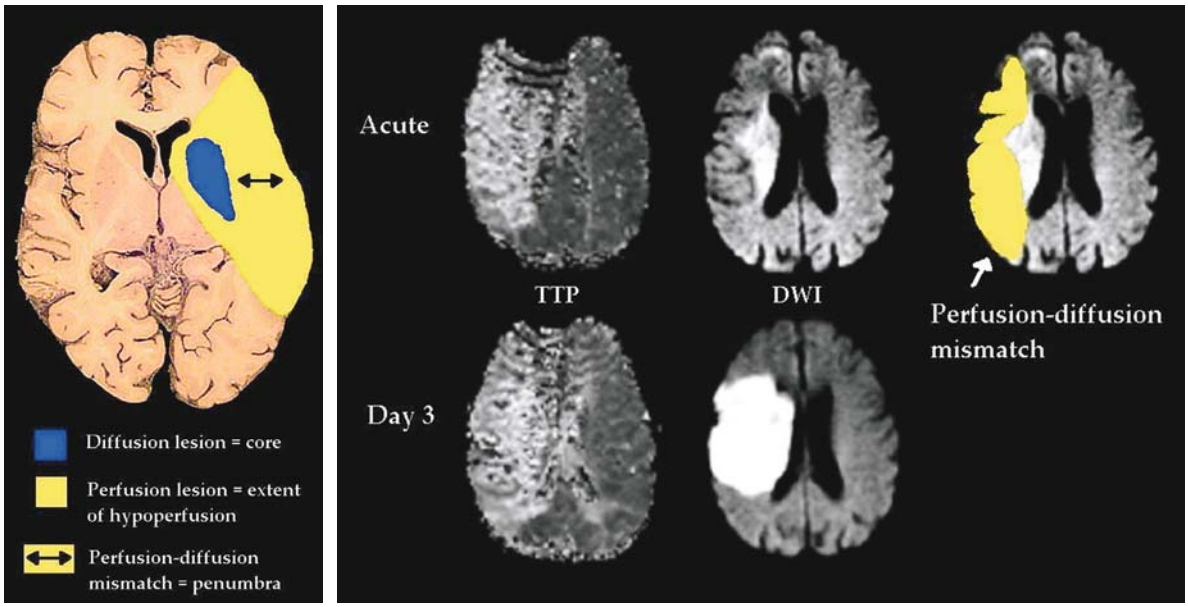

Fig. 3.1a,b. a The ischaemic penumbra. The perfusion (PI) lesion delineates the extent of hypoperfusion and the diffusion (DWI) lesion outlines the infarct core. The difference between the two lesions (perfusion-diffusion mismatch) represents the ischaemic penumbra, tissue at risk of progression to infarction. **b** Patient imaged at 3 h after onset of left hemiparesis and neglect with large PI (time to peak - *TTP*) lesion and smaller DWI lesion. At day 3 reperfusion has not occurred and the infarct core (diffusion lesion) has expanded greatly into the region of acute perfusion-diffusion mismatch. This is consistent with the perfusion-diffusion mismatch area representing the ischaemic penumbra

the evolution of perfusion lesions and clarify when reperfusion occurs. Earlier reperfusion correlates strongly with improved stroke outcome (Barber et al. 1998b). Most patients who do not receive thrombolytics have persisting perfusion deficits for > 24 h, whereas early reversal of PI lesions may be seen following thrombolysis (Kidwell et al. 2000; Marks et al. 1999).

Early PI lesions are typically larger than early DWI lesions (perfusion-diffusion mismatch) (Barber et al. 1998a; Warach et al. 1996). In acute stroke patients, the volume of the early PI lesion correlates more closely with the acute neurological deficit, suggesting that the acute PI lesion provides a more accurate estimate of the amount of brain tissue with impaired function (Baird et al. 1997; Barber et al. 1998a). However, if early reperfusion does not occur, the DWI lesion will expand to fill most of the volume of the acute PI lesion (Barber et al. 1998a). This expanded DWI lesion volume correlates closely with the patient's final neurological deficit and final infarct volume on T2-weighted imaging (Barber et al. 1998a). Thus, there is substantial evidence to indicate that perfusion-diffusion mismatch tissue is 'at risk' of progressing to infarction if rapid reperfusion does not occur (Baird et al. 1997; Barber et al. 1998a; Beaulieu et al. 1999; Schlaug et al. 1999; Warach et al. 1996). These observations provide compelling support for the mismatch model of the ischaemic penumbra as the natural history of early DWI lesions in untreated patients is to grow over time into the area of the initial PI lesion as the penumbra progressively fails and becomes recruited into the infarct (Fig. 3.2).

Some patients may undergo rapid irreversible injury to larger regions of brain, presumably due to poor collateral circulation. These patients may present with large acute DWI lesions that are of similar size to the acute PI lesion (non-mismatch pattern, see Fig. 3.3). It has been suggested that this group of

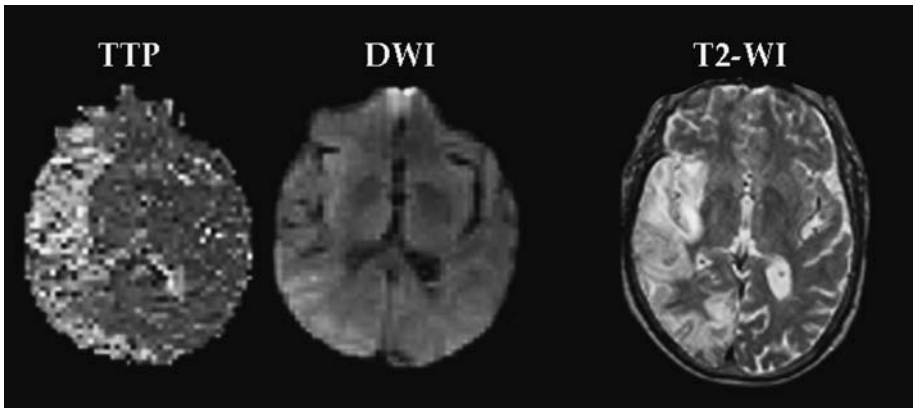

Fig. 3.2. Acute PI (*TTP*) and DWI scans demonstrate perfusion-diffusion mismatch. Follow-up T2-weighted imaging at 1 month documents major expansion of the infarct core into the original mismatch region

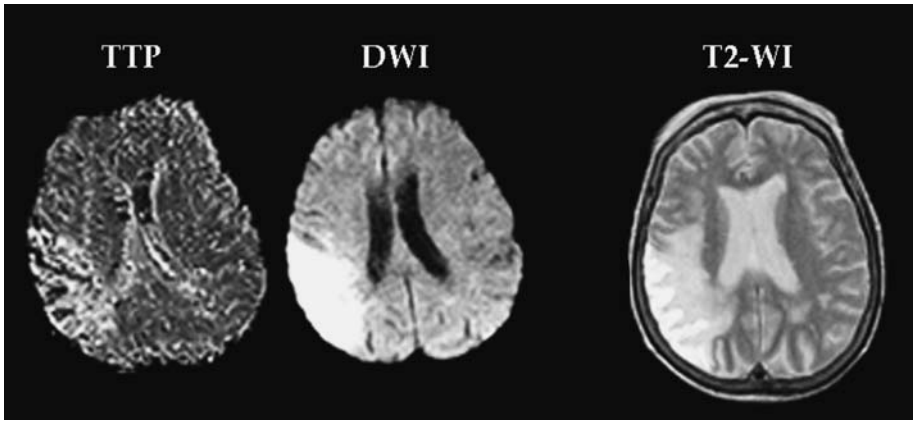

Fig. 3.3. There is no significant difference in size between the acute perfusion (*TTP*) and diffusion (*DWI*) lesion scans, non-mismatch. On follow-up T2-weighted imaging there has been no expansion of the infarct core

patients are unlikely to benefit from thrombolysis as there is little or no tissue at risk (Baird et al. 1997; Darby et al. 1999; Fisher 1997). Another PI/DWI pattern seen in stroke is where the acute DWI lesion is substantially larger than the PI lesion (Baird et al. 1997; Barber et al. 1998a). These patients may have experienced partial or complete reperfusion, implying that thrombolytic therapy will not be of benefit (Caplan et al. 1997).

Further natural history studies supported the mismatch model of the penumbra by demonstrating that if early reperfusion of the PI lesion occurs, growth of the acute DWI lesion is inhibited. Thus, there is salvage of the mismatch region and these patients may experience substantial clinical improvement (Barber et al. 1998b).

Of great relevance to the potential use of multimodal MRI in extending the time window for thrombolysis have been the observations that perfusion-diffusion mismatch was present for up to 24 h after symptom onset (Table 3.2). Whilst the presence and volume of mismatch decreases over time, at least 50% of patients still have significant tissue at risk 24 h after stroke onset (Fig. 3.4). This correlates well with positron emission tomography studies that show penumbral tissue persists up to 48 h after symptom onset, and that spontaneous survival of this tissue results in clinical improvement (Markus et al. 2003; Read et al. 2000). There is mounting evidence that the time window for salvage of the penumbra is well beyond 3 h and multimodal MRI can identify such patients.

The evolution of the mismatch model of the penumbra has led to a number of studies examining the response of acute DWI/PI patterns to thrombolytic therapy, particularly with respect to treatment beyond 3 h after stroke onset (Jansen et al. 1999; Kidwell et al. 2000; Parsons et al. 2002a; Schellinger et al. 2000). These studies supported the mismatch-penumbra hypothesis by demonstrating that thrombolysis rescues mismatch tissue from infarction. Furthermore, some reports have provided evidence that the natural history of tissue at risk can be altered by thrombolysis, and, that this may translate into improved clinical outcome (Hacke 2004; Parsons et al. 2002a).

Our group compared patients with and without perfusion-diffusion mismatch treated with intravenous tPA within 6 h to a group of matched controls (Parsons et al. 2002a). Mismatch patients treated with tPA had greater vessel recanalisation, enhanced reperfusion, greater penumbral salvage, and less infarct expansion than controls (Fig. 3.5). The positive effects of thrombolysis on lesion growth were reflected in mismatch patients treated with tPA having improved measures of clinical outcome. Of note, the MR endpoints of enhanced reperfusion, greater penumbral salvage, and reduced infarct expansion all correlated with a greater chance of clinically meaningful improvement. A particularly provocative finding was that the improvement in clinical outcome seen in the mismatch patients treated with tPA compared to controls was completely negated when non-mismatch patients were included in the analysis (Parsons et al. 2002a). This implies that patients with perfusion-diffusion mismatch have the most to gain from thrombolytic therapy.

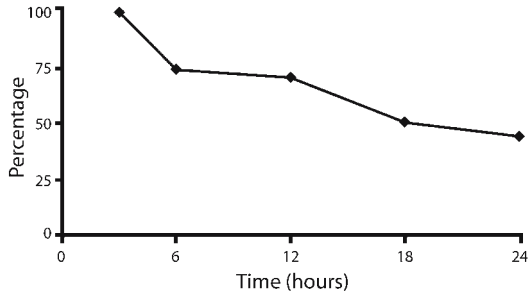

Fig. 3.4. Graph showing the proportion of patients with perfusion-diffusion mismatch at various time points after stroke onset. Although the proportion of patients with mismatch declines with time, 50% of patients still have at-risk tissue 24 h after symptom onset (Darby et al. 1999)

Table 3.2. Studies demonstrating the persistence of perfusion-diffusion mismatch

Author	Time window	Percentage with perfusion-diffusion mismatch	Type of PI map used to assess hypoperfusion
Baird et al. (1997)	24 h	70%	First moment time
Darby et al. (1999)	24 h	80% at 6 hours 65% at 12 hours 50% at 24 hours	First moment time
Neumann-Haefelin et al. (1999)	24 h	80%	Time to peak
Beaulieu et al. (1999)	7 h	50%	Time to peak
Sorenson et al. (1999)	12 h	65%	Mean transit time and cerebral blood flow
Schellinger et al. (2000)	6 h	80%	Time to peak
Parsons et al. (2001)	6 h	75%	Mean transit time and cerebral blood flow

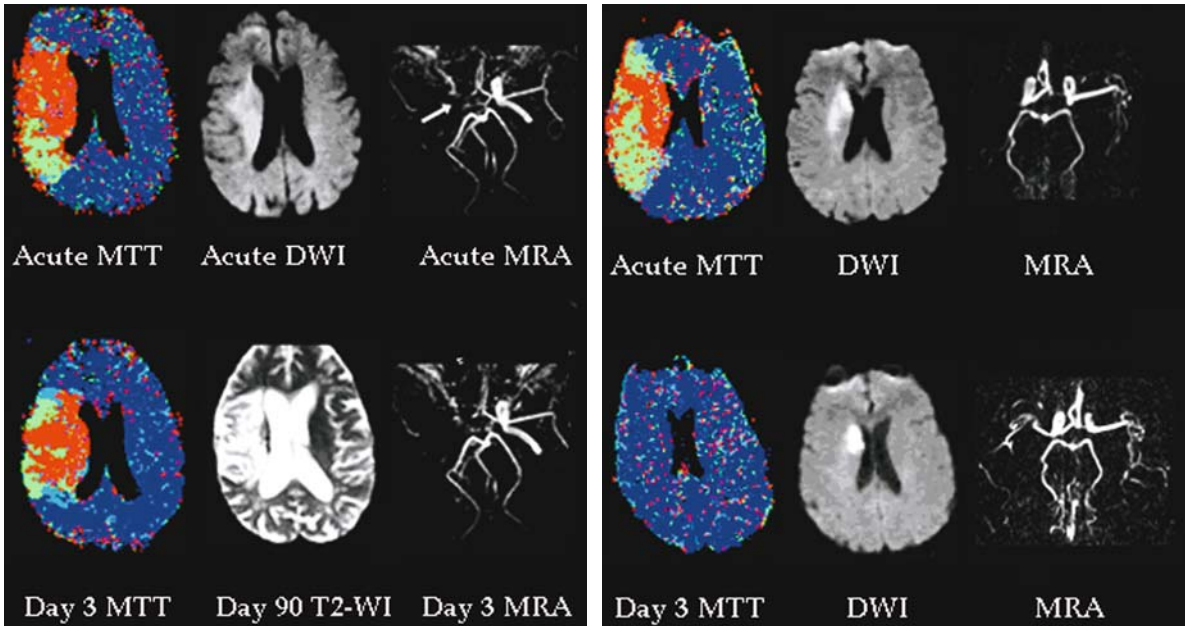

Fig. 3.5a,b. a Patient imaged at 3 h after stroke onset. There is a large perfusion lesion and extensive perfusion-diffusion mismatch. The PI map is a contrast mean transit time (*MTT*), green tissue is moderate contrast delay (4–6 s) and red is severe delay (> 6 s). The patient did not receive tPA, and at day 3 had persisting vessel occlusion on MRA (*arrow*) and large perfusion lesion. Consequently, there was major infarct expansion. **b** Patient treated with t-PA 5 h after symptom onset following MRI. Pre-therapy there is an occluded proximal M1 segment. Following tPA there is recanalization and reperfusion. In contrast to (**a**), there is salvage of a large amount of acute perfusion-diffusion mismatch tissue from infarction. Of interest, there is minor reduction in the DWI lesion after thrombolysis

A phase II study of a new thrombolytic agent, desmoteplase, has also recently been completed (Hacke 2004). A total of 104 patients were randomised to desmoteplase or placebo in a dose escalation study. Perfusion-diffusion mismatch was used as an inclusion criteria for the study. Patients who received desmoteplase had significantly higher reperfusion and reduced DWI lesion growth. A phase III study using perfusion-diffusion mismatch and perfusion CT to select patients is planned.

3.2 Refining the Mismatch Model of the Penumbra

In our view, the MRI patterns for identifying the ideal candidate for thrombolysis are straightforward. This particularly applies to treatment beyond the 3-h window. A small infarct core identified by DWI and a large perfusion deficit on PI indicate the potential for a major benefit from thrombolysis. This simple, practical mismatch model has, however, been challenged by partial normalisation of the DWI lesion, and because PI can exaggerate the area of truly ischaemic tissue (Fig. 3.6) (Kidwell et al. 2003; Parsons et al. 2001).

3.2.1 Perfusion Thresholds

PI may not necessarily differentiate between true penumbra and benign oligaemic tissue. The original experimental work by Astrup et al. (1981) identified three thresholds of hypoperfused tissue based on cerebral blood flow (CBF): core (CBF < 6–10 ml/100 g/min), penumbra (CBF < 10–20 ml/100 g/min), and oligaemic tissue (CBF below normal range but not at risk of infarction). It is clear that the commonly used PI contrast transit maps, time to peak (TTP) and mean transit time (MTT) include some benign oligaemic tissue at the border of the PI lesion (Barber et al. 1998a; Neumann-Haefelin et al. 1999; Parsons et al. 2001). Our group, and others, have demonstrated that the natural history of acute DWI lesion is to grow into the mismatch region, and that this growth encompasses a large proportion of the visible acute MTT or TTP lesion (Barber et al. 1998a; Neumann-

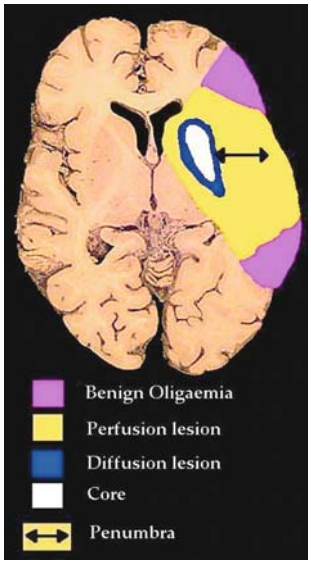

Fig. 3.6. The potential flaws in the mismatch hypothesis. The perfusion lesion probably overestimates truly hypoperfused tissue and includes some benign oligaemic tissue. The DWI lesion may overestimate the infarct core and be partially reversible

Haefelin et al. 1999; Parsons et al. 2001). However, these PI maps significantly overestimate final infarct size (Fig. 3.7) (Parsons et al. 2001).

How to best distinguish between penumbra and benign oligaemia at the border of the perfusion lesion has been the subject of intense research and debate. A range of perfusion (and apparent diffusion coefficient) thresholds have been identified that distinguish between penumbra and benign oligaemia with varying degrees of accuracy (Fig. 3.7) (Desmond et al. 2001; Grandin et al. 2002; Neumann-Haefelin et al. 1999; Parsons et al. 2001; Thijs et al. 2001). However, there is a number of difficulties with the predictive value of isolated ADC and perfusion thresholds. One major problem is that absolute quantification of cerebral perfusion with PI is not really possible, hence correlation with Astrup's experimental thresholds are impossible (Calamante et al. 1999, 2002). Simplistically, this relates to the fact that there is a non-linear relationship between contrast concentration and signal intensity with gadolinium-based PI (Calamante et al. 1999, 2002). Another major issue with perfusion thresholds is that they change with time. This has been demonstrated both experimentally, and in human stroke with PI (Butcher et al. 2003; Heiss 1983; Hossmann 1994; Hossmann et al. 1977). In research performed by our group, penumbral tissue with a contrast transit delay of up to 15 s was salvaged from infarction at 2 h after stroke onset, but at 6 h the threshold for salvage was less than 6 s delay in contrast transit (Fig. 3.8) (Butcher et al. 2003).

3.2.2 DWI Reversal

Much debate exists over the accuracy of the acute DWI lesion identifying the ischaemic core, that is, tissue that is irreversibly damaged. There is no doubt that diffusion lesions may be partially reversed with early reperfusion. This has been demonstrated in both animal and human stroke (Chalela et al. 2003; Kidwell et al. 2000; Li et al. 1999, 2000). However, in humans these lesion reversals in most instances are only minor or partial, and are quite often not permanent. Indeed, in our thrombolytic series, less than 5% of patients had what would be considered any significant reduction in ischaemic lesion volume between the pre-treatment DWI and outcome T2-weighted

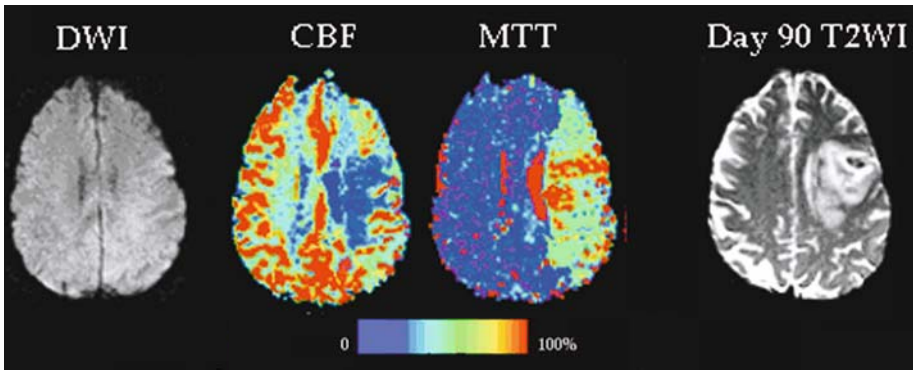

Fig. 3.7. Acute DWI and colour PI maps compared to outcome infarct size. Note that the acute CBF lesion is closest to final infarct size and the MTT lesion overestimates final infarct size, suggesting that the MTT map is demonstrating benign oligaemia as well as 'true penumbra'

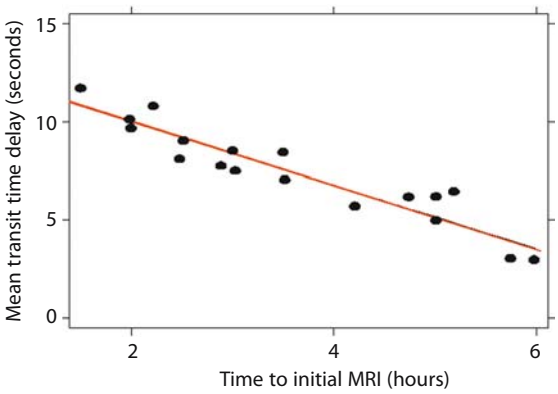

Fig. 3.8. Graph demonstrating that the perfusion threshold for mismatch tissue to be salvaged from infarction declines with time. These patients all had major reperfusion on follow-up imaging and tissue with severe hypoperfusion (mean transit time 15-s delay) was able to be salvaged from infarction within 3 h, but at 6 h, the threshold for salvage declined to only 3 s delay in mean transit time (Butcher et al. 2003)

scan (Parsons et al. 2002a). Most of these patients also had a large volume of acute perfusion-diffusion mismatch tissue salvaged from infarction. In fact, the reduction in volumes from the acute DWI lesion to outcome T2-weighted infarct were very small compared to the amount of mismatch tissue that was salvaged from infarction (Fig. 3.5b). Only one patient with non-mismatch was an exception to this rule (Fig. 3.9). We believe that acute perfusion-diffusion mismatch identifies the great majority of tissue at risk of infarction. The acute DWI lesion does not necessarily represent infarcted tissue. However, it is a very useful predictor of the minimum extent of tissue that eventually infarcts.

It has been proposed that the phenomenon of DWI lesion reversal means that patients without perfusion-diffusion mismatch may still benefit from thrombolytic therapy (Kidwell et al. 2000). However, others consider more research is needed before adopting such an approach into clinical practice (Schellinger et al. 2003). We have not found that non-mismatch patients benefited from thrombolysis compared to historical controls (Parsons et al. 2002a). The ongoing Australasian Echoplanar Imaging Thrombolysis Evaluation Trial (EPITHET) has been designed, in part, to answer the question of whether non-mismatch patients benefit from thrombolysis (Parsons et al. 2002a).

In an attempt to address the issues regarding PI overestimating at risk tissue and DWI overestimating the ischaemic core, multivariate models using different perfusion and ADC measures have been developed by several groups (Kidwell et al. 2003; Warach 2001). Kidwell et al. (2003) have shown that such a model using ADC and TTP values predicted infarction and salvage with 81% accuracy compared to 53% with the simple mismatch model. Although combined tissue viability models may be more accurate at predicting tissue fate than the mismatch model, their generalisability is yet to be proven. It is uncertain whether the improved precision is of clinical significance for patient selection. For example, one visualises an extensive area of acute perfusion-diffusion mismatch using PI and DWI maps at the MR console, how often would the availability of a co-registered quantitative tissue outcome map (appropriately) change the decision to treat with thrombolysis? This question can only be answered with further research. It is also important to recognise that perfusion-diffusion mismatch provides a good, rapidly available estimation of the penumbra and a practical means of selecting candidates for acute stroke therapy.

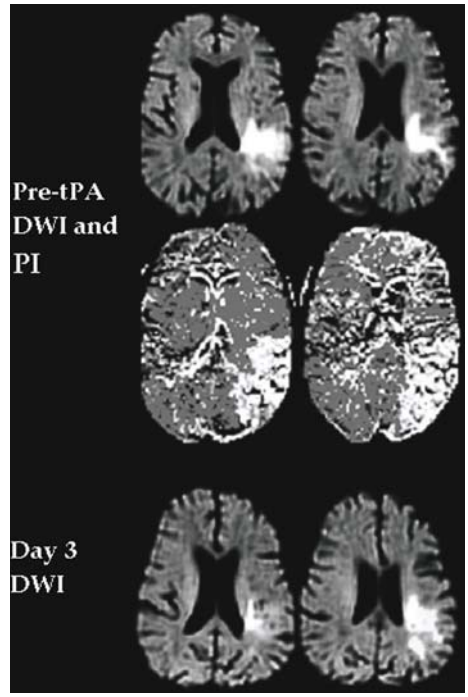

Fig. 3.9. Patient without acute perfusion-diffusion mismatch and significant DWI reversal following intravenous tPA

3.2.3 What Does MRA Add to PI/DWI/?

A previous study concluded that PI/DWI tissue at risk was always associated with a proximal vessel

occlusion on MRA (Schellinger et al. 2001). However, as our group has previously reported, about 25% of patients with perfusion-diffusion mismatch do not have an observable lesion on MRA (Barber et al. 1999b). These patients have PI lesions indicating probable branch MCA occlusion below the resolution of the MRA sequence. In our experience with acute stroke patients, the time invested in using longer MRA sequences (> 4 min) which may have greater resolution beyond the MCA division, is not productive. In our thrombolytic series, considerable at risk tissue was still present in the mismatch patients without visible MRA lesions (Parsons et al. 2002a). Indeed, this group of patients seems to have the most dramatic response to tPA, often with major reperfusion, complete penumbral salvage, and no infarct expansion (Fig. 3.10). Therefore, thrombolysis should still be considered for patients without a visible MRA lesion, provided that perfusion-diffusion mismatch is present.

Furthermore, a number of groups have now demonstrated that patients with distal vessel occlusion (including those without visible MRA lesions) have more complete reperfusion in response to tPA compared to those with proximal occlusion (Linfante et al. 2002; Neumann-Haefelin et al. 2004; Parsons et al. 2002a). This is consistent with conventional angiographic data (Furlan et al. 1999). These results emphasise that thrombolysis should not be withheld from patients with distal arterial occlusion (if perfusion-diffusion mismatch is present), but also that alternative treatment approaches might need to be considered for patients with ICA or proximal MCA occlusion. These might include intra-arterial (IA) thrombolysis and combined IV/IA thrombolysis. Such approaches might increase the risk of haemorrhagic transformation, however it is clear that the natural history of untreated distal ICA or proximal M1 MCA occlusion is very poor (Baird et al. 1997; Barber et al. 1999b; Darby et al. 1999; Linfante et al. 2002). Thus, MRA is complementary to DWI/PI in acute stroke. It is particularly useful in determining whether more aggressive reperfusion strategies are appropriate. However, it does not provide the valuable pathophysiologic information about cerebral perfusion in acute stroke that PI can.

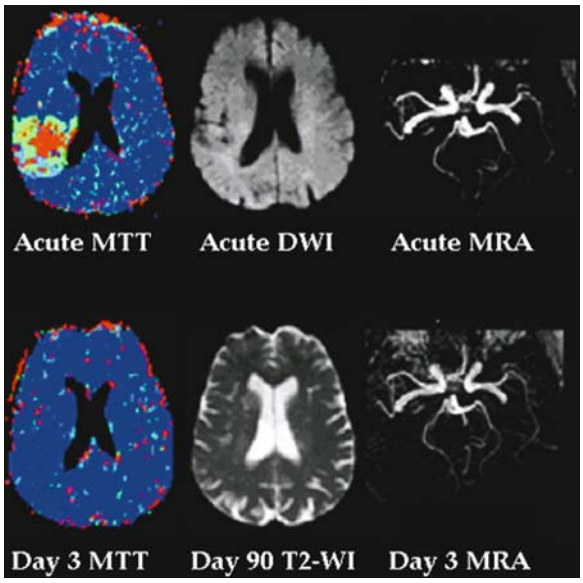

Fig. 3.10. Patient received intravenous tPA following MRI. PI map is a colour coded MTT map where mildly hypoperfused tissue is *light blue*, moderate hypoperfusion is *green*, and severe is *red*. Despite no visible vessel occlusion on acute MRA, there is still significant tissue at risk. Following thrombolysis, there is complete reperfusion and all mismatch tissue is salvaged from infarction on follow-up imaging

3.2.4 Clinical Diffusion Mismatch?

The relationship of sub-6 h PI and DWI lesion volumes with acute and outcome National Institutes of Health Stroke Scale (NIHSS) has been a source of recent controversy (Schellinger et al. 2001). Most reports, however, show a strong correlation between acute PI lesions and baseline clinical scores (Barber et al. 1998a; Tong et al. 1998; Warach et al. 1996, 1999). This has led to the suggestion that the discrepancy between stroke severity, assessed with the NIHSS, and the volume of the DWI lesion ('clinical-diffusion mismatch') could be used as a surrogate for perfusion-diffusion mismatch. Our group has examined this hypothesis and have found that an NIHSS > 7 and DWI lesion volume < 25 cm^3 predicts the presence of perfusion-diffusion mismatch with > 90% specificity, but low sensitivity. If PI had been omitted, more than 60% of patients with perfusion-diffusion mismatch would have been misdiagnosed as not having tissue at risk (Prosser et al. 2004). Indeed, other groups have demonstrated that up to 25% of patients with hyperacute stroke would have been incorrectly categorised as not having tissue at risk if PI was disregarded and DWI information alone was used (Sunshine et al. 2001). Therefore, combining PI with DWI dramatically increases the number of patients potentially eligible for acute stroke therapy.

3.2.5 False-Negative DWI

The other circumstance where PI is invaluable in acute stroke patients is where DWI is false-negative (Sunshine et al. 2001). This is a more common occurrence in hyperacute stroke, where decision making for therapy is critical (Sunshine et al. 2001). Overall, the sensitivity and specificity of DWI for ischemic lesions in acute stroke (< 24 hours) is very high, although false-negative DWI is more common in the posterior fossa (Ay et al. 1999; Lovblad et al. 1998; Oppenheim et al. 2000). In hyperacute stroke, the false-negative DWI rate may be above 10%, even in the anterior circulation (Sunshine et al. 2001). In this time window, combining PI with DWI provides essential diagnostic and therapy-guiding information that DWI alone does not.

3.3 Vertebrobasilar Stroke

The great majority of hyperacute stroke MRI studies have been limited to patients with supratentorial ischaemia. While much less frequent, vertebrobasilar infarction has a high mortality, up to 70%–80%. Both IA and IV thrombolysis in small, uncontrolled series have dramatically improved outcomes (Brandt et al. 1996; Grond et al. 1998; Hacke et al. 1988). Sensitivity of DWI, and especially PI, at the base of the skull is probably lower due to susceptibility artefacts. Recently of note, substantial regions of perfusion-diffusion mismatch have been demonstrated in the posterior fossa, with salvage of these regions after thrombolysis (Ostrem et al. 2004). Many stroke centres throughout the world use multimodal stroke MRI to confirm vertebrobasilar occlusion and exclude major brainstem and/or thalamic and occipital infarction before proceeding to thrombolytic therapy (Schellinger et al. 2003).

3.3.1 Prediction of Haemorrhagic Transformation with MRI

It is controversial whether ischaemic changes on CT involving > 33% of the MCA territory increases the risk of haemorrhagic transformation (HT) associated with tPA (Patel et al. 2001; von Kummer et al. 1997). This may partially reflect the insensitivity of CT for brain ischemia above 10 ml per 100 g/min. DWI more clearly identifies acute ischaemia below 30 ml per 100 g/min and thus may be a more reliable predictor of risk of thrombolysis-related HT (Barber et al. 1999a). A number of studies have now suggested that DWI findings can help to identify patients at increased risk for HT (Selim et al. 2002; Tong et al. 2001). In general, they have found that the number of voxels with an ADC $< 550 \times 10^{-6}$ mm^2/s is the best predictor. However, this is essentially a marker of overall DWI lesion volume (Selim et al. 2002). The problem with these predictors is that there is no absolute cut-off DWI/ADC lesion volume, and the overlap between patients with and without HT is significant. In our experience, an acute DWI lesion volume > 100 cm^3 (or qualitatively greater than 50% of the MCA territory) particularly if it is associated with no perfusion-diffusion mismatch (and regardless of vessel status on MRA), should probably be a contraindication to thrombolysis (Fig. 3.11). This requires further study, and EPITHET may provide more definitive answers to the question of HT prediction. The presence of prior microbleeds on T2*-weighted MRI may also be a risk factor for thrombolysis-related HT (Kidwell et al. 2002; Nighoghossian et al. 2002). This is a relatively infrequent finding (less than 10% of patients), and the association is not yet firmly established.

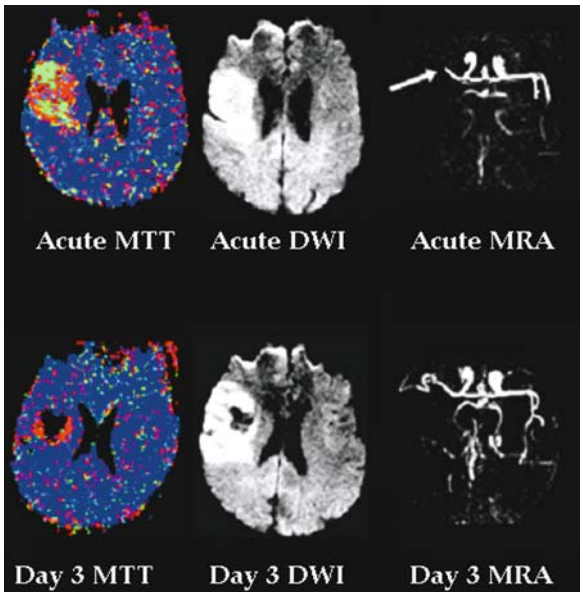

Fig. 3.11. Patient who received t-PA following MRI. *PI*, = quantitative MTT map. There is a distal M1 occlusion on MRA, but no obvious tissue at risk (no perfusion-diffusion mismatch). The baseline DWI lesion is quite large. Thrombolysis successfully achieves recanalization and reperfusion, but there is also haemorrhagic transformation apparent on day 3 imaging

3.4 Detection of ICH with MRI

Emerging data suggests that MRI may be able to detect hyperacute intra-parenchymal haemorrhage at least as accurately as CT (Fiebach et al. 2004; Linfante et al. 1999). So-called susceptibility-weighted T2* (gradient echo) sequences detect haemorrhage due to a profound signal loss caused by the paramagnetic effects of deoxyhaemoglobin, even when present in trace amounts (Linfante et al. 1999). In practice, the unprocessed gradient echo (T2*) images performed for PI, or the $b = 0$ images obtained from DWI echoplanar sequences can be used to sensitively detect ICH without adding any extra time to the stroke MRI protocol (Lin et al. 2001; Perl et al. 1999). Thus, stroke MRI probably obviates the need for a screening CT before thrombolysis.

3.4.1 Uncertain Stroke Onset

A not uncommon scenario is the acute stroke patient who has woken from sleep with a neurologic deficit, or is aphasic/obtunded and there is no corroborative history. Traditionally, such patients have been excluded from acute therapies, as the exact time of stroke onset is unclear. However, a significant proportion of these patients have perfusion-diffusion mismatch, suggesting recent stroke onset, and potential benefit from thrombolysis (Fink et al. 2002). As we are advocating that selection of patients for acute stroke therapy should be based on cerebral pathophysiology rather than a rigid time window it may well be that such patients will be treated in the future. However, at this point further evidence from randomised trials such as EPITHET and DIAS will be required to make such a major practice change.

3.4.2 Hyperacute Stroke MRI as a Practical Tool

Whilst the practicality of MRI as a neuroimaging tool for hyperacute stroke has been questioned in the past, there is now substantial data demonstrating its feasibility and practicality (Powers 2000; Powers and Zivin 1998). Current stroke MRI protocols take 15–20 min to perform (total 'table' time) and are part of the routine stroke workup in many academic centres (Kidwell et al. 2000; Parsons et al. 2001; Schellinger et al. 2003; Sunshine et al. 1999; Warach 2001). Although protocols vary somewhat, a streamlined hyperacute stroke MRI protocol need only include a T1 sagittal localising sequence, DWI, PI, T2* gradient echo, and MRA (usually time of flight). This allows determination of the presence of perfusion-diffusion mismatch, site of vessel occlusion, and exclusion of ICH.

3.4.2.1 Echoplanar MRI Thrombolysis Evaluation Trial

Although the mismatch hypothesis is a compelling one, randomised, prospective blinded trials are required as definitive evidence. The Royal Melbourne Hospital MRI Stroke Study group has designed the echoplanar imaging thrombolysis evaluation trial (EPITHET). This is a multicentre double blind, randomized, placebo controlled trial of tPA versus placebo in 100 eligible patients with hemispheric infarction 3–6 h after stroke onset (Davis and Donnan 2004). The trial is an example of a 'proof of concept' study discussed below, using (now established) biologically meaningful MR surrogate outcomes. The major hypothesis underlying EPITHET is that in patients treated with tPA between 3 and 6 h after stroke onset, the presence and extent of perfusion-diffusion mismatch will predict a therapeutic response. This response will be defined by the major MR outcome: reduced expansion of the ischaemic core between the acute DWI and outcome T2-weighted studies. Extent of reperfusion and penumbral salvage will also be used as MR outcome measures. In addition, an important secondary hypothesis being tested is that larger acute infarct cores (as represented by the DWI lesion) will be associated with an increased risk of haemorrhagic transformation in tPA treated patients. Twelve centres are currently involved (ten in Australia and two in New Zealand), it is anticipated that recruitment will be completed by the end of 2005.

It is important to note that this trial is not using perfusion-diffusion mismatch to select patients, but as a surrogate outcome measure. The rationale for this is that the mismatch hypothesis, whilst strongly supported by much data, remains unproven. Similarly, it is not yet established that patients with non-mismatch do not respond to thrombolysis (as there is at least a theoretical possibility of partial DWI reversal). Should either the mismatch hypothesis and/or the hypothesis that a large acute DWI lesion predicts ICH be proven in this trial, a logical next

step would be to use PI/DWI to select patients for tPA in the 3- to 6-h window in a phase III placebo-controlled RCT with primary clinical endpoints.

3.4.2.2 Future Stroke Patient Management: A Potential Thrombolysis Algorithm

Although ongoing trials may modify the following treatment algorithm, a possible role of combined PI and DWI as part of a multimodal MRI protocol in the near future for the selection of acute ischaemic stroke patient for thrombolysis is presented below. Indeed, many centres do use stroke MRI to select patients for thrombolysis beyond 3 h (Schellinger et al. 2003). At present, as the evidence is not conclusive, we prefer to randomise post-3-h patients to thrombolytic trials.

The thrombolysis algorithm is based on the assumption that the hypotheses discussed above are proven to be correct. That is, primarily: (1) the presence of significant perfusion-diffusion mismatch (qualitatively +/– quantitatively assessed) predicts treatment response, and (2) a 'large' DWI lesion (qualitatively > ½ MCA territory, and/or quantitatively > 100 cm^3) predicts haemorrhagic transformation. Patients excluded from thrombolysis because of extensive DWI lesions with or without perfusion-diffusion mismatch may be considered for more aggressive measures such as hypothermia or decompressive hemicraniectomy (Schwab et al. 1998, 2001).

A further possible scenario (particularly when thrombolysis later than 3 h after symptom onset is being considered) is that PI/DWI and MRA might be used to decide on the dose of tPA. This postulate is based on the early dose-finding tPA studies that smaller doses of tPA appeared to have significant efficacy, and possibly also a lesser risk of haemorrhage (Brott et al. 1992; Haley et al. 1992). Furthermore, our work, and angiographic studies, demonstrate that more proximal sites of occlusion are less likely to recanalize with thrombolysis (Alexandrov et al. 2001; Furlan et al. 1999; Parsons et al. 2002a). Therefore, a smaller dose of tPA might be as efficacious for distal vessel occlusions, and for more proximal occlusions (ICA, MCA stem) a higher dose of IV tPA, or (where available) a combined IV/IA approach might be used (Ernst et al. 2000). The risk of a higher dose of IV tPA (1.1 mg/kg as used in ECASS I) could be justified on two counts, patients with large baseline DWI lesions would be excluded, and the natural history of untreated proximal vessel occlusion is very poor (Hacke et al. 1995). New thrombolytic agents, or combined lower dose tPA and a platelet glycoprotein IIb/IIIa inhibitor (e.g., abciximab) might be alternative treatment arms (Abciximab in Ischemic Stroke Investigators 2000).

It is predicted that EPITHET will provide more information regarding the site of vessel occlusion and response to tPA. Should this trial confirm a lower rate of major reperfusion (and correspondingly greater infarct expansion and lower penumbral salvage) with intravenous tPA for proximal occlusions, then trials of more aggressive reperfusion strategies would be indicated. A safety proof of concept study using PI/DWI (and MRA) both to select patients and for surrogate measures of outcome, would be ideal for this purpose. In such a study, patients without large pre-treatment DWI lesions and perfusion-diffusion mismatch might, for example, be randomised to 0.9 mg/kg or 1.1 mg/kg IV tPA in a blinded manner. Rates of recanalization, major reperfusion, and ICH would be important outcome measures.

Pending safety confirmation of the higher tPA dose, the following thrombolysis algorithm could be also be tested in a randomised controlled trial, again using MRI surrogate outcomes, in the 3- to 6-h window (see below). The control group would probably receive standard dose tPA. It is envisaged that the following treatment algorithm might equally apply to ischaemic stroke patients presenting within 3 h of symptom onset. However, some might argue that

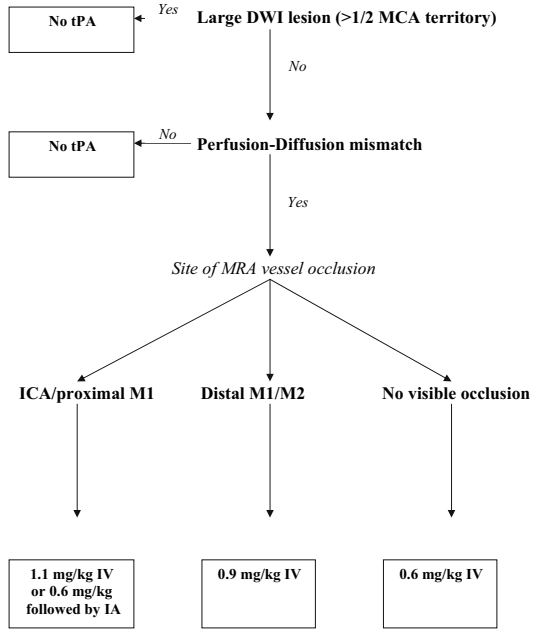

Potential future thrombolysis treatment algorithm using PI/DWI and MRA

clinically eligible patients presenting within 3 h do not need MRI to make a decision regarding thrombolysis. At the other end of the spectrum, if patients presenting after 6 h still have significant perfusion-diffusion mismatch without a large DWI lesion, it might also be reasonable to treat these patients as below. After all, the rationale for PI/DWI in acute stroke is to image ischaemic pathophysiology. Thus, treatment should be based on a 'tissue clock' rather than a time clock (Kidwell et al. 2000) (see Fig. 3.3).

Potential future thrombolysis treatment algorithm using PI/DWI and MRA for patients with unknown time of stroke onset or being admitted after 3 h.

3.4.2.3 Improving Acute Stroke Trial Design Using MRI

3.4.2.3.1 Patient Selection Using MRI

In the last few years, many unsuccessful acute stroke trials have been reported. Trials of intravenous tPA initiated up to 6 h from symptom onset have failed to demonstrate efficacy in patients without imaging confirmation of the diagnosis or pathophysiologic features most amenable to treatment (Albers and Clark 1999; Hacke et al. 1995, 1998). To demonstrate efficacy in stroke trials with a treatment time window greater than 3 h (including neuroprotective agents), trial design needs to be improved (Davis and Donnan 2002).

A number of factors may predict tissue response and clinical efficacy in stroke trials. Clearly, time is an important factor (Marler et al. 2000). However, the amount of ischaemic tissue at risk of infarction that is still potentially salvageable (the ischaemic penumbra) is another factor that is highly likely to predict clinical response. Much of the data presented above: (1) demonstrates that PI/DWI can identify such tissue at-risk, and (2) establishes that the ischaemic penumbra is a prime locus of ischaemic injury and a key target for acute stroke therapies. For example, we have shown that patients with significant perfusion-diffusion mismatch treated with thrombolysis have a significant degree of reperfusion and tissue salvage compared to similar controls (Parsons et al. 2002a). This also translated into a statistically significant clinical response (Parsons et al. 2002a). The sample size of this study (albeit not a randomised, placebo-controlled trial) was markedly smaller than that needed to show clinical benefit in the NINDS trial, which did not

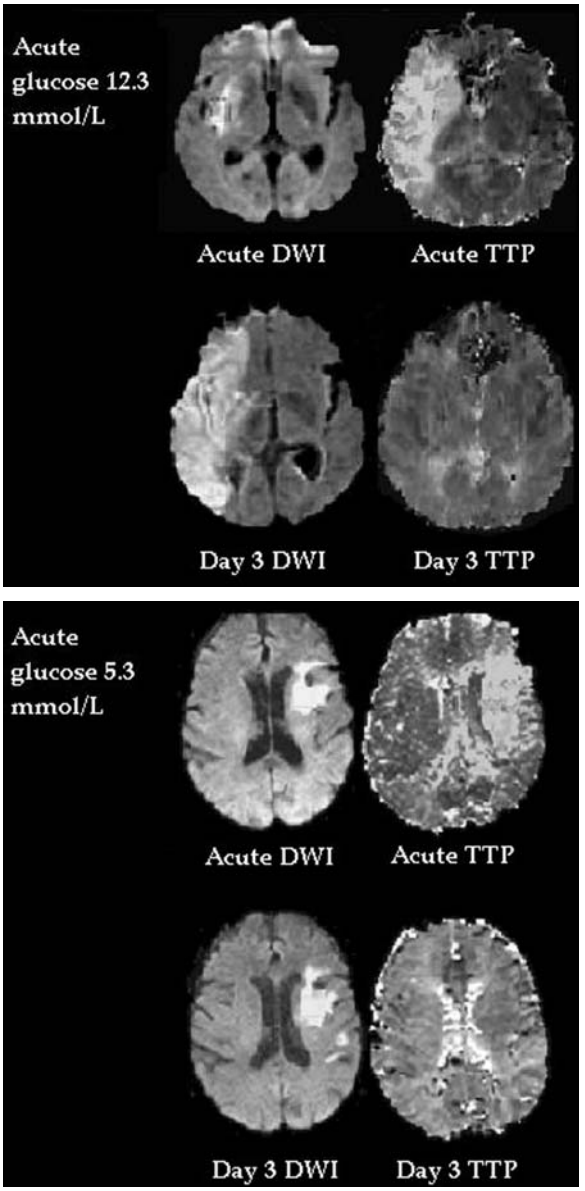

Fig. 3.12. Patient (*top*) with acute perfusion-diffusion mismatch and an acute blood glucose level of 12.3 mmol/l. Despite major reperfusion, much of the at-risk mismatch tissue progressed to infarction. In contrast, the bottom patient with an acute blood glucose of 5.3 mmol/l and a large area of mismatch, had major penumbral (mismatch) salvage on follow-up imaging

select an homogenous sample of patients based on imaging of pathology (The National Institute of Neurological Disorders and Stroke rt-PA Stroke Study Group 1995).

It is important to note that MRI selection of patients does not just apply to thrombolytic trials. In fact, selecting patients with an ischaemic penumbra may be critically important for trials of neuroprotective drugs, and other therapies such as manip-

ulation of physiologic variables (blood glucose, hypothermia) and decompressive hemicraniectomy (Fisher and Brott 2003). For example, our group has found that the adverse effect of acute hyperglycaemia on stroke outcome was seen predominantly in patients with an MR-defined ischaemic penumbra (Fig. 3.12). Acute hyperglycaemia in patients with perfusion-diffusion mismatch increased the progression of this at-risk tissue to infarction and was associated with worse clinical outcome, compared to normoglycaemic patients with mismatch (Parsons et al. 2002b). These results suggest that a trial of acute, aggressive glycaemic control in stroke might be optimised by using PI/DWI to select patients with salvageable at-risk tissue (Baird et al. 2003; Parsons et al. 2002b).

In a similar vein, decompressive hemicraniectomy has been shown to reduce mortality after malignant MCA infarction (Schwab et al. 1998). It appears the earlier the surgery is performed, the better the outcome. MRI is promising in predicting the likelihood of this complication within 6 h of stroke onset (Thomalla et al. 2003). An extensive DWI lesion predicts malignant MCA infarct very accurately, allowing ultra-early decompressive surgery. As suggested in the above thrombolysis treatment algorithm, patients with extensive acute DWI lesions would be excluded from thrombolytic treatment. However, such patients may still have perfusion-diffusion mismatch and other aggressive experimental treatments such as early decompression or hypothermia may salvage remaining at risk tissue (Schwab et al. 1998, 2001). This area deserves further study.

There seems little doubt that trials of neuroprotective drugs, of which there have been many negative results to date, might be more likely to succeed if patients with an ischaemic penumbra were selected using perfusion-diffusion mismatch (Lees et al. 2000; Muir and Lees 1995; Yamaguchi et al. 1998). This has a rational basis, as neuroprotective drugs are targeted at 'preserving' the penumbra (Davis and Donnan 2002; Fisher and Brott 2003).

3.4.2.3.2 PI/DWI as Surrogate Markers of Treatment Response – 'Proof of Concept'

As well as using PI/DWI to select an 'ideal' patient population to optimise the chances of efficacy of a therapeutic agent, PI/DWI may also have a role in the monitoring of ischaemic lesion evolution and therapeutic response in acute stroke trials. Reducing the functional disability associated with cerebral infarction is the clinical goal of acute stroke therapy. Therefore, reduction of infarct volume is the biological objective. A relative reduction in infarct volume in animal models is required to advance a drug into clinical trials. Replicating these observations in a clinical sample is the next logical step. However, this has often been bypassed in favour of very expensive, large clinical endpoint trials that have failed for treatments given beyond the 3-h window. Pilot 'proof-of-concept' studies using a biologically meaningful outcome variable, similar to EPITHET, may provide an important bridge between animal studies and the large phase III trials (Barber et al. 2004; Davis and Donnan 2002).

Although it seems intuitive, the surrogate outcome measures used in such proof-of-concept trials must have a tight correlation with clinical outcome. The first randomised-controlled trial of PI/DWI for outcome assessment did not definitively demonstrate efficacy of the experimental agent, but it did show a clear association between infarct expansion and poorer clinical outcome (Warach et al. 1999). The results of our case-control tPA series strengthen the case for using PI/DWI as biologically meaningful outcome measures (Parsons et al. 2002a). In the comparison between tPA treated patients and untreated controls; baseline to outcome infarct expansion, reperfusion, and penumbral salvage all had strong correlations with clinically meaningful improvement. These correlations were independent of treatment group, although a higher proportion of tPA treated patients had better MRI and clinical outcomes.

Other studies have also demonstrated the potential value of using PI/DWI in proof concept studies. Our group has shown, based on statistical modelling from a natural history stroke cohort with serial PI/DWI, that a therapy postulated to reduce infarct expansion by 50% would need 100 patients in each group to show a significant difference between treatment and placebo groups (Barber et al. 2004). Similarly, a therapy postulated to increase the chances of major reperfusion from acute to subacute PI by 50% would only need 50 patients in each group to demonstrate a significant difference between active treatment and placebo (Barber et al. 2004). Others have shown that the presence of recanalization (on MRA) or reperfusion (on PI) after thrombolysis are powerful predictors of eventual clinical outcome (Chalela et al. 2003, 2004; Schellinger et al. 2000). In fact, extent of reperfusion from pre- to post thrombolysis PI was a more sensitive predictor

of excellent outcome than MRA recanalization, and appears to be the ideal surrogate outcome for testing new reperfusion therapies (Chalela et al. 2004).

3.5 Conclusions

MRI is being increasingly used as a selection tool and an outcome measure in stroke trials, reflecting the growing evidence that direct pathophysiologic imaging may provide a more rational approach to acute stroke therapy than clinical diagnosis (and non-contrast CT scanning) alone. Stroke MRI is practical and feasible. Perfusion-diffusion mismatch provides a reliable estimation of the ischaemic penumbra. The future holds great promise. It is only a matter of time before MRI routinely assists the stroke clinician in making individual therapeutic decisions, and guides stroke researchers in identifying effective therapies that can be delivered well beyond the current 3-h window.

References

Abciximab in Ischemic Stroke Investigators (2000) Abciximab in acute ischemic stroke: a randomized, double-blind, placebo-controlled, dose-escalation study. Stroke 31:601–609

Albers GW, Clark WM (1999) For the ATLANTIS Study Investigators. The ATLANTIS rt-PA (Alteplase) acute stroke trial: final results. Cerebrovasc Dis 9:126

Alexandrov AV, Burgin WS, Demchuk AM, El-Mitwalli A, Grotta JC (2001) Speed of intracranial clot lysis with intravenous tissue plasminogen activator therapy: sonographic classification and short-term improvement. Circulation 103:2897–2902

Astrup J, Symon L, Siesjo BK (1981) Thresholds in cerebral ischemia - the ischemic penumbra. Stroke 12:723–725

Ay H, Buonanno FS, Rordorf G, Schaefer PW, Schwamm LH, Wu O, Gonzalez RG, Yamada K, Sorensen AG, Koroshetz WJ (1999) Normal diffusion-weighted MRI during stroke like deficits. Neurology 52:1784–1792

Baird AE, Benfield A, Schlaug G, Siewert B, Lovblad K, Edelman R, Warach S (1997) Enlargement of human cerebral ischemic lesion volumes measured by diffusion-weighted magnetic resonance imaging. Ann Neurol 41:581–589

Baird AE, Lovblad KO, Dashe JF, Connor A, Burzynski C, Schlaug G, Straroselskaya I, Edelman RR, Warach S (2000) Clinical correlations of diffusion and perfusion lesion volumes in acute ischemic stroke. Cerebrovasc Dis 10:441–448

Baird TA, Parsons MW, Phanh T, Butcher KS, Desmond PM, Tress BM, Colman PG, Chambers BR, Davis SM (2003) Persistent poststroke hyperglycemia is independently associated with infarct expansion and worse clinical outcome. Stroke 34:2208–2214

Barber PA, Darby DG, Desmond PM, Yang Q, Gerraty RP, Jolley D, Donnan GA, Tress BM, Davis SM (1998a) Prediction of stroke outcome with echoplanar perfusion- and diffusion-weighted magnetic resonance imaging. Neurology 51:418–426

Barber PA, Davis SM, Infeld B, Baird AE, Donnan GA, Jolley D, Lichtenstein M (1998b) Spontaneous reperfusion following ischemic stroke is associated with improved outcome. Stroke 29:2522–2528

Barber PA, Darby DG, Desmond PM, Gerraty RP, Yang Q, Li T, Jolley D, Donnan GA, Tress BM, Davis SM (1999a) Identification of major ischemic change. Diffusion-weighted imaging versus computed tomography. Stroke 30:2059–2065

Barber PA, Darby DG, Desmond PM, Yang Q, Gerraty RP, Jolley D, Donnan GA, Tress BM, Davis SM (1999b) Absent middle cerebral artery flow predicts the presence and evolution of the ischemic penumbra. Neurology 52:1125-1132

Barber PA, Parsons MW, Desmond PM, Bennet DA, Donnan GA, Tress BM, Davis SM (2004) The use of PWI and DWI measures in the design of "proof of concept" stroke trials. J Neuroimaging 14:123-132

Baron JC, von Kummer R, del Zoppo GJ (1995) Treatment of acute ischemic stroke: challenging the concept of a rigid and universal time window. Stroke 26:2219–2221

Beaulieu C, de Crespigny A, Tong DC, Moseley ME, Albers GW, Marks MP (1999) Longitudinal magnetic resonance imaging study of perfusion and diffusion in stroke: evolution of lesion volume and correlation with clinical outcome (see comments). Ann Neurol 46:568–578

Brandt T, Grau AJ, Hacke W (1996) Severe stroke. Baillieres Clin Neurol 5:515–541

Brott TG, Haley EC Jr, Levy DE, Barsan W, Broderick J, Sheppard GL, Spilker J, Kongable GL, Massey S, Reed R et al (1992) Urgent therapy for stroke. Part I. Pilot study of tissue plasminogen activator administered within 90 minutes. Stroke 23:632–640

Butcher K, Parsons M, Baird T, Barber A, Donnan G, Desmond P, Tress B, Davis S (2003) Perfusion thresholds in acute stroke thrombolysis. Stroke 34:2159–2164

Calamante F, Thomas DL, Pell GS, Wiersma J, Turner R (1999) Measuring cerebral blood flow using magnetic resonance imaging techniques. J Cereb Blood Flow Metab 19:701–735

Calamante F, Gadian DG, Connelly A (2002) Quantification of perfusion using bolus tracking magnetic resonance imaging in stroke: assumptions, limitations, and potential implications for clinical use. Stroke 33:1146–1151

Caplan LR, Mohr JP, Kistler JP, Koroshetz W (1997) Should thrombolytic therapy be the first-line treatment for acute ischemic stroke? Thrombolysis-not a panacea for ischemic stroke. N Engl J Med 337:1309–1310; discussion 1313

Chalela JA, Ezzeddine M, Latour L, Warach S (2003) Reversal of perfusion and diffusion abnormalities after intravenous thrombolysis for a lacunar infarction. J Neuroimaging 13:152–154

Chalela JA, Kang DW, Luby M, Ezzeddine M, Latour LL, Todd JW, Dunn B, Warach S (2004) Early magnetic resonance imaging findings in patients receiving tissue plasminogen activator predict outcome: insights into the pathophysiology of acute stroke in the thrombolysis era. Ann Neurol 55:105–112

Darby DG, Barber PA, Gerraty RP, Desmond PM, Yang Q, Parsons M, Li T, Tress BM, Davis SM (1999) Pathophysiological topography of acute ischemia by combined diffusion-weighted and perfusion MRI. Stroke 30:2043–2052

Davis SM, Donnan GA (2002) Neuroprotection: establishing proof of concept in human stroke. Stroke 33:309–310

Davis SM, Donnan GA (2004) Advances in penumbra imaging with MR. Cerebrovasc Dis 17 [Suppl 3]:23–27

Desmond PM, Lovell AC, Rawlinson AA, Parsons MW, Barber PA, Yang Q, Li T, Darby DG, Gerraty RP, Davis SM, Tress BM (2001) The value of apparent diffusion coefficient maps in early cerebral ischemia. AJNR Am J Neuroradiol 22:1260–1267

Donnan GA, Howells DW, Markus R, Toni D, Davis SM (2003) Can the time window for administration of thrombolytics in stroke be increased? CNS Drugs 17:995–1011

Ernst R, Pancioli A, Tomsick T, Kissela B, Woo D, Kanter D, Jauch E, Carrozzella J, Spilker J, Broderick J (2000) Combined intravenous and intra-arterial recombinant tissue plasminogen activator in acute ischemic stroke. Stroke 31:2552–2557

Fiebach JB, Schellinger PD, Gass A, Kucinski T, Siebler M, Villringer A, Olkers P, Hirsch JG, Heiland S, Wilde P, Jansen O, Rother J, Hacke W, Sartor K (2004) Stroke magnetic resonance imaging is accurate in hyperacute intracerebral hemorrhage: a multicenter study on the validity of stroke imaging. Stroke 35:502–506

Fink JN, Kumar S, Horkan C, Linfante I, Selim MH, Caplan LR, Schlaug G (2002) The stroke patient who woke up: clinical and radiological features, including diffusion and perfusion MRI. Stroke 33:988–993

Fisher M (1997) Characterizing the target of acute stroke therapy. Stroke 28:866–872

Fisher M, Brott TG (2003) Emerging therapies for acute ischemic stroke: new therapies on trial. Stroke 34:359–361

Furlan A, Higashida R, Wechsler L, Gent M, Rowley H, Kase C, Pessin M, Ahuja A, Callahan F, Clark WM, Silver F, Rivera F (1999) Intra-arterial prourokinase for acute ischemic stroke. The PROACT II study: a randomized controlled trial. Prolyse in acute cerebral thromboembolism. JAMA 282:2003–2011

Ginsberg MD, Pulsinelli WA (1994) The ischemic penumbra, injury thresholds, and the therapeutic window for acute stroke. Ann Neurol 36:553–554

Grandin CB, Duprez TP, Smith AM, Oppenheim C, Peeters A, Robert AR, Cosnard G (2002) Which MR-derived perfusion parameters are the best predictors of infarct growth in hyperacute stroke? Comparative study between relative and quantitative measurements. Radiology 223:361–370

Grond M, Rudolf J, Schmulling S, Stenzel C, Neveling M, Heiss WD (1998) Early intravenous thrombolysis with recombinant tissue-type plasminogen activator in vertebrobasilar ischemic stroke. Arch Neurol 55:466–469

Hacke W (2004) Desmoteplase In Acute Stroke Study (DIAS) - results of phase II trial. International Stroke Conference, San Diego

Hacke W, Warach S (2000) Diffusion-weighted MRI as an evolving standard of care in acute stroke. Neurology 54:1548–1549

Hacke W, Zeumer H, Ferbert A, Bruckmann H, del Zoppo GJ (1988) Intra-arterial thrombolytic therapy improves outcome in patients with acute vertebrobasilar occlusive disease. Stroke 19:1216–1222

Hacke W, Kaste M, Fieschi C, Toni D, Lesaffre E, von Kummer R, Boysen G, Bluhmki E, Hoxter G, Mahagne MH, Henerici M (1995) Intravenous thrombolysis with recombinant tissue plasminogen activator for acute hemispheric stroke. The European Cooperative Acute Stroke Study (ECASS). JAMA 274:1017–1025

Hacke W, Kaste M, Fieschi C (1998) Randomised double-blind placebo controlled trial of thrombolytic therapy with intravenous alteplase in acute ischaemic stroke (ECASS II). Lancet 352:1245–1251

Haley EC Jr, Levy DE, Brott TG, Sheppard GL, Wong MC, Kongable GL, Torner JC, Marler JR (1992) Urgent therapy for stroke. Part II. Pilot study of tissue plasminogen activator administered 91–180 minutes from onset. Stroke 23:641–645

Heiss WD (1983) Flow thresholds for functional and morphological damage of brain tissue. Stroke 14:329–331

Hossmann K-A (1994) Viability thresholds and the penumbra of focal ischemia. Ann Neurol 36:557–565

Hossmann K-A, Sakaki S, Zimmermann V (1977) Cation activities in reversible ischemia of the cat brain. Stroke 8:77–81

Jansen O, Schellinger P, Fiebach J, Hacke W, Sartor K (1999) Early recanalisation in acute ischaemic stroke saves tissue at risk defined by MRI. Lancet 353:2036–2037

Jovin TG, Yonas H, Gebel JM, Kanal E, Chang YF, Grahovac SZ, Goldstein S, Wechsler LR (2003) The cortical ischemic core and not the consistently present penumbra is a determinant of clinical outcome in acute middle cerebral artery occlusion. Stroke 34:2426–2433

Kidwell CS, Saver JL, Mattiello J, Starkman S, Vinuela F, Duckwiler G, Gobin YP, Jahan R, Vespa P, Kalafut M, Alger JR (2000) Thrombolytic reversal of acute human cerebral ischemic injury shown by diffusion/perfusion magnetic resonance imaging. Ann Neurol 47:462–469

Kidwell CS, Saver JL, Villablanca JP, Duckwiler G, Fredieu A, Gough K, Leary MC, Starkman S, Gobin YP, Jahan R, Vespa P, Liebeskind DS, Alger JR, Vinuela F (2002) Magnetic resonance imaging detection of microbleeds before thrombolysis: an emerging application. Stroke 33:95–98

Kidwell CS, Alger JR, Saver JL (2003) Beyond mismatch: evolving paradigms in imaging the ischemic penumbra with multimodal magnetic resonance imaging. Stroke 34:2729–2735

Lees KR, Asplund K, Carolei A, Davis SM, Diener HC, Kaste M, Orgogozo JM, Whitehead J (2000) Glycine antagonist (gavestinel) in neuroprotection (GAIN International) in patients with acute stroke: a randomised controlled trial. GAIN International Investigators. Lancet 355:1949–1954

Li F, Han SS, Tatlisumak T, Liu K-F, Garcia JH, Sotak C, Fisher M (1999) Reversal of acute apparent diffusion coefficient abnormalities and delayed neuronal death following transient focal cerebral ischemia in rats. Ann Neurol 46:333–342

Li F, Silva MD, Liu KF, Helmer KG, Omae T, Fenstermacher JD, Sotak CH, Fisher M (2000) Secondary decline in apparent diffusion coefficient and neurological outcomes after a short period of focal brain ischemia in rats. Ann Neurol 48:236–244

Lin DD, Filippi CG, Steever AB, Zimmerman RD (2001) Detection of intracranial hemorrhage: comparison between gradient-echo images and b(0) images obtained from diffusion-weighted echo-planar sequences. AJNR Am J Neuroradiol 22:1275–1281

Linfante I, Llinas RH, Caplan LR, Warach S (1999) MRI features of intracerebral hemorrhage within 2 hours from symptom onset. Stroke 30:2263–2267

Linfante I, Llinas RH, Selim M, Chaves C, Kumar S, Parker RA,

Caplan LR, Schlaug G (2002) Clinical and vascular outcome in internal carotid artery versus middle cerebral artery occlusions after intravenous tissue plasminogen activator. Stroke 33:2066–2071

Lovblad K, Baird AE, Schlaug G, Benfield A, Siewert B, Voetsch B, Connor A, Burzynski C, Edelman R, Warach S (1997) Ischemic lesion volumes in acute stroke by diffusion-weighted magnetic resonance imaging correlate with clinical outcome. Ann Neurol 42:164–170

Lovblad KO, Laubach HJ, Baird AE, Curtin F, Schlaug G, Edelman RR, Warach S (1998) Clinical experience with diffusion-weighted MR in patients with acute stroke. AJNR Am J Neuroradiol 19:1061–1066

Marks MP, Tong DC, Beaulieu C, Albers GW, de Crespigny A, Moseley ME (1999) Evaluation of early reperfusion and i.v. tPA therapy using diffusion- and perfusion-weighted MRI (see comments). Neurology 52:1792–1798

Markus R, Reutens DC, Kazui S, Read S, Wright P, Chambers BR, Sachinidis JI, Tochon-Danguy HJ, Donnan GA (2003) Topography and temporal evolution of hypoxic viable tissue identified by 18F-fluoromisonidazole positron emission tomography in humans after ischemic stroke. Stroke 34:2646–2652

Marler JR, Tilley BC, Lu M, Brott TG, Lyden PC, Grotta JC, Broderick JP, Levine SR, Frankel MP, Horowitz SH, Haley EC Jr, Lewandowski CA, Kwiatkowski TP (2000) Early stroke treatment associated with better outcome: the NINDS rt-PA stroke study. Neurology 55:1649–1655

Muir KW, Lees KR (1995) A randomized, double-blind, placebo-controlled pilot trial of intravenous magnesium sulfate in acute stroke. Ann NY Acad Sci 765:315–316

Muller TB, Haraldseth O, Jones RA, Sebastiani G, Godtliebsen F, Lindboe CF, Unsgard G (1995) Combined perfusion and diffusion-weighted magnetic resonance imaging in a rat model of reversible middle cerebral artery occlusion. Stroke 26:451–457; discussion 457–458

National Institute of Neurological Disorders and Stroke rt-PA Stroke Study Group (1995) Tissue plasminogen activator for acute ischemic stroke. N Engl J Med 333:1581–1587

Neumann-Haefelin T, Wittsack HJ, Wenserski F, Siebler M, Seitz RJ, Modder U, Freund HJ (1999) Diffusion- and perfusion-weighted MRI. The DWI/PWI mismatch region in acute stroke. Stroke 30:1591–1597

Neumann-Haefelin T, du Mesnil de Rochemont R, Fiebach JB, Gass A, Nolte C, Kucinski T, Rother J, Siebler M, Singer OC, Szabo K, Villringer A, Schellinger PD (2004) Effect of incomplete (spontaneous and postthrombolytic) recanalization after middle cerebral artery occlusion: a magnetic resonance imaging study. Stroke 35:109–114

Nighoghossian N, Hermier M, Adeleine P, Blanc-Lasserre K, Derex L, Honnorat J, Philippeau F, Dugor JF, Froment JC, Trouillas P (2002) Old microbleeds are a potential risk factor for cerebral bleeding after ischemic stroke: a gradient-echo T2*-weighted brain MRI study. Stroke 33:735–742

Oppenheim C, Logak M, Dormont D, Lehericy S, Manai R, Samson Y, Marsault C, Rancurel G (2000) Diagnosis of acute ischaemic stroke with fluid-attenuated inversion recovery and diffusion-weighted sequences. Neuroradiology 42:602–607

Ostrem JL, Saver JL, Alger JR, Starkman S, Leary MC, Duckwiler G, Jahan R, Vespa P, Villablanca JP, Gobin YP, Vinuela F, Kidwell CS (2004) Acute basilar artery occlusion: diffusion-perfusion MRI characterization of tissue salvage in patients receiving intra-arterial stroke therapies. Stroke 35:e30–e34

Parsons MW, Yang Q, Barber PA, Darby DG, Desmond PM, Gerraty RP, Tress BM, Davis SM (2001) Perfusion magnetic resonance imaging maps in hyperacute stroke: relative cerebral blood flow most accurately identifies tissue destined to infarct. Stroke 32:1581–1587

Parsons MW, Barber PA, Chalk J, Darby DG, Rose S, Desmond PM, Gerraty RP, Tress BM, Wright PM, Donnan GA, Davis SM (2002a) Diffusion- and perfusion-weighted MRI response to thrombolysis in stroke. Ann Neurol 51:28–37

Parsons MW, Barber PA, Desmond PM, Baird TA, Darby DG, Byrnes G, Tress BM, Davis SM (2002b) Acute hyperglycemia adversely affects stroke outcome: a magnetic resonance imaging and spectroscopy study. Ann Neurol 52:20–28

Patel SC, Levine SR, Tilley BC, Grotta JC, Lu M, Frankel M, Haley EC, Jr., Brott TG, Broderick JP, Horowitz S, Lyden PD, Lewandowski CA, Marler JR, Welch KM (2001) Lack of clinical significance of early ischemic changes on computed tomography in acute stroke. JAMA 286:2830–2838

Perl J 2nd, Tkach JA, Porras-Jimenez M, Lieber M, Obuchowski N, Ross JS, Ding XP, Ruggieri PM, Shearer DM, Khajavi K, Masaryk TJ (1999) Hemorrhage detected using MR imaging in the setting of acute stroke: an in vivo model. AJNR Am J Neuroradiol 20:1863–1870

Powers WJ (2000) Testing a test. A report card for DWI in acute stroke. Neurology 54:1549–1551

Powers WJ, Zivin JA (1998) Magnetic resonance imaging in acute stroke. Not ready for prime time. Neurology 50:842–843

Prosser J, Butcher K, Allport L, Parsons MW, Baird TA, MacGregor L, Tress BM, Davis SM (2004) Clinical-diffusion mismatch predicts the penumbra with high specificity. World stroke congress, Vancouver

Read SJ, Hirano T, Abbott DF, Markus R, Sachinidis JI, Tochon-Danguy HJ, Chan JG, Egan GF, Scott AM, Bladin CF, McKay WJ, Donnan GA (2000) The fate of hypoxic tissue on 18F-fluoromisonidazole positron emission tomography after ischemic stroke. Ann Neurol 48:228–235

Saunders DE, Howe FA, van den Boogaart A, McLean MA, Griffiths JR, Brown MM (1995) Continuing ischemic damage after acute middle cerebral artery infarction in humans demonstrated by short-echo proton spectroscopy. Stroke 26:1007–1013

Schellinger PD, Jansen O, Fiebach JB, Heiland S, Steiner T, Schwab S, Pohlers O, Ryssel H, Sartor K, Hacke W (2000) Monitoring intravenous recombinant tissue plasminogen activator thrombolysis for acute ischemic stroke with diffusion and perfusion MRI. Stroke 31:1318–1328

Schellinger PD, Fiebach JB, Jansen O, Ringleb PA, Mohr A, Steiner T, Heiland S, Schwab S, Pohlers O, Ryssel H, Orakcioglu B, Sartor K, Hacke W (2001) Stroke magnetic resonance imaging within 6 hours after onset of hyperacute cerebral ischemia. Ann Neurol 49:460–469

Schellinger PD, Fiebach JB, Hacke W (2003) Imaging-based decision making in thrombolytic therapy for ischemic stroke: present status. Stroke 34:575–583

Schlaug G, Benfield A, Baird AE, Siewert B, Lovblad KO, Parker RA, Edelman RR, Warach S (1999) The ischemic penumbra: operationally defined by diffusion and perfusion MRI. Neurology 53:1528–1537

Schwab S, Steiner T, Aschoff A, Schwarz S, Steiner HH, Jansen O, Hacke W (1998) Early hemicraniectomy in patients

with complete middle cerebral artery infarction. Stroke 29:1888–1893

Schwab S, Georgiadis D, Berrouschot J, Schellinger PD, Graffagnino C, Mayer SA (2001) Feasibility and safety of moderate hypothermia after massive hemispheric infarction. Stroke 32:2033–2035

Selim M, Fink JN, Kumar S, Caplan LR, Horkan C, Chen Y, Linfante I, Schlaug G (2002) Predictors of hemorrhagic transformation after intravenous recombinant tissue plasminogen activator: prognostic value of the initial apparent diffusion coefficient and diffusion-weighted lesion volume. Stroke 33:2047–2052

Sorensen AG, Copen WA, Ostergaard L, Buonanno FS, Gonzalez RG, Rordorf G, Rosen BR, Schwamm LH, Weisskoff RM, Koroshetz WJ (1999) Hyperacute stroke: simultaneous measurement of relative cerebral blood volume, relative cerebral blood flow, and mean tissue transit time. Radiology 210:519–527

Sunshine JL, Tarr RW, Lanzieri CF, Landis DM, Selman WR, Lewin JS (1999) Hyperacute stroke: ultrafast MR imaging to triage patients prior to therapy. Radiology 212:325–332

Sunshine JL, Bambakidis N, Tarr RW, Lanzieri CF, Zaidat OO, Suarez JI, Landis DM, Selman WR (2001) Benefits of perfusion MR imaging relative to diffusion MR imaging in the diagnosis and treatment of hyperacute stroke. AJNR Am J Neuroradiol 22:915–921

Thijs VN, Adami A, Neumann-Haefelin T, Moseley ME, Marks MP, Albers GW (2001) Relationship between severity of MR perfusion deficit and DWI lesion evolution. Neurology 57:1205–1211

Thomalla GJ, Kucinski T, Schoder V, Fiehler J, Knab R, Zeumer H, Weiller C, Rother J (2003) Prediction of malignant middle cerebral artery infarction by early perfusion- and diffusion-weighted magnetic resonance imaging. Stroke 34:1892–1899

Tong DC, Yenari MA, Albers GW, O'Brien M, Marks MP, Moseley ME (1998) Correlation of perfusion- and diffusion-weighted MRI with NIHSS score in acute (<6.5 hour) ischemic stroke (see comments). Neurology 50:864–870

Tong DC, Adami A, Moseley ME, Marks MP (2001) Prediction of hemorrhagic transformation following acute stroke: role of diffusion- and perfusion-weighted magnetic resonance imaging. Arch Neurol 58:587–593

Von Kummer R, Allen KL, Holle R, Bozzao L, Bastianello S, Manelfe C, Bluhmki E, Ringleb P, Meier D, Hacke W (1997) Acute stroke: usefulness of early CT findings before thrombolytic therapy. Radiology 205:327–333

Warach S (2001) Tissue viability thresholds in acute stroke: the 4-factor model. Stroke 32:2460–2461

Warach S, Gaa J, Siewert B, Wielopolski P, Edelman R (1995) Acute human stroke studied by whole brain echoplanar diffusion-weighted magnetic resonance imaging. Ann Neurol 37:231–141

Warach S, Dashe JF, Edelman RR (1996) Clinical outcome in ischemic stroke predicted by early diffusion-weighted and perfusion magnetic resonance imaging: a preliminary analysis. J Cereb Blood Flow Metab 16:53–59

Warach S, Pettigrew LC, Dashe JF, Pullicino P, Sabounjian L (1999) The effect of citicholine on lesion volume in acute stroke: a multicenter double blind placebo controlled trial. Stroke 30:243

Wardlaw JM (2001) Overview of Cochrane thrombolysis meta-analysis. Neurology 57:S69–S76

Yamaguchi T, Sano K, Takakura K, Saito I, Shinohara Y, Asano T, Yasuhara H (1998) Ebselen in acute ischemic stroke: a placebo-controlled, double-blind clinical trial. Ebselen Study Group. Stroke 29:12–17

Yenari MA, de Crespigny A, Palmer JT, Roberts S, Schrier SL, Albers GW, Moseley ME, Steinberg GK (1997) Improved perfusion with rt-PA and hirulog in a rabbit model of embolic stroke. J Cereb Blood Flow Metab 17:401–411

4 Insights from Experimental Studies

Tobias Back

CONTENTS

4.1 Basic Pathophysiology

Our insight into the development, evolution and the mechanisms of damage in cerebral ischemia is mainly based on animal studies. A large variety of experimental models have been developed that imitate conditions of stroke and cardiac arrest (Hossmann 1991). In the past, experiments had to be terminated at certain timepoints to obtain invasive measurements of lesion size, blood flow, metabolism or other markers of injury. Therefore, longitudinal observations required large animal numbers and the inter-individual differences complicated the analysis of results. The advent of MR techniques of imaging (MRI) and spectroscopy (MRS) has enabled us to perform longitudinal studies that document intra-individual disease progression and provide excellent contrast between normal and injured tissue, even in small animals such as rodents (Hoehn-Berlage 1995; Le Bihan et al. 1986; Moseley et al. 1990).

Especially the development of diffusion-weighted MR imaging (DWI) has triggered many investigations of cerebrovascular disease because ischemic lesions could be clearly delineated already in the hyperacute phase of ischemia (Moseley et al. 1990) when conventional staining methods are unable to display clear-cut tissue changes (Garcia et al. 1993). It is, therefore, conceivable that MRI has been widely applied to diagnose and study brain ischemia not only in animal experiments, but also in the clinical environment (Moseley et al. 1995; Warach et al. 1992, 1995) where it is now going to replace conventional CT scanning in many instances. The fact that ischemic brain lesions can be measured repeatedly by non-invasive MR techniques can be used not only to observe the natural course of stroke (Baird et al. 1997) or anoxic ischemia after cardiac arrest (Arbelaez et al. 1999), but also to detect treatment effects, e.g., by recanalizing interventions like thrombolytic therapy in stroke patients (Parsons et al. 2002). In the future, possibly only one complex MR investigation may provide information on all of the following: the morphology, perfusion state and metabolic condition of ischemic tissue as well as the functional status of perilesional brain. It may also enable us to distinguish old from new lesions, estimate the age of the latter and provide information on the prognosis of different tissue compartments in terms of viability. But this knowledge is largely, not exclusively, based on experimental studies that will be reviewed in this chapter.

4.1.1 Dimensions of Injury

It has been believed that ischemic lesions are basically static in nature unless reperfusion is rapidly initiated, and that it would be difficult to treat them

T. Back, MD
Department of Neurology, University Hospital Mannheim, Ruprecht-Karls University Heidelberg, Theodor-Kutzer-Ufer 1–3, 68167 Mannheim, Germany

because the process of irreversible tissue damage evolves within several minutes. We know today that brain ischemia behaves differently in a very dynamic manner with regard to its spatial and temporal patterns of evolution. This notion is particularly true for territorial infarcts, i.e., ischemia occurring in the territory of a major cerebral artery that is obstructed by a thrombus or embolus. However, our current knowledge is limited for other types of focal ischemia such as lacunar infarcts or hemodynamic infarction in which other patterns of lesion evolution might be seen. Repeated DWI combined with metabolic and blood flow imaging could show that territorial infarcts expand early over the initial 6–8 h (Gyngell et al. 1995; Kohno et al. 1995b). Similar observations were made in a cat model of middle cerebral artery (MCA) occlusion (Heiss et al. 1994) and patients with hemispheric stroke (Heiss et al. 1992) by using sequential multitracer positron emission tomography (PET).

Based on those and other investigations it has been suggested that primary ischemic damage (occurring within 8-12 h after onset of ischemia) should be differentiated from secondary damage that appears at later stages of infarct maturation. The search for mechanisms of damage has revealed that early injury is probably in large parts due to excitotoxic processes related to excessive glutamate release and calcium overload of cells whereas molecular and cellular responses like inflammation and the occurrence of pro-apoptotic gene products typically occur at later stages of the disease process. The obstruction of a major cerebral vessel causes a blood flow gradient that declines towards the center of the territory affected. The high vulnerability of neurons, that also shows a topical preference, leads to a similar gradient of neuronal loss: whereas in the periphery of ischemic regions neurons are selectively injured with normal appearing neuropil and astroglia (so-called scattered neuronal injury), the regions with dense ischemia suffer cell loss of all brain structures including neurons, glial cells and blood vessels also named pan-necrosis. Figure 4.1 shows frequency maps of complete and incomplete (scattered neuronal) infarction in a rat model of MCA occlusion to illustrate the spatial heterogeneity of tissue changes that may also change over time resulting in a small rim of selective neuronal damage that in the subacute phase may account for about 15% of the total lesion (Back et al. 1996). Figure 4.2 demonstrates histological sections that were obtained 6 h post embolic MCA occlusion in a rat: the clot obstruction of the MCA is visualized as well as the selective neuronal cell loss occurring in the infarct borderzone.

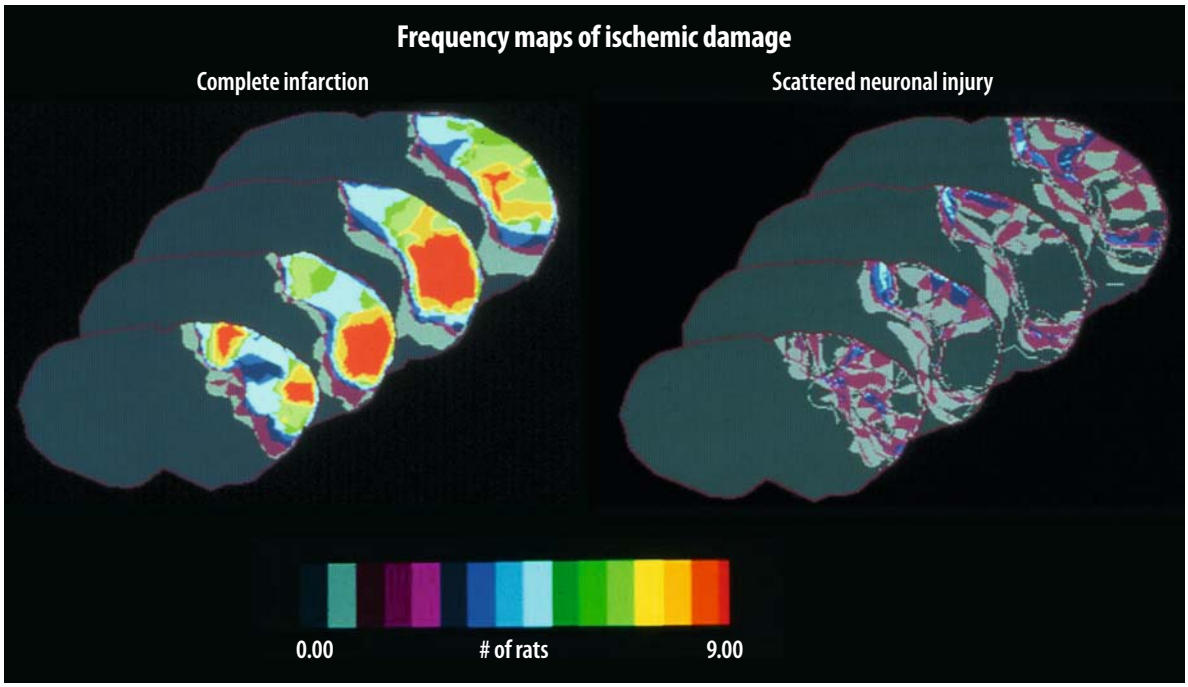

Fig. 4.1. Frequency maps of two types of ischemic damage: complete infarction (*left*) and scattered neuronal injury (*right*). Histology was obtained 24 h after left MCA occlusion in rats. Total number of animals was 9. Pseudocolor representation denotes the number of animals that showed the respective type of injury at this pixel. Note the widespread distribution of incomplete infarction over the affected left hemisphere. [Adapted from Alexis et al. (1996)]

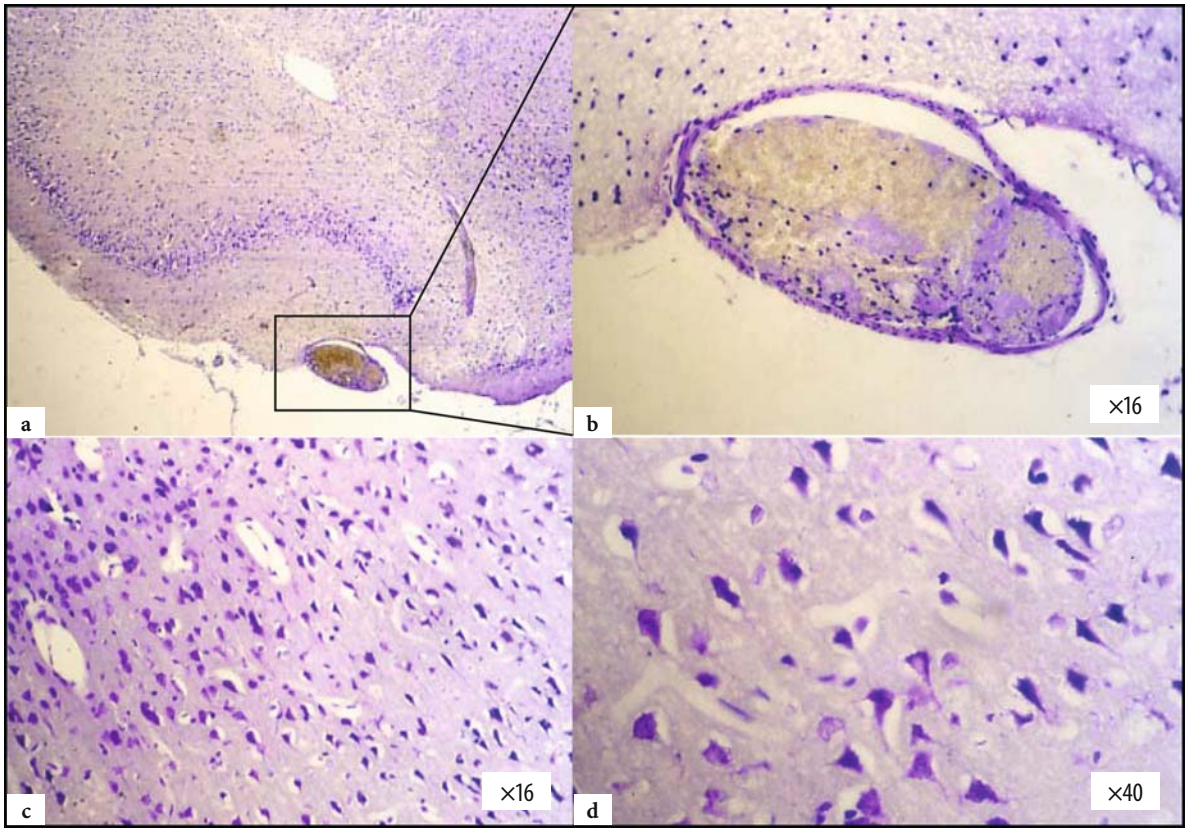

Fig. 4.2a-d. Histological staining with cresyl violet 6 h after embolic stroke in rats. Coronal section of the right temporobasal region (affected side, **a**) shows a fibrin-rich thrombus in the middle cerebral artery, MCA (**b**). Within the infarct borderzone of the same animal, selective neuronal loss is seen (condensed dark neurons with surrounding vacuoles) in the presence of preserved neurons and intact neuropil (**c**, higher magnification in **d**). This histological picture is typical for the ischemic penumbra of brain infarcts

Especially in models of *transient* cerebral ischemia, apoptotic cell death has been observed after 3–7 days post insult in selected brain regions in which basal energy metabolism has been preserved (Chen et al. 1997; Du et al. 1996). In the meantime, molecular "switches" have been identified that gate different populations of neurons with regard to the type of cell death they eventually undergo (Nicotera 2003). However, there is little doubt that in animal stroke the vast majority of cells would die from necrosis or, alternatively, secondary energy failure even in the presence of a pro-apoptotic genetic balance. The concept of thresholds of cerebral blood flow (CBF) for various functions of brain parenchyma (see below) explains why the infarct core suffers from pan-necrosis whereas the peri-infarct border in which function is suppressed, but structure initially preserved (the so-called ischemic penumbra), may show apoptotic cell death or a combination of both.

4.1.2 Infarct Maturation

In focal brain ischemia, the evolution of lesions has been investigated by using histopathological methods (Dereski et al. 1993; Garcia et al. 1993). These studies were able to demonstrate the phenomenon of infarct maturation, i.e., that there is time needed for the macroscopic and microscopic changes to appear on histological sections of the brain. At least 2-3 h following ischemia are necessary for cells to show distinct ischemic changes such as generalized swelling, shrinkage and scalloping of neurons and the formation of vacuoles in dendrites (Garcia et al. 1993). During the initial hours of ischemia, it is difficult to assess the lesion size by using histological means because the ischemic changes are sparse and – in the more peripheral regions – not well demarcated. Initial evidence of cell loss can be obtained as early as 1 h post occlusion (stria-

tum) and at 3 h post insult in the cortex. However, even in the center of the affected cortical regions, the majority of cells appears to be intact through the initial 6 h (Bartus et al. 1995). About 8-12 h after onset of ischemia, typical features appear that indicate irreversible tissue damage such as axonal swelling, eosinophilic, so-called red neurons, and the occurrence of neuronal and astrocytic 'ghost cells' (Fig. 4.3). Based on those and similar findings (see above) early lesion growth may differ from late growth (> 12 h post occlusion). This concept assumes that at later stages of the disease process morphologic alterations become irreversible, while very early changes such as astrocytic swelling with otherwise normal appearing neuropil and preserved neurons are considered as potentially reversible.

4.1.3 Thresholds of Cerebral Blood Flow

The working brain consumes about one-third of its energy for maintenance of synaptic transmission, one-third for transport of sodium and potassium, and one-third for preserving its structural integrity. In pathophysiological conditions, such as hypoxia or ischemia, the hierarchy of energy-dependent cell functions results in a characteristic sequence of events. The gradual decline of oxygen delivery induced functional deficits when cerebrovenous pO_2 fell below 60% of control in a model of hypoxic brain injury. With a further reduction below 50% of control structural damage occurred if this condition was prolonged (Opitz and Schneider 1950). In 1977, Astrup and colleagues extended the threshold concept of critical levels of hypoxia to cerebral ischemia (Astrup et al. 1977). They established precisely defined thresholds of CBF that are needed to support synaptic transmission in the upper flow range (electrical function) and ion homeostasis in the lower (structural integrity). Ischemic brain regions with flow rates that ranged between those two thresholds have been termed "ischemic penumbra" in analogy to the half-shaded zone around sunspots. The penumbra was characterized as a condition which causes functional suppression without structural damage (Astrup et al. 1981) and represents tissue in a state at-risk which bears the potential of complete recovery in terms of function and morphology. Alternatively, ongoing ischemia and/or the occurrence of further events in the pathophysiological cascade may eventually turn the ischemic penumbra into necrotic tissue.

The concept of critical flow thresholds provides the rational basis for attempts to salvage the ischemic penumbra. In the clinical environment, the successful application of thrombolysis in stroke patients (NINDS Study Group 1995) could be shown to be related to this issue: fair clinical outcome correlated positively with early recanalization (von Kummer et al. 1995) and even small improvements of local CBF in the 10% range predicted the reversibility of ischemic tissue changes (Butcher et al. 2003).

Following the occlusion of a major cerebral artery, the topographic features of the consecutive ischemic injury depend in the first instance on the extent, severity and duration of the perfusion deficit. The extent of ischemia is critically determined by the distribution of collateral blood vessels (varying greatly among human individuals and animal species and strains). In an MCA occlusion study, spontaneous single-cell activity and local CBF were measured to establish a discriminant curve relating severity and duration of ischemia to the resulting pathological outcome (Heiss and Rosner 1983). Neurons exposed to CBF ≤ 0.14 ml/g/min for more than 45 min recovered poorly. By contrast, even extreme degrees of ischemia – if followed by recirculation within 20 min – permitted recovery. It is, however, well accepted that brain tissue suffering from high-grade ischemia for sufficient lengths of time (> 60 min) will not survive.

Studies in primates employing MCA occlusion have established that local CBF values below 0.10-0.12 ml/g/min lasting 2 h or longer are associated with consistent infarction, whereas higher flows avert irreversible injury (Jones et al. 1981; Morawetz et al. 1978). In brain ischemia of cats, damage occurs below a flow rate of 0.15 ml/g/min (Strong et al. 1983). In the rat, flow rates below 0.25 ml/g/min produced well demarcated infarcts (Tyson et al. 1984) – a threshold value higher than the one defined in larger species, very likely related to the higher neuronal density of rat brain. Interestingly, spontaneously hypertensive rats are more susceptible to an ischemic insult than normotensive ones. In a hypertensive strain, overt infarction occurred below a CBF threshold of 0.50 ml/g/min probably due to inadequate collateral circulation (Jacewicz et al. 1992).

Of greater therapeutic relevance is the zone lying peripheral to the region of dense ischemia and perfused at somewhat higher CBF levels: the ischemic penumbra. In baboons subjected to MCA occlusion, CBF was measured along with the extracellular potassium concentration and sensory evoked poten-

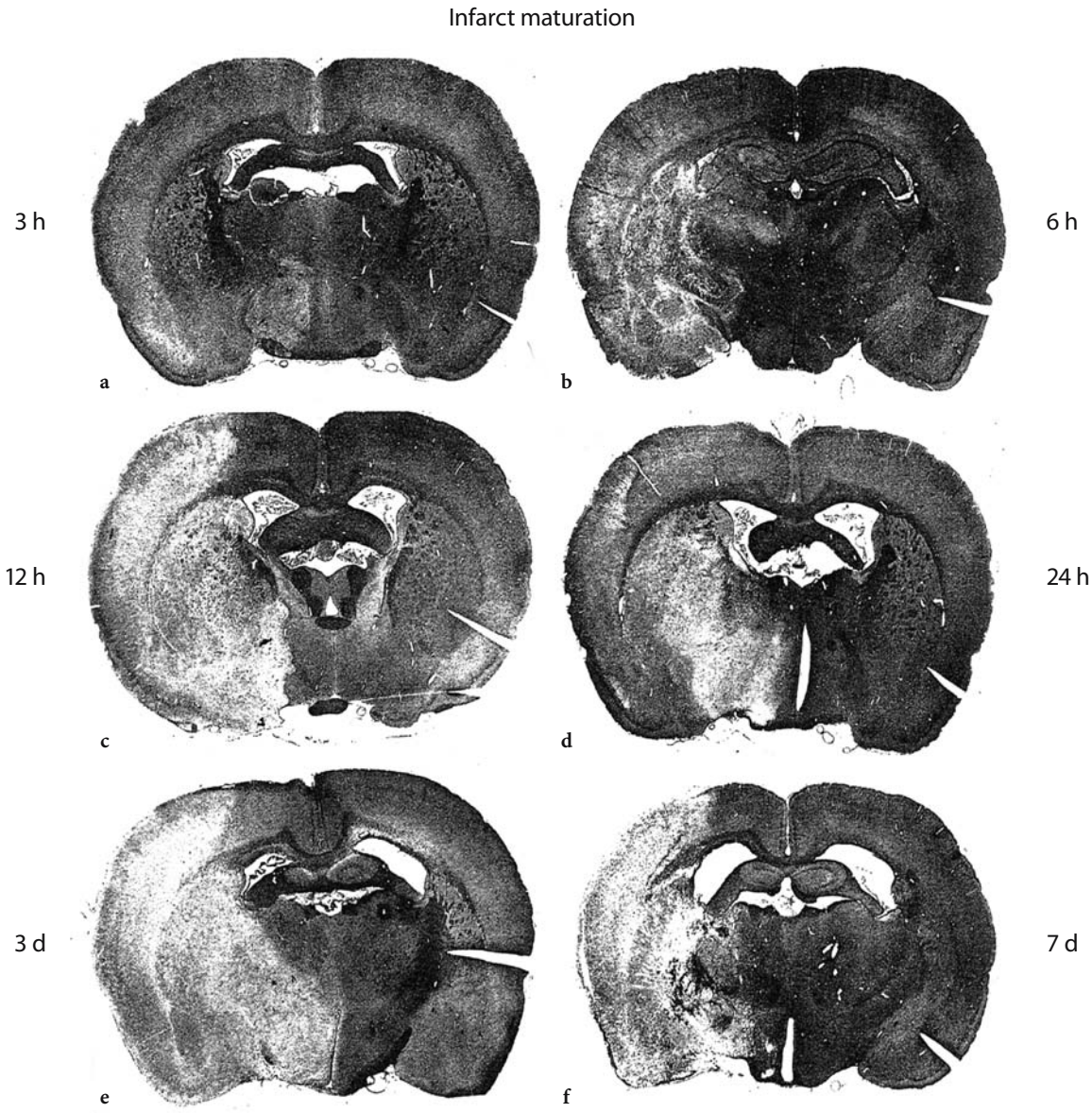

Fig. 4.3a-f. The phenomenon of infarct maturation is shown as macroscopic appearance on hematoxylin-eosin stained coronal brain sections. Right permanent middle cerebral artery occlusion was performed in rats and histology obtained between 3 h and 7 days. Note the sparse changes at 3 h and lesion shrinkage at 7 days. [Reproduced with permission from Garcia et al. (1993)]

tials (Astrup et al. 1977). In the borderzone around the densely ischemic core, the evoked potentials were affected when local CBF decreased below 0.20 ml/g/min (the upper threshold). A blood flow reduction below 0.15 ml/g/min induced complete electrical failure, but membrane function was still preserved as evidenced by near-to-normal extracellular potassium concentrations. The lower threshold (0.06 ml/g/min) was characterized as the CBF value below which massive release of potassium occurred that indicated irreversible loss of membrane function and subsequent cell death. The absolute CBF values defining the upper and lower thresholds of transmission or membrane failure, respectively, show a considerable variation depending on the method of flow measurement, the animal species, the ischemia model and the type of anesthesia used (Astrup et al. 1977; Branston et al. 1977, 1979, 1984; Heiss and Rosner 1983; Hossmann and Schuier 1980; Morawetz et al. 1978; Strong et al. 1983; Tamura et al. 1981).

Therefore, the CBF thresholds should be expressed in percent of control for better comparison: the upper one being about 40%, the lower one 12%-15% of control, respectively. Of note, the concept of flow thresholds could be successfully extended to a variety of physiological functions as presented in Figure 4.4 (Hossmann 1994), including pH regulation and tissue water diffusion. The simultaneous measurements of CBF, local ATP (adenosine triphosphate) content, pH and DWI in acute MCA infarcts revealed that tissue diffusion was disturbed below a CBF threshold of 0.34 ml/g/min (30 min post occlusion) and 0.41 ml/g/min (2 h post occlusion) which was distinctly higher than the threshold values for ATP depletion (0.13 ml/g/min after 30 min, and 0.19 ml/g/min after 2 h) (Kohno et al. 1995b). Most of the CBF thresholds, e.g., for overt infarction, ATP homeostasis or glutamate release, are also a function of time and rise with increasing durations of ischemia (Kohno et al. 1995b). This means that, for example, rodent brain with a CBF of 0.20 ml/g/min may escape infarction at 2 h post insult, but gets infarcted 1 h later if blood flow is not improved by then (Hossmann 1994). However, there are exceptions to this rule: the flow threshold for maintenance of protein synthesis does not change with ongoing ischemia (Hossmann 1994).

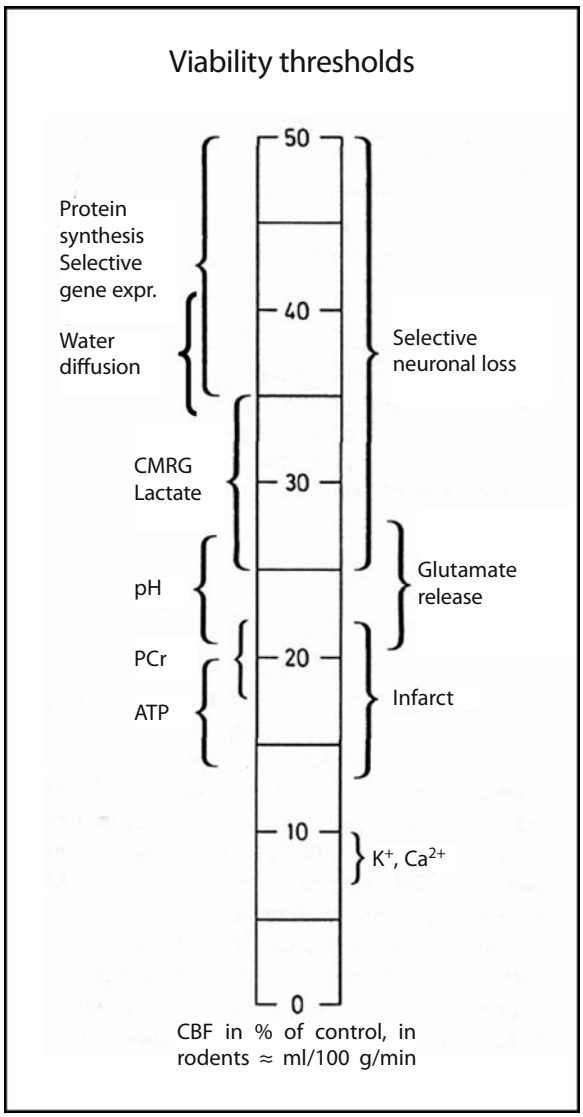

Fig. 4.4. Bar graph of viability thresholds of cerebral blood flow for a variety of functions and metabolites. Note that selective neuronal loss occurs at consistently higher flow values than overt infarction. *CMRG*, cerebral metabolic rate of glucose; *PCr*, phosphocreatine; *ATP*, adenosine triphosphate. [Adapted and reproduced with permission from Hossmann (1994)]

4.1.4 Cerebrovascular Reactivity and Functional Activation

The cerebral circulation is characterized by two phenomena that play a critical role in the presence of ischemic insults: (i) the ability of vessels to react to a variety of stimuli (the prototype of which is CO_2) by vasodilation or vasoconstriction, termed vasoreactivity, and (ii) the ability of the cerebral circulation to keep cerebral perfusion pressure constant within a wide range of the systemic arterial pressures, named autoregulation of CBF (reviewed in Hossmann 1987). Intact cerebral autoregulation and vasoreactivity is the basis for more complex responses that participate in the functional activation of distinct cortical regions triggered for example by sensory or motor functions. The development of blood oxygenation level-dependent (BOLD) imaging is based on the robust local blood flow increase that is triggered by local electrical activity. The BOLD effect allows us to visualize cortical representation fields in humans (Belliveau et al. 1991) and animals (Hyder et al. 1994). The coupling mechanism involves the interaction of a complex system of biochemical and neurogenic mediators that are subject to pathological interference. Therefore, pathological processes may modulate both, the effect of functional activation on metabolism and the response of blood flow to the change in local metabolic activity.

Blood flow regulation systems are disturbed in acute focal brain ischemia when an increase in blood pressure, but not of arterial $PaCO_2$, causes a rise of CBF (Shima et al. 1983). Disturbances of flow regulation are not confined to the ischemic focus

but may affect other parts of the hemisphere. The area with impaired autoregulation is larger than that of reduced CO_2 reactivity (Russell et al. 1970). The relationship between CBF and arterial blood pressure in focally ischemic brain areas is highly dependent on the severity of ischemia: autoregulation is lost in a gradual manner until CBF falls below 30% of normal (Dirnagl and Pulsinelli 1990). After experimental MCA occlusion, CO_2 reactivity partially recovered after 5 to 12 days (Waltz 1970). In another animal model, a complete recovery was already observed within 2 days (Dijkhuizen et al. 2001), but at this timepoint functional activation was still suppressed in the perilesional regions. At 2 weeks after the insult, signs of forelimb activation (that had recovered at this time) were evident in the infarct borderzone, both in and adjacent to the sensorimotor cortex. This finding may indicate the extension of forelimb representation fields into adjacent cortical areas during restoration of sensorimotor function (Dijkhuizen et al. 2001). We have, therefore, to take into account that functional plasticity of the cortex may interact with recovery patterns of vascular regulation.

In global cerebral ischemia different pathophysiological observations were made. Short periods of global ischemia cause extracellular acidosis that – as a potent vasodilator – induces a hyperemic phase in which autoregulation and CO_2 reactivity are both severely disturbed (Waltz and Sundt 1968). Frequently, brief hyperemia is relieved by a lasting phase of hypoperfusion (down to 50% of control) when autoregulation recovers, but vasoreactivity remains diminished (Hossmann 1997). Postischemic hypoperfusion that is characterized by an increased vascular tone, is not coupled any longer to metabolism and leads to the dissociation between oxygen supply and consumption, thereby inducing a gradual increase in oxygen extraction. Normal oxygen extraction fraction amounts to about 35% and may rise up to 80% which in turn stimulates anaerobic glycolysis. As a result, secondary lactacidosis and energy depletion may occur. Causal factors include the expression of adhesion molecules and the generation of free radicals, possibly also the down-regulation of endothelial nitric oxide (NO) synthase. It is conceivable that under those conditions, the coupling between blood flow and metabolism can be disturbed on two sides: functional activation may not trigger any longer a sufficient increase in local metabolism and/or metabolic activation may not be coupled to a sufficient increase in local CBF any more. These considerations are of particular importance for studies that utilize BOLD imaging to study perilesional brain areas.

4.1.5 Mechanisms of Injury

It is beyond the scope of this chapter to review the current knowledge of potential mechanisms of ischemic injury. However, we wish to point to key processes that can be also addressed by experimental studies applying MR methods. Here, our interest will be focussed on the pathophysiology of focal ischemia. Brain ischemia results in a cascade of events that affect the brain in a certain hierarchy of physiological functions (e.g., based on flow thresholds) and in a certain time sequence of processes resulting in very peculiar patterns of lesion evolution. As reviewed by Dirnagl et al. (1999), mechanisms of injury may be roughly divided into the following categories: (1) rapid excitotoxic mechanisms including the occurrence of spreading depression-like phenomena in the infarct border, (2) slower inflammatory responses triggered by the generation of oxygen free radicals, and (3) pro-apoptotic processes that may lead to a very delayed type of cell death, closely related to mitochondrial dysfunction (Fig. 4.5). Other potential causes for lesion evolution (studied mainly in focal cerebral ischemia) include the time-dependent increases in microcirculatory flow disturbances (Hakim et al. 1992; Kohno et al. 1995b), the glucose utilization/blood flow uncoupling in the infarct border (Back et al. 1995; Nedergaard et al. 1986) and the occurrence of severe lactacidosis in the infarct core (Back et al. 1994a, 2000b; Kobatake et al. 1984). It has to be mentioned that a vast variety of molecular responses to ischemia are under investigation the pathophysiological significance and role of which are only partially understood. For instance, serine proteases like tissue plasminogen activator, plasmin, and thrombin may play a role through activation of protease-activated receptor 1 (PAR-1) (Junge et al. 2003). Other interesting molecular targets are calcineurin, cytokines, apoptosis-inducing factor, nitric oxide, matrix metalloproteinases, and acid-sensing calcium permeable ion channels.

In experimental stroke, the zone of dense ischemia leads to the rapid exhaustion of substrates, particularly oxygen and glucose. The impaired energy yield cannot maintain the ion pumps so that cells loose their membrane potential (anoxic depolarization of glia and neurons). As a consequence, volt-

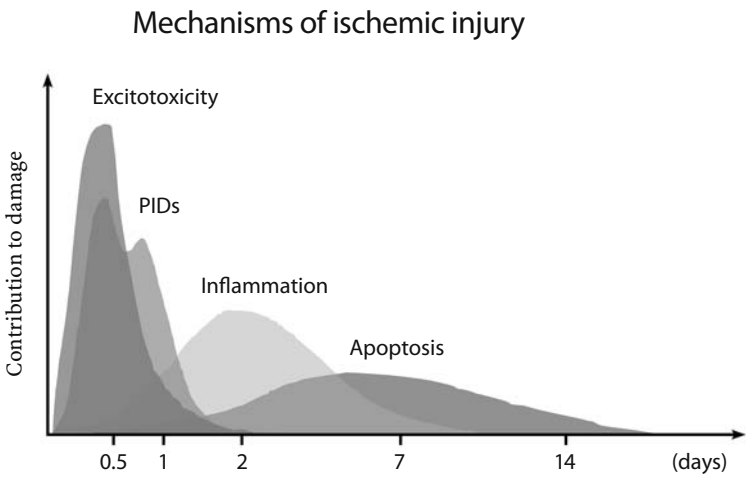

Fig. 4.5. Timecourse and impact of mechanisms that contribute to ischemic damage. Note that inflammatory responses and programmed cell death are processes of the subacute and chronic phase. *PIDs*, peri-infarct depolarizations. [Adapted from Dirnagl et al. (1999)]

age-dependent calcium channels are activated and excitatory amino acids are released into the extracellular space where the presynaptic reuptake is disturbed. What follows is the activation of NMDA receptors and other types of glutamate receptors that contribute to the accumulation of intracellular calcium and the influx of Na^+ and Cl^- via receptor-associated ion channels. A water hydrops of neurons can be observed that is associated with a dramatic (about 50%) decrease of the extracellular space. This early water shift from the extra- to the intracellular compartment is believed to be the basis of disturbed water diffusion imaged by DWI. This very early form of cell edema has also be termed cytotoxic edema and is *not* coupled to major changes of the blood–brain barrier permeability nor to a large net increase in brain water. The latter does occur with very low flow rates less than 0.10 ml/g/min when brain water content increases steeply along with the increase in the tissue ratio of sodium/potassium (Hossmann 1987). This type of more delayed edema development is accompanied by a break-down of the blood–brain barrier and termed vasogenic edema (for details see Chap. 8). However, it has to be stated that ischemic brain edema is a complex combination of cytotoxic and vasogenic elements depending on the type of ischemia, the timepoint of observation and the severity of the ischemic impact.

We have seen that sodium enters the cells, but potassium is set free into the extracellular space where it induces irregular depolarizations, particularly in the surroundings of an ischemic focus. Such transient depolarizations travel over the cortex like classical waves of spreading depression of electrical activity (Back et al. 1994b; Leao 1944; Nedergaard and Astrup 1986). The number of such peri-infarct depolarizations (PIDs) correlated well with final infarct size (Back et al. 1996; Mies et al. 1993) and could be effectively blocked by glutamate antagonists or initiation of recanalization that both reduced infarct volumes (Gill et al. 1992; Iijima et al. 1992; Schüler et al. 2001). By using repetitive DWI, the propagation and enlargement of the ischemic lesion, which is dependent on the occurrence of PIDs, has been demonstrated in a rat model of stroke (Busch et al. 1996; Takano et al. 1996). A recent attempt to measure similar changes in ADC (apparent diffusion coefficient of water) that would resemble PIDs in acute human stroke, was unsuccessful (Back et al. 2000a). Nevertheless, spreading depression has been irrefutably demonstrated in patients suffering from acute traumatic brain lesions (Strong et al. 2002). PIDs are closely related to cellular injury through mechanisms of excitotoxicity (Marrannes et al. 1988). The high number of glutamate receptors on the surface of cortical neurons but also in other parts of the brain explain that excessive glutamate release may over stimulate those neurons due to impaired clearance mechanisms for excitotoxic transmitters (Choi 1992).

Other factors that contribute to lesion growth are related to the progressive impairment of CBF and the associated derangement of glucose and energy metabolism (Back et al. 1998). A striking uncoupling between near-to-normal glucose utilization in the presence of compromised flow has been demonstrated in animal models of stroke (Back et al. 1995; Nedergaard et al. 1986). It seems unlikely that any brain tissue could survive this mismatch between energy demand and blood supply on longer terms. The high dependence of brain tissue on oxidative phosphorylation explains why primary or secondary energy failure is impending over flow-compromised areas. Another important pathophysiological factor

is the excess generation of lactate due to the initiation of anaerobic metabolism. We have seen above that the increase in oxygen extraction above 50% is a strong trigger of anaerobic metabolism. As a result, lactate is excessively produced and may spread by diffusion over adjacent parts of the affected hemisphere. Together with hydrogen ions that stem from ATP hydrolysis, lactate contributes to the severe acidosis that may further damage neurons (Back et al. 1994a, 2000b). Apart from these acute metabolic changes, a large variety of molecular responses like the upregulation of immediate-early genes, the formation of stress proteins, the upregulation of pro-apoptotic proteins and inflammatory changes occur that may modify the final extent of damage in the subacute phase. However, we may assume that this modification does not account for changes in lesion volume exceeding the 5%–10% range in human stroke (Heiss et al. 1999).

4.2 Evolution of Ischemic Lesions

The insight into the dynamic nature of ischemic brain lesions has raised growing attention over the past few years. Distinct temporal and spatial patterns of lesion evolution have been described for two types of cerebral ischemia that differ in many pathophysiological aspects: namely conditions of focal and global cerebral ischemia.

i) Territorial brain infarcts, the prototype of focal cerebral ischemia, tend to enlarge in size during an ongoing period of hypoperfusion. This has been shown in animal models of stroke (Dereski et al. 1993; Garcia and Kamijyo 1974; Garcia et al. 1993; Gyngell et al. 1995; Kohno et al. 1995b) and in clinical human studies using MRI (Baird et al. 1997; Barber et al. 1998; Karonen et al. 1999; Neumann-Haefelin et al. 1999; Parsons et al. 2002). Almost half of the patients who presented with acute hemispheric stroke showed an increase in lesion size by > 20% occurring over the initial 7 days post stroke (Baird et al. 1997). The lesion growth is clinically important and is associated with poor outcome. A better understanding of the underlying pathophysiological changes involved may guide future therapeutic interventions as reviewed in Chap. 3.
ii) In conditions of global cerebral ischemia, however, the changes are more complex. As shown in animal models, periods of global ischemia can either lead to the recovery or, alternatively, to secondary deterioration of the tissue status accompanied by a global reduction of energy metabolism (Hossmann et al. 1994; Paschen et al. 1983). The time course of changes in the brain parenchyma of patients with ischemic-anoxic brain damage after cardiac arrest is not well studied so far (Arbelaez et al. 1999; Schaafsma et al. 2003; Wijdicks et al. 2001). Repeated MRI studies may disclose parenchymal changes in those patients that are subtle and patchy in nature targeting selectively vulnerable neurons as reviewed in detail in Chap. 16.

4.2.1 Global Ischemia

Global brain ischemia results from transient low CBF below 0.5 ml/100g/min or severe hypoxia to the entire brain (Hossmann 1987; Siesjö 1988). The causes are mostly cardiac arrest, near drowning and hypotension as is often seen as a consequence of surgical procedures. After a few minutes of cardiac arrest, hypoxic encephalopathy becomes irreversible. The precise duration of global ischemia necessary for irreversible neuronal damage in humans is unknown (Heiss 1983; Zivin 1997), but for the most vulnerable areas it is about 5 min. Many animal models have confirmed cellular death within a few minutes after global ischemia onset (Siesjö 1978). On the other hand, Hossmann et al. demonstrated that global cessation of CBF in animals of up to 1 h can be followed by recovery of electrophysiological function and, in a few animals, recovery of neurological function (Hossmann et al. 1987; Hossmann and Zimmermann 1974). It remains unclear how neurons can respond so differently after an ischemic insult.

Besides the variable functional outcome after ischemia in animal models, it is well established that specific neuronal populations within an individual vary substantially in ischemic tolerance. Neurons in the CA1 region of the hippocampus and other distinct cellular populations of the caudate, thalamus, neocortex and cerebellum are selectively vulnerable to relatively brief periods of ischemia (Kirino and Sano 1984; Siesjö 1988). The reasons for this phenomenon are not fully elucidated, but for example in cerebellar Purkinje cells it could be shown that a reduced level of aldolase may trigger energy failure after brief periods of anoxia (Welsh et al. 2002). Changes in microcirculation, as seen in focal stroke,

do not occur in global ischemia. This may alter the dynamics, especially in the reperfusion phase after transient ischemia, and explain why models of global ischemia cannot fully represent stroke pathophysiology (Hossmann 1987; Kirino and Sano 1984; Smith et al. 1984).

Studies by Hossmann et al. have shown that prolonged global ischemia may result in secondary deterioration during the reperfusion phase followed by depletion of energy metabolites, acidosis and a dramatic increase in lactate content (Hossmann et al. 1994). However, in some animals recovery can be observed that is dependent on successful reperfusion. This pathologic condition that imitates cardiac arrest in man, results in a rapid (< 10 min) and marked (68% of control) decrease in the ADC when measured by repeated MR diffusion imaging (Hossmann et al. 1994) (Fig. 4.6).

If we apply the lesion assessment as used in focal ischemia, one would estimate a nearly 100% lesion spread after 1 h of global ischemia (visible after the initial 10 min) that may or may not resolve during a 180-min reperfusion period. Short-lasting periods of global ischemia, e.g., the four-vessel occlusion model in rats (Schmidt-Kastner et al. 1989), provoke a circumscribed damage to the CA1 sector of the hippocampal formation that appears after 3 days. The number of dead CA1 neurons has been shown to increase from 3 to 7 days post insult (Böttiger et al. 1998). Other selectively vulnerable regions in global ischemia are the thalamus, the basal ganglia and the cortical layers 3–5. Due to the subtlety of histopathologic changes that consist mainly of selective neuronal injury of the delayed type, it is difficult to assess lesion size in quantitative terms. Therefore, in the literature no solid numbers for affected volumes of this process are reported.

In global ischemia, cell death occurs due to apoptosis, and not necrosis as seen in focal ischemia (Böttiger et al. 1998; Ouyang et al. 1999). The morphological and imaging data on cardiac arrest patients are scarce (Arbelaez et al. 1999; Berek et al. 1995; Grubb et al. 2000; Schaafsma et al. 2003; Wijdicks et al. 2001) (see also Chap. 16). Arbaelez et al. (1999) published MR findings in a series of patients with global cerebral hypoperfusion following cardiac arrest. The anoxic-ischemic tissue changes were depicted in the acute and early subacute phase (up to 14 days post insult) on DWI. The same alterations were not visible on T1- or T2-weighted images or seen at a later stage of the disease (Arbelaez et al. 1999). To date, systematic longitudinal studies available to answer the questions of timepoint and localization of brain lesion appearance following human cardiac arrest are nearly lacking. However, there is clinical evidence that longer durations of global circulatory arrest exceeding the resuscitation time of ~ 10 min, almost uniformly result in fatal outcome with generalized brain edema, obscuration of grey–white matter junctions and widespread laminar necrosis of the cortex. In a series of ten patients who suffered from anoxic-ischemic coma, most individuals showed diffuse signal abnormalities in DWI and fluid-attenuated inversion recovery

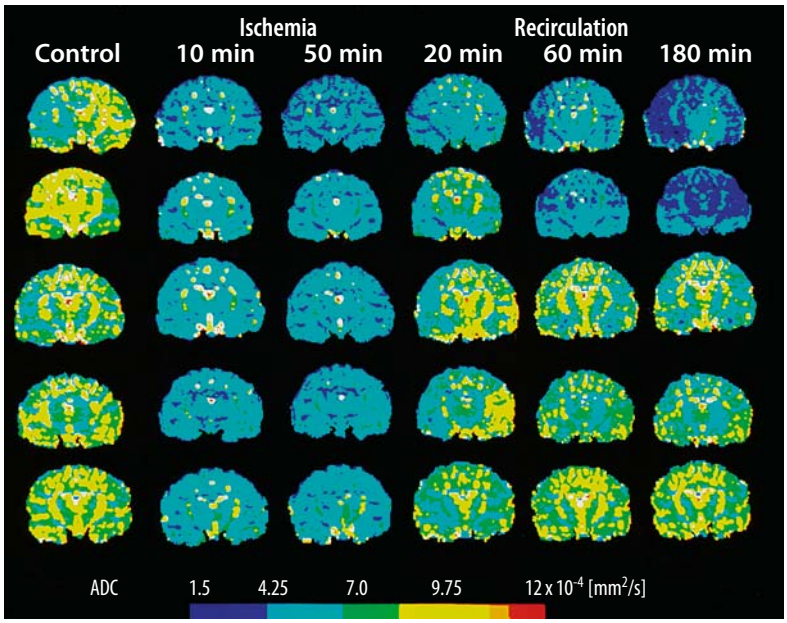

Fig. 4.6. Quantitative maps of the apparent diffusion coefficient (*ADC*) in cats subjected to 1-h complete cerebrocirculatory arrest followed by 180 min of recirculation. Each *row* represents one animal. The pre-ischemic condition is shown by the first *left column*. Images show a central coronal slice that was measured at six time points per animal. Note the early decline of ADC after onset of ischemia and the rapid post-ischemic normalization in the *lower three rows* indicating recovery in those animals. The *upper two rows* depict animals that did not recover during the reperfusion phase. [Reproduced with permission from Hossmann et al. (1994)]

(FLAIR) images that affected most severely areas of high vulnerability (cerebellum, hippocampus, thalamus, frontal and parietal cortices) (Singhal et al. 2002). Especially alterations in DWI seemed to correlate well with the distinct neuropathological features of anoxic-ischemic encephalopathy.

Another study used PET to measure perfusion and glucose metabolism after cardiac arrest (Schaafsma et al. 2003). It revealed a nearly 50% decrease of glucose consumption, but was unable to detect patterns of metabolic or perfusion changes that would predict clinical outcome or imaging abnormalities. See Chap. 16 for detailed information on this matter.

4.2.2 Focal Ischemia

4.2.2.1 Comparison of Diffusion Imaging with Changes in Relaxation Times

In states of focal cerebral ischemia, repetitive MRI has elucidated the natural course of brain lesions which – as a regular phenomenon – show considerable lesion enlargement over time. This observation was made by using DWI in animal models with occlusion of the middle cerebral artery. To date, we have little information on the natural course of ischemic lesions that are of hemodynamic origin or the result of small vessel disease. After the first publications on diffusion MRI of tissue water (Le Bihan et al. 1986), Moseley and coworkers (1990) could demonstrate that DWI offers a high contrast between normal and ischemic tissue, and that this contrast could be observed already several minutes after arterial obstruction (Moseley et al. 1990; Sevick et al. 1990). It became obvious that signal changes in DWI clearly preceded changes in T2-weighted images (Fig. 4.7). With a multi-slice approach it could be shown that over the initial 6 h both the signal intensity and the lesion volume increased over time (Gyngell et al. 1995; Hossmann and Hoehn-Berlage 1995). The increasing hyperintensity on DWI reflects the gradual decline of the apparent diffusion coefficient (ADC) that drops rapidly during the initial 30 min, thereafter decreasing more slowly along with an initial phase of rapid and afterwards slow lesion growth (Roussel et al. 1994). Figure 4.8 presents such an example in which the increase in affected tissue is visible on repeated DWI, but also the increase in signal intensity over time. The changes of ischemic lesion volume could be confirmed in a model of clot embolism of the MCA in rats by using repeated DWI. Compared to the lesion volume at 30 min, final lesion size at 8 h post occlusion had increased by ~ 70% (Brinker et al. 1999).

The quantitative measurement of the ADC has advantages over mere diffusion-weighting because

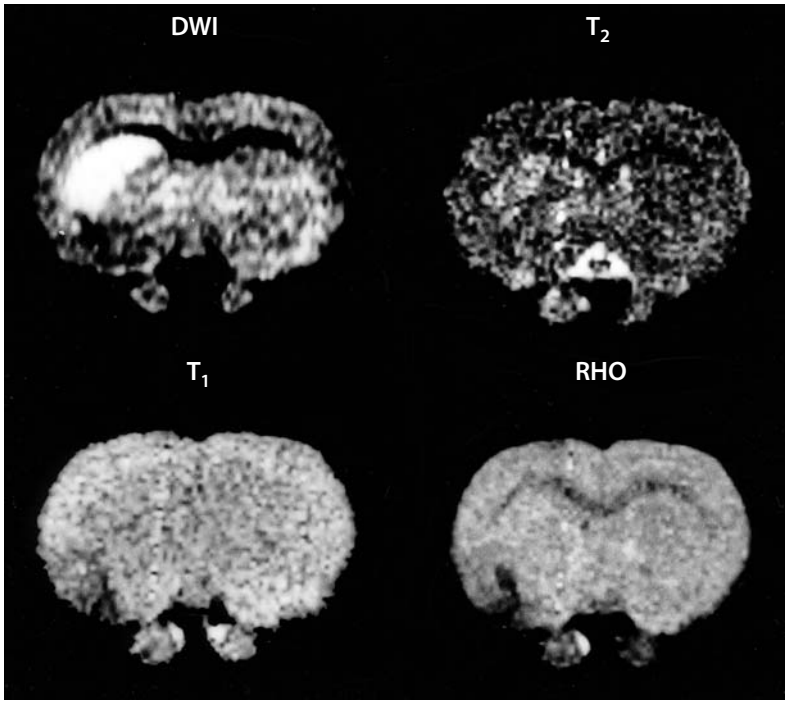

Fig. 4.7. Coronal measurements of diffusion, proton density (*RHO*), T1 and T2 relaxation times 30 min after occlusion of the middle cerebral artery in a rat. Note the clear-cut striatal signal increase in the diffusion-weighted image (*DWI*) compared to nearly unchanged images of the other MR modalities

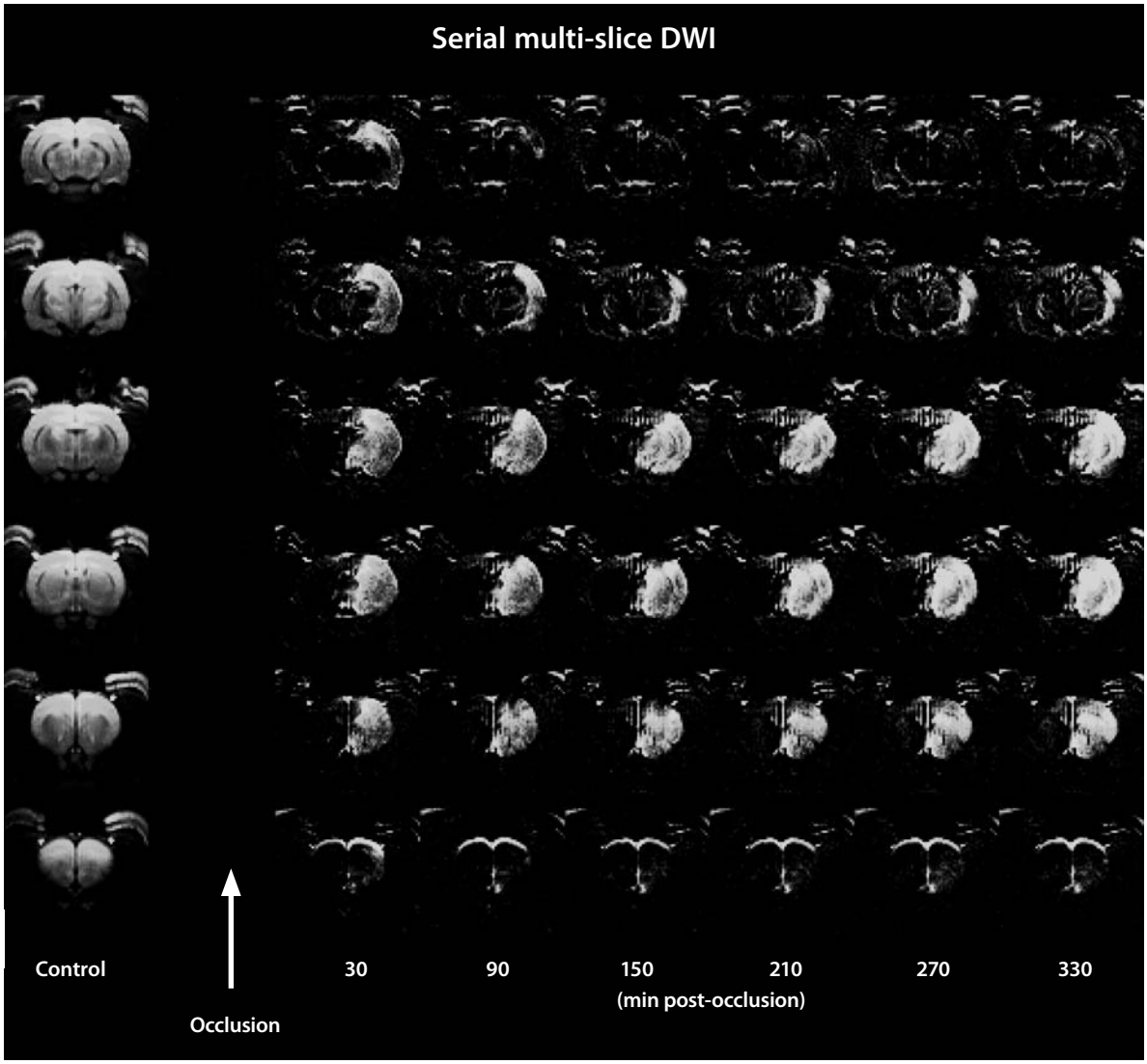

Fig. 4.8. Lesion development in permanent middle cerebral artery (MCA) occlusion in a rat measured by repeated MR diffusion-weighted imaging (DWI). *Left column*: Control condition pre-occlusion in coronal slices from posterior (*top*) to anterior (*bottom*). The *arrow* marks the timepoint of occlusion. Images shown in columns 2 to 7 are DWI (subtraction images) measured 30 to 330 min post-occlusion. Note the lesion growth and the increase in signal intensity within the lesion. (Courtesy Dr. M. Hoehn, Cologne)

influences of other MR parameters are eliminated. It requires the measurement of a whole set of images with increasing diffusion weighting (minimum: two) expressed by variable b-factors. Increased T2, for example, can be mistaken as a reduction of tissue diffusion. On the contrary, ischemia-induced T1 increases tend to diminish the contrast in DWI (with short recovery times). A disadvantage of ADC maps is that ischemic lesions present as "darker" brain regions that are not as easily depicted as hyperintense lesions in DWI. From experimental data there is good evidence that ADC values do not fall below 50% of control and that densely ischemic brain regions exhibit ADC values in the range of 60%-80% (for review see Hoehn-Berlage 1995). ADC above 80% is typically seen in the first hours of occlusion and/or in more peripheral borderzone regions of brain infarction (Back et al. 1994a; Jiang et al. 1993; Mintorovitch et al. 1991). Volume evaluations have to take into account that ADC values depend on the direction of the diffusion encoding gradient that is of particular importance for the study of white matter changes, but also affects grey matter (Hoehn-Berlage et al. 1995a). This effect has been

termed anisotropy of tissue diffusion. Strategies of diffusion tensor imaging have elucidated in great detail this phenomenon.

The observation of relaxation times revealed that increases in T1 and T2 could be seen a few hours after onset of focal ischemia onset, but not as early as changes in DWI or ADC (Hoehn-Berlage et al. 1995a; Knight et al. 1994). This observation has been confirmed in stroke patients in whom DWI changes are observed as early as 40 min post insult (Yoneda et al. 1999). However, T2 signal changes occur in the subacute phase and are nearly always indicative of irreversible tissue damage. Thus, the discovery of very early diffusion changes in experimental brain ischemia has filled out the *diagnostic gap* of conventional cranial MRI or CT in acute stroke. So far, stroke clinicians had been forced to search for very subtle signs in CT (early ischemic signs like obscuration of the lentiform nucleus) or MRI (e.g., slight T2 hyperintensity, discrete swelling) to detect focal ischemia during the initital hours after onset of symptoms.

The further timecourse of ischemia-related changes in ADC and relaxation times reveals striking differences, too. Experimentally, the initial reduction of ADC returns to normal within 48-72 h in models of MCA occlusion and rises thereafter to supranormal values that normalize after about 1 week (Helpern et al. 1993; Knight et al. 1991). By contrast, the subacute increases in relaxation times reach their peak at 24-48 h and decrease slowly thereafter (Helpern et al. 1993; Knight et al. 1994). In human stroke, the timecourse of ADC changes appears to be similar, but in a somewhat retarded fashion: the minimum ADC has been observed 12-24 hours after onset, the pseudonormalization of altered diffusion between 7 and 14 days and clearcut elevations of ADC from 30 days onward (Warach et al. 1992, 1995). Both in humans and animals, grey and white matter show differential profiles in the magnitude and timecourse of changes observed. Whereas the ADC is reduced by ≈ 30% in ischemic grey matter with more rapid pseudonormalization, the reduction is more profound in ischemic white matter (by ≈ 45%) that returns more slowly to "pseudonormal" values if it occurs at all (Kuroiwa et al. 1998; Mukherjee et al. 2000).

With regard to the spatial evolution of ischemic lesions heterogeneity was also observed. During the initial 4 h of experimental MCA stroke, the areas with increased relaxation times or proton density were significantly smaller than the regions showing altered ADC (Hoehn-Berlage et al. 1995a). At later timepoints, these differences merged to congruent lesion sizes and showed high congruence with histological infarcts at 7 h post occlusion (Back et al. 1994a). It is concluded from this data, that images of T1, T2 or proton density only reflect the correct infarct size after about 7-8 h after onset of ischemia. This notion is particularly true for a situation of permanent vessel obstruction.

4.2.2.2 Correlation Between Changes in Diffusion, Cerebral Metabolites and Tissue Injury

The signal change in diffusion-weighted images is induced by the reduction of the ADC of water in ischemic brain. Experimental studies employing rapid DWI and MRS have demonstrated that this change in ADC occurs within minutes after obstructing a brain artery (Dijkhuizen et al. 1999; van der Toorn et al. 1996). This hyperacute change in tissue water ADC was subject to many efforts to elucidate the underlying mechanisms. Moseley et al. (1990) had already suspected that the ischemia-induced water shift from the extra- to the intracellular space may be a key event that explains both, early cell swelling and restricted diffusion in the extracellular compartment. Very similar timecourses of changes in the extracellular space volume and in tissue water diffusion have been nicely shown in a model of acute brain injury (Verheul et al. 1994). By several other studies, the close relationship between cytotoxic cell swelling and disturbance of the energy metabolism has been shown. The abrupt reduction of tissue oxygen and/or glucose concentrations induce anoxic depolarization, caused by a failure of cation-pumping ATPases and leading to the disruption of transmembrane ionic gradients. Much of the ADC decrease occurs during anoxic depolarization, however, recent studies suggest that ADC may change already before anoxic depolarization occurs and may accompany conditions with elevated excitotoxins, but preserved energy metabolism and intact ion homeostasis (for review see Hoehn et al. 2001). It is conceivable that diffusion in the extracellular space is more rapid than within cells. On the other hand, the intracellular space comprises about 85% of total tissue water volume. Cell swelling by water shift would not only reduce the volume of the extracellular compartment, but also increase its tortuosity. Both effects would decrease the ADC. It seems, however, that the ischemia-dependent reduction in ADC is the result

of diminished water diffusivity in the extra- *and* the intracellular space (Szafer et al. 1995). Recently, the contribution of intra- and extracellular water ADC could be separated in normal and ischemic brain. In normal brain, the volume-localized ADC was about 10% lower in the intracellular compartment compared to the unseparated condition where both, the intra- and extracellular space contribute to the signal (Silva et al. 2002). Interestingly, in ischemic brain, this difference was frankly absent pointing to the notion that the intracellular ADC dominates and determines the overall water ADC under ischemic conditions (by part due to the drastic decrease of the extracellular space). To summarize, current knowledge links tissue diffusion changes to the development of cytotoxic cell swelling as an early hallmark of stroke pathology although the exact mechanisms remain unknown.

Histopathological studies have demonstrated in the rat MCA occlusion model that the ischemic area covered 10% of the hemisphere at 1 h, 22% at 2 h, 38% at 6 h and 50% at 12 h post occlusion (Garcia et al. 1993). It has to be taken into account that during the initial 3–6 h the lesion volume evaluations rather reflect gradual infarct maturation than actual growth as mentioned before. However, the observation of histological lesion enlargement between 6 and 24 h post-occlusion is a consistent finding (Fig. 4.9). The regional distribution of ATP or glucose as measured by bioluminescence techniques is a more reliable marker of ischemic lesions than histopathological changes in the very early stage of infarction. In a permanent MCA occlusion model, areas with grossly reduced ATP/glucose enlarge significantly during the initial 2 h following MCA occlusion (Kohno et al. 1995b). In this animal study, ATP reduction was present in 22% of the ischemic hemisphere at 30 min and in 50% at 2 h post ischemia (Fig. 4.10). This considerable magnitude of lesion enlargement was also demonstrated for other variables, i.e., areas with solid acidosis (61% at 30 min; 70% at 2 h post occlusion) or regions that exhibit a disturbance of diffusion as measured by DWI (Gyngell et al. 1995; Kohno et al. 1995b) (Table 4.1).

The alterations of ATP content, glucose content, tissue pH or tissue diffusion all were dependent on distinct thresholds of CBF that increase with increasing ischemia times. ADC was reduced if CBF fell short of 0.34 ml/g/min (30-min ischemia) or 0.41 ml/g/min (2-h ischemia), respectively (Kohno et al. 1995b). This relationship was recently confirmed by a study in stroke patients using simultaneous measurements of ADC and quantitative perfusion maps (Lin et al. 2003). The authors showed that in patients who were examined 2-4 h after stroke onset, ADC values dropped abruptly if CBF was lower than 0.15 ml/g/min. In a patient group imaged 4.5-6.5 h after symptom onset, the corresponding CBF threshold had increased to 0.24 ml/g/min (Lin et al. 2003). For a rough comparison between man and rat studies (as mentioned before), one has to double the human CBF values in order to meet comparable absolute values in small animal species. We recognize that there is a fair correspondence of CBF thresholds for altering diffusion in animals (35%-50% of control CBF) and man (30%-50% of control CBF). Decreased water diffusion

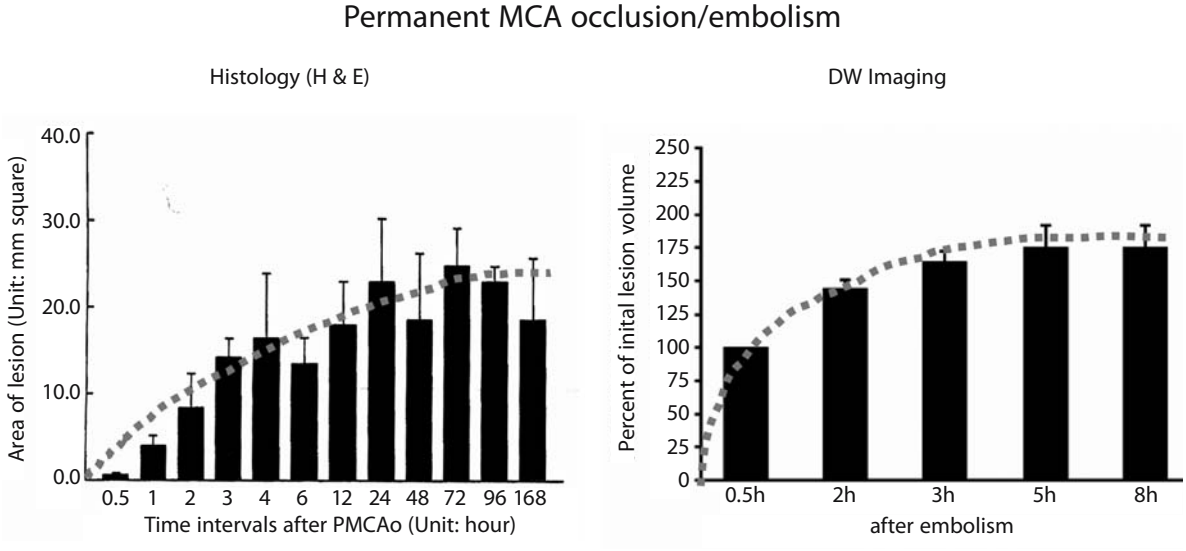

Fig. 4.9. Lesion development in stroke models of permanent focal ischemia (PMCAo) visualized by histology (*left*) and diffusion-weighted (DW) imaging. [Adapted from Garcia et al. (1993) and Brinker et al. (1999)]

Table 4.1. Lesion growth determined 30 min and 2 h after middle cerebral artery occlusion in rats. Tissue alterations are presented as hemispheric lesion areas (HLA) that were assessed at the level of striatum. [Adapted from Kohno et al. (1995b)]

	HLA at striatal level (% of hemisphere)	
	30 min	2 h
ATP depletion (Infarct core)	22%	50%
Perfusion deficit (CBF < 0.20 ml/g/min)	36%	52%
Diffusion lesion	54%	67%
Diffusion lesion minus ATP loss ("Metabolic penumbra")	32%	17%

CBF, local cerebral blood flow.

occurs at CBF rates that alter the electrical function of the brain (i.e., correspond to the upper threshold of the ischemic penumbra), but do not necessarily lead to morphologic damage (Busza et al. 1992; Hossmann 1994) (see also Fig. 4.4). This notion is of high importance to understand the potential for reversibility of diffusion changes.

Figure 4.9 shows that lesion expansion can be documented by histology (somewhat masked by infarct maturation during the first hours) and DWI, pointing to the very first hours of evolving infarcts as the target of therapy to interfere with the most rapid lesion dynamics. At later timepoints, excellent congruence between histological damage, breakdown of energy metabolism, tissue acidosis and diffusion lesions could be shown. In this study, DWI and biochemical imaging of the regional distribution of ATP, tissue pH and other metabolites were performed simultaneously with histological assessment 7 h post MCA occlusion (Back et al. 1994a). The close correlation between ATP loss, tissue acidosis and hyperintensity in DWI clearly shows that at this timepoint the rapid phase of infarct development is over and turns into subacute and more chronic processes involving inflammatory and molecular responses (Fig. 4.11).

4.2.2.3 Composition of Focal Ischemic Lesions

The close investigation of ischemic lesions and their correlates in MRI, CBF maps and biochemical imaging reveals that the response to ischemia is non-uniform. In accordance to the penumbra concept, the densely ischemic infarct core exhibits lower ADC values (Hoehn-Berlage et al. 1995b) compared to borderzone areas that are exposed to less severe reductions of CBF (Back et al. 1995). The lesions, therefore, show a gradient of CBF values ranging from normal to very low and a parallel gradient of ADC values ranging from normal to about 55% that cover the distance between unaffected surrounding tissue, the ischemic penumbra and the infarct core in three dimensions (Back et al. 1995, 2000a). During the first hours of stroke, special attention should be paid to borderzone regions in which DWI shows hyperintensity, pH is decreased, but ATP remains normal, even in the presence of increased lactate concentrations.

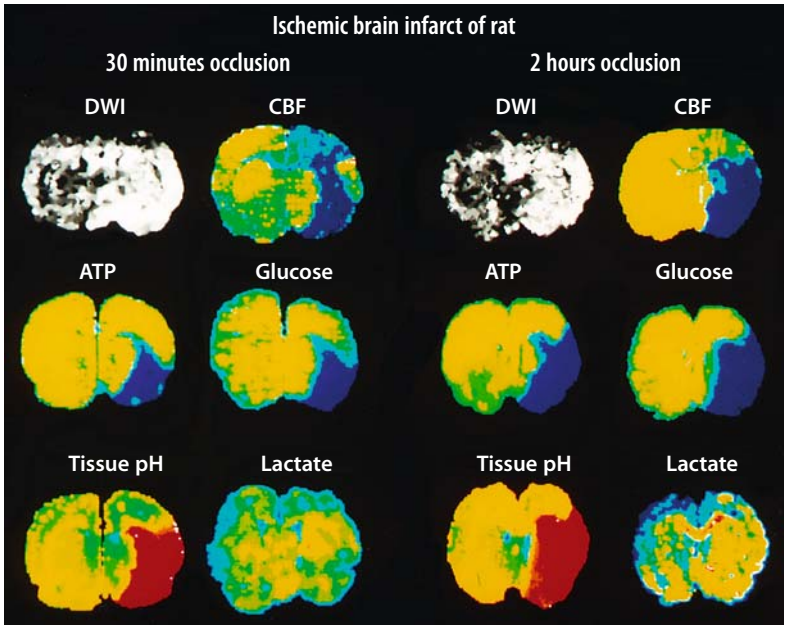

Fig. 4.10. Image combination showing diffusion-weighted images (*DWI*), maps of cerebral blood flow (*CBF*), bioluminescence images of ATP, glucose and lactate content, and tissue pH maps at 30-min (two *left columns*) and 2-h occlusion (two *right columns*) of the middle cerebral artery in rats. Hyperpintensity in DWI denotes ischemic changes; *blue* in CBF, ATP and glucose maps marks a reduction in flow, regional ATP and glucose content, respectively. *Red* in pH maps denotes tissue acidosis. *Bright yellow* indicates elevated tissue lactate levels. Note that the region with depleted ATP and glucose rapidly grows between 30 min and 2 h postocclusion. At both timepoints, hyperintensity in DWI corresponds well to the areas with diminished blood flow and tissue acidosis, but clearly exceeds the region with ATP loss. [Reproduced with permission from Kohno et al. (1995b)]

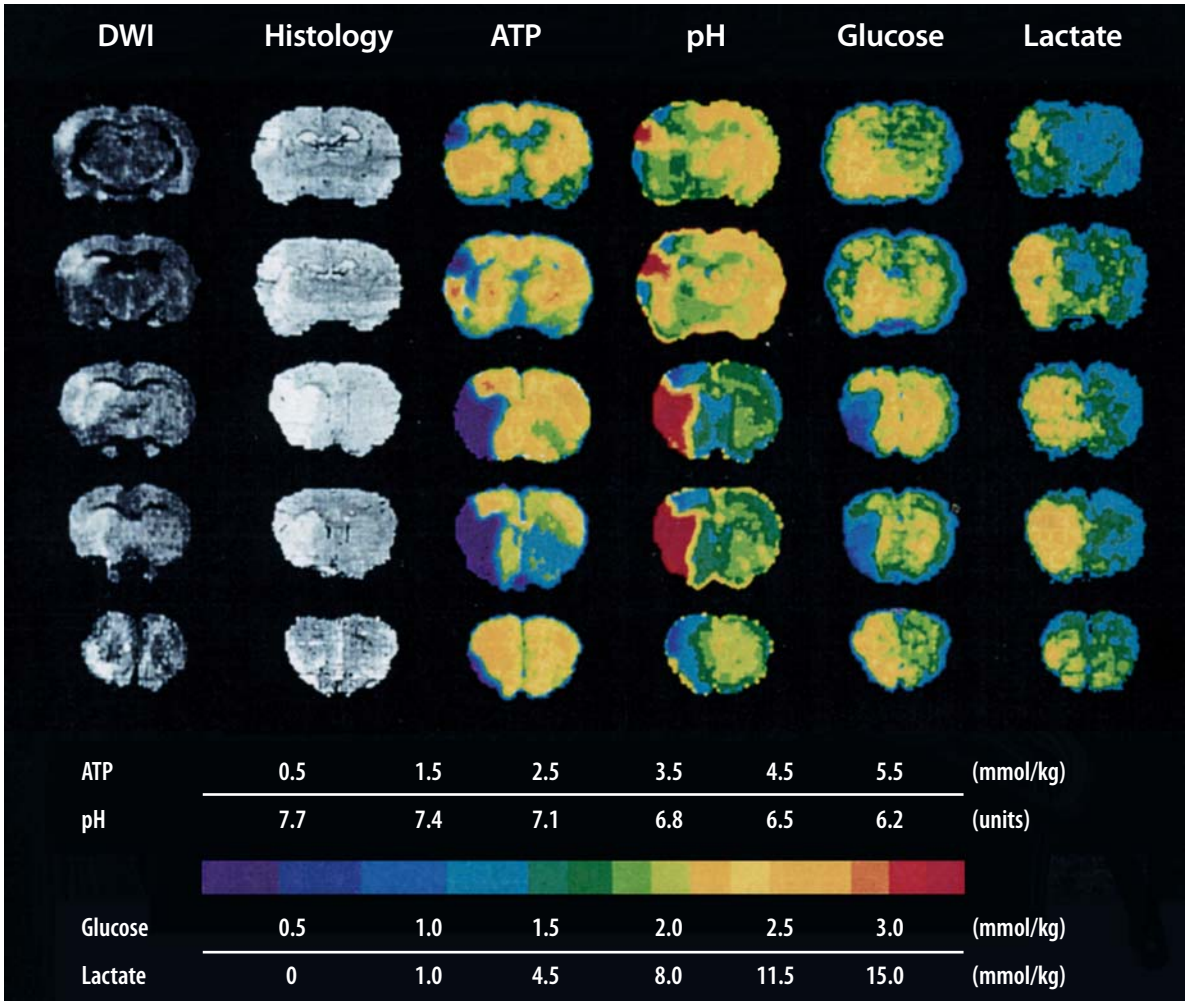

Fig. 4.11. Image combination showing diffusion-weighted images (*DWI*), histological sections and maps that display the regional distribution of ATP, glucose, lactate, and tissue pH. Permanent MCA occlusion was performed in a rat, all images were obtained 7 h postocclusion and are shown at five coronal levels ranging from posterior (*first row*) to anterior (*last row*). Note the high congruence of DWI, histology, ATP and pH maps, indicating that the rapid phase of infarct growth has ceased at this timepoint. [Reproduced with permission from Back et al. (1994a)]

By using a thresholding approach in a 3-D CBF data set, we could show that 54% of the total ischemic lesion volume could be attributed to the penumbra, only 46% to the infarct core at 1.5 h post MCA occlusion (Back et al. 1995). Those areas with pending infarction show potentially reversible changes that can be addressed by therapeutic interventions like recanalizing therapy and/or neuroprotective drugs.

Since the spatial progression of acute ischemic stroke is rather a common finding than exceptional, the ischemic penumbra is a "sleeping beauty" that may eventually die (Lassen and Vorstrup 1984). Penumbral regions are recruited into the infarct core during the initital hours of stroke development: the total lesion size expands, however, the ischemic penumbra is shifted to more peripheral parts of the affected territory and gets restricted in size whereas the infarct core grows at its expense (Table 4.1). In the more complex human brain, the ischemic penumbra may be composed of regions that do show early changes in DWI and those, in which blood flow is altered, but water diffusion remains to be normal (the so-called diffusion-perfusion mismatch region) (Kidwell et al. 2003). By combining DWI with bolus-track perfusion imaging, it could be noted in animal and human stroke that the area with a perfusion deficit was larger than the lesion depicted by DWI. The early identification of such a diffusion-perfusion mismatch zone (perfusion reduced, diffusion normal) has been regarded of high thera-

peutic interest because it may serve as a marker to properly select patients for thrombolytic therapy (Liu et al. 2000, Hacke et al. 2005). However, the consideration of the whole area with reduced perfusion also includes areas with oligemia that do not trigger pathology and, thus, leads to overestimate the tissue at-risk. A refined model of diffusion-perfusion mismatch is presented in Fig. 4.12. The advent of quantitative MR perfusion imaging (see Chap. 6) will enable investigators to transfer well defined flow thresholds from animal experiments (e.g., the penumbral CBF range between 20%-40% of control) to the human situation and improve the prognostic modeling.

Several studies have indicated that the early measurement of the water ADC provides a valuable predictor of final tissue injury (reviewed in Hoehn-Berlage 1995). This notion has to be extended by adding information on the perfusion status of the tissue: in models of permanent vessel occlusion, DWI may indeed be an excellent surrogate marker for chronic tissue damage. However, if reperfusion is installed either by using a reversible occlusion model or by administration of recanalizing drugs such correlations become much weaker as recently demonstrated (van Dorsten et al. 2002).

4.2.2.4 Transient Occlusion: Reversibility of Changes

In experiments with transient vessel obstruction, the lesion growth, as visualized on DWI, can be reversed if the brain is reperfused within 1 h post occlusion (Minematsu et al. 1992). Regions like the putamen and, depending on the stroke model, temporal parts of the cortex show consistent infarction. With ongoing ischemia, predominantly cortical areas are recruited into the process of lesion growth. This pattern may be explained first by the threshold relationship between flow reduction and ADC change which may be reversed if the critical CBF value is exceeded upon reperfusion. The protective or beneficial effect disappears if the duration of ischemia exceeds 2–3 h. To achieve reperfusion after defined durations of ischemia, procedures of mechanical reopening of obstructed arteries (e.g., by replacing an intraluminal filament) can be applied, even inside a magnet for MR investigations (Kohno et al. 1995a). The strong interest in thrombolysis has triggered many investigations of transient focal brain ischemia in which reperfusion is initiated by drug-induced clot lysis in animal models of embolic stroke (Busch et al. 1997; Zhang et al. 1997). The advantage of such models is, that the pathophysiology of intravascular thrombosis and thrombolytic therapy are well imitated; potential disadvantages are the reduced prediction of lesioned territories and the prolonged process of recanalization with delayed or undetermined timepoints of actual reperfusion (Schüler et al. 2001).

Figure 4.13 shows a rat brain undergoing 90-min occlusion of the MCA. It exhibits an initial diffusion abnormality that resolves nearly completely after reperfusion. At shorter occlusion times, the ADC is known to normalize throughout the entire brain. Interestingly, several hours up to 3 days after reperfusion of a mild ischemic insult, the lesion may reappear and, eventually, evolve into brain

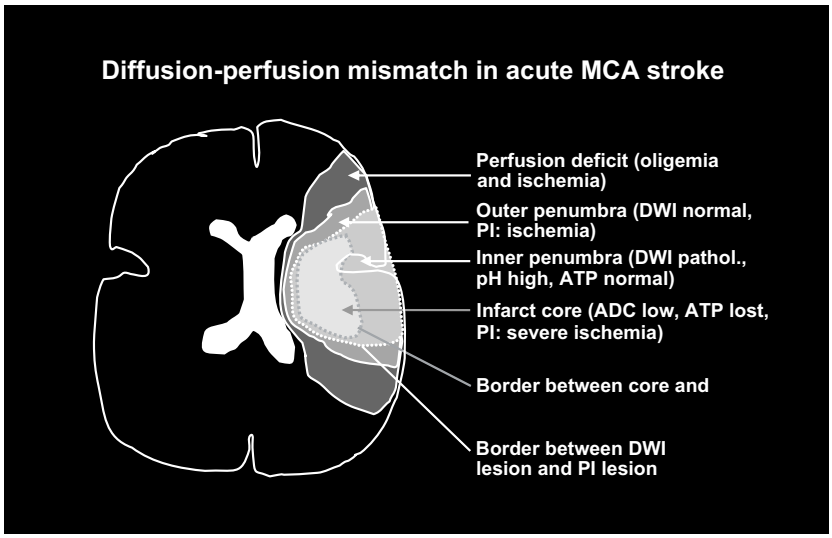

Fig. 4.12. Mismatch concept of diffusion lesion (smaller) and perfusion deficit (larger) in human territorial brain infarction. Acute MCA territory ischemia/oligemia with a smaller, centrally located diffusion disturbance showing the relationship between infarct core, ischemic penumbra and changes in DWI and PI. *DWI*, diffusion-weighted imaging; *PI*, perfusion imaging; *ADC*, apparent diffusion coefficient; *ATP*, high energy phosphates; *MCA*, middle cerebral artery

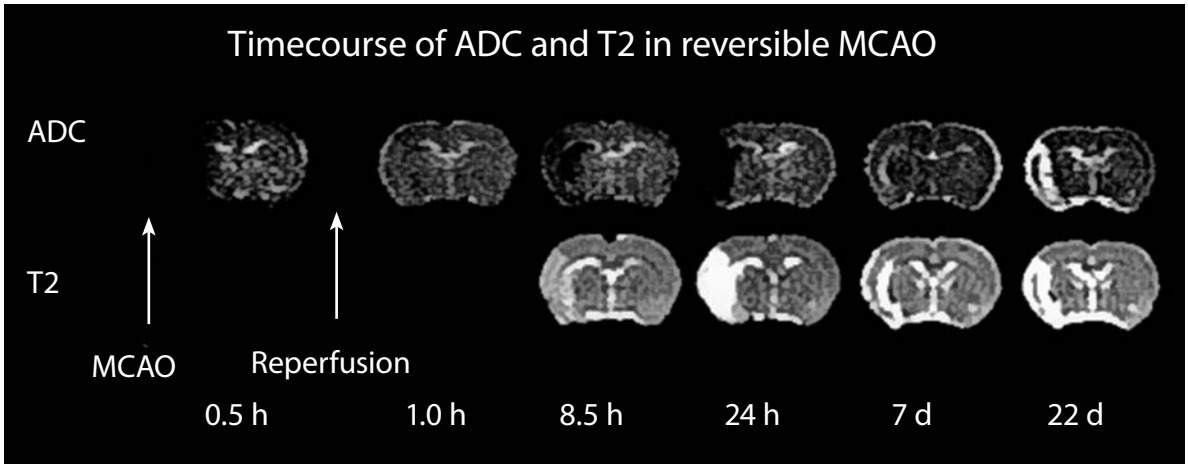

Fig. 4.13. Lesion evolution in reversible (90-min) middle cerebral artery occlusion (*MCAO*) in a rat. *Upper row*, quantitative images of the apparent diffusion coefficient (*ADC*); *lower row*, quantitative T2 images as measured serially over 22 days post stroke. Note the transient pseudo-normalization of the diffusion disturbance upon reperfusion and, second, after 7 days when initially reduced ADC values slowly shift to supernormal levels indicating the chronic infarct stage. [Reproduced with permission from Hoehn et al. (2001)]

infarction with reduced ADC and prolonged T2 signals completed at about 1 week post occlusion (Du et al. 1996; van Lookeren Campagne et al. 1999). Of note, the thrombolysis-induced reversal of DWI lesion volumes upon prompt recanalization has been also convincingly shown in acute human stroke (Kidwell et al. 2000) and confirmed in a larger patient cohort, recently (Parsons et al. 2002; see Chap. 2). The latter authors also observed that in a proportion of treated patients secondary DWI or ADC abnormalities would develop following early reversal. In those patients, hyperintensity in T2 images indicate the presence of ischemic infarcts. Kidwell and coworkers (2000), therefore, claim: "It is important for clinicians to be aware that some tissue that appears initially to be salvaged on early MRI scan when ADC normalizes, may nonetheless proceed to late tissue infarction."

Whereas the initial recovery of ADC or DWI lesions really reflects a normalization of tissue energy metabolism (Olah et al. 2000), several studies suggest that the tissue under focus remains to be abnormal even in the presence of re-established perfusion. Theoretically, potential mechanisms of this late secondary ADC decline include reperfusion injury, possibly related to inflammatory responses, oxygen free radical production, ongoing excitotoxic processes emanating from the infarct core, and apoptosis (Hallenbeck and Dutka 1990; Peters et al. 1998).

The application of metabolic imaging assays of cerebral protein synthesis (CPS) shows that, despite the normalization of energy metabolites, most of the territory affected by transient ischemia displays persisting suppression of CPS (Hata et al. 2000). With the exception of a small peripheral rim in the infarct border where CPS recovered between 6 h and 3 days, the sustained CPS suppression leads to secondary energy failure possibly mediated by mitochondrial dysfunction (Hata et al. 2000). In those secondary infarcts, the presence of prominent TUNEL staining and DNA fragmentation points to apoptosis as a major mechanism of cell death that could be diminished by inhibitors of protein synthesis (Du et al. 1996; Snider et al. 2001). Other authors have argued that the appearance of TUNEL-positive cells in this condition is associated with secondary energy failure due to DNA repair processes (Endres et al. 1997; Hata et al. 2000). Furthermore, in neonatal models of transient hypoxia/ischemia, the distinct and sustained increase of inorganic phosphate (P_i) over phosphocreatine (PCr) levels was documented by labeled phosphorous magnetic resonance spectroscopy (^{31}P-MRS) which, in turn, was associated with reduced water ADC (Thornton et al. 1998). The close link between local energy status and ADC abnormalities could be confirmed both for the intra-ischemic and post-ischemic phase of transient ischemia: if local ADC fell below 77% of normal values ATP was depleted (Olah et al. 2001).

Very brief episodes of ischemia (e.g., 15 min) trigger delayed hyperintensity on T1-weighted MRI visible 1–4 weeks after the ictus in the striatum of humans and rats. It could be shown that these MRI

changes correspond to striatal neurodegeneration with chronic inflammation and signs of oxidative stress associated with late-onset cognitive impairment (Fujioka et al. 2003). In the future, more detailed MRI studies exploring very mild ischemic insults will show which abnormalities can be depicted in more chronic stages. Such studies will elucidate more deeply the clinical condition of transient ischemic attacks (TIA) that, for a long time, have been regarded as fully reversible neurological deficits without long-term sequelae. Clinical MRI studies have found that up to 50% of TIA patients indeed show imaging abnormalities (Kidwell et al. 1999) the pathophysiological importance of which wait to be clarified in the future.

4.3 Treatment of Focal Cerebral Ischemia

The ischemic penumbra has been defined as the target of therapy in stroke. In principle, there are two strategies to address this issue. First, one can attempt to increase substrate availability above the threshold of irreversible tissue injury by recanalizing therapies. As we have seen, even slight increases in CBF may confer benefit to tissue in a state at-risk. Thrombolytic therapy is the prototype of this sort of intervention which has been successfully applied to stroke patients (NINDS Study Group 1995, Hacke et al. 2005). Second, there may be pharmacological strategies to decrease the vulnerability or increase the robustness of brain parenchyma, especially neurons, against ischemic injury without improving blood flow. The latter is termed neuroprotective therapy and has attracted strong interest after the discovery of glutamate antagonists that block excitotoxic actions in models of stroke (Choi 1992). It has to be mentioned, however, that tissue at-risk may not survive on longer terms unless perfusion is restored. Also, without reperfusion neuroprotective drugs have little chance to reach their target tissue in sufficient concentrations. This notion represents two reasons among others why so many clinical trials of neuroprotection in human stroke have failed (Grotta 1995).

4.3.1 Recanalizing Strategies and Risk of Hemorrhage

Animal models of embolic stroke enable us to study effects of fibrinolytic drugs like recombinant tissue plasminogen activator (tPA) (Brinker et al. 1999). Thrombolysis with tPA should be administered as long as the target brain tissue is viable and reperfusion can be expected to reduce or prevent tissue damage. With ongoing ischemia times and increasing disturbance of the blood–brain barrier, tPA treatment may loose its benefit and harm by the induction of parenchymal hemorrhage. In the section on transient occlusion models, we have already learnt about the complex primary and secondary imaging abnormalities that accompany reperfusion. Obviously, the failure of a fibrinolytic drug to recanalize the obstructed artery does *not* reverse ischemic injury, but other factors, such as breakdown of the blood–brain barrier, microembolism and reperfusion injury, may play an additional role. It is desirable to look for predictors of therapeutic outcome with regard to both, tissue recovery and hemorrhagic complications to early identify salvageable brain tissue.

Repeated MR measurements of diffusion and perfusion (perfusion imaging, PI) in embolic models of stroke have not shown differences in lesion development compared to other types of permanent MCA occlusion as long as thrombolysis was not applied (de Crespigny et al. 1993). In PI, the territorial perfusion deficit is observed followed by DWI abnormalities and, later, changes in T2 that expand over time (Brinker et al. 1999). Phosphorous (^{31}P) as well as proton MR spectroscopy are able to monitor the generation of lactate and high-energy phosphates due to anaerobic glycolysis that are coupled to a rapid consumption of glucose. When glucose availability drops, ATP production becomes compromised and causes the depletion of the PCr pool. The concentration of inorganic phosphate increases, eventually leading to a complete loss of ATP.

Several studies have evaluated the effect of tPA treatment administered at variable timepoints after clot embolization (Brinker et al. 1999; Busch et al. 1998; Franke et al. 2000; Jiang et al. 2000). Early lesion expansion as visible on DWI could only be reversed or slowed down if thrombolysis-induced reperfusion was initiated early after the onset of ischemia (Fig. 4.14). For example, if tPA was given at 1.5 h post occlusion the DWI lesion did not further enlarge whereas thrombolysis at later timepoints did not attenuate lesion growth (Brinker et al. 1999). Correlation analysis with other MR parameters revealed that areas with increased lactate or T2 values did not improve when tPA was started ≥ 3 h after the insult (Franke et al. 2000). By using histological means, other investigators however

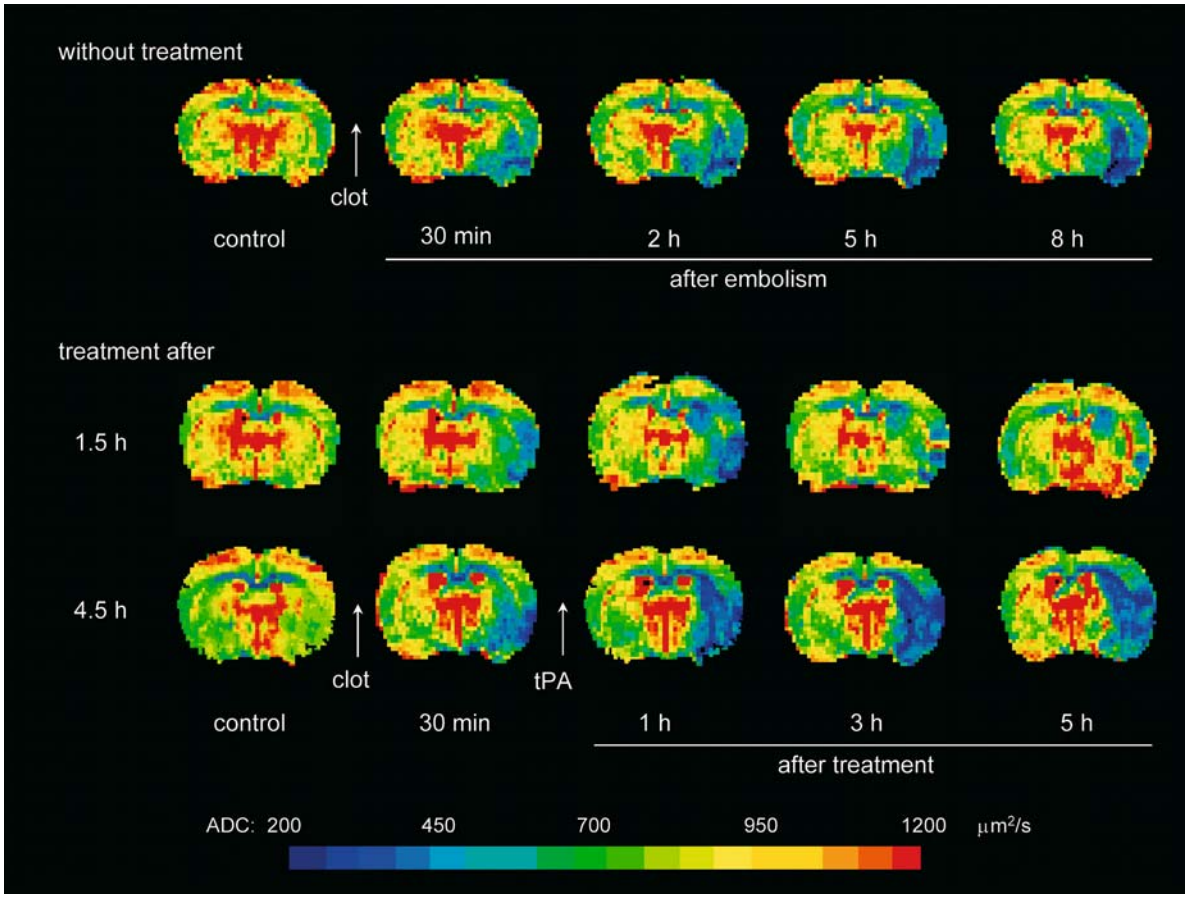

Fig. 4.14. Maps of the apparent diffusion coefficient (ADC) measured before and after embolic occlusion of the right middle cerebral artery in an animal without therapy (*upper row*) and in two animals with thrombolytic treatment initiated 1.5 h (*middle row*) and 4.5 h (*lower row*) after onset of ischemia. In the untreated animal, a decline of ADC was observed immediately after MCA occlusion that increased in size over time. Thrombolysis with recombinant tissue-type plasminogen activator (tPA) lead to the partial reversal of the ADC lesion over the first 5 h of therapy if started early. Late-onset thrombolysis at 4.5 h post occlusion did not reverse lesion growth, but was followed by a further lesion enlargement of the ischemic lesion. [Reproduced with permission from Hoehn et al. (2001)]

showed that tPA does reduce ischemic damage also at later timepoints as long as complete recanalization is achieved. In this study, the volume of complete infarction was significantly smaller in animals with successful reperfusion having a higher proportion of scattered neuronal injury of total lesion size (Back et al. 2002).

In contrast to the instantaneous and complete reperfusion as seen after removal of an occluding thread or filament, thrombolysis induces clot lysis in a delayed and often incomplete manner, both in humans and animals (Busch et al. 1998; Furlan et al. 1999; von Kummer et al. 1995; Schüler et al. 2001). This effect could be well monitored by PI showing that thrombolysis improves blood flow, but leads to incomplete reperfusion in a sense that pre-ischemic CBF values are rarely restored (Busch et al. 1998; Franke et al. 2000). Potential explanations for this observation include: (i) the possibility of clot fragmentation and down-stream embolism with more peripheral obstruction of the capillary bed, and (ii) too slow recanalization that prompts cell swelling but does not sufficiently supply glucose and oxygen to the ischemic tissue, thereby leading to a vicious circle of cell swelling, compression of the microcirculation and impaired blood flow. Indeed, MR angiography has been successfully applied to a thromboembolic stroke model of rats to characterize intracranial vessel occlusion patterns as well as the time lag between tPA treatment and vessel reopening. Combined occlusions of the circle of Willis and the MCA had recanalization times of 70–80 min post tPA treatment whereas selective MCA occlusion was recanalized after about 20 min. The type of occlu-

sion predicted outcome as evidenced by ADC and T2 relaxation time maps (Hilger et al. 2002). The efficacy of tPA treatment in an experimental setting seems to depend also greatly on composition and generation of the occluding clot: thrombin-induced blood clots injected into the internal carotid artery, induced a delayed type of cerebral reperfusion upon tPA therapy compared to spontaneously forming clots (Niessen et al. 2003). Incomplete reperfusion patterns lead to sustained reduction of ADC, increases in T2 and blood–brain barrier permeability, thereby triggering edema formation.

The combination of tPA therapy with other drugs may enhance the effect of thrombolysis. It could be shown that the addition of hirulog, a novel antithrombin, to tPA therapy improved and accelerated reperfusion, but did not result in a better outcome (Yenari et al. 1997). Antiadhesion molecule antibodies can be also combined with tPA. The anti-CD18 antibody in combination with tPA significantly reduced lesion volume (Chopp et al. 1999). To date, the combination of thrombolytics with antagonists of the glycoprotein IIb/IIIa receptor are expected to be of substantial benefit. In myocardial infarction, rate and degree of recanalization could be clearly improved although the dose of the fibrinolytic drug was half of the usual (Antman et al. 1999). This improvement was achieved without increasing the risk of major bleeding. Similarly, the first observations of combined thrombolysis with tPA and anti-GP IIb/IIIa drugs in brain ischemia have proven to be very promising in man and animal models of stroke (Shuaib et al. 2002; Straub et al. 2004). More detailed studies employing MR imaging and spectroscopy will be able to explore the potentials of this new therapeutic approach. Another novel development is the iv administration of high-dose albumin that has been shown to dramatically reduce ischemic edema along with a marked reduction of ischemic damage and better functional outcome (Belayev et al. 1998). Treated animals showed only very mild changes in ADC compared to saline treatment. Albumin also lead to higher ADC values within unlesioned brain regions – an effect as yet unexplained.

Alternatively, a better preselection of patients who may benefit from thrombolytic therapy or who may suffer from hemorrhagic complications, is an appealing approach. The idea is to characterize ischemic tissue subareas by information from DWI, PI, MRS, T1- or T2-weighted images in order to estimate the volume of tissue at-risk that may profit from recanalization. We have already reviewed the mismatch concept of diffusion lesion and perfusion deficit. Using a spectroscopic imaging sequence, Franke et al. (2000) could demonstrate that the probability of metabolic tissue recovery, defined as the reversal of an increased lactate concentration in the ischemic region, clearly declines with increasing tissue lactate content before thrombolysis (Fig. 4.15). This probability was shown to be independent of treatment delay. Metabolic recovery could be predicted knowing metabolic disturbances alone. In another study the relative ADC, T2, and perfusion values before thrombolysis were tested for their ability to predict outcome (Pillekamp et al. 2001). The probability of tissue damage 5 h after tPA treatment increased with the severity (i.e., degree of reduction) of ADC changes prior to thrombolysis. Pretreatment PI or T2 relaxometry also correlated with outcome, but – alone or in combination with pretreatment ADC maps – did not improve injury prediction over that obtained by ADC alone (Pillekamp et al. 2001). In a recent MR study in human stroke patients, the prolongation of the mean transit time (MTT) in PI indicating impaired CBF, differed significantly between the regions that became infarcted or salvaged tissue on day 90 (Butcher et al. 2003). Relative CBF was 10% lower in infarcted tissue than in salvaged regions. The authors also showed that – when reperfusion occurred – tissue with more severely prolonged MTT (i.e., lower CBF) was rescued from infarction relative to patients with persistent hypoperfusion. In addition, the magnitude of early reversal of the perfusion deficit proved to be the best predictor of favorable clinical outcome in another study (Chalela et al. 2004). MRI was performed prior to and soon after tPA therapy in acute stroke patients; the decrease of the hypoperfusion volume on MTT maps by > 30%, but not of DWI lesions, was a strong independent predictor of good clinical outcome evidenced by a 3-month Rankin score < 2 (Chalela et al. 2004).

The predictability of hemorrhagic complications remains a controversial issue. Knight et al. (1998) described that the post-reperfusion parenchymal enhancement of contrast agent on T1-weighted MRI predicted petechial hemorrhage after 24 h. By contrast, Neumann-Haefelin et al. (2001) could not predict the occurrence of hemorrhagic transformation between day 2 and 7 on the basis of early blood–brain barrier disruption or ADC changes in a reversible suture occlusion model of stroke. However, in an embolic stroke model the hemorrhagic transformation of infarction was significantly more frequent in tPA-treated animals. In those animals, hemorrhagic

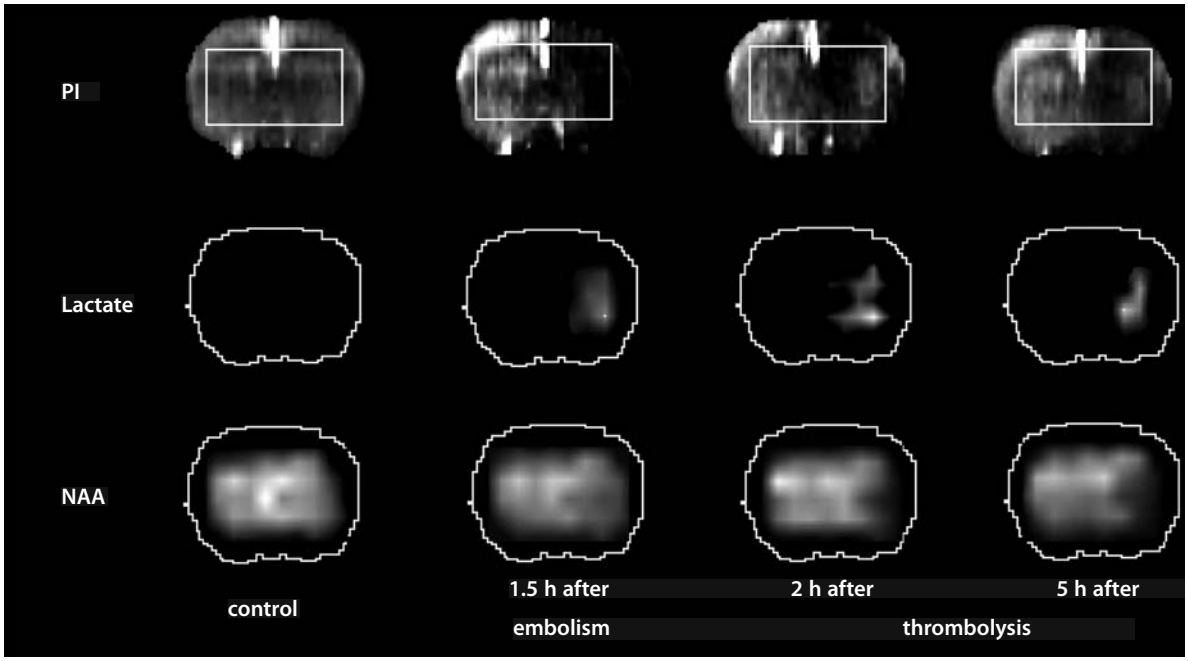

Fig. 4.15. Perfusion images (PI) and spectroscopic imaging maps of lactate and N-acetyl-aspartate (NAA) before and after embolic occlusion of the middle cerebral artery. Thrombolysis was applied 1.5 h after embolism and lead to a partial reperfusion of the affected territory (*upper row*). There was a clear increase in lactate that was partially reversed upon thrombolytic reperfusion. NAA maps showed a decreased signal in the ischemic hemisphere that did not recover. [Reproduced with permission from Franke et al. (2000)]

transformation occurred in the ischemic core region and could be predicted by a disturbance of the blood–brain barrier before treatment by Gadolinium-DTPA contrast enhancement, but not by ADC, T2, or perfusion imaging (Neumann-Haefelin et al. 2002). The region of bleeding co-localized with prior contrast enhancement in those animals.

It has to be mentioned, that in the clinical context the occurrence of hemorrhagic transformation is a part of the natural history of territorial infarcts occurring in 40%–60% of cases (Jorgensen and Torvik 1969) and behaving differently from parenchymal hematomas that are associated with worse outcome especially in the setting of thrombolytic therapy (Fiorelli et al. 1999). Molina et al. (2002) showed prospectively in a series of tPA-treated patients, that the occurrence of hemorrhagic transformation as visible on CT scans on day 3 to 4, was a marker of successful recanalization and lead to reduced infarct size and improved clinical outcome. Nonetheless, one would wish that the benefit of thrombolytic therapy could be conferred without producing mild hemorrhagic signs. It is also controversial whether or not the detection of old microbleeds by T2* imaging prior to thrombolytic treatment is of significance for outcome (Derex et al. 2004; Kidwell et al. 2002).

4.3.2 Neuroprotective Strategies

Interventions by drug application can be properly monitored by MRI, especially DWI. This is of particular interest because any therapeutical strategy will be most effective if applied during the early ischemic period, i.e., the initial 6 h after vessel occlusion when changes of lesion size and lesion composition are most rapid as already shown above. Table 4.2 lists the most important studies in this field showing that – depending on the animal model and the time of reperfusion – a drug-related reversal of the diffusion lesion is rather the exception than the rule (Busch et al. 2002; Ebisu et al. 2001; Gill et al. 1996; Hoehn-Berlage et al. 1997; Kucharczyk et al. 1991; Lo et al. 1994; Minematsu et al. 1993b; Muller et al. 1995; Seega and Elger 1993). Histologically confirmed positive treatment effects are in most cases reflected by a slowing of the lesion enlargement during the first hours of ischemia and/or reperfusion. Even in the case of early DWI lesion regression one has to consider the possibility of late lesion reappearance as shown earlier in this chapter.

Table 4.2. Selected studies that employ MRI to monitor drug effects in models of stroke

Authors	Year	Neuroprotective drug	Species	Animal model	Result
Kucharczyk et al.	1991	sodium-calcium channel blocker (RS-87476)	cat	perm MCAO	smaller DWI lesion, MRS: lactate reduced
Seega et al.	1993	serotonin antagonist (levemopamil)	rat	perm MCAO	reduced edema formation (T2)
Minematsu et al.	1993	non-comp NMDA antagonist (MK-801)	rat	3-h MCAO + reperfusion	better DWI lesion regression post reperfusion
Lo et al.	1994	non-comp NMDA antagonist (MK-801)	rat	perm MCAO + reperfusion	DWI lesion regression
Müller et al.	1995	free radical scavenger (U74389G)	rat	2-h MCAO + reperfusion	better DWI lesion regression post reperfusion
Gill et al.	1996	MK-801	rat	perm MCAO	slower lesion progression
Hoehn-Berlage et al.	1997	cation channel blocker (LOE 908 MS)	rat	perm MCAO	slower lesion progression
Ebisu et al.	2001	immunosuppressant FK 506	rat	perm MCAO	slower lesion progression
Busch et al.	2002	tPA	rat	embol MCAO	slower lesion progression

Perm, permanent; *embol*, embolic; *MCAO*, middle cerebral artery occlusion; *MRS*, magnetic resonance spectroscopy; *non-comp*, non-competitive

Several authors have investigated the cerebroprotective effects of NMDA receptor antagonists by using DWI. Minematsu et al. (1993a,b) studied CNS-1102 in two different models: permanent MCA occlusion and 3-h occlusion followed by 21 h of reperfusion. The drug was given 15 min after vascular occlusion and infusion was continued for 3 h to obtain constant plasma levels. The comparison of lesion size on DWI at 3 h post occlusion with histological analysis after 24 h showed a good spatial correspondence in the reversible ischemia model, both with and without treatment. In the permanent occlusion model, DWI hyperintensity at 3 h post occlusion slightly underestimated the lesion size as assessed on histological sections – due to a certain growth of lesions between the two timepoints. Reductions of infarct size by 66% in the permanent ischemia model and by 40% in the reversible model were observed. Similar observations were made with MK-801, a non-competitive NMDA receptor blocker (Gill et al. 1996; Lo et al. 1994). Gill et al. (1996) observed a progressive increase in the volume of hyperintensity over the total observation time for both, treated and placebo groups. However, the lesion size in MK-801 treated animals was consistently smaller on DWI with less marked signal changes. Hoehn-Berlage et al. (1997) made similar measurements when a cation channel blocker was applied (Fig. 4.16).

The development of the excitotoxicity hypothesis of ischemic damage along with the advent of potent glutamate antagonists provided the theoretical basis of what has been named neuroprotection. The failure of more than 40 clinical trials that have applied neuroprotectants to stroke patients, to show a clear clinical benefit has, however, raised concerns about this concept (Grotta 1995; Weir et al. 2004). Apart from considerations of correct drug dosage, limited therapeutic time window, and the heterogeneity of stroke syndromes, it is questionable whether the drugs can arrive at their target unless reperfusion is installed to some degree. Therefore, strategies to combine thrombolysis and neuroprotective agents have been developed and recently reviewed (Chen et al. 2002). In own experiments, the combination of tPA with the NMDA receptor antagonist memantine was unable to reduce tissue damage in embolic stroke (Back et al. 2004). Future studies that target molecular responses like the action of serine proteases on protease-activated receptor 1 (PAR-1) (Junge et al. 2003) or the activation of newly discovered acid-sensing ion channels that are calcium permeable (Chu et al. 2002), may reveal intriguing insights. The successful translation of experimentally proven strategies into the clinical field may require a better design of trials (Weir et al. 2004) that may – as one potent measure – implement MRI prior to treatment in order to better define and select stroke patients (Warach 2001).

4.4 Delayed Effects After Cerebral Ischemia

In the previous sections we have, by part, already reviewed delayed effects after cerebral ischemia, such as the risk of hemorrhagic complications that may occur as petechial bleedings or parenchymal hematoma. We have seen that the blood–brain barrier opens to various degrees with a substantial time

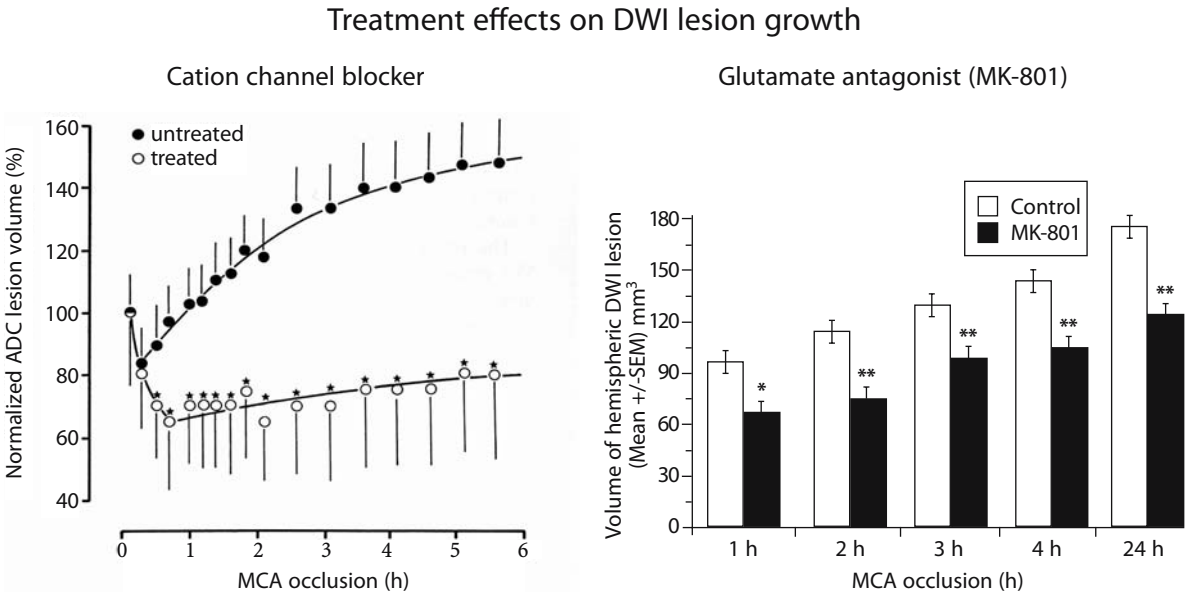

Fig. 4.16. Treatment effects by pharmacological intervention in models of permanent focal ischemia. Efficacy of cation channel blocker (*left*) or glutamate antagonist MK-801 (*right*) was monitored by using repetitive diffusion-weighted imaging (*DWI*). Lesions were defined by a change in the apparent diffusion coefficient (ADC, *left*) or by hyperintensity in DWI (*right*). Note that pharmacological intervention tends to slow down natural lesion enlargement rather than reversing ischemic lesions. [Reproduced with permission from Hoehn-Berlage et al. (1997), and Gill et al. (1996)]

lag from primary injury, also depending on the severity of the ischemic insult and the occurrence of reperfusion. Here, two aspects of delayed changes are to be addressed, namely the postischemic patterns of functional activation and the plasticity of the cortex as response to local injury. Of note, we stand at the very beginning of a better understanding of processes that reorganize injured brain.

4.4.1 Effects on Functional Activation

In Sect. 4.1.4 the detection of activated brain areas by BOLD or perfusion-weighted imaging was shown to depend on: (i) the ability of neurons to become activated and (ii) the neurovasculature to respond to neuronal activation by an (adequately matched) increase in local blood flow. During functional activation, a ≈ 6% increase in signal intensity is observed in BOLD images that is attributed to a decrease of the absolute concentration of dexoygenated hemoglobin (Hb_{deoxy}) per voxel (Grüne et al. 1999). Hb_{deoxy} is paramagnetic and thereby decreases signal intensity in T2*-weighted images. The signal increase is brought about by an excess increase in blood flow leading to excess concentration of oxygenated hemoglobin (Hb_{oxy}) overriding the oxygen demand of the activated tissue. As a consequence, a perfect match of local blood flow and oxygen extraction would result in an increase of absolute Hb_{deoxy} concentration per voxel (due to increased blood volume) and, thus, to a negative BOLD signal. Under physiological conditions this match is imperfect so that a positive BOLD response to functional activation is the normal finding. Apart from this, functionally activated brain regions can be monitored by application of PI (i.e., bolus tracking MRI) that reveals a 70% increase in local blood flow or blood volume that matches very well CBF measurements by other methods documenting flow changes in the range of 70%-90% above baseline during functional activation (Schmitz et al. 1997).

In a recent study, rats underwent permanent MCA occlusion and functional activation was studied by bilateral forepaw stimulation and MRI 24 h after the insult (Reese et al. 2000). The CBF response was monitored in both hemispheres by using a T2*-sensitive imaging sequence and intravascular bolus of contrast agent. In the non-ischemic hemisphere, a proper activation due to forepaw stimulation was recorded, but on the affected side no response could be elicited. This failure of activation was first attributed to ischemic damage of the somato-

sensory cortex. However, in animals that received neuroprotective treatment and in which the somatosensory cortex was spared from injury, still no response could be detected. The authors concluded that those cortical areas are functionally impaired although their afferent input remained to be unlesioned. More extended observations of functional recovery at 2 days and 2 weeks post occlusion were published by Dijkhuizen et al. (2001). At day 2 after stroke onset no functional activity was observed in the ischemic hemisphere. Interestingly, at this timepoint CO_2-reactivity was preserved (or had recovered) and baseline flow was not increased, indicating the absence of severe vasodilation that would prohibit a further stimulation-induced vascular response. After 2 weeks, bilateral signs of activation were present in the infarct borderzone, both in and adjacent to the sensorimotor cortex. Neurobehavioral tests revealed a nearly complete recovery of forelimb function. Obviously, the cortical forelimb representation field has recruited peri- and contralesional functional fields in order to regain near-to-normal function.

In the pathophysiological state of resuscitation after global ischemia, the pattern of recovery is different. During postischemic hyperemia, autoregulation and CO_2 reactivity are abolished and the former recovers earlier than the latter. The question arises whether the impaired functional coupling between metabolism and blood flow reflects disturbances of the functional integrity of the brain or just indicates impaired cerebrovascular reactivity. In studies by Schmitz et al. (1997, 1998), rats were exposed to 10-min cardiac arrest followed by reanimation and repeated MRI studies up to 7 days. ADC normalized within 45 min after resuscitation, but neurological scores and amplitudes of the sensory evoked potential (SEP) recovered at a much slower pace. While CO_2 reactivity had returned to normal at 5 h after reanimation, the stimulus-induced CBF increase due to electrical forepaw stimulation recovered to only 40% of normal within 1 week (measured by laser-Doppler flowmetry) (Schmitz et al. 1997). Laser-Doppler flow measurements were precisely confirmed by PI (Schmitz et al. 1998). After 3 h of reperfusion, functional activity began to reappear, but the recovery of the BOLD signal progressed faster than that of the perfusion-weighted signal: the stimulus-induced signal intensity increase in T2* images at day 1 after resuscitation was already comparable to normal. The differences in the recovery of ADC, BOLD, and perfusion imaging were interpreted to relate to differences between metabolic and functional recovery on one hand and between blood flow and oxygen extraction on the other. Thus, the much slower recovery of the CBF response to functional activation is not limited by an impaired cerebrovascular sensitivity. Since the BOLD signal is inversely proportional to the tissue oxygen extraction, it may be concluded that the decoupling between the T2*-weighted imaging behavior (rapidly restored) and PI responses to stimulation (sustainedly impaired) is due to reduced oxygen extraction upon activation.

4.4.2 Brain Plasticity and Stem Cell Implantation

Therapeutic strategies do not aim alone at preservation of lesioned tissue but also at functional restitution after completed stroke. There are two principle approaches to the latter: (i) mechanisms of brain plasticity and (ii) regeneration based on stem cell implantation.

The pattern and role of brain plasticity in stroke recovery has been incompletely characterized. Both ipsilesional and contralesional changes have been described in the previous section, but it remained unclear how these relate to functional recovery. In a recent investigation, brain activation patterns were correlated with tissue damage, hemodynamics, and neurologic status after temporary stroke, using functional MRI (Dijkhuizen et al. 2003). Functional activation and cerebrovascular reactivity maps were generated at days 1, 3 and 14 after 2-h MCA occlusion in rats. Significant activation responses in the contralesional hemisphere were detected at days 1 and 3. There was no correlation between activation parameters and perfusion status or cerebrovascular reactivity. The degree of shift of activation balance toward the contralesional hemisphere early after stroke increased with the extent of tissue injury. Functional recovery was associated mainly with preservation or restoration of activation in the ipsilesional hemisphere.

During neonatal development, the brain possesses the striking ability to transfer initially lost functions to new, unaffected cortical areas when irreversible lesions prohibit function of the original representation fields – an ability that is still to a lesser degree present in mature brain. This type of "plastic" response has been studied in rats with a well defined lesion of the somatosensory cortex that was induced 1 day after birth. Six months later functional MRI (fMRI) was performed with a forepaw stimulation paradigm when the animals showed no neurological

deficits. fMRI signal amplitude in activation areas was decreased on the ispilesional side with the occasional occurrence of contralesional activation in the secondary somatosensory cortex (Schwindt et al. 2004). Taking these and other results into account, neuromodulatory mechanisms enable the activation of previously inhibited but existing pathways that contribute to functional reorganization.

Stem cell implantation is a new intriguing way to promote regeneration. In vivo monitoring of stem cells after grafting is essential for a better understanding of their migrational dynamics and differentiation processes and of their regeneration potential. Using MRI at 78-μm spatial resolution and cell labeling by a lipofection procedure with a MR contrast agent, focal cerebral ischemia was studied (Hoehn et al. 2002). Over a 3-week period, cell migration was observed along the corpus callosum to the lesioned hemisphere, and cells massively populated the borderzone of the damaged brain tissue on the hemisphere opposite to the implantation sites (Fig. 4.17). Obviously, embryonic stem cells have high migrational dynamics, targeted to the cerebral lesion area. The translation of those results into clinical research needs to be shown in the future.

4.5 Outlook on Future Research

MRS is a promising tool to accompany imaging studies in cerebral ischemia. In vivo ^{31}P MRS provides information on energy metabolism (ATP, PCr) and can be used to estimate intracellular pH from the chemical shift difference between P_i (inorganic phosphate) and PCr. Due to its relatively low sensitivity (7% of that of ^{1}H) quite large voxels-of-interest have to be chosen which complicates studies in smaller animals. In vivo ^{1}H spectroscopy offers insight into other metabolic arenas: during ischemia/hypoxia a prominent peak due to lactate can be detected that is not visible under normal physiological conditions. N-acetyl-aspar-

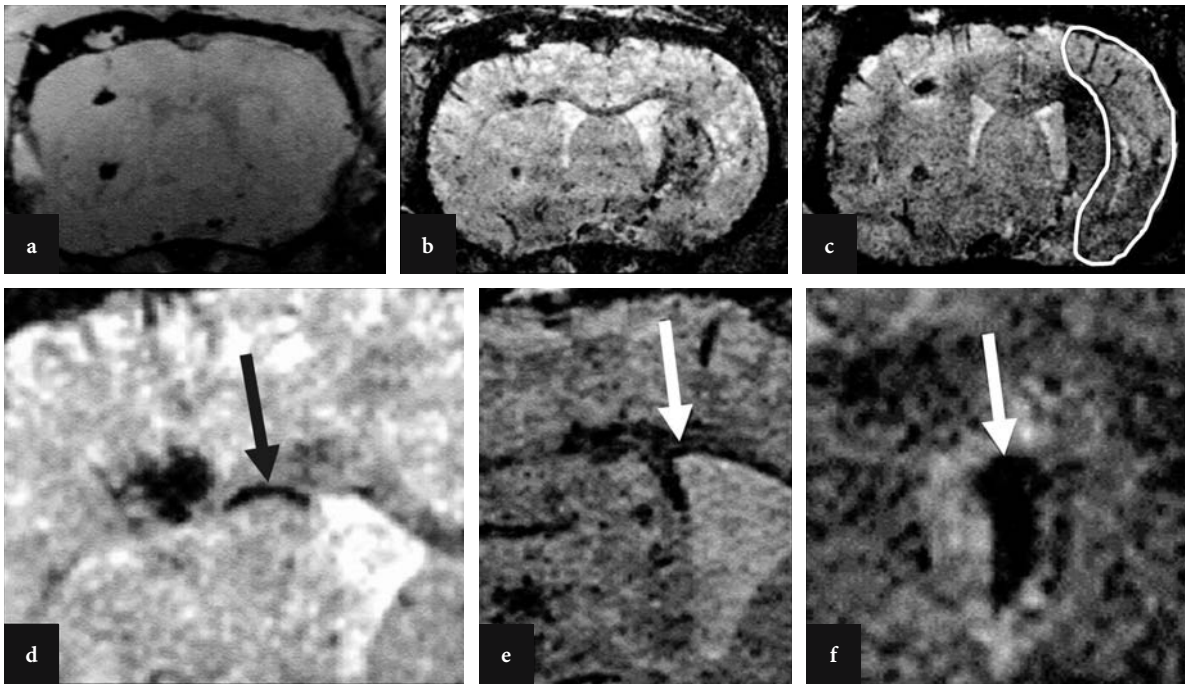

Fig. 4.17a–f. Coronal section through a rat brain at various times after implantation of embryonic stem cells contralateral to the induced focal ischemia. Data sets were recorded at the day of implantation (**a**) and at 6 (**b**) and 8 (**c**) days after implantation. The infarcted tissue area is outlined on (**c**). Note at 6 days (**b**) the discrete dark line (*arrow* in **d**, higher magnification) along the corpus callosum showing iron-oxide labeled cells migrating toward the lesioned hemisphere. At 8 days (**c**) a dark region becomes visible in the dorsal part of the lesioned territory reflecting first arrival of those cells. At higher magnification (**d**), the migration along the corpus callosum is better visible. The lining along the ventricular wall (**e**) and the accumulation of labeled stem cells on the choroid plexus (**f**) are presented in another example with high magnification. [With permission from Hoehn et al. (2002)]

tate (NAA) is a substrate almost exclusively localized in neurons, the function of which is widely unknown. Its characteristic peak in proton spectra decreases in ischemic states, probably due to neuronal loss. Other peaks derived from proton spectra are those for glucose, (phospho)creatine, choline-containing compounds, glutamate/glutamine, and myo-inositol. They provide information of other aspects of ischemia-dependent changes in metabolism. Choline derivatives are involved in membrane function and fluidity, glutamate/glutamine point to the activity of the tricarboxylic acid cycle, and myo-inositol plays a role in the ion homeostasis that is known to be disturbed in acute ischemia. Perhaps the most interesting application of MRS is the multi-voxel approach of proton spectra called spectroscopic imaging (SI) (Brown et al. 1982). SI provides metabolic maps of the brain with increasing spatial resolution and has been successfully applied to animal and human stroke (Fig. 4.15). The high regional heterogeneity of cerebral infarcts is reflected by differential metabolic responses from the ischemic core and borderzone areas (Franke et al. 2000). Such metabolic profiles have already been used to characterize subtypes of human stroke (Liu et al. 2003) (see Chap. 11).

Technical progress and higher spatial and temporal resolution of MRI and MRS is going to trigger MR studies in small animals, especially in mice, although high-resolution MR methods have predominantly been applied to rat and cat models of ischemia. Gene-manipulated mice (knock-out, knock-in) offer a powerful way to gain insight into complex molecular interactions and intracellular signaling. Zaharchuk et al. (1997) showed for the first time that MRI can be used in mouse MCA occlusion to detect changes in T1, T2 and DWI. They also demonstrated that mice deficient of neuronal nitric oxide synthase had a smaller periinfarct zone (defined by ADC threshold) and attributed this finding to less severe metabolic changes after ischemia. Van Dorsten et al. (1999) investigated different wild-type mouse strains using PI and DWI and found significantly smaller lesion volumes in SV129 mice compared to C57Black/6 mice probably due to the smaller MCA territory of the former strain. Hence, differences in vascular anatomy have to be considered in the future when parent strains are selected for genetic engineering.

Finally, we have little doubt that MR methods will play a dominant and innovative role in future research of brain ischemia covering alterations of perfusion, metabolism and molecular signaling.

References

Alexis NE, Back T, Zhao W, Dietrich WD, Watson BD, Ginsberg MD (1996) Neurobehavioral consequences of induced spreading depression following photothrombotic middle cerebral artery occlusion. Brain Res 706:273-282

Antman EM, Giugliano RP, Gibson CM, McCabe CH, Coussement P, Kleiman NS, Vahanian A, Adgey AAJ, Menown I, Rupprecht H-J, van der Wieken R, Ducas J, Scherer J, Anderson K, van de Werf F, Braunwald E (1999) Abciximab facilitates the rate and extent of thrombolysis-Results of the thrombolysis in myocardial infarction (TIMI) 14 trial. Circulation 99:2720-2732

Arbelaez A, Castillo M, Mukherji SK (1999) Diffusion-weighted MR imaging of global cerebral anoxia. Am J Neuroradiol 20:999-1007

Astrup J, Symon L, Branston NM, Lassen NA (1977) Cortical evoked potential and extracellular K+ and H+ at critical levels of brain ischemia. Stroke 8:51-57

Astrup J, Siesjö BK, Symon L (1981) Thresholds in cerebral ischemia - the ischemic penumbra. Stroke 12:723-725

Back T, Hoehn-Berlage M, Kohno K, Hossmann K-A (1994a) Diffusion NMR imaging in experimental stroke: Correlation with cerebral metabolites. Stroke 25:494-500

Back T, Kohno K, Hossmann K-A (1994b) Cortical negative DC deflections following middle cerebral artery occlusion and KCl-induced spreading depression: effect on blood flow, tissue oxygenation and electroencephalogram. J Cereb Blood Flow Metab 14:12-19

Back T, Zhao W, Ginsberg MD (1995) Three-dimensional image analysis of brain glucose metabolism/blood flow uncoupling and its electrophysiological correlates in the acute ischemic penumbra following middle cerebral artery occlusion. J Cereb Blood Flow Metab 15:566-577

Back T, Ginsberg MD, Dietrich WD, Watson BD (1996) Induction of spreading depression in the ischemic hemisphere following experimental middle cerebral artery occlusion: Effect on infarct morphology. J Cereb Blood Flow Metab 16:202-213

Back T, Nedergaard M, Ginsberg MD (1998) The ischemic penumbra: Pathophysiology, and relevance of spreading depression-like phenomena. In: Ginsberg MD, Bogousslavsky J (eds) Cerebrovascular disease: pathophysiology, diagnosis, and management. Blackwell Scientific Publications, Malden, MA, USA, pp 276-286

Back T, Hirsch JG, Szabo K, Gass A (2000a) Failure to demonstrate peri-infarct depolarizations by repetitive MR diffusion imaging in acute human stroke. Stroke 31:2901-2906

Back T, Hoehn M, Mies G, Busch E, Schmitz B, Kohno K, Hossmann KA (2000b) Penumbral tissue alkalosis in focal cerebral ischemia: relationship to energy metabolism, blood flow, and steady potential. Ann Neurol 47:485-492

Back T, Schüler OG, Otto D, Culmsee C, Plesnila N, Krieglstein J, Oertel WH, Baethmann A (2002) Early versus delayed thrombolysis in embolic stroke: effects on blood flow, DC potential and infarct morphology. In: Krieglstein J, Klumpp S (eds) Pharmacology of cerebral ischemia. MedPharm Scientific Publishers, Stuttgart, pp 159-169

Back T, Otto D, Kittner D, Hemmen T, Oertel WH (2004) Failure to enhance thrombolytic therapy by neuroprotection with memantine in embolic stroke. Cerebrovasc Dis 17:59

Baird AE, Benfield A, Schlaug G, Siewert B, Lövblad K-O, Edelman RR, Warach S (1997) Enlargement of human cerebral

ischemic lesion volumes measured by diffusion-weighted magnetic resonance imaging. Ann Neurol 41:581-589
Barber PA, Darby DG, Desmond PM, Yang Q, Gerraty RP, Jolley D, Donnan GA, Tress BM, Davis SM (1998) Prediciton of stroke outcome with echoplanar perfusion- and diffusion-weighted MRI. Neurology 51:418-426
Bartus RT, Dean RL, Cavanaugh K, Eveleth D, Carriero DL, Lynch G (1995) Time-related neuronal changes following middle cerebral artery occlusion: Implications for therapeutic intervention and the role of calpain. J Cereb Blood Flow Metab 15:969-979
Belayev L, Zhao W, Pattany PM, Weaver RG, Huh PW, Lin B, Busto R, Ginsberg MD (1998) Diffusion-weighted magnetic resonance imaging confirms marked neuroprotective efficacy of albumin therapy in focal cerebral ischemia. Stroke 29:2587-2599
Belliveau JW, Kennedy DN Jr, McKinstry RC, Buchbinder BR, Weisskoff RM, Cohen MS, Vevea JM, Brady TJ, Rosen BR (1991) Functional mapping of the human visual cortex by magnetic resonance imaging. Science 254:716-719
Berek K, Lechleitner P, Luef G, Felber S, Saltuari L, Schinnerl A, Traweger C, Dienstl F, Aichner F (1995) Early determination of neurological outcome after prehospital cardiopulmonary resuscitation. Stroke 26:543-549
Böttiger BW, Schmitz B, Wiessner C, Vogel P, Hossmann KA (1998) Neuronal stress response and neuronal cell damage after cardiocirculatory arrest in rats. J CerebBlood Flow Metab 18:1077-1087
Branston NM, Hope DT, Symon L (1979) Barbiturates in focal ischemia of primate cortex: effects on blood flow distribution, evoked potential and extracellular potassium. Stroke 10:647-653
Branston NM, Ladds A, Symon L, Wang AD (1984) Comparison of the effects of ischaemia on early components of the somatosensory evoked potential in brainstem, thalamus, and cerebral cortex. J Cereb Blood Flow Metab 4:68-81
Branston NM, Strong AJ, Symon L (1977) Extracellular potassium activity, evoked potential and tissue blood flow. Relationships during progressive ischaemia of baboon cerebral cortex. J Neurol Sci 32:305-321
Brinker G, Franke C, Hoehn M, Uhlenkuken U, Hossmann KA (1999) Thrombolysis of cerebral clot embolism in rat: effect of treatment delay. NeuroReport 10:3269-3272
Brown TR, Kincaid BM, Ugurbil K (1982) NMR chemical shift imaging in three dimensions. Proc Natl Acad Sci USA 79:3523-3526
Busch E, Gyngell M, Eis M, Hoehn-Berlage M, Hossmann K-A (1996) Potassium-induced cortical spreading depression during focal cerebral ischemia in rats: contribution to lesion growth assessed by diffusion-weighted NMR and biochemical imaging. J Cereb Blood Flow Metab 16:1090-1099
Busch E, Kruger K, Hossmann K-A (1997) Improved model of thromboembolic stroke and rt-PA induced reperfusion in the rat. Brain Res 778:16-24
Busch E, Kruger K, Allegrini PR, Kerskens CM, Gyngell ML, Hoehn-Berlage M, Hossmann KA (1998) Reperfusion after thrombolytic therapy of embolic stroke in the rat: magnetic resonance and biochemical imaging. J Cereb Blood Flow Metab 18:407-418
Busch E, Beaulieu C, de Crespigny A, Kreischer S, Diener HC, Moseley ME (2002) Combined X-ray angiography and diffusion-perfusion MRI for studying stroke evolution after rt-PA treatment in rats. Brain Res 953:112-118
Busza AL, Allen KL, King MD, van Bruggen N, Williams SR, Gadian DG (1992) Diffusion-weighted imaging studies of cerebral ischemia in gerbils: potential relevance to energy failure. Stroke 23:1602-1612
Butcher K, Parsons M, Baird T, Barber A, Donnan G, Desmond P, Tress B, Davis S (2003) Perfusion thresholds in acute stroke thrombolysis. Stroke 34:2159-2164
Chalela JA, Kang DW, Luby M, Ezzeddine M, Latour LL, Todd JW, Dunn B, Warach S (2004) Early magnetic resonance imaging findings in patients receiving tissue plasminogen activator predict outcome: insights into the pathophysiology of acute stroke in the thrombolysis era. Ann Neurol 55:105-112
Chen J, Jin K, Chen M, Pei W, Kawaguchi K, Greenberg DA, Simon RP (1997) Early detection of DNA strand breaks in the brain after transient focal ischemia: implications for the role of DNA damage in apoptosis and neuronal cell death. J Neurochem 69:232-245
Chen SD, Lee JM, Yang DI, Nassief A, Hsu CY (2002) Combination therapy for ischemic stroke: potential of neuroprotectants plus thrombolytics. Am J Cardiovasc Drugs 2:303-313
Choi DW (1992) Excitotoxic cell death. J Neurobiol 23:1261-1276
Chopp M, Zhang RL, Zhang ZG, Jiang Q (1999) The clot thickens-thrombolysis and combination therapies. Acta Neurochir Suppl (Wien) 73:67-71
Chu XP, Miesch J, Johnson M, Root L, Zhu XM, Chen D, Simon RP, Xiong ZG (2002) Proton-gated channels in PC12 cells. J Neurophysiol 87:2555-2561
De Crespigny AJ, Tsuura M, Moseley ME, Kucharczyk J (1993) Perfusion and diffusion MR imaging of thromboembolic stroke. J Magn Reson Imaging 3:746-754
Dereski MO, Chopp M, Knight RA, Rodolosi LC, Garcia JH (1993) The heterogeneous temporal evolution of focal ischemic neuronal damage in the rat. Acta Neuropathol (Berlin) 85:327-333
Derex L, Nighoghossian N, Hermier M, Adeleine P, Philippeau F, Honnorat J, Yilmaz H, Dardel P, Froment JC, Trouillas P (2004) Thrombolysis for ischemic stroke in patients with old microbleeds on pretreatment MRI. Cerebrovasc Dis 17:238-241
Dijkhuizen RM, de Graaf RA, Tulleken KA, Nicolay K (1999) Changes in the diffusion of water and intracellular metabolites after excitotoxic injury and global ischemia in neonatal rat brain. J Cereb Blood Flow Metab 19:341-349
Dijkhuizen RM, Ren J, Mandeville JB, Wu O, Ozdag FM, Moskowitz MA, Rosen BR, Finklestein SP (2001) Functional magnetic resonance imaging of reorganization in rat brain after stroke. Proc Natl Acad Sci USA 98:12766-12771
Dijkhuizen RM, Singhal AB, Mandeville JB, Wu O, Halpern EF, Finklestein SP, Rosen BR, Lo EH (2003) Correlation between brain reorganization, ischemic damage, and neurologic status after transient focal cerebral ischemia in rats: a functional magnetic resonance imaging study. J Neurosci 23:510-517
Dirnagl U, Pulsinelli W (1990) Autoregulation of cerebral blood flow in experimental focal brain ischemia. J Cereb Blood Flow Metab 10:327-336
Dirnagl U, Iadecola C, Moskowitz MA (1999) Pathobiology of ischaemic stroke: an integrated view. Trends Neurosci 22:391-397
Du C, Hu R, Csernansky CA, Hsu CY, Choi DW (1996) Very

delayed infarction after mild focal cerebral ischemia: a role for apoptosis? J Cereb Blood Flow Metab 16:195-201

Ebisu T, Katsuta K, Fujikawa A, Aoki I, Umeda M, Naruse S, Tanaka C (2001) Early and delayed neuroprotective effects of FK506 on experimental focal ischemia quantitatively assessed by diffusion-weighted MRI. Magn Reson Imaging 19:153-160

Endres M, Wang ZQ, Namura S, Waeber C, Moskowitz MA (1997) Ischemic brain injury is mediated by the activation of poly(ADP-ribose)polymerase. J Cereb Blood Flow Metab 17:1143-1151

Fiorelli M, Bastianello S, von Kummer R, del Zoppo GJ, Larrue V, Lesaffre E, Ringleb AP, Lorenzano S, Manelfe C, Bozzao L (1999) Hemorrhagic transformation within 36 hours of a cerebral infarct: relationships with early clinical deterioration and 3-month outcome in the European Cooperative Acute Stroke Study I (ECASS I) cohort. Stroke 30:2280-2284

Franke C, Brinker G, Pillekamp F, Hoehn M (2000) Probability of metabolic tissue recovery after thrombolytic treatment of experimental stroke: a magnetic resonance spectroscopic imaging study in rat brain. J Cereb Blood Flow Metab 20:583-591

Fujioka M, Taoka T, Matsuo Y, Mishima K, Ogoshi K, Kondo Y, Tsuda M, Fujiwara M, Asano T, Sakaki T, Miyasaki A, Park D, Siesjo BK (2003) Magnetic resonance imaging shows delayed ischemic striatal neurodegeneration. Ann Neurol 54:732-747

Furlan A, Higashida R, Wechsler L, Gent M, Rowley H, Kase C, Pessin M, Ahuja A, Callahan F, Clark WM, Silver F, Rivera F (1999) Intra-arterial prourokinase for acute ischemic stroke. The PROACT II study: a randomized controlled trial. Prolyse in acute cerebral thromboembolism. JAMA 282:2003-2011

Garcia JH, Kamijyo Y (1974) Cerebral infarction evolution of histopathological changes after occlusion of the middle cerebral artery in primates. Exp Neurol 33:408-421

Garcia JH, Yoshida Y, Chen H, Li Y, Zhang ZG, Lian J, Chen S, Chopp M (1993) Progression from ischemic injury to infarct following middle cerebral artery occlusion in the rat. Am J Pathol 142:623-635

Gill R, Andine P, Hillered L, Persson L, Hagberg H (1992) The effect of MK-801 on cortical spreading depression in the penumbral zone following focal ischemia in the rat. J Cereb Blood Flow Metab 12:371-379

Gill R, Sibson NR, Maskell L, Carpenter TA, Hall LD, Pickard JD (1996) The protective effect of MK-801 on infarct development over a period of 24 h as assessed by diffusion-weighted magnetic resonance imaging. NMR Biomed 9:241-248

Grotta J (1995) Why do all drugs work in animals but none in stroke patients? 2. Neuroprotective therapy. J Intern Med 237:89-94

Grubb NR, Fox KA, Smith K, Best J, Blane A, Ebmeier KP, Glabus MF, O'Carroll RE (2000) Memory impairment in out-of-hospital cardiac arrest survivors is associated with global reduction in brain volume, not focal hippocampal injury. Stroke 31:1509-1514

Grüne M, Pillekamp F, Schwindt W, Hoehn M (1999) Gradient echo time dependence and quantitative parameter maps for somatosensory activation in rats at 7 T. Magn Reson Med 42:118-126

Gyngell M, Busch E, Schmitz B, Kohno K, Back T, Hoehn-Berlage M, Hossmann K-A (1995) Evolution of acute focal cerebral ischaemia in rats observed by localised 1H-MRS, diffusion-weighted MRI, and electrophysiological monitoring. NMR Biomed 8:206-214

Hacke W, Albers G, Al-Rawi Y, Bogousslavsky J, Davalos A, Eliasziw M, Fischer M, Furlan A, Kaste M, Lees KR, Soehngen M, Warach S; DIAS Study Group (2005) The Desmoteplase in Acutic Ischemic Stroke Trial (DIAS): a phase II MRI-based 9-hour window acute stroke thrombolysis trial with intravenous desmoteplase. Stroke 36:66–73

Hakim AM, Hogan MJ, Carpenter S (1992) Time course of cerebral blood flow and histological outcome after focal cerebral ischemia in rats. Stroke 23:1138-1143

Hallenbeck JM, Dutka AJ (1990) Background review and current concepts of reperfusion injury. Arch Neurol 47:1245-1254

Hata R, Maeda K, Hermann D, Mies G, Hossmann KA (2000) Evolution of brain infarction after transient focal cerebral ischemia in mice. J Cereb Blood Flow Metab 20:937-946

Heiss W-D (1983) Flow thresholds to functional and morphological damage of brain tissue. Stroke 14:329-331

Heiss W-D, Rosner G (1983) Functional recovery of cortical neurons as related to degree and duration of ischemia. Ann Neurol 14:294-301

Heiss W-D, Huber M, Fink GR, Herholz K, Pietrzyk U, Wagner R, Wienhard K (1992) Progressive derangement of periinfarct viable tissue in ischemic stroke. J Cereb Blood Flow Metab 12:193-203

Heiss W-D, Graf R, Wienhard K, Lottgen J, Saito R, Fujita T, Rosner G, Wagner R (1994) Dynamic penumbra demonstrated by sequential multitracer PET after middle cerebral artery occlusion in cats. J Cereb Blood Flow Metab 14:892-902

Heiss W-D, Thiel A, Grond M, Graf R (1999) Contribution of immediate and delayed ischaemic damage to the volume of final infarcts. Lancet 353:1677-1678

Helpern JA, Dereski MO, Knight RA, Ordidge RJ, Chopp M, Qing ZX (1993) Histopathological correlations of nuclear magnetic resonance imaging parameters in experimental cerebral ischemia. Magn Reson Imaging 11:241-246

Hilger T, Niessen F, Diedenhofen M, Hossmann KA, Hoehn M (2002) Magnetic resonance angiography of thromboembolic stroke in rats: indicator of recanalization probability and tissue survival after recombinant tissue plasminogen activator treatment. J Cereb Blood Flow Metab 22:652-662

Hoehn M (2003) Functional magnetic resonance imaging. In: Van Bruggen N, Roberts T (eds) Biomedical imaging in experimental neuroscience. CRC Press, Boca Raton, FL, USA, pp 93-135

Hoehn M, Nicolay K, Franke C, van der Sanden B (2001) Application of magnetic resonance to animal models of cerebral ischemia. J Magn Reson Imaging 14:491-509

Hoehn M, Kustermann E, Blunk J, Wiedermann D, Trapp T, Wecker S, Focking M, Arnold H, Hescheler J, Fleischmann BK, Schwindt W, Buhrle C (2002) Monitoring of implanted stem cell migration in vivo: a highly resolved in vivo magnetic resonance imaging investigation of experimental stroke in rat. Proc Natl Acad Sci USA 99:16267-16272

Hoehn-Berlage M (1995) Diffusion-weighted NMR imaging: application to experimental focal cerebral ischemia. NMR Biomed 8:345-358

Hoehn-Berlage M, Eis M, Back T, Kohno K, Yamashita K (1995a) Changes of relaxation times T1, T2 and apparent diffusion coefficient ADC after permanent MCA occlusion in the rat:

Temporal evolution, regional extent, and comparison with histology. Magn Reson Med 34:824-834
Hoehn-Berlage M, Norris DG, Kohno K, Mies G, Leibfritz D, Hossmann KA (1995b) Evolution of regional changes in apparent diffusion coefficient during focal ischemia of rat brain: the relationship of quantitative diffusion NMR imaging to reduction in cerebral blood flow and metabolic disturbances. J Cereb Blood Flow Metab 15:1002-1011
Hoehn-Berlage M, Hossmann K-A, Busch E, Eis M, Schmitz B, Gyngell M (1997) Inhibition of nonselective cation channels reduces focal ischemic injury of rat brain. J Cereb Blood Flow Metab 17:534-542
Hossmann KA (1997) Reperfusion of the brain after global ischemia: hemodynamic disturbances. Shock 8:95-101
Hossmann K-A (1987) Pathophysiology of cerebral infarction. In: Vinken PJ, Bruyn GW, Klawans HL (eds) Handbook of clinical neurology. Elsevier, Amsterdam, pp 107-153
Hossmann K-A (1991) Animal models of cerebral ischemia. 1. Review of literature. Cerebrovasc Dis 1:2-15
Hossmann K-A (1994) Viability thresholds and the penumbra of focal ischemia. Ann Neurol 36:557-565
Hossmann KA, Hoehn-Berlage M (1995) Diffusion and perfusion MR imaging of cerebral ischemia. Cerebrovasc Brain Metab Rev 7:187-217
Hossmann KA, Schuier FJ (1980) Experimental brain infarcts in cats. I. Pathophysiological observations. Stroke 11:583-592
Hossmann KA, Zimmermann V (1974) Resuscitation of the monkey brain after 1 h complete ischemia. Brain Res 81:59-74
Hossmann KA, Schmidt-Kastner R, Ophoff BG (1987) Recovery of integrative central nervous function after one hour global cerebro-circulatory arrest in normothermic cat. J Neurol Sci 77:305-320
Hossmann KA, Fischer M, Bockhorst K, Hoehn-Berlage M (1994) NMR imaging of the apparent diffusion coefficient (ADC) for the evaluation of metabolic suppression and recovery after prolonged cerebral ischemia. J Cereb Blood Flow Metab 14:723-731
Hyder F, Behar KL, Martin MA, Blamire AM, Shulman RG (1994) Dynamic magnetic resonance imaging of the rat brain during forepaw stimulation. J Cereb Blood Flow Metab 14:649-655
Iijima T, Mies G, Hossmann K-A (1992) Repeaed negative DC deflections in rat cortex following middle cerebral artery occlusion are abolished by MK-801: effect on volume of ischemic injury. J Cereb Blood Flow Metab 12:727-733
Jacewicz M, Tanabe J, Pulsinelli WA (1992) The CBF threshold and dynamics for focal cerebral infarction in spontaneously hypertensive rats. J Cereb Blood Flow Metab 12:359-370
Jiang Q, Zhang ZG, Chopp M, Helpern JA, Ordidge RJ, Garcia JH, Marchese BA, Qing ZX, Knight RA (1993) Temporal evolution and spatial distribution of the diffusion constant of water in rat brain after transient middle cerebral artery occlusion. J Neurol Sci 120:123-130
Jiang Q, Zhang RL, Zhang ZG, Ewing JR, Jiang P, Divine GW, Knight RA, Chopp M (2000) Magnetic resonance imaging indexes of therapeutic efficacy of recombinant tissue plasminogen activator treatment of rat at 1 and 4 hours after embolic stroke. J Cereb Blood Flow Metab 20:21-27
Jones TH, Morawetz RB, Crowell RM, Marcoux FW, Fitzgibbon SJ, DeGirolami U, Ojemann RG (1981) Thresholds of focal cerebral ischemia in awake monkeys. J Neurosurg 54:773-782
Jorgensen L, Torvik A (1969) Ischaemic cerebrovascular diseases in an autopsy series. 2. Prevalence, location, pathogenesis, and clinical course of cerebral infarcts. J Neurol Sci 9:285-320
Junge CE, Sugawara T, Mannaioni G, Alagarsamy S, Conn PJ, Brat DJ, Chan PH, Traynelis SF (2003) The contribution of protease-activated receptor 1 to neuronal damage caused by transient focal cerebral ischemia. Proc Natl Acad Sci USA 100:13019-13024
Karonen JO, Vanninen RL, Liu Y, Ostergaard L, Kuikka JT, Nuutinen J, Vanninen EJ, Partanen PLK, Vainio PA, Korhonen K, Perki J, Roivainen R, Sivenius J, Aronen HJ (1999) Combined diffusion and perfusion MRI with correlation to single-photon emission CT in acute ischemic stroke. Ischemic penumbra predicts infarct growth. Stroke 30:1583-1590
Kidwell CS, Alger JR, Di Salle F, Starkman S, Villablanca P, Bentson J, Saver JL (1999) Diffusion MRI in patients with transient ischemic attacks. Stroke 30:1174-1180
Kidwell CS, Saver JL, Mattiello J, Starkman S, Vinuela F, Duckwiler G, Gobin YP, Jahan R, Vespa P, Kalafut M, Alger JR (2000) Thrombolytic reversal of acute human cerebral ischemic injury shown by diffusion/perfusion magnetic resonance imaging. Ann Neurol 47:462-469
Kidwell CS, Saver JL, Villablanca JP, Duckwiler G, Fredieu A, Gough K, Leary MC, Starkman S, Gobin YP, Jahan R, Vespa P, Liebeskind DS, Alger JR, Vinuela F (2002) Magnetic resonance imaging detection of microbleeds before thrombolysis: an emerging application. Stroke 33:95-98
Kidwell CS, Alger JR, Saver JL (2003) Beyond mismatch: evolving paradigms in imaging the ischemic penumbra with multimodal magnetic resonance imaging. Stroke 34:2729-2735
Kirino T, Sano K (1984) Selective vulnerability in the gerbil hippocampus following transient ischemia. Acta Neuropathol (Berl) 62:201-208
Knight RA, Ordidge RJ, Helpern JA, Chopp M, Rodolosi LC, Peck D (1991) Temporal evolution of ischemic damage in rat brain measured by proton nuclear magnetic resonance imaging. Stroke 22:802-808
Knight RA, Dereski MO, Helpern JA, Ordidge RJ, Chopp M (1994) Magnetic resonance imaging assessment of evolving focal cerebral ischemia. Comparison with histopathology in rats. Stroke 25:1252-1261; discussion 1261-1252
Knight RA, Barker PB, Fagan SC, Li Y, Jacobs MA, Welch KM (1998) Prediction of impending hemorrhagic transformation in ischemic stroke using magnetic resonance imaging in rats. Stroke 29:144-151
Kobatake K, Sako K, Izawa M, Yamamoto YL, Hakim AM (1984) Autoradiographic determination of brain pH following middle cerebral artery occlusion in the rat. Stroke 15:540-547
Kohno K, Back T, Hoehn-Berlage M, Hossmann K-A (1995a) A modified rat model of middle cerebral artery thread occlusion under electrophysiological control for magnetic resonance investigations. Magn Reson Imag 13:65-71
Kohno K, Hoehn-Berlage M, Mies G, Back T, Hossmann K-A (1995b) Relationship between diffusion-weighted magnetic resonance images, cerebral blood flow and energy state in experimental brain infarction. Magn Reson Imag 13:73-80

Kucharczyk J, Mintorovitch J, Moseley ME, Asgari HS, Sevick RJ, Derugin N, Norman D (1991) Ischemic brain damage: reduction by sodium-calcium ion channel modulator RS-87476. Radiology 179:221-227

Kuroiwa T, Nagaoka T, Ueki M, Yamada I, Miyasaka N, Akimoto H (1998) Different apparent diffusion coefficient: water content correlations of gray and white matter during early ischemia. Stroke 29:859-865

Lassen NA, Vorstrup S (1984) Ischemic penumbra results in incomplete infarction: is the sleeping beauty dead? Stroke 15:755

Le Bihan D, Breton E, Lallemand D, Grenier P, Cabanis E, Laval-Jeantet M (1986) MR imaging of intravoxel incoherent motions: application to diffusion and perfusion in neurologic disorders. Radiology 161:401-407

Leao AAP (1944) Spreading depression of activity in the cerebral cortex. J Neurophysiol 7:359-390

Lin W, Lee JM, Lee YZ, Vo KD, Pilgram T, Hsu CY (2003) Temporal relationship between apparent diffusion coefficient and absolute measurements of cerebral blood flow in acute stroke patients. Stroke 34:64-70

Liu Y, Karonen JO, Vanninen RL, Ostergaard L, Roivainen R, Nuutinen J, Perkio J, Kononen M, Hamalainen A, Vanninen EJ, Soimakallio S, Kuikka JT, Aronen HJ (2000) Cerebral hemodynamics in human acute ischemic stroke: a study with diffusion- and perfusion-weighted magnetic resonance imaging and SPECT. J Cereb Blood Flow Metab 20:910-920

Liu YJ, Chen CY, Chung HW, Huang IJ, Lee CS, Chin SC, Liou M (2003) Neuronal damage after ischemic injury in the middle cerebral arterial territory: deep watershed versus territorial infarction at MR perfusion and spectroscopic imaging. Radiology 229:366-374

Lo EH, Matsumoto K, Pierce AR, Garrido L, Luttinger D (1994) Pharmacologic reversal of acute changes in diffusion-weighted magnetic resonance imaging in focal cerebral ischemia. J Cereb Blood Flow Metab 14:597-603

Marrannes R, Willems R, DePrins E, Wauquier A (1988) Evidence for a role of the N-methyl-D-aspartate (NMDA) receptor in cortical spreading depression in the rat. Brain Res 457:226-240

Mies G, Iijima T, Hossmann K-A (1993) Correlation between periinfarct DC shifts and ischemic neuronal damage in rat. NeuroReport 4:709-711

Minematsu K, Li L, Sotak CH, Davis MA, Fisher M (1992) Reversible focal ischemic injury demonstrated by diffusion-weighted magnetic resonance imaging in rats. Stroke 23:1304-1311

Minematsu K, Fisher M, Li L, Davis MA, Knapp AG, Cotter RE, McBurney RN, Sotak CH (1993a) Effects of a novel NMDA antagonist on experimental stroke rapidly and quantitatively assessed by diffusion-weighted MRI. Neurology 43:397-403

Minematsu K, Fisher M, Li L, Sotak CH (1993b) Diffusion and perfusion magnetic resonance imaging studies to evaluate a noncompetitive N-methyl-D-aspartate antagonist and reperfusion in experimental stroke in rats. Stroke 24:2074-2081

Mintorovitch J, Moseley ME, Chileuitt L, Shimizu H, Cohen Y, Weinstein MD (1991) Comparison of diffusion- and T2-weighted MRI for early detection of cerebral ischemia and reperfusion in rats. Magn Reson Med 18:39-50

Molina CA, Alvarez-Sabin J, Montaner J, Abilleira S, Arenillas JF, Coscojuela P, Romero F, Codina A (2002) Thrombolysis-related hemorrhagic infarction: a marker of early reperfusion, reduced infarct size, and improved outcome in patients with proximal middle cerebral artery occlusion. Stroke 33:1551-1556

Morawetz RB, DeGirolami U, Ojemann RG, Marcoux FW, Crowell RM (1978) Cerebral blood flow determined by hydrogen clearance during middle cerebral artery occlusion in unanesthetized monkeys. Stroke 9:143-149

Moseley ME, Cohen Y, Mintorovitch J, Chileuitt L, Shimizu H, Kucharczyk JF, Wendland MF, Weinstein PR (1990) Early detection of regional cerebral ischemia in cats: comparison of diffusion- and T2-weighted MRI and spectroscopy. Magn Reson Med 14:330-346

Moseley ME, Butts K, Yenari MA, de Crespigny A (1995) Clinical aspects of DWI. NMR Biomed 8:387-396

Mukherjee P, Bahn MM, McKinstry RC, Shimony JS, Cull TS, Akbudak E, Snyder AZ, Conturo TE (2000) Differences between gray matter and white matter water diffusion in stroke: diffusion-tensor MR imaging in 12 patients. Radiology 215:211-220

Muller TB, Haraldseth O, Jones RA, Sebastiani G, Lindboe CF, Unsgard G, Oksendal AN (1995) Perfusion and diffusion-weighted MR imaging for in vivo evaluation of treatment with U74389G in a rat stroke model. Stroke 26:1453-1458

Nedergaard M, Astrup J (1986) Infarct rim: effect of hyperglycemia on direct current potential and [14C]2-deoxyglucose phosphorylation. J Cereb Blood Flow Metab 6:607-615

Nedergaard M, Gjedde A, Diemer NH (1986) Focal ischemia of the rat brain: autoradiographic determination of cerebral glucose utilization, glucose content, and blood flow. J Cereb Blood Flow Metab 6:414-424

Neumann-Haefelin T, Wittsack HJ, Wenserski F, Siebler M, Seitz R, Modder U, Freund H-J (1999) Diffusion- and perfusion-weighted MRI. The DWI/PI mismatch region in acute stroke. Stroke 30:1591-1597

Neumann-Haefelin T, Kastrup A, de Crespigny A, Ringer TM, Sun GH, Yenari MA, Moseley ME (2001) MRI of subacute hemorrhagic transformation in the rat suture occlusion model. Neuro Report 12:309-311

Neumann-Haefelin C, Brinker G, Uhlenkuken U, Pillekamp F, Hossmann KA, Hoehn M (2002) Prediction of hemorrhagic transformation after thrombolytic therapy of clot embolism: an MRI investigation in rat brain. Stroke 33:1392-1398

Nicotera P (2003) Molecular switches deciding the death of injured neurons. Toxicol Sci 74:4-9

Niessen F, Hilger T, Hoehn M, Hossmann KA (2003) Differences in clot preparation determine outcome of recombinant tissue plasminogen activator treatment in experimental thromboembolic stroke. Stroke 34:2019-2024

NINDS rt-PA Stroke Study Group (1995) Tissue plasminogen activator for acute ischemic stroke. N Engl J Med 333:1581-1587

Olah L, Wecker S, Hoehn M (2000) Secondary deterioration of apparent diffusion coefficient after 1-hour transient focal cerebral ischemia in rats. J Cereb Blood Flow Metab 20:1474-1482

Olah L, Wecker S, Hoehn M (2001) Relation of apparent diffusion coefficient changes and metabolic disturbances after 1 hour of focal cerebral ischemia and at different reperfusion phases in rats. J Cereb Blood Flow Metab 21:430-439

Opitz E, Schneider M (1950) Über die Sauerstoffversorgung des Gehirns und den Mechanismus der Mangelwirkungen. Ergeb Physiol 46:126-260

Ouyang YB, Tan Y, Comb M, Liu CL, Martone ME, Siesjo BK, Hu BR (1999) Survival- and death-promoting events after transient cerebral ischemia: phosphorylation of Akt, release of cytochrome C and activation of caspase-like proteases. J Cereb Blood Flow Metab 19:1126-1135

Parsons MW, Barber PA, Chalk J, Darby DG, Rose S, Desmond PM, Gerraty RP, Tress BM, Wright PM, Donnan GA, Davis SM (2002) Diffusion- and perfusion-weighted MRI response to thrombolysis in stroke. Ann Neurol 51:28-37

Paschen W, Hossmann K-A, van den Kerckhoff W (1983) Regional assessment of energy-producing metabolism following prolonged complete ischemia of cat brain. J Cereb Blood Flow Metab 3:321-329

Peters O, Back T, Lindauer U, Busch C, Megow D, Dreier J, Dirnagl U (1998) Increased formation of reactive oxygen species following permanent and reversible middle cerebral artery occlusion in the rat. J Cereb Blood Flow Metab 18:196-205

Pillekamp F, Grune M, Brinker G, Franke C, Uhlenkuken U, Hoehn M, Hossmann K (2001) Magnetic resonance prediction of outcome after thrombolytic treatment. Magn Reson Imaging 19:143-152

Reese T, Porszasz R, Baumann D, Bochelen D, Boumezbeur F, McAllister KH, Sauter A, Bjelke B, Rudin M (2000) Cytoprotection does not preserve brain functionality in rats during the acute post-stroke phase despite evidence of non-infarction provided by MRI. NMR Biomed 13:361-370

Roussel SA, van Bruggen N, King MD, Houseman J, Williams SR, Gadian DG (1994) Monitoring the initial expansion of focal ischaemic changes by diffusion-weighted MRI using a remote controlled method of occlusion. NMR Biomed 7:21-28

Russell RW, Simcock JP, Wilkinson IM, Frears CC (1970) The effect of blood pressure changes on the leptomeningeal circulation of the rabbit. Brain 93:491-504

Schaafsma A, de Jong BM, Bams JL, Haaxma-Reiche H, Pruim J, Zijlstra JG (2003) Cerebral perfusion and metabolism in resuscitated patients with severe post-hypoxic encephalopathy. J Neurol Sci 210:23-30

Schmidt-Kastner R, Paschen W, Ophoff BG, Hossmann KA (1989) A modified four-vessel occlusion model for inducing incomplete forebrain ischemia in rats. Stroke 20:938-946

Schmitz B, Bottiger BW, Hossmann KA (1997) Functional activation of cerebral blood flow after cardiac arrest in rat. J Cereb Blood Flow Metab 17:1202-1209

Schmitz B, Bock C, Hoehn-Berlage M, Kerskens CM, Bottiger BW, Hossmann KA (1998) Recovery of the rodent brain after cardiac arrest: a functional MRI study. Magn Reson Med 39:783-788

Schüler OG, Eriskat J, Baethmann AJ, Back T (2001a) Thrombolysis induces a reperfusion-dependent inhibition of perinfarct depolarizations in experimental thromboembolic stroke. J Cereb Blood Flow Metab 21:S396

Schüler OG, Plesnila N, Otto D, Baethmann AJ, Back T (2001b) Early thrombolysis inhibits periinfarct depolarizations in embolic MCA occlusion. NeuroReport 12:3943-3946

Schwindt W, Burke M, Pillekamp F, Luhmann HJ, Hoehn M (2004) Functional magnetic resonance imaging and somatosensory evoked potentials in rats with a neonatally induced freeze lesion of the somatosensory cortex. J Cereb Blood Flow Metab 24:1409-1418

Seega J, Elger B (1993) Diffusion- and T2-weighted imaging: evaluation of oedema reduction in focal cerebral ischaemia by the calcium and serotonin antagonist levemopamil. Magn Reson Imaging 11:401-409

Sevick RJ, Kucharczyk JF, Mintorovitch J, Moseley ME, Derugin N, Norman D (1990) Diffusion-weighted MR imaging in acute cerebral ischemia: Comparison and correlation with histopathology. Acta Neurochir [Suppl] 51:210-212

Shima T, Hossmann KA, Date H (1983) Pial arterial pressure in cats following middle cerebral artery occlusion. 1. Relationship to blood flow, regulation of blood flow and electrophysiological function. Stroke 14:713-719

Shuaib A, Yang Y, Nakada MT, Li Q, Yang T (2002) Glycoprotein IIb/IIIa antagonist, murine 7E3 F(ab') 2, and tissue plasminogen activator in focal ischemia: evaluation of efficacy and risk of hemorrhage with combination therapy. J Cereb Blood Flow Metab 22:215-222

Siesjö BK (1978) Brain energy metabolism. Wiley, New York

Siesjö BK (1988) Mechanisms of ischemic brain damage. Crit Care Med 16:954-963

Silva MD, Omae T, Helmer KG, Li F, Fisher M, Sotak CH (2002) Separating changes in the intra- and extracellular water apparent diffusion coefficient following focal cerebral ischemia in the rat brain. Magn Reson Med 48:826-837

Singhal AB, Topcuoglu MA, Koroshetz WJ (2002) Diffusion MRI in three types of anoxic encephalopathy. J Neurol Sci 196:37-40

Smith ML, Auer RN, Siesjö BK (1984) The density and distribution of ischemic brain injury in the rat following 2-10 min of forebrain ischemia. Acta Neuropathol (Berl) 64:319-332

Snider BJ, Du C, Wei L, Choi DW (2001) Cycloheximide reduces infarct volume when administered up to 6 h after mild focal ischemia in rats. Brain Res 917:147-157

Straub S, Junghans U, Jovanovic V, Wittsack HJ, Seitz RJ, Siebler M (2004) Systemic thrombolysis with recombinant tissue plasminogen activator and tirofiban in acute middle cerebral artery occlusion. Stroke 35:705-709

Strong AJ, Venables GS, Gibson G (1983) The cortical ischaemic penumbra associated with occlusion of the middle cerebral artery in the cat: 1. Topography of changes in blood flow, potassium ion activity, and EEG. J Cereb Blood Flow Metab 3:86-96

Strong AJ, Fabricius M, Boutelle MG, Hibbins SJ, Hopwood SE, Jones R, Parkin MC, Lauritzen M (2002) Spreading and synchronous depressions of cortical activity in acutely injured human brain. Stroke 33:2738-2743

Szafer A, Zhong J, Anderson AW, Gore JC (1995) Diffusion-weighted imaging in tissues: theoretical models. NMR Biomed 8:289-296

Takano K, Latour LL, Formato JE, Carano RAD, Helmer KG, Hasegawa Y, Sotak CH, Fisher M (1996) The role of spreading depression in focal ischemia evaluated by diffusion mapping. Ann Neurol 39:308-318

Tamura A, Graham DI, McCulloch J, Teasdale GM (1981) Focal cerebral ischemia in the rat: 2. Regional blood flow determined by [14C]iodoantipyrine autoradiography following middle cerebral artery occlusion. J Cereb Blood Flow Metab 1:61-69

Thornton JS, Ordidge RJ, Penrice J, Cady EB, Amess PN, Punwani S, Clemence M, Wyatt JS (1998) Temporal and anatomical variations of brain water apparent diffusion coefficient in perinatal cerebral hypoxic-ischemic injury: relationships to cerebral energy metabolism. Magn Reson Med 39:920-927

Tyson GW, Teasdale GM, Graham DI, McCulloch J (1984) Focal cerebral ischemia in the rat: Topography of hemodynamic and histopathological changes. Ann Neurol 15:559-567

Van der Toorn A, Sykova E, Dijkhuizen RM, Vorisek I, Vargova L, Skobisova E, van Lookeren Campagne M, Reese T, Nicolay K (1996) Dynamic changes in water ADC, energy metabolism, extracellular space volume, and tortuosity in neonatal rat brain during global ischemia. Magn Reson Med 36:52-60

Van Dorsten FA, Hata R, Maeda K, Franke C, Eis M, Hossmann KA, Hoehn M (1999) Diffusion- and perfusion-weighted MR imaging of transient focal cerebral ischaemia in mice. NMR Biomed 12:525-534

Van Dorsten FA, Olah L, Schwindt W, Grune M, Uhlenkuken U, Pillekamp F, Hossmann KA, Hoehn M (2002) Dynamic changes of ADC, perfusion, and NMR relaxation parameters in transient focal ischemia of rat brain. Magn Reson Med 47:97-104

Van Lookeren Campagne M, Thomas GR, Thibodeaux H, Palmer JT, Williams SP, Lowe DG, van Bruggen N (1999) Secondary reduction in the apparent diffusion coefficient of water, increase in cerebral blood volume, and delayed neuronal death after middle cerebral artery occlusion and early reperfusion in the rat. J Cereb Blood Flow Metab 19:1354-1364

Verheul HB, Balazs R, Berkelbach van der Sprenkel JW, Tulleken CA, Nicolay K, Tamminga KS, van Lookeren Campagne M (1994) Comparison of diffusion-weighted MRI with changes in cell volume in a rat model of brain injury. NMR Biomed 7:96-100

Von Kummer R, Holle R, Rosin L, Forsting M, Hacke W (1995) Does arterial recanalization improve outcome in carotid territory stroke? Stroke 26:581-487

Waltz AG (1970) Effect of Pa CO2 on blood flow and microvasculature of ischemic and nonischemic cerebral cortex. Stroke 1:27-37

Waltz AG, Sundt TM Jr (1968) Influence of systemic blood pressure on blood flow and microcirculation of ischemic cerebral cortex: a failure of autoregulation. Prog Brain Res 30:107-112

Warach S (2001) New imaging strategies for patient selection for thrombolytic and neuroprotective therapies. Neurology 57:S48-S52

Warach S, Chien D, Li W, Ronthal M, Edelman RR (1992) Fast magnetic resonance diffusion-weighted imaging of acute human stroke. Neurology 42:1717-1723

Warach S, Gaa J, Siewert B, Wielopowski P, Edelman RR (1995) Acute human stroke studied by whole brain echo planar diffusion-weighted magnetic resonance imaging. Ann Neurol 37:231-241

Weir CJ, Kaste M, Lees KR (2004) Targeting neuroprotection clinical trials to ischemic stroke patients with potential to benefit from therapy. Stroke 35:2111-2116

Welsh FA, Yuen G, Placantonakis DG, Vu TQ, Haiss F, O'Hearn E, Molliver ME, Aicher SA (2002) Why do Purkinje cells die so easily after global brain ischemia? Aldolase C, EAAT4, and the cerebellar contribution to posthypoxic myoclonus. Adv Neurol 89:331-359

Wijdicks EF, Campeau NG, Miller GM (2001) MR imaging in comatose survivors of cardiac resuscitation. Am J Neuroradiol 22:1561-1565

Yenari MA, de Crespigny A, Palmer JT, Roberts S, Schrier SL, Albers GW, Moseley ME, Steinberg GK (1997) Improved perfusion with rt-PA and hirulog in a rabbit model of embolic stroke. J Cereb Blood Flow Metab 17:401-411

Yoneda Y, Tokui K, Hanihara T, Kitagaki H, Tabuchi M, Mori E (1999) Diffusion-weighted magnetic resonance imaging: detection of ischemic injury 39 minutes after onset in a stroke patient. Ann Neurol 45:794-797

Zaharchuk G, Hara H, Huang PL, Fishman MC, Moskowitz MA, Jenkins BG, Rosen BR (1997) Neuronal nitric oxide synthase mutant mice show smaller infarcts and attenuated apparent diffusion coefficient changes in the peri-infarct zone during focal cerebral ischemia. Magn Reson Med 37:170-175

Zhang RL, Chopp M, Zhang ZG, Jiang Q, Ewing JR (1997) A rat model of focal embolic cerebral ischemia. Brain Res 766:83-92

Zivin JA (1997) Factors determining the therapeutic window for stroke. Neurology 50:599-603

Part 2:
MR Imaging of Stroke Pathology

5 Vascular Anatomy and Pathology

Dirk Petersen and Stefan Gottschalk

CONTENTS

5.1 Technical Considerations

The term MR angiography (MRA) does not denote a single imaging technique or MR-pulse sequence but it stands for a variety of different methods of vessel imaging, which are more or less comparable with classical angiographic examinations. As a robust method for the depiction of intracranial arterial stenoses the time-of-flight MRA (TOF-MRA) is widely accepted (Ozsarlak et al. 2004), while the contrast-enhanced MRA (CE-MRA) dominates the assessment of cervical stenoses (Wetzel and Bongartz 1999). It might be pointed out, that the best MRA technique does not exist. The selection of a suitable MRA technique depends on the technical equipment of the MR scanner, the vascular region of interest, the ratio of technical and temporal expense and of the clinical tasks. For instance protocols for hyperacute stroke diagnosis in emergency cases might differ from those for perfect vessel analysis in investigation of ischemic stroke in principle.

The terms 2D and 3D have different meanings, whether they are used for data acquisition techniques (i. e. pulse sequences) or for image display, respectively. 2D acquisition means for MR angiography that, for a a relatively short period of time, either a primary projection image of vessels from a thick volume [for instance in phase contrast MRA (PC-MRA)] or a single thin slice is produced. The sequential acquisition of a series of multiple thin slices with or without gaps is also termed 2D in this sense (for instance in sequential 2D TOF-MRA). In pulse sequences for 3D data acquisition, which are chosen in the majority of MRA purposes, so-called 3D Fourier transformation (3DFT) algorithms are applied, which allow the simultaneous acquisition of three-dimensionally defined volume data from a thick slab by use of a second phase encoding HF gradient. The image data are, however, also displayed primarily as thin, gapless subslices (partitions). In 3D measurements, image data for every single voxel of the volume are collected over the entire measurement time, which lasts up to several minutes. 3D measurements provide an improved signal-to-noise ratio and thus allow a better spatial resolution in a given time. Despite the 2D or 3D acquisition mode, the source images can be viewed and analyzed separately as single slices or after adequate postprocessing procedures (see Sect. 5.1.5) as three-dimensionally reconstructed projection images.

The MRA techniques discussed in the following base on gradient echo sequences and can generally be divided into flow-dependent and flow-independent ones . The main flow dependent techniques are: time-of-flight MRA (TOF-MRA) and phase contrast MRA. CE-MRA, in contrast, is blood flow-independent, although flow phenomena can still influence

D. Petersen, MD
S. Gottschalk, MD
Institute of Neuroradiology, University of Lübeck, Ratzeburger Allee 160, 23538 Lübeck, Germany

image quality. Flow-dependent high resolution MRA acquisition techniques normally require several minutes for data acquisition while flow-independent measurements can be performed within (and up to approximately 30) seconds. The higher the gradient system capability, the faster data acquisition is. The gradient system power on the other hand is limited by safety considerations in order to avoid stimulation effects in patients.

Very fast flow-independent MRA techniques require the intravenous application of MR contrast agents using extremely exact timing protocols. The same contrast media can be used for parenchymal and angiographic imaging. The choice of a contrast agent is mainly determined by its relaxation and viscosity parameters (Friese et al. 2001b). A group of specific contrast media with a prolonged intravenous circulation (blood pool agents) provide advantages for MRA with high spatial resolution but they are not yet commonly used (van Bemmel et al. 2003) for cerebral vessels.

Clinical MR tomographs work mostly with magnetic field strengths from 0.5 to 1.5 T. High field 3-T machines have also been used in recent years. They are characterized by a higher signal-to-noise ratio which enables an improvement of spatial resolution in order to depict smaller intracranial vessels (Al Kwifi et al. 2002). For MRA with inflow methods, the stronger saturation effect on stationary tissue improves the vessel signal-to-noise ratio. T1 shortening due to contrast agents, on the other hand, is less effective at higher field strengths.

For the examinations of intracranial vessels the same coil systems are used as for conventional MRI of the skull. For a combined examination of intracranial and cervical vessels specially integrated coil systems are needed which can receive signals from the circle of Willis down to the aortic arch. Improvements of coil design and high frequency (HF) capabilities allow remarkable reduction in acquisition times by the use of parallel acquisition techniques (Tintera et al. 2004).

5.1.1 Time-of-Flight MRA

Time-of-flight MRA is based on gradient echo sequences with very short repetition times (Laub and Kaiser 1988). The repeated HF excitations cause a relative spin saturation – i. e. signal reduction – in stationary tissue, while inflowing unsaturated blood is depicted with high signal. A saturation pulse cranially to the acquisition volume is usually applied to suppress the signal of venous downward flow, so that intracranial and cervical arteries can be depicted selectively within certain limits.

After the spins have entered the acquisition slab, the inflow-related high blood signal gradually decreases due to spin saturation according to the time period or number of excitations, respectively, rather than flow direction. Variations of the flip angle over the acquisition volume reduce saturation effects of moving blood protons (TONE = tilted optimized nonsaturating excitation). This homogenizes vessel contrast and elevates the signal in distal vessel segments. Despite TONE, however, the imaging of distal vessel segments is impaired. This limits the thickness of acquisition volumes and is a well known disadvantage of TOF-MRA. For the acquisition of larger volumes, the technique of multiple overlapping slice acquisition (MOTSA) was developed (Davis et al. 1993). This technique needs additional measurement time but can alternatively be used to enhance the signal in distal vessels.

Theoretically, 3D TOF-MRA can reach a spatial resolution of up to 0.2 mm voxels. With 1- to 1.5-T magnets this would not provide an acceptable signal-to-noise ratio and therefore in clinical routine the spatial resolution is realistically in a range of approximately 0.5 mm. 3D TOF-MRA is widely accepted as a standard for depiction of intracranial stenosis (Dagirmanjian et al. 1995; Oelerich et al. 1998). Intracranial TOF-MRA should depict the ves-

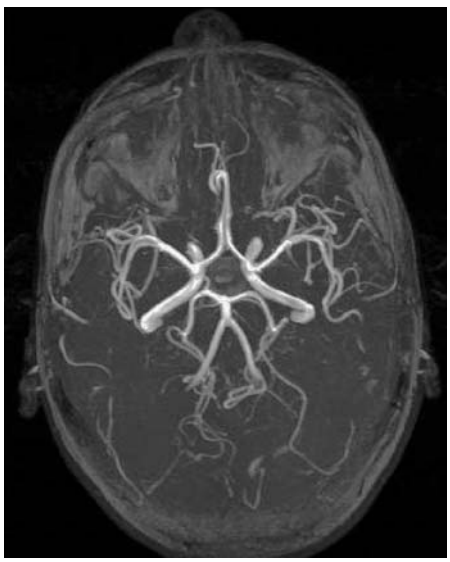

Fig. 5.1. Typical TOF-MRA (three overlapping slabs) of basal intracranial arteries. Maximum intensity projection. Slightly bright signal from fat tissue (orbits, skin)

sels from V4 vertebral artery segment through the M3 segments of the MCA (Fig. 5.1). Limitations of TOF-MRA in the assessment of stenoses are mainly caused by two factors: turbulence and slow or recirculating blood flow. These conditions can lead to overestimation of the stenosis grade, as well as of the length of an arterial stenosis. In patients with even physiologic vessel tortuosity (Fig. 5.2) or high flow velocities (children) non-existing stenoses can be simulated, so that a reliable quantification of stenosis remains problematic. The negative predictive value of a TOF-MRA, however, is high.

In maximum intensity projections of TOF-MRAs, typical overlaps of short T1 tissue (fat or subacute hemorrhages) can occur and affect diagnostic accuracy. Hematomas or thrombus material with short T1 have a high signal which can not be suppressed in TOF sequences (Fig. 5.3), but would not be signal intensive in PC-MRA. Specific excitation pulses can suppress the fatty high signal in bone marrow or within the orbits. So-called water excitation pulse sequences can provide an excellent fat signal suppression, but they are sensitive to typical artifacts due to susceptibility effects. This, for instance, leads to depiction of pseudostenosis, when the internal carotid artery comes close to the air in the sphenoid sinus (Fig. 5.4) (Gizewski et al. 2005). Certain regions with high fat signal such as the orbits can also be interactively removed before secondary reconstruction and then do not impair interpretation.

5.1.2 Phase Contrast MRA

Moving along a magnetic field gradient, spins experience a shift of the transverse magnetization. In phase contrast angiography, the phase shift of flowing blood is determined in several measurements in three directions in space and the vector of the differences is displayed as an image. The vector is proportional to velocity as long as the maximally expected flow velocity of blood is in a range that would cause phase shifts of less than 180°. If these conditions are fulfilled, the phase contrast can be assigned to

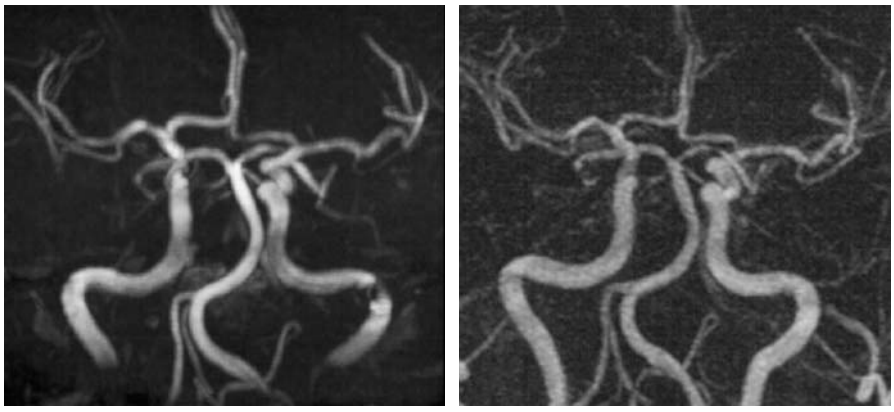

Fig. 5.2a,b. Pseudostenosis due to turbulent flow. Signal loss at the sharp bending of the left ICA entering the carotid canal on TOF image (**a**), smooth vessel enhancement on CE-MRA (**b**)

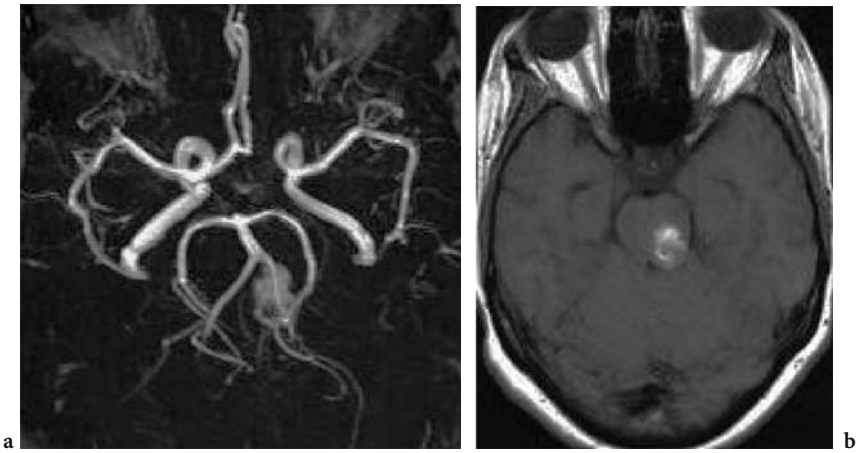

Fig. 5.3a,b. Bright pontine lesion on 3D reconstructed (MIP) TOF-MRA (**a**). T1-weighted precontrast spin echo reveals methemoglobin in a cavernous hemangioma as the source of bright signal (**b**)

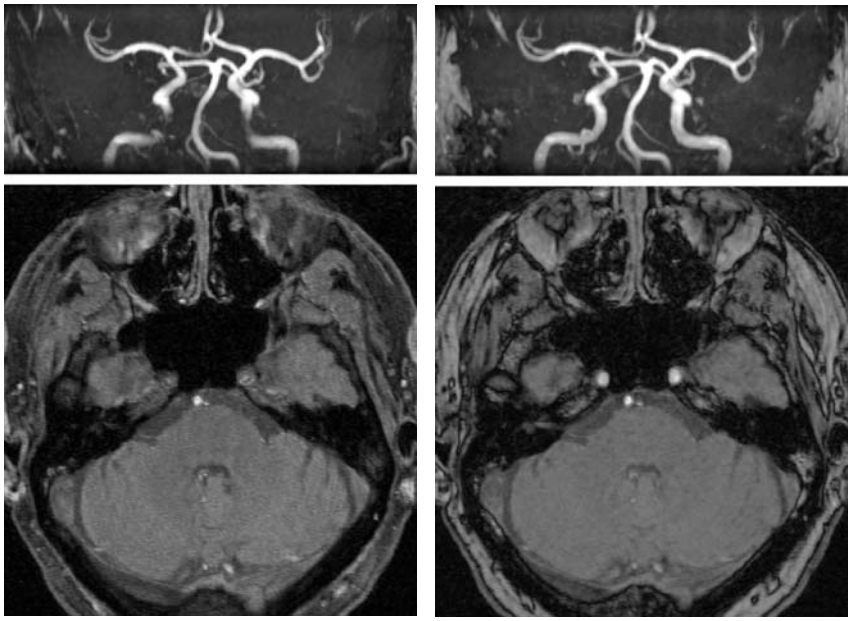

Fig. 5.4a,b. Susceptibility artifacts: due to the vicinity of air in the sphenoid sinus the flow signal of ICA is lowered symmetrically on the TOF images (**a**), when a fat-signal suppressing water excitation pulse sequence was used. The conventional TOF/TONE sequence shows no false vessel extinction, but a higher background signal from fat tissue (**b**)

a velocity encoding (VENC). Due to different flow velocities, arteries and veins are depicted with different contrast according to the selected VENC.

Drawbacks of PC-MRA are seen in its susceptibility for patient movements and its impairment by pulsatile or turbulent flow patterns. The diagnostic sensitivity of 3D PC-MRA in intracranial stenosis is markedly lower than with 3D TOF-MRA (Oelerich et al. 1998). Advantages are the good suppression of stationary tissue signal with the lack of interference with short T1 tissues, and the depiction of large volumes without limitations due to spin saturation effects.

Clinically, PC-MRA is often used for laminar flow with few pulsations as for example in the cerebral venous sinuses. Many users apply it as a thick slab 2D technique with short acquisition times and primary projective vessel depiction. 3D PC-MRA demands relatively long measurement times for data acquisition and is somewhat sensitive to patient movements. Principally, phase contrast methods additionally enable a quantification of blood flow velocity and the assessment of flow directions.

5.1.3 Contrast-Enhanced MRA

To overcome known drawbacks of TOF-MRA, fast contrast-enhanced 3D MRA was developed. Application of a paramagnetic contrast agent reduces spin saturation phenomena in large examination volumes but deals with the disadvantage of unwanted venous contrast overlap if measurement times exceed arteriovenous transit time. The development of very powerful gradient systems, however, enable application of strongly T1-weighted 3D gradient echo sequences with short acquisition times. Very short repetition times (TR) significantly reduce the signal of stationary tissue even more than in TOF-MRA. The native signal of flowing blood is also reduced. Intravenous application of a paramagnetic contrast agent bolus then produces a very strong intraluminal enhancement during the first pass, which is used for the depiction of vessels. If there is strong background signal, subtractions of pre- and post-contrast images make it possible to eliminate that signal almost entirely (Fig. 5.5). CE-MRA does not depict complex flow phenomena such as in TOF-MRA or PC-MRA but the intravascular blood itself, which provides a very short T1 due to a relatively high concentration of contrast agent during its first pass. To avoid the overlap of arterial and venous contrast, short data acquisition times must be maintained. Since 6–8 s of arteriovenous transit time would not be sufficient for the acquisition of high resolution 3D data sets in large volumes, only that portion of raw data is collected during the critical 6- to 8-s time period, which is most relevant for image contrasts. The portions of data most relevant for edge resolution are collected afterwards and do not count for venous signal. The very accurately performed individual timing of intravenous contrast agent application is mandatory for a perfect CE-MRA. It can be achieved by measuring

Fig. 5.5a,b. Image postprocessing: subtraction of pre- from post-contrast high resolution CE-MRA improves signal suppression from stationary tissue. Notice a mild blurring (smoothing) of the edges of the carotid arch and the proximal subclavian arteries, due to respiration and pulsations

the individual bolus arrival time using a test bolus or by using fluoroscopic bolus control and automated start of data acquisition. Failed bolus timing even in the range of 1–2 s does not only cause unsatisfactory vessel contrast but sometimes produces bizarre artifacts (Fig. 5.6) which can severely obviate correct interpretation.

Acquisition times of CE-MRA are determined by the desired spatial resolution. Given the physiologic arteriovenous transit time of approximately 8 s the use of an adequate read-out technique allows a total acquisition time of 25–30 s without impairment due to venous contrast. This leads to a maximum spatial resolution of 0.5–0.8 mm with partition thicknesses below 1 mm.

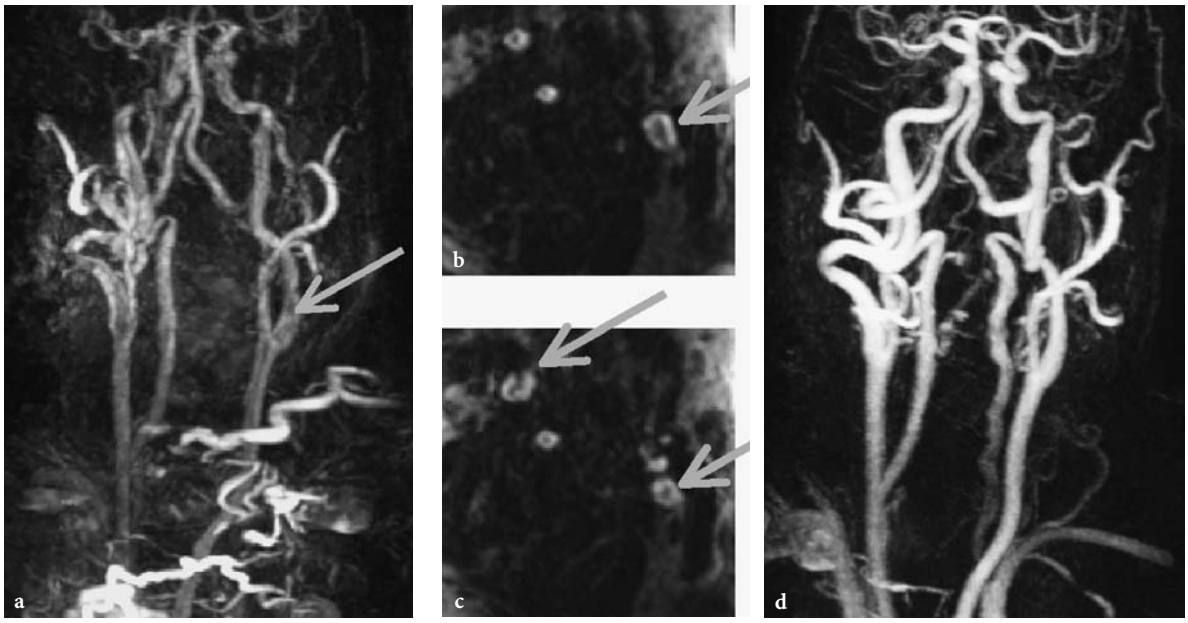

Fig. 5.6a–d. CE-MRA: failed bolus timing resulted not only in a weak artery signal, but also artificial enhancement of vessel walls (*ringing artifacts*), similar to intraluminal thrombus. Examination was repeated and revealed normal vessel enhancement

CE-MRA is currently the most used MRA technique for cervical carotids and other extracranial vessels of the body (Carr et al. 2002; Remonda et al. 2002). With 1.5-T magnets, however, the spatial resolution is still markedly inferior compared with TOF-MRA, since the time for data collection can not be extended over minutes. CE-MRA is increasingly used for intracranial indications as well (see below). The advantages are seen in a low sensitivity for signal loss due to turbulence (Fig. 5.2) or velocity displacements of streaming blood. This affords an opportunity to assess stenoses more reliably than with TOF or PC-MRA (Gottschalk et al. 2002), as long as sufficient anatomic resolution is provided.

CE-MRA also allows repetitive measurements to follow the passage of contrast bolus. Reduction in the number of slices and of in-plane resolution admits sequential measurements with a temporal resolution of less than 1 s (Krings and Hans 2004). In combination with high resolution measurements, thus dynamic processes in arteriovenous shunts or for instance in steal phenomena can be studied (Fig. 5.7).

5.1.4 Black Blood Angiography and Vessel Wall Imaging

While arterial flow causes an increase of signal in gradient echo sequences due to inflow effects (see Sect. 5.1.1), it leads to signal loss in spin echo sequences, known as flow void (Bradley, Jr. et al. 1984). The amount of signal loss is dependent on presaturation and on velocity of inflowing blood. Vessel lumens are homogeneously black when the presaturation is excellent. The high image contrast between vessel lumen, vessel wall, and surrounding tissue makes it possible to depict vessels as so-called black blood angiography (Edelman et al. 1990). The method did not become widely accepted in the first instance since spatial resolution and pre-saturation were often unsatisfactory to outline vessel contours sufficiently. Meanwhile the construction of specifically dedicated HF coils provided the preconditions for improved high resolution black blood MR studies of arteriosclerotic plaques in the carotid artery (Hayes et al. 1996). Studies now show that with the use of adequate

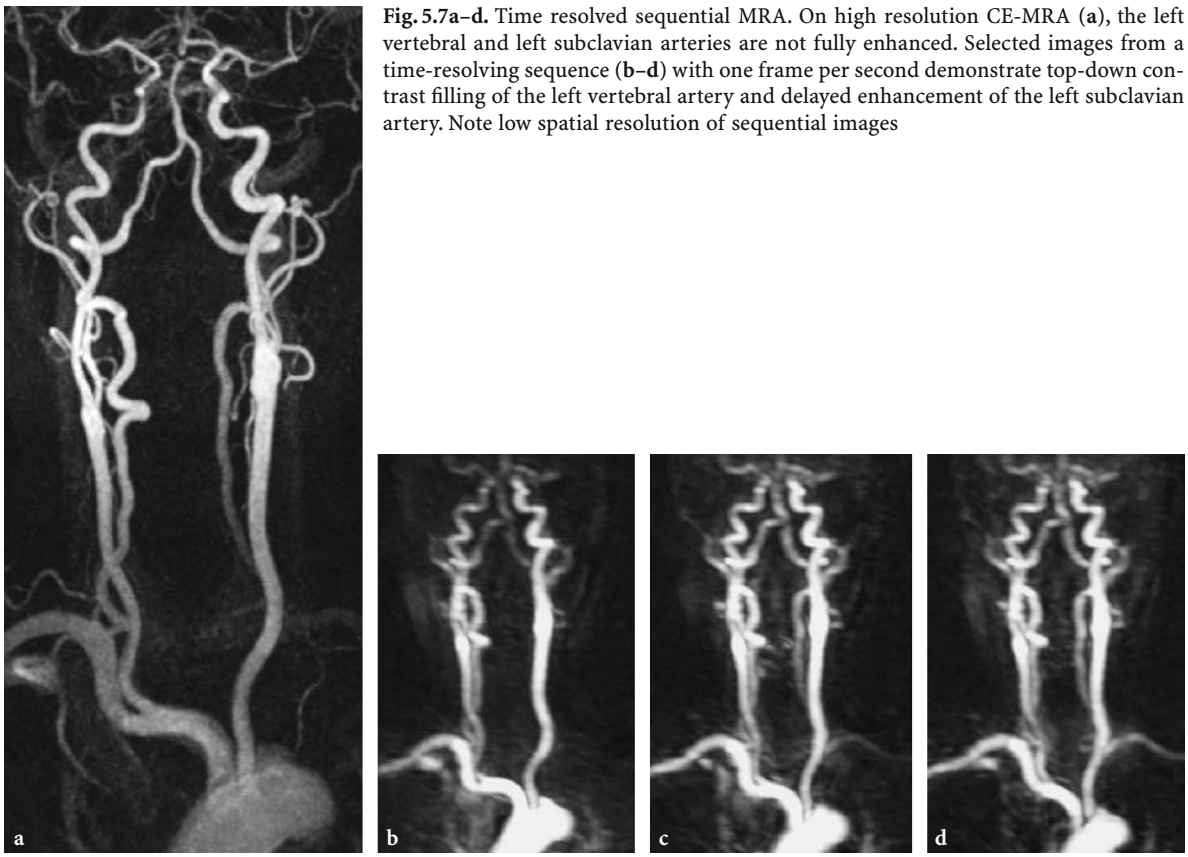

Fig. 5.7a–d. Time resolved sequential MRA. On high resolution CE-MRA (**a**), the left vertebral and left subclavian arteries are not fully enhanced. Selected images from a time-resolving sequence (**b–d**) with one frame per second demonstrate top-down contrast filling of the left vertebral artery and delayed enhancement of the left subclavian artery. Note low spatial resolution of sequential images

HF coils and optimized MR sequences a characterization of plaque structure can successfully be performed that possibly could help to predict the risk of plaque rupture (Figs. 5.8, 5.9) (Yuan et al. 2001).

Fig. 5.8a,b. Assumed signal intense plaque (**a**). Source image of TOF-MRA at the level of the carotid bulb displays bright material, ultrasound showed no evidence of a thrombus. On CE-MRA there is a short eccentric stenosis of the left ICA (**b**)

Fig. 5.9a,b. Subacute wall-adherent thrombus (**a**). After embolic infarction of the middle cerebral artery ultrasound has identified an echolucent structure within the ICA, highly suggestive of thrombus. T1-weighted spin echo image with fat saturation confirms an intraluminal thrombus (**a**) with a mild stenosis (**a, b**), gradually resolving over weeks

5.1.5 Postprocessing of MRA

MRA data sets typically consist of multiple (60–100) partitions, containing a large amount of detailed information. To achieve an overview, 3D vessel images are calculated from these data by the use

of different reconstruction algorithms. Maximum intensity projection (MIP) is the standard method. Signal intense vessels emerge from low signal background. MIP does not depend on a threshold value. Very small vessels, however, may have overly low contrast against background noise. In these cases a selective restriction of the volume of interest before MIP calculation can improve vessel depiction. Occasionally a diagnosis can be made from original source images alone which are optimally viewed on adequate postprocessing workstations. Multiplanar 2D reconstructions facilitate the evaluation of details in complex anatomic regions, while the overview is given by 3D reconstructions.

Alternatively, 3D images of MR angiographies can be calculated using volume rendering techniques (VRT) or shaded surface display (SSD). Both methods, however, depend on threshold values and therefore they carry the risk of unwanted manipulation. They are less suitable for the depiction of stenoses and are commonly used for aneurysms and other vascular malformations.

5.2 Vascular Anatomy

5.2.1 Supraaortic Vessels

The ascending aorta is approximately 5 cm long and merges smoothly into the aortic arch in the mediastinum. Under normal conditions, the truncus brachiocephalicus, the common carotid artery (CCA) and the left subclavian artery originate from the aortic arch. The right and left vertebral arteries have their origin in the proximal segment of the corresponding subclavian arteries. The aortic arch offers numerous variants:

The truncus brachiocephalicus and the left CCA show a combined origin from the aortic arch in approximately 25% of cases. The left vertebral artery rarely arises directly from the arch proximal to the subclavian artery. Infrequently an aberrant right subclavian artery leaves the aorta distal to the left subclavian artery and crosses the mediastinum dorsal to the esophagus and is then called the arteria lusoria (Fig. 5.10). Elongations and ectasias of the aortic arch and supraaortal vessels, which can impair the imaging quality of the vessels, are often seen in elderly patients.

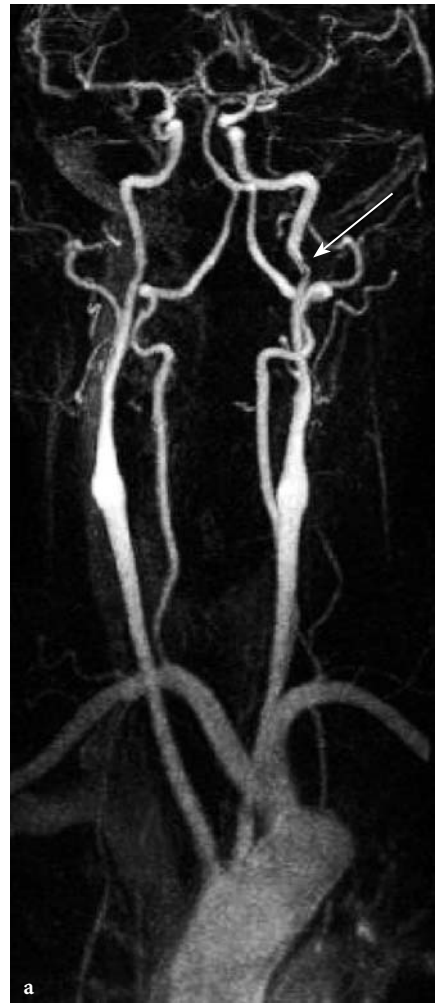

Fig. 5.10a-c. Fibromuscular dysplasia. CE-MRA (**a**) after right hemispheral TIA is suggestive of distal vessel wall irregularities (arrows). Diagnosis was made by DSA (**b, c**), showing bilateral 'string of beads' sign typical for FMD. As a variant, also note the aberrant course of the right subclavian artery with its origin distal of the left arteria lusoria

MR angiography of the aortic arch is provided in high quality by CE-MRA. Free projections and selective volume restrictions enable elaborate single vessels. Respiration movements can typically smooth the outlines of the arch (Fig. 5.5). This effect can be minimized by breath-hold techniques (Carr et al. 2002). Strong pulsations, however, also lead to blurred vascular outlines and can cause signal voids in tiny origins such as the vertebral arteries (Leclerc et al. 2000). ECG-triggered sequences can compensate pulsation artifacts in MRA (Arpasi et al. 2000) but they require shortened acquisition times which imply limited anatomic resolution.

The carotid bifurcation can be seen in 80% of the adult population at the level of cervical vertebrae 3–5. Distal to the physiologic dilatation of the carotid bulb the internal carotid artery (ICA) proceeds dorsally to the external carotid artery (ECA) into the petrous bone. Entering the bony carotid canal, it describes a sharp bend and thus causes turbulent flow patterns with somewhat typically symmetrical signal loss on TOF-MRA, which should not be misinterpreted as real stenoses (Fig. 5.2).

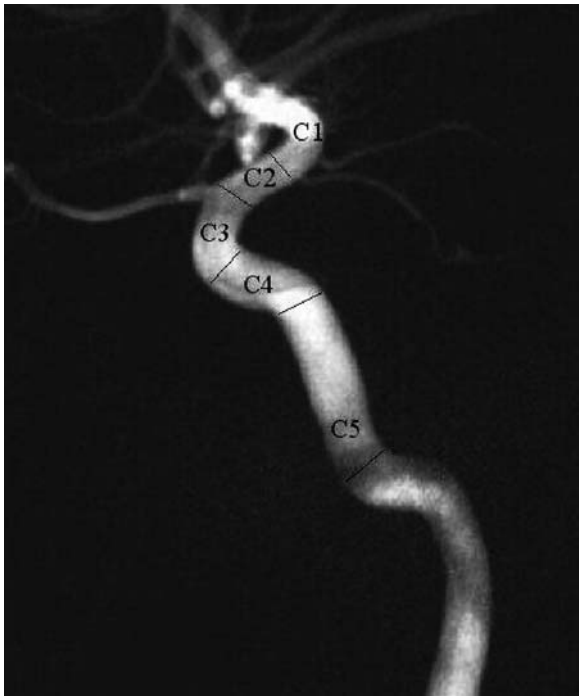

Fig. 5.11. Carotid segments according to Fischer (1938)

5.2.2 Intracranial Vessels

The internal carotid artery is anatomically divided into segments. Fischer (1938) primarily defined five intracranial segments (Fig. 5.11) beginning at the carotid T. A modern classification by Bouthillier et al. (1996) names seven segments instead of five which are counted in an anatomically reverse order in flow direction. In the following we use Fischer's nomenclature which is also still used in the ultrasound literature. The segments C2–C4 form the carotid siphon, which offers considerable variants in shape. It can resemble a "v" or an omega, or even a double siphon. Elongations of the siphon lead to artificial signal voids in flow-dependent MRA sequences, which express flow displacement effects (Pipe 2001).

Anomalies of the ICA are infrequent, and aplasia of the ICA is a rarity (Van de Perre et al. 2004). In hypoplasia, the vessel tapers off behind a normal proximal segment and can sometimes be followed up to the circle of Willis. Occasionally differential diagnosis is difficult against an arterial dissection or a very high grade stenosis with a collapsing distal lumen (pseudoocclusion). In cases of doubt, the CT shows the hypoplastic osseous carotid canal (Chen et al. 1998). An aberrant lateral course of ICA through the tympanum has no impact on the diagnosis of stenoses.

Small hypophyseal and meningeal branches of the ICA are not visible in MR angiographies. The first originating vessel is the ophthalmic artery from the C3 segment. Distally the posterior communicating artery and subsequently the anterior choroidal artery arise from the ICA. A direct origin of the posterior cerebral artery from the ICA is referred to as embryonic type.

The posterior communicating artery offers significant variations in size and is often not sufficiently visible in MRA. If it is utilized for a collateral circulation, it can increase in signal and size, but lacking detection in MR angiography in patients with proximal stenosis does not permit an assessment of the lack of collateral flow (Hartkamp et al. 1999; Hoksbergen et al. 2003).

The anterior choroidal artery is mostly detectable only on source images, not on MIP of a TOF-MRA (Wiesmann et al. 2001), because of its very small size. Consequently, definite statements about pathology can not be made.

The middle cerebral artery (MCA) is divided into four segments. The horizontal M1 segment reaches laterally to the bifurcation or trifurcation, the insular segments within the Sylvian fissure are named

as M2, the opercular vessels M3 and the peripheral cortical branches M4.

Intracranial MR angiography should be sensitive enough to depict stenosis at least in the M1 and M2 segments, even if exact quantification is not reliable. Small vessel diameters and signal loss due to spin saturation do not allow the diagnosis in peripheral MCA branches and lenticulostriatal vessels are normally not depicted. Nevertheless, an asymmetric signal loss within the peripheral MCA branches on MRA can be taken as an indicator for a high grade proximal M1 stenosis (Fujita et al. 1994). Relevant variants of the MCA are rare, differential problems can arise from duplications or fenestrations. The anterior cerebral artery (ACA) is much thinner than the MCA. The A1 segment reaches from the intracranial carotid bifurcation (carotid T) to the anterior communicating artery, the A2 segment up to the corpus callosum, where it divides into the pericallosal artery and the callosomarginal artery, also named as A3 segments. In most cases, a depiction of the ACA is sufficiently possible including the A2 segment, but a definitive evaluation of pathologic vessel wall lesions by means of MRA is not given in the majority of cases.

The vertebral artery normally originates from the subclavian artery. The first extraosseous segment is called V1, the intraforaminal section up to the first cervical vertebral body V2. V3 reaches from the exit of the first vertebral body to the dural passage, the V4 segment runs intradurally through the Foramen magnum and forms the vertebral junction with the contralateral vertebral to the basilar artery. The dural passage is occasionally marked by a small constriction of the vessel, which should not be taken as a stenosis.

Vertebral arteries vary in size and symmetry, where mostly the left vertebral artery is the dominant one. The coincidence of vertebral fenestrations and aneurysms is well known. The anterior spinal artery receives tiny vessels from the vertebral arteries which are physiologically not depicted by MRA due to their size. The posterior inferior cerebellar artery (PICA) as the largest, most important and most variable cerebellar artery; however, under normal conditions it is constantly depictable with TOF and CE-MRA.

The size of the basilar artery varies markedly. Given an embryonic type of PCA, the basilar artery can be extremely small and sometimes it appears to end at the level of the superior cerebellar arteries.

Persisting arterial anastomoses between the ICA and basilar artery occur as the primitive trigeminal artery (Fig. 5.12), rarely as the primitive acoustic artery, the primitive hypoglossal artery or as the proatlantal artery. They can easily be detected by MRA as well as the clinically relevant fenestrations of the basilar artery, which are seen atopically in more than 1%.

Fig. 5.12. Primitive trigeminal artery connecting the ICA and basilar artery (*arrow*)

The anterior cerebellar artery (AICA) is normally the thinnest cerebellar artery and in MR angiographies is often insufficiently depicted. The superior cerebellar artery on the other hand can almost constantly be identified and anomalies such as duplications are mostly recognized on MR angiographies (Uchino et al. 2003). For the numerous anomalies and potential collateral circulations see specific literature (Osborn and Anderson 1977).

5.3 Clinical Application of MRA in Stenoocclusive Arterial Diseases

Quality standards for diagnosis of stenosis are set by catheter DSA, and noninvasive methods have to be compared with these. In the majority of cerebrovascular diseases, however, invasive methods are no longer indicated and are replaced by MRA or CT angiography, respectively. To assure an optimal therapy of stroke, vascular imaging has to provide answers to a number of clinical questions:

- Is the sensitivity sufficient for detection or exclusion of a stenosis?
- Can stenoses be quantified by a standardized measure?
- Is it safe to differentiate between stenosis and occlusion?
- Is the underlying disease of a stenosis recognizable and are even mild lesions of the vessel wall visible?
- Can intravasal thrombosis be identified?
- Can collateral circulation be analyzed?
- Which technical limitations hamper the evaluation?

5.3.1 Atherosclerotic Diseases

Atherosclerosis mainly affects large- and medium-sized arteries. Extracranial manifestations at the carotid bifurcation statistically dominate the intracranial arteries. Besides typical manifestations at the carotid siphon or the vertebrobasilar junction, atherosclerosis is occasionally also found in peripheral intracranial vessel segments. Typical sequelae of atherosclerosis are stenosing plaque formations, ulcerations, dilatations or the evolution of fusiform aneurysms, which can be accompanied by extensive formation of thrombus.

5.3.1.1 Plaques

Superior to DSA, MRI can depict arterial flow or lumen as well as the vessel walls. Analysis of plaque morphology was improved in recent years by the development of specific MRI techniques. Plaques can now be characterized in vivo with regard to fibroid or lipid content or hemorrhagic lesions (Fig. 5.8). It can be expected that, in the future, plaque examination will influence stroke treatment protocols if the risk of plaque rupture can be reliably estimated (Cappendijk et al. 2005; Hayes et al. 1996; Trivedi et al. 2004; Yuan et al. 2001). Plaque examinations, however, are not yet clinical routine. Source images of TOF-MRA allow only limited assessment of vascular walls.

5.3.1.2 Extracranial Stenoses

The goal of optimized standard imaging protocols in stroke workup is to quantify carotid stenosis, recognize tandem stenosis or multifocal vessel pathology and possibly assess collateral circulation. Quality of flow-dependent MRA techniques for the evaluation of atherosclerotic stenosis of the carotid bifurcation was analyzed in a number of studies. In flow-dependent techniques, turbulent flow patterns and the high variance of flow velocities impair the quality of depiction as the main physiologic phenomena. PC-MRA showed an inferior sensitivity and diagnostic accuracy in the evaluation of stenosis compared with TOF techniques (Benjamin et al. 1997; Scarabino et al. 1998). With high resolution 3D TOF provided a better estimation of stenoses. The classification into <30%, <50%, 50%–70% and >70% proved to be reliable (Carriero et al. 1998; Rasanen et al. 1999). In stenoses higher than 85%, however, flow voids were seen (Anderson et al. 1994) even in transverse source images. A typical problem of 3D TOF-MRA is a mild overestimation of stenoses regarding their grade and length. The signal void in these cases is mainly induced by turbulence.

The main disadvantage of TOF angiography is the limited examination volumes. Even using multi-slab techniques it is problematic and extremely time consuming to depict the entire vessel tree from the aortic arch to the circle of Willis. Studies comparing TOF and CE-MRA proved the superiority of CE-MRA (Wetzel et al. 2001; Willig et al. 1998). CE-MRA provides a high sensitivity and no false positive findings in contrast to TOF-MRA, since turbulence and velocity variations do not remarkably influence the images (Stehling et al. 1997). To date, however, definitive standards for the technical performance of CE-MRA have not been established (Sundgren et al. 2002). While some examiners prefer sequences with very short acquisition times to avoid venous contrast overlap, a much better signal-to-noise ratio and spatial resolution are provided by longer data acquisitions in conjunction with a very exact contrast bolus timing. High spatial resolution techniques are necessary to depict short and high-grade stenoses with very complex flow patterns (Fig. 5.13) and to avoid unwanted signal disturbances in physiologically narrow vessel bends. Tandem stenoses of the ICA can thus also be reliably diagnosed (Fig. 5.14).

Fig. 5.13a,b. Detailed depiction of a rather complex carotid stenosis with several sharp plaques and an ulceration (*arrow*) on CE-MRA (**b**) to an extent matching DSA (**a**)

Fig. 5.14. Tandem stenoses of the left ICA demonstrated with CE-MRA. Approximately 80% proximal stenosis and high grade distal stenosis near the carotid canal (*arrows*)

Using MRA techniques with high spatial resolution, the correlation with DSA in the estimation of stenosis grades is excellent, with a tendency towards mild overestimation (Cosottini et al. 2003). By means of physical principles, however, a quantification of atherosclerotic stenoses with CE-MRA alone is not exactly possible. Even if there are no signal losses within a voxel, the spatial resolution is not sufficient to transfer the NASCET and ESCT quantification criteria to MRA. If, however, MRA is combined with ultrasound, the grading of carotid stenosis is reliable (Friese et al. 2001a). A remaining limitation of CE-MRA is still the diagnosis of very short, web-like stenoses (Fig. 5.15).

Subtotal stenoses greatly reduce post-stenotic flow and are called pseudoocclusions, since they are difficult to differentiate from true occlusions even with Doppler ultrasound (without the use of ultrasound contrast media). There are only a few studies on this problem with limited numbers of patients. In the majority of cases, CE-MRA could differentiate stenosis from occlusion (Friese et al. 2001a; Remonda et al. 2002) (Fig. 5.16). In these

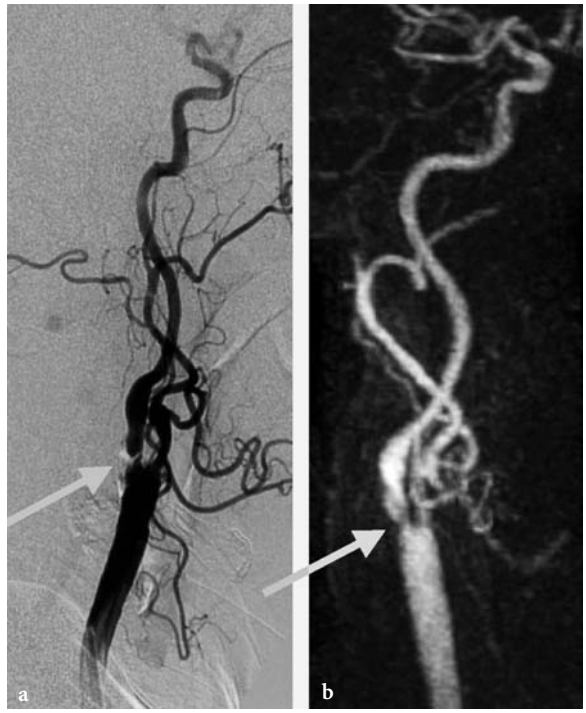

Fig. 5.15. High grade, very short web-like stenosis of ICA on high resolution CEMRA (**b**) compared to pre-interventional DSA (**a**). MRA depicts abnormality , but fails to sufficiently delineate the web. DSA indication should be discussed if ultrasound and MRA do not match

Fig. 5.16. Typical pseudoocclusion on CE-MRA. Note subtotal left proximal ACI stenosis (*arrow*). The distal vessel is collapsed and very thin, but relatively visible up to the circle of Willis

cases, it is less difficult to detect slow flowing blood in the distal ICA than not to confuse tiny extra-intracranial collaterals with residual post-stenotic flow in the ICA. This problem also occurs preferentially in MRA techniques with low spatial resolution. Thus, more false positive than false negative results occur.

After stent PTA, metallic artifacts hinder evaluation of restenosis due to metallic artifacts with all MRA sequences. Even with detailed knowledge of artifacts, a reliable assessment is possible only in few cases. The severity of artifacts is mainly dependent on stent material (Fig. 5.17) where steel stents disturb imaging more than those from nitinol (Cavagna et al. 2001; Teng et al. 2004).

Although MRI also depicts vessel walls, the detection of an intravascular thrombus remains a diagnostic dilemma. On CE-MRA the intraluminal signal gap due to a thrombus can not be distinguished from a plaque under certain conditions. This is especially true for the carotid bifurcation. In suggestive examination situations, conventional spin echo sequences could provide the evidence of thrombus. These sequences, however – including fat signal suppression and presaturation pulses – are time consuming and are not principally scheduled in standard examination protocols. Furthermore, the results are not always conclusive. Without the use of specially designed HF coils and sequence protocols the differentiation of thrombus against plaque remains difficult (Figs. 5.8, 5.9). Vessel wall

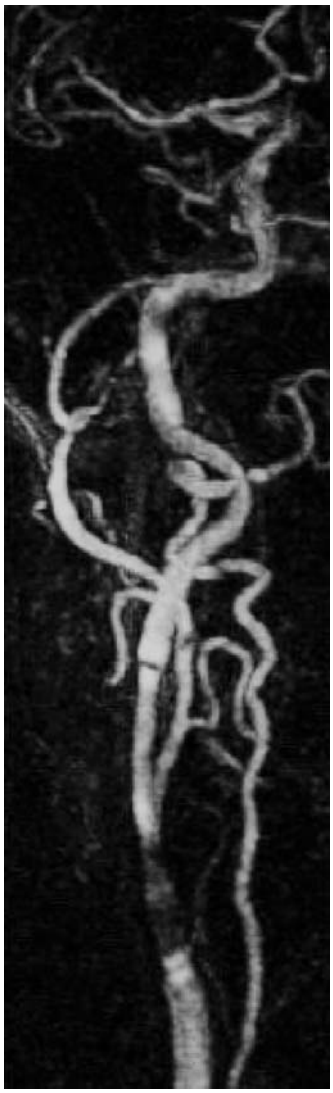

Fig. 5.17. Post-stent CE-MRA. Substantial signal loss due to metallic artifacts (a steel containing wall-stent was used). Note typical ring-like extinctions at proximal and distal tips of the stent. While CE-MRA did not really contribute to the problem of in-stent restenosis, ultrasound was normal in this case

lesions that have a configuration and localization untypical for a plaque should be suspected as thrombus. Intramural hematomas in cases of arterial dissections are much easier to recognize, as described later.

5.3.1.3 Intracranial Stenoses

The depiction of intracranial arterial stenosis by MRA requires a high sensitivity resolution technique, while the importance of an exact grading by MRA is not defined yet. A preventive anti-calculation for stenosis of proximal intracranial segments exceeding 50% is still a matter of debate (Sherman 2002).

In the diagnosis of intracranial stenosis, TOF-MRA is definitely superior to PC-MRA protocols. Oelerich et al. (1998) found a sensitivity of 87% for 3D TOF-MRA in intracranial stenoses. The correlation with DSA was 78%, and other authors found a correlation with MRA up to 88% (Dagirmanjian et al. 1995). While sensitivity is relatively high, false negative findings are rare, so that with sufficient examination quality, a good negative prediction is reached.

Despite high anatomical resolution TOF-MRA does not allow an authentic quantification of intracranial vessel stenoses. Stenoses are commonly overestimated, especially in small vessels (Figs. 5.18, 5.19). Turbulences and velocity displacement effects depending on flow velocity and the tortuosity of a vessel cause false positive stenoses. Typical localizations of pseudostenoses are the carotid siphon and the bent entrance into the carotid canal. In CE-MRA the contrast medium limits spin saturation effects and very short echo times reduce the negative signal effect of turbulent flow patterns, whereby false positive intracranial stenosis can be identified (Gottschalk et al. 2002). Currently, the spatial resolution of CE-MRA as obtained with sufficient signal-to-noise ratio and without relevant venous contrast overlap in the limited acquisition time, is still significantly lower than that of TOF-MRA. Therefore, CE-MRA should be used intracranially as an add-on and not as a substitute for TOF-MRA.

In many instances TOF-MRA provides indirect indicators on collateral circulation at the level of the circle of Willis. While the anatomic conditions for collateral circulation can be studied, the recognition of collateral flow itself is limited (Hoksbergen et al. 2003).

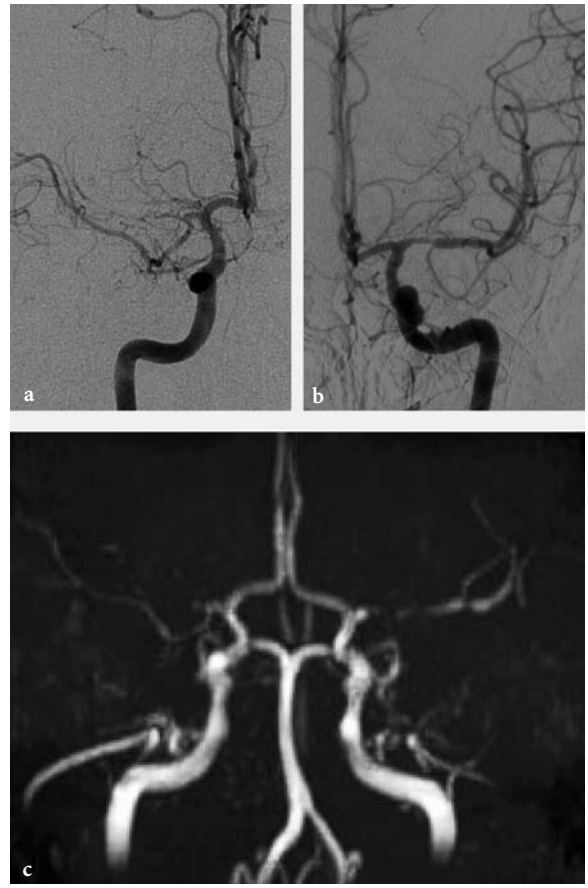

Fig. 5.18a-c. TOF-MRA versus DSA correlation in intracranial stenoses. Occlusion of the right MCA and only mild stenosis of the left one on DSA (**b, c**), while signal loss on CE-MRA (**a**) should not lead to an overestimation of stenosis grade

Preliminary studies of collateral circulation in high grade stenoses or occlusions using ultra fast dynamic MRA with temporal resolution in the range of a second did show delayed contrast enhancement in the affected vascular territory, but did not provide relevant additional information compared with conventional MRI and perfusion techniques probably due to the reduced spatial resolution (Wetzel et al. 2001). A dedicated analysis of collateral circulations, especially extra-intracranially, is still the domain of DSA as far as the exact depiction of anatomical connections is of importance. If the exact anastomotic vascular anatomy is not of primary interest, the collateral supply is better determined by MR perfusion techniques.

Patients with atherosclerosis present with stenoses and irregularities of vessel walls and elongated and ectatic arteries. Extreme dilative atherosclerotic pseudoaneurysms can typically occur with wall adherent thrombus. The differentiation of flow and thrombus signal can be difficult, although its age can fairly be estimated from the signal intensity in T1- and T2*-weighted images. If a high T1 signal of thrombus interferes with flow signal of TOF-MRA, then post-contrast TOF or post-contrast spin echo sequences or a CE-MRA should be performed in addition (Fig. 5.20).

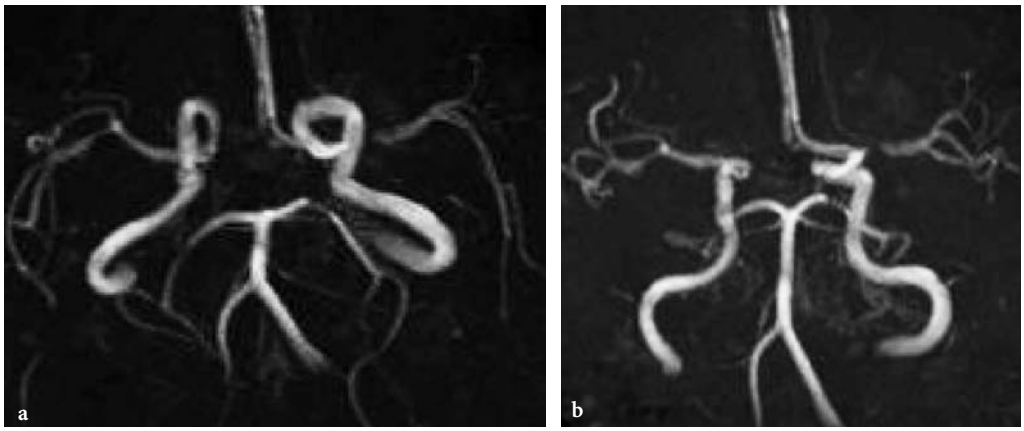

Fig. 5.19a,b. Multiple intracranial stenoses: TOF-MRA (**a,b**) with Doppler ultrasound correlation. High grade stenosis of left MCA (M1) was confirmed (>400 cm/s), suspected right M2 stenosis was estimated as mild by ultrasound and a left PCA stenosis was suspected only on MRA

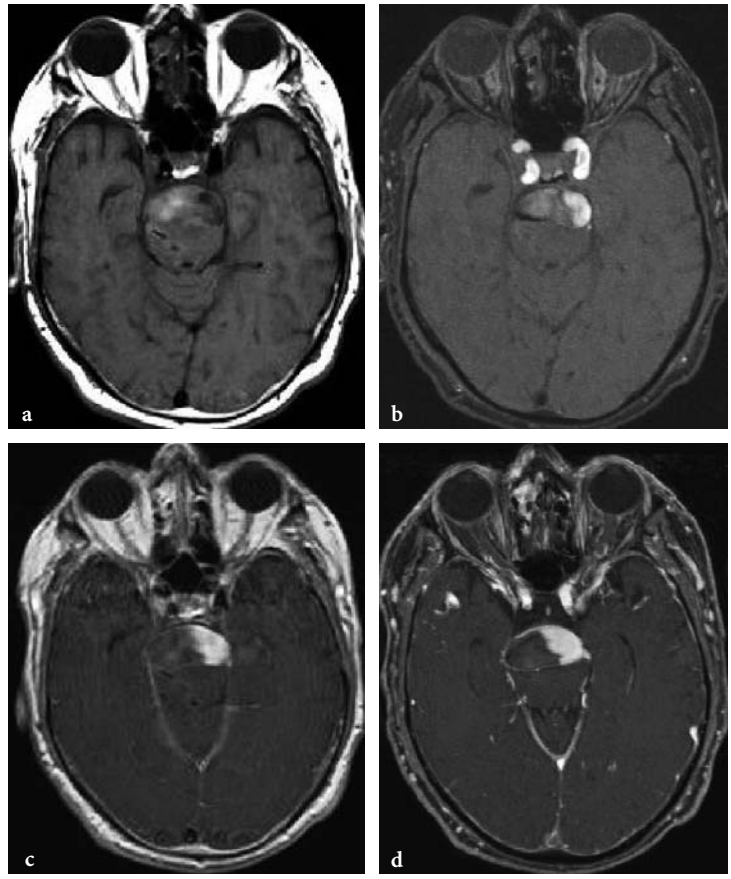

Fig. 5.20a–d. Subacute thrombus formation in a large fusiforme aneurysm of the basilar artery. Parts of the thrombus are still isointense to brain, while others are moderately hyperintense on spin echo T1-weighted image (**a**). Residual flow within the vessel is outlined against thrombus much better on post-contrast T1-weighted spin echo (**c**) and post-contrast TOF-MRA (**d**) than on unenhanced TOF-MRA (**b**)

5.3.2 Arterial Dissection

In young patients, non-atherosclerotic lesions of intra- and extracranial vessels are relevant causes for strokes (Bogousslavsky and Pierre 1992). An arterial dissection is an intimal lesion with hemorrhage into the vessel wall. A constriction of the vessel lumen can range from a minimal stenosis to total occlusion. Dissections occur post-traumatically or spontaneously, in conjunction with hypertension or with migraine, often with fibromuscular dysplasia or with other connective tissue diseases (Guillon et al. 1998). In contrast to atherosclerosis the carotid bulb is spared in most cases and the manifestations occur near the skull base or intracranially. Multiple simultaneous dissections of the ICA and vertebral arteries are possible. Besides the ICA , intracranial dissections can affect the MCA, the vertebral arteries and the basilar artery in rare instances. The typical angiographic image of a dissection is characterized by an increasing vessel stenosis. In typical localizations, the image is often suggestive, but not proof of an underlying dissection. Occasionally a false lumen, a pseudoaneurysm or a minimal lesion with intimal flap is detectable. Dissections can cause acute or subacute ischemic strokes and persisting pseudoaneurysms can remain as a source of embolism.

The examination strategy in MRA has to concentrate not only on the depiction of the vessel lumen by CE-MRA in analogy to DSA. The evidence of a dissection on MRA is given rather by the assessment of an intramural hematoma. Using noninvasive angiographies, dissections are recognized with best sensitivity in TOF-MRA (Levy et al. 1994; Oelerich et al. 1999). The depiction is easy, if a mural hematoma is already signal intense on T1-weighted images and provides a typical falciform configuration on axial slices below the skull base. An additional fat saturated T1 spin echo sequence facilitates the correct diagnosis (Fig. 5.21). Hematomas, however, provide short T1 signal not in the early phase, but only after 4–6 days. Acute hematomas are isointense on T1-weighted spin echo images and in the source images of TOF-MRA compared with brain and soft tissue and need to be analyzed accurately (Fig. 5.22). In cases of vessel occlusion or high grade stenosis, CE-MRA may demonstrate a pointed tapering of the vessel (Carr et al. 2002).

In the clinical setting, one should start with a TOF-MRA and an unenhanced T1-weighted sequence with fat saturation if possible, subsequently followed by a CE-MRA. It is important to mention that projection images and even single source images of CE-MRA constantly fail to show the intramural hematomas with high signal, even if very bright on TOF images (CE-MRA sequences are principally T1-weighted, but they are optimized for very short T1 values as they occur during the first pass of arterial contrast boluses). The typical bright signal of intramural hematoma is only seen on spin echo images or the source images of TOF-MRA (Fig. 5.23). Stenoses in patients without risk factors or in unusual distal

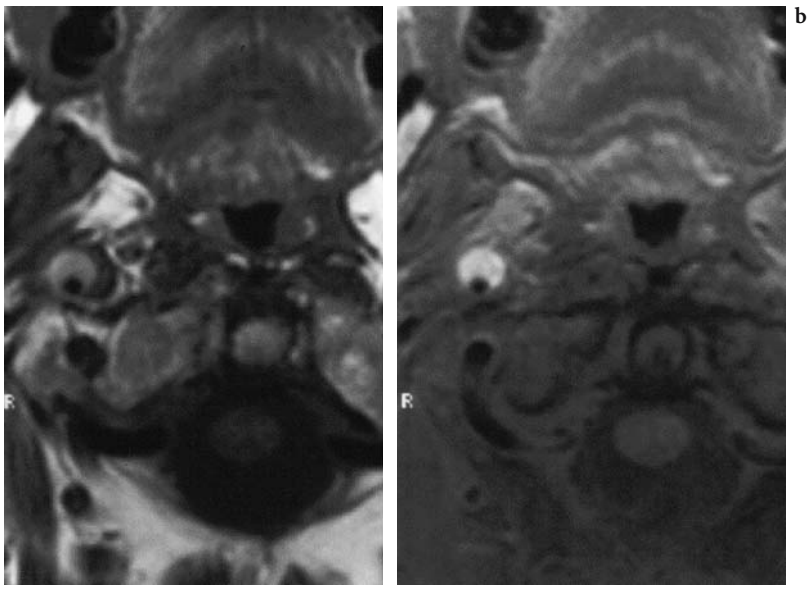

Fig. 5.21a,b. Subacute dissection of the extracranial right ICA. Spin-echo T1-weighted images pre- (**a**) and post-fat saturation (**b**)

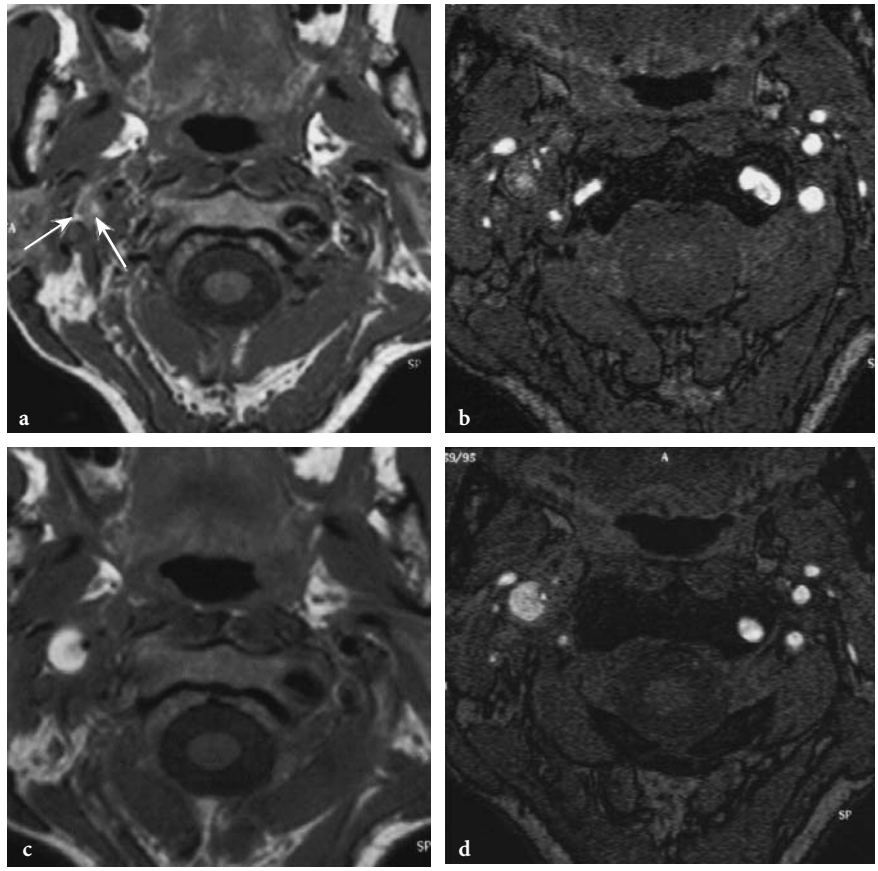

Fig. 5.22a–d. Time course of post-traumatic carotid dissection. Spin echo T1-weighted (**a,c**) and TOF single slices (**b,d**). The typically bright hematoma and stenosis are well seen 12 days after the trauma (**c,d**). On day 4, however, (**a,b**) there is already stenosis on both images, but signal intensity of hematoma is not yet markedly increased

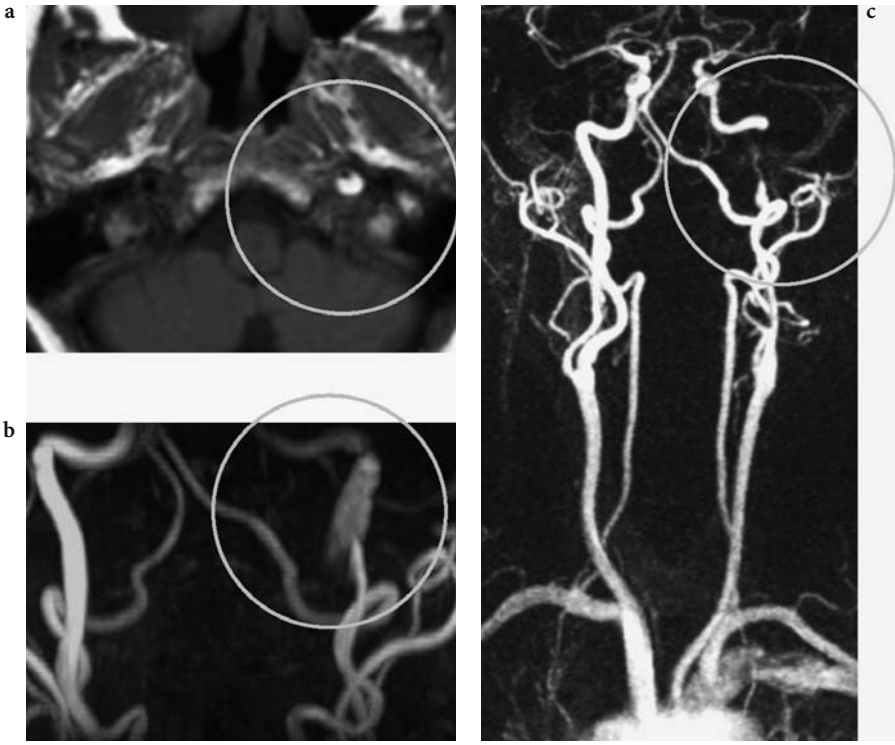

Fig. 5.23a–c. Carotid dissection. While the characteristic intramural hematoma is easily recognized as bright on TOF-MRA source images (**a**) and MIP (**b**), CE-MRA (**c**) outlines the long high grade stenosis of the distal extracranial vessel, but not the hematoma itself

localizations should always raise the suspicion of dissections and therefore be examined with the above mentioned adequate methods.

Smooth dissections (Lucas et al. 2000) or less impressive vessel lesions, especially in elongated vessels of the posterior circulation, are diagnostically problematic. In these cases, a DSA is sometimes necessary. False positive findings arise if vascular steps in secondary reconstructions of MR angiographic data sets are mistaken as pathologic wall lesions, which predominantly occur with insufficient spatial resolution.

5.3.3 Fibromuscular Dysplasia

Fibromuscular dysplasia (FMD) is a disease of medium-sized vessels, beginning in young to middle-aged patients with a predominance among females (Begelman and Olin 2000). The exact etiology is not clear, an association with a lack of alpha 1-antitrypsin is discussed as an indicator to a genetically mediated risk (Schievink et al. 1996). The radiological appearance of FMD depends on the histological type of disease and affects mainly the muscularis media, more rarely isolated the adventitia or the intima. FMD manifests through dissections or hyperplasia of the vessel walls with resulting stenosis. Stenosis and dilations with thinning of vascular walls alternate over longer distances, occasionally with aneurysms or luminal duplications. On DSA, this type of lesions was described as "string of beads". The carotid artery is often affected bilaterally, mostly sparing the bifurcation. There is an elevated incidence of intracranial aneurysms and additionally arteriovenous fistulae can occur (Mettinger and Ericson 1982; Osborn and Anderson 1977; Zimmerman et al. 1977).

Compared to high-resolution examinations of the vessel wall for plaque imaging there are no dedicated studies for the analysis of vessel wall alterations in FMD. MRA can provide evidence of dissections with high sensitivity and of alternating arterial dilatation and stenosed vessels. MRA may also to help identify the string of beads pattern. In source images of TOF-MRA, segmental changes in arterial wall thickness, however, are detected to only a limited extent. If the analysis is performed on the basis of CE-MRA source images, one should consider the restricted spatial resolution. Reconstruction artifacts have to be excluded, which can simulate vessel wall pathology.

MRA is recommended for FMD, particularly with regard to the cervical region (Heiserman et al. 1992; Link et al. 1996), but due to the frequently subtle lesions, DSA should still be considered for FMD (see Fig. 5.10) (Hurst 1996).

5.3.4 Moya Moya Phenomenon

Moya Moya disease is a chronic cerebral arteriopathy with progressive stenoses of the distal ICA mainly found in children and young adults (Chiu et al. 1998; Giroud et al. 1997). This idiopathic disease is rarely found outside of Asia. Typically, the progressive occlusion of the distal intracranial ICA causes the dilatation of small cloud-like collateral vessels around the circle of Willis. The angiographic image, however, is not specific for the idiopathic disease, but rather displays an etiologically unspecific pattern of collateral circulation, which can always develop when a stenosis of the distal ICA slowly progresses. This is specifically true for atherosclerosis and FMD. Since the grading of the stenosis is crucial for radiological diagnosis and very tiny collaterals have to be studied, a definite and reliable evaluation is most suitable with DSA. Nevertheless, MRA can also show stenoses and depict the collaterals to a certain degree (Fig. 5.24), if these vessels are dilated. In many of these cases with significantly slowed down flow with pre- and post-stenotic signal decrease, TOF-MRA is not able to sufficiently define the precise degree of stenosis nor to differentiate high grade stenosis from an occlusion (Fig. 5.25).

5.3.5 Vasculitis

With regard to the classification of primary and secondary forms of CNS vasculitis and the difficulties of confirming the diagnosis, we refer to specific literature (Younger 2004). The amount of vascular alterations might be relevant for the diagnosis, but the role of the pattern of vascular lesions for differential diagnosis is of different importance. The disease becomes manifest in different localizations and in differently sized group of arteries.

Takayasu arteritis affects medium-sized and large arteries, specifically the aorta and the supraaortic branches. The disease is usually not seen in intracranial vessels nor in the temporal artery. Although for a long time DSA was accepted as a diagnostic

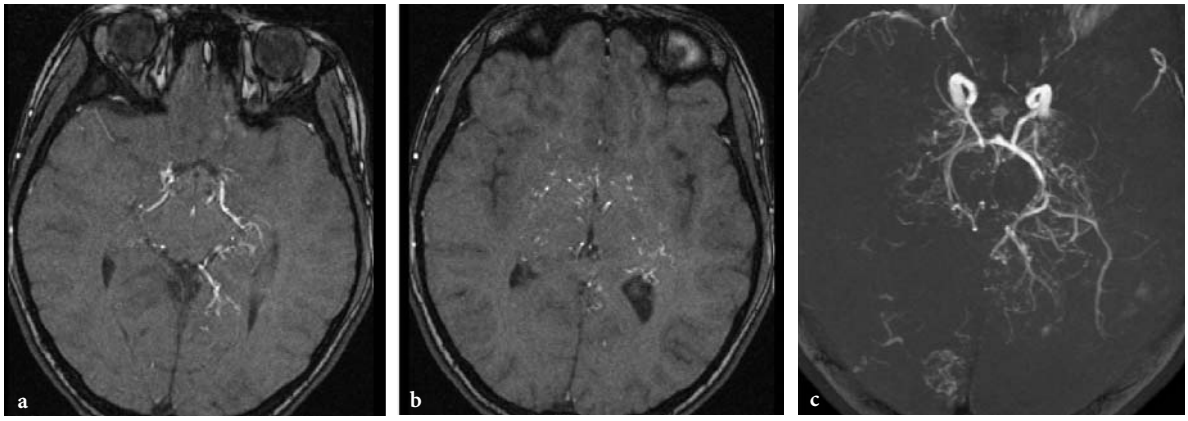

Fig. 5.24a–c. Moya Moya syndrome. TOF-MRA demonstrates on source images (**a,b**) and MIP image (**c**) multiple small collateral vessels and distal occlusions of the carotids

gold standard, MRI and MRA obviously provide the advantage not only to depict stenoses, but also to provide signs of inflammatory vessel disease. This provides new criteria for therapy monitoring. An appropriate examination consists of a CE-MRA, as well as acquisition of spin echo images (Andrews et al. 2004).

Primary angiitis of the CNS causes inflammation particularly in small leptomeningeal vessels, whereas larger vessels can also be affected. Systemic variants of vasculitis and secondary arteritis of the CNS affect mostly small or medium-sized arteries to different degrees, and occasionally the venous system is also afflicted as in Behcet disease. Segmental stenoses are frequently found, often not including bifurcations and alternating with arterial dilatations. This pattern is not definitively specific and can also be seen in atherosclerosis. Even with an optimal MRA technique, DSA still remains necessary for the depiction of tiny vessel lesions (Fig. 5.26).

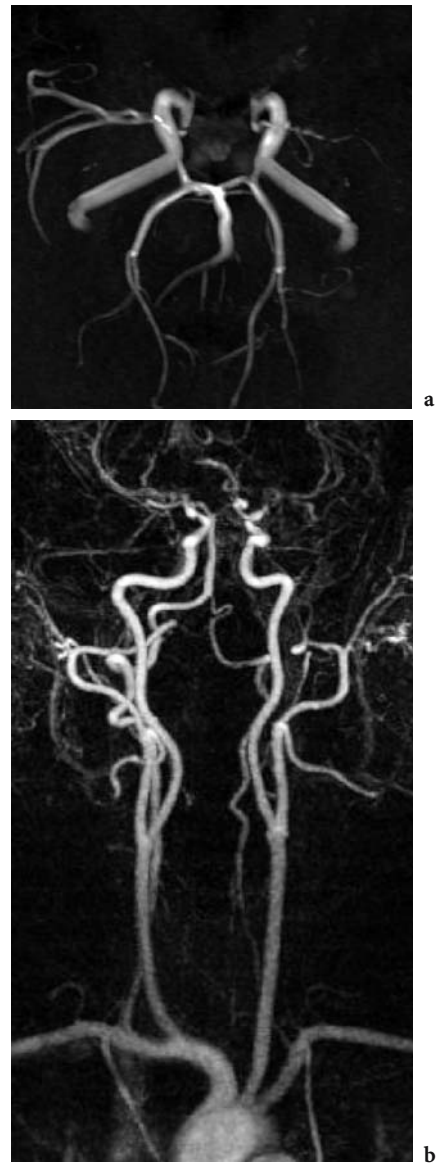

Fig. 5.25a,b. Moya Moya syndrome. Due to limited resolution as well as turbulence, TOF-MRA (**a**) and CE-MRA (**b**) do not enable definitive quantification of obstructions at the level of the distal intracranial carotids: TOF might be diagnosed as left occlusion and right high grade stenosis, while CE-MRA demonstrates bilateral enhancement of MCA branches

5.3.6 Stenoses of Other Etiologies

Vasospasms following subarachnoid hemorrhages are a frequent and highly relevant complication with significant morbidity. Spasms occur in the proximal

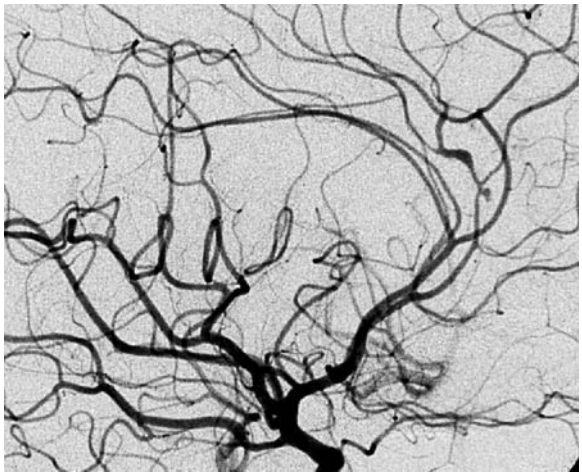

a

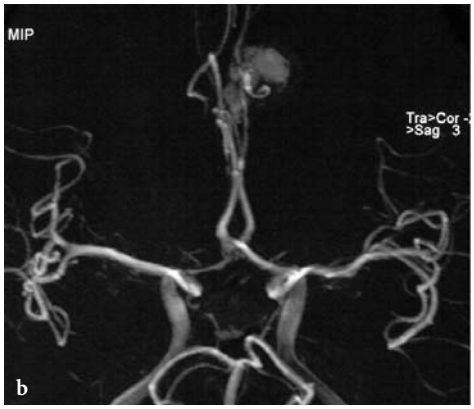

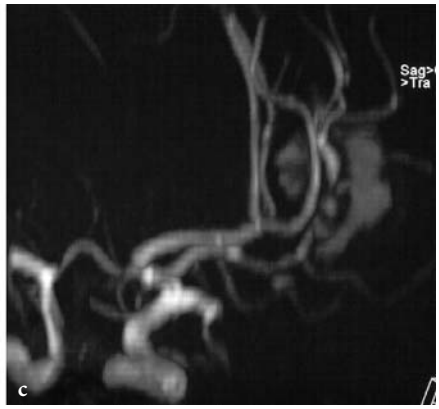

Fig. 5.26a–c. Vasculitis. After an atypical frontal hemorrhage, TOF projections (**a,b**) are slightly superimposed by short T1 blood, and they depict some vessel irregularities of the A3 segments. Due to limited spatial resolution a diagnosis cannot be made. DSA (**c**) reveals the findings of vasculitis with narrowed and widened vessel lumen and a small dissecting aneurysm on the callosomarginal artery

vicinity around the circle of Willis or far distally on peripheral segments. Although proximal spasms can be detected with high sensitivity by MRA (Grandin et al. 2000), this technique is – especially in the scope of bedside ultrasound facilities – of secondary importance due to its limited ability to objectively quantify flow obstructions. If an exact definition of stenosis and of the pattern of spasms is needed in order to schedule endovascular therapeutical measures, DSA still should be performed. The advantage of noninvasive MRI techniques on the other hand is rather seen in perfusion measurements (Hertel et al. 2005).

Some congenital diseases such as Marfan syndrome or Ehlers Danlos syndrome (type 4) can cause arteriopathies of cranial cervical vessels. In Ehlers Danlos syndrome, elongations, dissections, dilatation and aneurysms, as well as fistula in large and mid-size arteries, are found. Cystic medial necrosis (Ueda et al. 1999) leads to aortic dissections which can include supraaortic vessels (Fig. 5.27)

Cervical irradiations can yield carotid wall damage as an important delayed complication of tumor treatment. This would result in arterial sclerotic alterations with stenosis or vessel wall necrosis. Significant high grade stenosis, bilateral carotid stenoses and carotid occlusions have been described (Steele et al. 2004). The angiographic image itself is not specific, but the localization of stenoses is relevant since they correlate with the irradiation fields (Fig. 5.28). CE-MRA can be used as the primary method as in atherosclerotic stenosis.

5.3.7 MRA in Clinical Protocols

As shown above, MRA techniques are susceptible to artificial effects. High resolution time consuming measurements such as TOF-MRA are usually not suitable for the agitated patient suffering from acute stroke. Very fast and robust measurements, on the other hand, might be less detailed. In acute stroke with suspected arterial occlusion, the question of localization in the anterior or posterior circulation is of particular significance.

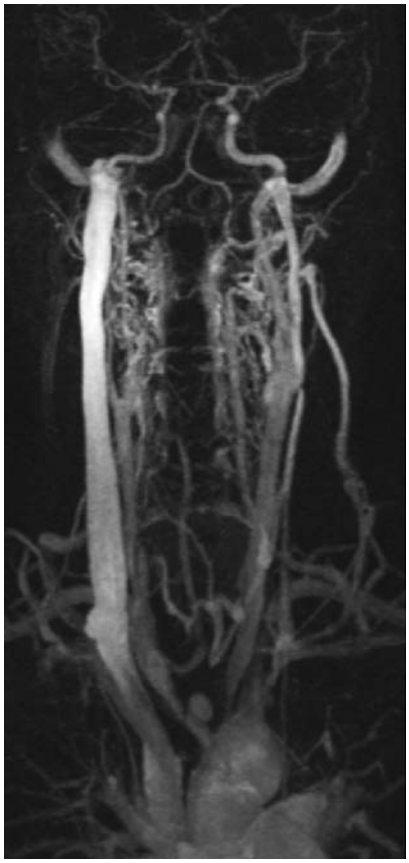

a

b

Fig. 5.27a,b. Cystic medial necrosis. Due to the high grade proximal stenoses, test bolus measurement prior to CE-MRA failed in this case, leading to superimposition of venous contrast (**a**). Evaluation is nevertheless possible on original source slices (**b**), showing stenoses and aneurysms along the proximal supraaortic vessels (*arrows*)

While theoretically CE-MRA could be the method of choice, there are currently no sufficient studies relating to MRA in acute vertebrobasilar occlusion. The emergency situation and the difficult management of patients with impaired consciousness still cause many examiners to begin their diagnostic investigations with DSA. If the therapeutic decision depends on a non-invasive method, then CT angiography might be preferred as less susceptible to artifacts, robust and an extremely fast method. On the other hand MR parenchymal imaging including diffusion and perfusion parameters provides relevant information rather than angiography.

For the acute occlusion in the anterior circulation, no large comparative studies have been carried out to date to validate MRA, perhaps because therapeutic decisions were not dependent on evidence of an arterial occlusion or from its exact localization

Fig. 5.28. Radiogenic carotid stenosis. CE-MRA depicts atypically located proximal high grade stenosis of the right common carotid artery

within the anterior circulation (Hacke et al. 1999; Hacke et al. 2004). Liu et al. (2004) applied 2D PC-MRA as a fast technique in acute stroke cases. The lack of flow signal in the MCA correlated well with impaired diffusion and perfusions, but the authors did not prove the validity of arterial occlusion using other diagnostic modalities. Schellinger et al. (2005) transferred the CT characteristics of the "arterial hyperdense media sign" (Tomsick et al. 1996; von Kummer et al. 1996) to MRI and defined an "early MR imaging vessel sign in hyperacute stroke". These vessel signs correlated in MRA with occlusion of the middle cerebral artery, but they could not predict the clinical outcome, eventual recanalization, nor the incidence of cerebral hemorrhage. The accuracy of MRA in this regard has not been tested.

5.3.8 Limitations and Pitfalls of MRA

Although MRA projection images may look much like classic DSA, they are based upon completely different facts. MRA provides a wide variety of examination techniques for different diagnostic purposes. Evaluation and interpretation require experience in the physical basics of the respective method in order to understand potentialities and limitations of MRA. It is particularly important to understand the origin of typical pitfalls and artifacts, which have been pointed out above.

Compared with DSA, spatial and dynamic information is also limited. Flow phenomena, however, influence vessel depiction markedly and lead to overestimation or even false positive depiction of stenoses. If the contrast bolus in CE-MRA does not exactly match the timing of the particular readout technique, false contrasts are generated at anatomic edges, which can simulate intraluminal thrombus (see Fig. 5.6). It is mandatory to recognize the technical origin of a finding like this and rather to repeat the examination than to trust imperfect images. While TOF-MRA depicts intramural short T1 hematoma in arterial dissections with high signal intensity, CE-MRA shows only the luminal abnormality in these cases and hematoma signal often does not differ from that of surrounding tissue even on single slices (Fig. 5.23). In clinically or radiologically suspicious cases, additional spin echo or TOF images are indispensable. One of the main problems with 3D inflow-MRA is spin saturation, which affects not only slow flow, but also recirculating flow. Large aneurysms for instance, whether saccular or fusiform, present with multiple recirculations of intraaneurysmal blood and appear therefore often largely obscured in TOF-MRA. Contrast agent administration makes the full extent of these aneurysms visible (Fig. 5.29). The high sensitivity of TOF sequences for short T1 tissue, on the other hand, also brings with it the risk of misdiagnosis, when intravascular signal due to thrombus is taken for inflow signal (Fig. 5.30).

a b

Fig. 5.29a,b. Giant aneurysm of the posterior communicating artery in an infant. Due to recirculating blood, there is marked spin saturation within the aneurysm on unenhanced TOF-MRA (**a**). The entire aneurysm is visualized after contrast enhancement (**b**)

Fig. 5.30a–d. TOF-MRA pitfall. Although the TOF projection (**a**) could erroneously be taken for a distal intracranial stenosis of the left ICA, the correct diagnosis is complete occlusion of this vessel. High signal intensity of the vessel is not caused by inflow, but is due to short T1 of the subacute inravascular thrombus. Note the similar signal of inflow and short T1 thrombus on TOF source image (**c**) and respectively the flow void of the right artery on spin echo image (**d**). CE-MRA proves complete occlusion of the vessel (**b**)

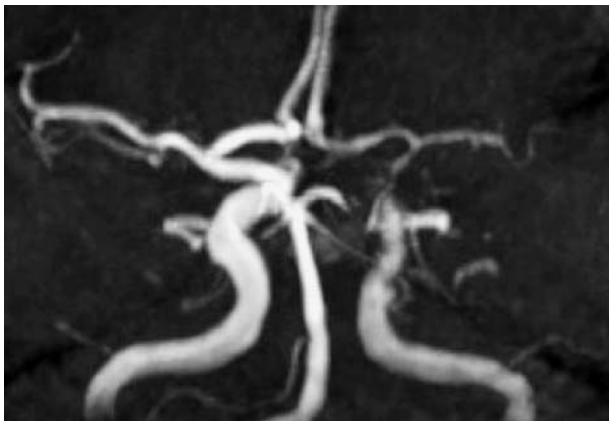

a

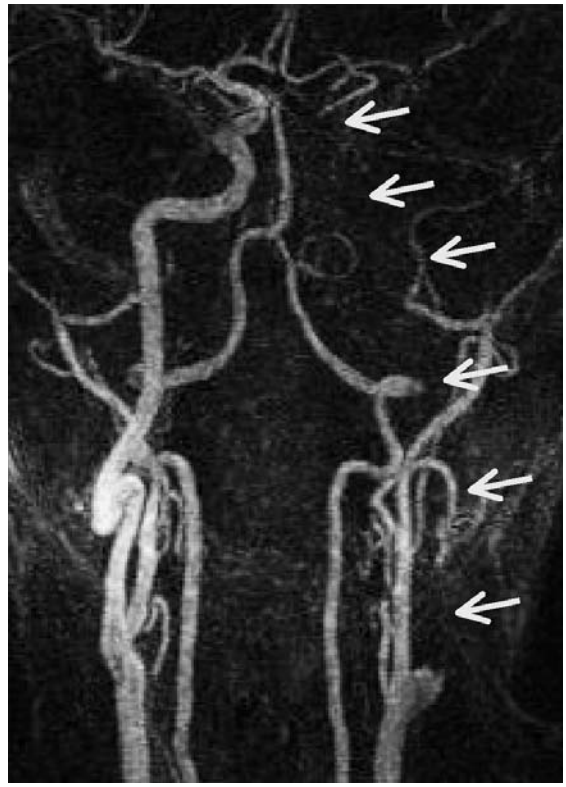

b

c

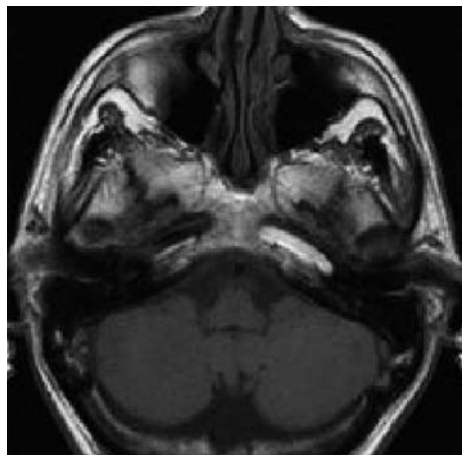

d

References

Al Kwifi O, Emery DJ, Wilman AH (2002) Vessel contrast at three Tesla in time-of-flight magnetic resonance angiography of the intracranial and carotid arteries. Magn Reson Imaging 20:181–187

Anderson CM, Lee RE, Levin DL et al. (1994) Measurement of internal carotid artery stenosis from source MR angiograms. Radiology 193:219–226

Andrews J, Al Nahhas A, Pennell DJ et al. (2004) Non-invasive imaging in the diagnosis and management of Takayasu's arteritis. Ann Rheum Dis 63:995–1000

Arpasi PJ, Bis KG, Shetty AN et al. (2000) MR angiography of the thoracic aorta with an electrocardiographically triggered breath-hold contrast-enhanced sequence. Radiographics 20:107–120

Begelman SM, Olin JW (2000) Fibromuscular dysplasia. Curr Opin Rheumatol 12:41–47

Benjamin MS, Gillams AR, Carter AP (1997) Carotid MRA – what advantages do the turbo field-echo and 3D phase-contrast sequences offer? Neuroradiology 39:469–473

Bogousslavsky J, Pierre P (1992) Ischemic stroke in patients under age 45. Neurol Clin 10:113–124

Bouthillier A, van Loveren HR, Keller JT (1996) Segments of the internal carotid artery: a new classification. Neurosurgery 38:425–432

Bradley WG Jr, Waluch V, Lai KS et al. (1984) The appearance of rapidly flowing blood on magnetic resonance images. AJR Am J Roentgenol 143:1167–1174

Cappendijk VC, Cleutjens KB, Kessels AG et al. (2005) Assessment of human atherosclerotic carotid plaque components with multisequence MR imaging: initial experience. Radiology 234:487–492

Carr JC, Ma J, Desphande V et al. (2002) High-resolution breath-hold contrast-enhanced MR angiography of the entire carotid circulation. AJR Am J Roentgenol 178:543–549

Carriero A, Scarabino T, Magarelli N et al. (1998) High-resolution magnetic resonance angiography of the internal carotid artery: 2D vs 3D TOF in stenotic disease. Eur Radiol 8:1370–1372

Cavagna E, Berletti R, Schiavon F (2001) In vivo evaluation of intravascular stents at three-dimensional MR angiography. Eur Radiol 11:2531–2535

Chen CJ, Chen ST, Hsieh FY et al. (1998) Hypoplasia of the internal carotid artery with intercavernous anastomosis. Neuroradiology 40:252–254

Chiu D, Shedden P, Bratina P et al. (1998) Clinical features of moyamoya disease in the United States. Stroke 29:1347–1351

Cosottini M, Calabrese R, Puglioli M et al. (2003) Contrast-enhanced three-dimensional MR angiography of neck vessels: does dephasing effect alter diagnostic accuracy? Eur Radiol 13:571–581

Dagirmanjian A, Ross JS, Obuchowski N et al. (1995) High resolution, magnetization transfer saturation, variable flip angle, time-of-flight MRA in the detection of intracranial vascular stenoses. J Comput Assist Tomogr 19:700–706

Davis WL, Warnock SH, Harnsberger HR et al. (1993) Intracranial MRA: single volume vs. multiple thin slab 3D time-of-flight acquisition. J Comput Assist Tomogr 17:15–21

Edelman RR, Mattle HP, Wallner B et al. (1990) Extracranial carotid arteries: evaluation with "black blood" MR angiography. Radiology 177:45–50

Fischer E (1938) Die Lageabweichungen der vorderen Hirnarterie im Gefaessbild. Zentralbl Neurochir 3:300–313

Friese S, Krapf H, Fetter M et al. (2001a) Ultrasonography and contrast-enhanced MRA in ICA-stenosis: is conventional angiography obsolete? J Neurol 248:506–513

Friese S, Krapf H, Fetter M et al. (2001b) [Contrast enhanced MR-angiography (CE-MRA): do contrast media with higher T1 relaxation improve imaging of carotid stenoses?]. Rofo 173:542–546

Fujita N, Hirabuki N, Fujii K et al. (1994) MR imaging of middle cerebral artery stenosis and occlusion: value of MR angiography. AJNR Am J Neuroradiol 15:335–341

Giroud M, Lemesle M, Madinier G et al. (1997) Stroke in children under 16 years of age. Clinical and etiological difference with adults. Acta Neurol Scand 96:401–406

Gizewski ER, Ladd ME, Paul A et al. (2005) Water excitation: a possible pitfall in cerebral time-of-flight angiography. AJNR Am J Neuroradiol 26:152–155

Gottschalk S, Gaebel C, Haendler G et al. (2002) [Contrast-enhanced intracranial 3 D MR angiography (CE-MRA) in assessing arterial stenoses and aneurysms]. Röfo 174:704–713

Grandin CB, Cosnard G, Hammer F et al. (2000) Vasospasm after subarachnoid hemorrhage: diagnosis with MR angiography. AJNR Am J Neuroradiol 21:1611–1617

Guillon B, Levy C, Bousser MG (1998) Internal carotid artery dissection: an update. J Neurol Sci 153:146–158

Hacke W, Brott T, Caplan L et al. (1999) Thrombolysis in acute ischemic stroke: controlled trials and clinical experience. Neurology 53:S3–14

Hacke W, Donnan G, Fieschi C et al. (2004) Association of outcome with early stroke treatment: pooled analysis of ATLANTIS, ECASS, and NINDS rt-PA stroke trials. Lancet 363:768–774

Hartkamp MJ, van Der GJ, van Everdingen KJ et al. (1999) Circle of Willis collateral flow investigated by magnetic resonance angiography. Stroke 30:2671–2678

Hayes CE, Mathis CM, Yuan C (1996) Surface coil phased arrays for high-resolution imaging of the carotid arteries. J Magn Reson Imaging 6:109–112

Heiserman JE, Drayer BP, Fram EK et al. (1992) MR angiography of cervical fibromuscular dysplasia. AJNR Am J Neuroradiol 13:1454–1457

Hertel F, Walter C, Bettag M et al. (2005) Perfusion-weighted magnetic resonance imaging in patients with vasospasm: a useful new tool in the management of patients with subarachnoid hemorrhage. Neurosurgery 56:28–35

Hoksbergen AW, Majoie CB, Hulsmans FJ et al. (2003) Assessment of the collateral function of the circle of Willis: three-dimensional time-of-flight MR angiography compared with transcranial color-coded duplex sonography. AJNR Am J Neuroradiol 24:456–462

Hurst RW (1996) Angiography of non-atherosclerotic occlusive cerebrovascular disease. Neuroimaging Clin N Am 6:651–678

Krings T, Hans F (2004) New developments in MRA: time-resolved MRA. Neuroradiology 46 Suppl 2:s214–s222

Laub GA, Kaiser WA (1988) MR angiography with gradient motion refocusing. J Comput Assist Tomogr 12:377–382

Leclerc X, Nicol L, Gauvrit JY et al. (2000) Contrast-enhanced MR angiography of supraaortic vessels: the effect of voxel size on image quality. AJNR Am J Neuroradiol 21:1021–1027

Levy C, Laissy JP, Raveau V et al. (1994) Carotid and vertebral artery dissections: three-dimensional time-of-flight MR angiography and MR imaging versus conventional angiography. Radiology 190:97–103

Link J, Steffens JC, Muller-Hulsbeck S et al. (1996) [MR angiography in fibromuscular dysplasia of the cervical arteries]. Röfo 164:201–205

Liu Y, Karonen JO, Vanninen RL et al. (2004) Acute ischemic stroke: predictive value of 2D phase-contrast MR angiography–serial study with combined diffusion and perfusion MR imaging. Radiology 231:517–527

Lucas C, Leclerc X, Pruvo JP et al. (2000) [Vertebral artery dissections: follow-up with magnetic resonance angiography and injection of gadolinium]. Rev Neurol (Paris) 156:1096–1105

Mettinger KL, Ericson K (1982) Fibromuscular dysplasia and the brain. I. Observations on angiographic, clinical and genetic characteristics. Stroke 13:46–52

Oelerich M, Lentschig MG, Zunker P et al. (1998) Intracranial vascular stenosis and occlusion: comparison of 3D time-of-flight and 3D phase-contrast MR angiography. Neuroradiology 40:567–573

Oelerich M, Stogbauer F, Kurlemann G et al. (1999) Craniocervical artery dissection: MR imaging and MR angiographic findings. Eur Radiol 9:1385–1391

Osborn AG, Anderson RE (1977) Angiographic spectrum of cervical and intracranial fibromuscular dysplasia. Stroke 8:617–626

Ozsarlak O, Van Goethem JW, Maes M et al. (2004) MR angiography of the intracranial vessels: technical aspects and clinical applications. Neuroradiology 46:955–972

Pipe JG (2001) Limits of time-of-flight magnetic resonance angiography. Top Magn Reson Imaging 12:163–174

Rasanen HT, Manninen HI, Vanninen RL et al. (1999) Mild carotid artery atherosclerosis: assessment by 3-dimensional time-of-flight magnetic resonance angiography, with reference to intravascular ultrasound imaging and contrast angiography. Stroke 30:827–833

Remonda L, Senn P, Barth A et al. (2002) Contrast-enhanced 3D MR angiography of the carotid artery: comparison with conventional digital subtraction angiography. AJNR Am J Neuroradiol 23:213–219

Scarabino T, Carriero A, Magarelli N et al. (1998) MR angiography in carotid stenosis: a comparison of three techniques. Eur J Radiol 28:117–125

Schellinger PD, Chalela JA, Kang DW et al. (2005) Diagnostic and prognostic value of early MR Imaging vessel signs in hyperacute stroke patients imaged <3 hours and treated with recombinant tissue plasminogen activator. AJNR Am J Neuroradiol 26:618–624

Schievink WI, Puumala MR, Meyer FB et al. (1996) Giant intracranial aneurysm and fibromuscular dysplasia in an adolescent with alpha 1-antitrypsin deficiency. J Neurosurg 85:503–506

Sherman D (2002) Long-term Anticoagulation Therapy in Prevention of Stroke. Curr Treat Options Neurol 4:411–416

Steele SR, Martin MJ, Mullenix PS et al. (2004) Focused high-risk population screening for carotid arterial stenosis after radiation therapy for head and neck cancer. Am J Surg 187:594–598

Stehling MK, Niedermeyer M, Laub G (1997) [Contrast medium enhanced magnetic resonance angiography. Theory, technique and practical implementation]. Radiologe 37:501–507

Sundgren PC, Sunden P, Lindgren A et al. (2002) Carotid artery stenosis: contrast-enhanced MR angiography with two different scan times compared with digital subtraction angiography. Neuroradiology 44:592–599

Teng MM, Tsai F, Liou AJ et al. (2004) Three-dimensional contrast-enhanced magnetic resonance angiography of carotid artery after stenting. J Neuroimaging 14:336–341

Tintera J, Gawehn J, Bauermann T et al. (2004) New partially parallel acquisition technique in cerebral imaging: preliminary findings. Eur Radiol 14:2273–2281

Tomsick T, Brott T, Barsan W et al. (1996) Prognostic value of the hyperdense middle cerebral artery sign and stroke scale score before ultraearly thrombolytic therapy. AJNR Am J Neuroradiol 17:79–85

Trivedi RA, King-Im JM, Graves MJ et al. (2004) Noninvasive imaging of carotid plaque inflammation. Neurology 63:187–188

Uchino A, Sawada A, Takase Y et al. (2003) Variations of the superior cerebellar artery: MR angiographic demonstration. Radiat Med 21:235–238

Ueda T, Shimizu H, Aeba R et al. (1999) Prognosis of Marfan and non-Marfan patients with cystic medial necrosis of the aorta. Jpn J Thorac Cardiovasc Surg 47:73–78

van Bemmel CM, Wink O, Verdonck B et al. (2003) Blood pool contrast-enhanced MRA: improved arterial visualization in the steady state. IEEE Trans Med Imaging 22:645–652

van de Perre S, Vanhoenacker FM, Van Breusegem L et al. (2004) Congenital agenesis of the internal carotid artery. JBR -BTR 87:258

von Kummer R, Holle R, Gizyska U et al. (1996) Interobserver agreement in assessing early CT signs of middle cerebral artery infarction. AJNR Am J Neuroradiol 17:1743–1748

Wetzel S, Bongartz G (1999) MR angiography: supra-aortic vessels. Eur Radiol 9:1277–1284

Wetzel SG, Haselhorst R, Bilecen D et al. (2001) Preliminary experience with dynamic MR projection angiography in the evaluation of cervicocranial steno-occlusive disease. Eur Radiol 11:295–302

Wiesmann M, Yousry I, Seelos KC et al. (2001) Identification and anatomic description of the anterior choroidal artery by use of 3D-TOF source and 3D-CISS MR imaging. AJNR Am J Neuroradiol 22:305–310

Willig DS, Turski PA, Frayne R et al. (1998) Contrast-enhanced 3D MR DSA of the carotid artery bifurcation: preliminary study of comparison with unenhanced 2D and 3D time-of-flight MR angiography. Radiology 208:447–451

Younger DS (2004) Vasculitis of the nervous system. Curr Opin Neurol 17:317–336

Yuan C, Mitsumori LM, Beach KW et al. (2001) Carotid atherosclerotic plaque: noninvasive MR characterization and identification of vulnerable lesions. Radiology 221:285–299

Zimmerman R, Leeds NE, Naidich TP (1977) Carotid-cavernous fistula associated with intracranial fibromuscular dysplasia. Radiology 122:725–726

6 Disturbed Brain Perfusion

Sabine Heiland

CONTENTS

6.1 Introduction

Blood flow in the vascular network, particularly within the capillaries, may be severely disturbed as a result of an occluded cerebral artery, but may also be impaired in case of hemodynamic infarction caused by high grade stenosis of cervical arteries. Up to the early 1990s, it was not possible to determine such changes in cerebral blood flow on the basis of radiological imaging techniques in clinical routine, despite the fact that Axel had developed a technique in 1980 using iothalamate sodium as contrast agent and computed tomography (CT) for visualization of the contrast agent bolus (Axel 1980; Norman et al. 1981). This method has not become a routine technique before multislice CT was developed, but it has constituted the methodological basis for the development of dynamic susceptibility contrast-enhanced (DSC) MRI, which is often falsely referred to as perfusion weighted MRI (PWI), but is better designated as MR perfusion imaging (PI).

S. Heiland, PhD
Division of Experimental Neuroradiology, Department of Neuroradiology, Ruprecht-Karls University of Heidelberg, Im Neuenheimer Feld 400, 69120 Heidelberg, Germany

6.2 Perfusion Measurements with the Dynamic Susceptibility Contrast-Enhanced Method

After the advent of MR systems with powerful gradient hardware, dynamic scans with a repetition rate of at least one image or image stack per 2 s have become possible. By use of such sequences it has become feasible to visualize the transit of a bolus of paramagnetic or superparamagnetic contrast agent through the brain (Moseley et al. 1990; Rosen et al. 1990). For DSC, the bolus is injected intravenously.

In contrast to conventional MR imaging, the contrast agent is not visualized on the basis of the T1 signal change, because the signal alteration in T1-weighted images is rather small in brain tissue with intact blood–brain barrier (BBB). This is due to the fact that T1 relaxation of water molecules is only changed, if a contrast agent molecule is present in the immediate vicinity. This means that water molecules in the extravascular compartment do not "see" the contrast agents in the case of intact BBB; only intravascular water molecules, which are about 3%–5% of the total tissue water, contribute to the T1 signal change.

A much larger signal change can be observed during contrast agent passage, if T2*-weighted (T2*w) sequences are used. The concentration difference between intravascular and extravascular contrast agent ($conc_{intr} > 0$, $conc_{extr} = 0$ for intact BBB) leads to local magnetic field gradients, which in turn results in a decrease of T2* signal. Therefore, in T2w sequences a distinct signal drop can be seen during bolus passage through the capillaries (Fisel et al. 1991).

The signal decrease in brain tissue largely depends on the perfused cerebral blood volume: The signal drop in gray matter (GM) exceeds that of white matter (WM). Therefore WM is hyperintense relatively to GM on the image data set acquired during the bolus maximum (Fig. 6.1). In ischemic tissue, where only a small amount of contrast agent passes the capillaries, the signal intensity during bolus maximum passage is even brighter than normally perfused WM. If perfusion has dropped completely, the signal during bolus passage equals the pre-contrast signal (Fig. 6.2).

6.3 Sequences for Dynamic Susceptibility Contrast-Enhanced Imaging

For PI, basically all fast and strongly T2*w sequences can be used. In the early days of PI, measurements were performed using fast, T2*w gradient-echo sequences, particularly the fast low angle shot (FLASH) sequences. A small flip angle should be chosen (10–20°) to reduce flow effects. Furthermore, echo time (TE) should exceed 20 ms to ensure strong T2*-weighting, whereas repetition time (TR) should not exceed 30 ms to enable a high image repetition rate. This sequence type, however, has the disadvantage, that with a required minimum image repetition rate of one image per 2 s it is limited to the acquisition of one slice only; even in-plane resolution has to be reduced to meet the demands of high time resolution.

Nowadays, echo planar imaging (EPI) sequences are widely used for DSC imaging. The general advantage of this sequence type over FLASH sequences is their ability to acquire multi-slice datasets within the required time resolution. They do, however, require an advanced gradient hardware with a maximum gradient of > 25 mT/m and a slew rate of > 50 mT/m/ms. There are basically two types of EPI sequences using different RF excitation schemes: gradient-echo EPI sequences and spin-echo EPI sequences. Gradient-echo EPI sequences are strongly T2*-weighted and therefore produce the highest signal drop for a

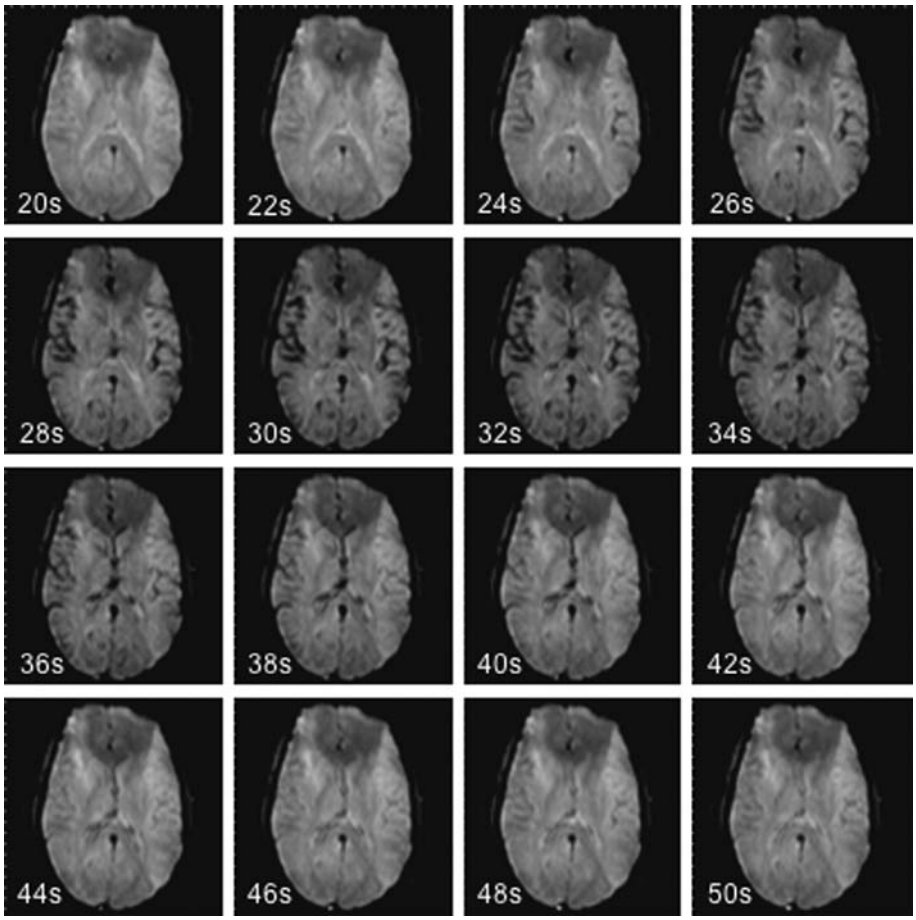

Fig. 6.1. Source images of a dynamic susceptibility contrast-enhanced series in a healthy volunteer, acquired 20–50 s after bolus injection: during the bolus passage the signal decrease in gray matter is more prominent than that in white matter. After the bolus passage, the signal returns to normal

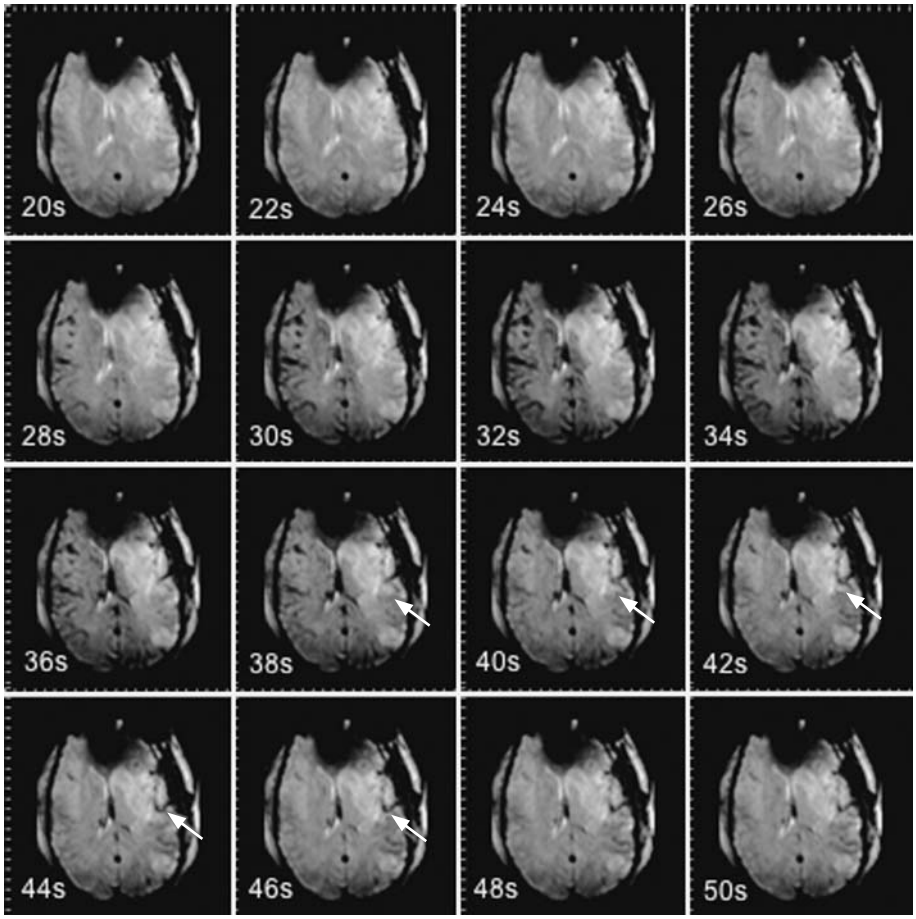

Fig. 6.2. Source images of a dynamic susceptibility contrast-enhanced series in a patient with focal cerebral ischemia, acquired 20–50 s after bolus injection: within the ischemic territory in the left hemisphere the signal decreases later and less than in the normal tissue (*arrows*)

given contrast agent concentration within the vessels (Heiland et al. 1998). This sequence type, however, is sensitive to contrast agent in both capillaries and larger vessels. The T2*-weighting of spin-echo EPI sequences is less than that of gradient-echo EPI sequences; spin-echo EPI sequences are predominantly T2-weighted. The signal-time course therefore shows a much smaller signal drop compared to that of gradient-echo EPI; this signal drop is, however, largely related to contrast agent molecules in capillaries, whereas contrast agent in larger vessels produces much less signal changes (Speck et al. 2000). Therefore spin-echo EPI sequences are well suited to study perfusion selectively in capillaries. The TR of EPI sequences equals the time resolution of the dynamic scan and should not exceed 2 s. To ensure a high sensitivity for the contrast agent and a reasonable signal-noise ratio (SNR) echo time should be chosen between 50 and 70 ms in case of gradient-echo EPI, whereas for spin-echo EPI it should be slightly longer (70–100 ms) (Boxerman et al. 1997).

6.4 Postprocessing of Dynamic Susceptibility Contrast-Enhanced Data

The visual analysis of the dynamic signal change gives the radiologist initial information about the existence of focal alterations in cerebral perfusion; tissue with very low or no perfusion, in particular, can be well distinguished from normal tissue. If one needs more detailed information about the cerebrovascular parameters, however, some mathematical operations need to be done. At first, from the signal-time-course – either determined in a user-defined region of interest (ROI) or on a pixel-by-pixel basis (Fig. 6.3) – the time course of the (relative) contrast agent concentration is calculated by

$$C(t) \propto -\ln\frac{S(t)}{S_0},$$

where C(t) is the relative concentration of the contrast agent within the ROI or the respective voxel, S(t) is the signal intensity and S_0 is the mean signal

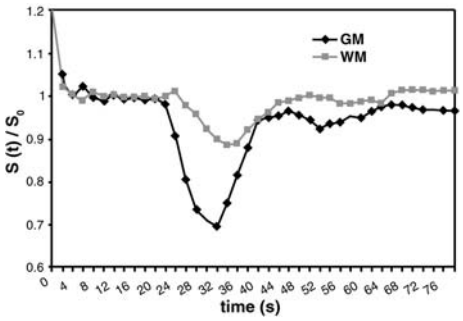

Fig. 6.3. Signal-time course in normally perfused gray and white matter: The signal drop of gray matter is larger than that of white matter

intensity before the bolus appears within the region of interest. This equation has been proposed by numerical simulation (Fisel et al. 1991) and verified by in vivo measurements (Rosen et al. 1990).

In the concentration time curve the first pass of the bolus appears after the pre-contrast baseline (Fig. 6.4a). After the first pass, concentration does not return to zero, but remains increased (Fig. 6.4b). This effect is due to contrast agent molecules remaining within the capillary network and to second pass effects. One way to avoid these effects is to fit a gamma-variate function to the measured values of contrast agent concentration (Belliveau et al. 1991; Thompson et al. 1964) (Fig. 6.4c):

$$C_T(t) = \begin{cases} A\,(t - T_A)^B\, e^{-D(t-T_A)}, & t \geq t_0 \\ 0, & t < t_0 \end{cases}$$

The parameters A, B, D and T_A are determined using a least squares fitting procedure. While A, B, and D are phenomenological parameters, T_A equals the so-called time to arrival which is the time between contrast agent injection and appearance of the first contrast agent molecules within the ROI.

Some MR manufacturers use numerical algorithms to process the concentration-time curves. In such algorithms, user interaction is mandatory for definition of the end of the first pass. The numerical algorithms, however, are much faster than algorithms based on curve fitting, because they avoid the time-consuming non-linear fitting procedure.

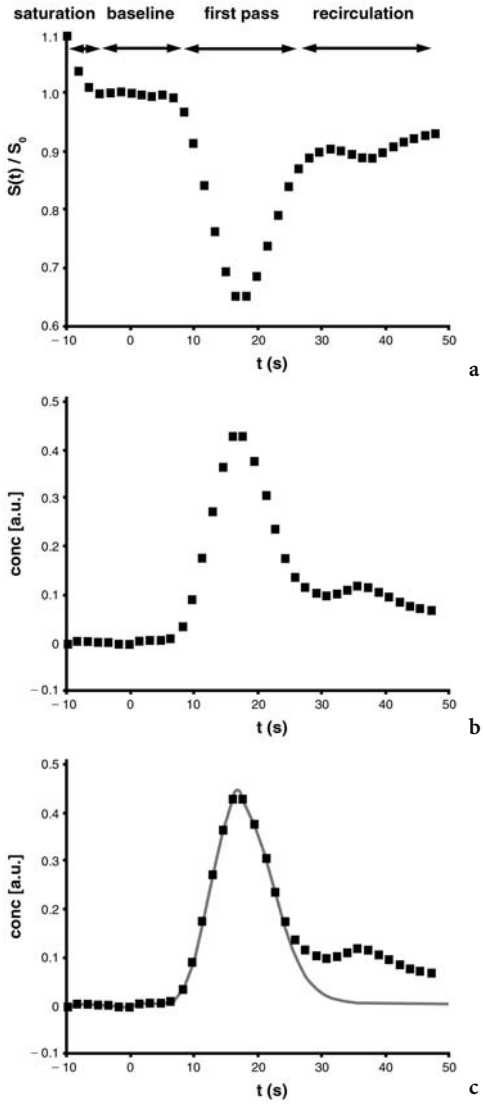

Fig. 6.4a–c. Postprocessing of the signal-time curve. **a** The baseline is determined from the signal before bolus arrival. During first pass, there is a sharp signal decrease. The first pass is often followed by a second pass, with a signal decrease that is less steep than in the first pass. **b** From the signal-time curve, the time course of the relative contrast agent concentration is calculated. **c** A gamma variate function is fitted to the curve to avoid effects of persistent contrast agent and of the second pass

6.4.1 Semiquantitative Parameters

From the time course of relative contrast agent concentration several cerebrovascular parameters can be calculated. They reflect different physiological parameters and make it possible to diagnose and monitor pathophysiological processes. Figure 6.5 visualizes how these parameters are calculated from the concentration-time curve.

Indicator-dilution theory (Axel 1980; Rosen et al. 1989) leads to the formula for calculation of the relative regional cerebral blood volume (rrCBV)

$$rrCBV = \int_{T_A}^{T_{FP}} C_T(t)\,dt$$

and $$rrCBV = \int_0^{\infty} C_T(t)\,dt = \frac{A}{D^{B+1}} \cdot \Gamma(B+1)$$

when using the numerical algorithm and the curve fitting algorithm, respectively. T_{FP} is the interactively determined end-point of the first pass. A, B, and D are the fitting parameters of the gamma variate function Γ.

A second, very important parameter is the normalized first momentum of the concentration time curve, which corresponds to the relative mean transit time (rMTT). This parameter is defined by

$$rMTT = \frac{\int_{T_A}^{T_{FP}} t \cdot C_T(t)\,dt}{\int_{T_A}^{T_{FP}} C_T(t)\,dt}$$

and

$$rMTT = \frac{\int_0^{\infty} t \cdot C_T(t)\,dt}{\int_0^{\infty} C_T(t)\,dt} = \frac{B+1}{D} + T_A$$

when using the numerical algorithm and the curve fitting algorithm, respectively (Thompson et al. 1964).

Parallel to rMTT, the parameter time to peak (TTP) is widely used:

$$TTP = T_{max} - T_{KM}.$$

T_{max} is the time-point when the bolus maximum passes the region of interest, while T_{KM} is the time-point of contrast agent injection.

Furthermore, the time to arrival (TTA) can be calculated as time difference between appearance of the first contrast agent molecules in the tissue of interest and contrast agent injection. When using the curve fitting method, TTA equals T_A.

Although the cerebral blood flow (CBF) is defined as

$$CBF = \frac{CBV}{MTT},$$

assuming that the bolus is an ideal δ-shaped function, the relative regional cerebral blood flow

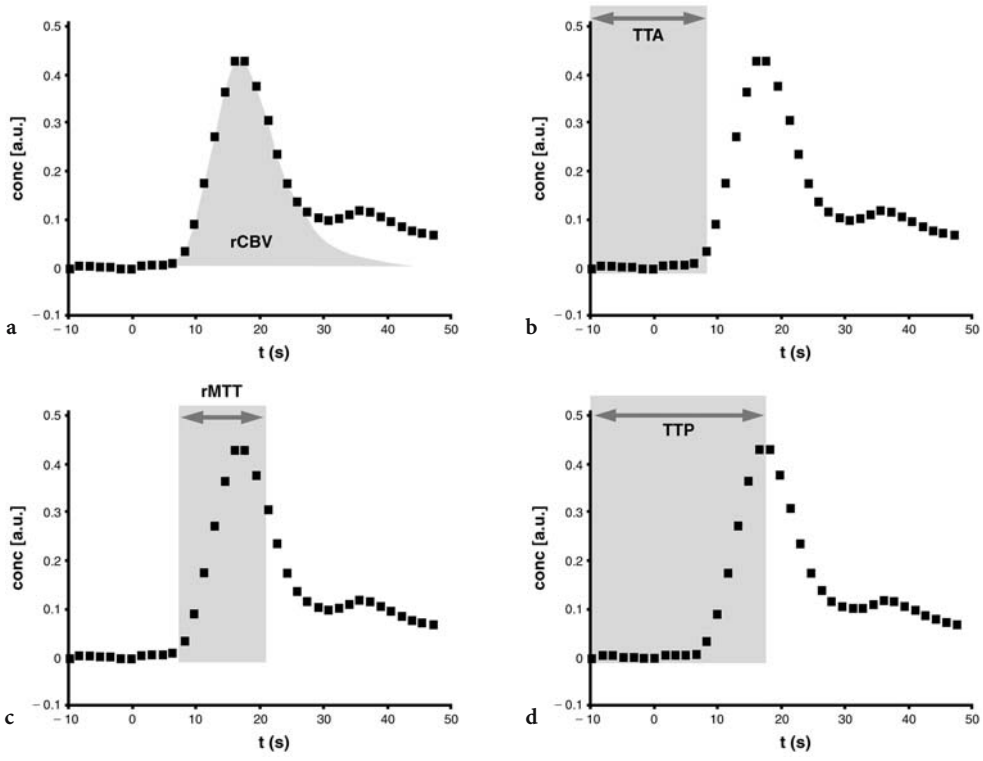

Fig. 6.5a–d. Various cerebrovascular parameters can be calculated from the concentration-time curve. **a** *rrCBV* is defined as the area under the concentration-time curve. **b** *TTA* is the time between contrast agent injection and arrival of the first contrast agent molecules within the region of interest. **c** *rMTT* is the first momentum of the curve. **d** *TTP* is the time between contrast agent injection and the maximum contrast agent concentration within the region of interest

(rrCBF) cannot be calculated on the basis of rMTT and rrCBV as shown by Weisskoff et al. (1993). This is because rMTT is contaminated by the bolus dispersion on its way between injection site and brain. The parameter rMTT, however, yields indirect information about the change of blood flow: An increase in rMTT indicates that CBF has decreased.

6.4.2 Quantification

The parameters mentioned above are only semi-quantitative values, i.e. focal changes of these parameters can be depicted by comparing the parameters within the lesion to those in normal tissue. If one is interested in quantitative values, knowledge about the arterial input function (AIF) is mandatory. When using gradient echo sequences for DSC imaging, measurement of the AIF needs a special sequence design, because two slices must be acquired simultaneously: one within the interesting tissue and one on the level of major feeding vessels (Perman et al. 1992; Rempp et al. 1994). If DSC imaging is performed with EPI sequences, one does not need to acquire additional slices to determine AIF, because normally the stack of slices contains several major feeding vessels. The AIF can be measured both in the carotid arteries and the middle cerebral arteries. Although it has been shown to be advantageous to determine the AIF within the carotid arteries (Scholdei et al. 1999), it has turned out that it is more convenient to use the middle cerebral arteries for AIF determination, because the image data mostly contain these vessels.

Voxels that represent the AIF must meet the following conditions: (a) The maximum signal drop is larger, (b) the TTA is shorter, and (c) the rMTT is lower than that of normal brain tissue (Fig. 6.6). Furthermore only voxels in the vicinity of the feeding vessels are considered, whereas voxels within the feeding vessels suffer from pulsation artifacts and therefore cannot contribute to the calculation of AIF.

When the AIF and the concentration time curve within the tissue are determined, quantitative values of the cerebrovascular parameters can be calculated by deconvolution under consideration of the relationship:

$$C(t)=\frac{\rho}{k_H}\cdot CBF\cdot\left(AIF(t)\otimes R(t)\right)$$

where ρ is the density of brain tissue, k_H is a parameter that accounts for the hematocrit difference between large vessels and capillaries, CBF is the cerebral blood flow and R(t) is the residue function. For deconvolution, several methods have been used, but the singular value decomposition (SVD) has turned out to be the most reliable method (Ostergaard et al. 1996a,b).

Although it would be methodologically correct to determine the AIF of all major feeding arteries and to use these AIFs separately for deconvolution of the concentration time curves measured in their respective territory, this is not done in clinical routine due to practicability reasons. This, however, leads to systematical errors in patients with pathologies of the feeding arteries, e.g. unilateral high grade stenoses: Because both MTT and CBF are influenced by a potential delay of the AIF (Calamante et al. 2000), the CBF of the ipsilateral tissue may be underestimated by more than 50% and MTT may be overestimated, if the AIF is determined on the contralateral hemisphere (Lythgoe et al. 2000; Calamante et al. 2002). Determination of the AIF on the ipsilateral side leads to correct CBF and MTT values of the ipsilateral hemisphere, but this in turn produces systematic errors on the contralateral side. Also other factors, as partial volume effects and the orientation of the vessel, that is used for AIF determination, with respect to the magnetic field, lead to systematic errors in quantification (Boxerman et al. 1995; van Osch et al. 2001). Although some work has been done to correct for these errors, it is important to be aware of the limitations of the methods used for quantification; otherwise over-interpretation or misinterpretation might be the result.

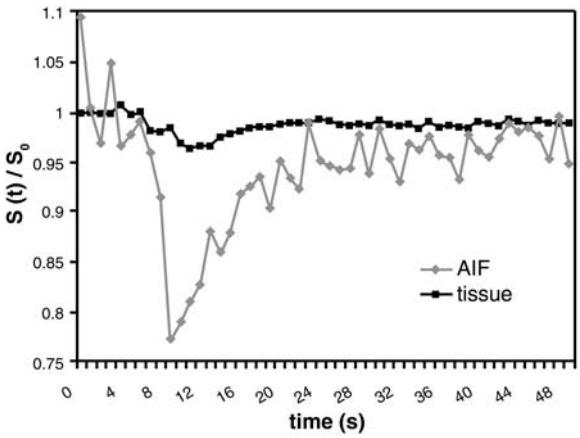

Fig. 6.6. Signal-time curves determined in normal tissue and in the feeding arteries (*AIF*). The signal drop in the arteries is much larger than in tissue

6.5 Diagnosis of Cerebrovascular Diseases with DSC

In most cerebrovascular diseases, the semiquantitative Parameters MTT, TTP, TTA and rrCBV provide important diagnostic information for prognosis and decision about therapy.

Even shortly after artery occlusion, the territory supplied by the respective artery can be defined by means of the change in rMTT and TTP, respectively. Both rMTT and TTP are increased significantly due to the decline of CBF (Heiland and Sartor 1999; Schellinger et al. 2000b) (Fig. 6.7). Patient studies have shown that rMTT is an important parameter for prognosis of the lesion growth: If recanalization therapy is not performed or is not successful, the infarction is likely to comprise the whole volume of initial hypoperfusion (Baird et al. 1997). In the very early phase of ischemia, the volume of hypoperfused tissue often exceeds the volume of the ischemic core, where tissue injury is irreversible. The latter can roughly be delineated by diffusion-weighted MRI (DWI) (Moseley et al. 1990; Schellinger et al. 2001, see Chap. 7). This has lead to the "mismatch-concept": The decision, whether or not a thrombolytic therapy is applied in a patient, depends on the size of the tissue volume, that is hypoperfused, but not yet irreversibly damaged (Jansen et al. 1999): presumably, only patients with a perfusion-diffusion mismatch are likely to benefit from recanalization (Marks et al. 1999; Schellinger et al. 2001, see Chap. 3). For follow-up examinations, rMTT and TTP are also well suited to assess whether reperfusion has occurred (Schellinger et al. 2000a). Even if magnetic resonance angiography (MRA) shows re-opening of the artery, this does not necessarily mean that the whole territory supplied by this artery is reperfused. Depending on occlusion time and collateralization, the lumen of the capillaries might be blocked due to endothelial cell swelling after a longer period of ischemia (Reith et al. 1995; Kempski and Behmanesh 1997). Some groups have studied whether there is a threshold for TTP and rMTT in order to depict the ischemic lesion in patients with hyperacute stroke. Neumann-Haefelin et al. (1999) have found that the area showing a TTP delay of ≥ 6 s compared to the contra-lateral hemisphere corresponds well to the infarcted tissue volume in follow-up scans, if the patient is not treated (Neumann-Haefelin et al. 1999). Although this method has worked well in the patients examined by Neumann-Haefelin et al. (1999), there is a major methodological concern with regard to this method: TTP and rMTT are only semiquantitative parameters and they depend strongly on the circulation parameters (e.g., pulse rate, cardiac output) and on the injection rate as well as the contrast agent dosage. Even if injection rate and contrast agent dosage is kept constant, the interindividual variability of the circulation parameters does not support the approach to use an absolute threshold. Additional to the interindividual variations, the change in rMTT after artery occlusion or high grade stenosis is different for gray and white matter (Kluytmans et al. 1998). This again leads to systematic errors in the method of Neumann-Haefelin et al. (1999).

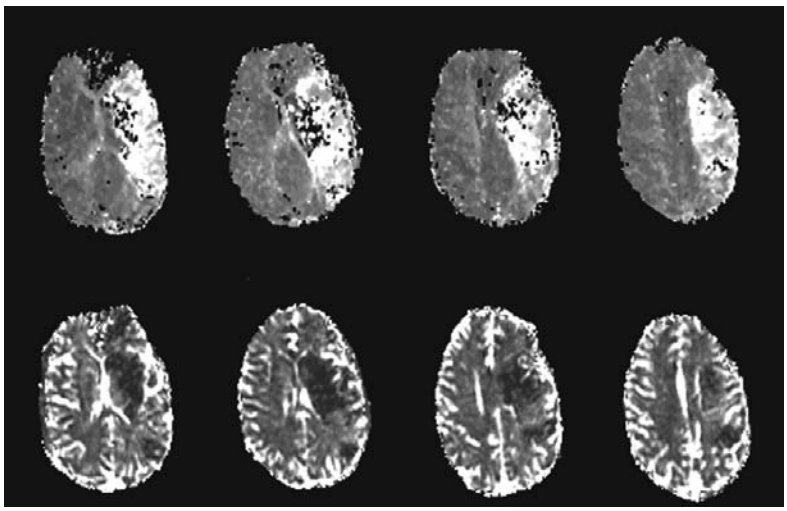

Fig. 6.7. Maps of rMTT (*upper row*) and rrCBV (*lower row*) in a patient with occlusion of the left middle cerebral artery. The territory with decreased CBV is smaller than the territory with increased MTT. In the periphery of the infarction core, CBV is slightly increased. This is due to compensatory vasodilatation as a response to the decreased perfusion pressure

While rMTT can depict changes in cerebral hemodynamics, which are due to vessel occlusion of cerebral arteries and the respective compensation mechanisms, the time to arrival of contrast (TTA) is sensitive to vessel diseases, which are more upstream of the arterial flow, most commonly high grade stenoses or occlusions of the carotid arteries. In such patients, blood flow in the hemisphere ipsilateral to the stenosis is mainly supplied by the contralateral carotid artery via the circle of Willis. Due to this detour, TTA is prolonged in the ipsilateral hemisphere (Reith et al. 1997). At the same time, rMTT may be prolonged in the ipsilateral hemisphere resulting from decreased blood flow (Dörfler et al. 2001). If TTP is calculated instead of MTT, the effect of the bolus delay cannot be separated from that of the perfusion decrease, because TTP is influenced by both rMTT and TTA.

Studies in animals have shown, that rrCBV within the ischemic core decreases immediately after occlusion and is likely to raise to values above the baseline, if early reperfusion is achieved (Hamberg et al. 1994). Studies in patients have shown, however, that rrCBV does not depict the ischemic lesion reliably (Tong et al. 1998). Particularly in very small ischemic lesions ($< 1\ cm^3$) the map of rrCBV does not show distinct signal changes (Flacke et al. 1998). In tissue with increased rMTT or TTP, particularly within the penumbra, rrCBV is likely to increase due to compensatory vasodilatation as a response to the decreased perfusion pressure (Tsuchida et al. 1997) (Figs. 6.7, 6.8).

CBV of the ischemic penumbra and of reperfused tissue might be overestimated by PI, particularly in measurements after successful reperfusion. One possible explanation is the fact that the gadolinium chelates that are normally used for DSC are so small, that they can passage through a capillary, even if corpuscular blood flow is no longer possible due to endothelial cell swelling (Reith et al. 1995). This shows that rrCBV measured by DSC represents the vasculature, where the plasma flow is restored or is still possible. Another potential source of systematic errors is the fact, that gradient-echo EPI sequences, which are widely used for DSC in the clinical setting, do not only measure the blood volume within the capillaries, but also in the larger vessels. On CBV maps, high values that arise from larger arteries and arterioles may mask a CBV deficit in adjacent capillaries that is due to endothelial cell swelling.

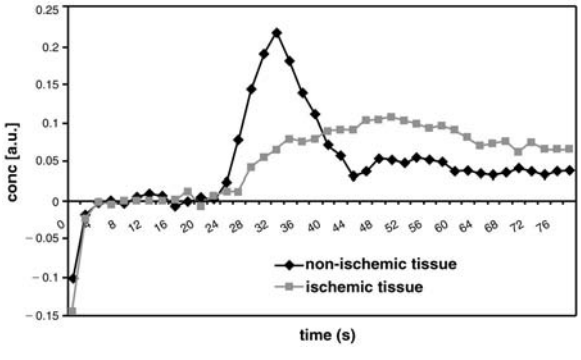

Fig. 6.8. Time course of the contrast agent concentration determined in non-ischemic tissue and in ischemic tissue (penumbra). The maximum concentration in the ischemic tissue is significantly lower than that in normal tissue, and the peak is delayed. The area under the curve of the ischemic tissue is larger than that of the normal tissue, being a sign of the increased CBV within the penumbra

Quantification is not necessarily needed for the diagnosis of acute stroke, because the decision whether or not the patient should be treated can be made on the basis of the volume with prolonged rMTT or TTP (Fig. 6.7). Animal studies suggested, however, that the amount of perfusion deficit correlates with the cellular damage. Vexler et al. (1997) have compared PI and histology and found that the perfusion deficit correlates with the number of the apoptosis-positive cells during occlusion. Patient studies have shown that quantitative parameters, particularly CBF, help to predict infarction growth in hyperacute stroke and to select the patients who will profit from therapy (Smith et al. 2000a; Grandin et al. 2001, 2002; Rose et al. 2001). Grandin et al. (2001) examined patients with acute stroke and compared CBF and CBV values in different regions that were defined on the basis of follow-up examinations: the area of the initial infarction core, the area of infarction growth, the area with disturbed perfusion that remained viable and the contralateral healthy tissue. They found that the CBF in the area of infarction growth [CBF=36±20 ml/(min·100 g)] was significantly lower than CBF in the tissue with transiently perfusion disturbance [CBF=50±17 ml/(min·100 g)]. Additionally they found that CBV in the infarction growth region (CBV=8.9±3.1%) was lower than in the oligemic tissue (CBV=11.2±3.0%). Compared to this, CBF and CBV in the initial infarction core were significantly lower (CBF=28±16 ml/(min·100 g); CBV=6.9±2.7%). From these observations they propose using a multiparametric analysis with thresholds of CBF_{thres}=35 ml/(min·100 g) and CBV_{thres}=8.2% to predict the evolution of infarction (Grandin et al. 2001). Based on another patient study, Fiehler et al. (2002) found that the presence of a tissue volume 50 mL with a CBF value 12 mL/100 g per minute (50 mL CBF_{12}) was predictive for further lesion enlargement in acute stroke

patients. (Fiehler et al. 2002). Other groups found the best sensitivity and accuracy by definition of thresholds based on ratios of CBF and CBV relative to the contralateral hemisphere (Rose et al. 2001), based on ratios of CBF and MTT (Rohl et al. 2001; Butcher et al. 2003), and based on the peak contrast agent concentration and TTP (Grandin et al. 2002). The contradictory results of these studies show that there is up to now no reliable, site-independent procedure for prediction of infarction growth by using quantitative perfusion parameters. The reason for the huge differences between the results of these studies might be the different methods used for data acquisition and post-processing. This in turn shows that CBF, CBV and MTT measured by PI are not really 'quantitative' parameters in the way of site-, operator- and method-independent parameters that do exactly correlate to the physiological parameters. CBV for example is influenced by the sequence used for DSC imaging and by the post-processing method: if a gradient-echo EPI sequence is used, not only the capillary network, but also the feeding and draining vessels contribute to the measured CBV, whereas spin-echo EPI sequences comprise only the volume of the capillaries (Speck et al. 2000). Therefore CBV and CBF measured with gradient-echo EPI will in general overestimate the capillary CBV dramatically by a factor 2 to 3 (Simonsen et al. 2000); the degree of this overestimation, however, is not constant but is highest in the vicinity of larger vessels, and is low in the territory of an occluded artery.

Also the method used for post-processing can influence the CBV: The reliability and stability of the results depend among other things on the fact, whether or not curve fitting is used to fit the concentration time curve of tissue and arterial input function (Smith et al. 2000b). As long as there is no universally accepted procedure for PI measurement and post-processing, all thresholds for prediction of infarction growth will therefore be of very limited value, because these thresholds can only be used in the very exact hardware and software setting as used for the respective study.

6.6 Practical Issues for DSC Imaging

In order to obtain reliable results, data acquisition and post-processing needs to be performed in consideration of methodological and technical constraints. Simulation studies based on signal-time curves of patient examinations have shown that there is a variety of factors that influence the quality and significance of the cerebrovascular parameters such as dosage and concentration of the contrast agent, sequence type and time resolution, and the post-processing method used (Smith et al. 2000b; Benner et al. 1997).

6.6.1 Contrast Agent

One of the most important factors influencing the reliability of the estimated cerebrovascular parameters is the maximum signal drop during bolus passage through the capillaries. Benner et al. (1997) have shown that the maximum signal drop should be at least 20%. The signal drop depends on the contrast agent concentration within a voxel, which in turn is influenced by dosage and concentration of the injected contrast agent as well as by the injection rate. Among these factors, the most important is the contrast agent dosage (Heiland et al. 2001).

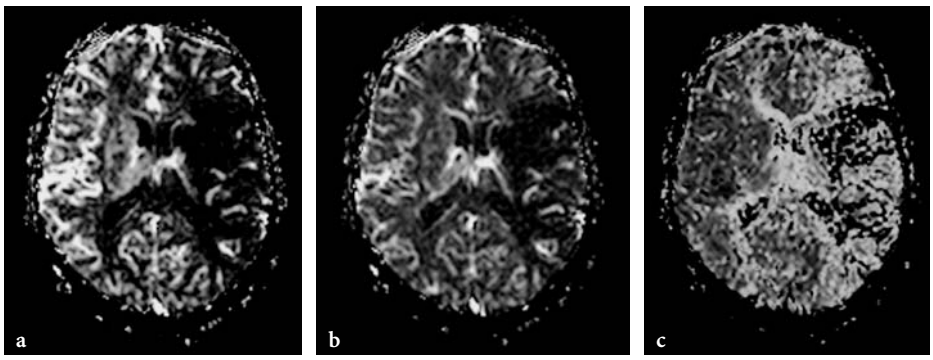

Fig. 6.9a–c. Maps of (**a**) CBF, (**b**) CBV and (**c**) MTT of a patient with an occlusion of the left middle cerebral artery. The maps were calculated based on both the tissue concentration-time curve and the AIF

It is, however, impossible to make a recommendation that is universally valid. This is because the optimum contrast agent dosage depends on other factors such as the field strength and the T2*-weighting of the sequence. There are several dose finding patient studies performed at 1T with FLASH sequences. The low field strength and the fact that the echo time and hence the T2*-sensitivity of this sequence type is limited, are the reason for the optimum contrast agent dosage being 0.3 mmol/kg bodyweight (Erb et al. 1997; Benner et al. 2000). Nowadays, the most common setting to perform PI is to use gradient-echo EPI sequences on a 1.5-T scanner; under these circumstances patient examinations are normally performed using 0.1 mmol/kg bodyweight, although a multicenter study has found that 0.2 mmol/kg bodyweight is the optimum dosage (Bruening et al. 2000). If a spin-echo EPI sequence is used instead of a gradient-echo EPI sequence, the contrast agent dosage should be increased to compensate for the lower T2*-sensitivity of the spin-echo EPI sequences (Heiland et al. 1998; Marstrand et al. 2001). In quantitative perfusion measurements it is important to limit the contrast agent dosage, because the signal drop corresponding within or adjacent to the arteries is much higher than that within the tissue. The signal drop in the region used to determine the AIF should not exceed 70% (Benner et al. 1997), because otherwise the linear relationship between contrast agent concentration and logarithmic signal decrease is no longer valid, which in turn leads to systematic errors in the calculated cerebrovascular parameters.

Compared to the effect of the contrast agent dosage, contrast agent concentration has only a minor effect upon maximum signal drop and hence the reliability of PI. It has been shown in animal and patient studies, that measurements performed with a higher concentrated contrast agent lead to a smaller bolus width and a higher maximum contrast agent concentration (Heiland et al. 1997; Tombach et al. 2003). These effects, however, are very small.

For contrast agent injection an MR compatible power injector should be used to ensure a high and reproducible injection rate. Injection rate should be at least 3 ml/s. Injection should be started parallel to the dynamic scan. This ensures a sufficient number of measurements for calculation of the pre-contrast baseline and guarantees that the whole first pass is comprised, if the scans are repeated for at least 1 min.

6.6.2 Time Resolution

Another important factor influencing the reliability of the calculated cerebrovascular parameters is the repetition rate of the dynamic scan. It has been shown by a simulation study, that at least eight measurements have to be performed during the first pass to limit the inaccuracy of the cerebrovascular parameters to less than 10% (Benner et al. 1997). The width of the first pass within the brain tissue ranges from 12 to 20 s; therefore, the image repetition rate should be at least one image (or image stack) per 1.5 s. This in turn restricts the number of slices. If PI is performed to calculate quantitative values, one has to choose an even higher repetition rate, because the width of the AIF is smaller than that of the concentration-time curve in tissue. This leads to an optimum image repetition rate of one image (or image stack) per second. A further increase of the repetition rate is not advisable, because the SNR drops dramatically for TR less than 1 s.

6.6.3 Data Postprocessing

The postprocessing methods described above (nonlinear fitting, numerical integration, quantification by deconvolution algorithms) are time-consuming. Some MR manufacturers provide post-processing algorithms that avoid these time-consuming procedures but do instead need user interaction to define the bolus arrival and the end of the first pass. These methods, however, are highly susceptible to systematic errors by second pass- and re-flow effects. A further disadvantage of these methods is that they yield only phenomenological parameters, which do not have a physiological correlate and are influenced by circulation parameters and sequence parameters. Some studies have shown that maps of phenomenological parameters as the maximum concentration, or the percentage of baseline at peak are well correlated to physiological parameters such as the CBV and yield similar diagnostic results in special applications (Berchtenbreiter et al. 1999; Teng et al. 2001). In general, however, the quantitative, automatic deconvolution methods are superior all other methods, because they are highly sensitive to lesion even in presence of a steno-occlusive disease (Perkio et al. 2002; Yamada et al. 2002). A standardized, fully automated post-processing method is desirable, particularly in evaluating and defin-

ing thresholds for prediction of infarction growth, because only such methods will allow an inter-site comparison of clinical results.

6.7 Perfusion Measurements with Arterial Spin Labeling

DSC is not the only MRI technique that enables perfusion measurement. An alternative technique is arterial spin labeling (ASL). In ASL, the blood is used as an intrinsic contrast agent (Detre et al. 1992, Zhang et al. 1993). Special pre-pulses invert the spins of brain supplying vessels. The labeled spins in the blood cause a change of tissue magnetization and relaxation in the downstream areas, because there is a magnetization exchange between spins in the blood compartment and spins in the tissue compartment even if the BBB is intact. Fast imaging techniques, usually EPI, acquire images of the interesting area in brain tissue. The labeling prepulse does not only cause changes in magnetization of the water spins in blood, but influences the magnetization of the macromolecules within the tissue. Therefore one has to perform a control experiment with a saturation slice that is equidistantly separated from the imaging slice, but does not cover the supplying vessels (Fig. 6.10).

There are two ways to perform arterial spin labeling experiments: The first one is the continuous spin labeling (CASL), where the blood is continuously inverted upstream. Therefore the magnetization within the tissue is in a steady state (Williams et al. 1992). The second class of ASL techniques is pulsed spin labeling (PASL), where a short pulse is used to invert the spins in a thick slab. After the inversion there is a time gap, TI, before the image acquisition of the interesting slices starts. During TI the labeled blood flows to the region of interest and exchanges magnetization with the tissue. In both methods, one can calculate CBF by comparing the magnetization of the control experiment and the magnetization of the experiment, where spin labeling has been performed. However, the calculation methods depend on the labeling scheme.

For both PASL and CASL there is a variety of sequence types, which differ in the pulse scheme used for labeling and in the way the control experiment is performed. Commonly labeling and imaging are performed using the same coil, but there are also techniques using a separate coil for labeling. Due to this diversity of sequence schemes, a large number of acronyms exists for ASL techniques, e.g. FAIR, UNFAIR, EPISTAR, PICORE, QUIPSS (Barbier et al. 2001).

The main advantage of ASL is that it allows measuring CBF quantitatively. There are, however, some methodological problems that lead to systematic errors in CBF at high flow rates (> 80 ml/100 g/min). Particularly the variability of the BBB permeability to water in different species and different pathologies and the subtotal magnetization exchange at high flow rates are factors that limit the accuracy of ASL. Nevertheless, validation studies have shown that low and medium CBF can accurately be determined by ASL (Walsh et al. 1994).

It is of further advantage that ASL does not need any contrast agent. Therefore, ASL measurements can be repeated several times. This makes ASL a useful method for measuring CBF changes during

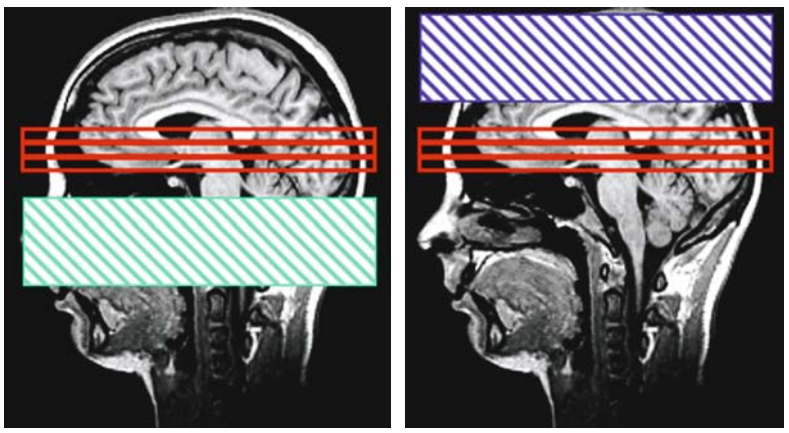

a b

Fig. 6.10a,b. Schematic diagram of an ASL experiment. Labeling experiment (**a**) and control experiment (**b**). The imaged slices are marked in *red*, the inversion slab is marked in *green* for the labeling experiment and in *blue* for the control experiment

Fig. 6.11. CBF map calculated from an ASL experiment in a healthy volunteer. Images were acquired with a CASL sequence (labeling duration: 2.2 s, post-labeling delay 1 s) on a 1.5-T MR scanner

brain activation, for animal studies with repeated perfusion measurements and for pharmacological studies.

The disadvantage of ASL is the low signal change, which in turn results in high statistical errors in CBF and therefore in poor quality of the calculated CBF maps. The use of high-field MR systems may help to overcome this problem: As T1 increases with the magnetic field strength, less relaxation takes place between labeling and imaging. This leads to a higher concentration of labeled spins in the region of interest.

References

Axel L (1980) Cerebral blood flow determination by rapid-sequence computed tomography. Radiology 137:679–686

Baird AE, Benfield A, Schlaug G et al (1997) Enlargement of human cerebral ischemic lesion volumes measured by diffusion-weighted magnetic resonance imaging. Ann Neurol 41:581–589

Barbier EL, Lamalle L, Decorps M (2001) Methodology of brain perfusion imaging. J Magn Reson Imaging 13:496–520

Belliveau JW, Kennedy DN Jr, McKinstry RC et al (1991) Functional mapping of the human visual cortex by magnetic resonance imaging. Science 254:716–719

Benner T, Heiland S, Erb G et al (1997) Accuracy of gamma-variate fits to concentration-time curves from dynamic susceptibility-contrast enhanced MRI: influence of time resolution, maximal signal drop and signal-to-noise. Magn Reson Imaging 15:307–317

Benner T, Reimer P, Erb G et al (2000) Cerebral MR perfusion imaging: first clinical application of a 1 M gadolinium chelate (Gadovist 1.0) in a double-blinded randomized dose-finding study. J Magn Reson Imaging 12:371–380

Berchtenbreiter C, Bruening R, Wu RH et al (1999) Comparison of the diagnostic information in relative cerebral blood volume, maximum concentration, and subtraction signal intensity maps based on magnetic resonance imaging of gliomas. Invest Radiol 34:75–81

Boxerman JL, Hamberg LM, Rosen BR, Weisskoff RM (1995) MR contrast due to intravascular magnetic susceptibility perturbations. Magn Reson Med 34:555–566

Boxerman JL, Rosen BR, Weiskoff RM (1997) Signal-to-noise analysis of cerebral blood volume maps from dynamic NMR imaging studies. J Magn Reson Imaging 7:528–537

Bruening R, Berchtenbreiter C, Holzknecht N et al (2000) Effects of three different doses of a bolus injection of gadodiamide: assessment of regional cerebral blood volume maps in a blinded reader study. AJNR Am J Neuroradiol 21:1603–1610

Butcher K, Parsons M, Baird T et al (2003) Perfusion thresholds in acute stroke thrombolysis. Stroke 34:2159–2164

Calamante F, Gadian DG, Connelly A (2000) Delay and dispersion effects in dynamic susceptibility contrast MRI: simulations using singular value decomposition. Magn Reson Med 44:466–473

Calamante F, Gadian DG, Connelly A (2002) Quantification of perfusion using bolus tracking magnetic resonance imaging in stroke: assumptions, limitations, and potential implications for clinical use. Stroke 33:1146–1151

Detre JA, Leigh JS, Williams DS, Koretsky AP (1992) Perfusion imaging. Magn Res Med 23:37–45

Dörfler A, Eckstein HH, Eichbaum M et al (2001) Perfusion-weighted magnetic resonance imaging in patients with carotid artery disease before and after carotid endarterectomy. J Vasc Surg 34:587–593

Erb G, Benner T, Heiland S et al (1997) Untersuchungen zur Kontrastmitteldosierung bei der perfusionsgewichteten MRT. RÖFO Fortschr Geb Rontgenstr Neuen Bildgeb Verfahr 167:599–604

Fiehler J, von Bezold M, Kucinski T et al (2002) Cerebral blood flow predicts lesion growth in acute stroke patients. Stroke 33:2421–2425

Fisel CR, Ackerman JL, Buxton RB et al (1991) MR contrast due to microscopically heterogeneous magnetic susceptibility: numerical simulations and applications to cerebral physiology. Magn Reson Med 17:336–347

Flacke S, Keller E, Hartmann A et al (1998) Verbesserte Diagnostik des frühen Hirninfarktes durch den kombinierten Einsatz von Diffusions- und Perfusions-Bildgebung. RÖFO Fortschr Geb Rontgenstr Neuen Bildgeb Verfahr 168:493–501

Grandin CB, Duprez TP, Smith AM et al (2001) Usefulness of magnetic resonance-derived quantitative measurements of cerebral blood flow and volume in prediction of infarct growth in hyperacute stroke. Stroke 32:1147–1153

Grandin CB, Duprez TP, Smith AM et al (2002) Which MR-derived perfusion parameters are the best predictors of infarct growth in hyperacute stroke? Comparative study between relative and quantitative measurements. Radiology 223:361–370

Hamberg LM, Macfarlane R, Tasdemiroglu E et al (1994) Measurement of cerebrovascular changes in cats after transient ischemia using dynamic magnetic resonance imaging. Stroke 24:444–450

Heiland S, Sartor K (1999) Magnetresonanztomographie beim Schlaganfall - methodische Grundlagen und klinische Anwendung. RÖFO Fortschr Geb Rontgenstr Neuen Bildgeb Verfahr 171:3–14

Heiland S, Benner T, Reith W et al (1997) Perfusion-weighted MRI using gadobutrol as a contrast agent in a rat stroke model. J Magn Reson Imaging 7:1109–1115

Heiland S, Kreibich W, Reith W et al (1998) Comparison of different EPI-sequence types in perfusion-weighted MR imaging: which one is the best? Neuroradiology 40:216–212

Heiland S, Reith W, Forsting M, Sartor K (2001) How do concentration and dosage of the contrast agent affect the signal change in perfusion-weighted magnetic resonance imaging? A computer simulation. Magn Reson Imaging 19:813–820

Jansen O, Knauth M, Sartor K (1999) Advances in clinical neuroradiology. Akt Neurol 26:1–7

Kempski O, Behmanesh S (1997) Endothelial cell swelling and brain perfusion. J Trauma 42 [Suppl]:38–40

Kluytmans M, van der Grond J, Folkers PJ et al (1998) Differentiation of gray matter and white matter perfusion in patients with unilateral internal carotid artery occlusion. J Magn Reson Imaging 8:767–774

Lythgoe DJ, Ostergaard L, Williams SC et al (2000) Quantitative perfusion imaging in carotid artery stenosis using dynamic susceptibility contrast-enhanced magnetic resonance imaging. Magn Reson Imaging 18:1–11

Marks MP, Tong D, Beaulieu C et al (1999) Evaluation of early reperfusion and IV rt-PA therapy using diffusion- and perfusion-weighted MRI. Neurology 52:1792–1798

Marstrand JR, Rostrup E, Rosenbaum S et al (2001) Cerebral hemodynamic changes measured by gradient-echo or spin-echo bolus tracking and its correlation to changes in ICA blood flow measured by phase-mapping MRI. J Magn Reson Imaging 14:391–400

Moseley ME, Kucharczyk J, Mintorovitch J et al (1990) Diffusion-weighted MR imaging of acute stroke: correlation with T2-weighted and magnetic susceptibility-enhances MR imaging in cats. AJNR Am J Neuoradiol 11:423–429

Neumann-Haefelin T, Wittsack HJ, Wenserski F et al (1999) Diffusion- and perfusion-weighted MRI. The DWI/PWI mismatch region in acute stroke. Stroke 30:1591–1597

Norman D, Axel L, Berninger WL et al (1981) Dynamic computed tomography of the brain: techniques, data analysis, and applications. AJR 136:759–770

Ostergaard L, Weisskoff RM, Chesler DA et al (1996a) High resolution measurement of cerebral blood flow using intravascular tracer bolus passages, part I. Mathematical approach and statistical analysis. Magn Reson Med 36:715–725

Ostergaard L, Sorensen AG, Kwong KK et al (1996b) High resolution measurement of cerebral blood flow using intravascular tracer bolus passages, part II. Experimental comparison and preliminary results. Magn Reson Med 36:726–736

Perkio J, Aronen HJ, Kangasmaki A et al (2002) Evaluation of four postprocessing methods for determination of cerebral blood volume and mean transit time by dynamic susceptibility contrast imaging. Magn Reson Med 47:973–981

Perman WH, Gado MH, Larson KB, Perlmutter JS (1992) Simultaneous MR acquisition of arterial and brain signal-time curves. Magn Reson Med 28:74–83

Reith W, Forsting M, Vogler H et al (1995) Contrast enhanced MR for early detection of cerebral ischemia: an experimental study. Am J Neuroradiol 16:53–60

Reith W, Heiland S, Erb G et al (1997) Dynamic contrast-enhanced T2*-weighted MRI in patients with cerebrovascular disease. Neuroradiology 39:250–257

Rempp KA, Brix G, Wenz F et al (1994) Quantification of regional cerebral blood flow and volume with dynamic susceptibility contrast-enhanced MR imaging. Radiology 193:637–641

Rohl L, Ostergaard L, Simonsen CZ et al (2001) Viability thresholds of ischemic penumbra of hyperacute stroke defined by perfusion-weighted MRI and apparent diffusion coefficient. Stroke 32:1140–1146

Rose SE, Chalk JB, Griffin MP et al (2001) MRI based diffusion and perfusion predictive model to estimate stroke evolution. Magn Reson Imaging 19:1043–1053

Rosen BR, Belliveau JW, Chien D (1989) Perfusion imaging by nuclear magnetic resonance. Magn Reson Q 5:263–281

Rosen BR, Belliveau JW, Vevea JM, Brady TJ (1990) Perfusion imaging with NMR contrast agents. Magn Reson Med 14:249–265

Schellinger PD, Jansen O, Fiebach JB et al (2000a) Monitoring intravenous recombinant tissue plasminogen activator thrombolysis for acute ischemic stroke with diffusion and perfusion MRI. Stroke 31:1318–1328

Schellinger PD, Jansen O, Fiebach JB et al (2000b) Feasibility and practicality of MR imaging of stroke in the management of hyperacute cerebral ischemia. AJNR Am J Neuroradiol 21:1184–1189

Schellinger PD, Fiebach JB, Jansen O et al (2001) Stroke magnetic resonance imaging within 6 hours after onset of hyperacute cerebral ischemia. Ann Neurol 49:460–469

Scholdei R, Wenz F, Essig M et al (1999) The simultaneous determination of the arterial input function for dynamic susceptibility-weighted magnetic resonance tomography of the A. carotis interna and the A. cerebri media. RÖFO Fortschr Geb Rontgenstr Neuen Bildgeb Verfahr 171:38–43

Simonsen CZ, Ostergaard L, Smith DF et al (2000) Comparison of gradient- and spin-echo imaging: CBF, CBV, and MTT measurements by bolus tracking. J Magn Reson Imaging 12:411–416

Smith AM, Grandin CB, Duprez T et al (2000a) Whole brain quantitative CBF, CBV, and MTT measurements using MRI bolus tracking: implementation and application to data acquired from hyperacute stroke patients. J Magn Reson Imaging 12:400–410

Smith AM, Grandin CB, Duprez T et al (2000b) Whole brain quantitative CBF and CBV measurements using MRI bolus tracking: comparison of methodologies. Magn Reson Med 43:559–564

Speck O, Chang L, DeSilva NM, Ernst T (2000) Perfusion MRI of the human brain with dynamic susceptibility contrast: gradient-echo versus spin-echo techniques. J Magn Reson Imaging 12:381–387

Teng MM, Cheng HC, Kao YH et al (2001) MR perfusion studies of brain for patients with unilateral carotid stenosis or occlusion: evaluation of maps of “time to peak” and “percentage of baseline at peak”. J Comput Assist Tomogr 25:121–125

Thompson HK, Starmer CF, Whalen RE, McIntosh H (1964) Indicator transit time considered as a gamma variate. Circ Res 14:502–515

Tombach B, Benner T, Reimer P et al (2003) Do highly concentrated gadolinium chelates improve MR brain perfusion imaging? Intraindividually controlled randomized

crossover concentration comparison study of 0.5 versus 1.0 mol/L gadobutrol. Radiology 226:880–888
Tong DC, Yenari MA, Albers GW et al (1998) Correlation of perfusion- and diffusion-weighted MRI with NIHSS score in acute (<6.5 hour) ischemic stroke. Neurology 50:864–870
Tsuchida C, Yamada H, Maeda M et al (1997) Evaluation of peri-infarcted hypoperfusion with T2*-weighted dynamic MRI. J Magn Reson Imaging 7: 518–522
Van Osch MJ, Vonken EJ, Bakker CJ, Viergever MA (2001) Correcting partial volume artifacts of the arterial input function in quantitative cerebral perfusion MRI. Magn Reson Med 45:477–485
Vexler ZS, Roberts TP, Bollen AW et al (1997) Transient cerebral ischemia. Association of apoptosis induction with hypoperfusion. J Clin Invest 99:1453–1459
Walsh EG, Minematsu K, Leppo J, Moore SC (1994) Radioactive microsphere validation of a volume localized continuous saturation perfusion measurement. Magn Reson Med 31:147–153
Weisskoff RM, Chesler D, Boxerman JL, Rosen BR (1993) Pitfalls in MR measurement of tissue blood flow with intravascular tracers: which mean transit time? Magn Reson Med 29:553–558
Williams DS, Detre JA, Leigh JS, Koretsky AP (1992) Magnetic resonance imaging of perfusion using spin inversion of arterial water. Proc Natl Acad Sci USA 89:212–216
Yamada K, Wu O, Gonzalez RG et al (2002) Magnetic resonance perfusion-weighted imaging of acute cerebral infarction: effect of the calculation methods and underlying vasculopathy. Stroke 33:87–94
Zhang W, Williams DS, Koretsky AP (1993) Measurement of rat brain perfusion by NMR using spin labeling of arterial water: in vivo determination of the degree of spin labeling. Magn Reson Med 29:416–421

7 Disturbed Proton Diffusion

Tobias Neumann-Haefelin

CONTENTS

7.1 Molecular Basis of Disturbed Proton Diffusion

7.1.1 Basics of Diffusion

Diffusion is a physical process that involves the random motion of molecules as they collide with other molecules (Brownian motion) and, on a macroscopic scale, move from one part of a system to another. The average distance that molecules move per unit time is described by a physical constant called the diffusion coefficient, D (in units of mm^2/s). In pure water, molecules diffuse at a rate of approximately $3\times10^{-3}\,mm^2\,s^{-1}$ at 37°C. The factors influencing diffusion in a solution (or self-diffusion in a pure liquid) are molecular weight, intermolecular interactions (viscosity), and temperature (Beaulieu 2002; le Bihan 2003; Moseley and Butts 1999). For comparison, at 20°C the diffusion coefficient of water is approximately $2\times10^{-3}\,mm^2\,s^{-1}$.

In MRI, *water* protons are of principal interest due to their abundance and dominant contribution to the MR signal. The remainder of this chapter will focus on physiological and pathophysiological aspects of water proton diffusion, although it should be mentioned that proton diffusion of other metabolites has also been investigated with MR spectroscopy (Nicolay et al. 2001).

In the brain, diffusion of water molecules is substantially slower than in pure water. This is in part due to cellular membranes and fiber tracts hindering the free movement of water molecules. In addition, even in the extracellular space where diffusion is less restricted than intracellularly, there exists a matrix consisting of "sticky" macromolecules such as proteoglycans and glycosaminoglycans leading to slower diffusion than in pure liquids. Therefore, it is the *apparent* diffusion coefficient (ADC) that is measured in biological tissue and not the physical diffusion coefficient as measured in pure liquids. The ADC in normal brain (as measured with MRI) varies between 0.67 and $0.83\times10^{-3}\,mm^2\,s^{-1}$ in gray matter and 0.64 and $0.71\times10^{-3}\,mm^2\,s^{-1}$ in white matter (Fiehler et al. 2002a). During diffusion times of about 50–100 ms, as they are used in diffusion imaging with MRI, water molecules move in the brain on average over distances around 10–15 µm, bouncing into, crossing or interacting with many tissue components (le Bihan and van Zijl 2002).

If there is a systematic (i.e., highly ordered) tissue substructure such as in white matter, diffusion is usually more restricted in one than in another direction, i.e., the molecular mobility of water is not the same in all directions. In white matter, diffusion is less restricted parallel to than perpendicular to fiber tracts. If diffusion is different along various directions, then it is termed *anisotropic* diffusion. In stroke imaging the avoidance of the confounding effects of anisotropy is a common goal. However,

T. Neumann-Haefelin, MD
Department of Neurology, Goethe University of Frankfurt, Schleusenweg 2–16, 60528 Frankfurt/Main, Germany

diffusion anisotropy can also be exploited (with diffusion tensor imaging) to map out the orientation of white matter tracts, assuming that the direction of the fastest diffusion indicates the overall orientation of the fibers (le Bihan and van Zijl 2002).

The molecular basis of diffusion anisotropy in white matter is still only partially understood, although numerous studies have provided a better understanding of the relationship between diffusion and the underlying microstructural components (for review see Beaulieu 2002). Anisotropic diffusion is clearly related to the ordered arrangement of myelinated fibers in nerve and white matter. However, the relative contributions of various structural components of white matter are not known in detail. Experimental work indicates that axonal membranes are critical structures determining the degree of anisotropy. Myelination can modulate the degree of anisotropy, but is not necessary for significant anisotropy. Other structural or physiological components such as neurofilaments and microtubules as well as fast axonal transport are probably not critical for diffusion anisotropy (Beaulieu 2002).

7.1.2 Molecular Pathophysiology of Restricted Diffusion During Cerebral Ischemia

During cerebral ischemia, water proton mobility declines rapidly, which may be measured with diffusion-weighted imaging (DWI) or other methods (Nicholson and Sykova 1998). In animal models of focal ischemia, the ADC declines by about 30%–50% starting within a few minutes following onset of ischemia, the exact time course depending on the severity of ischemia. In global ischemia models (in particular cardiac arrest models), where the degree of ischemia can be controlled better than in focal ischemia models, a pronounced drop of the ADC occurs at 1–2 min following complete circulatory arrest and occurs at the time of anoxic depolarization, which in turn is the result of energy failure. The rapid and pronounced drop of the ADC is preceded by an earlier, more modest ADC decline (of only ~ 5%), which occurs almost immediately and may reflect intracellular water shifts from a gradual predepolarization leakage of sodium ions or a gradual build up of intracellular lactate, resulting from anaerobic metabolism (de Crespigny et al. 1999, 2001). The time course of diffusion changes during ischemia is probably very similar in humans, although data on the initial phase of stroke are limited. In humans, diffusion changes have been found as early as ~ 39 min following stroke onset (Neumann-Haefelin et al. 2000b).

Pathophysiologically, the pronounced ADC decline during ischemia occurs at the same time as anoxic depolarization. Anoxic depolarization is the consequence of energy failure with secondary failure of ion pumps (in particular Na^+/K^+-ATPase), which are necessary to maintain ion gradients over cell membranes. The resulting influx of Na^+-ions is accompanied by a water shift from the extra- to the intracellular space (cytotoxic edema) without a net uptake of water (Fig. 7.1).

While this association between the ischemia-associated ADC decline and energy failure/anoxic depolarization is undisputed, it is still a matter of debate what exactly leads to the restriction in water proton diffusion. As already mentioned above, water

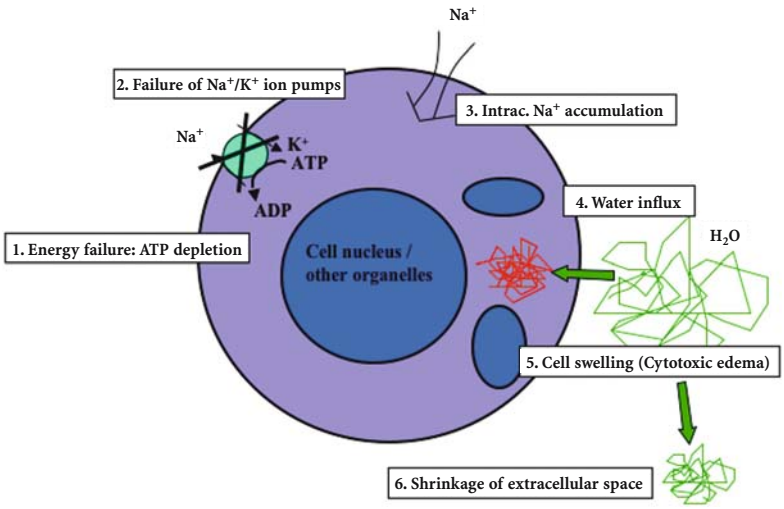

Fig. 7.1. Pathophysiology of abnormal diffusion in cerebral ischemia. Cascade of metabolic changes leading to a decrease in diffusion of water protons in cerebral ischemia. The main steps leading to significant diffusion reductions are shown, while modest changes may also be found with incomplete energy failure. [Reproduced with permission from Neumann-Haefelin and Moseley (2003)]

diffusion in the extracellular space (ECS) is faster than in the intracellular space (ICS). Thus, the shift of water from the fast-diffusing ECS compartment to the slow-diffusing ICS could be responsible for the net decrease of the ADC (Benveniste et al. 1992; Moseley et al. 1990a; van der Toorn et al. 1996a,b; van Gelderen et al. 1994). This initial hypothesis has been the most popular one in the past. Alternatively, assuming that water diffusion in the ECS dominates the ADC signal, the changes of the ECS could theoretically explain the ADC decrease during ischemia. The ECS shrinks by about 50% during the early phase of ischemia (from 20% to 10% of a given volume) and is associated with a parallel ICS increase from 80% to 90%. This ECS shrinkage leads to an increase in tortuosity, which could potentially explain part of the ADC decrease during ischemia (Latour et al. 1994; Sykova et al. 1994). Recent studies, however, using methods that allow separate determination of extra- and intracellular ADC, indicate that the ICS contribution to the ADC dominates the DWI signal, both under normal conditions and during ischemia, while the decrease of extracellular ADC from ~ 1.6 $mm^2 s^{-1}$ to 1.3 $mm^2 s^{-1}$ cannot (fully) explain the *global* ADC decrease during ischemia (Duong et al. 1998; Silva et al. 2002).

On a cellular level, there is evidence that the ICS contribution to the ADC is in part an active process including energy-dependent "cytoplasmic streaming" (Wheatley 1985), i.e., – from a cellular point of view – a purposeful movement of cytoplasm within the cell rather than passive diffusion. Hypothetically, energy failure during ischemia may result in a sudden termination of this process abruptly stopping active intracellular water movements. The relative contribution of the various processes to the ADC decline during ischemia will need further investigation; fortunately, although interesting from an academic point of view, the exact mechanisms underlying disturbed diffusion at the cellular level are of only limited relevance for the clinical interpretation of diffusion changes, which may be safely viewed as an indicator of severe tissue compromise during ischemia.

Disturbances of proton diffusion are not unique to cerebral ischemia. Reduced diffusion has also been found in various experimental conditions including spreading depression (Busch et al. 1995) and periinfarct depolarizations (Gyngell et al. 1994; Rother et al. 1996), hypoglycemia (Hasegawa et al. 1996), following cortical application of noxious substances [blockers of the Na^+-/K^+-ATPase (Benveniste et al. 1992), excitotoxins (Verheul et al. 1994)] and after electrical cortical stimulation (Prichard et al. 1995). In humans, reduced diffusion has been reported in patients with seizures by several groups, mostly in status epilepticus (Lansberg et al. 1999). In addition, visual stimulation as typically used in fMRI experiments was shown to lead to minimal ADC reductions (Darquie et al. 2001; Flacke et al. 2000). The common feature of these non-ischemic states is that they are associated with relative energy failure and disturbances of cellular ion homeostasis leading to (at least some degree of) cell swelling.

7.1.3 Relationship Between Restricted Diffusion and Cerebral Blood Flow

The relationship between ADC change and regional cerebral blood flow (rCBF) has been studied in detail (for review see Hossmann and Hoehn-Berlage 1995). In experimental studies low ADC (~ < 80% of normal) was found in areas with severely reduced rCBF and depletion of high energy phosphates (i.e., ATP) (Hoehn-Berlage et al. 1995). Moderately reduced ADC (~ 90% of normal) was found in areas with less severe rCBF reduction and tissue acidosis (mainly due to lactate accumulation). Different perfusion thresholds for ADC changes have been reported, ranging between 15 to 20 ml/100g/min in gerbils (Busza et al. 1992) and 34–41 ml/100 g/min in rats (Kohno et al. 1995). Partially, this difference may be due to species differences, but may also reflect differences in defining thresholds for ADC change. In addition, the perfusion threshold for ADC changes has been shown to increase as a function of time.

Recent studies in humans have largely confirmed the (non-linear) relationship between ADC and rCBF found in experimental studies. After a gradual decline (with the ADC not falling below 90% of normal), an abrupt drop occurs below an rCBF threshold of 15–24 ml/100 g × min, depending on the time after symptom onset (Fig. 7.2) (Lin et al. 2003). However, these rCBF threshold values are based on perfusion measurements with MRI and the reliability of absolute perfusion measurements with MR perfusion imaging (PI) is still debated (Calamante et al. 2002). Assuming the thresholds are correct, ADC may drop below 90% when rCBF is still in the penumbral range (~12–22 ml/100 g /min). This is in line with a back-to-back MRI and positron emission tomography (PET) studies (Guadagno et al. 2004) showing that some areas with reduced dif-

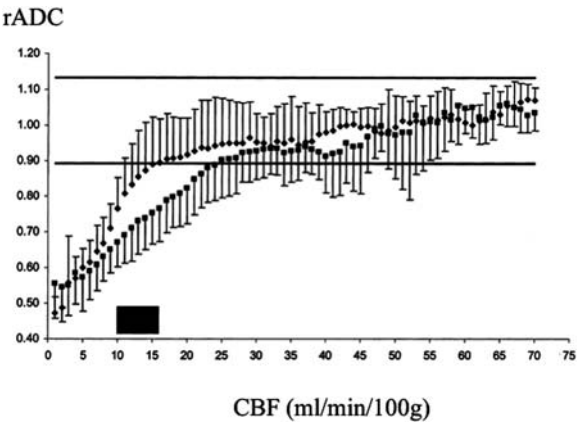

Fig. 7.2. Relationship between relative (rADC) and cerebral blood flow (CBF). ADC drops to below normal at CBF values around 15–24 ml/min/100 g, as shown in a pixel-wise comparison between diffusion and perfusion imaging in acute stroke patients. A lower threshold (15 ml/min/100 g) was found for patients imaged earlier (up to 4 h; ◆) compared to the value (24 ml/min/100 g) of those patients imaged between 4.5 and 6.5 h (■). The data show that the ADC threshold increases with time. [Reproduced with permission from Lin et al. (2003)]

fusion may have increased oxygen extraction fraction (OEF), which is a clear indicator of tissue viability and a characteristic finding of the penumbra. Together with the studies correlating CBF measurements with DWI, these findings conclusively show that reduced diffusion does not necessarily mean irreversible tissue damage.

7.2 Imaging of Diffusion

7.2.1 Diffusion-weighted Imaging

Historically, the first diffusion-weighted NMR pulse sequences were described as early as 1965 by Stejskal and Tanner, long before MR imaging was introduced. The theoretical foundations of DWI and the introduction as a clinical imaging technique were laid out in the mid-1980s (for review see le Bihan 1995), by combining MRI pulse sequences with methods that had been previously developed to encode molecular diffusion effects through the use of pairs of magnetic field gradient pulses. In 1990, Moseley and coworkers first demonstrated in two land-mark articles (Moseley et al. 1990a,b) that DWI could detect regional ischemia (in cats) earlier than conventional MRI techniques. In subsequent years, Warach and coworkers (1992, 1995, 1996a), as well as others (Marks et al. 1996; Sorensen et al. 1996), demonstrated successful application of DWI to human stroke patients. Particularly the development of ultra-fast imaging techniques (such as echo-planar imaging, EPI) and improvements in MR hard- and software have now lead to a situation where DWI is a very fast and robust technique that is easily applicable in the acute stroke situation [for general reviews on DWI in acute stroke see Baird and Warach (1998); Beauchamp et al. (1999) Neumann-Haefelin et al. (2000b)].

The vast majority of DWI studies are still performed by adding "Stejskal Tanner" pulse gradients to a spin-echo imaging sequence (Fig. 7.3). These extra gradient pulses are located symmetrically before and after the 180° refocusing pulse of a spin-echo sequence. The first gradient pulse causes molecules to acquire phase shifts, while the second gradient pulse will cancel the phase shifts by rephasing the (stationary) spins. In the case of moving spins, signal

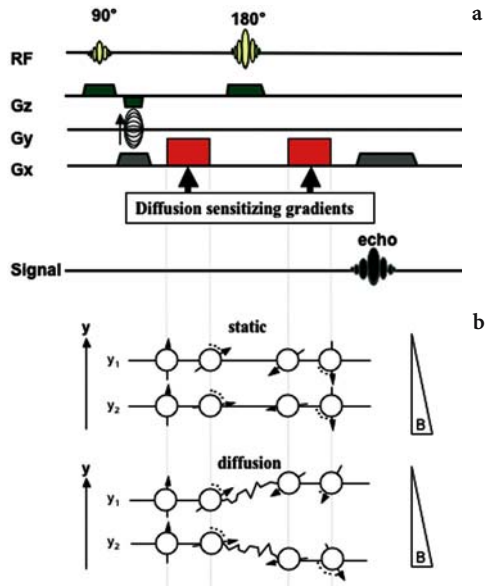

Fig. 7.3a,b. Diffusion-weighted imaging. **a** A typical pulse sequence is shown with two strong diffusion-sensitizing gradients arranged symmetrically around the 180° radio-frequency pulse. The first of the two diffusion-sensitizing gradients leads to dephasing of water protons, while the second gradient leads to an exact rephasing, provided the water protons do not move between the gradients. If the water protons change their location between the two gradients, as in diffusion, the second gradient will lead to incorrect rephasing (**b**). Therefore, the spins will not perfectly realign after the second gradient, which results in a smaller signal. Conversely, if diffusion is restricted, the spins will rephase more accurately, leading to a stronger signal on the diffusion weighted images. [Reproduced with permission from Neumann-Haefelin and Moseley (2003)]

amplitude is attenuated by the incomplete rephasing during gradient 2 of the dephasing induced by gradient 1. For thorough recent reviews on technical aspects of DWI see Bammer et al. (2003); Huisman (2003); Roberts and Rowley (2003).

The degree of diffusion weighting can be quantified by a parameter known as the b-value and is influenced by characteristics of the diffusion gradients including their strength (G), duration (δ) and the interval between the two gradients (Δ). The relationship between signal intensity (SI) on DWI and the b-value is characterized by the following equation:

$$SI = SI_0 \times e^{-bD}, \text{ with} \quad (7.1)$$

$$b = \gamma^2\delta^2G^2(\Delta - 1/3\delta) \quad (7.2)$$

where SI_0 is the signal intensity on the T2-weighted image without diffusion weighting, D the diffusion coefficient and γ is the gyromagnetic ratio. As can be seen from Eq. 7.1, SI in DWI is equal to the signal intensity on a T2-weighted image (or b = 0 image) decreased by an amount of signal drop related to the diffusion coefficient and the applied b-value. In clinical practice, DWI is typically performed with a b-value of around 1000 s/mm^2.

To calculate ADC maps (by solving Eq. 7.1 for D), at least one corresponding set of images is required with a low b-value (near to 0) to determine SI_0. Clinically, ADC maps are useful to absolutely quantify the severity of diffusion abnormalities. In addition, they are used to rule out that high signal on DWI images is due to "T2 shine-through". This phenomenon is due to the residual T2 contrast in DWI images, as the sequence rests on a T2-weighted sequence. Thus, if there is a strong signal on T2-weighted images, the signal drop induced by normal (or even supranormal) diffusion in DWI may not suffice to reduce the DWI signal to levels lower than normal.

On modern scanners diffusion gradient pulses can be applied in (at least) three orthogonal sampling directions (x, y, z), resulting in images selectively sensitized to diffusion along these directions. In acute stroke, DWI is often performed with diffusion-sensitizing gradients applied in all three orthogonal directions, followed by averaging of the resulting images to suppress effects due to anisotropy (Fig. 7.4). The average images are commonly termed "trace" images, although – in a strict sense – the "trace" is a measure derived from diffusion tensor imaging characterizing the average diffusivity after removal of effects due to anisotropy and fiber orientation. The use of "trace" images is particularly useful in small subcortical lacunar stroke close to fiber tracts, since these lesions may otherwise be obscured by high signal due to anisotropic diffusion.

Another method to optimize image contrast includes the addition of an inversion recovery pulse before the typical SE sequence to suppress signal from cerebrospinal fluid (CSF). This yields so-called fluid-attenuated inversion recovery (FLAIR)- or CSF-suppressed DWI images or ADC maps. With this approach, the partial-volume effect of cerebrospinal fluid can be substantially reduced, which is particularly relevant in cortical regions due to the frequent CSF contribution to individual voxels (Latour and Warach 2002). The technique may enhance lesion conspicuity in the vicinity of CSF and has been shown to be of value in research studies utilizing pixel-wise analyses to predict tissue fate. The technique is not yet implemented in many centers, although this may change in the near future.

DWI based on SE-sequences can be combined with different read-out strategies, but single-shot echo planar imaging (EPI) is by far the most widely used method clinically. With this ultra-fast imaging approach, in which the entire k-space is filled with a single read-out train, images can be acquired in fractions of a second. A DWI study covering the whole brain (~ 20 slices) with diffusion sensitizing gradients applied in three directions and two b-values will typically take less than 1 min. Earlier

Fig. 7.4. "Trace" ADC maps. Averaging of ADC maps obtained with diffusion gradients applied in the three orthogonal directions in space (x, y, z) yields "trace" ADC maps with relative suppression of anisotropic diffusion. (Courtesy of Prof. M. E. Moseley, Stanford University)

problems with motion artifacts are no longer a relevant issue.

However, EPI is susceptible to off-resonance effects, such as main field inhomogeneity, local susceptibility gradients, and chemical shift, which all may lead to severe image degradation (Bammer 2003). Image distortions due to susceptibility artifacts affect particularly brain regions near air cavities, such as around the posterior fossa and the skull base. Several strategies have been developed to overcome this problem, including parallel imaging using techniques such as SENSE as well as optimized ways of sampling k-space such as PROPELLER and spiral imaging. A detailed discussion of these imaging methods has been published (Bammer 2003).

7.2.2 Diffusion Tensor Imaging

Diffusion tensor imaging (DTI) is a "sophisticated" form of diffusion imaging that is not yet routinely used in clinical stroke. However, it is becoming increasingly popular as a research tool (Sotak 2002), particularly in small lacunar stroke (Gillard et al. 2001; Lie et al. 2004) and in patients with ischemic leukoaraiosis (O'Sullivan et al. 2001, 2004), and will, thus, be shortly described here.

In DTI, diffusion is no longer described by a single diffusion coefficient, but by an array of nine coefficients that fully characterize how diffusion in space varies according to direction (Basser 1995). With this approach, diffusion anisotropy can be exploited to provide details on tissue microstructure and fiber tracts (le Bihan 2003). To obtain sufficient information on the direction of diffusion, the full diffusion tensor needs to be sampled [for a review on theoretical foundations of DTI see Basser and Jones (2002)].

The tensor has three degrees of freedom and is represented by a 3×3 symmetric matrix (Dxx, Dxy, Dxz, Dyx, Dyy, Dyz, Dzx, Dzy, Dzz) (see Fig. 7.5a). To obtain the full diffusion tensor, diffusion measurements in all of these directions are required (minus those that are mathematically the same, i.e. Dxy=Dyx); therefore, the diffusion gradients need to be applied in at least six different non-collinear directions (at high b-values) to sample the full tensor data plus an additional image that needs to be sampled at a low b-value.

As it is difficult to display tensor data, the concept of "diffusion ellipsoids" has been proposed (le Bihan 2003). An ellipsoid is a three-dimensional representation of the diffusion distance covered in space by molecules in a given diffusion time. This ellipsoid may also be viewed as a three-dimensional vector. The form of the ellipsoid may vary in tissue: isotropic diffusion is best represented by a sphere, while anisotropic diffusion may result in cigar- or pancake-shaped ellipsoids.

DTI data contains specific information not only on the magnitude of diffusion, but also on the relative contribution of anisotropic vs. isotropic diffusion, as well as on the direction of diffusion. Each of these features of DTI data can be analyzed and displayed separately. First, the magnitude of overall diffusion within individual voxels may be displayed by maps showing the "mean diffusivity". Secondly, the relative contributions of isotropic and anisotropic diffusion can be calculated and depicted in maps displaying various mathematically different, but qualitatively similar anisotropy indices, such as the fractional anisotropy (FA), relative anisotropy (RA) and volume ratios (VR) (see Fig. 7.5a); for information on the mathematical derivation of these indices from the diffusion tensor refer to le Bihan et al. (2001). As may be expected, higher anisotropy indices are found in white matter, particularly in fiber tracts. Finally, the spatial direction of anisotropic diffusion can be color-coded on eigenvector-maps, with different colors assigned to the three main orthogonal directions in space (typically: red for predominant left-right, green for anterior-posterior and blue for superior-inferior directions).

Finally, one of the most interesting extensions of DTI is the potential to track fibers ["in vivo MR tractography" (Bammer et al. 2003; Mori and van Zijl 2002)], by using the information on anisotropic directionality contained in the diffusion tensor. With these mathematically complex methods, it has become possible to track fibers from an initial set of seed points, which can be used to track the pyramidal tract or corpus callosum as shown in Fig. 7.5b.

7.3 Diffusion-weighted Imaging (DWI) – Pathophysiological and Clinical Aspects

7.3.1 Time Course of Diffusion Changes in Acute Stroke

The time course of diffusion changes in acute cerebral ischemia has been studied in detail (Lansberg

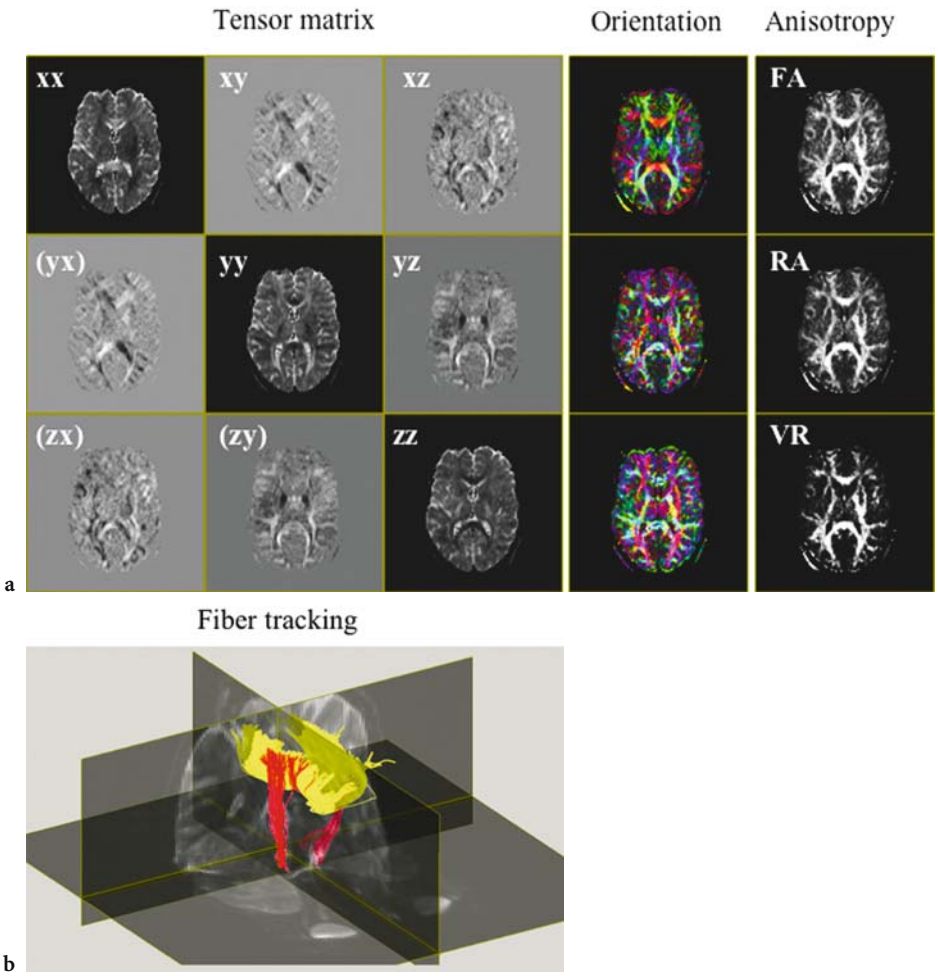

Fig. 7.5a,b. Diffusion tensor imaging (DTI). Example of a DTI study in a normal volunteer obtained at 3 Tesla. The tensor matrix with diffusion gradients applied in six directions is displayed on the *left*. The three images in parentheses (*yx*, *zx*, *zy*) were not acquired separately, as they are the same as those in the right upper part of the matrix (*xy*, *xz*, *yz*). From these images as well as one b0-image (not shown), the full tensor can be calculated. Three common indices of anisotropy, which can be extracted from the tensor, are displayed on the *right side* of (**a**). *FA*, fractional anisotropy; *RA*, relative anisotropy; *VR*, volume ratio. In addition, the fiber orientation is displayed on the color maps in the middle with *red* for predominant left-right, *green* for anterior-posterior and *blue* for superior-inferior directions (with color intensity based on the FA, RA and VR values, respectively). **b** An example of fiber tracking is shown with the pyramidal tract depicted in *red* and the corpus callosum in *yellow*. (Images acquired by Dr. C. Lienerth, Brain Imaging Center, Frankfurt)

et al. 2001; Schlaug et al. 1997; Warach et al. 1996b). In human stroke, as a rule of thumb, ADC remains low for about 1 week, is pseudonormal for another week and then becomes supranormal (Fig. 7.6). Pseudonormal values may be found starting from day four after symptom onset. On the other hand, although there is substantial interindividual variability, it is relatively safe to assume that lesions are less than 10 days old if the ADC is still low (Lansberg et al. 2001). On DWI images, however, signal intensity may remain increased beyond 10 days due to the T2 contribution to the diffusion signal. Pathophysiologically, the subacute pseudonormalization of the ADC and subsequent increase to supranormal values is believed to correspond to cell lysis of necrotic neurons and astrocytes, associated with an increase in extracellular space. This increase in ADC is accompanied by a decrease in diffusion anisotropy, particularly in white matter.

A more complex time course of ADC changes is seen in the presence of early reperfusion (see Fig. 7.7). In animal experiments, ADC abnormalities resolve during the early reperfusion phase following ischemia of short duration (e.g., in the rat suture occlu-

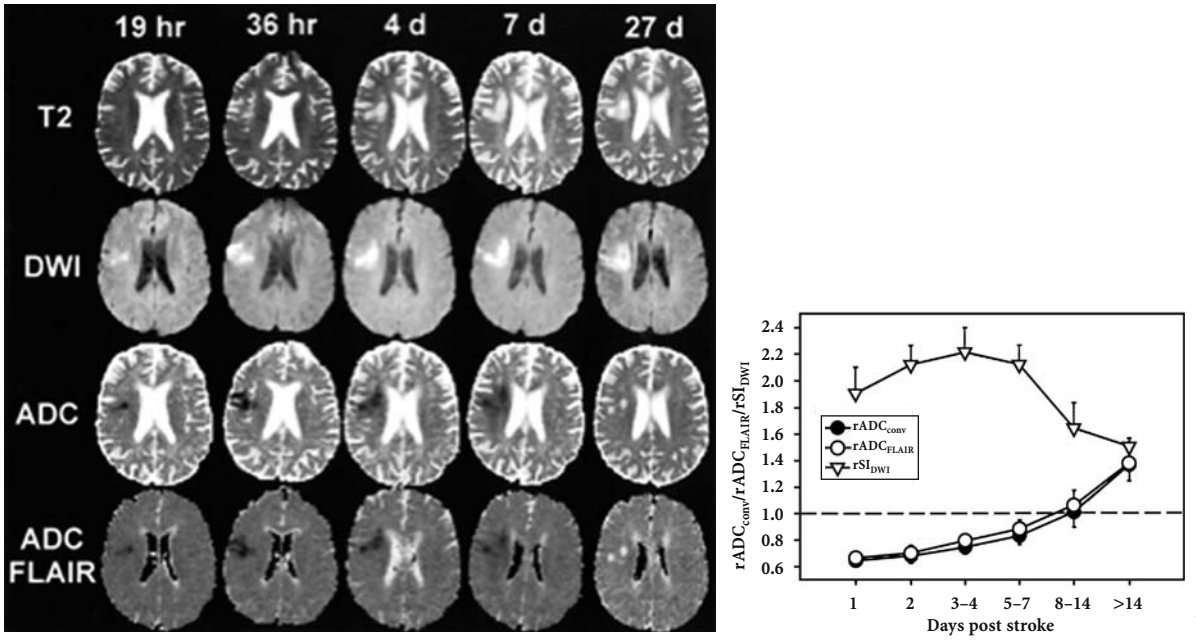

Fig. 7.6a,b. Evolution of DWI, ADC, and FLAIR-ADC signal changes over time. **a** Example of T2-weighted images, DWI, ADC and FLAIR-ADC in a single patient imaged at five time points during the first month following symptom onset. The area with increased signal intensity on DWI corresponds to low signal on ADC and FLAIR-ADC maps. Note the pseudonormalization of the ADC at 27 days despite persistently high signal on DWI due to "T2 shine-through". **b** The average time course of DWI and ADC changes over time for a group of acute stroke patients. rSI_{DWI}, relative signal intensity on DWI; $rADC_{conv}$, relative signal intensity on conventional ADC maps; $rADC_{FLAIR}$, relative signal intensity on FLAIR-ADC maps. [Reproduced with permission from Lansberg et al. (2001)]

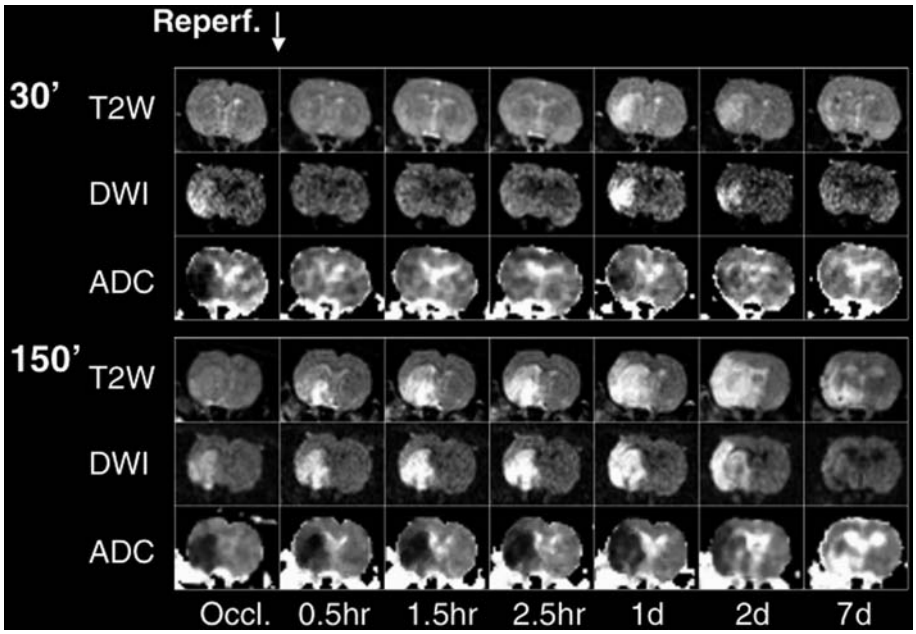

Fig. 7.7. Transient ADC recovery and secondary ADC decline. Time course of ADC changes in a rat model of focal cerebral ischemia, as shown in two examples (30-min and 150-min suture occlusion). After 30 min of ischemia both DWI and ADC changes resolve during the early reperfusion period. This is followed by evolution of a secondary DWI abnormality at day 1 following ischemia, which is associated with a lesion seen on T2-weighted imaging. In contrast, no resolution of DWI or ADC changes is observed following 150-min occlusion (see *lower part* of the image). (The data were acquired in collaboration with A. Kastrup, A. de Crespigny and M.E. Moseley, Stanford University)

sion model after up to ~ 90 minutes) (Li et al. 1999; Li et al. 2000b; Neumann-Haefelin et al. 2000a). If the duration of ischemia is very short (~ 10 min), the ADC recovers permanently (Li et al. 2000a). With intermediate occlusion times, ADC may recover initially and decrease again slowly during the following 24 h to values similar to those found during ischemia (Olah et al. 2000). This is in striking contrast to permanent ischemia (in rats), where areas of diffusion abnormality reflect precisely the region of histological injury, breakdown of energy metabolism, and tissue acidosis at 7 h indicating completion of infarct evolution (Back et al. 1994). A generally similar time course of ADC changes following reperfusion has also been found in humans treated with intraarterial recanalizing therapies (Kidwell et al. 2000, 2002). In humans, this pattern may be seen with occlusion times of up to several hours, probably due to the somewhat slower evolution of ischemic changes in humans compared to rodents.

The pathophysiology behind the secondary ADC decline following transient ADC recovery is not fully understood. It is intriguing to speculate that the initially ischemic tissue remains salvageable during the phase of transient ADC recovery, since this suggests a longer time window for (e.g., neuroprotective) treatment than commonly assumed. Experimentally, normalization of ATP levels has been found during the recovery period (Olah et al. 2001) as well as resolution of intraischemic lactate accumulation (unpublished own observations). However, although this suggests metabolic tissue recovery, subtle histological abnormalities are found during the early reperfusion period (Li et al. 2002; Ringer et al. 2001), and ADC recovery is not associated with functional recovery , indicating that there are ongoing tissue changes, which are not detected with current imaging methods. Potential mechanisms underlying the phenomenon include apoptosis, deranged mitochondrial metabolism and failure of protein synthesis.

7.3.2 Enlargement of DWI Lesions

Enlargement of diffusion abnormalities during the acute phase of stroke (Fig. 7.8) occurs in a substantial proportion of stroke patients. In a study by Baird et al. (1997), almost half of the patients showed DWI lesion enlargement. This lesion enlargement occurs more frequently in patients receiving their first DWI image very early during stroke evolution and was found to be particularly prominent in patients with proximal vessel occlusion (Rordorf et al. 1998). DWI lesion enlargement is not restricted to the first few hours, but may occur over several days, although the most prominent increases are found at early time points.

Despite the frequent increase in DWI lesion size, there is consensus that – at any given time point – areas outside acute diffusion abnormalities, although threatened in the presence of hypoperfusion, are still viable. Thus, the increase in DWI lesion size reflects the evolution of tissue injury during stroke.

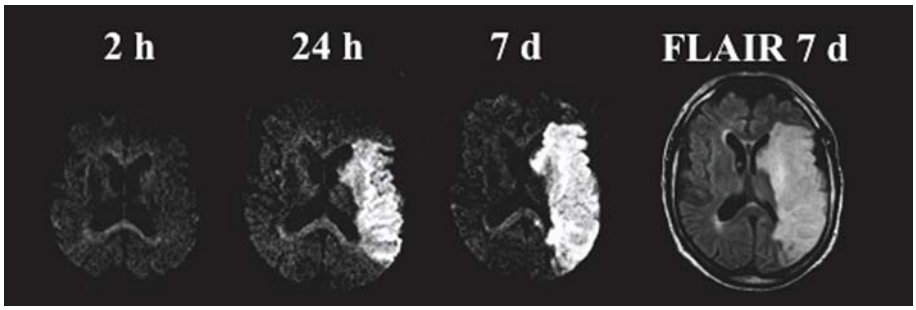

a

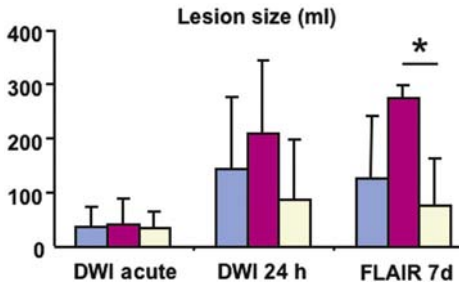

b

Fig. 7.8a,b. DWI lesion enlargement in patients with M1 occlusion. DWI lesion enlargement is frequent in patients with proximal vessel occlusion (M1 occlusion). **a** A prominent example is shown with dramatic lesion growth between the acute imaging time point and follow-up. **b** In addition to showing the lesion growth for unselected patients with M1 occlusions (symptom onset < 6 h), the profound influence of early recanalization is demonstrated (*blue*, all patients; *violet*, subgroup with persistent M1 occlusion; *bright yellow*, early recanalization within 24 h). (The data were acquired in collaboration with O.C. Singer, Neurology, Frankfurt, and R. du Mesnil de Rochemont, Neuroradiology, Frankfurt)

DWI lesions expand into surrounding hypoperfused tissue (the DWI/PI mismatch). Lesion expansion is much more frequent in patients with a DWI/PI mismatch than in patients without mismatch. However, predicting the exact degree of lesion expansion is still challenging. Several semiquantitative perfusion parameters have been proposed including measurements of bolus delay ("time-to-peak," TTP) (Grandin et al. 2002; Neumann-Haefelin et al. 1999) and relative CBF (Grandin et al. 2002), in an attempt to better define the severity of the perfusion deficit and, thus, the risk of infarction in the mismatch region. All studies found an association between the severity of perfusion abnormalities in the mismatch region and the likelihood of lesion expansion, but defining the outer borders of tissue at risk in individual patients is only possible with a substantial degree of uncertainty. Absolute quantification of PI, which would allow defining CBF ranges that are known to correspond to tissue at risk from PET studies, is still difficult (Calamante et al. 2002) due to theoretical problems with bolus delay and dispersion (see Chap. 6), particularly in the presence of proximal vessel occlusion.

In addition, factors other than the severity of the perfusion deficit are known to influence lesion dynamics (Warach 2001). Several studies have now shown that lesion expansion may be arrested by timely reperfusion, either occurring spontaneously or as a consequence of successful intervention (Jansen et al. 1999; Neumann-Haefelin et al. 2004; Schellinger et al. 2001). In addition, there are many other factors influencing lesion growth to a certain extent, such as intrinsic tissue factors (preexisting determinants of susceptibility), induced ischemic tissue tolerance induced by preceding vascular events, age, gender, serum glucose, temperature and blood pressure. Thus, it is not surprising that predicting lesion development is a complex issue.

7.3.3 Potential Reversibility of Diffusion Abnormalities

One of the intensely debated issues during the past few years was the issue of potential DWI lesion reversibility. Initially, it was believed that DWI abnormalities depict irreversibly damaged tissue in humans, i.e., the ischemic core. Only few convincing cases had been reported in the literature with resolution of DWI lesions (mostly small lesions, often located in white matter). There is still no doubt that disturbed diffusion is a sign of severe ischemia and that DWI lesions are a good predictor of final infarct size. However, it became clear recently that – similar to the situation in animals – DWI abnormalities can also reverse in humans. Following the initial observation of DWI lesion reversal in patients treated by intra-arterial thrombolysis (Kidwell et al. 2000), another study found DWI lesion reversal (defined as shrinkage of the DWI lesion by more than 20%) in roughly 20% of hyperacute stroke patients (< 6 h) (Fiehler et al. 2004). Only patients with early recanalization showed significant regions with ADC normalization. Partial ADC normalization was much more frequent in patients imaged very early (< 3 h) indicating that time is the other important parameter determining potential viability of tissue with disturbed diffusion. Taken together, it may be safe to assume that only few patients will have diffusion abnormalities containing viable tissue ("tissue at risk") beyond the first 3 h.

7.3.4 ADC as a Predictor of Infarction?

Predicting the fate of diffusion abnormalities (infarction or recovery) during the first few hours following symptom onset based on the severity of the acute ADC decline (or other imaging parameters) is not straightforward. It has been shown, both in experimental and clinical studies, that a relatively greater ADC decrease (compared to contralateral tissue) is associated with a greater risk of infarction (Pillekamp et al. 2001). This confirms the general experience that mild diffusion abnormalities – often located in the lesion periphery – are the first to reverse following reperfusion. However, there is no ADC threshold below which tissue will progress to infarction with certainty (Fiehler et al. 2002b). Even tissue with ADC reductions to 50% of contralateral values can occasionally survive, but this is comparatively rare. On a voxel basis, ADC values combined with CBF values (or other perfusion parameters) may be better at predicting tissue fate (Kidwell et al. 2003). In addition, various more complicated models using combinations of parameters have been proposed, but none of them are in widespread use. Possibly, in addition to current standard methods such as DWI and PI, spectroscopic imaging will be helpful in the future for the evaluation of tissue viability within DWI lesions; a recent study showed clear differences in lactate accumulation within the region of decreased ADC, again indicating that the severity

of tissue injury is not uniform within DWI lesions (Nicoli et al. 2003).

Clinically, assessment of tissue viability is most important in acute stroke patients who are potential candidates for thrombolysis. In this context, a relatively common problem for stroke physicians is the patient presenting in a time window acceptable for thrombolysis, but with a large diffusion lesion. Is it justified to treat these patients with extensive DWI lesions with thrombolysis? Here, it would be crucial to know the true extent of irreversible tissue damage within the diffusion lesion. However, as mentioned above, assessing tissue viability within DWI lesions and predicting tissue fate is not possible with certainty yet. Nevertheless, several parameters may be taken into consideration to make a rational guess: (1) time from symptom onset, (2) degree of ADC decline (or the brightness of the DWI signal) and (3) severity of the perfusion abnormality. For example, the chances of reversing a faint DWI lesion with an ADC decline to 85% 1 h after symptom onset are much better than those of reversing an ADC lesion with reductions to 50%–60% at 5 h after onset. Although MR algorithms for selecting patients for thrombolysis need to be evaluated more systematically in the future, these rough guidelines may already be helpful in current patient management.

7.3.5 DWI as Part of Integrated MR Examinations in Acute Stroke

In addition to DWI, integrated stroke examinations typically consist of perfusion imaging (PI), T2*- or susceptibility-weighted imaging (=bleed screen), T2-weighted imaging and MR angiography. DWI covering the whole brain can be performed in less than 1 min, and complete stroke MRI examinations take about 10–15 min on modern machines.

Although DWI is nearly always used in combination with other sequences, DWI alone will reveal at least one lesion in the majority of acute stroke patients, even in the first hours after symptom onset. A low ADC identifies the acute (and often clinically relevant) lesion and allows differentiation from older infarcts.

Lesion conspicuity is often better on DWI than on ADC maps, which is the reason why DWI images are preferred by many neuroradiologists for clinical image interpretation. DWI alone may be sufficient in most cases, but differentiation from T2 shine-through effects can be difficult, particularly with lesions located in white matter. From a practical point of view, primary interpretation of DWI images followed by analysis of ADC maps in cases of doubt is probably the most convenient approach.

DWI has been shown to yield clinically relevant information in a substantial number of patients even at subacute time points (i.e., after the first 6 h), which are not apparent on standard MRI. In a careful study on the additional benefit of DWI over standard MRI, Albers and colleagues (2000) investigated how often the following three combinations of findings, which were viewed as being clinically relevant, occurred in patients imaged between 6 and 48 h after stroke onset: (1) the acute symptomatic lesion could be identified only on DWI and it was in a different vascular territory than expected clinically; (2) DWI alone identified acute ischemic lesions in multiple vascular territories suggestive of a proximal source of embolism; or (3) DWI demonstrated that a lesion, thought to be acute on conventional MRI, was not acute. In this study, DWI demonstrated the symptomatic lesion in a different vascular territory than suspected clinically or by conventional MRI in seven patients (18%) and showed acute lesions in multiple vascular distributions in five patients (13%). In eight patients (20%), DWI clarified that lesions thought to be acute on conventional MRI were actually old. Clearly, although most of the benefit of DWI is believed to be due to the increased sensitivity in the first hours after symptom onset, the information obtained in the subacute period may also change patient management.

7.3.6 DWI Negative Stroke

DWI is a very sensitive technique for the detection of ischemia. However, in a minority of patients presenting with stroke-like deficits, normal DWI scans are obtained, even though the clinical deficits are (still) present. Ay et al. (1999) found DWI negative studies in ~ 3.5% (n = 27/782) of consecutively investigated patients with stroke-like deficits; the best final diagnosis in 63% of these patients was "cerebral vascular event" including both reversible ischemic attacks and stroke.

DWI negative scans can be obtained in one of three pathophysiological situations:

i) Hypoperfusion is present and can be detected by PI, but is not severe enough to cause diffusion changes. This situation represents a lesion that consists of an isolated "mismatch" without

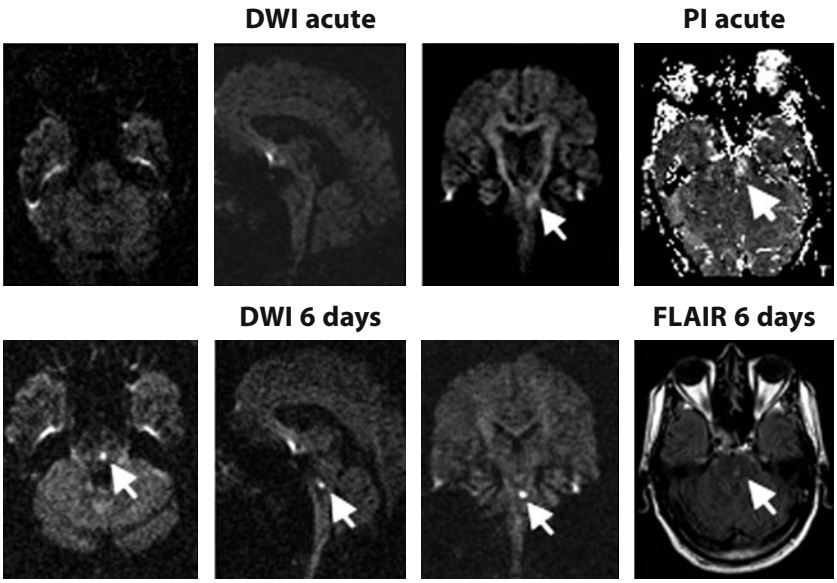

Fig. 7.9. Lacunar brain stem stroke. Typical example of a lacunar brain stem stroke that would be missed if only transverse DWI images were obtained ("DWI negative stroke"). In this case, a faint DWI lesion was seen on coronal sections at the acute time point, but both transverse and sagittal planes did not show an unequivocal lesion. PI, on the other hand, showed a clear-cut perfusion deficit in the brain stem. Follow-up images confirmed a small infarct in the brain stem. (Images were acquired in collaboration with P. Sterzer, Neurology, Frankfurt, and R. du Mesnil de Rochemont, H. Lanfermann, Neuroradiology, Frankfurt)

a diffusion core. Probably, this is the underlying pathophysiology in many patients with TIA (although diffusion changes have also been found in a relevant number of TIA patients [Kidwell et al. 1999]). At the time an "isolated mismatch" is revealed by MRI, symptoms usually already persist for longer than 60 min (which is the maximum duration of TIAs according to a recent definition), and the fate of these regions is hard to predict. Both spontaneous resolution of perfusion changes with tissue recovery as well as progression to infarction may occur.

ii) Hypoperfusion is present, but DWI *and* PI fail to detect it. This situation is rare and is most often encountered in brain stem lacunar stroke. Due to susceptibility artifact, the brain stem may be difficult to assess on EPI images. Occasionally, coronal DWI images may help to identify small brain stem lacunar strokes that were missed on standard axial sections (pseudo-negative DWI; see Fig. 7.9). These brain stem lacunes may or may not be associated with perfusion deficits on PI.

iii) Finally, the stroke-like deficits are due to a non-ischemic cause (i.e., a stroke mimic, see Chap. 19). In most cases no DWI or PI deficit is seen, although PI deficits may be found in some stroke mimics such as migraine with aura.

Thus, PI is a particularly important tool in DWI negative vascular events and non-ischemic stroke-like episodes and may, indeed, clarify the underlying pathology. The majority of patients with DWI negative scans can be classified correctly based on PI as suffering from a cerebrovascular event or from a stroke mimic. Negative DWI and PI studies should intensify the search for non-ischemic conditions. However, in the majority of stroke patients DWI will reveal the clinically relevant lesion and has now become the centerpiece of integrated stroke MRI examinations.

References

Albers GW, Lansberg MG, Norbash AM, Tong DC, O'Brien MW, Woolfenden AR, Marks MP, Moseley ME (2000) Yield of diffusion-weighted MRI for detection of potentially relevant findings in stroke patients. Neurology 54:1562–1567

Ay H, Buonanno FS, Rordorf G, Schaefer PW, Schwamm LH, Wu O, Gonzalez RG, Yamada K, Sorensen GA, Koroshetz WJ (1999) Normal diffusion-weighted MRI during stroke-like deficits. Neurology 52:1784–1792

Back T, Hoehn-Berlage M, Kohno K, Hossmann KA (1994) Diffusion nuclear magnetic resonance imaging in experimental stroke. Correlation with cerebral metabolites. Stroke 25:494–500

Baird AE, Benfield A, Schlaug G, Siewert B, Lovblad KO, Edelman RR, Warach S (1997) Enlargement of human cerebral ischemic lesion volumes measured by diffusion-weighted magnetic resonance imaging. Ann Neurol 41:581–589

Baird AE, Warach S (1998) Magnetic resonance imaging of acute stroke. J Cereb Blood Flow Metab 18:583–609

Bammer R (2003) Basic principles of diffusion-weighted imaging. Eur J Radiol 45:169–184

Bammer R, Acar B, Moseley ME (2003) In vivo MR tractography using diffusion imaging. Eur J Radiol 45:223–234

Basser PJ (1995) Inferring microstructural features and the physiological state of tissues from diffusion-weighted images. NMR Biomed 8:333–344

Basser PJ, Jones DK (2002) Diffusion-tensor MRI: theory, experimental design and data analysis – a technical review. NMR Biomed 15:456–467

Beauchamp NJ Jr, Barker PB, Wang PY, van Zijl PC (1999) Imaging of acute cerebral ischemia. Radiology 212:307–324

Beaulieu C (2002) The basis of anisotropic water diffusion in the nervous system – a technical review. NMR Biomed 15:435–455

Benveniste H, Hedlund LW, Johnson GA (1992) Mechanism of detection of acute cerebral ischemia in rats by diffusion-weighted magnetic resonance microscopy. Stroke 23:746–754

Busch E, Hoehn-Berlage M, Eis M, Gyngell ML, Hossmann KA (1995) Simultaneous recording of EEG, DC potential and diffusion-weighted NMR imaging during potassium induced cortical spreading depression in rats. NMR Biomed 8:59–64

Busza AL, Allen KL, King MD, van Bruggen N, Williams SR, Gadian DG (1992) Diffusion-weighted imaging studies of cerebral ischemia in gerbils. Potential relevance to energy failure. Stroke 23:1602–1612

Calamante F, Gadian DG, Connelly A (2002) Quantification of perfusion using bolus tracking magnetic resonance imaging in stroke: assumptions, limitations, and potential implications for clinical use. Stroke 33:1146–1151

Darquie A, Poline JB, Poupon C, Saint-Jalmes H, Le Bihan D (2001) Transient decrease in water diffusion observed in human occipital cortex during visual stimulation. Proc Natl Acad Sci USA 98:9391–9395

De Crespigny AJ, Rother J, Beaulieu C, Moseley ME, Hoehn M (1999) Rapid monitoring of diffusion, DC potential, and blood oxygenation changes during global ischemia. Effects of hypoglycemia, hyperglycemia, and TTX. Stroke 30:2212–2222

De Crespigny AJ, Rother J, Beaulieu C, Neumann-Haefelin T, Moseley ME (2001) Comparison of diffusion, blood oxygenation, and blood volume changes during global ischemia in rats. Magn Reson Med 45:10–16

Duong TQ, Ackerman JJ, Ying HS, Neil JJ (1998) Evaluation of extra- and intracellular apparent diffusion in normal and globally ischemic rat brain via 19F NMR. Magn Reson Med 40:1–13

Fiehler J, Fiebach JB, Gass A, Hoehn M, Kucinski T, Neumann-Haefelin T, Schellinger PD, Siebler M, Villringer A, Rother J (2002a) Diffusion-weighted imaging in acute stroke-a tool of uncertain value? Cerebrovasc Dis 14:187–196

Fiehler J, Foth M, Kucinski T, Knab R, von Bezold M, Weiller C, Zeumer H, Rother J (2002b) Severe ADC decreases do not predict irreversible tissue damage in humans. Stroke 33:79–86

Fiehler J, Knudsen K, Kucinski T, Kidwell CS, Alger JR, Thomalla G, Eckert B, Wittkugel O, Weiller C, Zeumer H, Rother J (2004) Predictors of apparent diffusion coefficient normalization in stroke patients. Stroke 35:514–519

Flacke S, Wullner U, Keller E, Hamzei F, Urbach H (2000) Reversible changes in echo planar perfusion- and diffusion-weighted MRI in status epilepticus. Neuroradiology 42:92–95

Gillard JH, Papadakis NG, Martin K, Price CJ, Warburton EA, Antoun NM, Huang CL, Carpenter TA, Pickard JD (2001) MR diffusion tensor imaging of white matter tract disruption in stroke at 3 T. Br J Radiol 74:642–647

Grandin CB, Duprez TP, Smith AM, Oppenheim C, Peeters A, Robert AR, Cosnard G (2002) Which MR-derived perfusion parameters are the best predictors of infarct growth in hyperacute stroke? Comparative study between relative and quantitative measurements. Radiology 223:361–370

Guadagno JV, Warburton EA, Aigbirhio F, Smielewski P, Fryer T, Day D, Price CJ, Gillard JH, Carpenter A, Baron J-C (2004) Understanding the metabolic counterpart of the DWI lesion in acute ischemic stroke: a combined MR / PET study. Cerebrovasc Dis 17:1127

Gyngell ML, Back T, Hoehn-Berlage M, Kohno K, Hossmann KA (1994) Transient cell depolarization after permanent middle cerebral artery occlusion: an observation by diffusion-weighted MRI and localized 1H-MRS. Magn Reson Med 31:337–341

Hasegawa Y, Formato JE, Latour LL, Gutierrez JA, Liu KF, Garcia JH, Sotak CH, Fisher M (1996) Severe transient hypoglycemia causes reversible change in the apparent diffusion coefficient of water. Stroke 27:1648–1655; discussion 1655–1646

Hoehn-Berlage M, Norris DG, Kohno K, Mies G, Leibfritz D, Hossmann KA. (1995) Evolution of regional changes in apparent diffusion coefficient during focal ischemia of rat brain: the relationship of quantitative diffusion NMR imaging to reduction in cerebral blood flow and metabolic disturbances. J Cereb Blood Flow Metab 15:1002–1011

Hossmann K-A, Hoehn-Berlage M (1995) Diffusion and perfusion MR imaging of cerebral ischemia. Cerebrovasc Brain Metab Rev 7:187–217

Huisman TA (2003) Diffusion-weighted imaging: basic concepts and application in cerebral stroke and head trauma. Eur Radiol 13:2283–2297

Jansen O, Schellinger P, Fiebach J, Hacke W, Sartor K (1999) Early recanalisation in acute ischaemic stroke saves tissue at risk defined by MRI Lancet 353:2036–2037

Kidwell CS, Alger JR, di Salle F, Starkman S, Villablanca P, Bentson J, Saver JL (1999) Diffusion MRI in patients with transient ischemic attacks. Stroke 30:1174–1180

Kidwell CS, Saver JL, Mattiello J, Starkman S, Vinuela F, Duckwiler G, Gobin YP, Jahan R, Vespa P, Kalafut M, Alger JR (2000) Thrombolytic reversal of acute human cerebral ischemic injury shown by diffusion/perfusion magnetic resonance imaging. Ann Neurol 47:462–469

Kidwell CS, Saver JL, Starkman S, Duckwiler G, Jahan R, Vespa P, Villablanca JP, Liebeskind DS, Gobin YP, Vinuela F, Alger JR (2002) Late secondary ischemic injury in patients receiving intraarterial thrombolysis. Ann Neurol 52:698–703

Kidwell CS, Alger JR, Saver JL (2003) Beyond mismatch: evolving paradigms in imaging the ischemic penumbra with multimodal magnetic resonance imaging. Stroke 34:2729–2735

Kohno K, Hoehn-Berlage M, Mies G, Back T, Hossmann KA (1995) Relationship between diffusion-weighted MR images, cerebral blood flow, and energy state in experimental brain infarction. Magn Reson Imaging 13:73–80

Lansberg MG, O'Brien MW, Norbash AM, Moseley ME, Morrell M, Albers GW (1999) MRI abnormalities associated with partial status epilepticus. Neurology 52:1021–1027

Lansberg MG, Thijs VN, O'Brien MW, Ali JO, de Crespigny AJ, Tong DC, Moseley ME, Albers GW (2001) Evolution of apparent diffusion coefficient, diffusion-weighted, and T2-weighted signal intensity of acute stroke. AJNR Am J Neuroradiol 22:637–644

Latour LL, Warach S (2002) Cerebral spinal fluid contamination of the measurement of the apparent diffusion coefficient of water in acute stroke. Magn Reson Med 48:478–486

Latour LL, Svoboda K, Mitra PP, Sotak CH (1994) Time-dependent diffusion of water in a biological model system. Proc Natl Acad Sci USA 91:1229–1233

Le Bihan D (1995) Molecular diffusion, tissue microdynamics and microstructure. NMR Biomed 8:375–386

Le Bihan D (2003) Looking into the functional architecture of the brain with diffusion MRI. Nat Rev Neurosci 4:469–480

Le Bihan D, van Zijl P (2002) From the diffusion coefficient to the diffusion tensor. NMR Biomed 15:431–434

Le Bihan D, Mangin JF, Poupon C, Clark CA, Pappata S, Molko N, Chabriat H (2001) Diffusion tensor imaging: concepts and applications. J Magn Reson Imaging 13:534–546

Li F, Han SS, Tatlisumak T, Liu KF, Garcia JH, Sotak CH, Fisher M (1999) Reversal of acute apparent diffusion coefficient abnormalities and delayed neuronal death following transient focal cerebral ischemia in rats. Ann Neurol 46:333–342

Li F, Liu KF, Silva MD, Omae T, Sotak CH, Fenstermacher JD, Fisher M, Hsu CY, Lin W (2000a) Transient and permanent resolution of ischemic lesions on diffusion-weighted imaging after brief periods of focal ischemia in rats: correlation with histopathology. Stroke 31:946–954

Li F, Silva MD, Sotak CH, Fisher M (2000b) Temporal evolution of ischemic injury evaluated with diffusion-, perfusion-, and T2-weighted MRI. Neurology 54:689–696

Li F, Liu KF, Silva MD, Meng X, Gerriets T, Helmer KG, Fenstermacher JD, Sotak CH, Fisher M (2002) Acute postischemic renormalization of the apparent diffusion coefficient of water is not associated with reversal of astrocytic swelling and neuronal shrinkage in rats. AJNR Am J Neuroradiol 23:180–188

Lie C, Hirsch JG, Rossmanith C, Hennerici MG, Gass A (2004) Clinicotopographical correlation of corticospinal tract stroke: a color-coded diffusion tensor imaging study. Stroke 35:86–92

Lin W, Lee JM, Lee YZ, Vo KD, Pilgram T, Hsu CY (2003) Temporal relationship between apparent diffusion coefficient and absolute measurements of cerebral blood flow in acute stroke patients. Stroke 34:64–70

Marks MP, de CA, Lentz D, Enzmann DR, Albers GW, Moseley ME (1996) Acute and chronic stroke: navigated spin-echo diffusion-weighted MR imaging (published erratum appears in Radiology 1996, 200:289). Radiology 199:403–408

Mori S, van Zijl PC (2002) Fiber tracking: principles and strategies – a technical review. NMR Biomed 15:468–480

Moseley ME, Butts K (1999) Diffusion and perfusion. In: Stark D, Bradley WG (eds) Magnetic resonance imaging. Mosby, St Louis, pp 1515–1538

Moseley ME, Cohen Y, Mintorovitch J, Chileuitt L, Shimizu H, Kucharczyk J, Wendland MF, Weinstein PR (1990a) Early detection of regional cerebral ischemia in cats: comparison of diffusion- and T2-weighted MRI and spectroscopy. Magn Reson Med 14:330–346

Moseley ME, Kucharczyk J, Mintorovitch J, Cohen Y, Kurhanewicz J, Derugin N, Asgari H, Norman D (1990b) Diffusion-weighted MR imaging of acute stroke: correlation with T2-weighted and magnetic susceptibility-enhanced MR imaging in cats. AJNR Am J Neuroradiol 11:423–429

Neumann-Haefelin T, Wittsack HJ, Wenserski F, Siebler M, Seitz RJ, Modder U, Freund HJ (1999) Diffusion- and perfusion-weighted MRI: the DWI/PWI mismatch region in acute stroke. Stroke 30:1591–1597

Neumann-Haefelin T, Kastrup A, de Crespigny A, Yenari MA, Ringer T, Sun GH, Moseley ME (2000a) Serial MRI after transient focal cerebral ischemia in rats: dynamics of tissue injury, blood-brain barrier damage, and edema formation. Stroke 31:1965–1973

Neumann-Haefelin T, Moseley ME, Albers GW (2000b) New magnetic resonance imaging methods for cerebrovascular disease: emerging clinical applications. Ann Neurol 47:559–570

Neumann-Haefelin T, Moseley ME (2003) MRI in acute stroke. In: Hennerici M (ed) Imaging in stroke. Remedica, London, pp 43-62

Neumann-Haefelin T, du Mesnil de Rochemont R, Fiebach JB, Gass A, Nolte C, Kucinski T, Rother J, Siebler M, Singer OC, Szabo K, Villringer A, Schellinger PD (2004) Effect of incomplete (spontaneous and postthrombolytic) recanalization after middle cerebral artery occlusion: a magnetic resonance imaging study. Stroke 35:109–114

Nicholson C, Sykova E (1998) Extracellular space structure revealed by diffusion analysis. Trends Neurosci 21:207–215

Nicolay K, Braun KP, Graaf RA, Dijkhuizen RM, Kruiskamp MJ (2001) Diffusion NMR spectroscopy. NMR Biomed 14:94–111

Nicoli F, Lefur Y, Denis B, Ranjeva JP, Confort-Gouny S, Cozzone PJ (2003) Metabolic counterpart of decreased apparent diffusion coefficient during hyperacute ischemic stroke: a brain proton magnetic resonance spectroscopic imaging study. Stroke 34:e82–e87

Olah L, Wecker S, Hoehn M (2000) Secondary deterioration of apparent diffusion coefficient after 1-hour transient focal cerebral ischemia in rats. J Cereb Blood Flow Metab 20:1474–1482

Olah L, Wecker S, Hoehn M (2001) Relation of apparent diffusion coefficient changes and metabolic disturbances after 1 hour of focal cerebral ischemia and at different reperfusion phases in rats. J Cereb Blood Flow Metab 21:430–439

O'Sullivan M, Summers PE, Jones DK, Jarosz JM, Williams SC, Markus HS (2001) Normal-appearing white matter in ischemic leukoaraiosis: a diffusion tensor MRI study. Neurology 57:2307–2310

O'Sullivan M, Morris RG, Huckstep B, Jones DK, Williams SC, Markus HS (2004) Diffusion tensor MRI correlates with executive dysfunction in patients with ischaemic leukoaraiosis. J Neurol Neurosurg Psychiatry 75:441–447

Pillekamp F, Grune M, Brinker G, Franke C, Uhlenkuken U, Hoehn M, Hossmann K (2001) Magnetic resonance prediction of outcome after thrombolytic treatment. Magn Reson Imaging 19:143–152

Prichard JW, Zhong J, Petroff OA, Gore JC (1995) Diffusion-weighted NMR imaging changes caused by electrical activation of the brain. NMR Biomed 8:359–364

Ringer TM, Neumann-Haefelin T, Sobel RA, Moseley ME, Yenari MA (2001) Reversal of early diffusion-weighted magnetic resonance imaging abnormalities does not necessarily reflect tissue salvage in experimental cerebral ischemia. Stroke 32:2362–2369

Roberts TP, Rowley HA (2003) Diffusion weighted magnetic resonance imaging in stroke. Eur J Radiol 45:185–194

Rordorf G, Koroshetz WJ, Copen WA, Cramer SC, Schaefer PW, Budzik RF Jr, Schwamm LH, Buonanno F, Sorensen AG, Gonzalez G (1998) Regional ischemia and ischemic injury in patients with acute middle cerebral artery stroke as defined by early diffusion-weighted and perfusion-weighted MRI. Stroke 29:939–943

Rother J, de CA, D'Arceuil H, Iwai K, Moseley ME (1996) Recovery of apparent diffusion coefficient after ischemia-induced spreading depression relates to cerebral perfusion gradient. Stroke 27:980–986

Schellinger PD, Fiebach JB, Jansen O, Ringleb PA, Mohr A, Steiner T, Heiland S, Schwab S, Pohlers O, Ryssel H, Orakcioglu B, Sartor K, Hacke W (2001) Stroke magnetic resonance imaging within 6 hours after onset of hyperacute cerebral ischemia. Ann Neurol 49:460–469

Schlaug G, Siewert B, Benfield A, Edelman RR, Warach S (1997) Time course of the apparent diffusion coefficient (ADC) abnormality in human stroke. Neurology 49:113–119

Silva MD, Omae T, Helmer KG, Li F, Fisher M, Sotak CH (2002) Separating changes in the intra- and extracellular water apparent diffusion coefficient following focal cerebral ischemia in the rat brain. Magn Reson Med 48:826–837

Sorensen AG, Buonanno FS, Gonzalez RG, Schwamm LH, Lev MH, Huang-Hellinger FR, Reese TG, Weisskoff RM, Davis TL, Suwanwela N, Can U, Moreira JA, Copen WA, Look RB, Finklestein SP, Rosen BR, Koroshetz WJ (1996) Hyperacute stroke: evaluation with combined multisection diffusion-weighted and hemodynamically weighted echo-planar MR imaging. Radiology 199:391–401

Sotak CH (2002) The role of diffusion tensor imaging in the evaluation of ischemic brain injury - a review. NMR Biomed 15:561–569

Stejskal EO, Tanner JE (1965) Spin diffusion measurements: spin-echo in the presence of a time dependent field gradient. J Chem Phys 42:288–292

Sykova E, Svoboda J, Polak J, Chvatal A (1994) Extracellular volume fraction and diffusion characteristics during progressive ischemia and terminal anoxia in the spinal cord of the rat. J Cereb Blood Flow Metab 14:301–311

Van der Toorn A, Dijkhuizen RM, Tulleken CA, Nicolay K (1996a) Diffusion of metabolites in normal and ischemic rat brain measured by localized 1H MRS. Magn Reson Med 36:914–922

Van der Toorn A, Sykova E, Dijkhuizen RM, Vorisek I, Vargova L, Skobisova E, van Lookeren Campagne M, Reese T, Nicolay K (1996b) Dynamic changes in water ADC, energy metabolism, extracellular space volume, and tortuosity in neonatal rat brain during global ischemia. Magn Reson Med 36:52–60

Van Gelderen P, de Vleeschouwer MH, DesPres D, Pekar J, van Zijl PC, Moonen CT (1994) Water diffusion and acute stroke. Magn Reson Med 31:154–163

Verheul HB, Balazs R, Berkelbach van der Sprenkel JW, Tulleken CA, Nicolay K, Tamminga KS, van Lookeren Campagne M (1994) Comparison of diffusion-weighted MRI with changes in cell volume in a rat model of brain injury. NMR Biomed 7:96–100

Warach S (2001) Tissue viability thresholds in acute stroke: the 4-factor model. Stroke 32:2460–2461

Warach S, Chien D, Li W, Ronthal M, Edelman RR (1992) Fast magnetic resonance diffusion-weighted imaging of acute human stroke. Neurology 42:1717–1723

Warach S, Gaa J, Siewert B, Wielopolski P, Edelman RR (1995) Acute human stroke studied by whole brain echo planar diffusion-weighted magnetic resonance imaging. Ann Neurol 37:231–241

Warach S, Dashe JF, Edelman RR (1996a) Clinical outcome in ischemic stroke predicted by early diffusion-weighted and perfusion magnetic resonance imaging: a preliminary analysis. J Cereb Blood Flow Metab 16:53–59

Warach S, Mosley M, Sorensen AG, Koroshetz W (1996b) Time course of diffusion imaging abnormalities in human stroke (letter; comment). Stroke 27:1254–1256

Wheatley DN (1985) Mini-review. On the possible importance of an intracellular circulation. Life Sci 36:299–307

8 Ischemic Edema and Necrosis

Susanne Wegener, Mathias Hoehn, and Tobias Back

CONTENTS

S. Wegener, MD
In-vivo NMR Laboratory, Max Planck Institute for Neurological Research, Gleueler Strasse 50, 50931 Cologne, Germany
M. Hoehn, PhD
In-vivo NMR Laboratory, Max-Planck Institute for Neurological Research, Gleueler Strasse 50, 50931 Cologne, Germany
T. Back, MD
Department of Neurology, University Hospital Mannheim, Ruprecht-Karls University Heidelberg, Theodor-Kutzer-Ufer 1–3, 68167 Mannheim, Germany

8.1 Vasogenic Edema and Necrosis Formation: Pathophysiology

8.1.1 The Blood Brain–Barrier and Brain Edema Subtypes

Ischemic injury of the brain initiates a cascade of events that involves formation of brain edema and culminates in tissue destruction (Endres and Dirnagl 2002). Brain edema is defined as swelling of the brain tissue due to an increase in water content. In 1967, Klatzo classified edema based on the localization and biochemical features of fluid as either cytotoxic (intracellular, plasma ultrafiltrate) or vasogenic (extracellular, plasma filtrate including serum proteins) edema (Klatzo 1967). Disruption of blood flow to the brain results in energy depletion and consecutive ion pump failure at the cell membranes resulting in disturbance of ion and water homeostasis, which in consequence leads to cell swelling (for more details see Chap. 7). This cytotoxic edema develops within minutes after the ischemic onset and has emerged as the hallmark of stroke due to its early detectability in diffusion-weighted MRI (DWI).

Vasogenic edema occurs after various brain injuries besides ischemia, such as in trauma, hemorrhage, encephalitis, and tumors. It is preceded by an increase in permeability of the blood–brain barrier (BBB). Specialized endothelial cells located on the luminal side of capillaries constitute the BBB (Go 1997; Rubin and Staddon 1999). These cells are characterized by very few endocytotic vesicles and so called tight junctions, composed of five-layered structures tightly occluding the intercellular clefts. Under normal, physiological conditions, the BBB prevents passage of substances from the blood circulation into the brain, and thereby governs influx and efflux of fluids and solutes between the vascular system and the brain parenchyma. While gases and small (especially lipophilic) molecules pass the

BBB easily, molecules with a molecular weight above 500 Dalton are kept outside the barrier. Some ions and particles needed for cell metabolism, such as glucose, are actively shuttled through the BBB via respective transporters. The amount of water and other molecules crossing the BBB depends on the cerebral blood flow (CBF) and hydrostatic as well as osmotic forces.

8.1.2 Vasogenic Edema and Necrosis after Cerebral Ischemia

After ischemia, the BBB breaks down and plasma constituents enter the brain parenchyma through the opened tight junctions. Up regulation of matrix metalloproteinases (MMPs), zinc-containing enzymes directly degrading components of the vascular basement membrane, and the thrombolytic enzyme endogenous tissue-type plasminogen activator (tPA) appear to be involved in the early steps of BBB opening (Rosenberg et al. 1996; Yepes et al. 2003). The brain tissue, swollen because of the edema fluid, contains more water with a higher Na^+ and a lower K^+ ion concentration. Due to the presence of plasma proteins, the edema fluid has a high colloid-oncotic pressure. It spreads within the intercellular tissue space, preferentially along fiber structures in white matter. Unlike the cytotoxic edema, the vasogenic edema distributes anisotropically (i.e., parallel to the fiber tracts) and leads to an increased compliance of edematous white matter, probably the correlate of the moist and soft macroscopic appearance of the "*Hirnödem*" described by Reichardt in 1904 (Kuroiwa et al. 1994a,b; Reichardt 1904). This excessive extracellular fluid can be cleared by reuptake into capillaries or glial cells, or drained into CSF and the lymphatic system (Klatzo 1967).

Experimentally, the BBB disruption can be assessed by the administration of dyes (e.g., Evans blue, Fluorescein) or radioactive tracers (e.g., [^{14}C] sucrose) and visualization or measurement of their distribution in the brain parenchyma on tissue sections (Fig. 8.1). To estimate brain water content, the weight of a brain is determined with the "wet-and-dry-weight method", i.e., weighing the tissue speci-

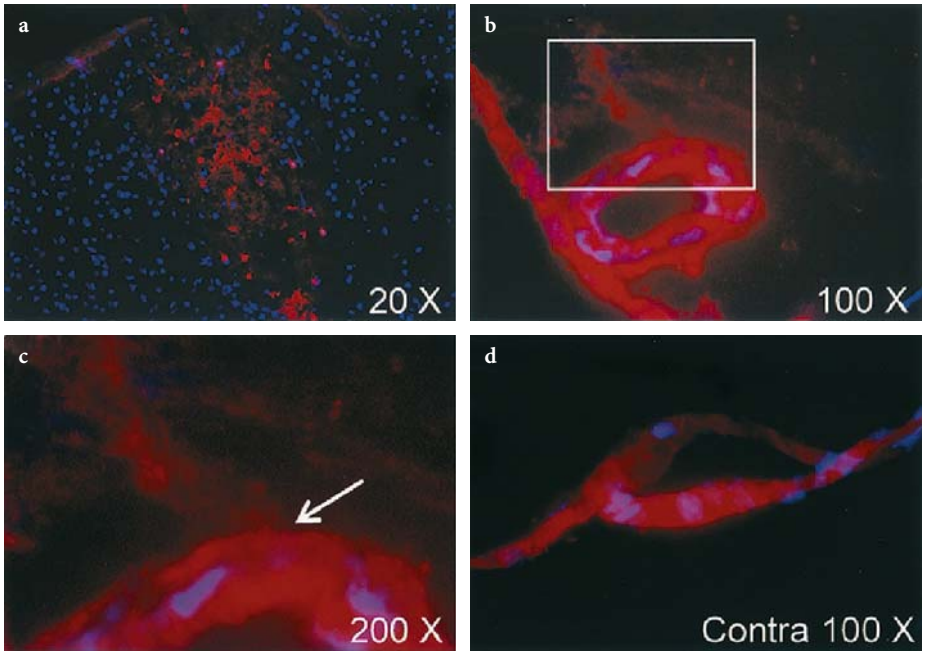

Fig. 8.1a-d. Evans blue extravasation 6 h after permanent middle cerebral artery occlusion (MCAO) in Sprague-Dawley rats. Evans blue extravasation is shown in *red* and cell nuclei in *blue* labeled by 4'-6-diamidino-2-phenylindole (DAPI), a compound that binds to DNA. (**a**) A low-magnification view of the entire ischemic area. (**b**) Evans blue extravasation from a vessel located in the area adjacent to the ischemic area. (**c**) Electronic magnification of the box in (**b**) (*arrow* is pointing at a leakage of Evans blue from the vessel). (**d**) No extravasation of Evans blue is seen in a vessel from the same section seen in (**b**) and (**c**) but located in the corresponding region of the contralateral hemisphere *Contra*, contralateral. [Reproduced with permission from Yepes et al. (2003)]

men before and after drying in an oven at 90–100°C (Hatashita and Hoff 1990; Uyama et al. 1988).

When cerebral blood flow drops below a critical threshold for a longer period of time (e.g., 10 ml/100 mg/min for more than 30 min in animal models of cortical ischemia), necrosis is the consequence (Neumar 2000). Necrosis refers to the "accidental" form of cell death. It is characterized by initial cellular and organelle swelling, membrane disruption, and disintegration of nuclear structure and cytoplasmatic organelles, ending up with extrusion of cell contents into the extracellular space. Necrosis develops from 6 h up to 4 days following ischemia and is further aggravated by inflammatory processes such as secretion of toxic substances by activated inflammatory cells and obstruction of microvessels by these cells (Dirnagl et al. 1999; Garcia et al. 1993; Persson et al. 1989) (see Chap. 4). For selective destruction of neurons after mild cerebral ischemia the term "selective neuronal necrosis" has been coined (Garcia et al. 1996), while in pannecrosis all cell types (neuronal, glial, endothelial) are irreversibly damaged.

More recently, apoptosis has been described as a mechanism of cell death, especially after mild ischemia and in the lesion borderzone (Dirnagl et al. 1999; Snider et al. 1999). In this form of programmed cell death cell bodies are phagocytosed by macrophages and therefore do not enter the extracellular space, thus minimizing deleterious effects on surrounding tissue. Both forms of cell death may be found in coexistence.

During the days following the focal ischemic event, macrophages and glial cells infiltrate the lesion. After about 1–2 weeks, a loose connective tissue matrix is formed along the infarct borders. The necrotic cells have completely resolved 2 weeks later, with macrophages remaining in the tissue adjacent to the infarcted area (Clark et al. 1993).

8.1.3 Temporal Profile of Vasogenic Edema Formation in Experimental Ischemia

A number of animal models have been developed to mimic cerebral ischemia experimentally. They can be roughly categorized into global (bilateral arterial occlusion) and focal (unilateral arterial occlusion) cerebral ischemia models. Probably the widest applied method is the middle cerebral artery occlusion (MCAO), performed by transiently blocking the arterial blood flow with a removable thread or clip, or by permanently occluding the artery (e.g., by ligation or electrical cauterization of the vessel) (Hossmann 1998). Further factors influencing the development of tissue injury are animal strain and age as well as surgical procedure and duration of the ischemic impact.

With respect to brain edema formation, differentiation between transient and permanent vascular occlusion models is very important. In the latter approach blood flow into the ischemic area remains cut off, while reperfusion is restored in the former, similar to the clinical setting of successful thrombolysis or spontaneous reperfusion. Early reperfusion can salvage tissue at risk of infarction (ischemic penumbra). However, when tissue damage has progressed further, reperfusion can have detrimental effects because more water drains from the circulation through the damaged BBB into the already edematous tissue. In consequence, the vasogenic edema develops with a different temporal profile and to a different degree in these cerebral ischemia models.

8.1.3.1 Permanent Occlusion Models

Already 1 h after the onset of permanent ischemia, activity of tPA increases in the ischemic territory, particularly in the perivascular tissue within the penumbra (Yepes et al. 2003). This then activates a cascade of molecular events that finally lead to an increase in permeability of the BBB. In an elaborate study, Hatashita and Hoff (1990) investigated changes in BBB function after permanent ischemia in rats. They found that edema fluid, as estimated by the wet to dry weight method, is significantly elevated already 1 h after MCAO, with an intermittent plateau at day 1, only to rise further to its maximum after 3 days. From there it gradually decreases again. They confirmed earlier findings by Schuier and Hossmann (1980) in the cat MCA occlusion model. It is of importance to note that the early phase of ischemic brain edema is not an isolated shift of water from the extracellular space into neurons. A net uptake of water is observed in brain regions with CBF below 10 ml/100 g/min. Such a net uptake of water can be regarded as a marker for irreversibly injured brain tissue. Extravasation of the micromolecular dye sodium fluorescein was first observed at 6 h, while Evans blue, a dye that binds to plasma molecules and indicates escape of larger molecules, was first noted

in the extracellular space at 12 h after MCAO. To analyze BBB permeability quantitatively, [I^{125}]-labeled bovine serum albumin (^{125}I-BSA) and [C^{14}]-labeled sucrose (^{14}C-sucrose) were applied, and transfer indices were calculated (radioactivity of brain tissue divided by that of blood). This allowed estimation of serum protein (^{125}I-BSA) or small molecular (^{14}C-sucrose) extravasation. Both transfer indices started to increase 12 h after ischemia onset and reached a maximal value around day 8. These findings indicate that despite an early increase in water content, the BBB remains impermeable to serum proteins for at least several hours after MCAO. Permeability becomes maximal only after the peak of edema fluid levels has already been reached.

8.1.3.2 Transient Occlusion Models

In contrast to the gradually increasing BBB permeability in permanent ischemia, transient MCAO has been reported to result in a biphasic opening of the BBB (Kuroiwa et al. 1985). Kuriowa and colleagues found leakage of Evans blue in cats subjected to 1 h of focal occlusion promptly (within minutes) after reperfusion, but only in animals with a severe CBF reduction during ischemia (CBF below 15 ml/100 g/min) and pronounced increase in blood flow after reperfusion (Kuroiwa et al. 1985). A "refractory period" in which no extravasation of dye was observed, was followed by a second BBB opening at about 5 h after ischemia. Time to barrier opening appears to depend on the duration of vascular occlusion. Other groups suggested other time frames, employing 2-h MCA occlusion [3 h and 48–50 h after reperfusion (Belayev et al. 1996; Rosenberg et al. 1998), or 30 min and 22–48 h after reperfusion (Huang et al. 1999)]. The first phase of BBB disturbance has been ascribed to reactive hyperemia or damage through oxygen free radicals after reperfusion. For the delayed, second phase of BBB disturbance inflammatory processes have been implicated, but mechanisms remain to be elucidated (Kuroiwa et al. 1985; Nelson et al. 1992).

It was noted in spontaneously hypertensive rats, subjected either to permanent or transient (2-h) MCAO that vasogenic edema and gliosis, as visualized immunohistochemically, were more widespread after transient occlusion although infarctions were larger after permanent occlusion (Nordborg et al. 1994).

8.2 Correlation of MRI Parameter Changes to the Formation of Vasogenic Edema in Animal Models

8.2.1 MRI Parameters with Sensitivity to Vasogenic Edema and Necrosis

MRI can provide valuable information on the progression of vasogenic edema and necrosis in the living organism. "Free" and "bound" water (e.g., water in the ventricles vs. water bound to cellular structures) can be discriminated based on different T1 and T2 relaxation times (Bakay et al. 1975; Naruse et al. 1982). Typical T1 and T2 relaxation times of normal rat brain at 4.7 T are 869±145 ms and 72±2 ms (caudate putamen) and 928±117 ms and 73±2 ms (cortex), while more liquid structures such as edematous tissue, cysts or CSF will lead to significantly elevated T1 and T2 relaxation times (Hoehn-Berlage et al. 1995).

In consequence, such increases in free, extracellular water can be picked up on T1- and T2-weighted (T1-w, T2-w) images (Dijkhuizen and Nicolay 2003; Horikawa et al. 1986). Proton density images (PD) reflect the concentration of water protons in tissue, and therefore indicate regions with a high water content, such as in edema. When paramagnetic contrast agents such as gadolinium chelates are injected, their T1-shortening effect is used to visualize BBB damage on T1-w MRI: signal enhancement on these images indicates leakage of the tracer into the brain parenchyma (Runge et al. 1985) (Fig. 8.2). Magnetization transfer imaging (MT-MRI) is based on magnetization exchange between "free" and "bound" water protons. The broad resonance of bound protons is saturated using a prolonged off-resonance RF pulse, and only the free proton magnetization is observed. The increase in interstitial water and breakdown of macromolecular structures as it occurs in cerebral ischemia with vasogenic edema are characterized by a reduction in the MT ratio (ratio between free and bound proton pools) (Ewing et al. 1999; Ordidge et al. 1991). The reason for only very few MT-MRI studies lies in the required long RF pulse which causes the risk of unacceptably high RF power deposits into the tissue. Diffusion-weighted imaging (DWI), the "classical" MR parameter to follow the cytotoxic edema after stroke, may also indicate the areas of vasogenic edema by the increased water diffusivity in the larger pools of free water (Fig. 8.2). These regions display increased

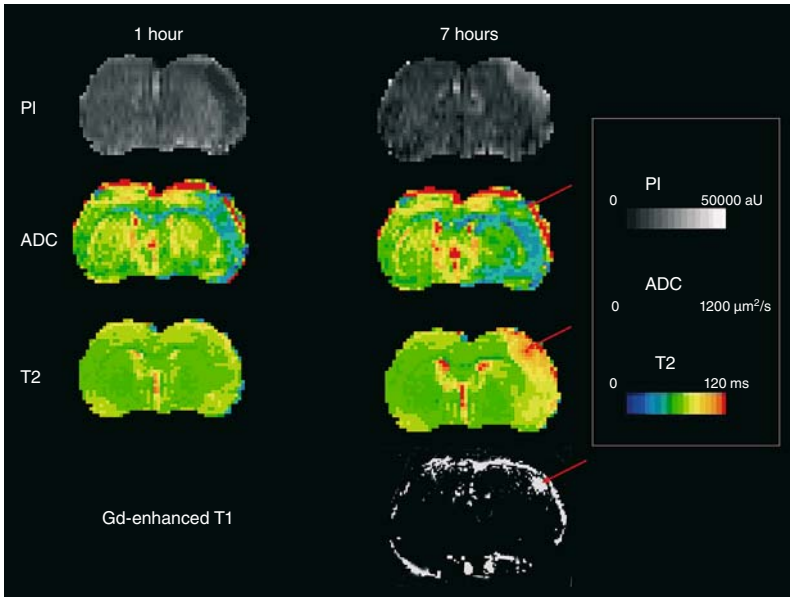

Fig. 8.2. Coronal perfusion images (PI) and quantitative ADC and T2 relaxation time maps of rat brain at 1 h after embolic stroke (*left column*) and 7 h after onset of tPA lysis (*right column*). Note the perfusion deficit in the early ischemic phase which is reversed into a hyperperfusion by the thrombolytic treatment. The maps of the apparent diffusion coefficient show the lesion as decreased ADC value in the right hemisphere (depicted in *blue*). The lesion persists despite the successful recanalization and tissue reperfusion. The T2 parameter map is insensitive to the ischemic alteration in the early phase. At later times (7 h after embolic stroke) a clear, pronounced increase in T2 is observed across the ischemic territory (as determined on ADC maps). At 7 h, a subtraction image of T1-weighted images after and before Gd-DTPA application (Gd-enhanced) shows an area of BBB disturbance (*arrow*) as a strong hyperintensity in the right parietal cortex. Note that this area sticks out in the T2 map with the highest T2 rise (*arrow*). The same region on the ADC map at the later time point is characterized by a pseudo-normalization (*arrow*): the increasing water content of the vasogenic edema counteracts the ADC decrease caused by the cytotoxic edema, thus leading to a re-increase from the early ADC minimum

values of the apparent diffusion coefficient (ADC) (please see Chap. 7 for a closer description of DWI). When effects of cytotoxic and vasogenic edema are coexisting (at subacute timepoints), DWI may be less conclusive because of the two counteracting mechanisms (Fig. 8.2).

8.2.2 MRI Changes Corresponding to Vasogenic Edema after Experimental Brain Ischemia

Earliest proof of an ischemic situation on MRI can be obtained within seconds after stroke onset by perfusion imaging (PI), depicting the area of reduced cerebral blood flow (Fig. 8.2; see also Chap. 6). This is followed within minutes by a rapid delineation of the early ischemic injury (cytotoxic edema) on DWI. Focus of this chapter will be on data acquired in animal ischemia models, using PD-w, T1-w, and T2-w MRI, and their correlation with histopathology.

As discussed above, due to the influence of reperfusion, vasogenic edema develops differently in permanent and transient ischemia models. Therefore, we will also discuss MRI findings in these two models separately (Fig. 8.3).

8.2.2.1 Permanent Occlusion Models

Hoehn-Berlage and colleagues (1995) investigated changes in T1, T2, and proton density in comparison to DWI at an acute time period after permanent occlusion. They demonstrated elevated T1- and T2-values in the ischemic area as early as 2 h after permanent MCAO (pMCAO), which continued to rise during the observation period of 7 h, leading to 29±20% (T1) and 51±41% (T2) above control. This was not paralleled by significant changes in PD, although small increases were detectable in individual animals. Together with the early rise in T1 and T2 relaxation times, before Evans blue leakage demonstrates BBB disruption in histological studies, the unchanged PD argues against vasogenic edema as the source of relaxation time increase at this time.

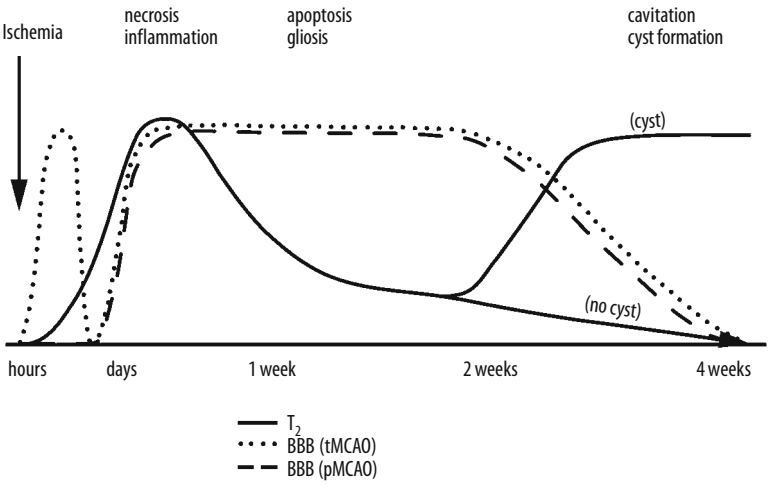

Fig. 8.3. Schematic overview of T2-weighted MRI changes and blood–brain barrier (BBB) opening after experimental ischemia. The x-axis reflects the evolution of events over time while the y-axis illustrates relative intensity of the variable under investigation. *tMCAO*, transient middle cerebral artery (MCA) occlusion; *pMCAO*, permanent MCA occlusion

More likely, the "state" of water as "free" or "bound" or other macromolecular restructuring processes in the tissue early after ischemia must be assumed to cause the observed parameter changes. The rise in relaxation times was more pronounced in the caudate putamen than in the cortex. In concert with absolute relaxation time values, lesion areas on T1 and T2 maps grew during the observation period.

Depending on the experimental setting, different groups reported different time points of initial changes in relaxation times after ischemia, ranging from minutes (Brant-Zawadzki et al. 1986, Kavec et al. 2004) up to about 4 h, rarely later (Bose et al. 1988; Helpern et al. 1993; Knight et al. 1991, 1994; Loubinoux et al. 1997). T1 has been found to increase after T2, and changes to a lesser degree (Bose et al. 1988; van Bruggen et al. 1994).

In a photothrombotic stroke model, in which thrombosis of cortical microvessels is initiated by a laser beam through the intact skull activating rose bengal, a substance that damages endothelial cells and leads to microvascular occlusion, T2 values were elevated at the lesion already 15 min after light exposure (Pierpaoli et al. 1993). However, this procedure, even though leading to permanent vascular occlusion, is governed by different pathophysiological mechanisms that make it difficult to compare to MCAO approaches: the direct endothelium damage in this model leads to rapid disturbance of the BBB, thus explaining the fast T2 relaxation time increase. There is general agreement about the following steady rise in T1 and T2 times, until a peak is reached between 24–72 h (Bose et al. 1988; Helpern et al. 1993; Knight et al. 1991, 1994; Loubinoux et al. 1997; Quast et al. 1993; van Bruggen et al. 1994). Over the following 1–2 weeks, this maximum in relaxation time values gradually declines, but values remain above control levels (Helpern et al. 1993; Knight et al. 1991; Quast et al. 1993). Proton density was found to increase in a study by Knight and colleagues (1991) after pMCAO, but "lagged behind" T1 and T2 times (rise after 24 h, maximum at 96 h, return to control levels at 168 h). The same group reported similar delayed increases in PD in some rat brain regions (e.g., primary somatosensory cortex), but no changes in other areas (e.g., medial portion of caudate putamen) in a later work (Knight et al. 1994). Correspondingly, relaxation times rose to a different degree and at different time points, depending on the region of interest under investigation. In addition to a region-specific macromolecular structure of brain tissue, such as lipid-rich myelin sheaths within subcortical areas, the degree of ischemic severity may well vary within the brain.

Using 2,3,5-triphenyltetrazolium chloride (TTC) stain for the mapping of tissue viability, Bose and colleagues (1988) demonstrated a good correlation of relaxation times with loss of TTC stain (which matches loss of metabolic cell viability in vasogenic edema) earlier than with neuropathological signs of cell damage. Histologically determined brain swelling was estimated with high accuracy from T2-w images in another study at early time points (1–3 days) after pMCAO (Barone et al. 1991; Loubinoux et al. 1997). Nevertheless, there is also data suggesting that the MR parameters T1 and T2 do not reliably reflect histological tissue status after pMCAO (Knight et al. 1994). The appearance of large numbers of shrunken, dark-stained eosinophilic neurons (indicative of irreversible damage) corresponded with peak T1 and T2 values, but no significant correlation was found between histologic score and MR parameter at any time point (Knight et al. 1994).

8.2.2.2 Transient Occlusion Models

Temporary occlusion of an artery offers important insights into the phenomenon of reperfusion. Although transient MCAO (tMCAO) by a thread or clip is a common approach, the injection of blood clots and the consecutive attempt of a successful clot breakdown with thrombolytic therapy is even closer to the clinical situation (Niessen et al. 2002) (Fig. 8.2). Varying temporary occlusion times have been investigated with regard to histologic outcome and MRI pattern of infarct evolution. The phenomenon of reperfusion injury and secondary energy failure was described on diffusion-weighted images and has drawn attention to more chronic observation time points for the characterization of ischemic injury (Hata et al. 2000; Olah et al. 2000). Furthermore, short-term arterial flow restriction gave rise to the discovery of incomplete infarction and selective neuronal death as injury mechanisms, limited to a subpopulation of neurons, but potentially growing at later time points (Garcia et al. 1996).

In a study by Olah and colleagues (2000), T2 relaxation times were followed for 10-h reperfusion after 1 h of MCAO. Similar to the earlier results on permanent MCAO by the same group (Hoehn-Berlage et al. 1995), T2 values increased steadily starting within the first hour after reperfusion. While relative T2 values (% preischemic control) did not reach the level of corresponding observation times after permanent occlusion, the amount of early T2 increase in a voxel was predictive of its later chance for recovery. The major factor influencing relaxation time dynamics in transient MCA occlusion is occlusion time. When applying transient MCA occlusion for 20, 30, 45, and 90 min to a distal branch of the MCA, leading to cortical infarctions, van Lookeren-Campagne and colleagues (1999) found that 20 min did not induce MR parameter changes, but that 90 min lead to profound increases in T2 times at 6 h after reperfusion, culminating towards 48 h. The intermediate occlusion times 30 and 45 min lead to a delayed increase in T2 24 h after reperfusion, accompanied by a secondary decline of the ADC on DWI. Infarctions of the 90-min occlusion group were 50% larger compared to the 30- or 45-min occlusion group, when assessed histologically after 18 days (van Lookeren Campagne et al. 1999). Other investigators observed time courses of relaxation parameters after tMCAO that can be summarized as follows: early (30 min–4.5 h) T1 and T2 increases follow after longer (1–2.5 h) occlusion times, while late (12–24 h) increases follow after shorter (30–45 min) occlusion times. As in permanent MCAO, peak changes of relaxation time values are reached at around 48 h, after which the values decrease over the following week, only to either remain stable or to rise to a second peak around 2 weeks after ischemia (Fig. 8.3). This secondary increase in T2 was correlated to "tissue liquification" and cyst formation (Ishii et al. 1998; Li et al. 2000; Lin et al. 2002a,b; Neumann-Haefelin et al. 2000; Palmer et al. 2001; van Dorsten et al. 2002; Virley et al. 2000). Proton density maps depicted signal increases in some brain regions (Virley et al. 2000) only at time points (several days) much later than T2. Neumann-Haefelin and colleagues (2000) used contrast agent-enhanced T1-w MRI to detect BBB damage after different occlusion times. Their results demonstrate an early leakage of contrast agent in animals subjected to 2.5 h of MCAO, that was not detected after a short occlusion time of 30 min.

At longer survival times, it was noted by some groups that T2-w MRI underestimated true infarct volume to some extent (Ishii et al. 1998; Neumann-Haefelin et al. 2000), while others found a good correlation with histology (Palmer et al. 2001). Factors that could potentially shorten T2 have been discussed: resolution of vasogenic edema and ischemic tissue, accumulation of paramagnetic substances (e.g., iron) in the lesioned area, or increased gliosis. Closer investigation of this so-called MR fogging effect by Lin and colleagues (2002a) revealed that a decrease in water content rather than iron deposits causes this partial T2 normalization. The issue is still under debate, as others have found that T2 is influenced by glial infiltration (Ishii et al. 1998), and own results using T2*-w MRI and histology demonstrate the appearance of iron-loaded macrophages at chronic ischemic lesions with effects on relaxivity (Weber et al. 2005). Since areas of selective neuronal necrosis frequently appear normal (and therefore might be missed) on conventional T1-w and T2-w MRI, application of T2*-w sequences could be a way to reveal inflammatory changes involving iron deposition in these ischemic lesions and facilitate their detection.

Recent fast and quantitative relaxation time studies led to new observations regarding relaxivity parameters after MCAO: within minutes after occlusion a decrease in T2 and an increase in T1 were observed at 8.5 T by Calamante and colleagues (1999), bringing up other causes of relax-

ivity changes, such as flow effects and the amount of oxy- and deoxyhemoglobin (deoxyhemoglobin accumulates) in tissue after ischemia. Support for a region-specific lesion evolution, in analogy to pMCAO, was also raised for transient occlusion models (Dijkhuizen et al. 1998).

8.2.2.3 Relaxation Time Changes and Function

In transient MCAO models, T2 relaxation time values and lesion sizes based on T2 changes have been shown to correlate to somatosensory test scores at different time points (Palmer et al. 2001; Virley et al. 2000). This bears great clinical relevance, because the alleviation of a patient's functional deficits is the primary motivation of experimental stroke studies. However, reliable prediction of functional impairment by MRI is not undisputed. We noted positive striatal T2-w MRI findings in the absence of functional deficits and concluded dissociation between these two diagnostic variables in certain stroke patterns (Wegener et al. 2005).

8.3 Translation of Experimental Results to Human Stroke

Results obtained by MRI and MRS in the setting of experimental stroke have to be translated to human brain ischemia in order to apply new knowledge to clinically important situations. This translation has to take into account that the human cortex is much more complex (e.g., number of gyri, cytoarchitecture of cortical areas etc.) compared to rodent brain or brains of other animal species. There are also considerable differences in the density of neurons per tissue volume and in the vascular anatomy that provides collateral circulation on different levels of the brain-supplying arteries in the case of obstructed perfusion. Animal experiments are frequently carried out in healthy adults whereas stroke patients often suffer from comorbidity (e.g., hypertension, diabetes mellitus) and show signs of chronic and widespread arteriosclerotic changes in various vascular territories including the brain and heart. Therefore, a larger variability of the temporal profile and magnitude of changes visible on MRI may be expected in human stroke pathology.

8.3.1 Correlation of MRI Changes to Human Brain Pathology

In the 1970s and 1980s, many investigations addressed the histopathological changes associated with stroke in man. The histological assessments aimed to characterize the age of recent brain infarcts (Chuaqui and Tapia 1993), to quantify the distribution and frequency of microthromboemboli that were seen also contralaterally to the main site of infarction (Heye and Cervos-Navarro 1996) and to correlate brain pathology to imaging results (Parisi et al. 1988; Nedergaard et al. 1986). A stroke case was reported that showed hyperdensity within the infarct on a second CT scan taken 18 days after the insult. Autopsy revealed no hemorrhage as suspected, but early calcification of infarcted regions (Parisi et al. 1988). A small, but distinct transitional zone between infarct and surrounding unlesioned tissue was described in which necrotic neurons were seen comprising a rim of maximal 10 mm width (Torvik and Svindland 1986). This infarct borderzone was thought to represent regions that had suffered from a lesser degree of ischemia compared to more centrally located infarct areas. The direct comparison of CT findings, tomographic measurement of CBF and neuropathological sections was performed in one case of a small old brain infarct (Nedergaard et al. 1986). A peri-lesional reduction of CBF was described although peri-infarct neuronal density seemed intact.

With the clinical availability of MRI comparisons have been drawn between CT and MRI findings (Barber et al. 1999; Kucinski et al. 2002; Saur et al. 2003; Wardlaw et al. 2004). However, direct comparisons between MRI changes and human brain pathology are lacking. To date, clinicians and researcher take it for granted that hyperintensity on T2-weighted MRI (and/or hypointensity in T1-weighted images) in the chronic phase of stroke would represent destroyed tissue. However, there is no correlative proof of this assumption to the best of our knowledge. There may be good reasons to assume such a relationship, but it remains unclear from which time point post-insult onward this could be valid. Also, it remains to be shown by correlative autopsy studies whether reperfusion alters the correlation of MRI findings to histological changes. It may be expected from animal studies that early reperfusion would reverse by part histological changes, thereby increasing the percentage of scattered neuronal injury in borderzone regions (Back et al. 2002).

8.3.2 Temporal Profile of Blood–Brain Barrier Disruption

Several investigators have described the time course of contrast enhancement with gadolinium chelate in patients with ischemic stroke (Crain et al. 1991; Elster 1991; Essig et al. 1996; Karonen et al. 2001; Vo et al. 2003). Contrast-enhanced MRI on days 1, 2 and 7 post-stroke revealed two different patterns, namely intravascular and parenchymal enhancement of the contrast agent. Whereas intravascular enhancement in the infarcted area was detected in 78% of the cases on day 1 and in 30% of cases at 1 week, parenchymal enhancement was observed with increasing frequency over 7 days (Karonen et al. 2001).

The pattern of intravascular enhancement was only seen in larger territorial infarcts that involved regions with good collateral supply, not in regions that are supplied by deep perforating end arteries (Elster 1991). The presence of intravascular enhancement over a larger area than the infarcted core (as seen on DWI) on the first day did not predict infarct growth (Karonen et al. 2001). It is widely accepted that intravascular contrast enhancement is caused by decreased blood flow in arteries surrounding the ischemic tissue and resulting in decreased flow void as a sign of acute ischemia (Essig et al. 1996). Local vasodilation may also contribute to this effect.

Of greater importance for the assessment of the disturbed BBB are the patterns of parenchymal contrast enhancement. CT studies showed that parenchymal enhancement is commonly seen 2–4 weeks after stroke, sometimes already during the first week (Norton et al. 1978). The higher spatial resolution and sensitivity of contrast-enhanced MRI enabled the detailed study of different forms of contrast enhancement during the acute phase of stroke. Disruption of the BBB could be visualized by leakage of contrast material into the brain parenchyma in 26% (day 1), in 56% (day 2) and in 100% of stroke cases at 1 week (Karonen et al. 2001). The changes observed increased not only with regard to their incidence, but also with regard to intensity of enhancement. In a recent MRI study, 3 of 22 stroke patients showed signs of ischemic tissue enhancement within 5 h of symptom onset (Vo et al. 2003). Interestingly, two of the three patients developed large symptomatic hemorrhage after thrombolysis with tissue plasminogen activator. To compare experimental data, breakdown of the BBB could be shown in about half of animals subjected to embolic MCA occlusion and investigated by contrast-enhanced T1-w imaging 3 h following the insult (Neumann-Haefelin et al. 2002). The detection of disrupted BBB prior to thrombolysis predicted the hemorrhagic transformation of infarcts following tPA therapy in those animals. It seems as if very early parenchymal enhancement may be a predictor of increased risk for subsequent symptomatic hemorrhage after thrombolytic therapy, but this notion needs further confirmation.

Also technical aspects may contribute to the variable incidence of parenchymal enhancement in acute human stroke. With double dose contrast medium and a time lag between injection and imaging, every fourth stroke patient showed tissue enhancement within 24 h of stroke onset (Karonen et al. 2001). Widespread parenchymal enhancement in T1-w images seems to gradually develop over the first week when simultaneously the diffusion changes tend to pseudonormalize. Without precise clinical history confounding with tumor enhancement may occur and should be ruled out by observation of the time profile of MR contrast enhancement and DWI.

To summarize, BBB disruption occurs in humans at earlier time points than previously believed, develops progressively over the initial 7 days and, probably, is more dominant in stroke cases of permanent ischemia. It should be regarded as a key event for the development of vasogenic edema.

8.3.3 Temporal Profile of Ischemic Brain Edema

As reviewed in Chap. 4, the ischemic brain edema is a mixture of cytotoxic and vasogenic edema elements. Whereas the cytotoxic edema is not associated with a marked net increase in brain water content, disruption of the BBB triggers the vasogenic component of ischemic edema formation. This involves a gradual increase in brain water content. Depending on the magnitude of the territory affected, edema formation leads to focal occupation of space. The narrowing of CSF-containing compartments of the brain (e.g., ventricles, basal cisterns) adjacent to ischemic lesions is a well recognized sign of this process visible on CT and MR scans. The exact time course of edema formation in large brain infarcts of rats has been determined by MRI showing that edema peaks at 24 h post-occlusion (Hofmeijer et al. 2004). MR studies with quantitative assessment of ischemic edema formation in humans are lacking. However, it is clinically well established that edema formation in territorial brain infarcts peaks

between 3–5 days post-stroke and can be readily detected by MRI.

The development of "malignant" middle cerebral artery infarction associated with a 80% mortality can be regarded as an extreme case of ischemic edema progression. The intracranial space is surrounded by tight bone structures that do not permit expansion, and contains three compartments: brain, blood and CSF (Monro-Kellie doctrine) (Mokri 2001). Since blood and CSF are non-compressible liquids, the volume increase of brain can be compensated for by narrowing of CSF containing spaces. But when those spaces are pressed out, further volume increases lead directly to increased intracranial pressure (ICP) finally resulting in herniation of brain and brain stem compression. Mostly due to the proximal obstruction of the MCA or the carotid T-branch, the occurrence of malignant MCA infarction can be predicted by using quantitative analysis of early DWI and PI. As strong MRI-based predictors the following items were identified: ADC lesion size > 82 ml; severe perfusion deficit size > 162 ml (defined by increases in time-to-peak time > 4 s); low ADC in the infarct core (< 300 $\mu m^2/s$), and relatively small diffusion-perfusion mismatch area (Thomalla et al. 2003). We may deduce that the larger and more severe the perfusion deficit is, the more pronounced the disruption of the BBB and subsequent vasogenic edema formation. As a consequence, midline shift of brain occurs as an important indicator of significant hemispheric swelling. In a rat model of malignant MCA infarction, the drop of contralateral (contralesional) blood flow was observed upon the peak of midline shift at 24 h post-occlusion (Hofmeijer et al. 2004). Therefore, formation of ischemic edema is always associated with compensatory processes that try to minimize an increase in ICP on the expense of the blood or CSF containing compartments. Compression of the capillary bed or larger brain vessels (that both lead to reduced CBF) are sequelae of focal brain edema. In order to interact with this type of pathology, surgical procedures like hemicraniectomy have been performed and been proven useful in experimental settings (Doerfler et al. 1996) and in humans (Schwab et al. 1998).

8.3.4 Probability Approach to Define Irreversible Damage

We have seen that MR parameters like T1, T2, proton density, diffusion-weighting or apparent diffusion coefficient, and perfusion signals all follow different time profiles of change that reflect different aspects of ischemic injury. Histological correlations are only available from animal experimentation confirming those differential profiles (Helpern et al. 1993). It became clear that there is not one single MR marker specific for tissue necrosis valid at all time points after stroke (see Chaps. 4 and 7). Especially after reversible ischemia, whether prompted by therapy or occurring spontaneously, MRI reveals complicated signal changes that may involve partial reversal as well as the eventual secondary appearance of injury visible on T2-w or DWI. Also, infarct growth as a regular phenomenon of developing territorial stroke (Baird et al. 1997) complicates the prediction of outcome by using early MRI measured within the first hours after onset of symptoms.

If we put all this information together it is conceivable to choose a multiparametric MRI approach in order to predict irreversible damage on the basis of probabilities of various MR signal changes. The simplest strategy would be to start with one MRI modality and look for tissue outcome subsequently. Oppenheim et al. (2001) provide such an approach for the early measurement of ADC within 6 h of stroke onset. Follow-up MRI was performed between day 2 and 4 using fluid attenuated inversion recovery (FLAIR) images to assess final infarct volumes. The authors showed that ADC values gradually increased from the infarct core to the periphery of the ischemic lesion. There were distinct significant differences in mean ADC values as measured within the initial DWI hyperintense lesion (660 $\mu m^2/s$), within the infarct growth area (780 $\mu m^2/s$), and in the oligemic area that remained viable despite initially reduced perfusion (820 $\mu m^2/s$). The latter values were nearly identical to contralateral normal ADC. Of the total cohort of 48 patients, 14 patients had an apparent infarct growth, 29 showed a stable lesion, and the remaining five patients had a partially reversible lesion. Tissue damage could be predicted if the initial ADC was < 750 $\mu m^2/s$, if relative ADC was < 0.91, if local CBF was < 37 ml/100 g/min or if mean transit time MTT was > 16.4 s (Oppenheim et al. 2001) (Fig. 8.4). On the basis of the absolute or relative ADC threshold values, 88% and 95% of the final damage could be correctly predicted, respectively. In this study, ADC-based prediction was more accurate and robust than prediction based on hemodynamic parameters.

A change in the perfusion state of ischemic tissue may alter its response to ischemia as shown previously in this and other chapters (see Chaps. 4, 6

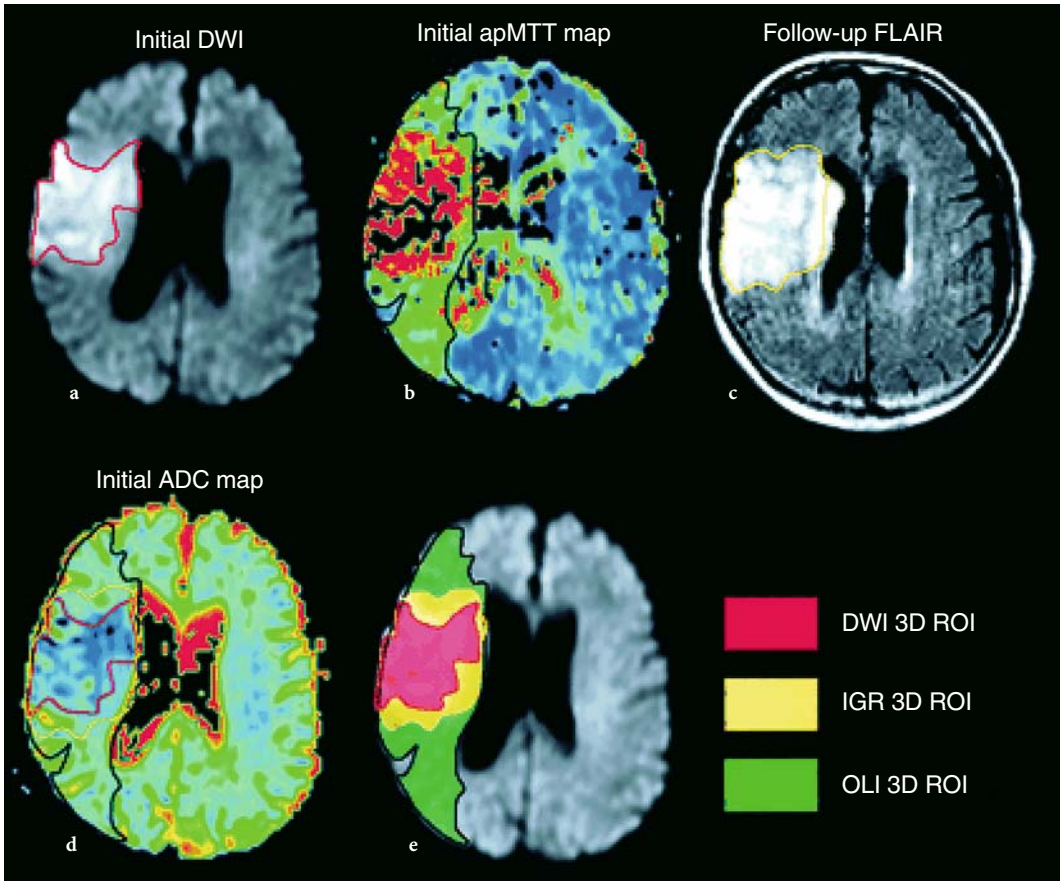

Fig. 8.4a-e. A 4-h post-onset MRI (**a**, **b**, and **d**) and 3-day follow-up FLAIR (**c**) in a patient with acute right MCA infarction. Initially, the area of reduced perfusion on the apparent mean transit time map (apMTT, **b**) was larger than the DWI hyperintensity (**a**) and larger than the final infarct on follow-up FLAIR (**c**). The large perfusion-diffusion mismatch was divided into an area showing infarct growth (IGR) and an area with oligemia (OLI) and copied onto the initial ADC map (**d**, **e**). [Reproduced with permission from Oppenheim et al. (2001)]

and 7). This is particularly true if reperfusion is initiated rapidly by thrombolytic therapy. Therefore, in an alternative approach both data from DWI and PI have been used to model and estimate stroke evolution (Rose et al. 2001). A novel automated strategy for predicting infarct development was created the validity of which was tested on novel patient data. Regions-of-interest (ROIs) defining the initial diffusion lesion and tissue with abnormal hemodynamic function as defined by the mean transit time abnormality were automatically extracted from DWI/PI maps. Quantitative measures of cerebral blood flow (CBF) and volume (CBV) along with ratio measures defined relative to the contralateral hemisphere (rCBF and rCBV) were calculated for the MTT ROIs (Fig. 8.5). A parametric normal classifier algorithm incorporating these measures was used to predict infarct growth or lesion reversal. The mean rCBF and rCBV values for eventually infarcted MTT tissue were 0.70 and 1.20, respectively. For recovered tissue the mean values were 0.99 (rCBF) and 1.87 (rCBV), respectively (Rose et al. 2001). Both measures were significantly different in these two regions. Mean absolute measure of CBF for the total infarcted territory was 34 ml/100 g/min and for recovered MTT tissue 42 ml/100 g/min, also being significantly different. Those CBF values correspond to 58% and 71% of control. When testing novel patient data, a sensitivity of 72% and a specificity of 97% was observed.

In this study, the authors state that optimal predictive efficiency was achieved if an eight-dimensional model was applied utilizing the metrics of rDWI, DWI, rMTT, MTT, rCBF, CBF, rCBV and CBV (Rose et al. 2001). A quantitative diffusion measure like ADC was not applied and may have further improved prediction if we regard the findings of Oppenheim et al. (2001) as shown above.

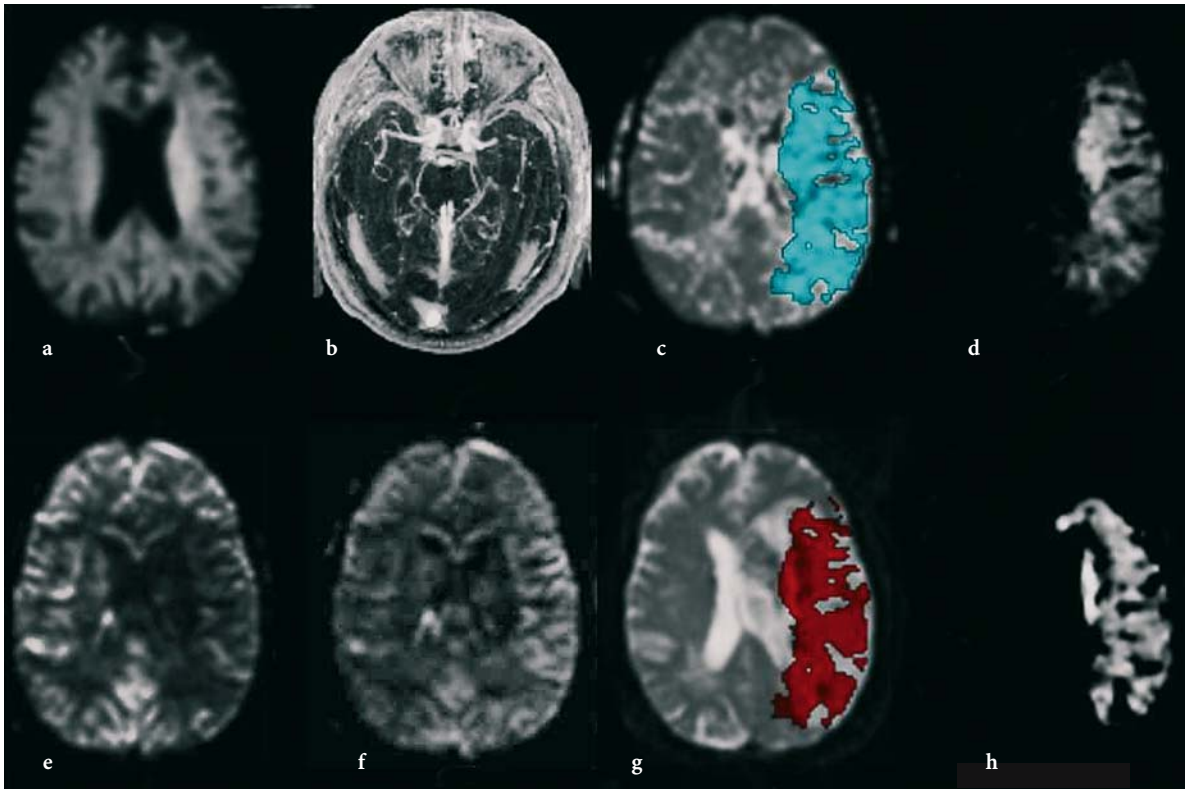

Fig. 8.5a-h. Diffusion and perfusion images acquired from a stroke patient 2 h after onset of symptoms. *Top*, *left* to *right*, (**a**) the DWI scan showing a poorly defined diffusion lesion in the deep white matter in the left hemisphere, (**b**) the MR angiography showing occlusion of the left middle cerebral artery, (**c**) the mean transit time (MTT) map with the extracted MTT mask given in blue and (**d**) the composite MTT map. *Bottom left* to *right*, (**e**) cerebral blood flow map, (**f**) cerebral blood volume map, (**g**) the follow-up T2-weighted scan with predicted lesion colored red and (**h**) the final lesion volume derived by subtraction of the initial T2 image from the follow-up scan. [Reproduced with permission from Rose et al. (2001)]

Finally, we would like to draw attention to another approach combining MRI and positron emission tomography (PET) technologies. Heiss et al. (2001) investigated ten acute hemispheric stroke patients by early (within 12 h) PET measurements of CBF and labeled flumazenil (FMZ) that binds as ligand to benzodiazepine receptors and serves as a marker for neuronal integrity (Heiss et al. 2001). Morphological outcome was defined by late T1-w MRI 3 weeks post-insult. ROIs were placed on co-registered maps of CBF, FMZ binding, and T1-w images to identify various subcompartments: a 55% portion of the final infarct showed critically decreased FMZ binding that predicted necrosis. In 21% of the final infarct, CBF was in the penumbral range (< 14 ml/100 g/min) and FMZ binding above the critical threshold of irreversible damage. Only 13% of the final infarct exhibited neuronal integrity and CBF values above the penumbral range (Heiss et al. 2001) (Fig. 8.6).

Therefore, most of the final infarct is already irreversibly damaged at the time of the first evaluation (i.e., within 12 h after symptom onset). A much smaller portion is still viable but suffers from insufficient blood supply which may be salvaged by effective reperfusion. Only an even smaller subarea is both viable and sufficiently perfused, but eventually becomes necrotic, mainly owing to delayed mechanisms. It represents the target for neuroprotective drugs or other means that prevent secondary damage.

8.4 Conclusions

Animal studies have substantially added to our understanding of the creation and development of vasogenic edema and necrosis after stroke onset. T2 has emerged as the most commonly applied MR parameter to study this aspect of infarct evolution in animal as well as in human stroke (Warach 2001). Although MRI monitoring of vasogenic edema is

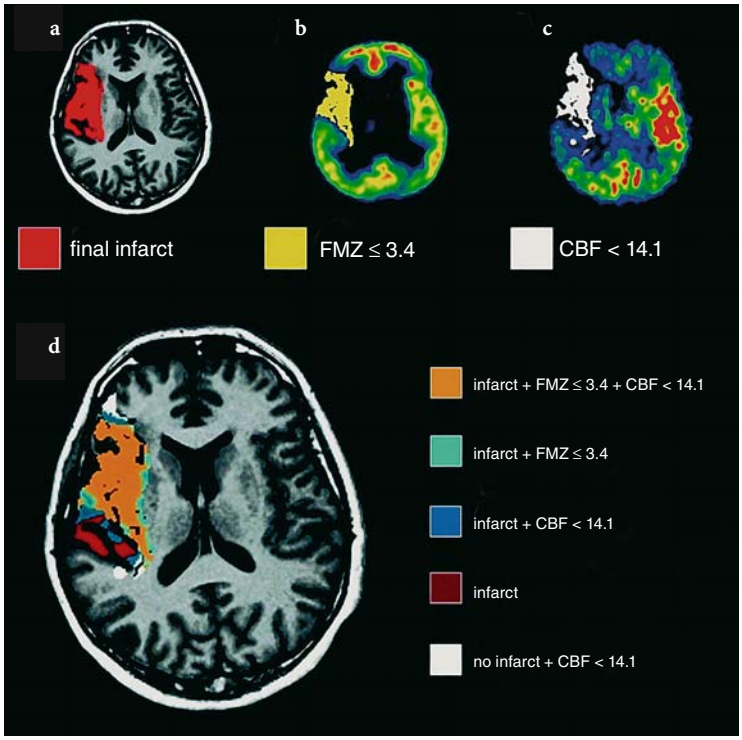

Fig. 8.6a-d. Various subareas within and outside of the final brain infarction as determined by PET measurements of CBF and flumazenil (FMZ) binding on benzodiazepine receptors: extension of final infarct as seen on MRI 3 weeks post-insult (**a**); subarea with severely decreased FMZ binding (**b**); subarea with CBF < 14 ml/100 g/min; combination of (**a**), (**b**) and (**c**) showing infarct subareas with decreased FMZ binding and reduced CBF in relation to final infarction. [Reproduced with permission from Heiss et al. (2001)]

possible, there are still open questions as concerns the conclusions about functional and tissue status that can really be drawn from MRI for the individual patient. Multiparametric MRI approaches (e.g., combined diffusion- and perfusion-weighted imaging) can be expected to greatly improve the diagnostic value of the method by modeling and predicting infarct evolution.

References

Back T, Schüler OG, Otto D, Culmsee C, Plesnila N, Krieglstein J, Oertel WH, Baethmann A (2002) Early versus delayed thrombolysis in embolic stroke: effects on blood flow, DC potential and infarct morphology. In: Krieglstein J, Klumpp S (eds) Pharmacology of cerebral ischemia. MedPharm Scientific Publishers, Stuttgart, pp 159–169

Baird AE, Benfield A, Schlaug G, Siewert B, Lövblad K-O, Edelman RR, Warach S (1997) Enlargement of human cerebral ischemic lesion volumes measured by diffusion-weighted magnetic resonance imaging. Ann Neurol 41:581–589

Bakay L, Kurland RJ, Parrish RG, Lee JC, Peng RJ, Bartkowski HM (1975) Nuclear magnetic resonance studies in normal and edematous brain tissue. Exp Brain Res 23:241–248

Barber PA, Darby DG, Desmond PM, Gerraty RP, Yang Q, Li T, Jolley D, Donnan GA, Tress BM, Davis SM (1999) Identification of major ischemic change. Diffusion-weighted imaging versus computed tomography. Stroke 30:2059–2065

Barone FC, Clark RK, Feuerstein G, Lenkinski RE, Sarkar SK (1991) Quantitative comparison of magnetic resonance imaging (MRI) and histologic analyses of focal ischemic damage in the rat. Brain Res Bull 26:285–291

Belayev L, Busto R, Zhao W, Ginsberg MD (1996) Quantitative evaluation of blood–brain barrier permeability following middle cerebral artery occlusion in rats. Brain Res 739:88–96

Bose B, Jones SC, Lorig R, Friel HT, Weinstein M, Little JR (1988) Evolving focal cerebral ischemia in cats: spatial correlation of nuclear magnetic resonance imaging, cerebral blood flow, tetrazolium staining, and histopathology. Stroke 19:28–37

Brant-Zawadzki M, Pereira B, Weinstein P, Moore S, Kucharczyk W, Berry I, McNamara M, Derugin N (1986) MR imaging of acute experimental ischemia in cats. Am J Neuroradiol 7:7–11

Calamante F, Lythgoe MF, Pell GS, Thomas DL, King MD, Busza AL, Sotak CH, Williams SR, Ordidge RJ, Gadian DG (1999) Early changes in water diffusion, perfusion, T1, and T2 during focal cerebral ischemia in the rat studied at 8.5 T. Magn Reson Med 41:479–485

Chuaqui R, Tapia J (1993) Histologic assessment of the age of recent brain infarcts in man. J Neuropathol Exp Neurol 52:481–489

Clark RK, Lee EV, Fish CJ, White RF, Price WJ, Jonak ZL, Feuerstein GZ, Barone FC (1993) Development of tissue damage, inflammation and resolution following stroke: an immunohistochemical and quantitative planimetric study. Brain Res Bull 31:565–572

Crain MR, Yuh WT, Greene GM, Loes DJ, Ryals TJ, Sato Y, Hart MN (1991) Cerebral ischemia: evaluation with contrast-enhanced MR imaging. Am J Neuroradiol 12:631–639

Dijkhuizen RM, Nicolay K (2003) Magnetic resonance imaging in experimental models of brain disorders. J Cereb Blood Flow Metab 23:1383–1402

Dijkhuizen RM, Knollema S, van der Worp HB, Ter Horst GJ, De Wildt DJ, Berkelbach van der Sprenkel JW, Tulleken KA, Nicolay K (1998) Dynamics of cerebral tissue injury and perfusion after temporary hypoxia-ischemia in the rat: evidence for region-specific sensitivity and delayed damage. Stroke 29:695–704

Dirnagl U, Iadecola C, Moskowitz MA (1999) Pathobiology of ischaemic stroke: an integrated view. Trends Neurosci 22:391–397

Doerfler A, Forsting M, Reith W, Staff C, Heiland S, Schabitz WR, von Kummer R, Hacke W, Sartor K (1996) Decompressive craniectomy in a rat model of "malignant" cerebral hemispheric stroke: experimental support for an aggressive therapeutic approach. J Neurosurg 85:853–859

Elster AD (1991) MR contrast enhancement in brainstem and deep cerebral infarction. Am J Neuroradiol 12:1127–1132

Endres M, Dirnagl U (2002) Ischemia and stroke. Adv Exp Med Biol 513:455–473

Essig M, von Kummer R, Egelhof T, Winter R, Sartor K (1996) Vascular MR contrast enhancement in cerebrovascular disease. Am J Neuroradiol 17:887–894

Ewing JR, Jiang Q, Boska M, Zhang ZG, Brown SL, Li GH, Divine GW, Chopp M (1999) T1 and magnetization transfer at 7 Tesla in acute ischemic infarct in the rat. Magn Reson Med 41:696–705

Garcia JH, Yoshida Y, Chen H, Li Y, Zhang ZG, Lian J, Chen S, Chopp M (1993) Progression from ischemic injury to infarct following middle cerebral artery occlusion in the rat. Am J Pathol 142:623–635

Garcia JH, Lassen NA, Weiller C, Sperling B, Nakagawara J (1996) Ischemic stroke and incomplete infarction. Stroke 27:761–765

Go KG (1997) The normal and pathological physiology of brain water. Adv Tech Stand Neurosurg 23:47–142

Hata R, Maeda K, Hermann D, Mies G, Hossmann KA (2000) Evolution of brain infarction after transient focal cerebral ischemia in mice. J Cereb Blood Flow Metab 20:937–946

Hatashita S, Hoff JT (1990) Brain edema and cerebrovascular permeability during cerebral ischemia in rats. Stroke 21:582–588

Heiss WD, Kracht LW, Thiel A, Grond M, Pawlik G (2001) Penumbral probability thresholds of cortical flumazenil binding and blood flow predicting tissue outcome in patients with cerebral ischaemia. Brain 124:20–29

Helpern JA, Dereski MO, Knight RA, Ordidge RJ, Chopp M, Qing ZX (1993) Histopathological correlations of nuclear magnetic resonance imaging parameters in experimental cerebral ischemia. Magn Reson Imaging 11:241–246

Heye N, Cervos-Navarro J (1996) Microthromboemboli in acute infarcts: analysis of 40 autopsy cases. Stroke 27:431–434

Hoehn-Berlage M, Eis M, Back T, Kohno K, Yamashita K (1995) Changes of relaxation times (T1, T2) and apparent diffusion coefficient after permanent middle cerebral artery occlusion in the rat: temporal evolution, regional extent, and comparison with histology. Magn Reson Med 34:824–834

Hofmeijer J, Veldhuis WB, Schepers J, Nicolay K, Kappelle LJ, Bar PR, van der Worp HB (2004) The time course of ischemic damage and cerebral perfusion in a rat model of space-occupying cerebral infarction. Brain Res 1013:74–82

Horikawa Y, Naruse S, Tanaka C, Hirakawa K, Nishikawa H (1986) Proton NMR relaxation times in ischemic brain edema. Stroke 17:1149–1152

Hossmann KA (1998) Experimental models for the investigation of brain ischemia. Cardiovasc Res 39:106–120

Huang ZG, Xue D, Preston E, Karbalai H, Buchan AM (1999) Biphasic opening of the blood–brain barrier following transient focal ischemia: effects of hypothermia. Can J Neurol Sci 26:298–304

Ishii H, Arai T, Morikawa S, Inubushi T, Tooyama I, Kimura H, Mori K (1998) Evaluation of focal cerebral ischemia in rats by magnetic resonance imaging and immunohistochemical analyses. J Cereb Blood Flow Metab 18:931–934

Karonen JO, Partanen PL, Vanninen RL, Vainio PA, Aronen HJ (2001) Evolution of MR contrast enhancement patterns during the first week after acute ischemic stroke. Am J Neuroradiol 22:103–111

Kavec M, Grohn OHJ, Kettunen MI, Silvennoinen MJ, Garwood M, Kauppinen RA (2004) Acute cerebral ischemia in rats studied by Carr-Purcell spin-echo magnetic resonance imaging: assessment of blood oxygenation level-dependent and tissue effects on the transverse relaxation. Magn Reson Med 51:1138-1146

Klatzo I (1967) Presidental address. Neuropathological aspects of brain edema. J Neuropathol Exp Neurol 26:1–14

Knight RA, Ordidge RJ, Helpern JA, Chopp M, Rodolosi LC, Peck D (1991) Temporal evolution of ischemic damage in rat brain measured by proton nuclear magnetic resonance imaging. Stroke 22:802–808

Knight RA, Dereski MO, Helpern JA, Ordidge RJ, Chopp M (1994) Magnetic resonance imaging assessment of evolving focal cerebral ischemia. Comparison with histopathology in rats. Stroke 25:1252–1261

Kucinski T, Vaterlein O, Glauche V, Fiehler J, Klotz E, Eckert B, Koch C, Rother J, Zeumer H (2002) Correlation of apparent diffusion coefficient and computed tomography density in acute ischemic stroke. Stroke 33:1786–1791

Kuroiwa T, Ting P, Martinez H, Klatzo I (1985) The biphasic opening of the blood-brain barrier to proteins following temporary middle cerebral artery occlusion. Acta Neuropathol (Berl) 68:122–129

Kuroiwa T, Ueki M, Chen Q, Ichinose S, Okeda R (1994a) Is the swelling in brain edema isotropic or anisotropic? Acta Neurochir Suppl (Wien) 60:155–157

Kuroiwa T, Ueki M, Chen Q, Suemasu H, Taniguchi I, Okeda R (1994b) Biomechanical characteristics of brain edema: the difference between vasogenic-type and cytotoxic-type edema. Acta Neurochir Suppl (Wien) 60:158–161

Li F, Liu KF, Silva MD, Omae T, Sotak CH, Fenstermacher JD, Fisher M, Hsu CY, Lin W (2000) Transient and permanent resolution of ischemic lesions on diffusion-weighted imaging after brief periods of focal ischemia in rats : correlation with histopathology. Stroke 31:946–954

Lin SP, Schmidt RE, McKinstry RC, Ackerman JJ, Neil JJ (2002a) Investigation of mechanisms underlying transient T2 normalization in longitudinal studies of ischemic stroke. J Magn Reson Imaging 15:130–136

Lin TN, Sun SW, Cheung WM, Li F, Chang C (2002b) Dynamic changes in cerebral blood flow and angiogenesis after transient focal cerebral ischemia in rats. Evaluation with serial magnetic resonance imaging. Stroke 33:2985–2991

Loubinoux I, Volk A, Borredon J, Guirimand S, Tiffon B, Seylaz

J, Meric P (1997) Spreading of vasogenic edema and cytotoxic edema assessed by quantitative diffusion and T2 magnetic resonance imaging. Stroke 28:419-426; discussion 426–417

Mokri B (2001) The Monro-Kellie hypothesis: applications in CSF volume depletion. Neurology 56:1746–1748

Naruse S, Horikawa Y, Tanaka C, Hirakawa K, Nishikawa H, Yoshizaki K (1982) Proton nuclear magnetic resonance studies on brain edema. J Neurosurg 56:747–752

Nedergaard M, Vorstrup S, Astrup J (1986) Cell density in the borderzone around old small human brain infarcts. Stroke 17:1129–1137

Nelson CW, Wei EP, Povlishock JT, Kontos HA, Moskowitz MA (1992) Oxygen radicals in cerebral ischemia. Am J Physiol 263:H1356–1362

Neumann-Haefelin T, Kastrup A, de Crespigny A, Yenari MA, Ringer T, Sun GH, Moseley ME (2000) Serial MRI after transient focal cerebral ischemia in rats: dynamics of tissue injury, blood-brain barrier damage, and edema formation. Stroke 31:1965–1972; discussion 1972–1963

Neumann-Haefelin C, Brinker G, Uhlenkuken U, Pillekamp F, Hossmann KA, Hoehn M (2002) Prediction of hemorrhagic transformation after thrombolytic therapy of clot embolism: an MRI investigation in rat brain. Stroke 33:1392–1398

Neumar RW (2000) Molecular mechanisms of ischemic neuronal injury. Ann Emerg Med 36:483–506

Niessen F, Hilger T, Hoehn M, Hossmann KA (2002) Thrombolytic treatment of clot embolism in rat: comparison of intra-arterial and intravenous application of recombinant tissue plasminogen activator. Stroke 33:2999–3005

Nordborg C, Sokrab TE, Johansson BB (1994) Oedema-related tissue damage after temporary and permanent occlusion of the middle cerebral artery. Neuropathol Appl Neurobiol 20:56–65

Norton GA, Kishore PR, Lin J (1978) CT contrast enhancement in cerebral infarction. Am J Roentgenol 131:881–885

Olah L, Wecker S, Hoehn M (2000) Secondary deterioration of apparent diffusion coefficient after 1-hour transient focal cerebral ischemia in rats. J Cereb Blood Flow Metab 20:1474–1482

Oppenheim C, Grandin C, Samson Y, Smith A, Duprez T, Marsault C, Cosnard G (2001) Is there an apparent diffusion coefficient threshold in predicting tissue viability in hyperacute stroke? Stroke 32:2486–2491

Ordidge RJ, Helpern JA, Knight RA, Qing ZX, Welch KM (1991) Investigation of cerebral ischemia using magnetization transfer contrast (MTC) MR imaging. Magn Reson Imaging 9:895–902

Palmer GC, Peeling J, Corbett D, Del Bigio MR, Hudzik TJ (2001) T2-weighted MRI correlates with long-term histopathology, neurology scores, and skilled motor behavior in a rat stroke model. Ann NY Acad Sci 939:283–296

Parisi J, Place C, Nag S (1988) Calcification in a recent cerebral infarct-radiologic and pathologic correlation. Can J Neurol Sci 15:152–155

Persson L, Hardemark HG, Bolander HG, Hillered L, Olsson Y (1989) Neurologic and neuropathologic outcome after middle cerebral artery occlusion in rats. Stroke 20:641–645

Pierpaoli C, Righini A, Linfante I, Tao-Cheng JH, Alger JR, Di Chiro G (1993) Histopathologic correlates of abnormal water diffusion in cerebral ischemia: diffusion-weighted MR imaging and light and electron microscopic study. Radiology 189:439–448

Quast MJ, Huang NC, Hillman GR, Kent TA (1993) The evolution of acute stroke recorded by multimodal magnetic resonance imaging. Magn Reson Imaging 11:465–471

Reichardt M (1904) Zur Entstehung des Hirndrucks. Dtsch Z Nervenheilkd 28:306

Rose SE, Chalk JB, Griffin MP, Janke AL, Chen F, McLachan GJ, Peel D, Zelaya FO, Markus HS, Jones DK, Simmons A, O'Sullivan M, Jarosz JM, Strugnell W, Doddrell DM, Semple J (2001) MRI based diffusion and perfusion predictive model to estimate stroke evolution. Magn Reson Imaging 19:1043–1053

Rosenberg GA, Navratil M, Barone F, Feuerstein G (1996) Proteolytic cascade enzymes increase in focal cerebral ischemia in rat. J Cereb Blood Flow Metab 16:360–366

Rosenberg GA, Estrada EY, Dencoff JE (1998) Matrix metalloproteinases and TIMPs are associated with blood-brain barrier opening after reperfusion in rat brain. Stroke 29:2189–2195

Rubin LL, Staddon JM (1999) The cell biology of the blood-brain barrier. Annu Rev Neurosci 22:11–28

Runge VM, Price AC, Wehr CJ, Atkinson JB, Tweedle MF (1985) Contrast enhanced MRI. Evaluation of a canine model of osmotic blood-brain barrier disruption. Invest Radiol 20:830–844

Saur D, Kucinski T, Grzyska U, Eckert B, Eggers C, Niesen W, Schoder V, Zeumer H, Weiller C, Rother J (2003) Sensitivity and interrater agreement of CT and diffusion-weighted MR imaging in hyperacute stroke. Am J Neuroradiol 24:878–885

Schuier FJ, Hossmann KA (1980) Experimental brain infarcts in cats. II. Ischemic brain edema. Stroke 11:593–601

Schwab S, Steiner T, Aschoff A, Schwarz S, Steiner HH, Jansen O, Hacke W (1998) Early hemicraniectomy in patients with complete middle cerebral artery infarction. Stroke 29:1888–1893

Snider BJ, Gottron FJ, Choi DW (1999) Apoptosis and necrosis in cerebrovascular disease. Ann NY Acad Sci 893:243–253

Thomalla GJ, Kucinski T, Schoder V, Fiehler J, Knab R, Zeumer H, Weiller C, Rother J (2003) Prediction of malignant middle cerebral artery infarction by early perfusion- and diffusion-weighted magnetic resonance imaging. Stroke 34:1892–1899

Torvik A, Svindland A (1986) Is there a transitional zone between brain infarcts and the surrounding brain? A histological study. Acta Neurol Scand 74:365–370

Uyama O, Okamura N, Yanase M, Narita M, Kawabata K, Sugita M (1988) Quantitative evaluation of vascular permeability in the gerbil brain after transient ischemia using Evans blue fluorescence. J Cereb Blood Flow Metab 8:282–284

Van Bruggen N, Roberts TP, Cremer JE (1994) The application of magnetic resonance imaging to the study of experimental cerebral ischaemia. Cerebrovasc Brain Metab Rev 6:180–210

Van Dorsten FA, Olah L, Schwindt W, Grune M, Uhlenkuken U, Pillekamp F, Hossmann KA, Hoehn M (2002) Dynamic changes of ADC, perfusion, and NMR relaxation parameters in transient focal ischemia of rat brain. Magn Reson Med 47:97–104

Van Lookeren Campagne M, Thomas GR, Thibodeaux H, Palmer JT, Williams SP, Lowe DG, van Bruggen N (1999) Secondary reduction in the apparent diffusion coefficient of water, increase in cerebral blood volume, and delayed neuronal death after middle cerebral artery occlusion and early reperfusion in the rat. J Cereb Blood Flow Metab 19:1354–1364

Virley D, Beech JS, Smart SC, Williams SC, Hodges H, Hunter AJ (2000) A temporal MRI assessment of neuropathology after transient middle cerebral artery occlusion in the rat: correlations with behavior. J Cereb Blood Flow Metab 20:563–582

Vo KD, Santiago F, Lin W, Hsu CY, Lee Y, Lee JM (2003) MR imaging enhancement patterns as predictors of hemorrhagic transformation in acute ischemic stroke. AJNR Am J Neuroradiol 24:674–679

Warach S (2001) New imaging strategies for patient selection for thrombolytic and neuroprotective therapies. Neurology 57:S48–S52

Wardlaw JM, Keir SL, Seymour J, Lewis S, Sandercock PA, Dennis MS, Cairns J (2004) What is the best imaging strategy for acute stroke? Health Technol Assess 8:iii, ix-x, 1–180

Weber R, Wegener S, Ramos-Cabrer P, Wiedermann D, Hoehn M (2005) MRI detection of macrophage activity after experimental stroke in rats: new indicators for late appearance of vascular degradation? Magn Rreson Med 54(1):59-66

Wegener S, Weber R, Ramos-Cabrer P, Uhlenkueken U, Wiedermann D, Kandal K, Villringer A, Hoehn M (2005) Subcortical lesions after transient thread occlusion in the rat: T2-w magnetic resonance imaging findings without corresponding sensorimotor deficits. JMRI 21(4):340-346

Yepes M, Sandkvist M, Moore EG, Bugge TH, Strickland DK, Lawrence DA (2003) Tissue-type plasminogen activator induces opening of the blood-brain barrier via the LDL receptor-related protein. J Clin Invest 112:1533–1540

9 MR Imaging of White Matter Changes

Johanna Helenius and Turgut Tatlisumak

CONTENTS

9.1 Cerebral White Matter

The cerebral white matter (WM) surrounds the subcortical gray matter (GM) and intervenes between it and the cerebral cortex. The cerebral WM consists of fibers of axons and their myelin sheaths. The whitish color is given by the myelin content. Approximately half of the brain weight and volume is formed by the WM. The WM is developed from the external marginal zone of neural tube, as the marginal zone consists of nerve cell processes that evolve into WM when myelinated. Each neuron has a single axon that may have a length of micrometers to over 1 m and a diameter of 0.1 μm to more than 20 μm. Most axons are covered by multiple concentric layers of myelin, a lipid- and protein-rich insulating material formed by oligodendrocytes in the central nervous system. Their function is to provide neurons with structural support and maintain local conditions for neuronal function. Myelinization starts about the middle of fetal life; some tracts are not completely myelinated until 20 years of age. However, most myelinization is completed by 18 months of life. The phylogenetically oldest tracts myelinate first (e.g. tracts within the spinal cord) whereas the corticospinal tracts myelinate largely during the first and the second years of life. The WM contains less water and more lipid than the GM. While average cerebral blood flow (CBF) is approximated to be 45–55 ml/100 g/min, it is about 80 ml/100 g/min in the GM, and only 20 ml/100 g/min in the WM (Lassen 1985; Moody et al. 1990).

The dense intermingling of nerve fibers within the WM connects different regions of the brain with each other. Projectional fibers connect cerebral cortex and subcortical structures as well as cerebellum; commissural fibers connect homologous areas between the two hemispheres of brain, and the association fibers connect various regions within the same cerebral hemisphere. The major function of the cerebral WM is simply to interconnect various regions of brain and transmit signals in-between them.

9.2 White Matter Changes (Leukoaraiosis)

9.2.1 What Is Leukoaraiosis?

Cerebral WM changes (WMC) are found in a number of diseases of adulthood, such as the debated Binswanger's disease, multiple sclerosis, acute demyelinating encephalomyelitis, posterior reversible leukoencephalopathy syndrome, cerebral anoxia, leukodystrophies, and mitochondrial encephalopathies, among others. The term leukoaraiosis (LA) is applied for nonspecific WMC, primarily in the elderly, that cannot be attributed to a

J. Helenius, MD, PhD
T. Tatlisumak, MD, PhD
Department of Neurology, Helsinki University Central Hospital, Haartmaninkatu 4, 00290 Helsinki, Finland

specific disease. Several terms other than LA, such as unidentified bright objects and incidental subcortical lesions, are also used to describe these lesions. In 1987, Hachinski and coworkers used the term leukoaraiosis (from the Greek; leuko = white and araiosis = rarefied, of loose texture, or rarefaction) to describe an abnormal computed tomography (CT) appearance of the subcortical brain WM in elderly or demented individuals, seen as bilateral patchy or diffuse areas of reduced X-ray attenuation (hypointense) with ill-defined margins, limited to the periventricular regions or extended to the centrum ovale (Fig. 9.1). On the contrary, LA appears as hyperintense lesions in periventricular or subcortical regions on T2-weighted or fluid attenuated inversion recovery (FLAIR) magnetic resonance imaging (MRI) sequences.

9.2.2 Epidemiology

The frequency of LA increases considerably with age. Under 50 years of age, prevalence on CT is only a few percent, and over the age of 50 the prevalence increases two- to three-fold with every decade. LA is a common finding, and its frequency in older patient groups has ranged between 21% and 100% depending on the imaging method used and on the study population; its exact frequency is still under debate since no agreement between the various rating scales exists between centers, and CT and different sequences of MRI detect LA differently. In healthy subjects, it is found in 1%–10% when studied with CT and in 27% with MRI (Breteler et al. 1994). In the Cardiovascular Health Study, among 3660 community-living elderly participants, the incidence of LA increased more rapidly with age in the group of individuals with some risk factors or findings of cardiovascular disease than in the healthier subgroup (Yue et al. 1997). Furthermore, the degree of LA was higher in women than in men in both this and the later Rotterdam Scan Study where 1077 subjects aged between 60 to 90 were randomly sampled from the general population and evaluated by MRI (de Leeuw et al. 2001). In the Rotterdam Scan Study, only 5% of the individuals were completely free of LA (de Leeuw et al. 2001).

9.2.3 Pathophysiological and Clinical Aspects

Chronic cerebral ischemia and hypoperfusion due to various reasons are thought to be the main etiologies for LA (Pantoni and Garcia 1997). Some individuals, regardless of the severity of LA, remain neurologically and neuropsychologically asymptomatic for prolonged periods, while others develop cognitive impairment, mood and psychiatric disorders, gait disturbance, urinary dysfunctions, disability, and even dementia. LA has been found to be associated with significantly lower scores on neuropsychological test batteries (Breteler et al. 1994), and an independent risk factor for dementia. As depicted in the Cardiovascular Health Study (Bryan et al. 1997) and later in the Rotterdam Scan Study (Vermeer et al. 2003), LA does seem to increase morbidity and mortality, and to enhance the risk for ischemic stroke even in neurologically asymptomatic elderly patients.

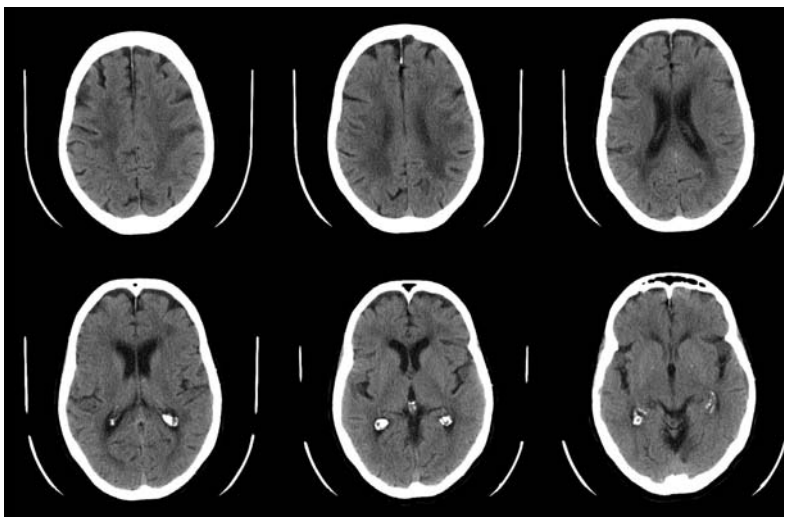

Fig. 9.1. Computed tomography (CT) images of a 75-year-old patient with widespread and symmetrical leukoaraiotic changes

In autopsy studies, leukoaraiotic regions have been found to consist of periventricular venous collagenosis, perivascular degeneration with widening of extracellular and perivascular spaces, arteriolar tortuosity, lacunar infarcts, incomplete infarctions, apoptosis, gliosis, axonal loss with loosening of the WM structure, and proliferation of glial cells (Moody et al. 1995; Brown et al. 2000, 2002; Murdoch 2000). Axonal loss leads to an increase in water content of affected brain tissue. The findings suggest that an inflammatory reaction, changes in myelin, and compromised axonal transport, all of which are affected in chronic ischemia, may play important roles in the pathophysiology of LA. Further support for the role of chronic ischemia comes from the markers of chronic endothelial dysfunction and prothrombic changes in patients with LA (Hassan et al. 2003).

Wallerian degeneration, seen in the cerebral and spinal WM, is the descending destruction of axons and myelin sheaths resulting from more proximal neuronal damage, such as that due to ischemic infarction or hemorrhage and is different from LA. It is characterized by disintegration of axonal structures within days after injury, followed by degradation of myelin due to infiltration of macrophages, leading finally to fibrosis and atrophy of the affected fiber tracts. In the chronic stage of Wallerian degeneration, the destruction of myelin sheaths can be detected by CT. Conventional MRI detects varying signal intensity changes during the time course of Wallerian degeneration several weeks after the injury. Short phase of hypointensity of T2-weighted images is followed by hyperintensity along the affected tracts. However, in the first days and weeks, Wallerian degeneration can be detected neither by CT nor by conventional MRI. Instead, diffusion tensor imaging, being particularly suitable for imaging white matter tracts in vivo, seems to display characteristic changes of water diffusion already within the first weeks after the injury. A decrease of the fractional anisotropy indicates disintegration of axonal structuresand myelin (Thomalla et al. 2004).

Many individuals with LA also harbor lacunar and/or cortical infarcts. Presence of LA serves as an intermediate surrogate both for ischemic stroke and intracerebral hemorrhage as they all share similar risk factors and similar pathophysiological mechanisms (Inzitari 2003). LA is widely found in dementing illnesses, such as Alzheimer's disease, vascular dementia, and cerebral autosomal dominant arteriopathy with subcortical infarcts and leukoencephalopathy (CADASIL). Failure of blood supply in the small arteries of the brain, chronic brain ischemia due to various reasons, diabetes mellitus, brain blood pressure dysregulation, and especially high systemic arterial blood pressure are associated with LA (Pantoni and Garcia 1995).

9.3 Computed Tomography Findings

The application of CT for three decades revealed an unexpected amount of LA in both healthy and cognitively impaired individuals. Originally, the term LA was introduced to describe the WMC in periventricular or subcortical regions seen hypointense on CT. Therefore, the term LA is originally described based upon CT findings, and some of the findings with MRI may be of doubtful significance. CT shows the most pronounced findings of LA (Fig. 9.1), while MRI detects the lesions in smaller and in earlier stages (Fig. 9.2). In general, MRI is overwhelmingly more sensitive than CT in detecting LA.

9.4 Conventional Magnetic Resonance Imaging Findings

Conventional MRI detects LA with low specificity but high sensitivity. However, most of the diseases of the WM are far less frequent than leukoaraiotic changes that are found usually in healthy but aging brain and with cerebrovascular risk factors. Additionally, most of the diseases affecting the WM manifest themselves with characteristic clinical features unlike incidental LA.

T2-weighted, proton-density-weighted, and FLAIR imaging are highly sensitive in the detection of LA. Since T2-weighted imaging is sensitive to liquid, gliosis, and the effects of demyelination, some of the lesions seen on T2-weighted imaging may represent Virchow-Robin (VR) spaces instead of leukoaraiotic lesions or have no neuropathological correlates at all (Fig. 9.3). T1-weighted imaging is the least sensitive, as leukoaraiotic changes are seen as hypointense regions or no change at all.

VR space, or perivascular space, is an invagination of the subpial space surrounding a vessel going into the brain. VR spaces surround arteries, veins, arterioles, and venules. VR spaces enlarge and become numerous by advancing age, hypertension,

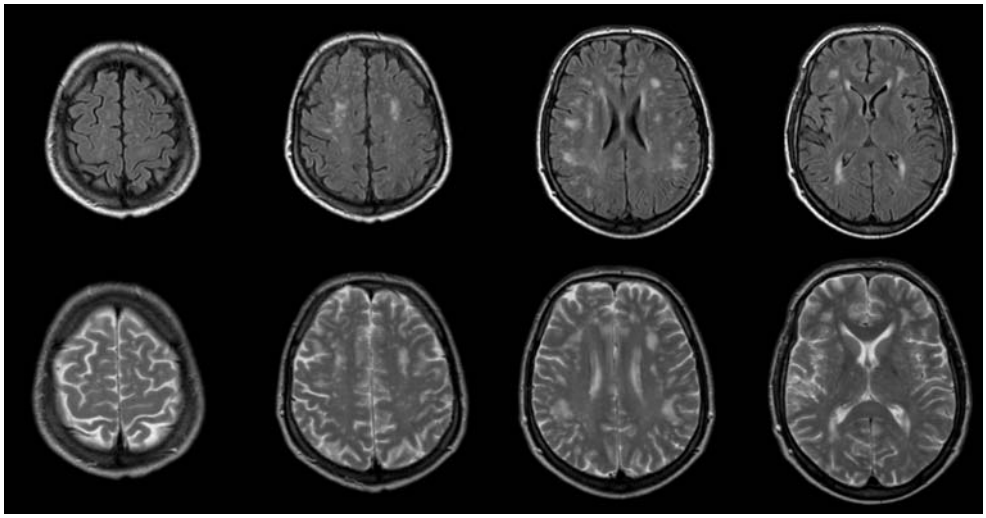

Fig. 9.2. Fluid-attenuated inversion recovery (FLAIR, upper row) and T2-weighted (lower row) magnetic resonance images demonstrating early small focal lesions of leukoaraiosis

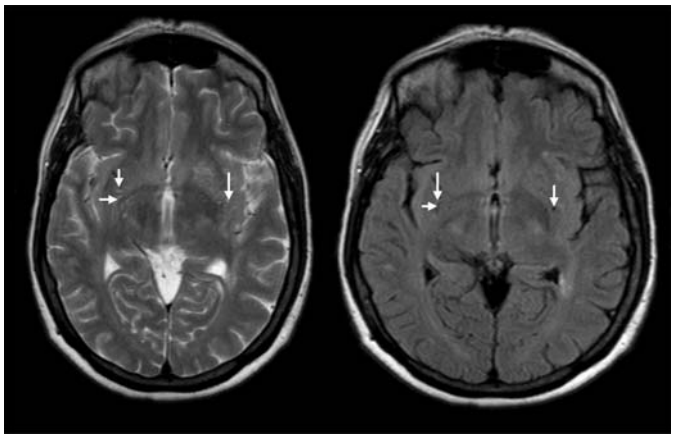

Fig. 9.3. Virchow-Robin spaces marked with *arrows* on T2-weighted (left) and FLAIR (right) images. They appear bright on T2-WI and can be differentiated from pathological changes only when both images are evaluated simultaneously

and dementia (Heier et al. 1989). The significance of VR spaces is not to confuse them with lacunar infarcts or with LA. Because perivascular spaces are filled with extracellular fluid, their signal is similar to that of cerebrospinal fluid on all pulse sequences. On FLAIR images, the CSF is hypointense compared to brain tissue and VR spaces also appear dark (hypointense) whereas they appear bright (hyperintense) on T2-weighted images (Fig. 9.3).

FLAIR is an inversion recovery sequence with long repetition and echo times and an inversion time that is tailored to null the signal from CSF. Most pathologic processes including LA show increased signal intensities on T2-weighted images and the conspicuity of lesions located close to interfaces between brain parenchyma and CSF may be poor (Rumboldt and Marotti 2003). Additionally, the high signal of CSF on T2-weighted images makes it difficult to differentiate VR spaces from true lesions. FLAIR images are heavily T2-weighted with CSF signal suppression, highlighting hyperintense lesions and improving their detection when located adjacent to CSF-containing spaces and differentiating VR spaces from lesions as these spaces appear as hypointense like CSF on FLAIR images.

Previously, it has been thought that LA is limited to the supratentorial part of the brain, and even in that case they do not affect the internal capsule. However, with advancements in neuroimaging and research work, it recently became evident that similar lesions can be seen in the pons (Fig. 9.4) and the internal capsule (Fig. 9.5). The LA lesions around the horns of ventricles are usually homogeneous, while those in other regions of WM tend to appear as mul-

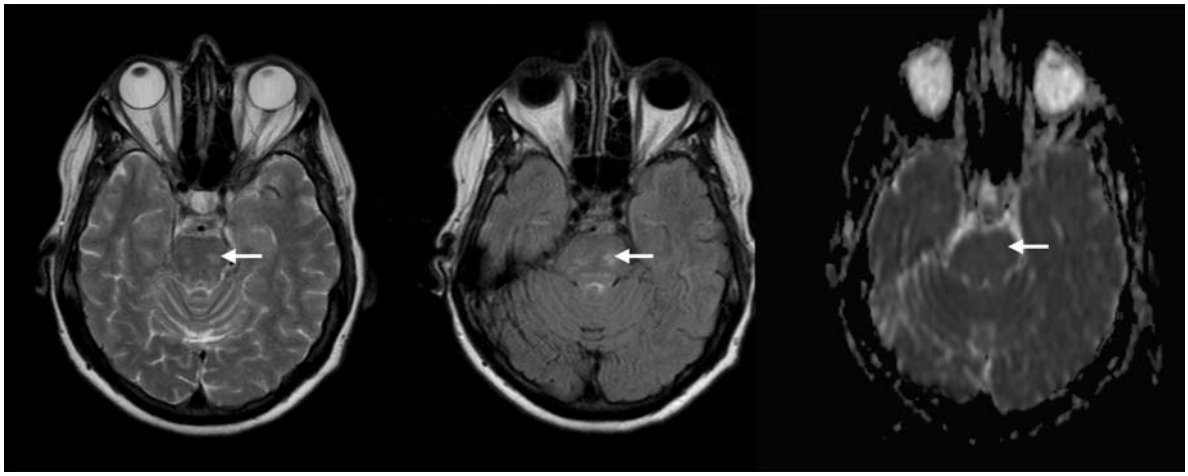

Fig. 9.4. Pontine leukoaraiosis appearing hyperintense on T2-weighted (left) and FLAIR (middle) images and on an ADC map (right)

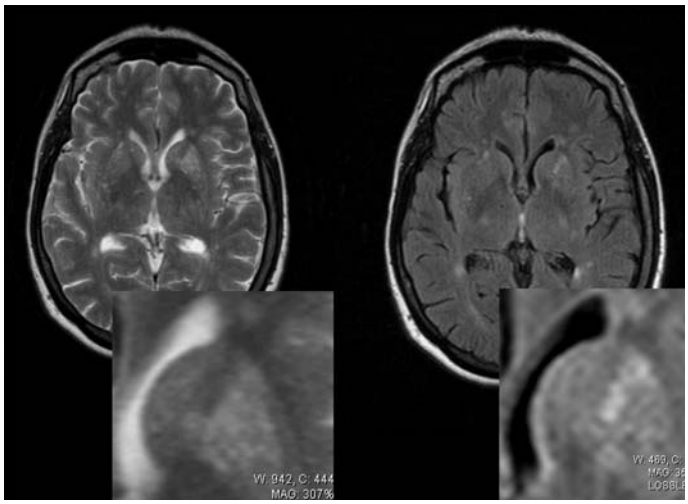

Fig. 9.5. T2-weighted (left) and FLAIR (right) images demonstrating a leukoaraiotic lesion in the left internal capsule (on the *right side* of the image)

tiple smaller lesions unless LA is extremely severe. The subcortical u-fibers and corpus callosum are usually spared from LA changes due to their favorable blood supply.

9.4.1 Rating Scales for Leukoaraiotic Changes

The classification of LA according to its severity and extent is a real challenge. Several rating scales with varying approaches exist. Some make a distinction between different regions, while others use an overall estimate of LA. The scales often refer to definite pulse sequences or imaging methods. A previously validated rating scale utilizing MRI that was developed at our hospital will be presented below, since it takes widely into account the number, size, and shape of the leukoaraiotic lesions. Although the numerous rating scales in the literature have different approaches to evaluating the LA, comparison of the results between studies has been deemed to be reasonable.

WM lesions are rated separately in four WM areas: periventricular, deep, watershed, and subcortical WM. By definition, periventricular WM foci have to be in contact with the ventricular wall, deep WM foci separated from the ventricles by a strip of normal-appearing WM and located outside watershed regions. Watershed regions are the areas located between the territories of two of the main cerebral arteries, like middle cerebral artery and anterior cerebral artery or middle cerebral artery and posterior cerebral artery. The subcortical

region represents the area less than 5 mm beneath the cortex. Foci, which affect some part of this area and are located outside watershed regions, should be rated as subcortical changes.

Periventricular hyperintensities (PVH) are classified based on size and shape into small cap, large cap, and extending cap. Small cap is a hyperintensity lesion of 5 mm or less in diameter, rounded and with regular margins, large cap is 6–10 mm in diameter and has mostly regular margins, while extending cap is over 10 mm in diameter and has irregular margins (Fig. 9.6). The size of the cap is measured in a direction parallel to the axis of the ventricular horn.

PVHs along the bodies of lateral ventricles are classified based on thickness and shape into thin lining, smooth halo, and irregular halo. Thin lining is a hyperintense lining 5 mm or less and has regular margins, smooth halo is 6–10 mm broad and has mostly regular margins, and irregular halo is over 10 mm broad, has irregular margins and extends into the deep WM (Fig. 9.6).

Hyperintensities over other WM regions (HI) are classified based on size and shape into small focal, large focal, focal confluent, diffusely confluent, and extensive WM changes. Small focal lesions are punctate hyperintensities of 5 mm or less and are mostly rounded. Large focal lesions are 6–10 mm in diameter and are mostly rounded; focal confluent lesions are 11–25 mm, have often various shapes and may have irregular borders. Diffusely confluent lesions are over 25 mm, mostly with irregular borders, while extensive WM changes are diffuse regions without distinct focal lesions affecting the majority of the WM area (Fig. 9.7). The number of each type of leukoaraiotic change is counted, and extensive WM changes are rated as absent or present.

PVHs are graded into four categories: 0, absence of PVH; 1, small caps or thin lining; 2, large caps or smooth halo; 3, extending caps or irregular halo. The side, which is more affected, is taken into account. HIs are rated separately in watershed, deep and subcortical white matter into six grades: 0, absence of HI; 1, only small focal lesions; 2, at least one large focal, no confluent lesions; 3, at least one focal confluent, no diffusely confluent lesions; 4, at least one diffusely confluent lesion; 5, extensive HI lesions (Table 9.1).

9.5 Diffusion-Weighted (DWI) and Diffusion Tensor Magnetic Resonance Imaging Findings

Diffusion-weighted magnetic resonance imaging (DWI) provides an image contrast that is dependent on the molecular motion of water (diffusion), which is called Brownian movement. After Stejskal and Tanner described a diffusion-weighted spin-echo T2-weighted pulse sequence with two extra gradient pulses equal in magnitude and opposite in

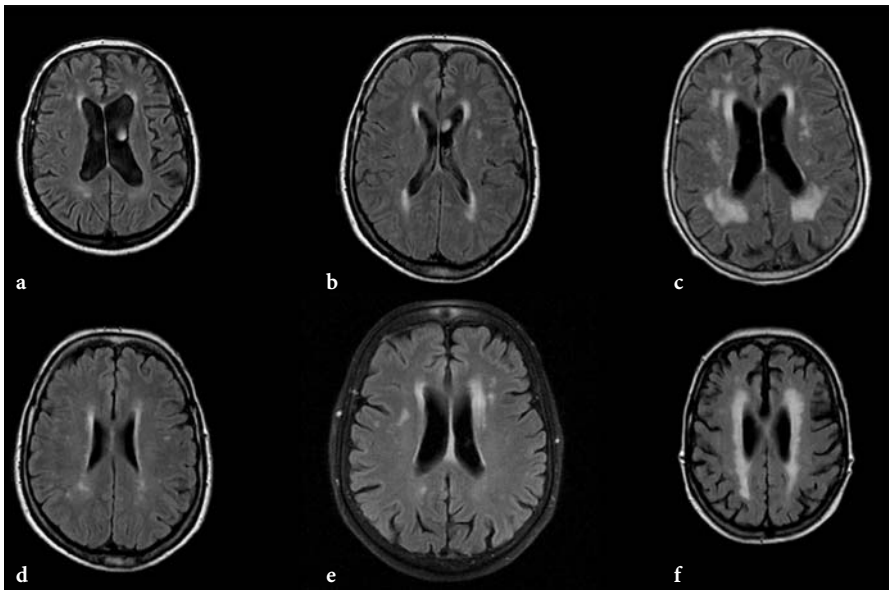

Fig. 9.6a–f. Periventricular white matter changes (FLAIR images). **a** Small caps around the frontal horns of lateral ventricles. **b** Large caps. **c** Extending caps. **d** Thin lining along the bodies of the lateral ventricles. **e** Smooth halo. **f** Irregular halo

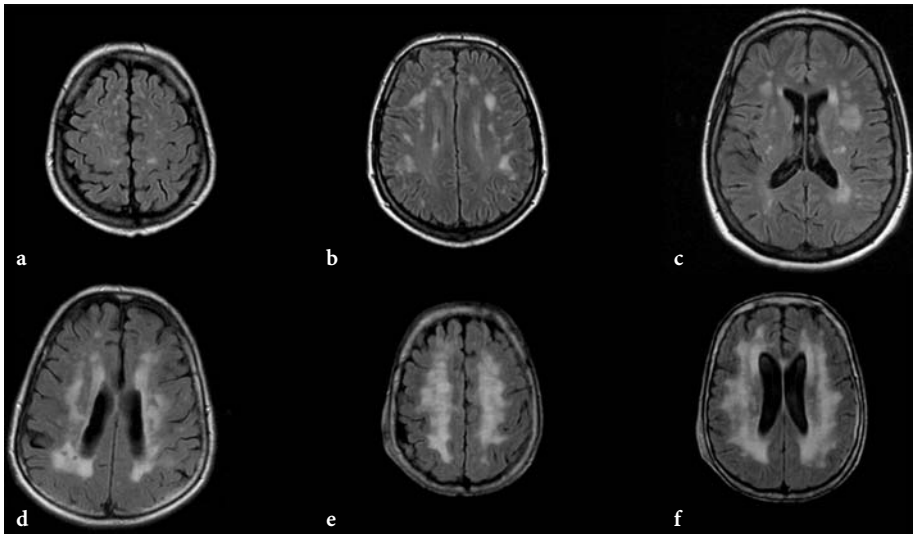

Fig. 9.7a-f. White matter changes in regions other than the periventricular area (FLAIR images). **a** Multiple small focal lesions. **b** Multiple large focal lesions. **c** Multiple focal confluent lesions. **d** Diffusely confluent lesions irregular in shape. **e,f** Extensive WM changes

Table 9.1. Rating scale for leukoaraiotic changes

Periventricular Hyperintensities (PVH)
Around frontal and occipital horns:
Small cap: ≤ 5 mm, rounded, regular margins
Large cap: 6–10 mm, mostly regular margins
Extending cap: >10 mm, irregular margins
Along the bodies of lateral ventricles:
Thin lining: ≤ 5 mm, regular margins
Smooth halo: 6–10 mm, mostly regular margins
Irregular halo: >10 mm, irregular margins
Hyperintensities in the Regions Other Than Periventricular White Matter (HI)
Small focal lesions: ≤ 5 mm, mostly rounded
Large focal lesions: 6–10 mm, mostly rounded
Focal confluent lesions: 11–25 mm, various shapes, may have irregular borders
Diffusely confluent lesions: >25 mm, mostly with irregular borders
Extensive white matter change: diffuse hyperintensity without focal lesions

direction, it took several decades for that sequence to become clinically feasible due to limitations of early MR equipment. The methodology of DWI is discussed in detail in Chap. 7.

Axons transport materials from the cell body to the synaptic terminals (anterograde transport) and in the opposite direction (retrograde transport). Anterograde transport may occur slowly (a few millimeters/day only) or fast (up to 400 mm/day), whereas retrograde transport is always fast. Diffusion in the perpendicular direction (not along axons) is much more limited as the membranes and the myelin sheath form obstacles. Therefore, diffusion is not isotropic (same in all directions) in the WM. This phenomenon is known as "diffusion anisotropy". In contrast, diffusion is relatively isotropic in the GM. Since only the molecular displacement that occurs along the direction of gradient pulses is visible, the effect of diffusion anisotropy can easily be detected by observing variations in diffusion measurements after the direction of gradient pulses is changed. With diffusion tensor imaging, anisotropy effects can be extracted, characterized, and exploited, which provides more detailed information on tissue microstructure in healthy and diseased brains. WM tracts can be followed from the cerebral cortex to the spinal cord, and the diseases involving these tracts can be studied. Among the many indices that offer a numerical value for the degree of tissue anisotropy, the relative anisotropy (RA) index is the ratio of the variance of the eigen-values of their mean,

and is equal to zero in a perfectly isotropic medium. Fractional anisotropy (FA) is the ratio of the anisotropic component of the diffusion tensor and is equal to zero in a perfectly isotropic medium, but approaches 1 for a cylindrically symmetric anisotropic medium. The FA maps demonstrate hyperintensity in regions of brain with anisotropic diffusion, whereas regions with isotropic diffusion will appear hypointense. As diffusion is normally strongly anisotropic in the cerebral WM and anisotropy decreases as a result of LA, FA maps can quantify the degree of LA and may also be useful in a number of other WM disorders. As the WM disease progresses, the FA maps will become darker (hypointense) and the numerical FA value will decrease (Fig. 9.8).

DWI and diffusion tensor imaging provide information on the extent and formation of LA and elucidates the mechanism of LA in vivo. The apparent diffusion coefficient (ADC) value for healthy human brain has been reported to be 0.8 and 1.4×10^{-3} mm^2/s for the cortical GM, and 0.6 and 0.9×10^{-3} mm^2/s for the WM. However, we found significantly higher ADC values for the regions of LA ($0.92–1.27\times10^{-3}$ mm^2/s, Fig. 9.9) and slightly but significantly increased ADC values for the WM regions that appeared normal on T2-weighted images from patients with LA (Helenius et al. 2002). In the same study, ADC values of brain infarction were found to be 0.33 to 0.44×10^{-3} mm^2/s at 6 hours, 0.31 to 0.42×10^{-3} mm^2/s at 24 hours, 0.45 to 0.57×10^{-3} mm^2/s at 1 week, 0.56 to 1.60 at 1 month, and 1.26 to 1.93×10^{-3} mm^2/s at 3 months after the insult. Therefore, LA could easily be distinguished from early and chronic infarcts, but not of 1-month-old infarcts barely depending on ADC findings (Helenius et al. 2002). Leukoaraiotic regions appear hyperintense on ADC maps and hypointense on FA maps (Jones et al. 1999; Helenius et al. 2002). Even the normal-appearing WM regions on T2-weighted imaging in healthy individuals with LA (Helenius et al. 2002) and in patients with ipsilateral carotid artery stenosis (Soinne et al. 2003a) showed increased ADC values. These findings may account for an early change that might lead to LA in a long period of time, but yet undetectable on conventional images. Furthermore, the conventional images showed no change but ADC values decreased slightly but significantly following carotid endarterectomy in the latter patient group, suggesting that this elevation in ADC values is partly reversible (Soinne et al. 2003a). We therefore coined the term "pre-leukoaraiosis" to define this condition. Long-term observational studies are needed to demonstrate whether these WM regions actually go under leukoaraiotic changes overtime.

According to the neuropathological investigations, one of the consequences of LA is axonal loss, which may lead to an increase in the water content of the brain WM tissue, thereby increasing ADC values and decreasing FA of the regions of LA. One may, there-

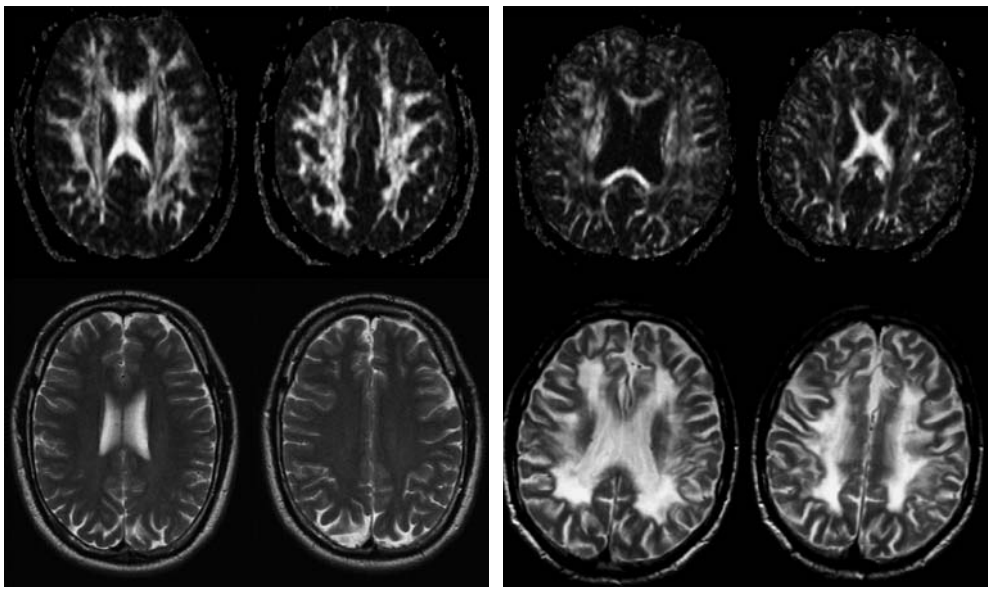

a b

Fig. 9.8a,b. Fractional anisotropy images and T2-weighted images of a healthy individual (**a**) and of a patient with leukoaraiosis (**b**). On the *left* (**a**) *upper row* demonstrates high anisotropy on FA maps and T2-weighted images on the *lower row* appear normal. On the *right side* (**b**) FA maps on the *upper row* demonstrate substantially decreased anisotropy within the WM and on the lower row T2-weighted images show widespread symmetrical leukoaraiosis. (Courtesy of Drs G. Thomalla and T. Kucinski, Hamburg, Germany)

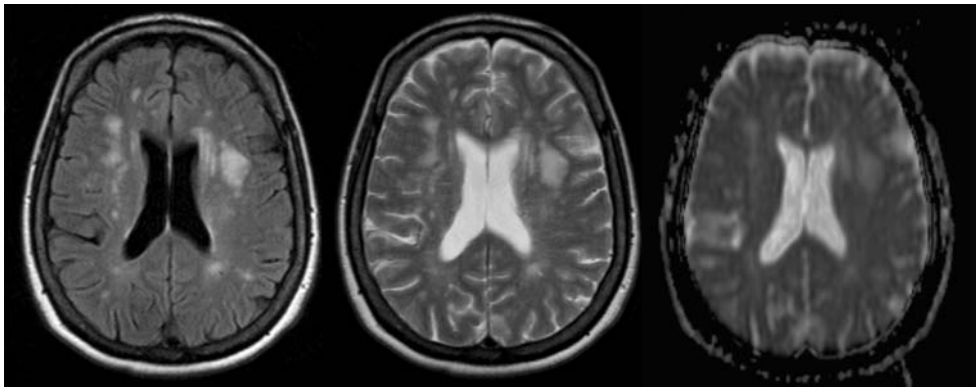

Fig. 9.9. FLAIR (left) and T2-weighted (middle) images, and apparent diffusion coefficient (ADC) map (right) of a patient with leukoaraiosis. Multiple small and large focal lesions can be detected better on the FLAIR image than on the T2-weighted image. Lesions appear hyperintense (bright) on the ADC map indicating increased diffusion

fore, hypothesize that the finding of a relationship between severity of LA and increasing ADC values reflects the extent of axonal loss (Helenius et al. 2002). The partly reversible, preoperatively elevated ipsilateral ADC values in the WM and watershed regions of the high-grade carotid stenosis patients in our study suggest the concomitant existence of both reversible and irreversible components in the pathogenesis of LA, which is triggered and maintained by severe carotid stenosis (hypoperfusion or chronic ischemia). The net decrease observed in ADC values following carotid endarterectomy in those regions supports the hypothesis of a corrective effect on cellular-level mechanisms, one of which could be chronic, ipsilaterally focused relative ischemia.

9.6 Perfusion Magnetic Resonance Imaging (PI) Findings

Brain perfusion refers to the microcirculation of the brain (see Chap. 6). Microcirculation comprises the blood circulation in capillary networks and the exchange of oxygen and nutrients between the blood and the brain tissue. The effectiveness of brain perfusion depends on blood pressure, blood velocity, characteristics of the capillary network, capillary wall permeability, and diffusion rates of oxygen and nutrients. In the healthy brain, perfusion is symmetrical, and is substantially higher in the GM than in the WM. It has been approximated that the CBF is about 80 ml/100 g/min in the GM, and 20 ml/100 g/min in the WM. Brain perfusion is usually quantified in terms of ml/100 g (cerebral blood volume, CBV), ml/100 g/min (CBF), or seconds (mean transit time, MTT). The methodology of perfusion imaging (PI) is discussed in detail in Chap. 6.

As the primary hypothesis for the etiology of LA is chronic ischemia of the brain, PI appears to be a suitable tool for investigating this state. Studies of LA with PI are few, but some preliminary conclusions can be drawn. The CBF seems to be the most sensitive perfusion parameter for leukoaraiotic changes. It is consistently lower both in leukoaraiotic regions and in normal-appearing WM of subjects with LA than in healthy controls (Markus et al. 2000; O'Sullivan et al. 2002), supporting hypoperfusion and chronic ischemia being involved in the pathogenesis of LA. Findings in other perfusion parameters have, however, been more variable. High-grade carotid stenosis leading to hypoperfusion and thus to chronic ischemia of the brain has been suspected of inducing LA, and some studies support this expectation (Oppenheimer et al. 1995; Yamauchi et al. 1999; Soinne et al. 2003b). However, PI in LA is still in its early days, and further studies are needed.

9.7 Management

Although the prognosis of an individual LA patient is largely unpredictable, the prognosis of leukoaraiotic patients in general, especially in the most severe groups, is worse than for individuals of similar age, but without this condition. Therefore, the need for primary and secondary preventive measures is clear. As the etiology and pathogenesis of leukoaraiosis seem to be manifold, a single best course of treat-

ment does not exist, but some basic guidelines can be followed. Since chronic brain ischemia is the most likely etiology, preventive and management methods should be targeted against it. Antithrombotic agents, such as aspirin with or without dipyridamole and clopidogrel, may represent an important component in prevention, especially in subjects with risk factors for vascular diseases. Equally important is aggressive treatment of risk factors for vascular diseases, such as arterial hypertension, diabetes mellitus, dyslipidemia, and heart diseases, and all subjects should be motivated to give up smoking and excessive consumption of alcohol. Therapies that help to stabilize the endothelium, such as statins and angiotensin converting enzyme inhibitors, may also have a role in treating patients with LA. There is not yet scientific evidence whether carotid endarterectomy in patients with coexisting severe carotid artery stenosis and LA may be beneficial in attenuating the progression of LA and/or slowing down the cognitive decline process.

References

Breteler MM, van Amerongen NM, van Swieten JC, Claus JJ, Grobbee DE, van Gijn J, Hofman A, van Harskamp F (1994) Cognitive correlates of ventricular enlargement and cerebral white matter lesions on magnetic resonance imaging. The Rotterdam Study. Stroke 25:1109–1115

Brown WR, Moody DM, Thore CR, Challa VR (2000) Apoptosis in leukoaraiosis. AJNR Am J Neuroradiol 21:79–82

Brown WR, Moody DM, Challa VR, Thore CR, Anstrom JA (2002) Venous collagenosis and arteriolar tortuosity in leukoaraiosis. J Neurol Sci 203-204:159–163

Bryan RN, Wells SW, Miller TJ, Elster AD, Jungreis CA, Poirier VC, Lind BK, Manolio TA (1997) Infarctlike lesions in the brain: prevalence and anatomic characteristics at MR imaging of the elderly - data from the Cardiovascular Health Study. Radiology 202:47–54

De Leeuw FE, de Groot JC, Achten E, Oudkerk M, Ramos LM, Heijboer R, Hofman A, Jolles J, van Gijn J, Breteler MM (2001) Prevalence of cerebral white matter lesions in elderly people: a population based magnetic resonance imaging study. J Neurol Neurosurg Psychiatry 70:9–14

Hachinski VC, Potter P, Merskey H (1987) Leukoaraiosis. Arch Neurol 44:21–23

Hassan A, Hunt BJ, O'Sullivan M, Parmar K, Bamford JM, Briley D, Brown MM, Thomas DL, Markus HS (2003) Markers of endothelial dysfunction in lacunar infarction and ischemic leukoaraiosis. Brain 126:424–432

Heier LA, Bauer CJ, Schwartz L, Zimmerman RD, Morgello S, Deck MD (1989) Large Virchow-Robin spaces: MR-clinical correlation. AJNR Am J Neuroradiol 10:929–936

Helenius J, Soinne L, Salonen O, Kaste M, Tatlisumak T (2002) Leukoaraiosis, ischemic stroke, and normal white matter on diffusion-weighted MRI. Stroke 33:45–50

Inzitari D (2003) Leukoaraiosis: an independent risk factor for stroke? Stroke 34:2067–2071

Jones DK, Lythgoe D, Horsfield MA, Simmons A, Williams SC, Markus HS (1999) Characterization of white matter damage in ischemic leukoaraiosis with diffusion tensor MRI. Stroke 30:393–397

Lassen NA (1985) Normal average value of cerebral blood flow in younger adults is 50 ml/100 g/min. J Cereb Blood Flow Metab 5:347–349

Markus HS, Lythgoe DJ, Østergaard L, O'Sullivan M, Williams SC (2000) Reduced cerebral blood flow in white matter in ischaemic leukoaraiosis demonstrated using quantitative exogenous contrast based perfusion MRI. J Neurol Neurosurg Psychiatry 69:48–53

Moody DM, Bell MA, Challa VR (1990) Features of the cerebral vascular pattern that predict vulnerability to perfusion or oxygenation deficiency: an anatomic study. AJNR Am J Neuroradiol 11:431–439

Moody DM, Brown WR, Challa VR, Anderson RL (1995) Periventricular venous collagenosis: association with leukoaraiosis. Radiology 194:469–476

Murdoch G (2000) Staining for apoptosis: now neuropathologists can "see" leukoaraiosis. AJNR Am J Neuroradiol 21:42–43

Oppenheimer SM, Bryan RN, Conturo TE, Soher BJ, Preziosi TJ, Barker PB (1995) Proton magnetic resonance spectroscopy and gadolinium-DTPA perfusion imaging of asymptomatic MRI white matter lesions. Magn Reson Med 33:61–68

O'Sullivan M, Lythgoe DJ, Pereira AC, Summers PE, Jarosz JM, Williams SC, Markus HS (2002) Patterns of cerebral blood flow reduction in patients with ischemic leukoaraiosis. Neurology 59: 321–326

Pantoni L, Garcia JH (1995) The significance of cerebral white matter abnormalities 100 years after Binswanger's report. A review. Stroke 26:1293–1301

Pantoni L, Garcia JH (1997) Pathogenesis of leukoaraiosis: a review. Stroke 28:652–659

Rumboldt Z, Marotti M (2003) Magnetization transfer, HASTE, and FLAIR imaging. Magn Reson Imaging Clin North Am 11:471–492

Soinne L, Helenius J, Saimanen E, Salonen O, Lindsberg PJ, Kaste M, Tatlisumak T (2003a) Brain diffusion changes in carotid occlusive disease treated with endarterectomy. Neurology 61:1061–1065

Soinne L, Helenius J, Tatlisumak T, Saimanen E, Salonen O, Lindsberg PJ, Kaste M (2003b) Cerebral hemodynamics in asymptomatic and symptomatic patients with high-grade carotid stenosis undergoing carotid endarterectomy. Stroke 34:1655–1661

Thomalla G, Glauche V, Koch MA, Beaulieu C, Weiller C, Rother J (2004) Diffusion tensor imaging detects early Wallerian degeneration of the pyramidal tract after ischemic stroke. Neuroimage 22:1767–1774

Vermeer SE, Hollander M, van Dijk EJ, Hofman A, Koudstaal PJ, Breteler MM (2003) Silent brain infarcts and white matter lesions increase stroke risk in the general population: the Rotterdam Scan Study. Stroke 34:1126–1129

Yamauchi H, Fukuyama H, Nagahama Y, Shiozaki T, Nishizawa S, Konishi J, Shio H, Kimura J (1999) Brain arteriolosclerosis and hemodynamic disturbance may induce leukoaraiosis. Neurology 53:1833–1838

Yue NC, Arnold AM, Longstreth WT Jr, Elster AD, Jungreis CA, O'Leary DH, Poirier VC, Bryan RN (1997) Sulcal, ventricular, and white matter changes at MR imaging in the aging brain: data from the cardiovascular health study. Radiology 202:33–39

10 MR Detection of Intracranial Hemorrhage

Thamburaj Krishnamoorthy and Marco Fiorelli

CONTENTS

10.1 Introduction

Intracranial hemorrhage in any form can produce devastating effects. Neuroimaging plays a decisive role in the management of patients with any type of intracranial bleeding, by showing the presence, the extent, the location and often the cause of the hemorrhage. Traditionally CT scan has been used as the imaging modality of choice to confirm or exclude intracranial hemorrhage. However, while in the acute setting CT performs admirably, it is much less accurate in the identification of subacute and chronic bleeds (Wardlaw et al. 2003). MRI is known to be exquisitely sensitive to the presence of stigmata related to old bleedings, and to malformations or other potential causes of hemorrhage, but until recently has been considered unreliable in the diagnosis of hyperacute brain hemorrhage, a notion that is becoming obsolete. This chapter addresses the basic MR physical principles determining the appearance of intracranial hemorrhage, the pathology of various types of hemorrhagic cerebrovascular conditions and the relevant MR findings.

T. Krishnamoorthy, MD
Department of Imaging and Interventional Radiology, Sree Chitra Tirunal Institute for Medical Sciences and Technology, Trivandrum 695011, Kerala, India
M. Fiorelli, MD, PhD
Department of Neurological Sciences, University La Sapienza, Viale dell'Universitá 30, 00185 Rome, Italy

10.2 Types of Intracranial Hemorrhage (ICH)

Intracranial hemorrhages can be classified according to their anatomic location (epidural, subdural, subarachnoid, intracerebral, and intraventricular) or to their etiology (spontaneous or traumatic). Because of its frequency, higher than for any other type of intracranial hemorrhage, and its complex evolution from the hyperacute to the chronic stage, spontaneous intracerebral hematoma (ICH) serves as the paradigm for the systematization of the complex MR appearance of intracranial bleedings. It will therefore be treated in greater detail.

10.3 Spontaneous Intracerebral Hematoma (ICH)

Primary ICH is responsible for 10%–15% of all cases of stroke in Western populations and for 20%–30% of strokes among Asian and Black populations (Qureshi et al. 2001). An ICH typically presents with the sudden onset of a focal neurological deficit, which rapidly progresses over minutes to hours. Headache, nausea, vomiting, elevated blood pressure and decreased level of consciousness are more frequently associated with ICH than with ischemic stroke but are by no means pathognomonic. Imaging is therefore mandatory for a proper diagnosis of ICH. Expansion of the hematoma is the most common cause of secondary deterioration within the first few hours after onset (Brott et al. 1997).

With only 38% of patients surviving the first year, and only 20% of survivors capable of living independently after 6 months (Qureshi et al. 2001), the prognosis of ICHs is generally worse than that of ischemic strokes.

Depending on the cause, spontaneous ICH is classified into primary or secondary. Primary hemorrhages account for 78%–88% of overall cases of ICH, and occur from rupture of small vessels damaged by either chronic hypertension (85% of primary ICHs) or cerebral amyloid angiopathy (CAA) (15% of primary ICHs). The most frequent sites of hypertensive ICH are putamen (50%), thalamus (15%), pons (10%–15%), and cerebellum (10%) (Broderick et al. 1999). On the other hand, CAA is the cause of hemorrhage in more than 50% of patients with lobar ICH above 70 years of age. Secondary ICH is due to vascular malformations, tumors, impaired anticoagulation, drugs, infections etc. ICH in young patients (≤ 45 years) is often lobar in location and is most commonly secondary to an underlying vascular malformation (Qureshi et al. 2001).

Primary ICHs arise from small arteries, which have undergone degenerative changes from chronic hypertension or CAA. Charcot and Bouchard attributed hypertensive ICHs to ruptured miliary microaneurysms, but hemorrhage can originate from the fragile perforators also without microaneurysm formation. The bleeding initially results in mass effect with compression of the adjacent microvasculature (Huckman et al. 1970). The blood then spreads along white matter tracts causing compressive rather than destructive tissue damage. Histology of early hematoma shows edema, neuronal damage, and inflammatory cell infiltration in the perihematoma region. Edema is initially due to release and accumulation of osmotically active serum proteins from the clot, and later from vasogenic and cytotoxic phenomena (Carhuapoma et al. 2002). Despite the presence of local hypoperfusion, probably no ischemia develops in the perihematoma region and neuronal death is predominantly necrotic. In fact, PET studies have shown lack of elevation of oxygen extraction fraction in the perihematoma region, a finding that is not compatible with true ischemia (Zazulia et al. 2001).

Much of the current knowledge about ICH pathology has been obtained from experimental works conducted using various animal models. In a classical study, Rosenberg et al. (1990) were able to induce an ICH in the rat brain using an intraparenchymal injection of the enzyme collagenase. At 24 h, the resulting lesion consisted of a central zone showing a mixture of red blood cells and normal brain parenchyma, and a peripheral zone with necrotic or viable neuronal and glial cells. By 48 h polymorphonuclear infiltration was observed at the periphery. By 1 week, intense macrophage activity was seen at the border of the peripheral zone with associated increased vascularity and evidence of small vessel formation. Only a few macrophages had hemosiderin within them. By 21 days, the lesion was converted into a cavity filled with fluid and traversed by delicate gliovascular trabeculae, that contained variable numbers of hemosiderin and lipid laden macrophages. It is likely that these findings can be extrapolated with good approximation to the evolution of a primary human ICH.

10.3.1 Determinants of MR Signals in ICH

The most important mechanism that underlies the MR appearance of ICH is the transformation of initially oxygenated hemoglobin into a series of breakdown products (deoxyhemoglobin, methemoglobin, and hemosiderin), that differ in terms of presence and number of unpaired electrons of the heme iron. Hereafter, we will discuss the influence of hemoglobin and its metabolites on T1 and T2 relaxation times. We will also briefly review the effects on MR signals of other factors such as protein concentration, clot formation and retraction, and red blood cell dehydration.

10.3.1.1 Paramagnetic Effects

Approximately 99% of biological tissues are diamagnetic, i.e. they do not interact significantly with magnetic fields and therefore do not modify T1 and T2 relaxation times. The characteristic of diamagnetic molecules, like oxyhemoglobin, is the lack of unpaired electrons in their outer orbital. On the other hand, paramagnetic materials like iron or gadolinium do have unpaired electrons in their outer orbital, which induce significant shortenings of T1 and T2 relaxation times. Relevant to hemorrhage, this paramagnetic effect is observed in the acute phase with deoxyhemoglobin, in the subacute phase with methemoglobin, and in the chronic phase with hemosiderin (Gomori et al. 1985).

The T2 shortening effect induced by paramagnetic substances is known as the susceptibility effect, which in hemorrhages is caused by the presence of either deoxyhemoglobin, or intracellular methemo-

globin, or ferritin/hemosiderin, but not of extracellular methemoglobin. Compartmentalization of deoxyhemoglobin or, at a later stage, methemoglobin inside intact red blood cells, or finally of hemosiderin inside the lysosomes of macrophages and astrocytes (Bradley 1993) creates heterogeneously varying local field gradients (Gomori et al. 1987; Brooks et al. 1989) and induces phase shifts in the water protons as they diffuse through these local gradients (Gomori et al. 1985). The dephasing of the protons results in transverse relaxation and produces signal loss on T2 (DeLaPaz et al. 1984; Gomori et al. 1985), and especially on T2*-weighted images, the latter being the most sensitive sequence for the detection of susceptibility-induced effects (Gomori et al. 1987; Hayman et al. 1991). In fast spin echo (FSE) sequences due to the shorter echo spacing, the time available for diffusion of water protons is shorter. This leads to a lesser sensitivity of FSE techniques in the detection of susceptibility effects (Feinberg and Oshio 1991). T2 relaxation effects are directly proportional to the square of the local field gradients (Gomori et al. 1985). The T2 shortening effect of high field is 100 times that of 0.15 T (low field) and 9 times that of 0.5 T (intermediate field). At low field (less than 0.5 T) acute hematomas may appear isointense to brain parenchyma while subacute and chronic hematomas appear hyperintense on all pulse sequences (Gomori et al. 1985). The preferential T2 proton relaxation enhancement of acute hematomas and the hemosiderin rim are observed only with high magnetic fields. In agreement with these principles, a recent report indicates that the susceptibility effects typical of acute and subacute hematomas are more prominent at 3.0 T compared to 1.5 T, which, however, does not seem to translate into a significant incremental diagnostic accuracy (Allkemper et al. 2004).

The other important paramagnetic effect involves the longitudinal relaxation. When a paramagnetic ion is added to the water protons, the routine proton-proton dipole-dipole interaction between water protons is converted to a proton-electron dipole-dipole (PEDD) interaction (Barkovich and Atlas 1988). The efficient exchange of energy from this interaction results in T1 shortening and consequently in bright signals on T1-weighted images (Bradley 1993). This phenomenon is also known as the relaxivity effect. Even though deoxyhemoglobin is paramagnetic, it does not promote PEDD interactions since the paramagnetic ion is shielded by the hydrophobic pocket of the globin protein (Gomori et al. 1985; Bradley 1993). Hence, acute hematomas which contain deoxyhemoglobin do not appear hyperintense on T1-weighted images (Bradley 1993). On the other hand, following the oxidative denaturation of deoxyhemoglobin to methemoglobin (Bradley 1993), the conformational change in the hemoglobin molecule makes the paramagnetic heme move to the surface, where it can be approached by water protons (Gomori et al. 1987). The ensuing PEDD interaction is responsible for the hyperintense appearance of hematomas containing methemoglobin in T1-weighted images. Unlike susceptibility effects, PEDD interaction occurs regardless of whether the methemoglobin is intracellular or extracellular. A further difference with susceptibility effects is that the paramagnetic T1 shortening is less dependent on field strength.

10.3.1.2 Other Effects

Proteins seem to provide some contribution to the signal intensities of hemorrhage in all stages. However, the effect of proteins is more evident in the very early phase, when paramagnetic effects are still minimal. In the first few hours after the bleeding, the iso- or mildly hypointense appearance on T1-weighted images and the hyperintensity on T2-weighted images is mainly due to the high concentration of proteins, predominantly oxyhemoglobin but also cell membrane lipoproteins and fibrinogen (Clark et al. 1990). In the following days and weeks, the influence of proteins on MR signals is overwhelmed by paramagnetic effects. Packing of more RBCs per unit volume of blood, formation and retraction of clot matrix, and dehydration of RBCs are all phenomena for which an effect on MR signals has been postulated (Hayman et al. 1991). This effect, however, is likely to be only mild, especially at high field.

10.3.2 The Evolution of MR Signals in ICH

Based on the most mature form of the hemoglobin present in the clot, five stages of evolving ICH have been described (Bradley 1993). The hyperacute stage lasts for 24 h, acute stage for 2–3 days, early subacute stage for 3–7 days, late subacute stage up to 2 weeks and chronic stage more than 2 weeks. The evolution of an ICH is a complex and dynamic process and the estimation of the time of onset based on MRI findings may be inaccurate (Alemany Ripoll et al. 2004). However, the classification into five stages still retains its practical utility.

10.3.2.1 Hyperacute ICH

It was initially believed that on MRI an ICH of less than 24 h duration could not be distinguished reliably either from a mass lesion or from an acute infarct, because of an unspecific pattern of isointensity in T1 and slight hyperintensity on T2 imparted by the predominance of oxyhemoglobin. However, due to a reduced oxygen tension at the periphery of the clot, some deoxygenation of hemoglobin occurs immediately after the bleeding, and several studies have demonstrated that the resulting susceptibility effects can be visualized very early on T2- and particularly on T2*-weighted images as a hypointense rim (Fig. 10.1). This finding may be less apparent or even not apparent at all with low-field systems, or if FSE T2 sequences are used. Linfante et al. (1999) reported the ability of high field MRI to reliably detect a spontaneous ICH as early as 20 min after onset and schematized the appearance of the hyperacute hemorrhage as consisting of three distinct concentric regions. The center of the hemorrhage appears isointense or heterogeneously hyperintense on T2- and T2*-weighted images, probably reflecting the presence of intact oxyhemoglobin. The periphery is hypointense on T2- and T2*-weighted images reflecting the susceptibility effects due to deoxyhemoglobin, and finally there is an outer rim that appears hypointense on T1-weighted images and hyperintense on T2- and T2*-weighted images, suggestive of edema. Such a 'target-like' pattern is also found on DWI sequences (Mrita et al. 2002). Within a hyperacute ICH, perfusion imaging (PI) may reveal a different time-contrast curve compared to hyperacute ischemic stroke, probably due to the early blood-brain barrier breakdown seen in ICH and to the consequent contrast extravasation (Wintermark et al. 2002).

Kidwell et al. (2004) recently reported the results of a prospective, multicenter study in which

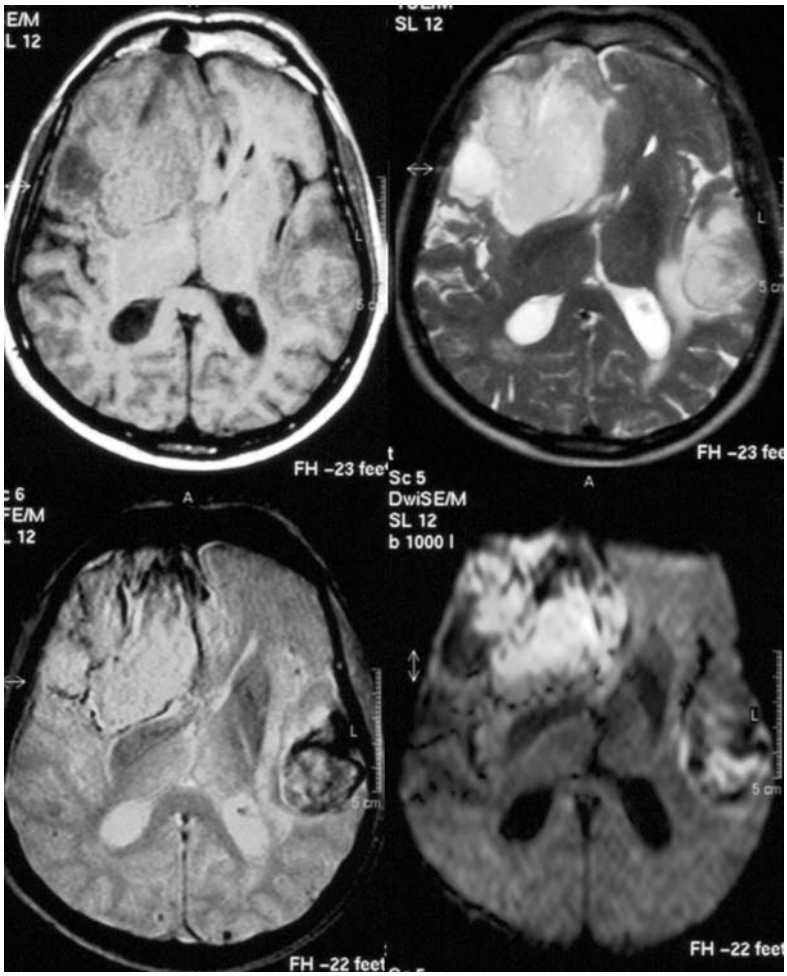

Fig. 10.1. Patient with a large hyperacute right frontotemporal hematoma and a smaller left temporal hematoma in transition from the hyperacute to the acute stage. *Top left*, T1; *top right*, T2; *bottom left*, T2*; *bottom right*; DWI

patients with focal stroke symptoms within 6 h of onset underwent brain MRI followed by non-contrast CT. Four blinded readers evaluated acute intracerebral hemorrhage and any intracerebral hemorrhage on gradient recalled echo MRI and CT scans by a consensus. After 200 patients were enrolled, it became apparent that MRI was detecting cases of hemorrhagic transformation not detected by CT. For the diagnosis of any hemorrhage, MRI was positive in 71 patients with CT positive in 29 patients ($p < 0.001$). For the diagnosis of acute hemorrhage, however, MRI and CT were equivalent (96% concordance). In three patients, regions interpreted as acute hemorrhage on CT were interpreted as chronic hemorrhage on MRI. In one patient, subarachnoid hemorrhage (SAH) was diagnosed on CT, but not on MRI. In 49 patients, chronic hemorrhage, most often microbleeds, was visualized on MRI, but not on CT.

These results indicate that, provided the appropriate imaging protocol is used, MRI can replace CT as the imaging modality of choice in acute stroke patients, if SAH is excluded.

10.3.2.2 Acute ICH

In the absence of rebleeding, deoxygenation of the clot is completed in most cases by 24 h (Brooks et al. 1989). At that time deoxyhemoglobin becomes the predominant blood breakdown product in the lesion. Due to its paramagnetic properties and its compartmentalization within still intact RBCs, deoxyhemoglobin exerts a strong susceptibility effect, which makes acute hematomas appear distinctly and characteristically dark on T2 weighted SE images (Gomori et al. 1985), and more so on T2* weighted GRE images (Hayman et al. 1991). On T1-weighted images, acute ICHs still appear isointense or mildly hypointense, as in the hyperacute stage. The parenchyma surrounding the clot exhibits a halo due to vasogenic edema and initial inflammatory reaction. The region of edema has long T1 and T2 relaxation times and appears hypointense on T1-weighted images and hyperintense on T2-weighted images. Edema is better shown by T2-weighted SE sequences than by T2* sequences. By the 5^{th} to 12^{th} day the hyperintense halo from edema begins to regress (Barkovich and Atlas 1988). These features of acute ICH last for about 3 days, after which formation of methemoglobin from deoxyhemoglobin begins and the clot evolves into the subacute stage (Bradley 1993).

10.3.2.3 Early and Late Subacute ICH

The appearance of methemoglobin in the clot marks the transition from the acute to the subacute phase. Too high or too low oxygen tension is likely to delay methemoglobin formation and the expected evolutionary changes of ICH (Barkovich and Atlas 1988). Unlike deoxyhemoglobin, methemoglobin allows water protons to approach the paramagnetic ion. This is possible due to a conformational change occurring in the structure of methemoglobin, which brings the ferric ion to the surface of the molecule. With this change PEDD interaction becomes possible and leads to the shortening of T1 that is characteristic of subacute hematomas. Since methemoglobin is formed initially at the interface of the hematoma with the parenchyma of the brain, the bright signals on T1-weighted images are observed initially at the periphery of the clot (Gomori et al. 1985). Later, the bright signal extends centripetally until the whole clot becomes hyperintense in T1. This paramagnetic T1 shortening effect is observed at all field strengths. In the early subacute phase, methemoglobin is still compartmentalized within red blood cells and hence generates local field gradients that maintain a T2 shortening effect similar to that induced by deoxyhemoglobin. Therefore, in the early subacute phase relaxivity effects and susceptibility effects coexist, i.e. the clot appears bright in T1, and dark in T2 and especially in T2*. This stage is expected to last for approximately 1 week.

As the clot ages, progressive fragmentation and osmotic phenomena damage RBC membranes until they eventually lyse. Hemolysis releases methemoglobin into the extracellular fluid compartment of the hematoma. The resulting dilution of methemoglobin in the extracellular fluids eliminates the biological field gradients (Barkovich and Atlas 1988), and with them the susceptibility phenomena, an effect that is observed initially at the periphery of the clot. When all methemoglobin is extracellular, the T2-shortening induced signal loss is no longer observed, so that the late subacute ICH is predominantly hyperintense in both T1- and T2-weighted images (Fig. 10.2). Focal brain lesions containing fat, calcium, or high concentrations of proteins can also appear hyperintense in T1 and T2 and therefore enter in the differential diagnosis of ICH at this stage.

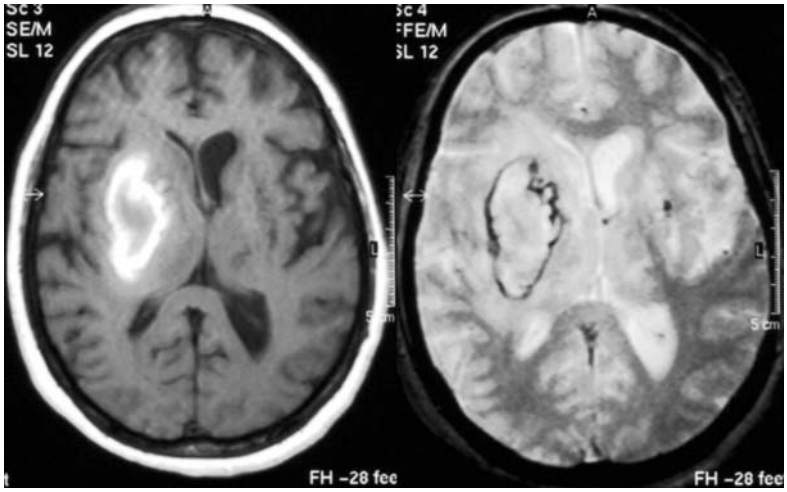

Fig. 10.2. Patient with late subacute hematoma in the right basal ganglia. *Left*, T1; *right*, T2*)

10.3.2.4 Chronic ICH

The beginning of the chronic phase is characterized by the appearance of modified macrophages (microglia), which phagocytose the ferritin and the hemosiderin formed from the breakdown of extracellular methemoglobin. These macrophages accumulate at the periphery of the hematoma and form a ring around the remnants of the clot. Hemosiderin is highly paramagnetic as it has five unpaired electrons. Its location inside the lysosomes of macrophages is responsible for the creation of field gradients and of marked T2 shortening. Hemosiderin is also insoluble in water, which prevents PEDD interaction. In the absence of T1 shortening no bright signals are observed from hemosiderin on T1-weighted images. However, at the beginning of the chronic stage there may still be free methemoglobin in the center of the clot giving bright signals on T1-weighted images. As a result, a chronic ICH initially shows a hypointense peripheral hemosiderin rim completely surrounding a central area hyperintense in all sequences due to the persistence of extracellular methemoglobin. The hemosiderin rim is less conspicuous on T1-weighted sequences and more conspicuous on T2- and T2*-weighted sequences. With time, the macromolecules in the hematoma cavity are slowly reabsorbed (Brooks et al. 1989). This results in a gradual disappearance of paramagnetic T1 shortening effects. With the elimination of all macromolecular components, the lesion becomes more fluid and the signal intensity of the inner part of the clot becomes isointense to CSF in all sequences. Finally, the cyst-like cavity collapses leaving a residual hemosiderin-containing scar.

10.4 Subdural and Epidural Hematomas

Chronic subdural hematoma (SDH) occurs in 1–2 per 100,000 people per year (Fogelholm et al. 1975) and is mainly related to a head trauma. The bridging veins that run between the surface of the brain and the intradural venous sinuses are torn from either direct injury or indirect injury with acceleration, which leads to accumulation of blood in the potential subdural space. Non-traumatic SDHs are rare. They may result from convexity vascular malformations, hemorrhagic diathesis or brain tumors such as meningioma or meningeal carcinomatosis (Markwalder 1981). As the inner membrane of the fluid collection lacks blood vessels, the expansion of a SDH is believed to be due to recurrent microhemorrhages from the vascularized outer membrane. Although the hyperattenuating acute phase of SDH can be reliably identified on CT, the isoattenuating subacute phase may be missed unless a contrast agent is used. CT may also be unable to reliably differentiate a hypoattenuating chronic SDH from a subdural hygroma (Markwalder 1981). Moreover, beam hardening artifacts of CT may interfere with diagnosis of posterior fossa SDH, and a routine axial CT scan may miss those SDHs that spread along the tentorium or along the inferior surface of cerebral hemispheres. Finally, SDH may occasionally be con-

fused with SAH on CT, and therefore erroneously give a mandate for angiography (Rabinstein et al. 2003). For all these reasons MR imaging is increasingly used in the assessment of possible SDHs.

The MR imaging features of acute and subacute SDHs resemble the changes seen in ICH (Fobben et al. 1989). However, the high oxygen tension found in a SDH may delay the evolutionary appearance on MRI. Acute hematomas (1 week) give dark signals in long TR/long TE images due to susceptibility effects. In the early subacute period (< 2 weeks) peripheral bright signals with central hypointensity may be observed on all sequences presumably due to formation of extracellular methemoglobin at the periphery. In the late subacute phase (> 2 weeks and < 1 month) the clot becomes uniformly hyperintense. Hemosiderin is infrequently observed in the subacute phase as the subdural space is lying outside the blood-brain barrier, so that hemosiderin is removed into the bloodstream. As the blood products are gradually absorbed, the signal intensity of chronic SDH decreases on T1-weighted images and appears hypointense or isointense relative to the gray matter, but still more intense than the CSF probably due to higher protein concentration. While this is considered to be the typical pattern of chronic SDH, Tsutsumi et al. (1997) reported that half the chronic SDHs among 199 patients showed mixed signals in T1. These authors also reported that chronic SDHs featuring homogeneous hyperintense signals on T1-weighted images were less likely to show recurrent bleedings following surgical evacuation than hematomas appearing predominantly iso- or hypointense. This may be related to the maturity of the outer vascular membrane, with immature membranes being more prone to bleeding (Tsutsumi et al. 1997). Even though hemosiderin formation is uncommon in chronic SDHs, large inhomogeneous hematomas can show a dark band along the inner membrane on T2*-weighted images (Imaizumi et al. 2003). The dark band results probably from the accumulation of hemosiderin-laden macrophages in the inner membrane and can disappear soon after successful evacuation of the hematoma. Finally, to differentiate a chronic SDH from a subdural hygroma, proton-density weighted sequences or FLAIR are required. In fact, SDHs may occasionally exhibit CSF-like signals on T1- and T2-weighted SE sequences, but will appear more intense than CSF on proton-density weighted and FLAIR images (Tsutsumi et al. 1997).

Epidural hematomas show signal changes similar to SDH. The displacement of the T2-hypointense dural membrane inward with lenticular shape of the clot is helpful in differentiating epidural bleedings from SDH, even though one may encounter difficulties in the acute phase since the clot and the dura both appear dark.

10.5 Subarachnoid Hemorrhage

With an incidence rate in the general population of around six cases per 100,000, SAH is responsible of 3% of all acute strokes and of 5% of stroke-related deaths (Sudlow and Warlow 1997; van Gijn and Rinkel 2001). Rupture of intracranial saccular aneurysm accounts for about 85% of cases of SAH. Perimesencephalic bleedings, a distinct and more benign type of SAH of probable venous origin, is responsible for a further 10% of cases. The remaining 5% of SAHs is due to miscellaneous conditions like trauma, intracranial arterial dissection, vascular malformations, vascular lesions of the spine, mycotic aneurysms, pituitary apoplexy, and cocaine abuse (van Gijn and Rinkel 2001).

Prompt identification of SAH and of the underlying aneurysm is crucial, as timely coiling or clipping will prevent re-bleed and the related morbidity and mortality. CT is considered the initial investigation of choice for diagnosis of acute SAH. Occasionally, lumbar puncture can be needed when the CT is negative in a patient whose clinical history is strongly suggestive of SAH (Macdonald et al. 2001; van Gijn and Rinkel 2001). CT shows the acute SAH as high attenuation areas filling the cisterns and sulci. About 90%–95% of CT will be positive for SAH in the first 24 h. However, this percentage drops to 80% at 3 days, to 70% at 5 days, to 50% at 1 week and to 30% at 2 weeks. After 3 weeks it is difficult to detect SAH with CT (van Gijn and van Dongen 1982; Adams et al. 1983), but even in the acute phase CT can miss the diagnosis if the amount of SAH is small (Noguchi et al. 2000). False negatives at CT can also be due to isolated SAH in the posterior fossa, where the hyperdense blood may be masked by beam hardening artifacts (Woodcock et al. 2001). Occasionally, a false positive diagnosis of SAH on CT may be due to diffuse cerebral edema (van Gijn and van Dongen 1982). At least in these situations MRI seems to hold an advantage over CT in diagnosing or ruling out SAH.

T1- and T2-weighted MR images are insensitive in the detection of acute SAH. In some cases T1 shortening effects from raised protein levels due

to SAH may be visible on T1-weighted SE images as signals relatively hyperintense to CSF and hypointense to brain parenchyma. However, as there is no methemoglobin formation in the acute stage, bright signals on T1-weighted sequence are not observed. T2-weighted images may occasionally show signals brighter than CSF (Rumboldt et al. 2003).

The skepticism on the ability of conventional MRI in detecting SAH is giving way to optimism as FLAIR imaging has been shown to be fairly accurate in the detection of acute subarachnoid bleedings. In fact, animal models suggest that FLAIR can be more sensitive than CT in the evaluation of acute SAH (Woodcock et al. 2001) even when the amount of blood is very small and diluted by CSF (Noguchi et al. 2000). In FLAIR an inversion pulse is utilized to null the bright CSF signals in T2-weighted images with long TE. Due to its high protein concentration and T1 shortening effect, the acute subarachnoid bleeding will appear bright on FLAIR.

As with intraparenchymal bleeds, a T2*-weighted GRE sequence may be expected to show signal loss from susceptibility effects in the cisterns and sulci in acute SAH. However, T2*-weighted sequences may not be sensitive enough within the first 24 h, either due to high oxygen levels in CSF which prevents formation of paramagnetic deoxyhemoglobin or to over hydration of RBCs (Noguchi et al. 1997). Nevertheless, one may observe susceptibility effects in the hyperacute stage in thick clots, where deoxyhemoglobin formation goes unimpeded.

While FLAIR may be very sensitive in the detection of acute SAH, its specificity for this disease is suboptimal. All conditions causing an elevation of CSF proteins, such as pyogenic meningitis, granulomatous meningitis, meningeal carcinomatosis etc., characteristically elevate the CSF protein levels and give rise to bright signals on FLAIR. Fat from ruptured dermoid or previous introduction of oily contrast media may also mimic SAH on FLAIR due to T1 shortening effects. Therefore, in order to confidently made a diagnosis of SAH on FLAIR, a careful appraisal of the clinical history is mandatory. Contrast may be helpful to exclude meningitis, while fat may be identified using chemical shift artifacts or fat saturation sequences. Another pitfall with FLAIR sequences may be represented by the CSF pulsation artifacts from inflow and misregistration effects (Noguchi et al. 1997). These artifacts create bright signals in the cisterns especially with fast FLAIR sequences. Hence, FLAIR may not be suitable to assess the posterior fossa SAH. IV propofol anesthesia in children (Filippi et al. 2001) or supplemental oxygen administered during anesthesia (Deliganis et al. 2001; Anzai et al. 2004) are further conditions which can give rise to bright CSF signals on FLAIR.

Proton density-weighted images seem to be as sensitive as FLAIR in detecting SAHs of less than 24 h . CSF flow artifacts in cisterns and ventricles are less likely to be observed with proton density than with FLAIR (Wiesmann et al. 2002). A recent report suggests that proton-density weighted sequences allow an accurate diagnosis of hyperacute SAH (Fiebach et al. 2004).

As the delay between SAH onset and imaging increases, susceptibility effects appear and T2*-weighted GRE images become more sensitive compared to FLAIR. Mitchell et al. (2001) have shown 94% sensitivity for T2* in the acute phase (less than 4 days) and 100% in the subacute phase (more than 4 days) compared to 81% and 87% for FLAIR. T2*-weighted images may also help localize previous SAH and locate the aneurysm. This may have an implication in diagnosing aneurysms with minor leak or to identify the culprit among multiple aneurysms (Imaizumi et al. 2003). Finally, contrast studies may exceptionally reveal an actual leakage of the contrast (Küker et al. 1999).

10.6 Intraventricular Hemorrhage

Most intraventricular hemorrhages (IVHs) are secondary to ICH or SAH. Isolated IVH is rare and usually due to the rupture of underlying vascular malformations (Zhu et al. 1997). Angiography is therefore strongly recommended for isolated IVHs (Broderick et al. 1999). Few data on MR features of IVH are available in the literature (Bakshi et al. 1999). Based on MR imaging, intraventricular bleedings have been classified into clotted IVH, usually unilateral, and layered IVH, usually bilateral. Since the CSF in ventricles has a higher content in oxygen and glucose, the layered form evolves more slowly compared to the clotted form. The latter evolves at a rate similar to ICH. However, in the chronic stage, unlike ICH, IVHs do not show hemosiderin formation. Among the conventional sequences, proton density depicts IVH better than T1- and T2-weighted images. In the acute stage FLAIR may have better sensitivity than CT scan to demonstrate IVH. On FLAIR, in the initial 48 h IVH appears hyperintense, but one should be aware of the CSF flow artifacts, which can mimic the presence of blood. Also, conditions like pyocephalus

or intraventricular tumors may exhibit signals similar to IVH. After the acute phase, IVHs may appear iso- or hypointense on FLAIR. At this stage, a bright signal on T1-weighted images and a hypointense signal on T2*-weighted image will mark the presence of an IVH (Bakshi et al. 1999).

10.7 Hemorrhagic Infarction

Hemorrhagic infarction (HI) may result either from the hemorrhagic conversion of an arterial ischemic stroke or, more rarely, from cerebral venous thrombosis (CVT). Autopsy studies indicate that hemorrhagic conversion occurs in 30% of recent ischemic brain infarcts (Hart and Easton 1986). The pathophysiological basis of hemorrhagic transformation is the microvascular injury to the blood-brain barrier due to ischemia and the subsequent reperfusion (del Zoppo et al. 1998). The two main types of hemorrhagic transformation are petechial hemorrhages (hemorrhagic infarction proper) or parenchymal hematoma. Hemorrhagic transformation is more commonly observed in the gray matter regions than in the subcortical white matter (Hornig et al. 1986).

The few existing studies on MR evaluation of HI emphasize the importance of T2*-weighted GRE sequences to detect hemorrhagic changes. Hermier et al. (2001) reported that these sequences are as effective or more effective than CT in the detection of acute HI. However, as for other types of parenchymal bleedings, one should be aware of other causes of signal loss on T2*-weighted images such as calcification, flow void, cavernomas, etc. Even chronic cerebral microbleeds (discussed in the following sections) may mimic hemorrhagic conversion. However, microbleeds usually measure less than 5 mm and are expected to be located outside the area of infarction.

Brain MRI in combination with venous MRA is considered as the gold standard for diagnosing CVT (Lee and Terbrugge 2003, see chapter 18). Cortical and subcortical bright (edema, necrosis) and dark (deoxyhemoglobin) signals on FLAIR, T2-weighted and especially T2*-weighted images not corresponding to any arterial territory, in the background of an appropriate clinical history (acute focal deficit, headache, and seizures), are suggestive of venous infarcts. The cortical veins or dural sinuses should be carefully scrutinized to identify the thrombosis. In the acute stage the thrombus in the veins or sinuses will appear iso- or hypointense on T1-weighted images and profoundly hypointense on T2-weighted images, which may mimic flow in T2-weighted SE/FSE sequences. It is often only after 3–7 days that the thrombus becomes hyperintense in T1.

10.8 Cerebral Microbleeds

Cerebral microbleeds (MBs) are chronic hemosiderin deposits caused by minor extravasations of blood from fibrohyalinized small arterioles (Fazekas et al. 1999). They are increasingly being recognized thanks to the increased use of T2*-weighted GRE sequences in the clinical practice. CT, but also conventional SE T2-weighted sequences, are insensitive in the detection of such microhemorrhages (Fig. 10.3). MBs have a strong association

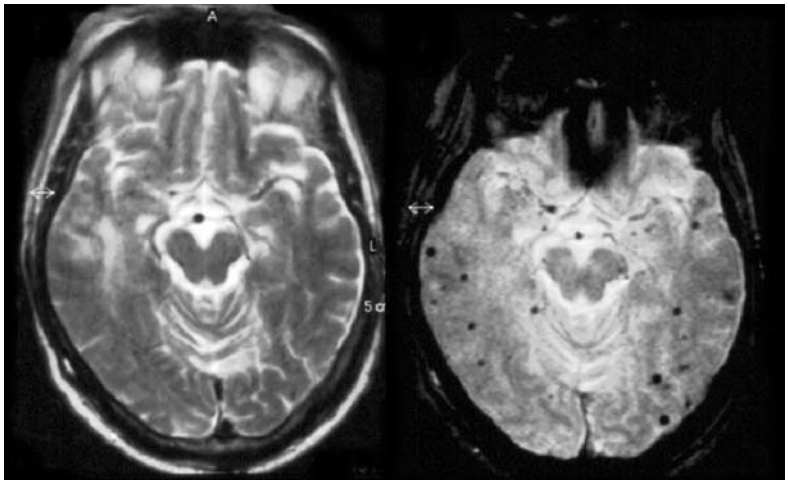

Fig. 10.3. Patient showing an unremarkable T2-weighted image (*right*) and multiple microbleeds on the T2*-weighted image (*left*)

with leukoaraiosis (Lee et al. 2002) and with chronic hypertension (Lee et al. 2004).

The incidence of these lesions among the healthy elderly population varies from 3.1% (Tsushima et al. 2002) to 6.4% (Roob et al. 1999). Among patients with ICH, MBs have a frequency of 30%–80% (Tsushima et al. 2003). MBs generally coexist with moderate-to-severe white matter changes (Kwa et al. 1998), which is explained by the fact that both leukoaraiosis and MBs have small vessel disease as a common denominator. MBs are found mainly in the basal ganglia, corona radiata, centrum semiovale, brainstem and cerebellum. Cerebral amyloid angiopathy (CAA) is another possible etiology of MBs (Fazekas et al. 1999; Kinoshita et al. 2000). CAA-related MBs are located in the cortex and the immediately subcortical white matter. The clinical importance of MBs is that they may identify patients prone to develop spontaneous ICH (Lee et al. 2004), and especially patients at higher risk of ICH after thrombolysis (Kidwell et al. 2002) or during chronic treatment with aspirin (Wong et al. 2003) or oral anticoagulants.

MBs appear as small sharply defined signal loss on T2*-weighted GRE sequences. They can also be demonstrated by T2-weighted SE sequences, albeit inconstantly and mainly at high field. Echo-planar T2*-weighted sequences can demonstrate MBs within seconds (Kinoshita et al. 2000), but they may fail to detect MBs at the basal regions of cerebral hemispheres and in the posterior fossa, due to susceptibility artifacts (Tsushima et al. 2003). T1-weighted images are insensitive to MBs, as they contain only hemosiderin and not other hemoglobin breakdown products.

References

Adams HP Jr, Kassell NF, Turner JC et al (1983) CT and clinical correlation in recent aneurysmal subarachnoid hemorrhage: a report of the cooperative aneurysm study. Neurology 33:981–988

Alemany Ripoll M, Stenborg A, Sonninen P et al (2004) Detection and appearance of intraparenchymal haematomas of the brain at 1.5 T with spin-echo, FLAIR and GE sequences: poor relationship to the age of the haematoma. Neuroradiology 46:435–443

Allkemper T, Tombach B, Schwindt W et al (2004) Acute and subacute intracerebral hemorrhages: comparison of MR imaging at 1.5 and 3.0 T. Initial experience. Radiology 232:874–881

Anzai Y, Ishikawa M, Shaw DW et al (2004) Paramagnetic effect of supplemental oxygen on CSF hyperintensity on fluid-attenuated inversion recovery MR images. AJNR Am J Neuroradiol 25:274–279

Bakshi R, Kamran S, Kinkel PR et al (1999) MRI in cerebral intraventricular hemorrhage: analysis of 50 consecutive cases. Neuroradiology 41:401–409

Barkovich AJ, Atlas SW (1988) Magnetic resonance imaging of intracranial hemorrhage. Radiol Clin North Am 26:801–820

Bradley WG Jr (1993) MR appearance of hemorrhage in the brain. Radiology 189:15–26

Broderick JP, Adams HP Jr, Barsan W et al (1999) Guidelines for the management of spontaneous intracerebral hemorrhage: a statement for healthcare professionals from a special writing group of The Stroke Council, American Heart Association. Stroke 30:905–915

Brooks RA, Di Chiro G, Patronas N et al (1989) MR imaging of cerebral hematomas at different field strengths: theory and applications. J Comput Assist Tomogr 13:194–206

Brott T, Broderick JP, Kothari R et al (1997) Early hemorrhage growth in patients with intracerebral hemorrhage. Stroke 28:1–5

Carhuapoma JR, Barker PB, Hanley DF et al (2002) Human brain hemorrhage: quantification of perihematoma edema by use of diffusion-weighted MR imaging. AJNR Am J Neuroradiol 23:1322–1326

Clark RA, Watanabe AT, Bradley WG Jr et al (1990) Acute hematomas: effects of deoxygenation, hematocrit and fibrin-clot formation and retraction on T2 shortening. Radiology 175:201–206

Del Zoppo GJ, von Kummer R, Hamann GF (1998) Ischemic damage of brain microvessels: inherent risks for thrombolytic treatment in stroke. J Neurol Neurosurg Psychiatry 65:1–9

DeLaPaz RL, New PF, Buonanno FS et al (1984) NMR imaging of intracranial hemorrhage. J Comput Assist Tomogr 8:599–607

Deliganis AV, Fisher DJ, Lam AM et al (2001) Cerebrospinal fluid signal intensity increase on FLAIR MR images in patients under general anesthesia: the role of supplemental oxygen. Radiology 218:152–156

Fazekas F, Kleinert R, Roob G et al (1999) Histopathologic analysis of foci of signal loss on gradient-echo T2*-weighted MR images in patients with spontaneous intracerebral hemorrhage: evidence of microangiopathy related microbleeds. AJNR Am J Neuroradiol 20:637–642

Feinberg DA, Oshio K (1991) GRASE (Gradient and Spin-Echo) MR imaging: a new fast clinical imaging technique. Radiology 181:597–602

Fiebach JB, Schellinger PD, Geletneky K et al (2004) MRI in acute subarachnoid haemorrhage; findings with a standardised stroke protocol. Neuroradiology 46:44–48

Filippi CG, Ulu AM, Lin D et al (2001) Hyperintense signal abnormality in subarachnoid spaces and basal cisterns on MR images of children anesthetized with propofol: new fluid-attenuated inversion recovery finding. AJNR Am J Neuroradiol 22:394–399

Fobben ES, Grossman RI, Atlas SW et al (1989) MR characteristics of subdural hematomas and hygromas at 1.5 T. AJNR Am J Neuroradiol 10:687–693

Fogelholm R, Heiskanen O, Waltimo O (1975) Chronic subdural hematoma in adults. Influence of patient's age on symptoms, signs, and thickness of hematoma. J Neurosurg 42:43–46

Gomori JM, Grossman RI, Goldberg HI et al (1985) Intracranial hematomas: imaging by high-field MR. Radiology 157:87–93

Gomori JM, Grossman RI, Yu-Ip C et al (1987) NMR relaxation

times of blood: dependence on field strength, oxidation state and cell integrity. J Comput Assist Tomogr 11:684–690
Hart RG, Easton JD (1986) Hemorrhagic infarcts. Stroke 17:586–589
Hayman LA, Taber KH, Ford JJ et al (1991) Mechanisms of MR signal alteration by acute intracerebral blood: old concepts and new theories. AJNR Am J Neuroradiol 12:899–907
Hermier M, Nighoghossian N, Derex L et al (2001) MRI of acute post-ischemic cerebral hemorrhage in stroke patients: diagnosis with T2*- weighted gradient - echo sequence. Neuroradiology 43:809–815
Hornig CR, Dorndorf W, Agnoli AL (1986) Hemorrhagic cerebral infarction. A prospective study. Stroke 17:179–185
Huckman MS, Weinberg PE, Kim KS et al (1970) Angiographic and clinico-pathologic correlates in basal ganglionic hemorrhage. Radiology 95:79–92
Imaizumi T, Chiba M, Honma T et al (2003a) Detection of hemosiderin deposition by T2*-weighted MRI after subarachnoid hemorrhage. Stroke 34:1693–1698
Imaizumi T, Horita Y, Honma T et al (2003b) Association between a black band on the inner membrane of a chronic subdural hematoma on T2*-weighted magnetic resonance images and enlargement of the hematoma. J Neurosurg 99:824–830
Kidwell CS, Saver JL, Villablanca JP et al (2002) Magnetic resonance imaging detection of microbleeds before thrombolysis: an emergency application. Stroke 33:95–98
Kidwell CS, Chalela JA, Saver JL et al (2004) Comparison of MRI and CT for detection of acute intracerebral hemorrhage. JAMA 292:1823–1830
Kinoshita T, Okudera T, Tamura H et al (2000) Assessment of lacunar hemorrhage associated with hypertensive stroke by echo-planar gradient-echo T2*-weighted MRI. Stroke 31:1646–1650
Küker W, Thiex R, Block F (1999) Hyperacute perimesencephalic subarachnoid hemorrhage: demonstration of blood extravasation with MRI. J Comput Assist Tomogr 23:521–523
Kwa VH, Franke CL, Verbeeten B Jr et al (1998) Silent intracerebral microhemorrhages in patients with ischemic stroke. Ann Neurol 44:372–377
Lee SK, Terbrugge KG (2003) Cerebral venous thrombosis in adults: the role of imaging evaluation and management. Neuroimag Clin North Am 13:139–152
Lee SH, Bae HJ, Yoon BW et al (2002) Concentration of serum total cholesterol is associated with multifocal signal loss lesions on gradient-echo magnetic resonance imaging. Analysis of risk factors for multifactorial signal loss lesions. Stroke 33:2845–2849
Lee SH, Bae HJ, Kwon SJ et al (2004) Cerebral microbleeds are regionally associated with intracerebral hemorrhage. Neurology 62:72–76
Linfante I, Linas RH, Caplan LR et al (1999) MRI features of intracranial hemorrhage within 2 hours from symptom onset. Stroke 30:2263–2267
Macdonald RL, Stoodley M, Weir B (2001) Intracranial aneurysms. Neurosurg Qtly 11:181–198
Markwalder TM (1981) Chronic subdural hematomas: a review. J Neurosurg 54:637–645
Mitchell P, Wilkinson ID, Hoggard N et al (2001) Detection of subarachnoid hemorrhage with magnetic resonance imaging. J Neurol Neurosurg Psychiatry 70:205–211
Mrita N, Harada M, Yoneda K et al (2002) A characteristic feature of acute hematomas in the brain on echo-planar diffusion weighted imaging. Neuroradiology 44:907–911
Noguchi K, Ogawa T, Seto H et al (1997) Subacute and chronic subarachnoid hemorrhage: diagnosis with fluid-attenuated inversion recovery MR imaging. Radiology 203:257–262
Noguchi K, Seto H, Kamisaki Y et al (2000) Comparison of fluid-attenuated inversion-recovery MR imaging with CT in a simulated model of acute subarachnoid hemorrhage. AJNR Am J Neuroradiol 21:923–927
Qureshi AI, Tuhrim S, Broderick JP et al (2001) Spontaneous intracerebral hemorrhage. N Engl J Med 344:1450–1460
Rabinstein AA, Pittock SJ, Miller GM et al (2003) Pseudosubarachnoid haemorrhage in subdural haematoma. J Neurol Neurosurg Psychiatry 74:1131–1132
Roob G, Schmidt R, Kapeller P et al (1999) MRI evidence of past cerebral microbleeds in a healthy elderly population. Neurology 52:991–994
Rosenberg GA, Mun-Bryce S, Wesley M et al (1990) Collagenase-induced intracerebral hemorrhage in rats. Stroke 21:801–807
Rumboldt Z, Kalousek M, Castillo M (2003) Hyperacute subarachnoid hemorrhage on T2-weighted MR images. AJNR Am J Neuroradiol 24:472–475
Sudlow C, Warlow CP (1997) Comparable studies of the incidence of stroke and its pathological types: results from an international collaboration. Stroke 28:491–499
Tsushima Y, Tanizaki Y, Aoki J et al (2002) Detection of microhemorrhage in neurologically healthy adults. Neuroradiology 44:31–36
Tsushima Y, Aoki J, Endo K (2003) Brain microhemorrhages detected on T2*-weighted gradient-echo MR images. AJNR Am J Neuroradiol 33:88–96
Tsutsumi K, Maeda K, Iijima A et al (1997) The relationship of preoperative magnetic resonance imaging findings and closed system drainage in the recurrence of chronic subdural hematoma. J Neurosurg 87:870–875
Van Gijn J, Rinkel GJ (2001) Subarachnoid hemorrhage. Diagnosis, causes and management. Brain 124:249–278
Van Gijn J, van Dongen KJ (1982) The time course of aneurysmal hemorrhage on computed tomograms. Neuroradiology 23:153–156
Wardlaw JM, Keir SL, Dennis MS (2003) The impact of delays in computed tomography of the brain on the accuracy of diagnosis and subsequent management in patients with minor stroke. J Neurol Neurosurg Psychiatry 74:77–81
Wiesmann M, Mayer TE, Yousry I et al (2002) Detection of hyperacute subarachnoid hemorrhage of the brain by using magnetic resonance imaging. J Neurosurg 96:684–689
Wintermark M, Maeder P, Reichart M et al (2002) MR pattern of hyperacute cerebral hemorrhage. J Magn Reson Imaging 15:705–709
Wong KS, Chan YL, Liu JY (2003) Asymptomatic microbleeds as a risk factor for aspirin-associated intracerebral hemorrhages. Neurology 60:511–513
Woodcock RJ Jr, Short J, Do HM et al (2001) Imaging of acute subarachnoid hemorrhage with a fluid-attenuated inversion recovery sequence in an animal model: comparison with non-contrast-enhanced CT. AJNR Am J Neuroradiol 22:1698–1703
Zazulia AR, Diringer MN, Videen TO et al (2001) Hypoperfusion without ischemia surrounding acute intracerebral hemorrhage. J Cereb Blood Flow Metab 21:801–810
Zhu XL, Chan MS, Poon WS (1997) Spontaneous intracranial hemorrhage: which patients need diagnostic cerebral angiography? A prospective study of 206 cases and review of the literature. Stroke 28:1406–1409

11 MR Spectroscopy in Stroke

Heinrich Lanfermann and Ulrich Pilatus

CONTENTS

11.1 ^{1}H-MR Spectroscopy in Stroke – Insight into Pathobiochemistry of Ischemic Brain

Only few of the complex pathophysiological and pathobiochemical processes during acute hypoperfusion of the brain can be accurately monitored by imaging techniques. The initial step in stroke can be monitored by mapping of the hypoperfused areas with perfusion MR imaging (PI). Resulting from the interception in nutrition supply, a cascade of biochemical events (Fig. 11.1) will finally cause cell swelling (cytotoxic edema) in the affected areas. The concomitant increase in the apparent water diffusion coefficient (ADC) can be exploited to visualize this area with diffusion weighted MR imaging (DWI). Thus, two advanced MR imaging methods are available to monitor either the initial or a rather late phase of stroke, but these methods, which are based on the water proton signal, can not resolve biochemical and physiological processes in between. In contrast, MR spectroscopy, which detects signals from water soluble metabolites provides information on concentration changes of key metabolites involved in ischemia (Beauchamp et al. 1999). Oxygen depletion will induce anaerobic glycolysis leading to an increase in lactate production which will accumulate especially in the presence of hypoperfusion. Lactate can be observed with MRS providing a sensitive biochemical marker for oxygen depletion due to hypoperfusion. Lactate accumulation and persisting lack in energy supply will cause drop in ATP and pH, both parameters are accessible by ^{31}P MRS. The following failure of Na^+-K^+-ATPase activity leads to Na^+ influx which in principle can be monitored by ^{23}Na MRS (Hilal et al. 1983). Since this is causing the cytotoxic edema, it can also be visualized by the above mentioned diffusion sensitive MRI method. Finally, monitoring the neuronal marker NAA with ^{1}H MRS will probe for integrity of neurons providing information on the last phase of infarcted tissue, the death of severely damaged cells.

The two MRI methods are already part of an advanced routine MRI stroke-protocol. At least, the ^{1}H MRS study could be performed in the framework of such a protocol without further equipment. As

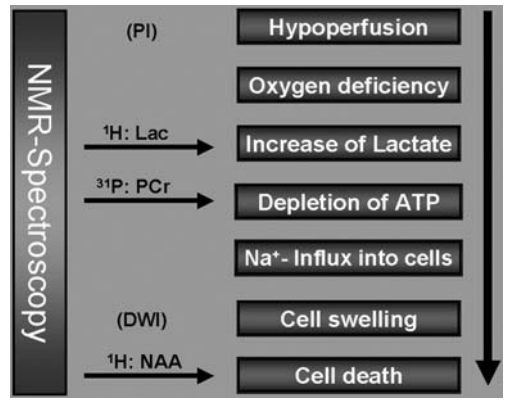

Fig. 11.1. Physiological and metabolic changes in stroke which can be targeted with ^{1}H-MR spectroscopy

H. Lanfermann, MD
Institute for Neuroradiology, Goethe University of Frankfurt, Schleusenweg 2–16, 60590 Frankfurt am Main, Germany
U. Pilatus, MD
Institute for Neuroradiology, Goethe University of Frankfurt, Schleusenweg 2–16, 60528 Frankfurt am Main, Germany

will be discussed below, modern MRS methods are now available, which allow the completion of such an MRS study in less than 10 min, which makes the examination acceptable even in the situation of acute stroke. The aim of this article is to describe the available methodology and discuss the benefits of such an examination for the pathophysiological analysis of stroke.

11.2 Introduction to MRS

Magnetic resonance imaging (MRI) depends on the signal of water protons (^{1}H nuclei) in the presence of magnetic field gradients, which, together with phase encoding, provides the localization. MRS detects water soluble metabolites thus presenting a method for in vivo monitoring of metabolic changes. Spectroscopy can be performed on all nuclei with a spin, leaving ^{23}Na, ^{15}N, ^{13}C, ^{31}P, and ^{1}H as main potential targets for biological applications. ^{15}N and ^{13}C are at low natural abundance and must be administered as labeled compounds. At clinical magnetic field strength, only the ^{1}H nuclei show sufficient sensitivity to be detectable in small volumes (< 4 ml) within reasonable acquisition time. However, measuring ^{1}H spectra requires efficient suppression of the dominant water signal which exceeds the metabolite signals by approximately 10^4. This can be achieved by selective saturation of the water. The first in vivo ^{1}H spectra of rat brain were recorded in 1983 using a surface coil in vertical bore high resolution NMR-spectrometer at 8 T (Behar et al. 1983). Human brain spectra were obtained in 1985 by Bottomley et al., which clearly demonstrated the superior sensitivity of ^{1}H nuclei compared to ^{31}P nuclei.

The first in vivo spectra were recorded with surface coils which detect signal from the entire region in the vicinity of the coil. For application to pathological lesions, it is required to obtain spectra from a targeted region of the brain (e.g. the DWI lesion). This can be achieved by pulse sequences with selective excitation of three orthogonal slabs resulting into spectra from single cuboid volume element localized at the intersection of the slabs (single voxel spectroscopy, SVS). Two methods are available, either PRESS (Bottomley 1987; Ordidge and van de Vyver 1985) or STEAM (Frahm et al. 1989a), each having their advantages and disadvantages as described by Moonen et al. (1989). The potential of measuring spatially resolved spectroscopic information (i.e. obtaining a matrix of spectra as demonstrated in Fig. 11.5) by combining spectroscopy with gradient phase encoding (spectroscopic imaging, SI or MRSI) was first demonstrated by Brown et al. (1982) for the ^{31}P nucleus. Maudsley et al. (1983) applied the same method to ^{23}Na which enabled Hilal et al. (1983) to map sodium increase in ischemic cat brains. One of the first applications in ^{1}H MRS in humans was focused on brain ischemia. The first SVS ^{1}H spectrum of stroke in humans was presented in 1988 (Berkelbach van der Sprenkel et al. 1988) whereas Duijn et al. (1992) showed first ^{1}H spectroscopic images of stroke patients in 1992. Especially with the development of thrombolytic therapies (Hacke et al. 1995; NINDS Stroke-Trial 1995) there is a high demand for a thorough analysis of the infarcted area. The concentration of key metabolites could play a pivotal role. Since MR spectroscopy can provide this information non-invasively in acute stroke, a considerable amount of effort was put in incorporating MRS into the MR examination protocol of acute stroke. However, technical demands and physical limits have prevented a real breakthrough of the method until today.

In the near future the signal to noise ratio (S/N) will gain by increased field strength (from 1.5 to 3.0 T) for clinical scanners. Also, implementation of fast SI techniques can reduce the acquisition time by more than a factor of two, which would turn SI to an applicable tool in a routine MRI protocol for stroke.

11.3 ^{1}H-MRS Methodology

11.3.1 Single-Volume ^{1}H-MRS Versus ^{1}H-MR Spectroscopic Imaging

Metabolic information of infarcted tissue can be retrieved by selecting a single cuboid volume of the pathological area for the spectroscopic examination using one of the above described SVS spectroscopy sequences. Results from an SVS MRS examination at 1.5 T with the PRESS sequence applying a TE of 144 ms are shown in Fig. 11.2. As expected, the infarcted area shows lactate which is visible as two inverted peaks (doublet) around 1.33 ppm while the contralateral tissue exhibits the spectrum of a healthy white matter. To achieve sufficient S/N for quantifiable SVS data from a 3 ml volume (approximately 1.5×1.5×1.5 cm^3), the data acquisition time will take approximately 4 min. This leads to a rather

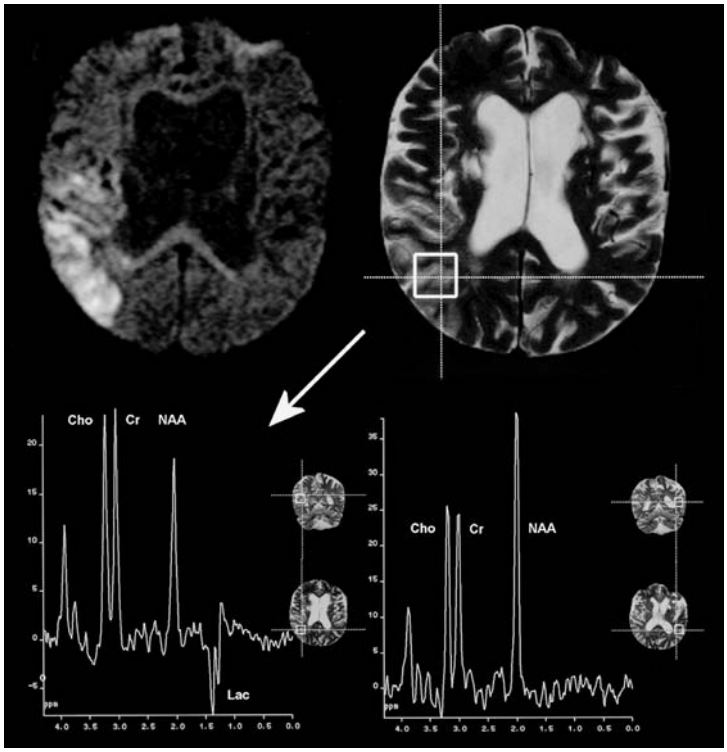

Fig. 11.2. ^{1}H single voxel MR spectroscopy of stroke. Data from a 60-year-old male were obtained at 1.5 T with 144 ms echo time. Respective volumes of interest are marked on T2-weighted image. *Left spectrum*, infarcted area. *Right spectrum*, contralateral healthy tissue. Note the appearance of lactate (two negative peaks at 1.3 ppm) as the most significant difference

long total measurement time since more representative voxels are required to characterize the infarcted area in size and severity, e.g. in Fig. 11.2 the area in the vicinity of the diffusion lesion would be of special interest. For ^{31}P MRS the S/N is even worse, which leaves this method – despite the expected high diagnostic impact of the detectable parameters like pH values, phosphocreatine and ATP concentration – less applicable for acute stroke.

With the lack of other methods to obtain sufficient information for a qualified choice of the position of the spectroscopic voxel, spectroscopic imaging (SI) techniques should be the method of choice. In SI all spectra of a selected slice are acquired simultaneously applying encoding gradients between the excitation pulse and the acquisition period. After spatial Fourier transformation the spectroscopic image is obtained as a matrix of the dimension A×B, where A and B denote the number of phase encoding steps in each direction within the slice. Each matrix element consists of a spectrum. A spectroscopic image can be visualized as a grid overlay on the anatomical image. The anatomical image, which should be recorded with a field of view (FOV), angulations and slice selection identical to the SI sequence, is divided by the grid in A×B voxels each carrying the respective spectroscopic information (Fig. 11.3). Such a map of spectra provides a retrospective definition of the center and the extension of infarcted tissue, while at the same time reference spectra are available from regular non-infarcted tissue. The spatial distribution of biochemical changes within the infarcted area can be exploited to discriminate irreversible damaged tissue from tissue at risk. Since Lac and NAA play a pivotal role for this discrimination, ^{1}H MRSI is already capable of adding important information to the conventional imaging techniques. SI can go down to resolution of 0.75×0.75×1.00 cm^3, but requires phase encoding of the respective matrix. Consequently, acquisition of a data set with conventional CSI technique takes more than 15 min (see below) which, in most cases, is not tolerated by acute stroke patients especially when performed in addition to the other modalities routinely applied in the MR examination of stroke. We will discuss modifications of the basic CSI sequence that can significantly reduce the data acquisition time and details of biochemical and clinical aspects of metabolic changes.

11.3.2 Impact of Fast Spectroscopic Imaging

For an in plane resolution of 7.5×7.5 mm^2, the 32×32 matrix shown in Fig. 11.3 had to be recorded at a

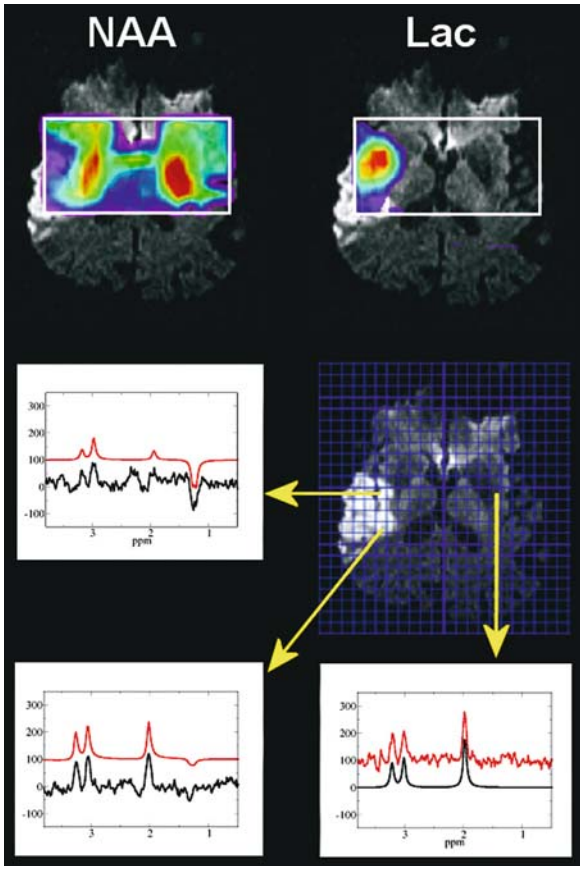

Fig. 11.3. Spectroscopic imaging of stroke. Data from a 71-year-old male were obtained at 3 T using conventional CSI with 144 ms echo time (17 min acquisition time). Metabolite intensities are plotted as color-coded overlay on diffusion-weighted images. Intensities of SI maps of NAA and lactate were obtained by time domain data fit using jMRUI. Representative spectra and fit results (*red line*) are shown in the lower part of the figure. The *arrows* indicate the position of the respective voxels. Low Lac values and persistent NAA signals in the posterior part of the area with increased signal on the DWI image may be caused by early reperfusion of an M3 branch of the middle cerebral artery and consecutive washout of Lac

240 mm^2 FOV. Acquisition of the entire *k*-space at a repetition time of 1.5 s would take 1024×1.5 s or 26 min. Together with the preparation period (extensive shimming, adjustments for water suppression), the MRS examination may add another 45 min to the conventional imaging examination. Sometimes, our early studies needed even 70 min in addition to the MRS protocol. Usually, patients with acute or subacute stroke are severely sick and not very compliant. Frequently, head movement during the MRS occurred, which will corrupt data, spoiling or at least complicating a reasonable evaluation. Reduction of measurement time and optimized automatic adjustments for the preparation period are therefore essential for a successful MRS protocol. The latter has been addressed in the modern scanners by use of image guided shimming procedures and implementations of routines for automatic adjustments of water suppression. These tools can reduce the preparation time to less then 5 min.

The rather extensive acquisition times required for the complete *k*-space can also be reduced. Without significant loss in spatial resolution, a 28×28 matrix can be recorded and extrapolated to 32×32 by adding zeroes before Fourier transformation, which will reduce the total acquisition time to 20 min. Selection of a circular (elliptical in case of rectangular FOV) *k*-space area centered around the origin, will save another 25% of acquisition time without seriously affecting the spatial resolution (Maudsley et al. 1994). The use of a rectangular FOV could also save up to 30% (Golay et al. 2002) resulting in a total acquisition time between 10 and 15 min. Further reduction in acquisition time can be achieved with fast imaging techniques like echo planar spectroscopic imaging (EPSI) (Posse et al. 1995) or multiple spin-echo spectroscopic imaging (MSESI) (Duyn et al. 1995; Duyn and Moonen 1993). These techniques scan more than one phase encoding step for a single excitation pulse, providing the respective acceleration factors. In a recent study (Stengel et al. 2004), our group could show that quantification of NAA and Lac concentrations can be obtained with 0.75×0.75×1.00 cm^3 resolution with a total acquisition time of 6 min using MSESI. A typical result of such an examination is shown in Fig. 11.4. Please note that due to the short sampling period at 144 ms echo repetition time the spectral resolution is rather limited, allowing detection of separate signals only for NAA and lactate. However, these metabolites are carrying the most valuable information about the infarcted area.

11.3.3 Partial Volume Effects Due to Low Resolution

Even with the application of the above mentioned fast imaging techniques, the spatial resolution is still limited by the minimum S/N which can be achieved in the time reserved for the spectroscopic examination. We feel that with the currently available instrumentation the maximum resolution should be around 0.6 cm^3. Representative spectra obtained with this resolution at 3 T magnetic field strength

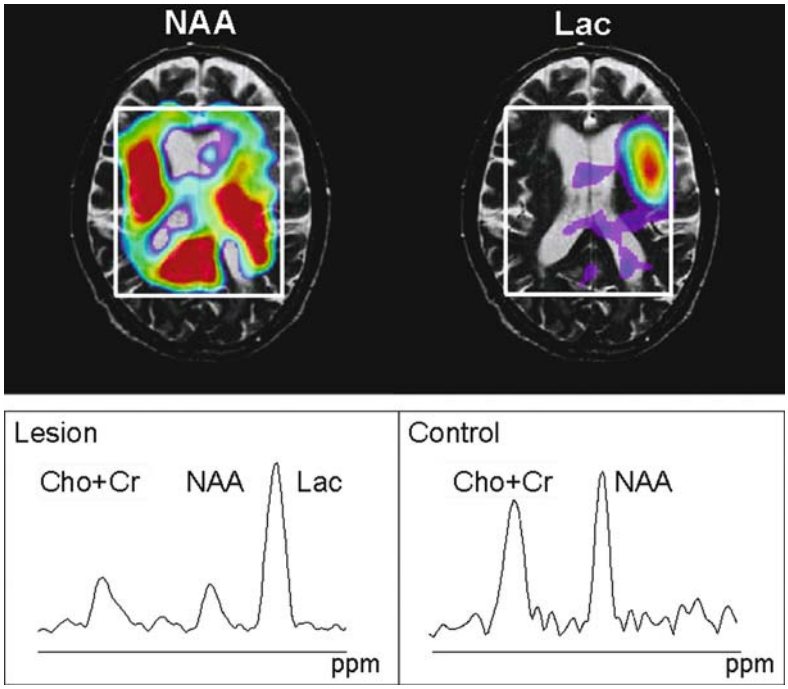

Fig. 11.4. Fast spectroscopic imaging of stroke. SI maps of lactate and NAA. Metabolite intensities are plotted as color-coded overlay on diffusion-weighted images. Intensities were obtained by numerical integration of the peak areas defined in the two spectra below. Data were acquired with the multiple spin echo SI sequence (7 min acquisition time), thus signal resolution is considerably reduced compared to single voxel spectra in Fig. 11.2 or conventional CSI in Fig. 11.3. (Data courtesy of A. Stengel)

are shown in Fig. 11.3. Metabolite concentrations from lesion smaller than the grid resolution will be affected by the concentration in the surrounding tissue and changes may be masked, i.e. Lac will be underestimated and NAA overestimated. However, since a slight increase above the background noise can be easier detected than signal variation of rather intensive signals, increased Lac can be observed in infarcted lesion with a size below the nominal resolution. Partial volume effects should also be taken into account when absolute quantification of spectroscopic data is considered (see below).

11.3.4 Evaluation of Metabolite Concentrations

Spectroscopic data reflect the concentration of a subset of brain metabolites. The accuracy of the related information depends crucially on the approach used for data quantification. Generally, the spectrum is evaluated by measuring the area under the metabolite signals. This can be done either by numerical integration of metabolite peaks in phased (real) or magnitude (modulus) spectra, or by using more sophisticated tools which basically perform a nonlinear fit of the entire spectrum. Depending on the tool, the fit is performed in the time domain [jMRUI (Naressi et al. 2001), offline] or frequency domain [online processing tools on the scanner console, LC-Model (Provencher 1993), offline]. All methods report signal intensities, which are proportional to the respective metabolite concentration in the volume of interest (VOI). Figure 11.5 shows the result of an online analysis of a SVS spectrum with the scanner software while red lines in the representative spectra of Fig. 11.3 depict calculated spectra of an offline analysis using jMRUI. Conversion of these hardware specific units to absolute concentrations (i.e., mmol/l) requires a set of correction factors which depend on the used pulse sequence, hardware parameters like signal amplification and coil loading, relaxation times (T1, T2) of the metabolites, as well as fractions of GM, WM and CSF in the VOI (partial volume effects). Hardware parameters can be corrected for by using either the so-called phantom replacement method (Michaelis et al. 1993) or scaling relative to the water signal (Barker et al. 1993). The water must be recorded in a separate measurement, either as a separate CSI data set or by an imaging sequence with proton density contrast. Relaxation terms for regular (healthy) tissue are available from several publications (e.g., Frahm et al. 1989b; Kugel et al. 2003). Changes due to pathological alterations may be less than 30% (Gideon and Hendriksen 1992; Kettunen et al. 2004). Correction for partial volume effects require at least one more additional imaging sequence and further calculations. A rather quick method which only takes into account

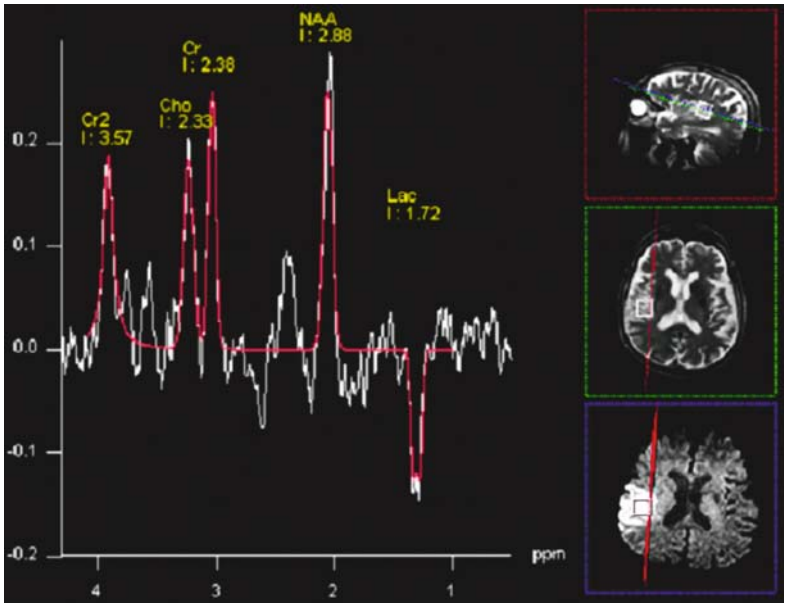

Fig. 11.5. Single voxel spectroscopic data at 3 T field strength. Same patient as presented in Fig. 11.3 (71-year-old man). The *red line* and signal intensities are results of an online frequency domain fit using the manufacturer provided software on the console (Siemens Allegra, Siemens, Erlangen, Germany). Images on the *right* show the voxel position in T2-weighted (transversal and sagittal) and diffusion weighted (transversal) images

the CSF fraction was described by Horska et al. (2002) while analysis of GM, WM, and CSF fraction requires tissue segmentation which can be very time consuming and are not applicable when immediate results are needed for a therapeutic decision. Therefore, a thorough data evaluation in terms of absolute concentrations should be reserved for research studies aimed at metabolic differences between different groups of patients (e.g. different size of infarct, different treatment) and longitudinal studies, while for diagnostic purposes in acute stroke a semi-quantitative approach should be sufficient. This can easily include correction for hardware sensitivity using either the phantom replacement or water reference scaling method where the phantom replacement method is not applicable with receive-only coils. Furthermore, relaxation corrections can be performed using parameters for healthy tissue. By inspection of a VOI with no CSF (preferentially WM) in a non-infarcted area the overall accuracy of the data can be evaluated. Immediate information of the extend of concentration change can then be visualized in the SI metabolite map. However, one should be aware of artifacts (see below).

11.3.5 Artifacts in Metabolite Maps

Spectroscopic imaging data are frequently visualized as metabolite maps, i.e. for each metabolite the concentration is displayed either as a gray image or as a color-coded overlay on an anatomical image. While this provides the most intuitive picture of the results, special care should be taken when interpreting these maps. The physician should be aware of the method used to calculate the metabolite maps: are they based on a simple integration of marked metabolite specific regions or was a fitting routine involved. Which processing steps were performed (baseline correction, frequency correction to account for susceptibility changes) before the final signal analysis was executed? All these points will affect the measured concentration, but can not be critically discussed based on the simple metabolite map. Local field inhomogeneities due to deposits of paramagnetic hemosiderin, can shift and distort signals spoiling the applied automatic data analysis algorithm. Especially for voxels crucial for diagnostic decision, a careful inspection of the entire spectrum is required in order to exclude artifacts, which may have caused the concentration change. Lactate metabolite maps are prone to contamination by lipids. Intensive lipid signals originating from fat deposits in the skull base and orbit can misleadingly be interpreted as high lactate in brain tissue. This may happen if the patient has moved during the examination so that lipid containing structures were inside the selected volume at least for a short period of time. Lipid signals can be easily distinguished from lactate, since only lactate shows a doublet signal (i.e., two peaks of identical intensity separated by 7.4 Hz) which may be inverted at an echo time of 144 ms (inversion is

not detectable in magnitude spectra). At B_0 field strength of 3 T, the doublet structure of lactate may be less visible due to increased line broadening at higher field strength but signal inversion can still be exploited for discrimination of lactate from lipid (see Figs. 11.3, 11.5).

11.4 Biochemical Alterations in Cerebral Infarcts

The infarcted area shows reduced concentrations of NAA, creatine, and choline compounds in single volume spectra as well as in one and two dimensional SI. An intensive signal of lactate could appear as well. The analysis of underlying biochemical processes is based on the following assumptions for the main observable metabolites:

- NAA is a marker for intact neurons
- Choline compounds are related to membrane turnover metabolism
- Creatine compounds are related to energy metabolism
- Lactate indicates insufficient oxidative phosphorylation by the TCA cycle. In this case, the pyruvate which is produced by glycolysis can not be transferred to the TCA cycle and is converted into lactate.

Metabolic changes occurring up to day 35 after stroke are presented in Fig. 11.6. Reduced NAA in the infarcted area is mainly detected in studies which include a significant fraction of patients with subacute infarct (Berkelbach van der Sprenkel et al. 1988; Bruhn et al. 1989; Duijn et al. 1992; Hugg et al. 1992; Lanfermann et al. 1995; Felber et al. 1992; Graham et al. 1995). Our recent publication with acute or hyperacute infarct patients (Stengel et al. 2004) indicate that NAA may not be a reliable marker for neuronal damage during early stage of stroke, a finding which confirms previous HPLC data of Sager et al. (1995).

Usually, NAA reduction in the subacute phase of stroke is accompanied by a decrease in choline and creatine compounds. However, the decrease is less significant. Duijn et al. (1992) could detect 47% remaining choline and 37% remaining creatine in a patient population with mean time after infarct of 400 days. Our own studies of acute and subacute infarcts showed even less pronounced decrease (down to 65% for choline and 69% for creatine) for infarcted areas larger than 2 cm diameter and a median time after infarct of 6.0 days. The concentrations dropped to 42% in the subacute phase indicating that remaining creatine and choline signals are predominantly a function of the time after infarct. A more detailed analysis comparing signal reduction in different areas of the infarct revealed more pronounced decrease of NAA compared to the other compounds in areas at the rim of the lesion. This would account for the existence of areas where ischemia had caused neuronal damage, but glial cells are still viable (Duijn et al. 1992; Hugg et al. 1992). Even an increase of choline had been observed. While there is no validated rational for this finding, one could speculate that enhanced membrane turnover rates occur in these areas, may be as result of repair mechanisms.

Elevated lactate seems to be the most reliable metabolic marker of acute stroke. Significantly increased lactate in ischemic tissue was observed within 30 s (Hetherington et al. 1994). Lactate is generally observed in the infarcted area which is defined by the diffusion lesion (Monsein et al. 1993; Nakada et al. 1991), but frequently, it can also be detected outside this lesion. In hyperglycemia, the elevated lactate concentration is correlated with blood glucose concentration (Parsons et al. 2000, 2001, 2002). While augmented lactate in areas with depletion of oxygen supply can be easily rationalized in terms of basic biochemistry, it's persistence for several weeks (Houkin et al. 1993; Lanfermann et al. 1995) needs further discussion and may critically depend on the time and extent of reperfusion. Regions adjacent to the infarcted area with ongoing hypoperfusion (the so-called penumbra, see below) may be the source of a permanent lactate production. However, MRSI data do not support this rational since areas of elevated lactate were rather homogeneous inside the infarcted tissue with no enhancements at the rim. For subacute strokes, slightly increased lactate concentrations were also observed in contralateral hemisphere and the ventricles (Duijn et al. 1992; Hugg et al. 1992; Lanfermann et al. 1995).

Several publications (Hugg et al. 1992; Levine et al. 1992; Sappey-Marinier et al. 1992) report increased pH values and augmented lactate in subacute infarcts. It has been speculated, that lactate, which has been produced during the first hour of ischemia can persist in dead cells and will be detected with ^{1}H-MRS. Furthermore, macrophages and microglia which infiltrate the infarcted area after the third day rely primarily on anaerobic glycolysis and may be responsible for the elevated lactate (Karnovsky 1962; Petroff et al. 1992).

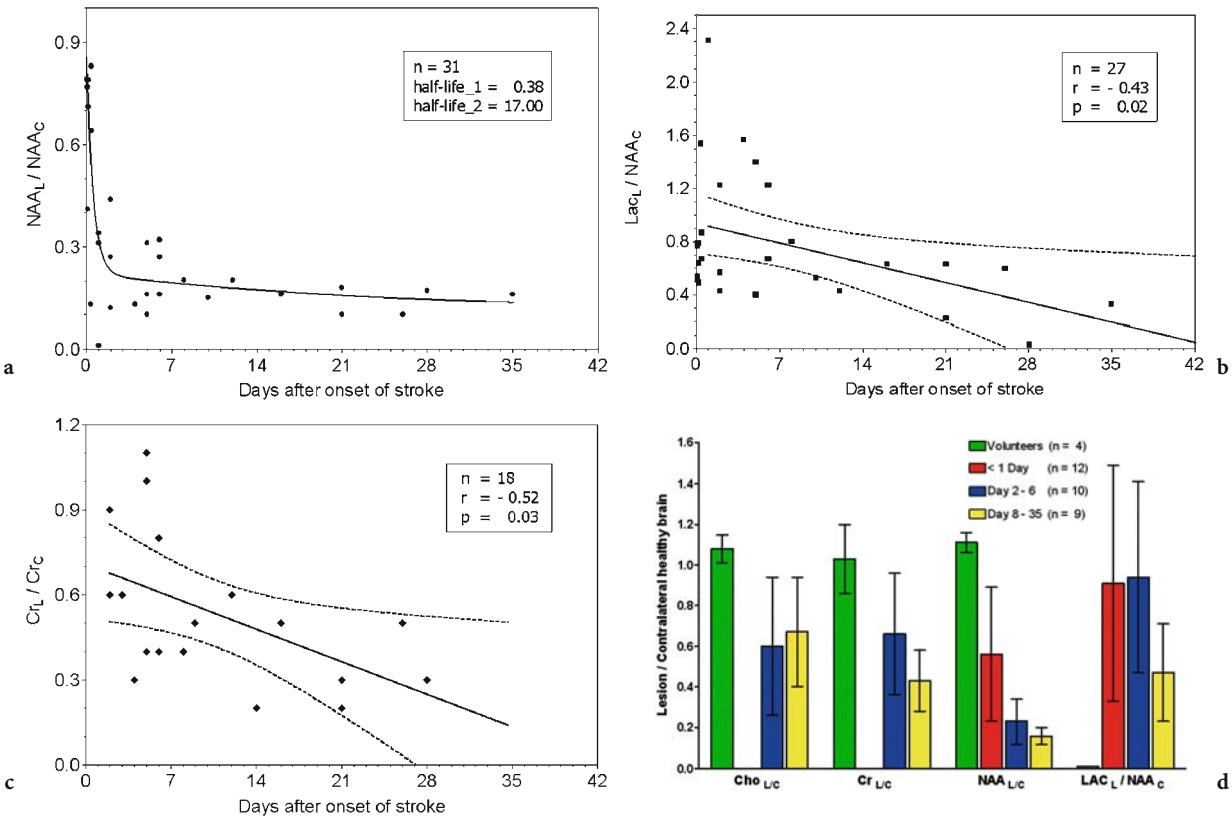

Fig. 11.6a-d. Metabolic changes in infarcted areas as a function of time after stroke onset: **a** NAA decrease. NAA concentration was referred to NAA peak intensity of the contralateral (healthy) side. The *line* shows a nonlinear fit of the data assuming a biexponential decay. The resulting *half-lives* were 0.38 days for the fast process and 17 days for the slow process. **b** Lactate concentration. The concentration was estimated by referring to the NAA signal of the contralateral (healthy) side. The straight line shows linear regression analysis. **c** Creatine concentration. The concentration was estimated referring to the creatine peak intensity of the contralateral (healthy) side. The *straight line* shows linear regression analysis. **d** Summary of (**a-c**) in a bar graph and comparison to healthy volunteers. Data for day 1 were calculated from our recently published data (Stengel et al. 2004). [With gratitude to H. Kugel (Münster, Germany) for support in acquisition and analysis of subacute data]

11.5 Clinical Impact of ^{1}H-MR Spectroscopic Imaging

Spectroscopic imaging is the only method which provides information on changes occurring during a very early stage of stroke up to neuronal cells death. A consistent interpretation of the data can be based on the following assumptions which are corroborated by most experiments:

- Increase in lactate indicates hypoxia, which is he first event in ischemic tissue
- Decrease in NAA indicates neuronal cells death. Tissue with NAA below a specific threshold should be irreversibly damaged.

Considering the final outcome of stroke as a cascade of consecutive biochemical events, step 1 may be considered as the initial physiological reaction to limited oxygen supply, which not necessarily indicates serious cell damage. On the other hand, NAA decrease reflects neuronal cell death as result of either serious ischemia (i.e. complete cessation of perfusion), or long term less severe ischemia, but also following reperfusion after a period of ischemia.

With the development of thrombolytic therapies (NINDS Stroke-Trial 1995; Hacke et al. 1995) there is a high demand for new methods which provide detailed information on the infarcted parenchyma, especially for those methods which enable characterization of tissue that is potentially salvageable by reperfusion therapy. Since the concentration of key metabolites may play a pivotal role, MR spectroscopy may have an impact on treatment decisions.

Basic pathophysiology of cerebral ischemia and infarcts was first studied using PET. In rather exten-

sive studies the complex relations between cerebral blood flow (CBF) cerebral blood volume (CBV), oxygen extraction fraction (OEF) and the metabolic rates for oxygen and glucose metabolism [cerebral metabolic rate of oxygen ($CMRO_2$), cerebral metabolic rate of glucose (CMR_{glc})] were analyzed (Baron et al. 1983, 1989; Heiss 1992; Heiss and Herholz 1994; Powers et al. 1985; Wise et al. 1983). In contrast to experimental systems with well defined parameters, stroke in human brain proposes a very complex situation with rather limited knowledge of the most important parameters like examination time after stroke onset, whether the occlusion is persistent or just temporary, and whether collateral perfusion is efficient or not. However, longitudinal studies revealed valuable information regarding the still viable tissue at depleted perfusion rates (Hakim 1987; Hakim and Shoubridge 1989; Heiss 1992). This area, the so called penumbra, depicts tissue at risk which may be rescued by adequate therapy. Due to inter-individual differences (collateral perfusion) and intra-individual differences [cell population (Heiss and Rosner 1983)], the differentiation between irreversibly damaged tissue and tissue at risk is difficult to pursue for each case. As already mentioned above, the increasing ability of therapeutic methods like thrombolysis, generated a growing demand for more accurate methods for staging of infarcted tissue. Consequently, a definition of the penumbra aroused from comparison of perfusion imaging (PI) and diffusion weighted imaging (DWI) data assigning those regions to tissue at risk which show depleted perfusion in PI but no increase in ADC. The PI based penumbra may overestimate the area for tissue at risk. In comparison to this penumbra definition, an MRSI penumbra can be postulated as the area which shows increased lactate but no decrease of NAA (at least not below a specific threshold). Adapted to the PET based penumbra definition of Astrup et al. (1981), early lactate increase would mark regions with impaired energy metabolism which potentially can be reversed, while a slowly developing NAA depletion in the center of regions with augmented lactate indicates irreversible cell damage with the well defined morphological changes. Both metabolites can therefore be considered as markers for threshold values verified in various PET studies which indicate the collapse of aerobic energy supply and finally irreversible damage of neurons.

The decrease in ADC in infarcted tissue can be assigned to a shift of water from the extracellular to intracellular compartment (see Chap. 7). While it is generally assumed that the final stage of energy cessation, the reduction of ATP followed by an inflow of Na^+ (cytotoxic cell swelling) is responsible for the massive ADC decrease, also augmented lactate production may induce cell swelling by increasing intracellular osmolality. Especially when the extracellular pH is decreased by accumulation of lactate while the intracellular pH is maintained due to pH homeostasis, the outward directed proton-gradient will further amplify intracellular lactate concentration since lactate as a weak acid will accumulate in the high pH compartment. Consequently, Hoehn-Berlage et al. (1995) and Kohno et al. (1995) could show that areas with decreased ADC values correspond to increased lactate concentrations and significantly extend the area of reduced ATP. Appropriately timed reperfusion confirmed that the ADC decrease can be reversed depending on the metabolic conditions of the tissue (Hossmann 1994; Minematsu et al. 1992). The question remains whether irreversible cell damage is explicitly linked to NAA decrease in acute or hyperacute stroke or whether NAA concentrations stay unaltered even after cytotoxic edema.

A combination of spectroscopy with DWI and PI data is probably the most promising approach for discrimination of tissue at risk from irreversible damaged tissue (Takegami et al. 2001). Both imaging methods require only short acquisition time and can easily be added to the spectroscopy examination. Within the time window of 3 h (Heiss and Graf 1994; Heiss and Herholz 1994) – depending on remaining perfusion – areas could be identified which show increased lactate but no measurable decrease in ADC. Accumulation of lactate as well as decrease in ADC depends on CBF. Below a CBF of 35-40 ml/100 g/min the cerebral lactate concentration is likely to increase (Allen et al. 1993; Kohno et al. 1995; Naritomi et al. 1988; Obrenovitch et al. 1988; Paschen et al. 1992) while values of less than 20 ml/100 g/min will usually correlate with a marked decrease in ADC (Busza et al. 1992). Thus, areas with increased lactate and decreased ADC represent regions with pronounced tissue ischemia within the larger territory of impaired perfusion (Nicoli et al. 2003; Takegami et al. 2001). A mismatch of lactate and ADC decrease (i.e., increased lactate but no change in ADC) in the first hours after stroke onset most probably reveals an area of brain tissue at high risk. Since NAA changes during the first hours are rather marginal we feel that with the current knowledge metabolic maps with lactate in combination with ADC weighted images provide the most suitable tool for detection of a penumbra which is restricted to brain tissue at high risk.

11.6 Limitations of ^{1}H-MR Spectroscopic Imaging

Compared to MR imaging techniques MRSI offers a rather coarse spatial resolution with a limit between 1.0 and 0.5 cm^3. On the one hand, this could lead to an underestimation of lactate concentrations in small lesions while on the other hand the size of the penumbra may be overestimated. Another problem is related to signals from lipids of the skull and bone marrow, which may mask lactate. Several options are available to discriminate the lipids from lactate. Most efficient is a fit of correctly phased spectra recorded at an TE of 144 ms, using an inverted doublet (two negative signals separated by 7.0 Hz). As discussed above, careful visual inspection of spectra to identify the typical lactate doublet in magnitude spectra or in multi-slice CSI with TE of 288 may also provide sufficient power for discrimination of lactate from lipids. However, if no such measures are taken [as it is usually the case for the MSESI technique applied by Stengel et al. (2004)] cortical regions close to the skull can not be incorporated into the ROI for SI.

11.7 Future of ^{1}H-MR Spectroscopic Imaging

State of the art spectroscopic imaging determines the spatial distribution of NAA, creatine, choline, and lactate concentrations with less than 1 cm^3 resolution. By monitoring biochemical changes, the method provides a unique tool for assessing ischemia related damage of brain tissue; however, for incorporation into a routine MR examination performed in the first hours after stroke, rather short data acquisition times are required. Currently, volume data (i.e., four slices with 1.5 cm thickness) can be recorded in less then 15 min while single slice data acquisition with a fast SI sequence will take less then 7 min. According to our experience, 7 min examination time is tolerable in most cases, thus, metabolic information can be obtained even with the constraints of an emergency MR examination of hyperacute stroke. Given the fact that the maximal MRS examination time should not exceed 10 min, the spatial resolution can not significantly be improved due to limited S/N. Future developments should focus on the following topics:

- Obtaining isotropic voxels by combination of fast SI techniques with concepts of parallel data acquisition.
- Extending the SI information to other metabolites, e.g., myo-inositol, glutamine, glutamate.
- Development of software tools for robust MRSI spectra analysis combined with easy and intuitively to use graphical user interfaces for interactively viewing and comparing MRSI, DWI, and PI data.

Feasibility studies are already published for topic 1 (Dydak et al. 2003). A potential solution for topic 2 would be a multislice (four slices) short TE ($\leq$ 30 ms) CSI sequence with rectangular FOV where the number of phase encoding steps is reduced by employing parallel data acquisition techniques. Enormous effort is currently put in development of software for analyzing and viewing different MRI modalities. The programs are either installed on the scanner or facilitate an offline analysis on workstations. Also the number of tools for sophisticated offline analysis of SI data is steadily growing (e.g., SI images in Fig. 11.3 are based on the time domain analysis tool jMRUI) while at the same time the software available on the scanner console is also improving. Thus we feel, that in the near future topic 3 will not be one of the limiting factors for MRSI studies.

References

Allen KL, Busza AL, Proctor E, King MD, Williams SR, Crockard HA, Gadian DG (1993) Controllable graded cerebral ischaemia in the gerbil: studies of cerebral blood flow and energy metabolism by hydrogen clearance and 31P NMR spectroscopy. NMR Biomed 6:181-186

Astrup J, Siesjo BK, Symon L (1981) Thresholds in cerebral ischemia – the ischemic penumbra. Stroke 12:723-725

Barker PB, Soher BJ, Blackband SJ, Chatham JC, Mathews VP, Bryan RN (1993) Quantitation of proton NMR spectra of the human brain using tissue water as an internal concentration reference. NMR Biomed 6:89-94

Baron JC, Bousser MG, Comar D, Rougemont D, Lebrun-Grandie P, Castaigne P (1983) [Positron emission tomography in the physiopathological study of cerebral ischemia in man]. Presse Med 12:3066-3072

Baron JC, Frackowiak RS, Herholz K, Jones T, Lammertsma AA, Mazoyer B, Wienhard K (1989) Use of PET methods for measurement of cerebral energy metabolism and hemodynamics in cerebrovascular disease. J Cereb Blood Flow Metab 9:723-742

Beauchamp NJ, Barker PB, Wang PY, van Zijl PCM (1999) Imaging of acute cerebral ischemia. Radiology 212:307-324

Behar KL, den Hollander JA, Stromski ME, Ogino T, Shulman RG, Petroff OA, Prichard JW (1983) High-resolution 1H

nuclear magnetic resonance study of cerebral hypoxia in vivo. ProcNatl Acad Sci USA 80:4945-4948

Berkelbach van der Sprenkel JW, Luyten PR, van Rijen PC, Tulleken CA, den Hollander JA (1988) Cerebral lactate detected by regional proton magnetic resonance spectroscopy in a patient with cerebral infarction. Stroke 19:1556-1560

Bottomley PA (1987) Spatial localization in NMR spectroscopy in vivo. Ann NY Acad Sci 508:333-348

Bottomley PA, Edelstein WA, Foster TH, Adams WA (1985) In vivo solvent-suppressed localized hydrogen nuclear magnetic resonance spectroscopy: a window to metabolism? Proc Natl Acad Sci USA 82:2148-2152

Brown TR, Kincaid BM, Ugurbil K (1982) NMR chemical shift imaging in three dimensions. Proc Natl Acad Sci USA 79:3523-3526

Bruhn H, Frahm J, Gyngell ML, Merboldt KD, Hanicke W, Sauter R (1989) Cerebral metabolism in man after acute stroke: new observations using localized proton NMR spectroscopy. Magn Reson Med. 9:126-131

Busza AL, Allen KL, King MD, van Bruggen N, Williams SR, Gadian DG (1992) Diffusion-weighted imaging studies of cerebral ischemia in gerbils. Potential relevance to energy failure. Stroke 23:1602-1612

Duijn JH, Matson GB, Maudsley AA, Hugg JW, Weiner MW (1992) Human brain infarction: proton MR spectroscopy. Radiology 183:711-718

Duyn JH, Frank JA, Moonen CT (1995) Incorporation of lactate measurement in multi-spin-echo proton spectroscopic imaging. Magn Reson Med 33:101-107

Duyn JH, Moonen CT (1993) Fast proton spectroscopic imaging of human brain using multiple spin-echoes. Magn Reson Med 30:409-414

Dydak U, Pruessmann KP, Weiger M, Tsao J, Meier D, Boesiger P (2003) Parallel spectroscopic imaging with spin-echo trains. Magn Reson Med 50:196-200

Felber SR, Aichner FT, Sauter R, Gerstenbrand F (1992) Combined magnetic resonance imaging and proton magnetic resonance spectroscopy of patients with acute stroke. Stroke 23:1106-1110

Frahm J, Bruhn H, Gyngell ML, Merboldt KD, Hanicke W, Sauter R (1989a) Localized high-resolution proton NMR spectroscopy using stimulated echoes: initial applications to human brain in vivo. Magn Reson Med 9:79-93

Frahm J, Bruhn H, Gyngell ML, Merboldt KD, Hanicke W, Sauter R (1989b) Localized proton NMR spectroscopy in different regions of the human brain in vivo. Relaxation times and concentrations of cerebral metabolites. Magn Reson Med 11:47-63

Gideon P, Hendriksen O (1992) In vivo relaxation of N-acetylaspartate, creatine plus phosphocreatine, and choline containing compounds during the course of brain infarction: a proton MRS study. Magn Reson Imaging 10:983-988

Golay X, Gillen J, van Zijl P, Barker P (2002) Scan time reduction in proton magnetic resonance spectroscopic imaging of the human brain. Magn Reson Med 47:384-387

Graham GD, Kalvach P, Blamire AM, Brass LM, Fayad PB, Prichard JW (1995) Clinical correlates of proton magnetic resonance spectroscopy findings after acute cerebral infarction. Stroke 26:225-9

Hacke W, Kaste M, Fieschi C, Toni D, Lesaffre E, von Kummer R, Boysen G, Bluhmki E, Hoxter G, Mahagne MH, Hennerici M (1995) Intravenous thrombolysis with recombinant tissue-plasminogen activator for acute hemispheric stroke – the European Cooperative Acute Stroke Study (Ecass). JAMA 274:1017-1025

Hakim AM (1987) The cerebral ischemic penumbra. Can. J.Neurol.Sci. 14:557-559

Hakim AM, Shoubridge EA (1989) Cerebral acidosis in focal ischemia. Cerebrovasc.Brain Metab Rev. 1:115-132

Heiss WD (1992) Experimental evidence of ischemic thresholds and functional recovery. Stroke 23:1668-1672

Heiss WD, Graf R (1994) The ischemic penumbra. Curr.Opin. Neurol. 7:11-19

Heiss WD, Herholz, K (1994) Assessment of pathophysiology of stroke by positron emission tomography. Eur.J.Nucl. Med. 21:455-465

Heiss WD, Rosner, G (1983) Functional recovery of cortical neurons as related to degree and duration of ischemia. Ann. Neurol. 14:294-301

Hetherington HP, Tan MJ, Luo KL, Pohost GM, Halsey JH, Conger KA (1994) Evaluation of lactate production and clearance kinetics by 1H NMR in a model of brief repetitive cerebral ischemia. J.Cereb.Blood Flow Metab 14:591-596

Hilal SK, Maudsley AA, Simon HE, Perman WH, Bonn J, Mawad ME, Silver AJ, Ganti SR, Sane P, Chien IC (1983) In vivo NMR imaging of tissue sodium in the intact cat before and after acute cerebral stroke. AJNR Am.J.Neuroradiol. 4:245-249

Hoehn-Berlage M, Norris DG, Kohno K, Mies G, Leibfritz D, Hossmann KA (1995) Evolution of regional changes in apparent diffusion coefficient during focal ischemia of rat brain: the relationship of quantitative diffusion NMR imaging to reduction in cerebral blood flow and metabolic disturbances. J Cereb Blood Flow Metab 15:1002-1011

Horska A, Calhoun VD, Bradshaw DH, Barker PB (2002) Rapid method for correction of CSF partial volume in quantitative proton MR spectroscopic imaging. Magn Reson Med 48:555-558

Hossmann KA (1994) Viability thresholds and the penumbra of focal ischemia. Ann Neurol 36:557-565

Houkin K, Kamada K, Kamiyama H, Iwasaki Y, Abe H, Kashiwaba T (1993) Longitudinal changes in proton magnetic resonance spectroscopy in cerebral infarction. Stroke 24:1316-1321

Hugg JW, Duijn JH, Matson GB, Maudsley AA, Tsuruda JS, Gelinas DF, Weiner MW (1992) Elevated lactate and alkalosis in chronic human brain infarction observed by 1H and 31P MR spectroscopic imaging. J.Cereb.Blood Flow Metab 12:734-744

Karnovsky ML (1962) Metabolic basis of phagocytic activity. Physiol Rev 42:143-168

Kettunen MI, Grohn OH, Kauppinen RA (2004) Quantitative T1rho NMR spectroscopy of rat cerebral metabolites in vivo: effects of global ischemia. Magn Reson Med 51:875-880

Kohno K, Hoehn-Berlage M, Mies G, Back T, Hossmann KA (1995) Relationship between diffusion-weighted MR images, cerebral blood flow, and energy state in experimental brain infarction. Magn Reson Imaging 13:73-80

Kugel H, Roth B, Pillekamp F, Krüger K, Schulte O, von Gontard A, Benz-Bohm G (2003) Proton spectroscopic metabolite signal relaxation times in preterm infants: a prerequisite for quantitative spectroscopy in infant brain. J Magn Reson Imaging 17:634-640

Lanfermann H, Kugel H, Heindel W, Herholz K, Heiss WD,

Lackner K (1995) Metabolic changes in acute and subacute cerebral infarctions: findings at proton MR spectroscopic imaging. Radiology 196:203-210

Levine SR, Helpern JA, Welch KM, Vande Linde AM, Sawaya KL, Brown EE, Ramadan NM, Deveshwar RK, Ordidge RJ (1992) Human focal cerebral ischemia: evaluation of brain pH and energy metabolism with P-31 NMR spectroscopy. Radiology 185:537-544

Maudsley AA, Hilal SK, Perman WH, Simon HE (1983) Spatially resolved high-resolution spectroscopy by "four-dimensional" NMR. J.Magn.Reson. 147-152

Maudsley AA, Matson GB, Hugg JW, Weiner MW (1994) Reduced phase encoding in spectroscopic imaging. Magn Reson Med 31:645-651

Michaelis T, Merboldt K, Bruhn H, Hänicke W, Frahm J (1993) Absolute concentrations of metabolites in the adult human brain in vivo: quantification of localized proton MR spectra. Radiology 187:219-227

Minematsu K, Li L, Sotak CH, Davis MA, Fisher M (1992) Reversible focal ischemic injury demonstrated by diffusion-weighted magnetic resonance imaging in rats. Stroke 23:1304-1310

Monsein LH, Mathews VP, Barker PB, Pardo CA, Blackband SJ, Whitlow WD, Wong DF, Bryan RN (1993) Irreversible regional cerebral ischemia: serial MR imaging and proton MR spectroscopy in a nonhuman primate model. AJNR Am J Neuroradiol 14:963-970

Moonen CT, von Kienlin M, van Zijl PC, Cohen J, Gillen J, Daly P, Wolf G (1989) Comparison of single-shot localization methods (STEAM and PRESS) for in vivo proton NMR spectroscopy. NMR Biomed 2:201-208

Nakada T, Houkin K, Hida K, Kwee IL (1991) Rebound alkalosis and persistent lactate: multinuclear (1H, 13C, 31P) NMR spectroscopic studies in rats. Magn Reson Med 18:9-14

Naressi A, Couturier C, Castang I, De Beer R, Graveron-Demilly D (2001) Java-based graphical user interface for MRUI, a software package for quantitation of in vivo/medical magnetic resonance spectroscopy signals. Comput Biol Med 31:269-286

Naritomi H, Sasaki M, Kanashiro M, Kitani M, Sawada T (1988) Flow thresholds for cerebral energy disturbance and Na+ pump failure as studied by in vivo 31P and 23Na nuclear magnetic resonance spectroscopy. J. Cereb. Blood Flow Metab 8:16-23

The National Institute of Neurological Disorders and Stroke rt-PA Stroke Study Group (1995) Tissue plasminogen activator for acute ischemic stroke. N Engl J Med 333:1581-1587

Nicoli F, Lefur Y, Denis B, Ranjeva JP, Confort-Gouny S, Cozzone PJ (2003) Metabolic counterpart of decreased apparent diffusion coefficient during hyperacute ischemic stroke: a brain proton magnetic resonance spectroscopic imaging study. Stroke 34:e82-e87

Obrenovitch TP, Garofalo O, Harris RJ, Bordi L, Ono M, Momma F, Bachelard HS, Symon L (1988) Brain tissue concentrations of ATP, phosphocreatine, lactate, and tissue pH in relation to reduced cerebral blood flow following experimental acute middle cerebral artery occlusion. J.Cereb. Blood Flow Metab 8:866-874

Ordidge RJ, Van de Vyver FL (1985) Re: Separate water and fat MR images. Radiology 157:551-553

Parsons M, Li T, Barber P, Yang Q, Darby D, Desmond P, Tress B, Davis S (2000) Acute hyperglycaemia in stroke leads to increased brain lactate production and greater final infarct size. Stroke 31:2795-2795

Parsons MW, Barber PA, Darby DG, Yang Q, Desmond PM, Gerraty RP, Tress BM, Davis SM (2001) Acute hyperglycemia in stroke leads to increased brain lactate production and greater final infarct size. Stroke 32:331-332

Parsons MW, Barber PA, Desmond PM, Baird TA, Darby DG, Byrnes G, Tress BM, Davis SM (2002) Acute hyperglycemia adversely affects stroke outcome: a magnetic resonance imaging and spectroscopy study. Annals of Neurology 52:20-28

Paschen W, Mies G, Hossmann KA (1992) Threshold relationship between cerebral blood flow, glucose utilization, and energy metabolites during development of stroke in gerbils. Exp.Neurol 117:325-333

Petroff OA, Graham GD, Blamire AM, al Rayess M, Rothman DL, Fayad PB, Brass LM, Shulman RG, Prichard JW (1992) Spectroscopic imaging of stroke in humans: histopathology correlates of spectral changes. Neurology 42:1349-1354

Posse S, Tedeschi G, Risinger R, Ogg R, Le Bihan D (1995) High speed 1H spectroscopic imaging in human brain by echo planar spatial-spectral encoding. Magn Reson Med 33:34-40

Powers WJ, Grubb RL Jr, Darriet D, Raichle ME (1985) Cerebral blood flow and cerebral metabolic rate of oxygen requirements for cerebral function and viability in humans. J.Cereb.Blood Flow Metab 5:600-608

Provencher SW (1993) Estimation of metabolite concentrations from localized in vivo proton NMR spectra. Magn Reson Med 30:672-9

Sager TN, Laursen H, Hansen AJ (1995) Changes in N-acetyl-aspartate content during focal and global brain ischemia of the rat. J Cereb Blood Flow Metab 15:639-646

Sappey-Marinier D, Hubesch B, Matson GB, Weiner MW (1992) Decreased phosphorus metabolite concentrations and alkalosis in chronic cerebral infarction. Radiology 182:29-34

Stengel A, Neumann-Haefelin T, Singer OC, Neumann-Haefelin C, Zanella FE, Lanfermann H, Pilatus U (2004) Multiple spin-echo spectroscopic imaging for rapid quantitative assessment of N-acetylaspartate and lactate in acute stroke. Magn Reson Med 52:228-238

Takegami T, Ebisu T, Bito Y, Hirata S, Yamamoto Y, Tanaka C, Naruse S, Mineura K (2001) Mismatch between lactate and the apparent diffusion coefficient of water in progressive focal ischemia. NMR Biomed. 14:5-11

Wise RJ, Rhodes CG, Gibbs JM, Hatazawa J, Palmer T, Frackowiak RS, Jones T (1983) Disturbance of oxidative metabolism of glucose in recent human cerebral infarcts. Ann Neurol 14:627-637

Part 3:

MR Correlates of Stroke Syndromes

12 Transient Ischemic Attacks

Hakan Ay and Achim Gass

CONTENTS

12.1 Clinical Features and the Role of Imaging in Transient Ischemic Attacks

Transient ischemic attack (TIA) is a clinical syndrome characterized by focal neurological symptoms presumed to be of vascular origin that last less than 24 h. Despite the transient nature of symptoms, the cerebrovascular thread is not over yet following a TIA. The mechanism that has given rise to the transient spell may also cause more severe ischemic syndromes if not properly treated. About 10% of patients with TIA suffer from stroke within the ensuing 3 months, 50% of which occur within the first 2 days (Johnston et al. 2003). Accurate and prompt recognition of ischemia as the cause of neurological symptoms is imperative to prevent subsequent strokes. This is, however, a complicated task as the current clinical criteria used for diagnosis are subjective and lack specificity for an ischemic etiology.

The 24-h time limit, despite lack of any scientific foundation, has been introduced as the key criterion for diagnosis of TIA. The usual duration of symptoms is, in fact, less than 1 h; spells typically last for 5–10 min (Levy 1988). Unavoidably, only a small fraction of patients can be examined by physicians at the height of their signs and symptoms; the neurological examination is often normal when patients are available for medical attention. The diagnosis is usually based on historical information provided by the patient or other observers. This historical information, however, is not always reliable because patients with TIA may suffer from no or inaccurate recollection of their spells, may not fully name their neurological symptoms, or may be even unaware of their spell. The proof of "vascular origin" is often decided by the clinician's best judgment as to whether the pattern of signs and symptoms fit into a specific arterial territory. Given that TIA-like symptoms also occur due to a variety of neurological disorders such as migraine, seizures, brain tumors (see Table 12.1 for the complete list of TIA mimics), transient neurological symptoms confined to a vascular territory should not be considered as specific for any particular etiology.

The use of arbitrary clinical criteria for TIA leads to a serious diagnostic confusion among physicians; up to 62% of TIA referrals by general practitioners are in fact non-vascular events by neurologists (Martin et al. 1997). Conversely, general practitioners misdiagnose a TIA as non-ischemic transient event in about half of the patients (Ferro et al. 1996). The agreement between two neurologists for the diagnosis of TIA by history varies from 42% to 73% (Tomasello et al. 1982).

Neuroimaging offers a tremendous utility in the evaluation of patients with transient neurological symptoms. In contrast to the long-standing notion that TIAs are associated with rapid and complete resolution of brain ischemia before any permanent

H. Ay, MD
Department of Neurology, Stroke Service, Massachusetts General Hospital, Harvard Medical School, CNY149-2301, 13th Sreet, Boston, MA 02129, USA
A. Gass, MD
Depts. of Neurology/Neuroradiology, University Hospitals Mannheim and Basle, 68165 Mannheim, Germany; 4031 Basle Switzerland

Table 12.1. Conditions that may mimic transient ischemic attacks

Subdural hematoma[a]
Intracerebral hemorrhage[a]
Brain tumors[a]
Cervical disc disease[a]
Multiple sclerosis[a]
Cerebral venous thrombosis[a]
Seizures
Neuropsychiatric syndromes (conversion disorder, panic disorder)
Compression neuropathies
Vasovagal syncope
Migraine or migraine accompaniments
Labyrinthine disorders
Transient global amnesia
Hypoglycemia
Drugs
Electrolyte abnormalities
Cardiac arrhythmia

[a]Central nervous system pathology identified by MRI

tissue injury occurs, recent imaging data supports the concept that clinically transient events are not necessarily transient at the tissue level and are associated with cerebral infarction in some patients. The goals in imaging patients with transient neurological symptoms are two-fold (Fig. 12.1): (1) To uncover an obvious condition other than ischemia as the cause of the transient event such as brain tumor, subdural hematoma, intracerebral hematoma, etc. (2) To identify ischemia as the operative mechanism responsible for symptoms in patients with no other obvious cause. Neuroimaging has proven its value in accomplishing the first goal. Many structural brain lesions listed in Table 12.1 that can mimic TIA are successfully identified with the current imaging technology (Fig. 12.2). The role of imaging in achieving the second goal is equally important. The aim is to capture the "footprints" of a recent, more widespread but reversible ischemia that has occurred transiently at the time of symptom. Given that some TIAs may not leave any footprints while others leave so subtle footprints that can easily escape from detection by the current neuroimaging techniques, one should not expect a very high yield of imaging in the study of TIAs. Nonetheless, the information provided by imaging serves as a crucial piece in clinical decision-making that justifies the use of imaging in patients with TIA. The remaining part of the current chapter will focus on the use of brain imaging in capturing the footprints of transient ischemia.

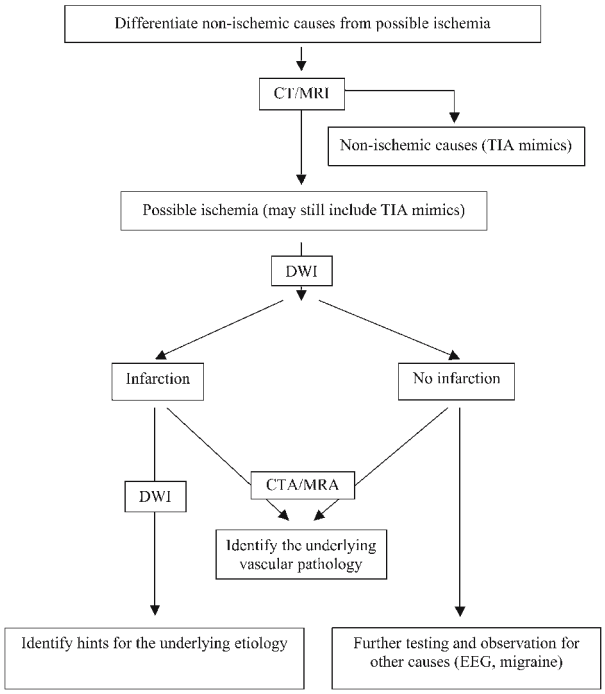

Fig. 12.1. An imaging algorithm for patients with the clinical syndrome of TIA. CT/MR angiography, CTA/MRA

12.2 CT and MRI to Identify TIA-Related Irreversible Brain Injury

Waxman and Toole (1983) first introduced the concept that the transient wave of ischemia that occurs during a TIA can leave footprints, small islands of permanent injury, on the brain. Their report of a patient with TIA who had an infarction on CT in a location consistent with symptoms has motivated the use of imaging to establish a link between such transient events and the ischemic pathophysiology. The past two decades have seen a number of imaging studies that consistently confirmed the presence of irreversible ischemic brain injury in victims of TIA. The infarction rate in these studies is variable, ranging from 4% to 77% with CT and conventional MRI (T1-, T2-, FLAIR-weighted images) (Awad et al. 1986; Bogousslavsky and Regli 1985; Douglas et al. 2003; Fazekas et al. 1996). A clinically-related infarction in these studies has traditionally been defined as being in the contralateral hemisphere or within a clinically expected arterial territory. This definition, however, remains short of establishing that the infarction and the TIA are in fact causally related in an individual patient. This is due to the fact that neither CT nor conventional MRI can reliably differentiate acute from chronic infarctions in patients with TIA since TIA-related infarctions are often very small. A volumetric analysis of TIA-related infarctions reveals that 96% of all infarc-

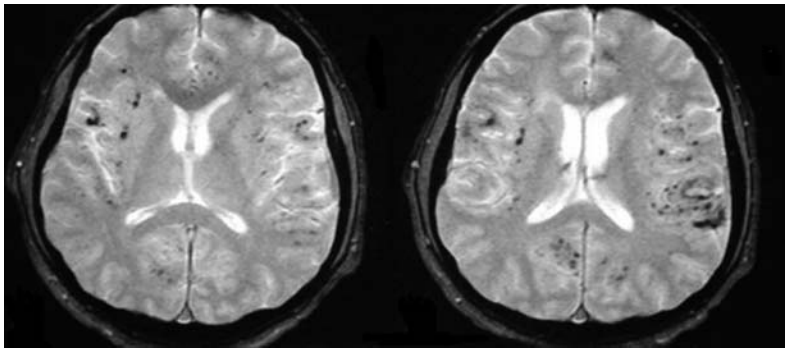

Fig. 12.2. MRI images of a 42 year-old man who presented with three stereotypic tingling spells in the right hand, each lasting for about 5–10 min, mimicking a TIA. Gradient-echo T2-weighted images [520/12.9 (TR/TE); flip angle, 30°], obtained through the level of lateral ventricles, show multiple millimetric hypointense foci of chronic hemorrhages, located in the cortical-subcortical region in both hemispheres. Pathologic examination of the biopsy material later showed severe destruction of leptomeningeal vessels with a mixed inflammatory cell infiltrate, consistent with the diagnosis of "primary angiitis of the CNS"

tions are smaller than 1 ml (Ay et al. 2004). Both acute and chronic infarctions of this size exhibit the same signal changes on CT and conventional MRI, do not demonstrate significant mass effect, and lack contrast enhancement. In addition, about one half of TIA patients harbor chronic multiple small silent infarctions that, in turn, further blurs confidence to call an infarction new and clinically-related to the TIA. As a result, conventional imaging techniques not only have the potential to misidentify a small chronic lesion as acute and clinically-related, but also pose a risk of missing TIA-related infarctions since they are extremely small.

DWI offers greater utility in identifying patients who have had ischemia as the cause of their transient neurological spell. The higher lesion to background contrast enables DWI to capture punctate infarctions (Gass et al. 2004; Gonzalez et al. 1999). Furthermore, DWI provides a unique opportunity to differentiate acute infarction from chronic lesions (Marks et al. 1996; Schlaug et al. 1997). This feature not only allows to age an infarction but also to temporally tie an imaging finding to the clinical transient event. Fueled by these advantages, DWI can identify infarctions related to the clinical symptoms in a subset of patients with TIA. To date, there are seven studies with DWI (Table 12.2) in TIAs that convincingly demonstrate that an acute infarction occurs during transient spells in about 50% of patients (range 21%-67%) (Ay et al. 2002; Bisschops et al. 2002; Crisostomo et al. 2003; Engelter et al. 1999; Kidwell et al. 1999; Rovira et al. 2002; Takayama et al. 2000).

12.3 Conventional MRI Versus DWI in Patients with TIA

The major drawback of conventional MRI in the study of patients with TIA is its limited sensitivity to detect as well as to age small infarctions. By comparing to DWI, it is possible to estimate the amount of error that could be imposed by the use of conventional MRI in patients with TIA. In a recent study (Ay et al. 2002), the examiners first reviewed T2-weighted images (T2w) with clinical information in hand and determined infarction(s) in the contra-lateral hemisphere to the symptoms or in the

Table 12.2. Studies of DWI in patients with TIA

Reference	Patient number	Number (%) with acute infarction on DWI	Number (%) with multiple acute infarctions on DWI	Mean time from symptom onset to MRI
Ay et al. (2002)	57	27 (47%)	11 (19%)	39 h
Bisschops et al. (2002)	44	21 (47%)	Not mentioned	< 72 h
Crisostomo et al. (2003)[a]	78	16 (21%)	Not mentioned	23 h
Engelter et al. (1999)	40	14 (35%)	5 (13%)	36.5 h
Kidwell et al. (1999)	42	20 (48%)	Not mentioned	17 h
Rovira et al. (2002)	58	39 (67%)	Not mentioned	5 days
Takayama et al. (2000)	19	7 (37%)	Not mentioned	Not mentioned

[a]This study underestimates the rate of infarction since some patients with infarction on DWI were called stroke and not included

arterial territory indicated by the symptoms (clinically appropriate lesion). The same procedure was repeated for FLAIR images in a blinded fashion with regard to DWI. Finally, diffusion-weighted images were rated in conjunction with T2w and FLAIR. T_2w missed the acute infarction on DWI in 42% and misidentified in 27% of the patients. Similarly, FLAIR images missed the acute infarction in 5% and misidentified in 32% of patients. Overall, conventional MRI misses or misidentifies the acute infarction on DWI in about one half of the patients with TIA. DWI should be the technique of choice for use in the evaluation of patients with TIA.

12.4 DWI Characteristics of TIA-Related Infarctions

1. TIA-related infarctions on DWI are often very small (Ay et al. 2002; Kidwell et al. 1999; Rovira et al. 2002). As mentioned before, 96% of infarctions on DWI are smaller than 1 ml in volume. The mean infarction load (total volume of all acute infarctions if there are multiple) on DWI has been reported to be 1.5±1.8 ml (Ay et al. 2005). An infarction load of less than 1.8 ml is associated with reversible clinical deficit within 24 h with 79% sensitivity and 78% specificity. Two other DWI studies have produced similar results. Ay et al. (2002) found that the infarction size was less than 15 mm in diameter in 85% of 27 TIA patients with infarction identified by DWI, of which 83% were punctate (< 5 mm). Rovira et al. (2002) estimated TIA-related infarctions range from 2 to 40 mm in diameter (mean, 15 mm). Figures 12.3 and 12.4 present examples of small hyperintense lesions on DWI that represent the remnants or "footprints" of a recent ischemia.
2. TIA-related infarctions do not occur, a priori, in silent parts of the brain. Acute infarctions in patients with TIA are distributed across a wide range of brain regions including brainstem, internal capsule, subcortical gray matter, cortex, and subcortical white matter (Ay et al. 2002; Kidwell et al. 1999). The volume of infarction, however, is not constant throughout the brain; it varies with respect to location. The volume that is associated with TIA is smallest for deep-brainstem penetrator infarctions, larger for isolated cortical infarctions, and the largest for those located in relatively silent brain regions (Ay et al. 2005).
3. TIA-related infarctions can be multiple. Estimates of multiple infarctions range from 13% to 19% of all TIAs (Ay et al. 2002, 2005; Engelter et al. 1999). DWI's ability to recognize the "plurality", and importantly, the bilaterality of small acute infarctions that are temporally related to each other and the symptoms, is important because multiple acute lesions on DWI are associated with an identifiable, and potentially modifiable stroke etiology in about 90% of the patients (Ay et al. 2002). In contrast, only about one third of TIA patients with normal DWI exhibit an identifiable stroke etiology. The presence of multiple small acute lesions within both hemispheres or both anterior and posterior circulation indicates a proximal source of embolism as the operative mechanism (such as cardiac or aortic embolism). A string of punctate DWI lesions in the internal watershed territories is often associated with low-flow state that results from severe stenosis or occlusion of proximal large arteries. Identification of multiple small infarctions on DWI serves as a powerful guide to institute the most appropriate algorithms for etiologic investigations as well as to determine the best means of preventive stroke care.
4. DWI lesions in patients with TIA represent permanent ischemic brain injury. Although it is possible that DWI changes can fully reverse with rapid reconstitution of the cerebral blood flow (usually within 6 h of symptom onset), either by means of early spontaneous reperfusion or pharmacological thrombolysis (Kidwell et al. 1999, 2000; Lo et al. 1994), it is often too late for such a reversal in patients with TIA; the mean time from symptom onset to MRI ranges from 17 h to 5 days in the DWI studies listed in Table 12.2, once again emphasizing that a timely evaluation in patients with TIA (during or soon after symptoms) is not quite possible due to delays in seeking medical attention.
5. The occurrence of infarction on DWI cannot be reliably predicted on the basis of symptom duration (Ay et al. 2005). Although, there are reports that suggest the presence of a relationship between symptom duration and probability of infarction on DWI, the association is not absolute (Crisostomo et al. 2003; Engelter et al. 1999; Kidwell et al. 1999; Rovira et al. 2002); a transient ischemia associated with symptoms lasting for as short as a few minutes can be associated with infarction whereas a spell lasting for as long as 20 h may not cause any signal changes on DWI. This is, in part, due to the fact that in addition to duration, sever-

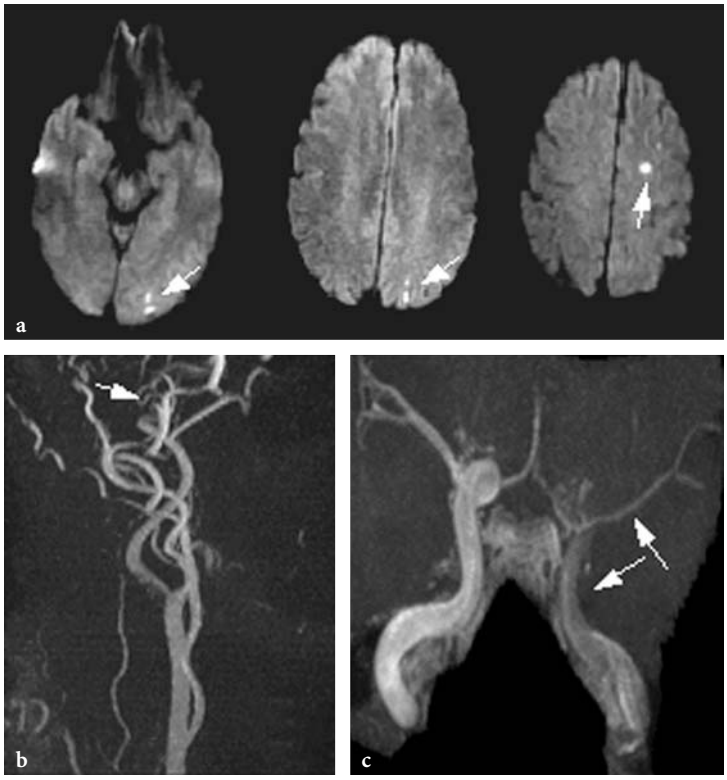

Fig. 12.3a-c. A 57-year-old man with right arm and leg weakness and right homonymous field defect for about 20 min. Diffusion weighted images (**a**) obtained 21 h after symptom onset demonstrate small acute infarctions in the left parieto-occipital region, the left parietal lobe, and the left frontal lobe (*arrows*). MR angiographic images through the neck (**b**) demonstrate signal loss in the left internal carotid artery at the skull base (*arrow*). This is associated with eccentric hyperintensity on T1-weighted images (not shown) consistent with a dissection. 3D time-of-flight imaging (**c**) demonstrates that there is compromise of the flow-related enhancement in the intracranial internal carotid artery as well as the left MCA branches (*arrow*). Further questioning revealed that the patient had been hit on the head by the bicycle rack of his car in the morning of admission

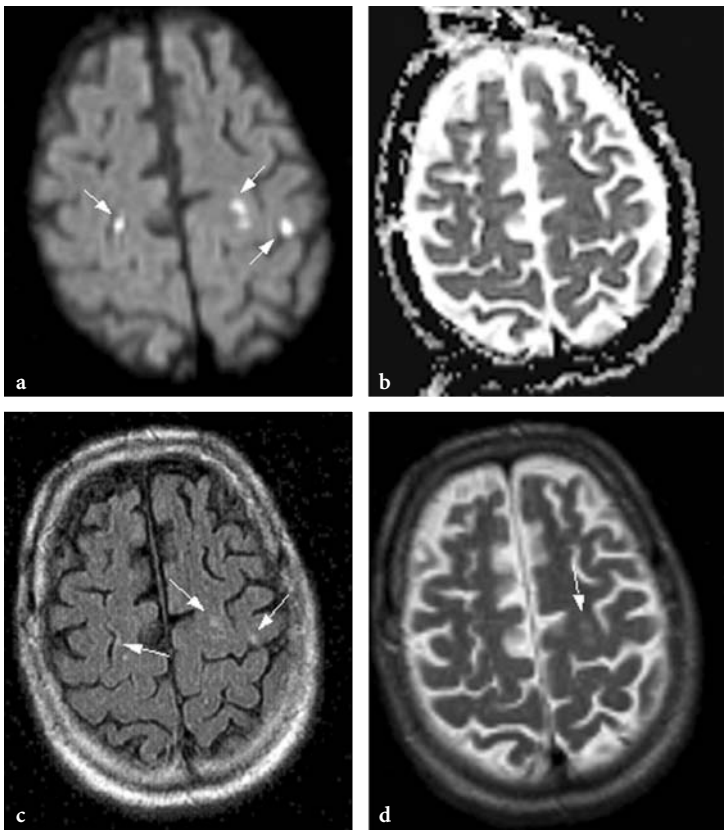

Fig. 12.4a-d. A 76-year-old man who presented with a transient episode of left lower extremity weakness lasting for 1 min. Diffusion weighted images (**a**) obtained 24 h after symptoms show several punctate foci of DWI bright areas in bilateral MCA territories (*arrows*). The volume of these small lesions ranges from 0.07 to 0.7 ml. These foci are difficult to distinguish on the ADC maps (**b**). Axial FLAIR images (**c**) demonstrate subtle hyperintensity in the regions hyperintense on DWI whereas only the lesion (*arrow*) not neighboring the cortical sulci is subtly distinguishable on T2-weighted images (**d**). Multiple embolism has been judged to be the mechanism as the patient had atrial fibrillation and was not on warfarin

ity of ischemia is also important in determining irreversible injury (Hossmann 1994; Kaplan et al. 1991) (see Chap. 4). Ischemia severe enough to cause symptoms but insufficient to cause irreversible tissue injury can result in long standing clinical deficit in the absence of any DWI abnormality (Ay et al. 1999). It is also possible that clinical symptoms can continue after the ischemia is corrected due to persistent failure in cortical synapses (Bolay and Dalkara 1998), further blurring the putative relationship between symptom duration and probability of infarction on DWI.

6. TIA-related infarctions on DWI can be predicted on the basis of certain clinical TIA features. Transient motor symptoms, preceding non-stereotypic attacks, the presence of an established cause of stroke, and presentation with aphasia are independent predictors of infarction on DWI (Ay et al. 2002; Crisostomo et al. 2003). In contrast, limb paresthesias, slurred speech, and brief attacks of dizziness or imbalance are not associated with occurrence of infarction. Of note, most symptoms that are not associated with infarction on DWI are based on patients' subjective feelings and sensations; in contrast to motor deficit or aphasia, it is not possible to objectively assess such symptoms and mark the brain as their origin. Of particular relevance to this point is that, according to a recent study, the independent predictors of infarction on DWI such as motor deficit and speech impairment are also independently associated with increased risk of stroke after TIA (Johnston et al. 2003), suggesting a potential role for DWI in the risk stratification for stroke following TIA.

12.5 Differential Diagnosis of Small Lesions on DWI in Patients with Transient Neurological Symptoms

In patients presenting with TIA-like symptoms (acute, focal, transient neurological deficits conforming to a specific vascular territory), a corresponding hyperintense lesion on DWI strongly favors the diagnosis of ischemia (Gonzalez et al. 1999). The great majority of such small hyperintense lesions on DWI is indeed due to arterial ischemia and can be easily identified for their vascular distribution in distal arterial territories or territorial borderzones. Hyperintensity on DWI and a reduced ADC have also been observed in a number of pathologies other than arterial ischemia including prolonged ictal activity (Wieshmann et al. 1997), venous thrombosis (Chu et al. 2001), multiple sclerosis (Tievsky et al. 1999), and phenylketonuria (Phillips et al. 2001). DWI hyperintense lesions in these pathologies tend to be much bigger, have a different shape and distribution and are frequently accompanied by chronic T2 lesions, which also provide circumstantial evidence for an underlying pathology other than ischemia. Non-ischemic lesions are frequently accompanied in their vicinity by signs of vasogenic edema (e.g., venous thrombosis, multiple sclerosis) different from the small well-defined lesions observed in arterial cerebral ischemia. Electroencephalography and further investigations are warranted in patients with transient symptoms and hyperintense lesion on DWI if clinical features are compatible with a seizure. In cases without informative clinical descriptions it must be kept in mind that hyperintense DWI lesions, even when accompanied by a reduced ADC, are highly suspicious of cerebral ischemia but not definite evidence.

12.6 Neuroimaging as a Marker of Subsequent Risk of Stroke Following TIA

Imaging promises for a potential use in identifying patients with TIA who harbor increased risk of subsequent stroke. Both in-hospital risk and short term (90-day) risk of stroke appears increased in the presence of acute infarction (Ay et al. 2002; Douglas et al. 2003). A retrospective review of 322 patients with TIA demonstrated that patients with TIA who had a new infarction on CT had increased risk of subsequent stroke (Douglas et al. 2003); 90-day risk of stroke was 38% and 10% in patients with or without a new infarction on CT, respectively. Using DWI, an earlier report of 57 patients described that the frequency of in-hospital stroke following TIA was 15% in patients with infarction (Ay et al. 2002). In contrast, no stroke was observed in patients with normal DWI. These data were further supported by a more recent study of 87 patients; the in-hospital recurrent stroke and TIA rate was 19.4% and 2.8% in patients with or without infarction on DWI (Ay et al. 2005). The only longitudinal study that provided long-term data included 83 patients with TIA (Purroy et al. 2004). The mean follow-up was 389 days. The combined stroke and TIA rate during this period was 29.6% and 14.3% in patients with or without infarction on DWI, respectively. The Kaplan-

Meier curves for event-free proportion continued to separate beyond 1 week suggesting that TIA with infarction conveys increased long-term risk of stroke as well. In conclusion, the current data support the concept that imaging might be used to identify TIA patients with high versus low risk of stroke.

12.7 Transient Ischemic Attacks with No Infarction on Imaging

Unlike TIA patients with infarction on DWI, it is not obvious that patients with normal DWI have suffered from ischemia as the cause of their transient symptoms. In these patients, TIA mimics should also be considered (see Chap. 19). However, an ischemic etiology for transient symptoms cannot be excluded by the lack of an associated hyperintense lesion on DWI. A short-lasting episode of ischemia without DWI changes, or with reversible DWI changes as demonstrated in animals (Minematsu et al. 1992; Mintorovitch et al. 1991), might have occurred at the time of symptoms. In addition, DWI may occasionally miss very small infarctions, especially in the brainstem location (Ay et al. 1999; Kuker et al. 2002; Lövblad et al. 1998). This is most likely due to susceptibility artifacts induced by surrounding bones at the skull base. New multi-array head coil systems and parallel imaging techniques promise to overcome this limitation and improve the detection rate of small infarctions in the brainstem.

12.8 Summary

Transient neurological syndrome, characterized by brief alterations in neurological functioning, is a serious public health problem occurring in about 4% of individuals over age 55 (Bots et al. 1997). Among many causes of transient neurological symptoms, TIA is presumably the leading one accounting for about one half of the cases (Bots et al. 1997). Approximately 300,000 people suffer from TIA annually in the US (Ovbiagele et al. 2003). However, these estimates are approximate as it is inherently impossible to be certain about ischemia as the cause of transient neurological symptoms in the absence of any gold standard. MRI offers tremendous utility in this regard. Fueled by the high lesion to background signal ratio, DWI detects small hyperintense lesions in approximately half of the patients with the clinical syndrome of TIA. Such hyperintense lesions indicate acute infarctions that occurred coincident with, or closely linked in time, to the TIA. This causal feature helps physicians more confidently establish the diagnosis of TIA in patients with transient neurological symptoms. Moreover, DWI is unique in its ability to demonstrate that multiple lesions are in fact linked temporally with each other and the TIA. The presence of acute infarctions in both hemispheres and in both anterior and posterior circulations indicates a proximal source of embolism. The knowledge of mechanism that engenders TIA helps to promptly introduce the most effective preventive stroke care. The future promises to yield an additional use for MRI in the risk stratification for subsequent stroke in patients with TIA.

References

Awad I, Modic M, Little JR et al (1986) Focal parenchymal lesions in transient ischemic attacks: correlation of computed tomography and magnetic resonance imaging. Stroke 17:399-403

Ay H, Buonanno FS, Rordorf G et al (1999) Normal diffusion-weighted MRI during stroke-like deficits. Neurology 52:1784-1792

Ay H, Oliveira-Filho J, Buonanno FS et al (2002) "Footprints" of transient ischemic attacks: a diffusion-weighted MRI study. Cerebrovasc Dis 14:177-186

Ay H, Koroshetz WJ, Benner T, Vangel MG, Wu O, Schwamm LH, Sorensen AG (2005)Transient ischemic attack with infarction: a unique syndrome? Ann Neurol 57:679-686.

Bisschops RH, Kappelle LJ, Mali WP, van der Grond J (2002) Hemodynamic and metabolic changes in transient ischemic attack patients: a magnetic resonance angiography and (1)H-magnetic resonance spectroscopy study performed within 3 days of onset of a transient ischemic attack. Stroke 33:110-115

Bogousslavsky J, Regli F (1985) Cerebral infarct in apparent transient ischemic attack. Neurology 35:1501-1503

Bolay H, Dalkara T (1998) Mechanisms of motor dysfunction after transient MCA occlusion: persistent transmission failure in cortical synapses is a major determinant. Stroke 29:1988-1993

Bots ML, van der Wilk EC, Koudstaal PJ, Hofman A, Grobbee DE (1997) Transient neurological attacks in the general population. Prevalence, risk factors, and clinical relevance. Stroke 28:768-773

Chu K, Kang DW, Yoon BW, Roh JK (2001) Diffusion-weighted magnetic resonance in cerebral venous thrombosis. Arch Neurol 58:1569-1576

Crisostomo RA, Garcia MM, Tong DC (2003) Detection of diffusion-weighted MRI abnormalities in patients with transient ischemic attack: correlation with clinical characteristics. Stroke 34:932-937

Douglas VC, Johnston CM, Elkins J, Sidney S, Gress DR, Johnston SC (2003) Head computed tomography findings predict short term stroke risk after transient ischemic attack. Stroke 34:2894-2899

Engelter ST, Provenzale JM, Petrella JR, Alberts MJ (1999) Diffusion MR imaging and transient ischemic attacks. Stroke 30:2762-2763

Fazekas F, Fazekas G, Schmidt R, Kapeller P, Offenbacher H (1996) Magnetic resonance imaging correlates of transient cerebral ischemic attacks. Stroke 27:607-611

Ferro JM, Falcao I, Rodrigues G et al (1996) Diagnosis of transient ischemic attack by the nonneurologist. A validation study. Stroke 27:2225-2229

Gass A, Ay H, Szabo K, Koroshetz WJ (2004) Diffusion weighted MRI for the small stuff: the details of acute cerebral ischaemia. Lancet Neurology 3:39-45

Gonzalez RG, Schaefer PW, Buonanno FS et al (1999) Diffusion-weighted MR imaging: diagnostic accuracy in patients imaged within 6 hours of stroke symptom onset. Radiology 210:155-162

Hossmann K (1994) Viability thresholds and the penumbra of focal ischemia. Ann Neurol 36:557-565

Johnston SC, Sidney S, Bernstein AL, Gress DR (2003) A comparison of risk factors for recurrent TIA and stroke in patients diagnosed with TIA. Neurology 60:280-285

Kaplan B, Brint S, Tanabe J, Jacewicz M, Wang XJ, Pulsinelli W (1991) Temporal thresholds for neocortical infarction in rats subjected to reversible focal ischemia. Stroke 22:1032-1039

Kidwell CS, Alger JR, Di Salle F et al (1999) Diffusion MRI in patients with transient ischemic attacks. Stroke 30:1174-80

Kidwell CS, Saver JL, Mattiello J et al (2000) Thrombolytic reversal of acute human cerebral ischemic injury shown by diffusion/perfusion magnetic resonance imaging. Ann Neurol 47:462-469

Kuker W, Weise J, Krapf H, Schmidt F, Friese S, Bahr M (2002) MRI characteristics of acute and subacute brainstem and thalamic infarctions: value of T2- and diffusion-weighted sequences. J Neurol 249:33-42

Levy DE (1988) How transient are transient ischemic attacks? Neurology 38:674-677

Lo EH, Matsumoto K, Pierce AR, Garrido L, Luttinger D (1994) Pharmacologic reversal of acute changes in diffusion-weighted magnetic resonance imaging in focal cerebral ischemia. J Cereb Blood Flow Metab 14:597-603

Lövblad KO, Laubach HJ, Baird AE et al (1998) Clinical experience with diffusion-weighted MR in patients with acute stroke. Am J Neuroradiol 19:1061-1066

Marks MP, de Crespigny A, Lentz D, Enzmann DR, Albers GW, Moseley ME (1996) Acute and chronic stroke: navigated spin-echo diffusion-weighted MR imaging. Radiology 199:403-408

Martin PJ, Young G, Enevoldson TP, Humphrey PR (1997) Overdiagnosis of TIA and minor stroke: experience in a regional neurovascular clinic. QJM 90:759-763

Minematsu K, Li L, Sotak CH, Davis MA, Fisher M (1992) Reversible focal ischemic injury demonstrated by diffusion-weighted magnetic resonance imaging in rats. Stroke 23:1304-1311

Mintorovitch J, Moseley ME, Chileuitt L, Shimizu H, Cohen Y, Weinstein PR (1991) Comparison of diffusion and T2-weighted MRI for the early detection of cerebral ischemia and reperfusion in rats. Magn Reson Med 18:39-50

Ovbiagele B, Kidwell CS, Saver JL (2003) Epidemiological impact in the United States of a tissue-based definition of transient ischemic attack. Stroke 34:919-924

Phillips MD, McGraw P, Lowe MJ, Mathews VP, Hainline BE (2001) Diffusion-weighted imaging of white matter abnormalities in patients with phenylketonuria. Am J Neuroradiol 22:1583-1586

Purroy F, Montaner J, Rovira A et al (2004) Higher risk of further vascular events among transient ischemic attack patients with diffusion-weighted imaging acute ischemic lesions. Stroke 35:2313-2319.

Righini A, Pierpaoli C, Alger JR, Di Chiro G (1994) Brain parenchyma apparent diffusion coefficient alterations associated with experimental complex partial status epilepticus. Magn Reson Imaging 12:865-871

Rovira A, Rovira-Gols A, Pedraza S, Grive E, Molina C, Alvarez-Sabin J (2002) Diffusion-weighted MR imaging in the acute phase of transient ischemic attacks. Am J Neuroradiol 23:77-83

Schlaug G, Siewert B, Benfield A, Edelman RR, Warach S (1997) Time course of the apparent diffusion coefficient (ADC) abnormality in human stroke. Neurology 49:113-119

Takayama H, Mihara B, Kobayashi M et al (2000) Usefulness of diffusion-weighted MRI in the diagnosis of transient ischemic attacks. No To Shinkei 52:919-923

Tievsky AL, Ptak T, Farkas J (1999) Investigation of apparent diffusion coefficient and diffusion tensor anisotrophy in acute and chronic multiple sclerosis lesions. AJNR Am J Neuroradiol 20:1491-1499

Tomasello F, Mariani F, Fieschi C et al (1982) Assessment of interobserver differences in the Italian Study on Reversible Cerebral Ischemia. Stroke 13:32-35

Waxman SG, Toole JF (1983) Temporal profile resembling TIA in the setting of cerebral infarction. Stroke 14:433-437

Wieshmann UC, Symms MR, Shorvon SD (1997) Diffusion changes in status epilepticus. Lancet 350:493-494

13 Microangiopathic Disease and Lacunar Stroke

Achim Gass and Hakan Ay

CONTENTS

13.1 Introduction

Cerebral microangiopathic disease – also termed small-vessel or white-matter disease, leukoaraiosis and subcortical vascular encephalopathy (SVE) – refers to lesions predominantly involving the cerebral white matter, basal ganglia, and the brainstem – as opposed to diseases also or exclusively affecting the cerebral cortex. The magnetic resonance imaging (MRI) correlates of microangiopathic disease are subcortical lesions with increased signal on T_2-weighted MRI sequences of the brain believed to be of ischemic origin and lacunar lesions caused by single perforating artery occlusion. Previously, leukoaraiosis has been a popular term to describe the CT correlate of such morphological changes. White matter lesions are of great interest for various research areas including the normal aging process, the detection of clinically silent or covert morphological changes, the differentiation of specific subgroups of vascular dementing syndromes (e.g., CADASIL, cerebral amyloid angiopathy, mixed cortical and subcortical dementias) and the relationship of white matter lesions to clinical phenomena in the highly prevalent subcortical vascular encephalopathy syndrome characterized by short term memory complaints and gait abnormality. Microangiopathic lesions are also found in up to 70% of individuals with vascular dementia and Alzheimer's disease and can occur in a large variety of clinical entities. Recently, mild cognitive impairment has attracted a lot of attention as it appears to define an early stage of cognitive decline in the continuum from normal cognitive functioning to overt dementia. In a similar fashion larger studies are on the way exploring the importance of white matter lesions, along with other morphological markers as potential prognostic markers of subclinical disease. However, given the high prevalence of white matter lesions in normal functioning elderly individuals their significance has also been compared as an equivalent to the "grey hair" occurring commonly with age. This chapter gives an overview of occurrence and pathophysiological concepts of white matter lesions with regard to MRI features.

A. Gass, MD
Depts. of Neurology/Neuroradiology, University Hospitals Mannheim and Basle, 68165 Mannheim, Germany; 4031 Basle, Switzerland
H. Ay, MD
Department of Neurology, Stroke Service, Massachusetts General Hospital, Harvard Medical School, CNY149-2301, 13th Street, Boston MA 02129, USA

13.2 Microangiopathic Disease

13.2.1 Incidence, Risk Factors, Pathology, Pathophysiology

White matter lesions have been already quite extensively studied with CT and the patchy or diffuse abnormalities in the deep white matter, which

show low density on CT have been termed "leukoaraiosis" (araiosis = rarefaction) (Hachinski et al. 1987). On MRI such changes can be identified with even higher sensitivity presenting as high intensity lesions on T2-weighted sequences. These abnormalities are seen characteristically in the periventricular regions, especially around the horns of the lateral ventricles, and in the centrum semiovale. Although not yet proven in larger studies, one may assume a continuity between an older person with just a few scattered white matter lesions and no clinical symptoms and a severely demented and neurologically disabled patient with a thick periventricular rim of abnormal white matter with some small lacunar infarctions in the centrum semiovale.

According to several population-based studies, the prevalence of cerebral white-matter hyperintensities on MRI in elderly people is in the range of 62%-95% (Breteler et al. 1994; Liao et al. 1997). In the Cardiovascular Health Study only 4.4% of 3301 participants did not have white matter lesions; about 20% had extensive lesions associated with impaired cognitive and lower extremity function (Longstreth et al. 1996). Increasing age is a potent risk factor for white matter lesions, suggesting that the phenomenon is acquired during the aging process (Pantoni and Garcia 1997; DeCarli et al. 1999; Wiszniewska et al. 2000; Breteler et al. 1994; Awad et al. 1986; Liao et al. 1997). Besides age, a history of cardiovascular disease and hypertension have been the most consistent risk factors across most studies; associations are less consistently demonstrated for other risk factors such as diabetes, serum glucose levels, hyperhomocysteinaemia, and smoking (de Leeuw et al. 1999; Liao et al. 1996; Vermeer et al. 2003). In one study, a history of hypertension was present in two-thirds of demented patients with leukoaraiosis compared with half that number in patients without leukoaraiosis (Inzitari 1987). However, hypotension, orthostatic hypotension, and labile hypertension have also been found to be significantly associated with the presence of white matter lesions on MRI and the impact of lowering the blood pressure in hypertensive patients needs to be further explored (van Dijk et al. 2004) (see also Chap. 9).

Histopathological features of white matter lesions include: diffuse myelin pallor (sparing the U-fibers, that are supplied by cortical branches), astrocytic gliosis, widening of perivascular spaces, and loss of oligodendrocytes leading to rarefaction, spongiosis, as well as loss of myelin and axons without definite necrosis, which has also been described as incomplete white matter infarction, which may finally cumulate in white matter necrosis (Erkinjutti et al. 1996; Pantoni and Garcia 1997; Révész et al. 1989). The mechanisms leading to these changes again may be complex: It is believed that critical stenosis and hypoperfusion of multiple medullary arterioles causes widespread incomplete infarction of deep white matter. An increasing size of the ventricles and altered CSF pressure states, as well as reduction of autoregulation may further contribute to the development of lesions in predilections sites (Fazekas et al. 1998). In contrast to grey matter the white matter has lower metabolic demand and lower tissue perfusion. It is less vulnerable to ischemia but also less well capillarized predisposing it to low perfusion damage. Pure incomplete white matter infarction – similar to that observed in the penumbra of large infarcts – is typically seen in hypoperfusion state (Roman et al. 1987; Englund 2002). Changes in the cerebral microvasculature occurring with age include lengthening, tortuosity, and lumen reduction due to arteriolosclerosis; histologically defined as concentric lamellar collagen fibres and fibrohyaline substance, especially in hypertensive individuals (Furuta et al. 1991; Ravens 1978). The cause of such findings is unknown – beginning in the fourth decade of life and increasing with age, they are most prominent in the frontal lobe, followed by changes in the parietal, occipital and temporal lobes (Furuta et al. 1991).

Another frequent morphological finding in patients with microangiopathic white matter lesions are small well defined infarcts in the course of small penetrating arteries, that on autopsy have been identified by Fisher and were described as "lacunar lesions" indicating the severe ischemic focal tissue injury in contrast to more diffuse and less severe tissue damage in the typical periventricular lesions. In many patients both can be seen, which is not surprising given that a large proportion shares a common origin. Lacunar lesions are part of this chapter and are discussed later. Furthermore, the combination of small and large vessel disease in the same patient is also common. The pathophysiological mechanisms are summarized in Table 13.1.

13.2.2 Symptomatology in Microangiopathic Disease

The clinical features of microangiopathic disease are increasingly better understood. This increase in knowledge on characteristic clinical types of cognitive worsening and their morphological correlates starts to improve the early identification of affected

Table 13.1. Subcortical ischemic vascular dementia. [Reprinted with permission from Roman et al. (2002)]

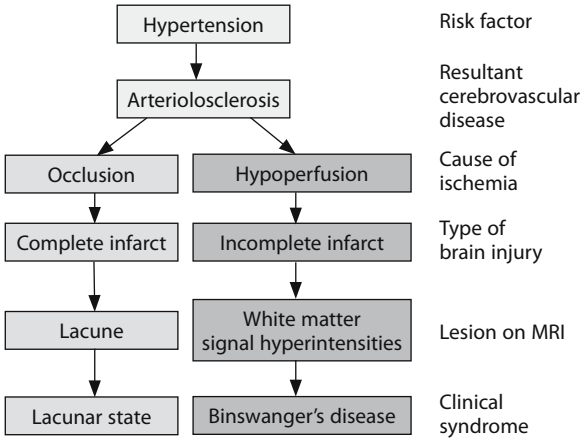

individuals and to guide and improve patient management. To date, therapies are only partially effective and improved treatment approaches are urgently needed. The hallmark of subcortical, predominantly white matter damage and basal ganglia disconnection are psychomotor slowing, possibly due to white matter damage sharing similarities with MS and other white matter pathologies. Loss of executive function, short term memory disturbances, and motor apraxia with a small-stepped gait are the common manifestation of subcortical vascular encephalopathy caused by microangiopathic white matter disease. Changes in affect, emotional lability, and urge incontinence are regularly seen (Roman and Royall 1999). As one would expect in focally accentuated tissue damage, focal neurological signs are regularly found including dysarthria, pseudobulbar palsy, grasp reflex, and pyramidal signs. To a large part symptoms are believed to be caused by interruption of prefrontal subcortical circuits (Ishii et al. 1986; Wolfe et al. 1990). These circuits are known to be involved in the executive control of working memory, organization, language, mood, regulation of attention, constructional skills, motivation and socially responsive behaviors (Alexander et al. 1986; Tekin and Cummings 2002; Mega and Cummings 1994). A population-based study of executive dysfunction in elderly people found a prevalence of mild impairment in about a third (33.7%) and moderate to severe deficits in 16.4% over the age of 60. Increasing levels of impairment of executive functioning were associated with lower education and advancing age. Besides a thorough neurological and psychiatric examination of these patients, special emphasis is usually put on the evaluation of gait and falls, timed-walk, timed finger-tapping, and frontal bladder control (urge incontinence and nocturia) to assess the functional status. Relatives and carers may report behavioral changes, but a detailed neuropsychological testing may be advisable to differentiate subcortical and/or cortical functional compromise and as a means for follow-up to monitor disease progression.

13.2.3 MRI in the Characterization of Cerebral Microangiopathy

White matter lesions are mainly seen as bilateral relatively symmetrical areas of T_2 hyperintensity in the periventricular or deep subcortical white matter and the pons on conventional T_2-weighted images and more easily outlined on FLAIR images. There is a continuum of morphological changes seen on MRI ranging from small punctate white matter lesions in the deep white matter to larger areas predominantly respecting a little distance to the posterior horns of the lateral ventricles. This is most likely an early phase and a mild form of a continuum of gradual increase in severity of tissue destruction. In these early phases, T_2 lesions show only little hypointensity on corresponding T_1-weighted images, again indicating that the severity of tissue changes is relatively mild at this point (Gass et al. 1998). Later on confluent lesions in the periventricular areas of the anterior and posterior horns of the lateral ventricles and in the deep white matter and in the centrum semiovale are seen (Fazekas et al. 1998). White matter atrophy is associated with more extensive white matter involvement. Indicators of subcortical tissue loss are enlargement of the lateral ventricles, loss of the normal anatomical shape and thinning of the corpus callosum, and enlargement and loss of the normal narrow appearance of the 3rd ventricle. It is important to differentiate the areas of predominant involvement and find indications for subcortical vs cortical or mixed forms of tissue changes, which are frequently seen once the subcortical damage has progressed. The improved knowledge on the clinical manifestations and the pathophysiological features of subcortical microangiopathic disease feed nicely back into a meaningful interpretation of morphological changes. Again only detailed information on the clinical status and inclusion of this information in all considerations of the MRI analysis will provide important hints as to the concordance or discordance of MRI findings, the clinical syndrome, and the clinical diagnosis and differential diagnostic considerations.

Differentiation of microangiopathic disease from territorial stroke is usually not difficult on FLAIR images (but may be rather more difficult on CT) due to the cortical involvement and the recognition of the shape of a vascular territory of a leptomeningeal arterial branch. Some atrophic reaction is often present in the vicinity of the infarction, which can be appreciated as ventricular enlargement or sulcal widening associated with the location of the chronic lesion. In territorial stroke, an obvious asymmetry in the hemispheric involvement should raise the suspicion of other macroangiopathic mechanisms even if no cortical territorial lesions are present. Proximal stenosis may give rise to lesions in subcortical hemodynamic risk zones very much overlapping with predilection sites of microangiopathy in the deep white matter (see Chap. 15). Embolic disease from proximal sources (cardiac, ascending aorta) is a frequent cause of cerebral ischemia in the elderly and overlapping mechanisms and comorbidity with microangiopathy is commonly seen in patients with acute ischemic symptoms. Diffusion-weighted MRI (DWI) is a most important modality in this regard. The ability to detect even very small lesions and to infer ischemic mechanisms from certain acute lesion patterns helps to detect uncommon features of microangiopathy and to distinguish different mechanisms of lesion development. This may well have important implications for patient management and treatment considerations.

For the purpose of rating the severity, for clinical or scientific purposes several rating scales have been suggested for MRI white matter changes (Scheltens et al. 1998). The Fazekas visual rating scale is simple, fast and reliable, and has been widely adopted as a means to describe the severity of morphological changes (Fazekas et al. 1998) (Fig. 13.1). Depending on the scientific question that needs to be answered (e.g., change in lesion volume), volumetric assessments may be preferable over visual rating scale, but descriptive scales may well suffice in many situations.

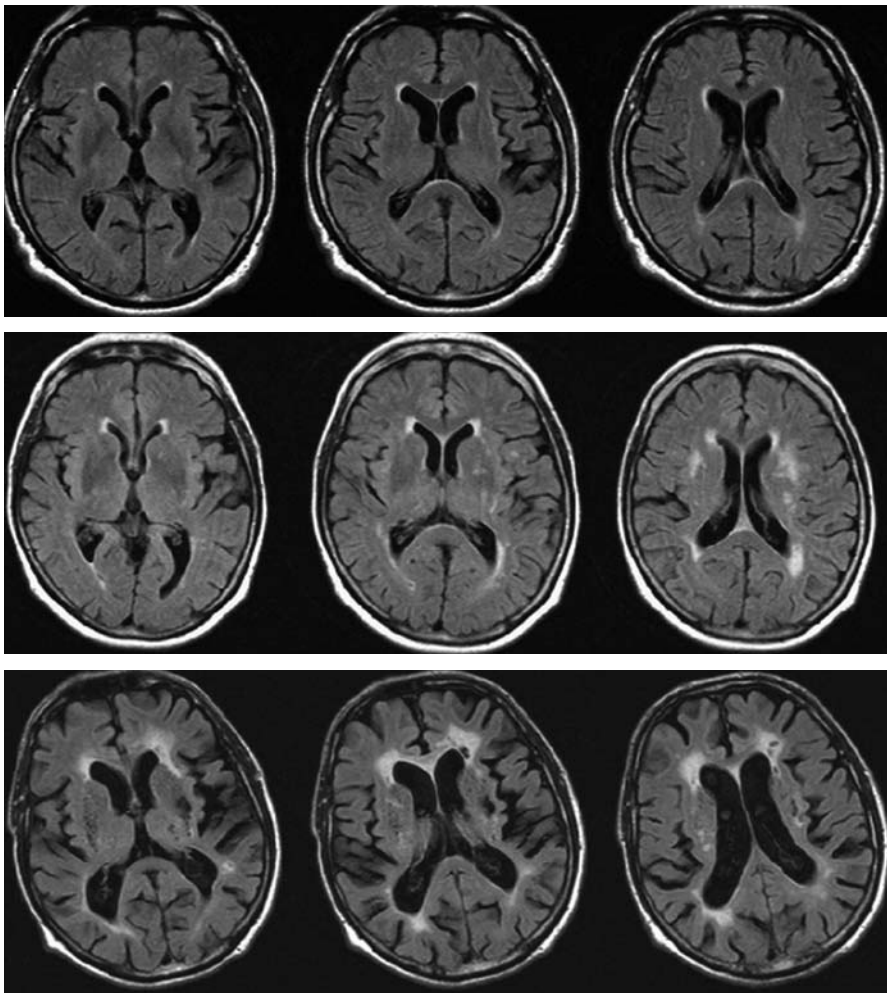

Fig. 13.1. Transverse FLAIR images demonstrating different degrees of characteristic microangiopathic subcortical lesions (and ventricular widening). In the *top row* a patient with grade 1 abnormalities consisting of punctate lesions is shown, the *center row* shows grade 2 abnormalities with earlier confluent lesions, while grade 3 with confluent lesions is shown in the *bottom row* (Fazekas et al. 1993)

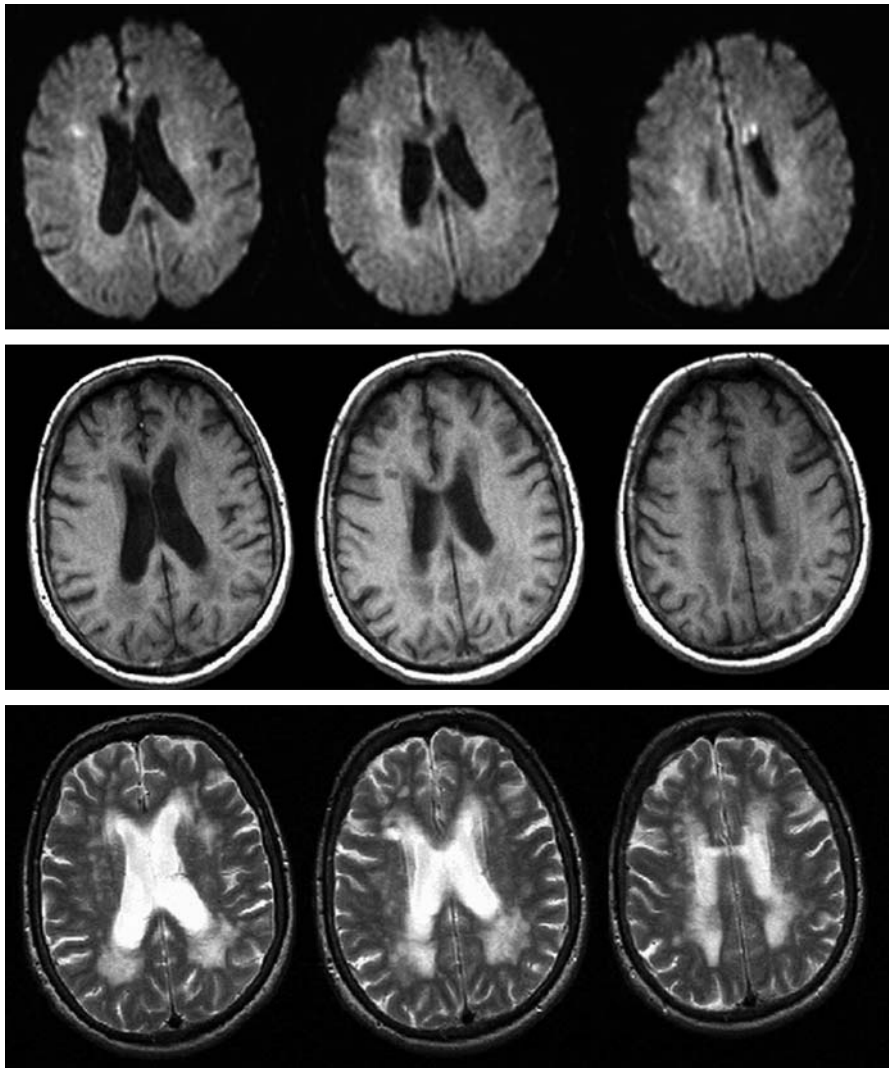

Fig. 13.2. Transverse diffusion weighted, T1-weighted, and T2-weighted images demonstrating different signal characteristics of subcortical lesions. Some T2 shine-through effects, probably from more recent tissue abnormality is seen on diffusion weighted images (*top row*), while different severities of T1 hypointensity are seen on T1-weighted images (*center row*), T2-weighted images provide high contrast between normal appearing tissue and lesions (*bottom row*)

13.3 Lacunar Stroke

13.3.1 Incidence, Risk Factors, Pathology, Pathophysiology

Lacunar infarctions represent 20%–25% of all strokes (Bamford et al. 1987; Bogousslavsky et al. 1988; Petty et al. 2000). They are usually single small infarcts (< 15 mm diameter) located subcortically in the basal ganglia, thalamus, internal capsule, corona radiata, and the brainstem. They are frequently the result of occlusion of a single perforating artery whose diameter ranges from 40 to 900 μm. Acute lesions on DWI often have a lengthy shape along the course of penetrators (Donnan et al. 2002; Lie et al. 2004). Fisher (1982) described two types of arterial pathology as a cause of lacunar infarctions: intracranial atherosclerosis and segmental lipohyalinosis secondary to the effects of hypertension. On occasion, an atheroma in the parent vessel or transient occlusion of the large arteries by a thrombus may block the origin of a penetrator giving rise to a lacunar infarction. It has also been suggested that a small embolus may lodge into a penetrating artery and results in a lacunar infarction (Fisher 1979). Lacunar infarcts and microangiopathic disease – which has a distinct pathology – commonly coincide in patients with vascular risk factors. Risk factors for lacunar stroke include age, gender, hypertension, diabetes, smoking, previous TIA, and possibly ischemic heart disease (You et al. 1995; Lodder and Boiten 1993).

13.3.2 Clinical Features of Lacunar Syndromes

While physicians may not recognize up to 80% of lacunes (Tuszynski et al. 1989), several clinical syndromes have been correlated with relevant lacunes detected at subsequent autopsy. Five of these are regarded as the classic lacunar syndromes: pure motor hemiparesis, sensorimotor stroke, pure sensory hemiparesis, dysarthria clumsy hand syndrome, and ataxic hemiparesis (Donnan et al. 2002; Fisher 1982; Bamford 2001). Pure motor stroke is the commonest lacunar syndrome in clinical practice, while pure sensory stroke is encountered less frequently. The involvement of the face, arm and leg of one side is the characteristic feature of the first three syndromes while reductions of consciousness, cognitive or visual field defects are absent. Even though lacunar infarcts have been linked to lacunar syndromes, the latter are of course not specific for this stroke subtype and mimicked by cortical infarcts, intracerebral hematomas, and non-vascular causes (Bogousslavsky et al. 1988; Bamford 2001).

13.3.3 MRI in the Diagnosis of Lacunar Lesions

Lacunar stroke lesions are characteristically small and usually lack extensive edema and subsequent mass effect. It should be noted that the size of lacunar infarction might be larger than the customarily accepted limit of 15 mm on acute imaging. This is because the conventional 15 mm limit was defined when lacunes were measured at the time of brain autopsy (Fisher 1965). Data from studies with serial imaging of lacunar infarctions show that infarct volumes shrink from acute to chronic phases of stroke by about 50% (Donnan et al. 1982; Lindgren et al. 2000). Assuming that penetrating artery infarctions are spherical in shape (though they are often comma shaped), a 15 mm lesion at chronic time point refers to an acute diameter of about 20 mm. Supporting this, a number of studies using MRI report that the volume of lacunar infarction could be as large as 4 ml during the acute period (Hommel et al. 1990; Kang et al. 2003), again referring to a diameter of about 20 mm. It is also our experience, along with others, to observe acute infarctions up to 20 mm in largest diameter on DWI within the territory of penetrating arteries in the absence of any mechanism other than small artery disease (Kang et al. 2003; Gerraty et al. 2002).

In the chronic stage, lacunar lesions show low signal, isointense to CSF on T_1-weighted, proton density-weighted and FLAIR images. Sometimes the separation from enlarged Virchow-Robin spaces can be difficult. In the acute phase, CT or MRI reveals no adequate lesion in up to 50% of patients (Donnan et al. 1982; Lindgren et al. 1994). Conventional MRI may not reliably identify the acute lacunar infarction related to the clinical symptoms because most patients with lacunar infarctions have chronic white matter lesions whose signal characteristics do not differ from acute lesions on conventional MRI (Arboix et al. 1990).

DWI with its ability to identify even small lesions and to provide temporal information in regard to the differentiation of acute and chronic lesions has been shown to be a valuable tool in the evaluation of patients with lacunar symptoms: By using the clinical criteria for subcortical infarctions, Singer and coworkers (1998) studied 39 patients with an acute syndrome. DWI obtained with a mean delay of 2 days revealed an infarction in the clinically appropriate brain regions of 37 patients. The sensitivity was calculated as 94.9% and specificity 94.1%. A recent study by Kuker and coworkers (2002) showed that DWI identified a clinically appropriate infarction in all of their 45 patients with signs and symptoms suggestive of infratentorial and thalamic infarction. However, DWI was negative in three patients scanned within the first 5 h of symptom onset, in whom a definite diagnosis could be reached by follow-up imaging. Medullar lesions revealed poor visibility compared to pons, midbrain, and thalamic lesions. This study along with other patient reports show that some caution should be exercised in interpreting negative DWI images obtained in the hyperacute phase in patients with symptoms highly suggestive of a brainstem location, especially the medulla oblongata (Lövblad et al. 1998; Ay et al. 1999).

To determine the benefit of adding DWI in the evaluation of lacunar infarctions, Oliveira-Filho and coworkers (2000) analyzed conventional MRI findings in 67 patients with DWI-proven lacunar infarction. The examiners were provided with clinical information, but unaware of the DWI findings and rated first T_2-, then FLAIR-weighted images for the presence of a clinically appropriate lacunar infarction. There was no lesion attributable to the symptoms in 9% of patients on each T_2- or FLAIR-weighted images. A lesion on T_2- and FLAIR-weighted images judged to be clinically appropriate did not overlap with the DWI lesion in an additional

13% and 16% of patients, respectively; the lesions on conventional MRI were indeed not acute and therefore not related to the clinical event. Overall, both T_2- and FLAIR-weighted images either missed or misidentified an acute lacunar infarction in about one quarter of the patients. A more recent study by Yonemura and coworkers (2002) showed that conventional MRI failed to identify the acute infarction on DWI in 13% of patients with a lacunar infarction due to occlusion of the perforators of the middle cerebral artery. Mean time to MRI was considerably longer in this study than in the previous study (5.8 days versus 50 h) indicating that the diagnostic performance of conventional MRI is largely dependent on the time of scanning. These findings establish that DWI is more reliable in accurately localizing the clinically relevant lesions, also improving clinical-anatomic correlations. One example for this is the capsular warning syndrome, a clinically distinct entity characterized by a cluster of repetitive, stereotypic, and typically short lasting lacunar spells. Standard imaging techniques have identified only internal capsule lesions in this entity (Donnan 1993). However, recent experiences with DWI show that a brainstem location can cause the same syndrome (Oliveira-Filho et al. 2001; Benito-Leon et al. 2001).

With the use of DWI, small acute lesions lying in different vascular territories in addition to lacunar infarction provides evidence for the possibility of an embolic mechanism in a subset of classic lacunar syndromes (Gerraty et al. 2002; Ay et al. 1999). This was systematically studied with DWI in 62 consecutive patients who presented with a classic lacunar syndrome (Ay et al. 1999). DWI showed subsidiary acute lesion(s) in addition to the index lacunar lesion in ten patients (16%). The additional lesions were punctuate and lay within the leptomeningeal arterial territories in the majority. Patients with subsidiary infarction(s) more frequently harbored an embolic cause of stroke. This finding is critical because underlying embolic cause may give rise to recurrent strokes with more extensive brain injury. Identification of subsidiary infarctions on DWI should have an impact in prompting the physician to introduce the best effective treatment for secondary stroke prevention in a patient with lacunar infarction.

DWI promises to have tremendous value in accurately localizing the subcortical or brainstem lesion(s). A summary of studies of DWI in patients with lacunar stroke is provided in Table 13.2. It is noteworthy that there is also a group of patients with lacunar infarction who harbor multiple chronic white matter lesions on the conventional MRI and present with non-specific syndromes that could not be attributed to a specific arterial territory. Such symptoms include worsening of a preexisting dysarthria, dysphagia or ataxia, sudden appearance of emotional incontinence or recent onset bowel or bladder problems. Excellent diagnostic performance of DWI in lacunar infarctions may help to prove ischemia as the cause of non-specific neurological symptoms in such patients.

Table 13.2. Studies of DWI in patients with lacunar stroke. [Reprinted with permission from Gass et al. (2004)]

Year and reference	n	Patients	Results and conclusions
Singer et al. (1998)	39	Clinical diagnosis of acute subcortical infarction	DWI has accuracy of 94.6% for acute subcortical infarction and differentiates acute from non-acute lesions
Kuker et al. (2002)	45	Clinical symptoms of akute infratentorial or thalamic infarction	Sensivity of DWI and T2 is lower earlier than 12 h after onset and for medulla-oblongata lesions
Oliveria-Filho et al. (2000)	67	Clinical syndrome consistent with infarct of small penetrating artery	Conventional MRI does not identify the clinically relevant infarct in almost 25% of patients with acute lesions on DWI
Yonemura et al. (2002)	106	SCOI or SBGI	Only 47% of SCOI and 87% of SBGIs were identified with conventional MRI, whereas DWI detected them all
Ay et al. (1999b)	62	Clinical diagnosis of lacunar syndrome	Almost one in six patients presenting with a classic lacunar syndrome has multiple lesions on DWI
Gerraty et al. (2002)	19	Clinical diagnosis of acute lacunar syndrome	In 13 cases DWI and PI altered the final diagnosis of infarct pathogenesis from small perforating artery occlusion to large artery embolism

PI = perfusion imaging; SCOI = small centrum-ovale infarct; SBGI = small based-ganglia infarct

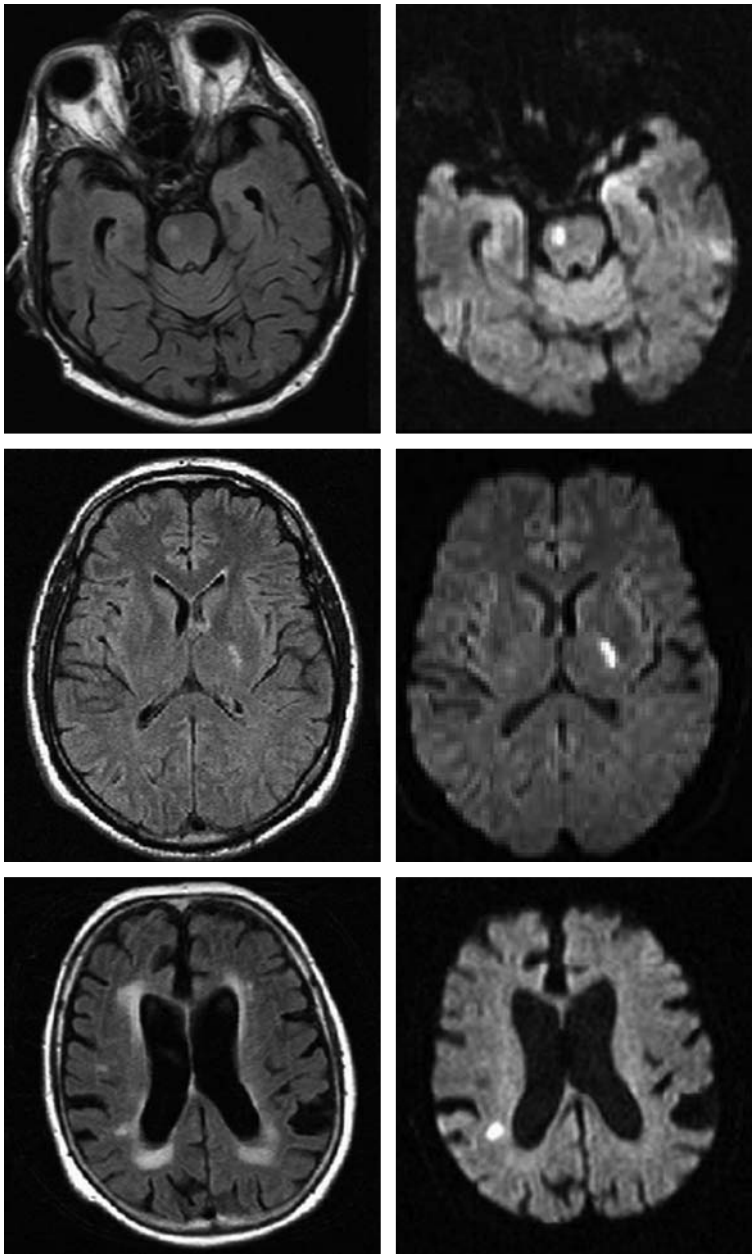

Fig. 13.3. FLAIR (*left column*) and diffusion-weighted transverse images (*right column*) in three patients with typical acute new ischemic subcortical lesions. Acute small subcortical lesions occurred in the pons (*top row*), internal capsule (*center row*), and lateral to the body of the right lateral ventricle

13.4 White Matter Lesions in the Elderly

In normal elderly controls, non-specific periventricular and subcortical T_2-hyperintense lesions of the brain are a common finding and are reported in 27%-92% of the elderly population (Breteler et al. 1994; de Leeuw et al. 2001). In asymptomatic individuals over 50 years of age, changes in the white matter on T_2-weighted, proton density and FLAIR images are frequently found, varying from a few scattered lesions in the centrum semiovale or periventricular region to a rim of high signal intensity around the ventricles, and to extensive hyperintense changes of most of the periventricular and lobar white matter. These changes increase with age, cerebrovascular disease and hypertension (Breteler et al. 1994; DeCarli et al. 1995).

The exact nature of these findings remains controversial. A number of investigators have postulated various explanations for this observation including atrophic perivascular demyelination (Kirkpatrick and Hayman 1987), ischemia (Meguro et al. 1990), and infarction with gliosis

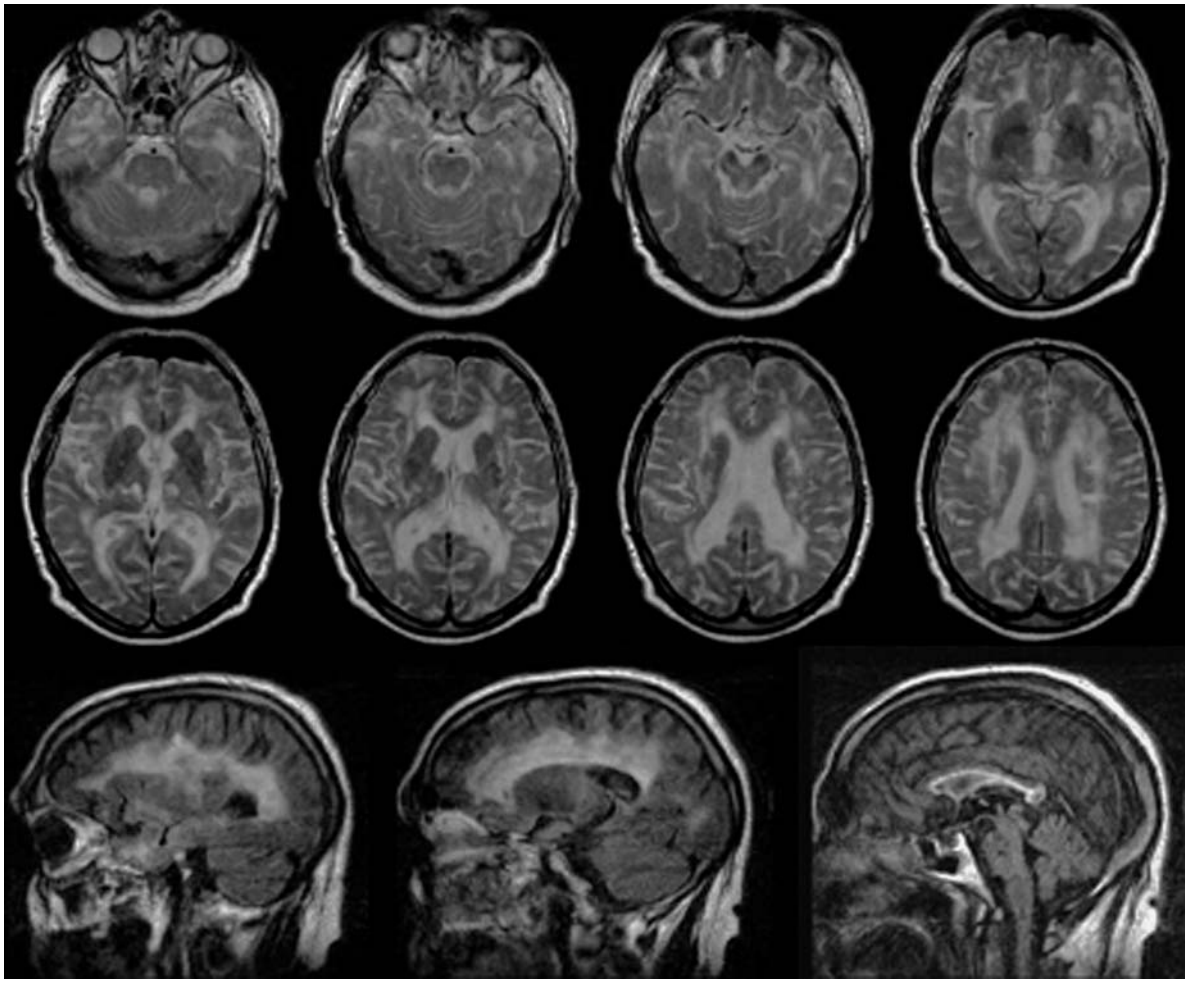

Fig. 13.4. Transverse FLAIR images of a CADASIL patient. Note the location of white matter lesions in the external capsule and close to the temporal pole anterior to the frontal horns of the lateral ventricles

(Marshall et al. 1988). Clinico-pathological studies indicate that diffuse hyperintensities on T_2-weighted scans represent ischemic damage of the subcortical fiber system (Awad et al. 1986; Fazekas et al. 1998; Scheltens et al. 1995). The Fazekas group related the histopathologic changes associated with incidental white matter signal hyperintensities on MRIs from 11 elderly patients (age range, 52–82 years) to a descriptive classification for such abnormalities (Fazekas et al. 1993). They found that punctuate, early confluent, and confluent white matter hyperintensities corresponded to increasing severity of ischemic tissue damage, ranging from mild perivascular alterations to large areas with variable loss of fibers, multiple small cavitations, and marked arteriolosclerosis. Microcystic infarcts and patchy rarefaction of myelin were also characteristic for irregular periventricular high signal intensity, while hyperintense periventricular caps and a smooth halo, however, were of nonischemic origin and constituted areas of demyelination associated with subependymal gliosis and discontinuity of the ependymal lining. In a recent study, similar regional distribution of white matter lesions in vascular dementia, Alzheimer's disease and healthy aging was found suggesting a common (vascular) pathogenic factor in all three groups (Gootjes et al. 2004). In a cohort of elderly normal controls with incidental white matter lesions, no hyperintense signal abnormality was identified on DWI which may be viewed as an indication that acute focal ischemia is a rather rare event in this group of patients and that white matter lesions can also be the result of more slowly evolving tissue degeneration not presenting with reductions of the ADC (Szabo et al. 2004).

White matter lesions in the healthy elderly population progress as shown in a study by Schmidt and coworkers (2003) who studied 296 volunteers aged 50-75 years at baseline, 3 years and 6 years. They found that the lesion grade at baseline was the only significant predictor of lesion progression. Punctuate white matter lesions showed no progression and may be viewed as comparably benign, whereas early confluent white matter abnormalities predicted new lesion accumulation and appear to be morphological and clinical predictors of worsening (Pantoni 2004). Several studies have reported a significant correlation between white matter lesions and reduced performance in specific cognitive domains in non-demented elderly subjects, particularly with a history of hypertension (Skoog et al. 1996; Ylikoski et al. 1993), while the Austrian Stroke Prevention Study did not find an association between the evolution of white matter lesions and cognitive functioning (Schmidt et al. 2002). A recent magnetization transfer MRI study also indicated that brain tissue abnormalities in otherwise normal elderly subjects with nonspecific white matter hyperintensities extend beyond the macroscopic white matter lesions visualized on conventional magnetic resonance images (Mezzapesa et al. 2003).

13.5 Subcortical Lesions and Dementia

In order of prevalence, vascular dementia is the second most common type of dementia after dementia in Alzheimer's disease (Dubois and Hebert 2001). Although concepts of vascular dementia have historically been based on stroke and the multi-infarct model (Hachinski et al. 1974) which requires multiple large cortical infarcts for dementia to develop, it is increasingly recognized that vascular dementia can result from several other – predominantly subcortical – vascular pathologies such as ischemic, hypoperfusive, or hemorrhagic brain lesions and can manifest with a spectrum of clinical dementia syndromes and psychiatric symptoms including depression, apathy, disinhibitive behavior, paranoia, and emotional lability (Esiri et al. 1997; Pohjasvaara et al. 2003; Rockwood et al. 2003). Subcortical vascular dementia may be caused by small vessel disease with lacunar infarct and ischemic white matter lesions as the primary types of brain lesions. The onset of dementia in these patients is insidious, and correlations between symptoms and MRI features are unclear. The clinical features include gait disorder/gait apraxia, urinary incontinence, personality changes, nighttime confusion, and difficulty with activities of daily living. Focal signs were also seen in the group of patients with pathologically confirmed subcortical arteriosclerotic encephalopathy and stroke-like episodes (Tarvonen-Schroder et al. 1996).

The relationship between white matter abnormalities detected by MRI and intellectual decline is less clear, probably because MRI detects preclinical stages, and decompensation due to loss of resources is a multifactorial process. Studies in patient groups with small vessel disease (Sabri et al. 1999; Mungas et al. 2001) found only relatively weak correlations between lesion load on T_2-weighted imaging and dementia, while in studies that only included moderate or severe periventricular white matter lesions, a clearer association between diffuse white matter abnormalities detected by MRI and dementia emerged (Brant-Zawadzki et al. 1985; Junque et al. 1990; Kertesz et al. 1990). This was also underlined in a comparative study of T2- and T1- hypointense lesion loads (indicative of severe tissue damage) (Gass et al. 1998). In patients with MRI-detected white matter lesions, the severity of intellectual decline correlated both with the size of the lateral ventricles (Tanaka et al. 1989) and with the degree of callosal atrophy (Yamauchi et al. 2000), presumably reflecting the severity of associated white matter tissue loss. In conclusion, the majority of small subcortical lesions seen in the white matter on MRI are not associated with clinical findings, but they may be early indicators of vascular disease that may progress to more extensive tissue changes and dementia. Recent evidence suggests, that morphological changes are important and that the degree and distribution of white matter damage separates the individuals with normal intellect from the patients with dementia.

New MR techniques may also have a role in this regard. In a recent study, diffusion tensor MRI (DTI) indices correlated more strongly with cognitive function than T_2 lesion volume in patients with white matter lesions (O'Sullivan et al. 2004). The correlation was strongest for diffusivity of normal appearing white matter and remained significant after controlling for conventional MRI parameters, including brain parenchymal volume and T1 and T2 lesion load.

13.6 Hereditary Disorders Associated with White Matter Lesions

The genetic contribution to stroke and vascular dementia is important. The underlying genetic defects for several monogenic disorders have already been identified (Joutel et al. 1996).

Cerebral autosomal dominant arteriopathy with subcortical infarcts and leukoencephalopathy (CADASIL) is a monogenic cause of ischemic small vessel disease and stroke in middle-aged individuals. Clinical manifestations include TIAs and strokes (80%), cognitive deficits (50%), migraine with aura (40%), psychiatric disorders (30%), and epilepsy (10%) (Dichgans et al. 1998). Mean age at onset is 46 years and MRI reveals a combination of small lacunar lesions and diffuse white matter abnormalities (Auer et al. 2001). T_2 hyperintensity of the white matter of the temporal poles and involvement of the external capsule is a MRI finding in CADASIL infrequent in other forms of microangiopathy that may help to raise the suspicion of the disease (O'Sullivan et al. 2001). Recently, a peculiar sign that appears to be of high specificity has been described in CADASIL patients with extensive white matter abnormality. It was best appreciated on FLAIR images that lacunar lesions can be present at the level of the junction of gray and white matter (van den Boom et al. 2002). The underlying vascular lesion is a unique non-amyloid angiopathy involving small arteries (100-400 μm) and capillaries primarily in the brain. Characteristically, ultrastructurally osmiophilic inclusion bodies are found in brain vessels, and these changes have also been seen on skin biopsy that is a standard diagnostic test for CADASIL. Mutations in the NOTCH3 gene which codes for a large transmembrane receptor have been identified (Joutel et al. 1996). Expression of NOTCH3 is restricted to vascular smooth muscle cells. The mutations result in a selective accumulation of the extracellular domain of the receptor within blood vessels (Joutel et al. 2000).

Another hereditary entity that has generated increasing interest in the past years is cerebral amyloid angiopathies (CAA). CAA are a heterogeneous group of disorders characterized by deposition of amyloid in the walls of leptomeningeal and cerebral cortical blood vessels. Clinical features include recurrent or multiple lobar hemorrhages, cogni-

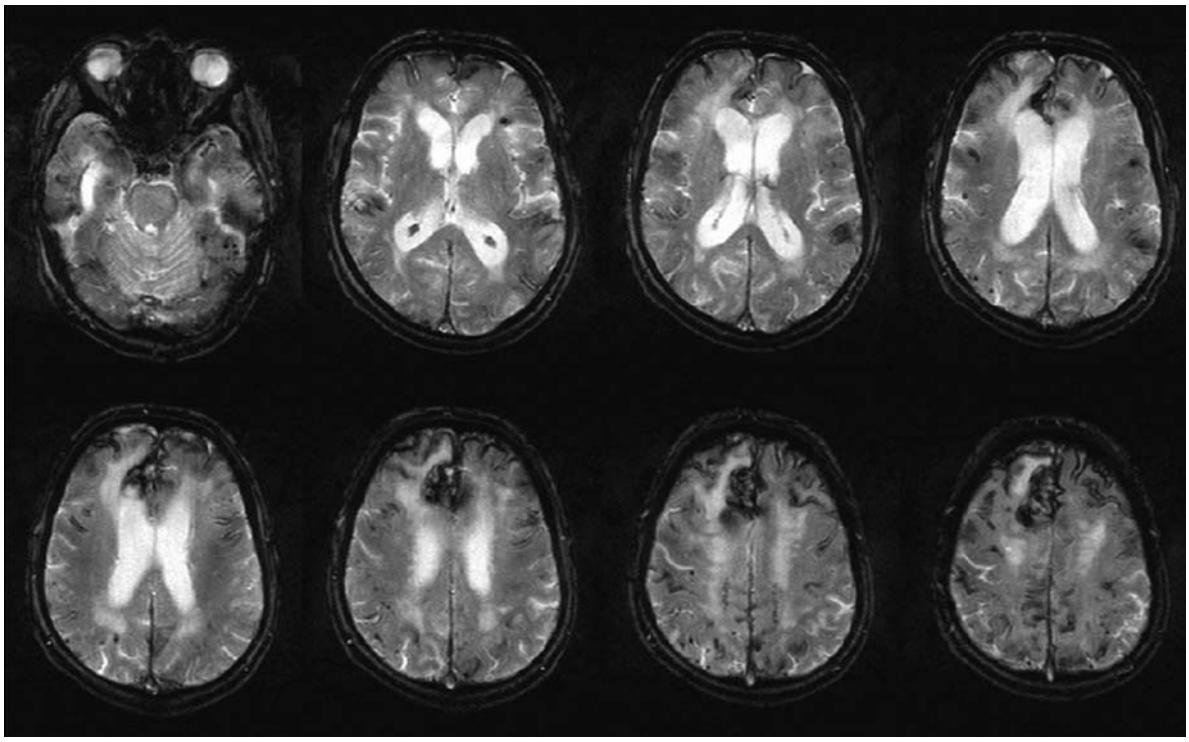

Fig. 13.5. T_{2^*}-weighted gradient echo images in a patient with biopsy proven cerebral amyloid angiopathy (CAA). Extensive low signal abnormality is noted on the brain surfaces and in the parenchyma indicating the previous hemorrhages. Periventricular high intensity lesions, a common finding in CAA is also noted

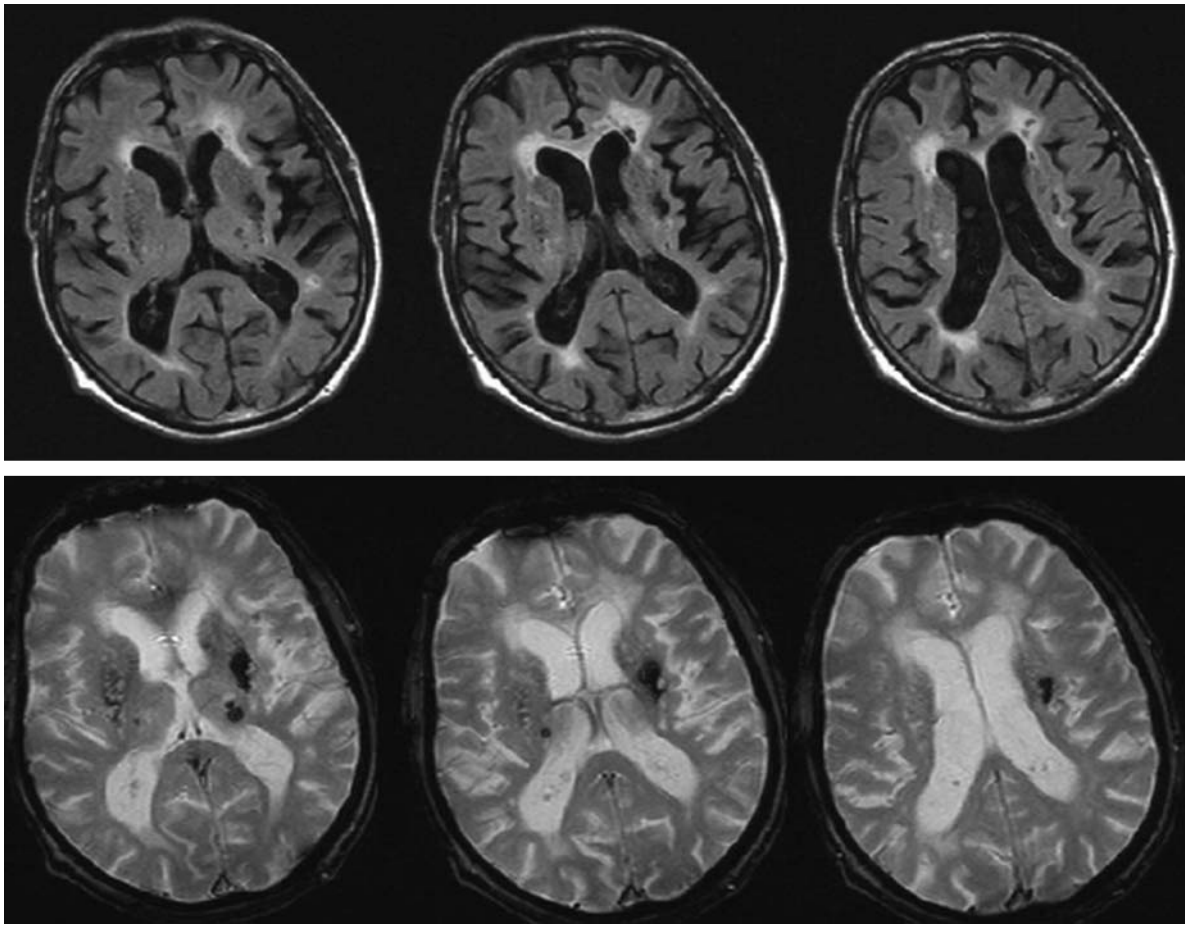

Fig. 13.6. FLAIR (*top row*) and T_{2^*}-weighted gradient echo images (*bottom row*) in a patient with hypertension showing a typical lesion pattern. Note subcortical lesions including lacunar lesions with severe tissue destruction and CSF like, low signal intensity (e.g. lateral to the anterior horn of the left lateral ventricle) on FLAIR images. On T_{2^*}-weighted images residuals from hemorrhagic lesions and small bleeds are appreciated mainly in the basal ganglia

tive deterioration, and ischemic stroke. MRI displays diffuse white matter abnormalities and focal lesions that can be ischemic or hemorrhagic. Vessels show amyloid deposition, cracking of single layers, microaneurysm formations and fibroid necrosis. The rupture of the structurally weakened arteries results in cerebral hemorrhage, characteristically in the cortices rather than the subcortical regions. CAA has usually been diagnosed postmortem. Although neuropathologic examination remains the definitive diagnostic approach to CAA, recent data suggest that a reliable diagnosis can be reached from clinical and MRI information alone using the Boston criteria (Greenberg et al. 1996; Knudsen et al. 2001), which include clinical data, MRI or CT demonstrating multiple hemorrhages restricted to lobar, cortical, or cortico-subcortical regions, and pathologic tissue (evacuated hematoma or cortical biopsy). Several autosomal dominantly inherited forms of cerebral amyloid angiopathy can be differentiated by genetic, biochemical and pathological findings (Greenberg et al. 1999).

13.7 Microangiopathic Disease and Hemorrhage

The presence of microhemorrhages has been reported in the last 5 years in patients with white matter disease and cognitive decline, with and lately also without a history of intracranial hemorrhage or cerebral infarction. The potential of MRI to reveal residues of intracerebral bleeding throughout life rests on its high sensitivity to iron-containing compounds. At the site of intracerebral hemorrhage

(ICH), hemosiderin remains stored in macrophages and leads to focal dephasing of the MRI signal. This causes areas of past bleeding to appear dark on T2*-weighted images. Techniques with high sensitivity to differences in magnetic susceptibility, such as the gradient-echo sequence, enhance these effects and allow detection of even minor hemosiderin deposition (Atlas et al. 1988). MRI is invaluable for obtaining this information because most small bleedings remain clinically undetected.

Scharf et al. (1994) were the first to present MRI evidence of previous, clinically silent intracerebral bleeds that they termed hemorrhagic lacunes. This type of lesion was significantly more frequent in patients with an intracerebral hematoma. In a series of 120 patients with primary ICH, Offenbacher and coworkers (1996) observed multiple foci of MRI signal loss compatible with old microbleeds in 28 individuals. In parallel, other investigators noticed similar MRI lesions in 9 of 15 patients with lobar hemorrhage (Greenberg et al. 1996). These abnormalities were considered to be evidence of previous petechial bleeds. Cortical and lobar ICH, predominantly of elderly patients, has been frequently related to amyloid angiopathy (Vinters 1987; Itoh et al. 1993). Also in this setting, MRI evidence of past bleedings has been reported (Greenberg et al. 1996). Furthermore, a cross-sectional study has also documented the accumulation of silent microbleeds over a short period of time in a series of patients with lobar hemorrhage and the diagnosis of probable or possible CAA (Greenberg et al. 1999).

Roob et al. (1999) noted focal areas of signal loss on gradient-echo T2*-weighted MRI in 18 of 280 (6.4%) participants in a cross-sectional study of neurologically asymptomatic elderly volunteers. These lesions were seen in cortico-subcortical regions of the brain, in the basal ganglia, and in infratentorial locations. Individuals with MRI evidence of microbleeds were significantly older, had a significantly higher frequency of hypertension, and had a higher rate of early confluent white matter lesions and lacunes. Foci of signal loss in cortico-subcortical regions were significantly less often associated with hypertension than microbleeds in the basal ganglia or infratentorial regions. These associations support the role of microangiopathy in the pathogenesis of focal T2* hypointensities.

Hypertension is regarded as the main clinically observable risk factor to cause microbleeds (Roob et al. 1999). Recent findings suggest that microbleeds on T2*-weighted MRI are an indicator of advanced small artery disease of the brain with an increased risk for bleeding (Kato et al. 2002). With more clinical significance of such findings, MRI demonstration of microbleeds could gain use to identify patients who have an increased risk for intracerebral bleeding complications resulting from therapy that affects blood clotting, This result should be taken into consideration when treating patients with stroke (Kidwell et al. 2002).

References

Alexander GE, DeLong MR, Strick PL (1986) Parallel organization of functionally segregated circuits linking basal ganglia and cortex. Annu Rev Neurosci 9:357-381

Arboix A, Marti-Vilalta JL, Pujol J, Sanz M (1990) Lacunar cerebral infarct and nuclear magnetic resonance. A review of sixty cases. Eur Neurol 30:47-51

Atlas SW, Mark AS, Grossman RI, Gomori JM (1988) Intracranial hemorrhage: gradient-echo MR imaging at 1.5 T. Comparison with spin-echo imaging and clinical applications. Radiology 168:803-807

Auer DP, Putz B, Gossl C, Elbel G, Gasser T, Dichgans M (2001) Differential lesion patterns in CADASIL and sporadic subcortical arteriosclerotic encephalopathy: MR imaging study with statistical parametric group comparison. Radiology 218:443-451

Awad IA, Spetzler RF, Hodak JA, Awad CA, Carey R (1986) Incidental subcortical lesions identified on magnetic resonance imaging in the elderly. I. Correlations with age and cerebrovascular risk factors. Stroke 17:1084-1089

Ay H, Buonanno FS, Rordorf G, Schaefer PW, Schwamm LH, Wu O, Gonzalez RG, Yamada K, Sorensen GA, Koroshetz WJ (1999a) Normal diffusion-weighted MRI during stroke-like deficits. Neurology 52:1784-1792

Ay H, Oliveira-Filho J, Buonanno FS, Ezzeddine M, Schaefer PW, Rordorf G, Schwamm LH, Gonzalez RG, Koroshetz WJ (1999b) Diffusion-weighted imaging identifies a subset of lacunar infarction associated with embolic source. Stroke 30:2644-2650

Bamford J (2001) Classical lacunar syndromes. In: Bogousslavsky J, Caplan L (eds) Sreoke syndromes. Cambridge University Press, Cambridge, pp 583-589

Bamford J, Bogousslavsky J (eds) (2002) Subcortical stroke, 2nd edn. Oxford Medical Publications, Oxford, pp 27-34

Bamford J, Sandercock P, Jones L, Warlow C (1987) The natural history of lacunar infarction: the Oxfordshire Community Stroke Project. Stroke 18:545-551

Benito-Leon J, Alvarez-Linera J, Porta-Etessam J (2001;Detection of acute pontine infarction by diffusion-weighted MRI in capsular warning syndrome. Cerebrovasc Dis 11:350-351

Bogousslavsky J, Van Melle G, Regli F (1988) The Lausanne Stroke Registry: analysis of 1,000 consecutive patients with first stroke. Stroke 19:1083-1092

Brant-Zawadzki M, Fein G, Van Dyke C, Kiernan R, Davenport L, de Groot J (1985) MR imaging of the aging brain: patchy white-matter lesions and dementia. Am J Neuroradiol 6:675-682

Breteler MM, van Swieten JC, Bots ML, Grobbee DE, Claus JJ,

van den Hout JH, van Harskamp F, Tanghe HL, de Jong PT, van Gijn J (1994) Cerebral white matter lesions, vascular risk factors, and cognitive function in a population-based study: the Rotterdam Study. Neurology 44:1246–1252

DeCarli C, Murphy DGM, Tranh M, Grady CL, Haxby JV, Gillette JA et al (1995) The effect of white matter hyperintensity volume on brain structure, cognitive performance, and cerebral metabolism of glucose in 51 healthy adults. Neurology 45:2077-2084

DeCarli C, Miller BL, Swan GE, Reed T, Wolf PA, Garner J, Jack L, Carmelli D (1999) Predictors of brain morphology for the men of the NHLBI Twin Study. Stroke 30:529–536

De Leeuw FE, de Groot JC, Oudkerk M, Witteman JC, Hofman A, van Gijn J, Breteler MM (1999) A follow-up study of blood pressure and cerebral white matter lesions. Ann Neurol 46:827–833

De Leeuw FE, de Groot JC, Achten E, Oudkerk M, Ramos LM, Heijboer R et al (2001) Prevalence of cerebral white matter lesions in elderly people: a population based magnetic resonance imaging study. The Rotterdam Scan Study. J Neurol Neurosurg Psychiatry 70:9-14

Dichgans M, Joutel A (2002) Cerebrovascular disorders. In: Rimoin D, Connor JM, Pyeritz RE, Korf B (eds) Emery and Rimoin's principles and practice of medical genetics. Churchill Livingstone, London, pp 3209-3230

Dichgans M, Mayer M, Uttner I, Bruning R, Muller-Hocker J, Rungger G, Ebke M, Klockgether T, Gasser T (1998) The phenotypic spectrum of CADASIL: clinical findings in 102 cases. Ann Neurol 44:731-739

Donnan GA, Tress BM, Bladin PF (1982) A prospective study of lacunar infarction using computerized tomography. Neurology 32:49-56

Dubois MF, Hebert R (2001) The incidence of vascular dementia in Canada: a comparison with Europe and East Asia. Neuroepidemiology 20:179-187

Englund E (2002) Neuropathology of white matter lesions in vascular cognitive impairment. Cerebrovasc Dis 13 [Suppl 2]:11-15

Erkinjuntti T, Benavente O, Eliasziw M, Munoz DG, Sulkava R, Haltia M, Hachinski V (1996) Diffuse vacuolization (spongiosis) and arteriolosclerosis in the frontal white matter occurs in vascular dementia. Arch Neurol 53:325-332

Esiri MM, Wilcock GK, Morris JH (1997) Neuropathological assessment of the lesions of significance in vascular dementia. J Neurol Neurosurg Psychiatry 63:749-753

Fazekas F, Kleinert R, Offenbacher H, Schmidt R, Kleinert G, Payer F, Radner H, Lechner H (1993) Pathologic correlates of incidental MRI white matter signal hyperintensities. Neurology 43:1683-1689

Fazekas F, Schmidt R, Kleinert R, Kapeller P, Roob G, Flooh E (1998) The spectrum of age-associated brain abnormalities: their measurement and histopathological correlates. J Neural Transm [Suppl] 53:31-39

Fisher CM (1965) Lacunes: small, deep cerebral infarcts. Neurology 15:774-784

Fisher CM (1979) Capsular infarcts: the underlying vascular lesions. Arch Neurol 36:65-73

Fisher CM (1982) Lacunar strokes and infarcts: a review. Neurology 32:871-876

Fisher CM (1991) Lacunar infarcts: a review. Cerebrovasc Dis 1:311-320

Furuta A, Ishii N, Nishihara Y, Horie A (1991) Medullary arteries in aging and dementia. Stroke 22:442-446

Gass A, Oster M, Cohen S, Daffertshofer M, Schwartz A, Hennerici MG (1998) Assessment of T2- and T1-weighted MRI brain lesion load in patients with subcortical vascular encephalopathy. Neuroradiology 40:503-506

Gass A, Ay H, Szabo K, Koroshetz WJ (2004) Diffusion-weighted MRI for the "small stuff": the details of acute cerebral ischaemia. Lancet Neurol 3:39-45

Gerraty RP, Parsons MW, Barber PA, Darby DG, Desmond PM, Tress BM, Davis SM (2002) Examining the lacunar hypothesis with diffusion and perfusion magnetic resonance imaging. Stroke 33:2019-2024

Greenberg SM, Finklestein SP, Schaefer PW (1996a) Petechial hemorrhages accompanying lobar hemorrhage: detection by gradient-echo MRI. Neurology 46:1751-1754

Greenberg SM, Briggs ME, Hyman BT et al (1996b) Apolipoprotein E e4 is associated with the presence and earlier onset of hemorrhage in cerebral amyloid angiopathy. Stroke 27:1333–1337

Greenberg SM, O'Donnell HC, Schaefer PW, Kraft E (1999) MRI detection of new hemorrhages: potential marker of progression in cerebral amyloid angiopathy. Neurology 53:1135-1138

Gootjes L, Teipel SJ, Zebuhr Y, Schwarz R, Leinsinger G, Scheltens P, Moller HJ, Hampel H (2004) Regional distribution of white matter hyperintensities in vascular dementia, Alzheimer's disease and healthy aging. Dement Geriatr Cogn Disord 18:180-188

Hachinski VC, Lassen NA, Marshall J (1974) Multi-infarct dementia. A cause of mental deterioration in the elderly. Lancet 2:207-210

Hachinski VC, Potter P, Merskey H (1987) Leukoaraiosis. Arch Neurol 44:21-23

Hommel M, Besson G, Le Bas JF, Gaio JM, Pollak P, Borgel F, Perret J (1990) Prospective study of lacunar infarction using magnetic resonance imaging. Stroke 21:546-554

Inzitari D, Diaz F, Fox A, Hachinski VC, Steingart A, Lau C, Donald A, Wade J, Mulic H, Merskey H (1987) Vascular risk factors and leuko-araiosis. Arch Neurol 44:42-47

Ishii N, Nishihara Y, Imamura T (1986) Why do frontal lobe symptoms predominate in vascular dementia with lacunes? Neurology 36:340-345

Itoh Y, Yamada M, Hayakawa M, Otomo E, Miyatake T (1993) Cerebral amyloid angiopathy: a significant cause of cerebellar as well as lobar cerebral hemorrhage in the elderly. J Neurol Sci 116:135-141

Joutel A, Corpechot C, Ducros A, Vahedi K, Chabriat H, Mouton P, Alamowitch S, Domenga V, Cecillion M, Marechal E, Maciazek J, Vayssiere C, Cruaud C, Cabanis EA, Ruchoux MM, Weissenbach J, Bach JF, Bousser MG, Tournier-Lasserve E (1996) Notch3 mutations in CADASIL, a hereditary adult-onset condition causing stroke and dementia. Nature 383:707-710

Joutel A, Andreux F, Gaulis S, Domenga V, Cecillon M, Battail N, Piga N, Chapon F, Godfrain C, Tournier-Lasserve E (2000) The ectodomain of the Notch3 receptor accumulates within the cerebrovasculature of CADASIL patients. J Clin Invest 105:597-605

Junque C, Pujol J, Vendrell P, Bruna O, Jodar M, Ribas JC, Vinas J, Capdevila A, Marti-Vilalta JL (1990) Leuko-araiosis on magnetic resonance imaging and speed of mental processing. Arch Neurol 47:151-156

Kang DW, Chalela JA, Ezzeddine MA, Warach S (2003) Association of ischemic lesion patterns on early diffusion-

weighted imaging with TOAST stroke subtypes. Arch Neurol 60:1730-1734
Kato H, Izumiyama M, Izumiyama K, Takahashi A, Itoyama Y (2002) Silent cerebral microbleeds on T2*-weighted MRI: correlation with stroke subtype, stroke recurrence, and leukoaraiosis. Stroke 33:1536-1540
Kertesz A, Black SE, Tokar G, Benke T, Carr T, Nicholson L (1988) Periventricular and subcortical hyperintensities on magnetic resonance imaging. 'Rims, caps, and unidentified bright objects'. Arch Neurol 45:404-408
Kertesz A, Polk M, Carr T (1990) Cognition and white matter changes on magnetic resonance imaging in dementia. Arch Neurol 47:387-391
Kidwell CS, Saver JL, Villablanca JP, Duckwiler G, Fredieu A, Gough K, Leary MC, Starkman S, Gobin YP, Jahan R, Vespa P, Liebeskind DS, Alger JR, Vinuela F (2002) Magnetic resonance imaging detection of microbleeds before thrombolysis: an emerging application. Stroke 33:95-98
Kirkpatrick JB, Hayman LA (1987) White-matter lesions in MR imaging of clinically healthy brains of elderly subjects: possible pathologic basis. Radiology 162:509-511
Knudsen KA, Rosand J, Karluk D, Greenberg SM (2001) Clinical diagnosis of cerebral amyloid angiopathy: validation of the Boston criteria. Neurology 56:537-539
Kuker W, Weise J, Krapf H, Schmidt F, Friese S, Bahr M (2002) MRI characteristics of acute and subacute brainstem and thalamic infarctions: value of T2- and diffusion-weighted sequences. J Neurol 249:33-42
Liao D, Cooper L, Cai J, Toole JF, Bryan NR, Hutchinson RG, Tyroler HA (1996) Presence and severity of cerebral white matter lesions and hypertension, its treatment, and its control. The ARIC study. Atherosclerosis risk in communities study. Stroke 27:2262–2270
Liao D, Cooper L, Cai J, Toole J, Bryan N, Burke G, Shahar E, Nieto J, Mosley T, Heiss G (1997) The prevalence and severity of white matter lesions, their relationship with age, ethnicity, gender, and cardiovascular disease risk factors: the ARIC Study. Neuroepidemiology 16:149–162
Lie C, Hirsch JG, Rossmanith C, Hennerici MG, Gass A (2004) Clinicotopographical correlation of corticospinal tract stroke: a color-coded diffusion tensor imaging study. Stroke. 35:86-92
Lindgren A, Norrving B, Rudling O, Johansson BB (1994) Comparison of clinical and neuroradiological findings in first-ever stroke. A population-based study. Stroke 25:1371-1377
Lindgren A, Staaf G, Geijer B, Brockstedt S, Stahlberg F, Holtas S, Norrving B (2000) Clinical lacunar syndromes as predictors of lacunar infarcts. A comparison of acute clinical lacunar syndromes and findings on diffusion-weighted MRI. Acta Neurol Scand 101:128-134
Lodder J, Boiten J (1993) Incidence, natural history, and risk factors in lacunar infarction. Adv Neurol 62:213-227
Longstreth WT Jr, Manolio TA, Arnold A, Burke GL, Bryan N, Jungreis CA, Enright PL, O'Leary D, Fried L (1996) Clinical correlates of white matter findings on cranial magnetic resonance imaging of 3301 elderly people. The cardiovascular health study. Stroke 27:1274-1282
Lovblad KO, Laubach HJ, Baird AE, Curtin F, Schlaug G, Edelman RR, Warach S (1998) Clinical experience with diffusion-weighted MR in patients with acute stroke. AJNR Am J Neuroradiol 19:1061-1066
Marshall VG, Bradley WG Jr, Marshall CE, Bhoopat T, Rhodes RH (1988) Deep white matter infarction: correlation of MR imaging and histopathologic findings. Radiology 167:517-522
McQuinn BA, O'Leary DH (1987) White matter lucencies on computed tomography, subacute arteriosclerotic encephalopathy (Binswanger's disease), and blood pressure. Stroke 18:900-905
Mega MS, Cummings JL (1994) Frontal-subcortical circuits and neuropsychiatric disorders. J Neuropsychiatry Clin Neurosci 6:358-70
Meguro K, Hatazawa J, Yamaguchi T, Itoh M, Matsuzawa T, Ono S, Miyazawa H, Hishinuma T, Yanai K, Sekita Y et al (1990) Cerebral circulation and oxygen metabolism associated with subclinical periventricular hyperintensity as shown by magnetic resonance imaging. Ann Neurol 28:378-383
Mezzapesa DM, Rocca MA, Pagani E, Comi G, Filippi M (2003) Evidence of subtle gray-matter pathologic changes in healthy elderly individuals with nonspecific white-matter hyperintensities. Arch Neurol 60:1109-1112
Mungas D, Jagust WJ, Reed BR et al (2001) MRI predictors of cognition in subcortical ischemic vascular disease and Alzheimer's disease. Neurology 57:2229–2235
O'Donnell HC, Rosand J, Knudsen KA, Furie KL, Segal AZ, Chiu RI, Ikeda D, Greenberg SM (2000) Apolipoprotein E genotype and the risk of recurrent lobar intracerebral hemorrhage. N Engl J Med 342:240-245
Offenbacher H, Fazekas F, Schmidt R, Koch M, Fazekas G, Kapeller P (1996) MR of cerebral abnormalities concomitant with primary intracerebral hematomas. Am J Neuroradiol 17:573-578
Oliveira-Filho J, Ay H, Schaefer PW, Buonanno FS, Chang Y, Gonzalez RG, Koroshetz WJ (2000) Diffusion-weighted magnetic resonance imaging identifies the "clinically relevant" small-penetrator infarcts. Arch Neurol 57:1009-1014
Oliveira-Filho J, Ay H, Koroshetz WJ, Buonanno FS (2001) Localization of clinical syndromes using DWI: two examples of the "capsular" warning syndrome. J Neuroimaging 11:44-47
O'Sullivan M, Jarosz JM, Martin RJ, Deasy N, Powell JF, Markus HS (2001) MRI hyperintensities of the temporal lobe and external capsule in patients with CADASIL. Neurology 56:628-634
O'Sullivan M, Morris RG, Huckstep B, Jones DK, Williams SCR, Markus HS (2004) Diffusion tensor MRI correlates with executive dysfunction in patients with ischaemic leukoaraiosis. J Neurol Neurosurg Psychiatry 75:441-447
Pantoni L, Garcia JH (1997) Pathogenesis of leukoaraiosis: a review. Stroke 28:652–659
Pantoni L, Basile AM, Pracucci G, Asplund K, Bogousslavsky J, Chabriat H, Erkinjuntti T, Fazekas F, Ferro JM, Hennerici M, O'brien J, Scheltens P, Visser MC, Wahlund LO, Waldemar G, Wallin A, Inzitari D (2005) Impact of age-related cerebral white matter changes on the transition to disability - the LADIS study: rationale, design and methodology. Neuroepidemiology 24:51-62
Petty GW, Brown RD Jr, Whisnant JP, Sicks JD, O'Fallon WM, Wiebers DO (2000) Ischemic stroke subtypes: a population-based study of functional outcome, survival, and recurrence. Stroke 31:1062-1068
Pohjasvaara T, Mantyla R, Ylikoski R, Kaste M, Erkinjuntti T (2003) Clinical features of MRI-defined subcortical vascular disease. Alzheimer Dis Assoc Disord 17:236-242

Ravens JR (1978) Vascular changes in the human senile brain. Adv Neurol 20:487-501

Révész T, Hawkins CP, du Boulay EP, Barnard RO, McDonald WI (1989) Pathological findings correlated with magnetic resonance imaging in subcortical arteriosclerotic encephalopathy (Binswanger's disease). J Neurol Neurosurg Psychiatry 52:1337-1344

Rockwood K, Burns A, Gauthier S, DeKosky ST (2003) Vascular cognitive impairment. Lancet Neurol 2:89-98

Roman GC (1987) Senile dementia of the Binswanger type. A vascular form of dementia in the elderly. JAMA 258:1782-1788

Roman GC, Royall DR (1999) Executive control function: a rational basis for the diagnosis of vascular dementia. Alzheimer Dis Assoc Disord 13 [Suppl 3]:S69-S80

Roman GC, Erkinjuntti T, Wallin A, Pantoni L, Chui HC (2002) Subcortical ischaemic vascular dementia. Lancet Neurol 1:426-436

Roob G, Schmidt R, Kapeller P, Lechner A, Hartung HP, Fazekas F (1999) MRI evidence of past cerebral microbleeds in a healthy elderly population. Neurology 52:991-994

Sabri O, Ringelstein EB, Hellwig D et al (1999) Neuropsychological impairment correlates with hypoperfusion and hypometabolism but not with severity of white matter lesions on MRI in patients with cerebral microangiopathy. Stroke 30:556–566

Scharf J, Brauherr E, Forsting M, Sartor K (1994) Significance of haemorrhagic lacunes on MRI in patients with hypertensive cerebrovascular disease and intracerebral haemorrhage. Neuroradiology 36:504-508

Scheltens P, Barkhof F, Leys D, Wolters EC, Ravid R, Kamphorst W (1995) Histopathologic correlates of white matter changes on MRI in Alzheimer's disease and normal aging. Neurology 45:883-888

Scheltens P, Erkinjunti T, Leys D, Wahlund LO, Inzitari D, del Ser T, Pasquier F, Barkhof F, Mantyla R, Bowler J, Wallin A, Ghika J, Fazekas F, Pantoni L (1998) White matter changes on CT and MRI: an overview of visual rating scales. European Task Force on Age-Related White Matter Changes. Eur Neurol 39:80-89

Schmidt R, Schmidt H, Kapeller P, Enzinger C, Ropele S, Saurugg R, Fazekas F (2002) The natural course of MRI white matter hyperintensities. J Neurol Sci 203-204:253-257

Schmidt R, Enzinger C, Ropele S, Schmidt H, Fazekas F (2003) Austrian stroke prevention study. Progression of cerebral white matter lesions: 6-year results of the Austrian stroke prevention study. Lancet 361:2046-2048

Singer MB, Chong J, Lu D, Schonewille WJ, Tuhrim S, Atlas SW (1998) Diffusion-weighted MRI in acute subcortical infarction. Stroke 29:133-136

Skoog I, Berg S, Johansson B, Palmertz B, Andreasson LA (1996) The influence of white matter lesions on neuropsychological functioning in demented and non-demented 85-year-olds. Acta Neurol Scand 93:142-148

Summergrad P, Peterson B (1989) Binswanger's disease, part I. The clinical recognition of subcortical arteriosclerotic encephalopathy in elderly neuropsychiatric patients. J Geriatr Psychiatry Neurol 2:123-133

Szabo K, Bäzner H, Kern R, Blahak C, Hennerici MG, Gass A (2004) Lack of incidental DWI hyperintensity in healthy elderly individuals. Cerebrovasc Dis [Suppl] 5:75

Tanaka Y, Tanaka O, Mizuno Y, Yoshida M (1989) A radiologic study of dynamic processes in lacunar dementia. Stroke 20:1488-1493

Tarvonen-Schroder S, Roytta M, Raiha I, Kurki T, Rajala T, Sourander L (1996) Clinical features of leuko-araiosis. J Neurol Neurosurg Psychiatry 60:431-436

Tekin S, Cummings JL (2002) Frontal-subcortical neuronal circuits and clinical neuropsychiatry: an update. J Psychosom Res 53:647-654

Tuszynski MH, Petito CK, Levy DE (1989) Risk factors and clinical manifestations of pathologically verified lacunar infarctions. Stroke 20:990-999

Van den Boom R, Lesnik Oberstein SA, van Duinen SG, Bornebroek M, Ferrari MD, Haan J, van Buchem MA (2002) Subcortical lacunar lesions: an MR imaging finding in patients with cerebral autosomal dominant arteriopathy with subcortical infarcts and leukoencephalopathy. Radiology 224:791-796

Van Dijk EJ, Breteler MM, Schmidt R, Berger K, Nilsson LG, Oudkerk M, Pajak A, Sans S, de Ridder M, Dufouil C, Fuhrer R, Giampaoli S, Launer LJ, Hofman A; CASCADE Consortium (2004) The association between blood pressure, hypertension, and cerebral white matter lesions: cardiovascular determinants of dementia study. Hypertension 44:625-630

Vermeer SE, Hollander M, van Dijk EJ, Hofman A, Koudstaal PJ, Breteler MM (2003) Silent brain infarcts and white matter lesions increase stroke risk in the general population: the Rotterdam scan study. Stroke 34:1126-1129

Wiszniewska M, Devuyst G, Bogousslavsky J, Ghika J, van Melle G (2000) What is the significance of leukoaraiosis in patients with acute ischemic stroke? Arch Neurol 57:967–973

Wolfe N, Linn R, Babikian VL, Knoefel JE, Albert ML (1990) Frontal systems impairment following multiple lacunar infarcts. Arch Neurol 47:129-132

Yamauchi H, Fukuyama H, Shio H (2000) Corpus callosum atrophy in patients with leukoaraiosis may indicate global cognitive impairment. Stroke 31:1515-1520

Ylikoski R, Ylikoski A, Erkinjuntti T, Sulkava R, Raininko R, Tilvis R (1993) White matter changes in healthy elderly persons correlate with attention and speed of mental processing. Arch Neurol 50:818-824

Yonemura K, Kimura K, Minematsu K, Uchino M, Yamaguchi T (2002) Small centrum ovale infarcts on diffusion-weighted magnetic resonance imaging. Stroke 33:1541-1544

You R, McNeil JJ, O'Malley HM, Davis SM, Donnan GA (1995) Risk factors for lacunar infarction syndromes. Neurology 45:1483-1487

14 Territorial and Embolic Infarcts

José M. Ferro

CONTENTS

14.1 Introduction

Despite the advances in neuroimaging, the early identification of ischemic stroke subtypes and patterns has several heuristic values, besides academic and research interest. It helps the physician to answer the patient's and their relatives' anxieties concerning the risk of early death, disability, stroke recurrence and length of hospital stay. It guides the neurologist to choose the most cost-effective ancillary procedures and the therapy with best efficacy. It also helps the hospital manager to calculate the average cost of care for stroke subtypes.

Prior to the use of magnetic resonance (MR) and in particular diffusion-weighted (DWI) MR, our clinico-anatomic concepts of acute stroke patterns were based on post-mortem correlations and on computerized tomography (CT). Post-mortem correlations are an accurate method with two obvious biases: (1) delay between acute clinical stroke pattern and death and (2) mortality bias. The introduction and dissemination of MR provided the neurological community with an opportunity to verify the validity of the classical description of acute stroke patterns. The yield of DWI for the detection of potentially relevant findings in acute stroke patients includes: (1) detecting an acute ischemic lesion in a territory different from that suspected clinically; (2) revealing multiple lesions in different vascular territories, when clinical examination and CT indicated a unifocal lesion; (3) clarifying whether a lesion seen on CT or MR is indeed acute or long-standing (Albers et al. 2000; Lee et al. 2000; Lindgren et al. 2000; Oliveira-Filho et al. 2000).

The early identification of the clinical and MR patterns of acute territorial infarcts can help the managing physician concerning prediction of outcome, risk of early death and dependency, risk of recurrence, stroke mechanism and etiology, selection of ancillary procedures, selection of best (effective and safe) anti-thrombotic treatment, risk of complications, length of stay and cost of hospital care.

Using only a few neurological findings the Oxfordshire Community Stroke Project (OCSP) classification allocates strokes to four subgroups, locating them either in the territory of the anterior (total anterior circulation infarct, TACI; partial anterior circulation infarct, PACI; lacunar infarct, LACI) and the posterior circulation, (posterior circulation infarct, POCI) (Bamford et al. 1991). The OCSP is a clinical syndromic classification, which

J. M. Ferro, MD, PhD
Neurology Service, Department of Neurosciences and Mental Health, Hospital de Santa Maria, University of Lisbon, Av. Prof. Egas Moniz, 1649–035 Lisbon, Portugal

does not include imaging information. The correspondence between the clinical classification and the imaging findings is not perfect, the positive predictive value ranging from 71 to 83 (Mead et al. 2000). Nevertheless the OCSP is very useful clinically because it is easy to communicate and predicts etiology (Mead et al. 1998), case fatality, functional recovery and risk of recurrence of stroke patients. TACIs have a highest mortality while LACIs have the lowest. The risk of recurrence is higher for PACI and POCI. The OSCP classification was validated in other populations (Wardlaw et al. 1996) and has a good inter-observer concordance (Lindley et al. 1993). The OSCP can also predict medical and neurological complications, therapeutic interventions and average cost of hospitalization (Pinto et al. 1998).

Impaired consciousness at onset or at presentation is the most powerful predictor of early death. Other predictors of death and disability include increasing age, male gender, previous dependency, dysphagia, pupil abnormality, gaze paresis, extensor plantars, dense hemiplegia, urine incontinence, breathing abnormalities, hypotension, hypertension, hypoglycemia, hyperglycemia (> 7 mmol/L), high hematocrit (> 50%), congestive heart failure, atrial fibrillation, medical complications, post-stroke seizures, early deterioration, stroke severity as measured by a stroke scale (NIHSS 4–7 < 8–14 < 15–22), TACI subtype, extensive [> 1/3 middle cerebral artery (MCA) territory] early infarct size and mass effect on admission CT (Ebrahim and Harwood 1999a,b; Moulin et al. 2000; Warlow et al. 2001; Wolf 2002).

The TOAST classification is commonly used to classify ischemic stroke subtypes. However, the accuracy of the early clinical diagnosis of stroke subtypes is below 2/3 and is not significantly improved by CT findings which are often unrevealing. Early DWI has a higher detection rate of ischemic lesions than other imaging modalities. Ischemic lesion patterns on DWI can indicate a specific etiology such as carotid occlusion or cardioembolism. There is also an overall significant relationship between DWI lesion patterns and TOAST stroke subtypes (Kang et al. 2003): cortico-subcortical single lesions, multiple lesions in anterior and posterior circulation, multiple lesions in multiple vascular territories are associated with cardioembolism; unilateral multiple lesions in the anterior circulation and small scattered lesions in one vascular territory are related to large artery atherosclerosis. A total of 50% of subcortical lesions being 15 mm or larger are cryptogenic or have a classical lacunar syndrome without cortical hypoperfusion.

In the first part of this chapter we will review the clinical-imaging patterns of acute territorial infarcts and their clinical relevance.

In the second part we will describe the clinical MR features of embolic stroke, with emphasis on cardioembolic stroke.

14.2 Clinical MR Patterns of Acute Territorial Infarcts

14.2.1 Middle Cerebral Artery (MCA) Infarcts

Middle cerebral artery (MCA) territorial infarcts are the most common type of ischemic stroke. They can be divided in superficial (involving the cortex and the underlying white matter), deep (involving the basal ganglia, the internal capsule and the deep white matter) and combined (Bogousslavsky and Caplan 2001; Gorelick 1996).

MCA infarcts are mainly caused by cardioembolism, internal carotid artery (ICA) thrombosis, dissection or embolism and rarely (in Caucasians) by intrinsic MCA disease. MCA atherothrombotic territory infarctions related to intrinsic MCA disease often cause concomitant small cortical (territorial or borderzone) and subcortical infarcts (Min et al. 2000).

14.2.1.1 Superficial Middle Cerebral Artery (MCA) Infarcts

The most common stroke patterns of superficial (pial) MCA infarcts are those due to complete pial infarction and infarcts in the distribution of the anterior division and posterior division of the MCA. Clinical presentation differs depending on whether the left (dominant for language) or the right (non-dominant) hemisphere is involved. In left hemispheric stroke the clinical picture is dominated by oral and written language disturbances, while after right MCA hemispheric strokes neglect is almost always present. The MCA has in general 12 pial branches and the syndromes corresponding to the infarcts in the distribution of such branches are also identifiable clinically.

14.2.1.2 Large Middle Cerebral Artery (MCA) Infarcts

Large supratentorial infarcts covering at least two subterritories of the MCA (deep, superficial, anterior or superior, and posterior or inferior) carry an unfavorable vital and functional prognosis and produce a severe neurological deficit (gaze deviation, hemiplegia, global aphasia or neglect with anosognosia, hemianopia) including reduced consciousness from onset. They are caused by cardioembolism, ICA occlusion or ICA dissection (Heinsius et al. 1998). Cardioembolic stroke tends to involve the three subterritories simultaneously. Poor collateral blood flow is an additional predictor of lethal outcome (Schwarz et al. 2001).

14.2.1.3 MCA Anterior or Superior Division Infarcts

They produce a contralateral hemiparesis with predominant faciobrachial deficit, hemisensory loss, gaze deviation towards the lesion or decreased visual exploration toward the opposite side. Left-sided infarcts also produce a non-fluent aphasia, ranging from mutism to typical Broca's aphasia and to articulatory, syntactical and naming difficulties. Buccofacial apraxia is very common. Neglect with anosognosia is an inconstant finding in right hemispheric strokes.

14.2.1.4 MCA Posterior or Inferior Division Infarcts

Motor deficits are absent, transient or mild. Hemisensory loss is more common and visual field defects (homonymous hemianopia or upper quadrantanopia) are usually present. In left-sided strokes, fluent aphasia of variable severity dominates the clinical picture. In the more severe form it is a Wernicke's aphasia with anosognosia and behavioral disturbances including persecutory delusions. In right hemispheric stroke, neglect, anosognosia and an agitated confusional state usually occur. Constructional apraxia can be demonstrated.

14.2.1.5 Cortical Branch Syndromes

These infarcts can occur isolated or in combination.

Infarcts in the distribution of the orbitofrontal and prefrontal arteries can produce a frontal syndrome. Left prefrontal infarcts can result in transcortical aphasia, while right prefrontal infarcts can produce motor neglect.

Precentral artery territory infarcts result in a hemiparesis with predominant proximal arm involvement. In left sided strokes, non-fluent aphasia, usually transcortical motor aphasia, apraxia and agraphia are present, while in right sided strokes, neglect and motor impersistence can be found.

Central sulcus or rolandic artery territory infarcts produce contralateral motor and sensory defects with face and arm predominance when the occlusion is proximal. If the occlusion is distal, motor deficit may be restricted to the arm or distal upper extremity. Cheiro-oral sensory loss may result from predominant involvement of the post central gyrus. Mild Broca's aphasia (left sided strokes) combined with dysarthria and transient tongue, palatal and pharyngeal as well as faciobrachial weakness are a typical pattern of a central sulcus artery territory infarct. Bilateral central sulcus infarcts cause the cortical form of the anterior opercular syndrome (Foix-Chavany-Marie), with bilateral voluntary paresis of the facial, masticatory, lingual and pharyngeal muscles, featuring bilateral lower facial weakness, anarthria or severe dysarthria and dysphagia.

There are three parietal MCA branches: anterior, angular and posterior. Anterior parietal or postcentral sulcus artery infarct causes a contralateral sensory loss, with upper limb predominance (pseudothalamic syndrome) with involvement of the touch, pain, temperature and vibration senses. Pain and hyperpathia and parietal ataxia can also be present. Conduction aphasia, which is a fluent form of aphasia with disproportionate impairment of repetition, anomia, agraphia and apraxia are present in left hemispheric infarcts while neglect follows in right hemispheric ones.

Posterior parietal artery territory infarcts are rare and usually occur in combination with angular gyrus territory artery infarcts. These infarcts cause lower quadrantanopia, cortical sensation dysfunction with astereognosia and impairment of position sense, two-point discrimination and graphesthesia, but with sparing of light touch, vibration, pain and temperature senses. On the left side, fluent aphasia with alexia, Gerstmann's syndrome (agraphia, acalculia, digitoagnosia and left–right disorientation) and ideomotor apraxia occur, while on the right, neglect and constructional apraxia result. If the upper parietal lobe is involved the patient shows elements of Balint's syndrome, including disturbance in manual reaching (optic or visuo-motor ataxia), visual attention and

"psychic paralysis of gaze", as they have difficulty in directing their gaze towards targets of interest and lose fixation easily.

There are usually five temporal branches of the MCA. Temporal MCA infarcts are often combined with lower posterior parietal infarcts. They cause upper quadrantanopia. Vertigo has occasionally been reported in association with superior temporal or insular infarcts. On the left side, the clinical picture is dominated by Wernicke's aphasia. On the right, limited infarcts can be pauci-symptomatic. Extended infarcts cause amusia, neglect, acute agitation and confusion and sometimes delusions and manic symptoms.

14.2.2 Subcortical Hemispheric Infarcts

These include infarcts in the territory of: (1) the deep perforators of the MCA, anterior cerebral artery (ACA) and posterior cerebral artery (PCA), posterior communicating artery (PcomA), the lenticulostriate arteries and the anterior choroidal artery; (2) the superficial perforators (white matter medullary branches) of the superficial pial arteries; (3) borderzone or junctional infarcts between 1 and 2; (4) combined infarcts. Small (< 1.5 mm infarcts – lacunes) are usually caused by single perforator disease while larger infarcts have a more diverse pathophysiology including embolism and MCA stenosis (Bang et al. 2002).

MCA stenosis causes subcortical stroke either by occlusion of a single penetrating artery to produce a small lacunar infarct or by artery to artery embolism with impaired clearance of emboli that produces multiple small cerebral infarcts, mainly in borderzone regions (Wong et al. 2002).

Large striato-capsular infarcts produce a clinical picture similar to that of pial infarcts overlying their territory, including non-fluent aphasia and neglect. These cortical signs may be due to cortical diaschisis, cortical hypoperfusion or scattered cortical lesions not apparent on CT. These additional lesions may be evident on MR, in particular in DWI (Singer et al. 1998). In the MCA territory, the most common combination is a deep small striato-capsular infarct and a distal small cortical infarct. In large subcortical infarcts, cortical perfusion defects are apparent on MR perfusion imaging (PI) (Gerraty et al. 2002), while they are not detected in single perforator infarcts (lacunes). However, patients with lacunes can have subsidiary cortical lesions in DWI.

Subcortical white matter infarcts may mimic a superficial MCA infarct causing a partial anterior circulation syndrome or present as a lacunar syndrome (pure motor, ataxic hemiparesis or sensori motor stroke). Superficial perforating artery infarcts (medullary branches) are often accompanied by cortical spotty lesions. Borderzone and white matter medullary branches infarctions are usually caused by hypoperfusion due lo large vessel occlusion or stenosis (Bogousslavsky 1993; Donnan and Yasaka 1998), but white matter medullary branches infarction can also be caused by cardioembolism (Lee et al. 2003).

14.2.2.1 Anterior Choroidal Artery Infarcts

Aphasia and neglect can be found following respectively dominant and non-dominant anterior choroidal artery infarcts. Anterior choroidal artery infarcts usually cause the classical 3H syndrome: hemiparesis, hemihypesthesia, hemianopia. Pure motor hemiparesis and isolated hemianopia can also occur (Han et al. 2000). Anterior choroidal artery territory infarcts are rarely caused by small vessel occlusion. In general they are caused by cardioembolism or large artery disease with occlusion or artery-to-artery embolism (Leys et al. 1994).

Recently, using color-coded diffusion tensor imaging five different patterns of corticospinal tract stroke were identified that fall into two clinical subgroups with either little recovery or good recovery. Patients with poor motor recovery had lesions centered in the pyramidal tract (anterior choroidal artery). Patients with good recovery had either very small lesions or lesions located anteriorly or medially (Lie et al. 2004).

14.2.2.2 Thalamic Infarcts

There are four main types of large thalamic infarcts: (1) Tuberothalamic (anterior or polar), in the territory of the tuberothalamic artery that arises from the posterior communicating artery; (2) Paramedian (thalamoperforate or posterior thalamic-subthalamic), in the territory of the paramedian artery that originates from the P1 segment of the PCA (Fig. 14.1); (3) Inferolateral (thalamogeniculate), in the territory of the inferolateral artery that originates from the P2 segment of the PCA; (4) Posterior

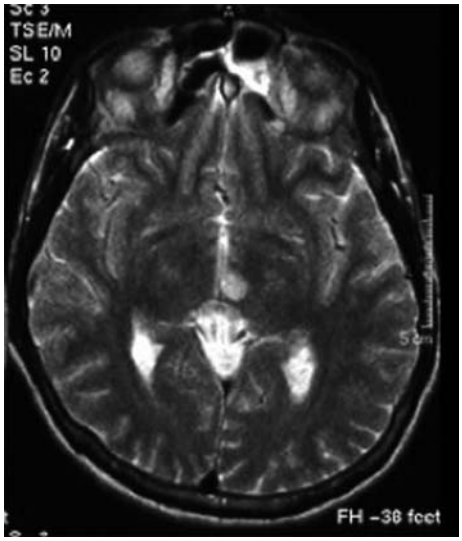

Fig. 14.1. Left paramedian thalamic infarct

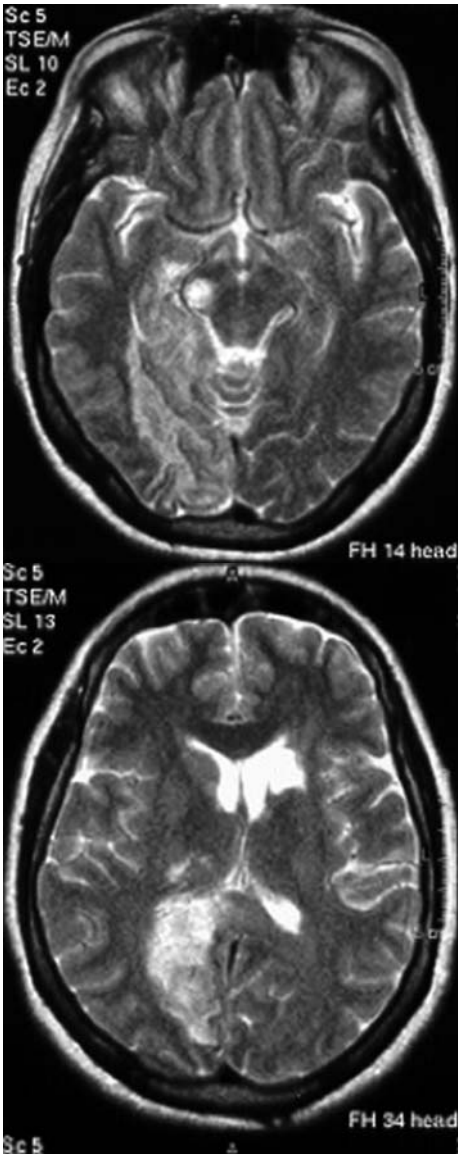

Fig. 14.2. Complete right posterior cerebral artery (PCA) territorial infarct. Notice the anterolateral mesencephalic and the inferolateral thalamic infarcts. Old left striatocapsular infarct

(posterior choroidal artery) which arises from the P2 segment of PCA (Bogousslavsky et al. 1988; Schmahmann 2003). Sometimes two territories are involved simultaneously. Bilateral infarcts, in particular tuberothalamic or paramedian, are not infrequent. They may be due to simultaneous emboli to a common unilateral origin of the arterial branches supplying the anterior and the paramedian thalamus. The four major topographical patterns of bilateral thalamic infarcts are: bilateral paramedian, bilateral inferolateral, combined unilateral paramedian and inferolateral and combined unilateral tuberothalamic and inferolateral. Panthalamic infarcts, involving the four arterial territories of the thalamus are exceptional. Occlusion of the PCA in the absence of an ipsilateral posterior communicating artery may explain this unusual type of arterial infarct (Studer et al. 2003).

Inferolateral or thalamogeniculate infarcts usually present as a hemisensory loss with pain or dysesthesia, plus hemiataxia (Melo et al. 1992) [hemiataxia-hypesthesia (Melo and Bogousslavsky 1992), hypesthetic ataxic hemiparesis and ataxic hemiparesis] and involuntary movements (chorea or dystonia). Tuberothalamic infarcts usually cause drowsiness, apathy, executive deficits, personality changes, amnesia and aphasia or neglect (depending on the involved side). In paramedian infarcts drowsiness is prominent. Impaired memory and learning, altered social skills and personality are also apparent. Oculomotor troubles may be present (Bogousslavsky and Caplan 1993; Bogousslavsky et al. 1988). Posterior choroidal artery infarcts result in visual field defects, variable sensory loss, hemiparesis, dystonia, hand tremor and occasionally amnesia and aphasia. Visual field defects, commonly quadrantanopia or hemianopia, are found if the lateral posterior choroidal arteries branches are involved in isolation. Unusual field defects such as homonymous horizontal sectoranopia or wedge shaped homonymous hemianopia, may also be found and may be explained by the dual blood supply to the lateral geniculate body by

the lateral posterior choroidal arteries and the anterior choroidal artery (Saeki et al. 1999). Bilateral thalamic infarcts cause a typical and devastating clinical picture of drowsiness, amnesia, abulia and vertical eye movement disorders. The neuropsychological and psychic changes tend to be permanent, causing a strategic infarct vascular dementia syndrome (Kumral et al. 2001).

14.2.3 Posterior Cerebral Artery (PCA) Infarcts

The predominant clinical findings of PCA infarcts are hemianopia or other visual field defects. Headache is rather frequent, in general unilateral and may be severe. PCA infarcts can be superficial (cortical) (Cals et al. 2002) or combined with lateral thalamic or rostral mesencephalic infarcts (Fig. 14.2). The thalamic infarct produces a sensory defect in variable combination with ataxia or involuntary movements. The midbrain lesion is usually limited and responsible for a transient motor deficit. More extensive midbrain lesions will produce vigilance and oculomotor troubles. Sensory abnormalities in PCA stroke are associated with ventrolateral thalamic infarcts in the thalamogeniculate or lateral posterior choroidal arteries or less frequently to ischemia to the white matter tracts to the somatosensory motor cortex (Georgiadis et al. 1999). The presence of hemiparesis in PCA infarcts can make the clinical differential diagnosis with MCA infarcts difficult. Hemiparesis can be due, as mentioned above, to the infarction of the cerebral peduncle and less frequently to infarction of the anterior segment of the posterior limb of the internal capsule, due to impaired perfusion in the distribution of the inferolateral thalamic branches of the PCA, which can include that part of the internal capsule (Montavont et al. 2003). The inferior striate cortex is more susceptible to ischemia due to poor collateral circulation. Therefore superior quadrantanopia is more common than inferior one. Neuropsychological manifestations are common and, when the dominant (usually left) hemisphere is damaged, include: (1) transcortical sensory aphasia or anomic aphasia, (2) alexia with or without agraphia; the lesion producing alexia without agraphia combines damage to the left calcarine cortex and to splenium of the corpus callosum or to the outflow of the callosum originating from the right visual cortex, (3) visual or color agnosia; infarcts causing persistent associative visual agnosia are usually large and involve the parahippocampal and fusiform gyrus. On the non-dominant side neglect, prosopagnosia (often transient) and topographical amnesia can be found. On either side visual perseverations, visual illusions or hallucinations and agitation can occur. Declarative memory defects, concerning verbal (left sided infarcts), visual (right sided infarcts) material or both are usually present. Such infarcts usually involve the hippocampus. Bilateral occipitotemporal infarcts can cause cortical blindness without or with anosognosia (Anton's syndrome), associative or apperceptive visual agnosia and severe memory defect (Brandt et al. 2000; Cals et al. 2002). PCA infarcts are due to cardiac embolism in about 1/3 of patients. Significant vertebrobasilar atheroma with occlusion or artery-to-artery embolism accounts for additional 25%. Local PCA stenosis or occlusions are much less frequent. In many PCA infarcts, embolism is suspected but cannot be confirmed and the cause remains undetermined. Complete infarction of the posterior branches of the PCA and hemorrhagic transformation are more frequent in cardioembolic strokes (Steinke et al. 1997). Migraine account for a few cases (migrainous infarcts). MELAS stroke-like events are predominantly located in the occipital lobes, but do not respect the territorial borders of PCA distribution. Anatomical variations may predispose to PCA infarct. Exclusive supply of the PCA territory via the carotid system; a patent posterior communicating artery with anteroposterior flow are less common in patients with PCA infarcts than in controls (Jongen et al. 2004).

14.2.4 Anterior Cerebral Artery (ACA) Infarcts

Strokes in the ACA territory are uncommon (< 2% in stroke registries). Left sided infarcts cause mutism, transcortical motor aphasia, hemiparesis and occasionally left arm apraxia and other callosal disconnection syndromes. Right-sided infarcts cause acute confusional state, hemiparesis and motor neglect (Kumral et al. 2002d). Hemiparesis predominates in the lower limb when the precentral gyrus is involved. If the infarction extends more posteriorly sensory loss in the leg can be found. In some cases the paresis may be proportional and the ACA stroke pattern will be indistinguishable from an MCA pattern. Proportional hemiparesis occurs when there is occlusion of the recurrent artery of Heubner that supplies the internal capsule. Abulia can be present with unilateral or bilateral infarcts that involve the

cingulum and the supplementary motor area. Bilateral infarcts may produce akinetic mutism (Wolff et al. 2002), gait apraxia (Della Sala et al. 2002), paraparesis and sphincter dysfunction and carry a bad prognosis for functional recovery (Fig. 14.3). Grasp reflex, utilization behavior (Boccardi et al. 2002) and executive deficits may be more or less prominent. Hand grasping correlates with orbitofrontal lesions. An expanding ACA infarct was recently reported (Ay et al. 2002).

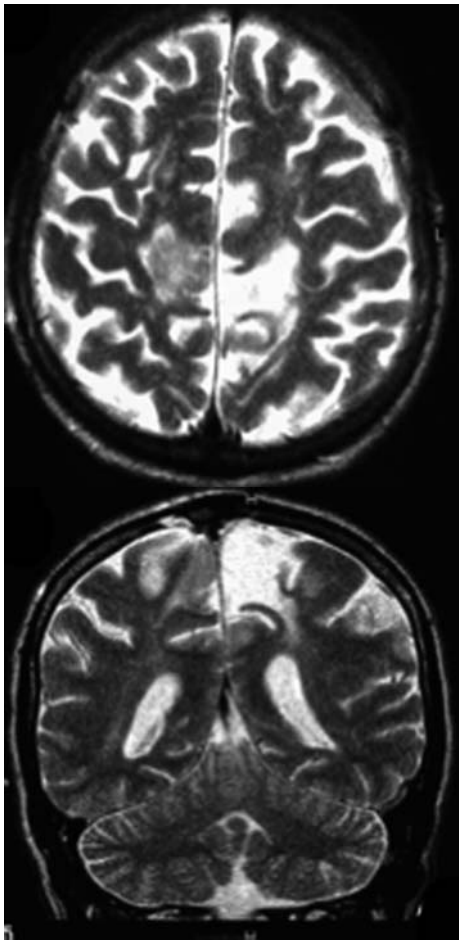

Fig. 14.3. Bilateral (acute and non-recent) anterior cerebral artery infarcts causing paraparesis

14.2.5 Combined Hemispheric Infarcts

Combined ACA-MCA infarcts can result from embolic occlusion of the distal ICA (carotid T). Combined MCA-PCA infarcts may be due to simultaneous embolism to the two territories, to a fetal (internal carotid) origin of the PCA or to compression of the PCA by a herniating hemisphere at the edge of the tentorial foramen.

These combined infarcts, as well as massive MCA infarcts, are often complicated within 24 to 96 h from onset by edema which will produce mass effect. In young and middle-aged patients, this may cause clinical deterioration and death due to brain stem compression (malignant MCA infarct). Predictors of fatal brain edema include > 50% MCA hypodensity, involvement of additional vascular territories (ACA; PCA; anterior choroidal artery), hypertension and heart failure and increased white blood cell count (Kasner et al. 2001). Such patients are candidates to aggressive live saving treatments such as decompressive hemicraniectomy and hypothermia.

14.2.6 Brain Stem Infarcts

14.2.6.1 Mesencephalic Infarcts

The mesencephalon has four arterial territories: anteromedial (paramedian branches of the basilar artery; anterolateral (branches from the P2 segment of the PCA); lateral (branches from P2 segment of PCA and from posterior choroidal arteries) and dorsal (branches from P1 segment of PCA and superior cerebellar artery). Isolated mesencephalic infarcts are rare because the arteries supplying blood to the mesencephalon (basilar artery, posterior cerebral artery and superior cerebellar artery) also serve other infratentorial and supratentorial anatomical sites (Fig. 14.4). Midbrain infarcts are more likely to be accompanied by infarcts in other structures than to occur alone (Martin et al. 1998; Kumral et al. 2002b). Patients with mesencephalic infarcts can be classified into four groups: (1) those with isolated mesencephalic infarcts, and those whose mesencephalic infarct is accompanied by (2) proximal infarcts involving the medulla and the posterior inferior cerebellar artery (PICA) territory (Kumral et al. 2002a), by (3) "middle" infarcts including the pons and the anterior inferior cerebellar artery (AICA), and by (4) distal lesions comprising the thalamus and the PCA territory (Martin et al. 1998). "Middle" infarcts are the most common. Patients with isolated mesencephalic infarcts have a combination of unsteadiness/dizziness, diplopia due to ipsilesional 3rd cranial nerve palsy, vertical gaze palsy, contralateral or four-limb ataxia, hemiparesis

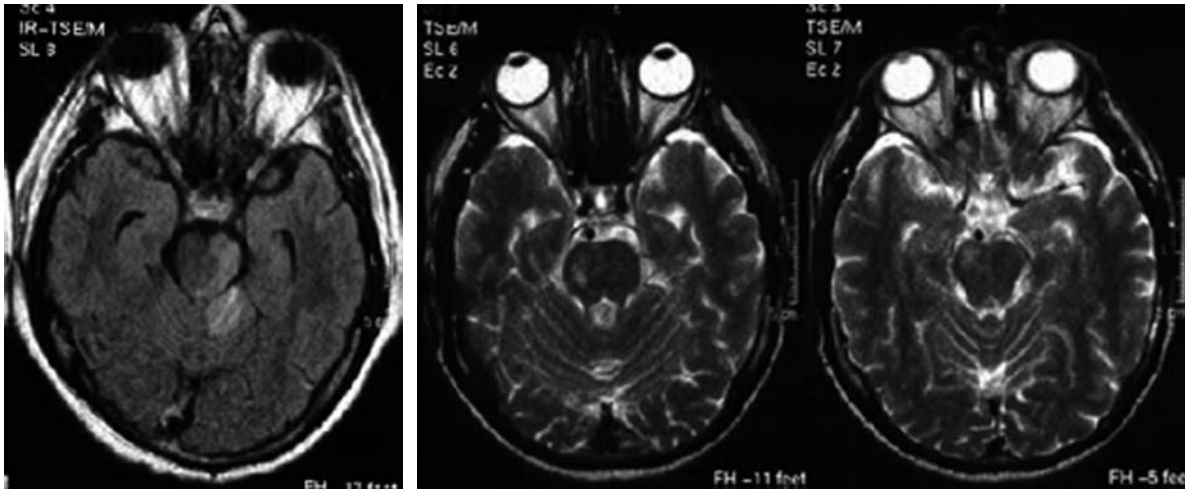

Fig. 14.4. Mesencephalic infarcts: anterolateral (*right*); extensive combined anteromedial and anterolateral involving also the vermis (*left*)

or hypesthetic ataxic hemiparesis or a combination of both and involuntary movements (tremor and chorea-like). Patients with isolated upper or lower midbrain infarcts have no localizing clinical findings, but patients with middle midbrain infarcts had a localizing clinical picture mainly with III nerve palsies that often occur in isolation (Bogousslavsky et al. 1994). The palsy of the 3rd cranial nerve can be nuclear or fascicular. A unilateral 3rd cranial nerve nuclear lesion causes bilateral ptosis and superior rectus weakness, divergent strabismus and mydriasis. In fascicular lesions there is unilateral findings with divergent strabismus, unilateral ptosis and mydriasis. The classic clinical picture of Claude's syndrome (ipsilesional 3rd cranial nerve palsy and contralateral ataxia) or Benedikt's syndrome (3rd cranial nerve palsy plus contralateral involuntary movements) are very rare. "Distal" mesencephalic infarcts are associated with disturbances of consciousness, gait ataxia, oculomotor disturbances and visual field defects. "Middle" strokes have disturbances of consciousness, dysarthria, horizontal oculomotor disorders and paresis, while "proximal" infarcts produce acute unsteadiness, vertigo, dysphagia, dysphonia, limb ataxia and paresis. Patients with mesencephalic infarcts can present involuntary repetitive stereotyped movements that may be confused with seizures (Saposnik and Caplan 2001; Lee et al. 2002). About 25% of midbrain strokes are bilateral (Kumral et al. 2002b). Such bilateral infarcts have a poorer outcome than unilateral infarcts. Large artery disease, producing artery-to-artery embolism or in situ thrombosis are the most common mesencephalic infarct mechanisms. Cardioembolism and small vessel disease account for 25% of the cases each.

14.2.6.2 Pontine Infarcts

Pontine infarcts (Kumral et al. 2002c) can have five main clinical patterns: anteromedial, anterolateral, tegmental, unilateral multiple and bilateral. (Fig. 14.5). The anteromedial and anterolateral territories are supplied from the basilar artery, while the lateral territory also receives blood from the superior and anterior inferior cerebellar arteries. The small posterior territory is supplied by the superior cerebellar artery. The most frequent syndrome is the anteromedial pontine syndrome presenting with motor deficit with dysarthria, ataxia plus mild tegmental symptoms in 1/3 of the patients. The second most common is the anterolateral pontine syndrome, featuring motor-sensory deficits associated with tegmental signs in more than half of the patients. Tegmental pontine syndromes (mild motor and sensory deficits together with eye movement and vestibular symptoms/signs) are less common. Unilateral multiple pontine infarcts are always associated with severe sensorimotor deficits and tegmental signs. Bilateral infarcts cause an ominous clinical pattern of transient loss of consciousness, tetraparesis, pseudobulbar palsy and, in some cases, locked-in syndrome. The main stroke mechanisms of pontine infarcts are basilar artery branch and

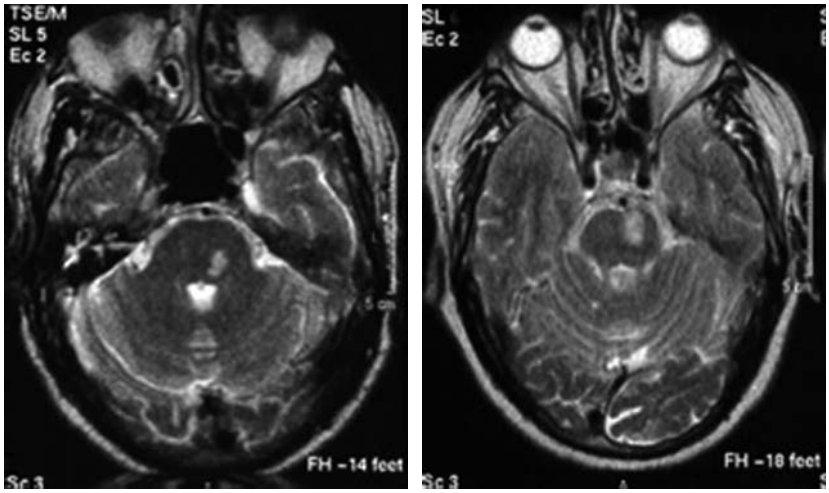

Fig. 14.5. Pontine infarcts: anteromedial (*right*) and tegmental (*left*)

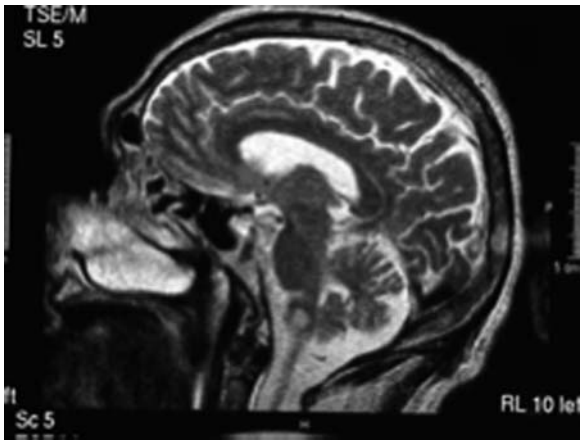

Fig. 14.6. Lateral medullary infarct causing a Wallenberg's syndrome

small artery disease occlusions (Kumral et al. 2002a).

14.2.6.3 Medullary Infarcts

Medullary infarcts can be medial, lateral or combined (Fig. 14.6). The medial territory is supplied by penetrating vessels from the anterior spinal artery and the distal vertebral artery. The lateral territory main arterial supply comes from penetrating arteries from the distal vertebral artery and the posterior inferior cerebellar artery. The small posterior territory is supplied by the posterior spinal artery and the posterior inferior cerebellar artery. Medial medullary infarcts have four major clinical patterns: (1) Dejerine's syndrome (contralateral hemiparesis and pain/thermal sensory loss plus ipsilateral lingual palsy, (2) sensorimotor stroke without lingual palsy, (3) hemiparesis, often combined with nystagmus, (4) bilateral syndromes. Lateral infarcts produce a more or less complete Wallenberg's syndrome: ipsilateral paralysis of the 9^{th} and 10^{th} cranial nerves, loss of pain and temperature sense on the face, ataxia, vestibular signs (nystagmus, ipsilesional lateropulsion) and Horner's syndrome, and contralateral dissociated hemianesthesia. Nausea and vomiting, hiccups and headache are frequent. Diplopia and oscillopsia are common complaints. Medial medullary infarcts are often accompanied by a cerebellar infarct. The most common mechanisms are vertebral artery thrombosis or dissection, and embolism. Combined (hemi-medullary) infarcts cause a Babinski-Nageotte syndrome (all the components of the Wallenberg syndrome plus ipsilateral tongue palsy and contralateral hemiplegia). They are usually secondary to occlusion of the vertebral artery.

14.2.6.4 Stroke Patterns in Basilar Artery Occlusion

The most feared vertebrobasilar stroke is occlusion of the basilar artery. Patients with lesions in the basilar artery are five times more likely to have a poor outcome independent of other factors (Glass et al. 2002). The importance of its early recognition is the possibility of performing intra-arterial throm-

bolysis. Basilar artery thrombosis may present as a locked-in syndrome, as a midbrain syndrome, a top-of-the-basilar syndrome or as partial syndromes. Basilar artery occlusion can have a sudden onset without warning signs, causing within minutes a dramatic and disabling neurological picture. More often it has a subacute onset with heralding TIAs or a progressive course with worsening or additive neurological deficits. The final neurological picture is reached within 6 h in about 1/3 of the patients, in 6–24 h in another 1/3 and up to 72 h in the remaining. The most common initial symptoms are motor weakness, dysarthria, vertigo, nausea/vomiting, and headache. The most common initial signs are motor deficits, facial palsies, eye movement abnormalities, lower cranial nerve deficits, altered level of consciousness and bilateral extensor plantar responses (von Campe et al. 2003). The prognosis of basilar artery occlusion is diverse. The outcome is invariably poor in patients with disorders of consciousness or a combination of dysarthria, pupillary disorders and involvement of the lower cranial nerves, while if these factors are absent only 11% have a poor outcome (Devuyst et al. 2002). The typical syndrome of basilar artery embolism (Schwarz et al. 1997) is an acute loss of consciousness followed by multiple brainstem symptoms and infarcts at several levels (thalamus, PCA, midbrain, pons). Usually, clinical symptoms improve quickly and even completely. Outcome correlates with the intensity of consciousness disorder and the number of infarcts.

14.2.7 Cerebellar Infarcts

Cerebellar infarcts can be grouped in territorial (superior cerebellar artery, anterior inferior cerebellar artery, posterior inferior cerebellar artery and combined), borderzone and lacunar. They are often combined with brain stem infarcts and with superficial posterior cerebral artery or thalamic infarcts. The most common isolated cerebellar infarcts are located in the superior cerebellar artery and posterior inferior cerebellar artery territories (Amarenco 1993; Amarenco et al. 1993, 1994).

14.2.7.1 Superior Cerebellar Artery (SCA)

The SCA territory has two divisions: lateral and medial. Full SCA infarcts are usually accompanied by PCA or brainstem infarcts. They can be edematous and have a malignant course. Partial infarcts are often pure cerebellar infarcts and have a benign course. Both are usually cardioembolic. Their clinical presentation ranges from severe, dramatic patterns such as coma with tetraplegia and oculomotor disturbances due to simultaneous brain stem infarct, or top-of-the-basilar syndrome with concomitant involvement of the mesencephalon and PCA territories, to more limited and benign presentations. The classical Mills-Guillain syndrome (ipsilateral cerebellar ataxia and Horner's syndrome and contralateral pain/temperature sensory loss and 4th cranial nerve palsy) is rare and in fact due to concomitant involvement of the pontine territory of the SCA. Tremor and other involuntary movements can be present and are due to ischemia of the superior cerebellar peduncle. Other patients have only a cerebello-vestibular syndrome. Dysarthria is almost always present. Lateral SCA infarcts involve the anterior rostral cerebellum and cause ipsilateral limb ataxia and lateropulsion and dysarthria. Medial SCA infarcts are less well described and cause ataxia and dysarthria.

14.2.7.2 Anterior Inferior Cerebellar Artery (AICA)

Symptoms of AICA territory infarct are related to damage to the inferolateral pons, the middle cerebellar peduncle and the flocculus. AICA infarcts are small and less frequent than the other cerebellar territorial infarcts. They almost always have a concomitant pontine infarct and their main cause is basilar artery occlusion, hence the importance of their recognition. Their clinical presentation has four major patterns: (1) coma with tetraplegia due to pontine infarct, (2) the classic AICA syndrome, which is the most frequent presenting pattern featuring ipsilateral involvement of the 5th, 7th and 8th cranial nerves with vertigo, vomiting, tinnitus, facial palsy and facial sensory loss, Horner's syndrome and appendicular ataxia and contralateral temperature/pain sensory loss, (3) pure vestibular syndrome, including exceedingly rare cases of isolated vertigo, and (4) isolated cerebellar signs.

14.2.7.3 Posterior Inferior Cerebellar Artery (PICA)

The classic clinical pattern of PICA territorial infarct is the Wallenberg's syndrome. However, symptoms

and signs in Wallenberg's syndrome are due to the lateral medullary infarct, which can also be due to occlusion of branches arising directly from the vertebral artery. The clinical pattern of PICA infarcts is therefore dependent on whether or not the medulla is also involved. Infarcts restricted to the cerebellum are in general small and have a benign course. They can involve the medial and less often the lateral PICA subterritories. PICA infarcts combined with AICA or SCA can assume a pseudotumoral form or present as coma with tetraplegia. If the medulla is involved, a more or less complete dorsal lateral medullary syndrome results: ipsilesional vestibular (vertigo, vomiting, nystagmus, lateropulsion), 5th, 9th, 10th cranial nerve palsies, Horner's syndrome and appendicular ataxia with contralesional loss of pain and temperature sensation. Hiccups are frequent and prolonged. If the medulla is spared, patients present with headache, vertigo, nystagmus, ipsilateral axial lateropulsion, gait and appendicular ataxia. There are a few reported cases of infarcts involving the nodulus and causing an isolated acute vertigo mimicking a vestibular disease. Medial PICA infarcts have a triangular shape on the dorsomedial rostral cerebellum with a ventral top pointing towards the 4th ventricle. They can produce: isolate vertigo; vertigo, axial lateropulsion and dysmetria; Wallenberg's syndrome, if the medulla is also involved. Lateral PICA infarcts are very rare and present with vertigo and ipsilateral dysmetria.

14.2.7.4 Pseudotumoral Cerebellar Infarcts

Some large cerebellar infarcts can produce mass effect and lead to clinical deterioration and eventual death. These patients usually have combined territorial cerebellar infarcts, a full territorial PICA or SCA infarct, or infarcts confined to the medial vermian branches of the PICA or SCA. Isolated lateral hemispheric branches of the PICA or SCA and infarcts confined to the AICA territory do not produce clinically relevant mass effect. Pseudotumoral cerebellar infarcts are usually large (> 1/3 of the cerebellar hemisphere). The most frequent mechanisms of infarction are large vessel occlusion due to large artery disease or cardioembolism with reperfusion. Such patients progress from a cerebellar syndrome to a stage where brain stem signs develop and the level of consciousness fluctuates. If untreated, the patient will progress to coma. These infarcts with mass effect cause increased intracranial pressure in the posterior fossa with compression of the basal cisterns and brain stem, hydrocephalus and/or downward or more rarely upward herniation. Clinical deterioration may start hours or days after stroke onset. Decompressive surgery is life-saving (Amarenco 1991; Hornig et al. 1994; Rieke et al. 1993; van Horn and Hawes 1982; Koh et al. 2000).

14.2.8 Acute Multiple Brain Infarcts (AMBI)

DWI revealed that acute multiple infarcts were much more frequent than expected clinically or on CT (Altieri et al. 1999). In the vertebro-basilar circulation the commonest form of acute multiple infarcts is the top-of-the basilar syndrome due to embolism of the junction of the basilar and the PCA producing occipital, thalamic and midbrain (or midbrain-superior cerebellar) lesions. Multi-level vertebro-basilar strokes can be related to cardioembolism or artery-to-artery embolism. Multiple, bilateral infarcts strongly suggest cardioembolism and are occasionally the herald of infective endocarditis (Timsit et al. 1992). Unilateral combined MCA-PCA or MCA-ACA infarcts are more often due to internal carotid artery (ICA) occlusion or embolism. Certain clinical syndromes are suggestive of simultaneous double ipsilateral infarction secondary to ICA occlusion: ipsilateral ocular ischemia (retinal or anterior) plus ipsilateral hemispheric infarct (optocerebral syndrome); hemiplegia-hemianopia syndrome and conduction aphasia with hemiparesis, due to combined anterior or deep MCA plus posterior MCA affection; mixed transcortical aphasia (isolation of the speech areas) results from the combination of anterior and posterior borderzone infarcts. Acute global aphasia without hemiparesis results from embolism to the anterior and posterior speech areas. Acute anarthria and pseudobulbar syndrome can be secondary to bi-opercular infarcts related to bilateral ICA occlusion (Kumral 2001).

Different topographical patterns of AMBI are associated with different vascular pathologies. Hemorheologic abnormalities or vascular anatomic variations may be contributing factors of AMBI in both hemispheres or in both the anterior and the posterior circulation (Roh et al. 2000). A scattered lesion pattern on DWI in patients with an initial negative CT is indicative of an arterial or embolic source and associated with favorable clinical outcome (Koennecke et al. 2001). Occlusion of the

internal carotid artery produces mainly multiple infarcts with three distinctive patterns: (1) territorial, either multiple cortical, cortical and deep or single, (2) borderzone, alone or in combination with a territorial infarct (Fig. 14.7), (3) bilateral lesions (Kang et al. 2003).

14.3 Cardioembolic Infarcts

Decreased consciousness at onset, sudden onset to maximal defect, rapid regression of symptoms, aphasia, neglect and visual field defects are more common in cardioembolic than other types of stroke, Headache, seizure at onset or onset during activity are not specific for cardioembolic stroke (Arboix et al. 1999; Kittner et al. 1992; Minematsu et al. 1992; Ramirez-Lassepas et al. 1987; Timsit et al. 1992). Stroke syndromes such as isolated Wernicke's aphasia, global aphasia without hemiparesis, Wallenberg's syndrome and top-of-the-basilar syndrome are suggestive of cardioembolism.

Simultaneous or sequential strokes in different arterial territories, multi-level posterior circulation infarcts, simultaneous infarcts in the three subterritories (superficial anterior, superficial posterior and deep) of the MCA, and hemorrhagic transformation of an ischemic infarct also point to a cardiac origin of the stroke (Arquizan et al. 1997; Ay et al. 1999; Ferro 2003a,b). Occlusion of the carotid artery by a mobile thrombus, early recanalization of an occluded vessel and the identification of microembolism in both MCAs are all highly indicative of a cardiac source of emboli.

DWI can demonstrate scattered lesions in acute stroke patients with initial negative CT (Koennecke et al. 2001) associated with an embolic etiology. In patients presenting with classical lacunar syndromes, DWI can demonstrate lesions not apparent in CT or conventional MR in addition to the lesion in the territory of a single perforator. The most common associated lesions are punctuate subsidiary lesions in the territory of the leptomeningeal arteries (Ay et al. 1990).

Multiple scattered cerebral infarcts can be demonstrated by DWI in highly emboligenic conditions

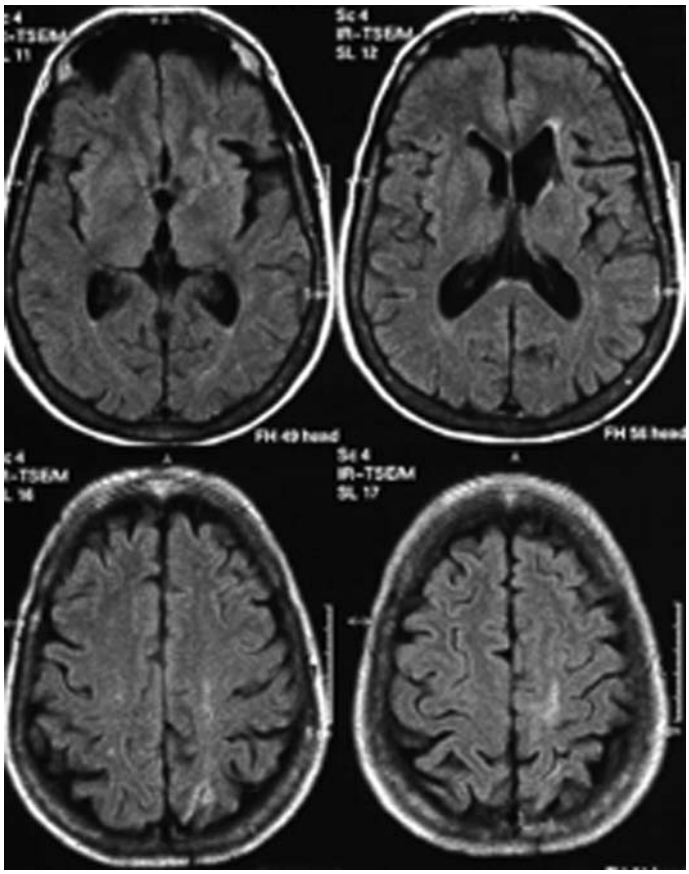

Fig. 14.7. Combined junctional and cortical infarcts in a case of carotid occlusion

such as endocarditis (Singhal et al. 2002) and cardiac surgery, and cause both focal syndromes and diffuse encephalopathy which are often found in such conditions (Wityk et al. 2001).

14.3.1 Infarcts with Hemorrhagic Transformation

About 40% of ischemic infarcts show hemorrhagic transformation on CT; this proportion is even higher on MRI (Egelhof et al. 1998). Cardioembolism accounts for the vast majority of infarcts with hemorrhagic transformation. TACIs, patients who are not fully alert, severe strokes (NIHSS > 14 points), proximal occlusion and delayed recanalization (> 6 h) predict hemorrhagic transformation. Hypodensity on CT > 1/3 of MCA territory and diabetes are associated with an increased risk of hemorrhagic transformation after thrombolysis (Alexandrov et al. 1997; de Freitas et al. 2001; Ferro 2003a,b; Fisher and Adams 1951; Jörgensen and Torvic 1969; Molina et al. 2001; Moulin et al. 2000; Nighoghossian et al. 2002). In MR imaging, ischemic brain regions destined to hemorrhagic transformation have lower apparent diffusion coefficient values and persistently delayed perfusion compared to regions which will not suffer hemorrhagic transformation (Tong et al. 2000, 2001; Selim et al. 2002). Old microbleeds detected by T2*-weighted sequences, indicating severe microangiopathy or amyloid angiopathy (Fig. 13.5, Chap. 13), are also a marker for hemorrhagic transformation in particular after thrombolytic therapy. Gadolinium enhancement patterns (vascular, meningeal and parenchymal) are also predictors of hemorrhagic transformation. Vascular enhancement defined as tubular enhancing vessels located in the sulci supplying the ischemic territory, is the most common pattern (Vo et al. 2003).

References

Albers GW, Lansberg MG, Norbash AM et al (2000) Yield of diffusion-weighted MRI for detection of potentially relevant findings in stroke patients. Neurology 54:1562–1567

Alexandrov AV, Black SE, Ehrlich LE et al (1997) Predictors of hemorrhagic transformation occurring spontaneously and on anticoagulants in patients with acute ischemic stroke. Stroke 28:1198–1202

Altieri M, Metz RJ, Muller C et al (1999) Multiple brain infarcts: clinical and neuroimaging patterns using diffusion-weighted magnetic resonance. Eur Neurol 42:76–82

Amarenco P (1991) The spectrum of cerebellar infarctions. Neurology 41:973–979

Amarenco P (1993) Les infarctus du cervelet et leurs mécanismes. Rev Neurol (Paris) 149:728–748

Amarenco P, Rosengart A, de Witt LD et al (1993) Anterior inferior cerebellar artery territory infarcts: mechanisms and clinical features. Arch Neurol 50:154–161

Amarenco P, Lévy C, Cohen A et al (1994) Causes and mechanisms of territorial and nonterritorial cerebellar infarcts in 115 consecutive cases. Stroke 25:105–112

Arboix A, Oliveres M, Massons J et al (1999) Early differentiation of cardioembolic from atherothrombotic cerebral infarction: a multivariate analysis. Eur J Neurol 6:677–683

Arquizan C, Lamy C, Mas J-L (1997) Infarctus cérébraux multiples simultanés sus-tentoriels. Rev Neurol (Paris) 153:748–753

Ay H, Oliveira-Filho J, Buonanno FS et al (1999) Diffusion-weighted imaging identifies a subset of lacunar infarction associated with embolic source. Stroke 30:2644–2650

Ay H, Uluc K, Arsava EM et al (2002) Unusually prolonged progressing stroke: an expanding anterior cerebral artery infarction. Cerebrovasc Dis 13:64–66

Bamford J, Sandercock P, Dennis M et al (1991) Classification and natural history of clinically identifiable subtypes of cerebral infarction. Lancet 337:1521–1526

Bang OY, Heo JH, Kim JY et al (2002) Middle cerebral artery stenosis is a major clinical determinant in striatocapsular small, deep infarction. Arch Neurol 59:259–263

Boccardi E, Della Sala S, Motto C et al (2002) Utilisation behaviour consequent to bilateral SMA softening. Cortex 38:289–308

Bogousslavsky J (1993) Subcortical infarcts. In: Fisher M, Bogousslavsky J (eds) Current review of cerebrovascular diasease. Current Medicine, Philadelphia, pp 31–40

Bogousslavsky J, Caplan LR (1993) Vertebrobasilar occlusive disease: review of selected aspects. 3 thalamic infarcts. Cerebrovasc Dis 3:193–205

Bogousslavsky J, Caplan LR (2001) Stroke syndromes, 2nd edn. Cambridge University Press, Cambridge

Bogousslavsky J, Regli F, Uske A (1988) Thalamic infarcts: clinical syndromes, etiology and prognosis. Neurology 38:837–848

Bogousslavsky J, Maeder P, Regli F et al (1994) Pure midbrain infarction: clinical syndromes, MRI, and etiologic patterns. Neurology 44:2032–2040

Brandt T, Steinke W, Thie A et al (2000) Posterior cerebral artery territory infarcts: clinical features, infarct topography, causes and outcome. Multicenter results and a review of the literature. Cerebrovasc Dis 10:170–182

Cals N, Devuyst G, Afsar N et al (2002) Pure superficial posterior cerebral artery territory infarction in The Lausanne Stroke Registry. J Neurol 249:855–861

De Freitas GR, Carruzzo A, Tsiskaridze A et al (2001) Massive haemorrhagic transformation in cardioembolic stroke: the role of arterial wall trauma and dissection. J Neurol Neurosurgery Psychiatry 70:672–674

Della Sala S, Francescani A, Spinnler H (2002) Gait apraxia after bilateral supplementary motor area lesion. J Neurol Neurosurg Psychiatry 72:77–85

Devuyst G, Bogousslavsky J, Meuli R et al (2002) Stroke or transient ischemic attacks with basilar artery stenosis or occlusion: clinical patterns and outcome. Arch Neurol 59:567–573

Donnan GA, Yasaka M (1998) Lacunes and lacunar syndromes. In: Ginsberg MD, Bogousslavsky J (eds) Cerebrovascular diseases. Pathophysiology, diagnosis and management, vol II. Blackwell Science, Massachusetts, pp 1090–1102

Ebrahim S, Harwood R (1999a) Mortality. In: Ebrahim S, Harwood R (eds) Stroke. Epidemiology, evidence and clinical practice. Oxford University Press, Oxford, pp 217–228

Ebrahim S, Harwood R (1999b) Recovery. In: Ebrahim S, Harwood R (eds) Stroke. Epidemiology, evidence and clinical practice. Oxford University Press, Oxford, pp 264–281

Egelhof T, Essig M, von Kummer R, Dörfler A, Winter R, Sartor K (1998) Der acute ischämische Hirninfarkt: eine prospective, serielle Untersuchung mit der Magnetresonanztomographie. Fortschr Röntgenstr 168:222–227

Ferro JM (2003a) Brain embolism - answers to practical questions. J Neurol 250:139–147

Ferro JM (2003b) Cardioembolic stroke: an update. Lancet Neurol 2:177–188

Fisher CM, Adams RD (1951) Observations on brain embolism with special reference to the mechanism of hemorrhagic infarction. J Neuropathol Exp Neurol 10:92–93

Georgiadis AL, Yamamoto Y, Kwan ED et al (1999) Anatomy of sensory findings in patients with posterior cerebral artery territory infarction. Arch Neurol 56:835–838

Gerraty RP, Parsons MW, Barber A et al (2002) Examining the lacunar hypothesis with diffusion and perfusion magnetic resonance imaging. Stroke 33:2019–2024

Glass TA, Nennessey PM, Pazdera L et al (2002) Outcome at 30 days in the New England Medical Center Posterior Circulation Registry. Arch Neurol 59:369–376

Gorelick PB (1996) Atlas of cerebrovascular disease. Current Medicine, Philadelphia

Han SW, Sohn YH, Lee PH et al (2000) Pure homonymous hemianopia due to anterior choroidal artery territory infarction. Eur Neurol 43:35–38

Heinsius T, Bogousslavsky J, van Melle G (1998) Large infarcts in the middle cerebral artery territory. Etiology and outcome patterns. Neurology 50:341–350

Hornig CR, Rust DS, Busse O et al (1994) Space-occupying cerebellar infarction: clinical course and prognosis. Stroke 25:372–374

Jongen JCF, Franke CL, Ramos LMP et al (2004) Direction of flow in posterior communicating artery on magnetic resonance angiography in patients with occipital lobe infarcts. Stroke 35:104–108

Jörgensen L, Torvik A (1969) Ischaemic cerebrovascular disease in an autopsy series: part prevalence, location, pathogenesis and clinical course of cerebral infarcts. J Neurol Sci 9:285–320

Kang DW, Chalela JA, Ezzeddine MA et al (2003a) Association of ischemic lesion patterns on early diffusion-weighted imaging with TOAST stroke subtypes. Arch Neurol 60:1730–1734

Kang DW, Chu K, Ko SB et al (2003b) Lesion patterns and mechanism of ischemia in internal carotid artery disease: a diffusion-weighted imaging study. Arch Neurol 59:1577–1582

Kasner SE, Demchuk AM, Berrouschot J et al (2001) Predictors of fatal brain edema in massive hemispheric ischemic stroke. Stroke 32:2117–2123

Kittner SJ, Sharkness CM, Sloan MA et al (1992) Infarcts with a cardiac source of embolism in the NINDS Stroke Data Bank: neurologic examination. Neurology 42:299–302

Koennecke H-C, Bernarding J, Braun J et al (2001) Scattered brain infarct pattern on diffusion-wheighted magnetic resonance imaging in patients with acute ischemic stroke. Cerebrovasc Dis 11:157–163

Koh MG, Phan TG, Atkinson JLD et al (2000) Neuroimaging in deteriorating patients with cerebellar infarcts and mass effect. Stroke 31:2062–2067

Kumral E (2001) Multiple, multilevel and bihemispheric infarcts. In: Bogousslavsky J, Caplan L (eds) Stroke syndromes. Cambridge University Press, Cambridge, pp 499–511

Kumral E, Evyapan D, Balkir K et al (2001) Bilateral thalamic infarction. Clinical, etiological and MRI correlates. Acta Neurol Scand 103:35–42

Kumral E, Afsar N, Kirbas D et al (2002a) Spectrum of medial medullary infarction: clinical and magnetic resonance imaging findings. J Neurol 249:85–93

Kumral E, Bayulkem G, Akyol A et al (2002b) Mesencephalic and associated posterior circulation infarcts. Stroke 33:2224–2231

Kumral E, Bayulkem G, Evyapan D (2002c) Clinical spectrum of pontine infarction clinical-MRI correlations. J Neurol 249:1659–1670

Kumral E, Bayulkem G, Evyapan D et al (2002d) Spectrum of anterior cerebral artery territory infarction: clinical and MRI findings. Eur J Neurol 9:615–624

Lee LJ, Kidwell CS, Alger J et al (2000) Impact on stroke subtype diagnosis of early diffusion-weighted magnetic resonance imaging and magnetic resonance angiography. Stroke 31:1081–1089

Lee MS, Oh SH, Lee KR (2002) Transient repetitive movements of the limbs in patients with acute basilar artery infarction. Neurology 59:1116–1117

Lee PH, Bang OY, Oh SH et al (2003) Subcortical white matter infarcts. Comparison of superficial perforating artery and internal borderzone infarcts using diffusion-weighted magnetic resonance imaging. Stroke 34:2630–2635

Leys D, Mounier-Vehier F, Lavenu I et al (1994) Anterior choroidal artery territory infarcts. Study of presumed mechanisms. Stroke 25:837-842

Lie C, Hirsch JG, Roßmanith C et al (2004) Clinicotopographical correlation of corticospinal tract stroke. A color-coded diffusion tensor imaging study. Stroke 35:86–93

Lindgren A, Staaf G, Geijer B et al (2000) Clinical lacunar syndromes as predictors of lacunar infarcts. A comparison of acute clinical lacunar syndromes and findings on diffusion-weighted MRI. Acta Neurol Scand 101:128–134

Lindley RI, Warlow CP, Wardlaw JM et al (1993) Interobserver reliability of a clinical classification of acute cerebral infarction. Stroke 24:1801–1804

Martin PJ, Chang HM, Wityk R et al (1998) Midbrain infarction: associations and aetiologies in the New England Medical Center Posterior Circulation Registry. J Neurol Neurosurg Psychiatry 64:392–395

Mead GE, Shingler H, Farrell A et al (1998) Carotid disease in acute stroke. Age Ageing 27:677–682

Mead GE, Lewis SC, Wardlaw JM et al (2000) How well does Oxfordshire Community Stroke Project classification predict the site and size of the infarct on brain imaging? J Neurol Neurosurg Psychiatry 68:558–562

Melo TP, Bogousslavsky J, Moulin T et al (1992) Thalamic ataxia. J Neurol 239:331–337

Melo TP, Bogousslvasky J (1992) Hemiataxia-hypesthesia:

a thalamic stroke syndrome. J Neurol Neurosurg Psych 55:581–584
Min WK, Park KK, Kim YS et al (2000) Atherothrombotic middle cerebral artery territory infarction. Topographic diversity with common occurrence of concomitant small cortical and subcortical infarcts. Stroke 31:2055–2061
Minematsu K, Yamaguchi T, Omae T (1992) Spectacular shrinking deficit: rapid recovery from a major hemispheric syndrome by migration of an embolus. Neurology 42:157–162
Molina CA, Montaner J, Abilleira S et al (2001) Timing of spontaneous recanalization and risk of hemorrhagic transformation in acute cardioembolic stroke. Stroke 32:1079–1084
Montavont A, Nighoghossian N, Hermier M et al (2003) Hemiplegia in posterior cerebral artery occlusion: acute MRI assessment. Cerebrovasc Dis 16:452–453
Moulin T, Crepin-Leblond T, Chopard JL et al (1993) Hemorrhagic infarcts. Eur Neurol 34:64–77
Moulin T, Tatu L, Vuillier F et al (2000) Role of a stroke data bank in evaluating cerebral infarction subtypes: patterns and outcome of 1.776 consecutive patients from the Besancon stroke registry. Cerebrovasc Dis 10:261–271
Nighoghossian N, Hermier M, Adeleine P et al (2002) Old microbleeds are a potential risk factor for cerebral bleeding after ischemic stroke. A gradient-echo T2* - weighted brain MRI study. Stroke 33:735–742
Oliveira-Filho J, Ay H, Schaefer PW et al (2000) Diffusion-weighted magnetic resonance imaging identifies the "clinically relevant" small-penetrator infarcts. Arch Neurol 57:1009–1014
Pinto AN, Melo TP, Lourenço ME et al (1998) Can a clinical classification of stroke predict complications and treatments during hospitalization? Cerebrovasc Dis 8:204–209
Ramirez-Lassepas M, Cipolle RJ, Bjork RJ et al (1987) Can embolic stroke be diagnosed on the basis of neurologic clinical criteria? Arch Neurol 44:87–89
Rieke K, Kreiger D, Adams HP et al (1993) Therapeutic strategies in space-occupying cerebellar infarction based on clinical, neuroradiological and neurophysiological data. Cerebrovasc Dis 3:45–55
Roh JK, Kang DW, Lee SH et al (2000) Significance of acute multiple brain infarction on diffusion-weighted imaging. Stroke 31:688–694
Saeki N, Shimazaki K, Yamaura A (1999) Isolated infarction in the territory of lateral posterior choroidal arteries. J Neurol Neurosurg Psychiatry 67:413–415
Saposnik G, Caplan LR (2001) Convulsive-like movements in brainstem stroke. Arch Neurol 58:654–657
Schmahmann JD (2003) Vascular syndromes of the thalamus. Stroke 34:2264–2278
Schwarz S, Egelhof T, Schwab S et al (1997) Basilar artery embolism. Clinical syndrome and neuroradiologic patterns in patients without permanent occlusion of the basilar artery. Neurology 49:1346–1352
Schwarz S, Schwab S, Hacke W (2001) Large and panhemispheric infarcts. In: Bogousslavsky J, Caplan L (eds) Stroke syndromes. Cambridge University Press, Cambridge, pp 490–498
Selim M, Fink JN, Kumar S et al (2002) Predictors of hemorrhagic transformation after intravenous recombinant tissue plasminogen activator: prognostic value of the initial apparent diffusion coefficient and diffusion-weighted lesion volume. Stroke 33:2047–2052
Singer MB, Chong J, Lu D et al (1998) Diffusion-weighted MRI in acute subcortical infarction. Stroke 29:133–136
Singhal AB, Topcuoglu MA, Buonanno FS (2002) Acute ischemic stroke patterns in infective and nonbacterial thrombotic endocarditis: a diffusion-weighted magnetic resonance imaging study. Stroke 33:1267–1273
Steinke W, Mangold J, Schwartz A et al (1997) Mechanisms of infarction in the superficial posterior cerebral artery territory. J Neurol 244:571–578
Studer A, Georgiadis D, Baumgartner RW (2003) Ischemic infarct involving all arterial territories of the thalamus. Acta Neurol Scand 107:423–425
Timsit SG, Sacco RL, Mohr JP et al (1992) Early clinical differentiation of cerebral infarction from severe atherosclerotic stenosis and cardioembolism. Stroke 23:486–491
Tong DC, Adami A, Moseley ME et al (2000) Relationship between apparent diffusion coefficient and subsequent hemorrhagic transformation following acute ischemic stroke. Stroke 31:2378–2384
Tong DC, Adami A, Moseley ME et al (2001) Prediction of hemorrhagic transformation following acute stroke: role of diffusion-and perfusion-weighted magnetic resonance imaging. Arch Neurol 58:587–593
Van Horn G, Hawes A (1982) Global aphasia without hemiparesis: a sign of embolic encephalopathy. Neurology 32:403–406
Vo KD, Santiago F, Lin W et al (2003) MR imaging enhancement patterns as predictors of hemorrhagic transformation in acute ischemic stroke. Am J Neuroradiol 24:674–679
Von Campe G, Regli F, Bogousslavsky J (2003) Heralding manifestations of basilar artery occlusion with lethal or severe stroke. J Neurol Neurosurg Psychiatry 74:1621–1626
Wardlaw JM, Dennis MS, Lindley RI et al (1996) The validity of a simple clinical classification of acute ischaemic stroke. J Neurol 1996:274–279
Warlow CP, Dennis MS, van Gijn J et al (2001) A practical approach to the management of stroke patients. In: Warlow CP, Dennis MS, van Gijn J, Hankey GJ, Sandercock PAG, Bamford JM, Wardlaw JM (eds) Stroke. A practical guide to management. Blackwell Science, Oxford, pp 414–441
Wityk RJ, Goldsborough MA, Hillis A et al (2001) Diffusion- and perfusion-weighted brain magnetic resonance imaging in patients with neurologic complications after cardiac surgery. Arch Neurol 58:571–576
Wolf PA (2002) Mortality in patients with stroke. In: Bogousslavsky (ed) Long-term effects of stroke. Dekker, New York, pp 93–104
Wolff V, Saint Maurice JP, Ducros A et al (2002) Akinetic mutism and anterior bicerebral infarction due to abnormal distribution of the anterior cerebral artery. Rev Neurol (Paris) 158:377–380
Wong KS, Gao S, Chan YL et al (2002) Mechanisms of acute cerebral infarctions in patients with middle cerebral artery stenosis: a diffusion-weighted imaging and microemboli monitoring study. Ann Neurol 52:74–81

15 Hemodynamic Infarcts and Occlusive Carotid Disease

Kristina Szabo and Michael G. Hennerici

CONTENTS

15.1 Introduction

"The observation that misfortunes rarely come single, was verified in Handel. His fortune was not more impaired, than his health and his understanding. His right-arm was become useless to him, from a stroke of the palsy; and how greatly his senses were disordered at intervals, for a long time, appeared from an hundred of instances, which are better forgotten than recorded" (Mainwaring 1760).

Georg Friedrich Händel's recurrent stroke is a well-documented historical case of cerebrovascular disease. He suffered from repeated palsies on his right side accompanied by speech impairment occurring in stroke-like episodes that must be considered left hemispheric ischemic events, possibly caused by left internal carotid artery disease (Bäzner and Hennerici 2004).

K. Szabo, MD; M. G. Hennerici, MD
Department of Neurology, University Hospital Mannheim, Ruprecht-Karls University Heidelberg, Theodor-Kutzer-Ufer 1–3, 68167 Mannheim, Germany

Atherosclerotic narrowing of the extracranial internal carotid artery (ICA) is a well-recognized cause of cerebral ischemia. The annual stroke risk for patients with asymptomatic ICA stenosis amounts to approximately 1%–2% (Chambers and Norris; Hennerici et al. 1987). Many natural history studies and prospective treatment trials with large patient samples have focused on optimal patient assessment in regard to medical or interventional measures, i.e., carotid endarterectomy, percutaneous transluminal angioplasty and carotid stenting (Barnett et al. 1998; Rothwell and Warlow 1999; Brown and Hacke 2004). Management of patients with carotid stenosis should focus on the occurrence and identification of neurological symptoms, the best possible identification of the degree and morphology of the stenosis and the determination of the mechanism of ischemic symptoms (Sacco 2001; Rothwell et al. 2004). Since such a differentiated approach is not always taken and patients undergo surgical or interventional treatment far too often without a proper neurological evaluation, the material presented in this chapter will demonstrate that a critical approach concerning the clinical relevance of a stenosis of the ICA is mandatory in the view of imaging procedures such as magnetic resonance imaging (MRI) and improves outcome based on a better understanding of the pathophysiology and mechanisms of ischemic symptoms. Therapeutic decisions should be largely based nowadays on the identification, visualization, and grading of the vascular situation and the identification of neurological symptoms related to carotid disease – thus neuroimaging studies are an integral part of the neurologist's assessment of the patient. Recent technological progress of MRI has made it possible to obtain data from magnetic resonance angiography (MRA), T2-, diffusion-weighted (DWI), and perfusion MRI (PI). Multi-parameter MRI "background" information may become a basis for an optimized risk–benefit assessment in individual patients. Adding information regarding the circle of Willis, acute and chronic tissue damage, severity of hemodynamic compromise, collateral

supply and the cerebral reserve capacity may potentially help identify the most appropriate candidates for interventional therapies.

15.2 Stroke Patterns in Occlusive Carotid Disease

In the past, two different basic mechanisms have been proposed to account for ischemic events in ICA occlusive disease: (1) intracranial embolism and (2) a low-perfusion state also referred to as hemodynamic insufficiency. In the post-mortem arteriographic and pathologic study by Rodda and Path (1986), massive infarcts involving two major cerebral artery territories were associated with distal ICA occlusion, middle cerebral artery (MCA) territory infarcts were seen when the ICA was occluded or stenosed, and borderzone infarcts were characterized by ICA disease and limited circle of Willis anastomosis.

Studies based on computed tomography have suggested that hemodynamically significant stenosis or obstructions of the extracranial ICA may cause hemodynamic changes in the distal regions of the hemispheric blood supply, the so-called watershed areas between major vascular territories, while embolism from ICA stenosis is believed to disproportionately affect the MCA stem and distal branches producing territorial infarction, often including the lenticulostriate territory (Pessin et al. 1979). In other studies, small borderzone infarcts were seen as markers for high-grade ICA stenosis and occlusion (Bogousslavsky 1986a; Del Sette et al. 2000), while this association was denied in a larger trial (Hupperts et al. 1997). The concept of borderzone ischemia as a cause of stroke in patients with severe ICA stenosis has been challenged (Hennerici et al. 1998), and recently the coexistence of hypoperfusion and arterial embolism in patients with borderzone stroke and ICA disease – as opposed to two independent mechanisms – has been postulated (Caplan and Hennerici 1998).

Using DWI and PI in acute stroke patients with the detection of the acute lesion and the delineation of the area of hemodynamic compromise, the understanding of pathophysiological mechanisms leading to cerebral ischemia in patients with ICA disease has been improved. DWI offers a better chance of detecting not only gross abnormalities but also very subtle acute ischemic lesions. In a systematic study using DWI in 102 consecutive patients with ICA stenosis > 50% or ICA occlusion and acute stroke, we defined certain patterns of acute infarctions (Szabo et al. 2001): Pattern 1 was identified as a large ischemic lesion involving the cerebral cortex and subcortical structures in one or more major cerebral artery territories, referred to as "cortical territorial infarction". This stroke subtype is assumed to be a partial MCA infarction if a distal middle cerebral artery branch is occluded, to be a large MCA infarction in the case of proximal occlusion at the level of the MCA bi- or trifurcation and in the absence of an efficient collateral system (Heinsius et al. 1998), or to be a complete anterior cerebral artery (ACA) and MCA territory infarction in the case of an embolism to the distal ICA. Pattern 2 was defined as "subcortical infarction" in the territory of the deep perforating branches from the distal ICA or the MCA trunk. This pattern has been explained by the occlusion of the MCA in the presence of patent collaterals, either due to the embolization into the middle cerebral artery resulting in a large striatocapsular lesion or due to the occlusion of a deep perforating artery of the carotid system leading to a subcortical lesion (Weiller et al. 1990; Nakano et al. 1995). Pattern 3 ("territorial infarction with fragmentation") represented a large ischemic lesion with additional smaller lesions either in cortical or in subcortical regions, probably due to partial fragmentation of the embolus (Roh et al. 2000). In pattern 4, several disseminated small lesions were sprinkled in random fashion in the distal territory of the middle cerebral artery involving mainly cortical regions. The possible cause of this pattern may be a fragmented embolus or multiple microemboli in smaller vessels (Baird et al. 2000). Pattern 5 ("borderzone infarction") exhibited lesions either completely or predominantly located in regions considered to be one of the hemodynamic risk zones between major cerebral vascular territories (Zülch 1963; Mull et al. 1997). An example for each pattern is given in Fig. 15.1. Our data showed that ischemic lesions on DWI in patients with ICA occlusive disease are by far more heterogeneous than hitherto suspected. Various stroke patterns represented very different characteristics from small embolic lesions to large territorial ischemia. Although the degree of ICA stenosis significantly influenced the pattern of cerebral ischemia seen on DWI, half of the patients with high-grade or subtotal stenosis had lesions of different types and extent in hemodynamic risk zones. In high-grade ICA stenosis, multiple small embolic lesions were a common feature of cerebral ischemia. However, although each of these patterns raises the initial suspicion of a specific underlying

mechanism, their specificity is by far not absolute. In contrast, various lesion patterns might be caused by a single mechanism, while a single lesion pattern might be associated with different mechanisms.

The study of stroke patterns in ICA occlusive disease has been addressed by other groups: Kastrup et al. (2002) prospectively analyzed 107 patients with high-grade (> 70%) ICA disease and found that the majority of patients had multiple, small cortical and/or subcortical DWI lesions. They conclude that this common lesion type supports large artery thromboembolism in symptomatic high-grade ICA stenosis. In a study by Kang et al. (2002), examining 35 consecutive patients with acute stroke and > 70% stenosis or occlusion of the ipsilateral ICA, similarly multiple DWI lesions were noted in 83%. They describe a common association of borderzone lesions with territorial infarction (Fig. 15.2), and therefore also suggest embolism in low perfusion territories as a predominant stroke mechanism in ICA occlusive disease. The new aspects of these DWI studies show that lesion characterization in carotid disease might be more complex and underline the concept that different pathomechanisms interact. However, neither of the latter two studies provided additional information on possible hemodynamic alterations leaving any interpretation of stroke mechanism incomplete. Our approach to definitively identify hemodynamic lesions is described below. Table 15.1 summarizes DWI findings in symptomatic ICA disease in these studies.

15.3 Hemodynamic Stroke

15.3.1 Pathophysiological Concepts

Infarcts occurring as a consequence of cardiac arrest or severe hypotension (see Chap. 16) follow similar topographical patterns with bilateral lesions in the borderzones between the major cerebral arteries – a

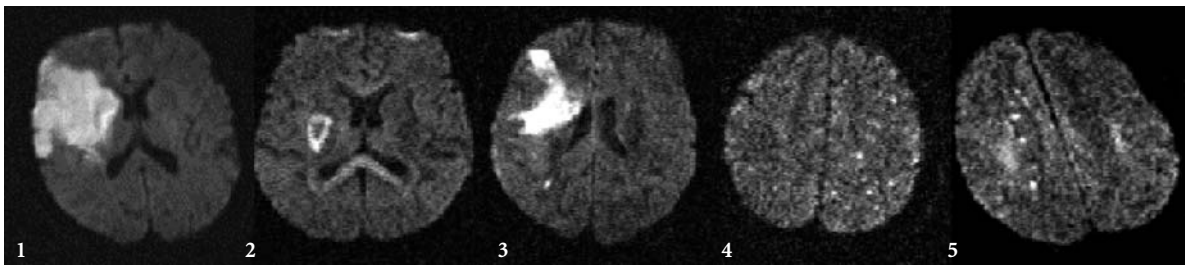

Fig 15.1. Diffusion-weighted imaging demonstrates different patterns of acute stroke in occlusive internal carotid artery disease: *1*, territorial stroke; *2*, subcortical stroke; *3*, territorial stroke with fragmentation; *4*, disseminated small lesions; *5*, borderzone infarction

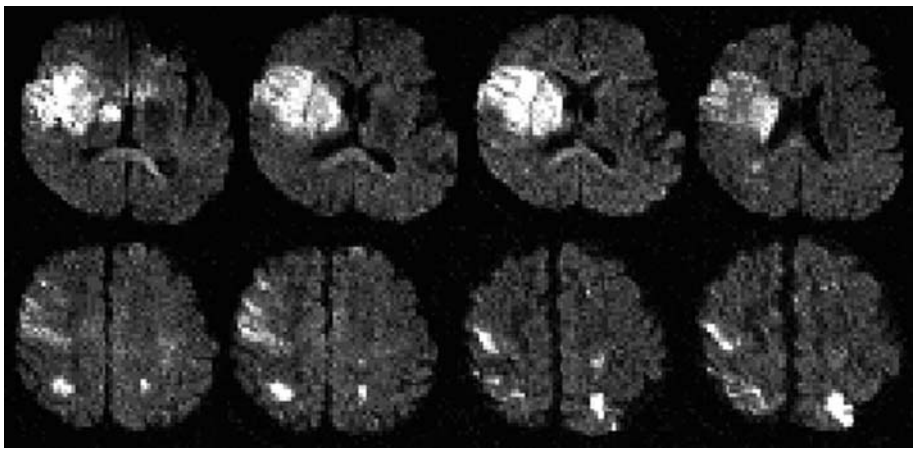

Fig. 15.2. Diffusion-weighted imaging in a 54-year-old patient with acute onset of severe left-sided hemiplegia shows a territorial infarction in the right middle cerebral artery territory, as well as additional bilateral hemodynamic lesions. Ultrasound examination in this patient showed high-grade internal carotid artery stenosis on both sides

Table 15.1. Diffusion-weighted imaging in symptomatic occlusive carotid disease

Study	Number of patients	Stenosis grade	Lesions identified	Conclusions
Kastrup et al. (2002)	107	≥ 70% or occlusion	• Single lesion (*n*=18) • Multiple lesions (*n*=37) • No lesion (retinal or hemispheric TIA, *n*=52)	The majority of patients with symptomatic high-grade stenosis had multiple, frequently very small DWI lesions
Kang et al. (2002)	35	≥ 70% or occlusion	• Territorial lesion (*n*=21) • Borderzone lesion with or without a territorial lesion (*n*=10) • Bilateral hemispheric lesions (*n*=4)	Acute ischemic lesion in ICA occlusive disease is mainly multiple; borderzone infarction was mostly associated with territorial infarction
Szabo et al. (2001)	102	≥ 50 or occlusion	• Territorial stroke (*n*=30) • Subcortical stroke (*n*=13) • Territorial infarction with fragmentation (*n*=11) • Disseminated small lesions (*n*=15) • Borderzone lesions (*n*=33)	The degree of ICA stenosis may favor certain stroke patterns. In patients with high-grade stenosis the highest frequency of lesions occurs in the hemodynamic risk zones

phenomenon also confirmed by early experimental studies with primates (Brierley and Excell 1966). Borderzone infarcts were identified in brains of patients who died shortly after cardiac surgery and ascribed to episodes of abrupt arterial hypotension (Adams et al. 1966). In patients with occlusive ICA disease alike stroke lesions have been described and are believed to be caused by a similar, yet gradual compromise of cerebral perfusion, especially under the conditions of limited collateral circulation (Bogousslavsky 1986b). These so-called borderzones are divided into the superficial or cortical borderzones wedged between the territory of ACA and the MCA, or between the MCA and posterior cerebral artery (PCA) territory, and the deep or subcortical borderzone located in the vascular territory between deep and superficial arterial systems (Waterston et al. 1990; Bogousslavsky 1986a; Torvik 1984).

More recently, not only hemodynamic compromise, but also embolism was found to play an important role in the pathogenesis of borderzone infarcts. Caplan and Hennerici (1998) postulated the coexistence of hypoperfusion and intra-arterial embolism in borderzone infarcts and suggested that emboli lodged in hypoperfused regions may contribute to local ischemia and infarction. A similar theory was expressed by Pollanen and Deck (1989) who proposed that small thromboemboli may not be randomly distributed in the cerebral artery supply, but may be preferentially distributed to the small arterial branches of the borderzone due to anatomical features of vessel branches. Supporting the theory of microembolism, using the Doppler ultrasound phenomenon of "high intensity transient signals" (HITS) for detecting microemboli in the middle cerebral artery in patients with occlusive carotid disease, HITS were significantly more often associated with severe (> 70%) (23.5%) than with moderate (50%–70%) internal carotid artery stenosis (3.4%) (Ries et al. 1996).

Yet, since the territories of the major cerebral arteries have been shown to possibly vary considerably, lesion localization alone may not be enough to identify borderzone lesions. Van der Zwaan and Hillen (1991) described different variations of the cortical distributions in all 25 human brains obtained at autopsy through injecting different colored substances into the six major arteries of the human brain. He also noted an inter-individual difference with remarkable asymmetrical territorial distribution in both hemispheres. With the clinical use of novel MRI techniques, however, it is possible to identify acute ischemic lesions in individual hemodynamic risk zones.

15.3.2 Diffusion-weighted and Perfusion Imaging Correlates of Hemodynamic Stroke

DWI is sensitive to changes of water molecule mobility and detects reduced proton mobility due to cytotoxic cell swelling, an early event in the cascade of ischemic tissue change, before T2-weighted MRI shows abnormality (LeBihan 1991; Sakuma et al. 1991; Tanner 1983). The regional reduction of diffusion is visible as hyperintensity on DWI images and as hypointensity on quantitative maps of the apparent diffusion coefficient (ADC) (see Chap. 7). DWI images provide a higher lesion-to-background contrast than conventional MRI facilitating lesion detection in early stages of stroke and allowing differentiation of acute and chronic tissue change. Current

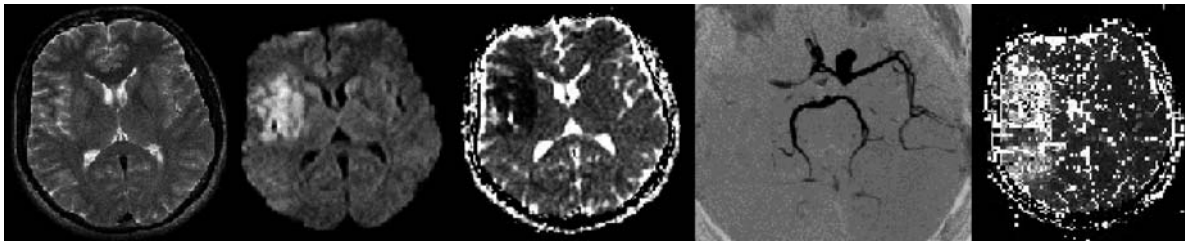

Fig. 15.3. Acute stroke MRI in a 34-year-old patient with acute-onset (1.5 h) right side hemiparesis. *From left to right*: the T2-weighted image shows no definite parenchymal abnormality, only subtle signs such as lack of flow void in the MCA branches of the temporal region; the DWI image demonstrates the acute ischemic lesion involving the insular region of the right MCA territory with corresponding reduction of the ADC; the MIP-TOF MRA depicts signal loss in the occluded proximal right MCA and distal ICA, while the perfusion map (time-to-peak) demonstrates different grades of hypoperfused tissue in the complete MCA territory

evidence suggests that reduced diffusion is caused by cell swelling associated with cytotoxic edema formation, caused by failure of energy dependent pumps and influx of sodium and calcium, possibly accentuated by metabolic stress due to periinfarct depolarization. It is likely that both the narrowing of extracellular space and intracellular changes contribute to reduced diffusion. At present single shot echo planar (EP) MRI techniques are most widely used for DWI (Edelmann et al. 1994; Gass et al. 1999). Only a single nuclear spin excitation is required and a whole head (e.g., 24 slices, slice thickness of 5 mm) DWI study can typically be generated within 4–5 s. EP images are prone to specific artifacts (susceptibility artifact, N/2 or Nyquist ghost artifact, chemical shift artifact, eddy current artifact) that also need to be considered when interpreting DWI. Figure 15.3 shows an example of acute stroke MRI and the benefit of the different MRI techniques.

Figure 15.4 shows typical examples of hemodynamic acute stroke patterns in four different patients with carotid disease as identified by DWI. Lesions can be either located in the anterior or posterior superficial hemodynamic risk zone or in both, they can be located in the subcortical borderzones or, as in Fig. 15.5, they can affect all areas considered to be regions vulnerable to hemodynamic compromise. Commonly, these lesions are small and dot-like or confluent distributed in a chain-like fashion and can be either single or multiple. It is important to acknowledge that some of these lesions would probably be missed using conventional imaging techniques. Even though these stroke patterns bear very characteristic features and may allow an experienced clinician to suspect hemodynamic pathogenesis, with lesions located in the paraventricular region it is sometimes difficult to distinguish between superficial perforating artery and internal borderzone lesions. In an interesting study Lee et al. (2003) compared MRI characteristics of these topographically well-defined types of deep cerebral infarcts and found that borderzone infarcts were larger, appeared in a chain-like distribution and had a higher degree of stenosis or occlusion of the ICA or the MCA, while superficial perforating artery strokes were more frequently accompanied by cortical spotty lesions and more frequent potential cardio-embolic sources.

For the exact description of hemodynamic stroke and identification of individual hemodynamic risk zones, as mentioned earlier, the assessment of the hemodynamic situation is essential. PI offers a means to obtain semiquantitative hemodynamic information in cerebral ischemia with relatively high resolution and short acquisition times covering all cerebral vascular territories. In acute cerebral ischemia dynamic susceptibility contrast

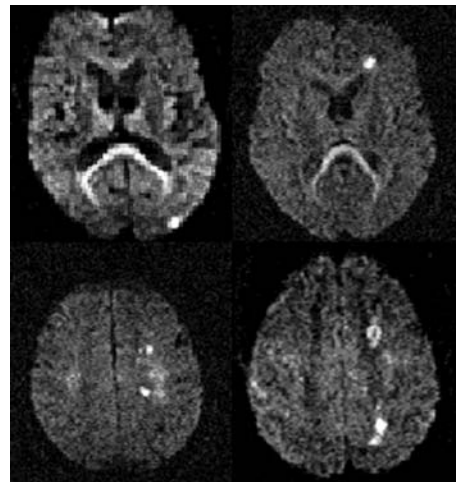

Fig. 15.4. DWI shows examples of acute borderzone lesions, namely in the posterior (upper row left) or anterior (*upper row right*) hemodynamic risk zones and in the subcortical or deep borderzone (*bottom row*)

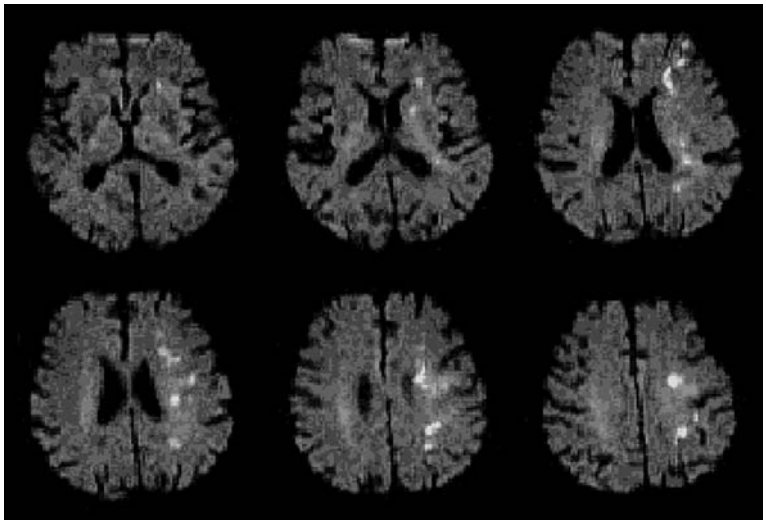

Fig. 15.5. As in this 68-year-old man with a high-grade stenosis of the left internal carotid artery presenting with a fluctuating mild left-hemispheric syndrome, acute ischemic lesions can affect all areas considered to be hemodynamic risk zones

(DSC) MRI is the most widely evaluated technique (see Chap. 6). It uses information from transient local changes of magnetic field homogeneity (susceptibility effects) induced by the bolus passage of a paramagnetic contrast agent in dynamic T2*-weighted MRI acquisitions (Rosen et al. 1990). The extent of hemodynamically compromised tissue is readily provided by the temporal characteristics of the contrast bolus arrival in 'time to peak' or 'mean transit time' maps (Ostergaard et al. 1996; Röther et al. 1996). In the first few hours after stroke onset, PI abnormalities are often larger than the DWI lesions. This pattern (PI > DWI) is frequently associated with lesion growth into the PI/DWI mismatch region and is therefore suggested to show "tissue at-risk" and is often found in critical carotid artery stenosis or occlusion (Neumann-Haefelin et al. 2000). It is well established that impaired hemodynamics can be demonstrated with PI in patients with ICA disease. Compromise of autoregulation in patients with high-grade carotid stenosis has been demonstrated (Guckel et al. 1996; Maeda et al. 1999). As a compensatory mechanism of high-grade carotid stenosis, cerebral blood volume (CBV) maps may show a local increase of CBV. PI has been a reliable method for assessing perfusion changes in patients with unilateral carotid stenosis and patients with good collateral supply have been distinguished from those with poor collateral supply (Reith et al. 1997). Recently, large territorial perfusion deficits have been found with a predisposition to borderzone infarction in high-grade ICA stenosis (Chaves et al. 2000). The authors examined the MRI data of 17 patients with borderzone infarcts and identified three patterns of perfusion abnormalities associated with the diffusion lesions. They found that the perfusion abnormality varied according to the mechanism of the borderzone infarction: (1) Transient perfusion deficits occurring with hypotension in the absence of significant large artery disease may not be revealed by PI; (2) embolism may cause some cases of small borderzone perfusion deficits; (3) critical large artery disease may cause large territorial perfusion deficits and predispose to borderzone infarction.

Frequently, visual analysis of DWI images allows the experienced reader to identify hemodynamic stroke patterns. However, this is not always reliable due to the fact that lesions are sometimes punctuated and small and it can be difficult to detect helpful anatomical landmarks on DWI. Sometimes only with help from PI is it possible to recognize lesions in the hemodynamic risk zones. Figure 15.6 gives an example of computerized superimposing of DWI and PI, to determine where the diffusion lesion is located with respect to the perfusion deficit. After aligning the time-to-peak and DWI images, it becomes clear that the lesions are indeed located in the borderzone area where the extent of the perfusion deficit is the greatest. Further studies to characterize these "dot-like" lesions with regard to the hypoperfused region are in the process and should shed new light on the role of microembolism in hemodynamically compromised regions. Figure 15.7 demonstrates two theoretical concepts of stroke in hemodynamic risk zones – microembolic lesions in the most distal arterial branches and the infarction of the compromised borderzone territory.

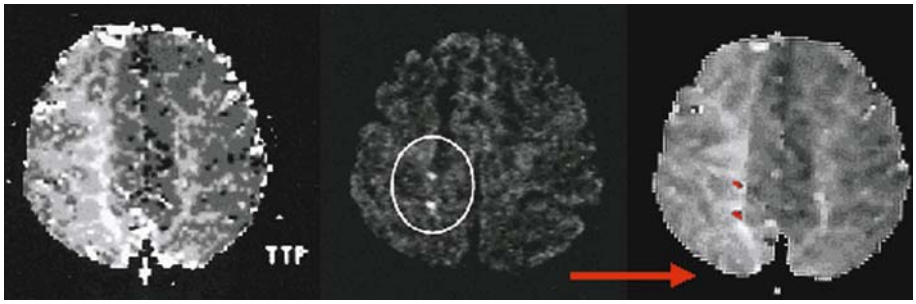

Fig. 15.6. Computerized registration and overlay of DWI lesions on PI images, to determine the exact location of the diffusion lesion with respect to the perfusion deficit. The alignment of the time-to-peak (TTP) and DWI images demonstrates that the lesions are indeed located in the borderzone area where the extent of the perfusion deficit is most pronounced

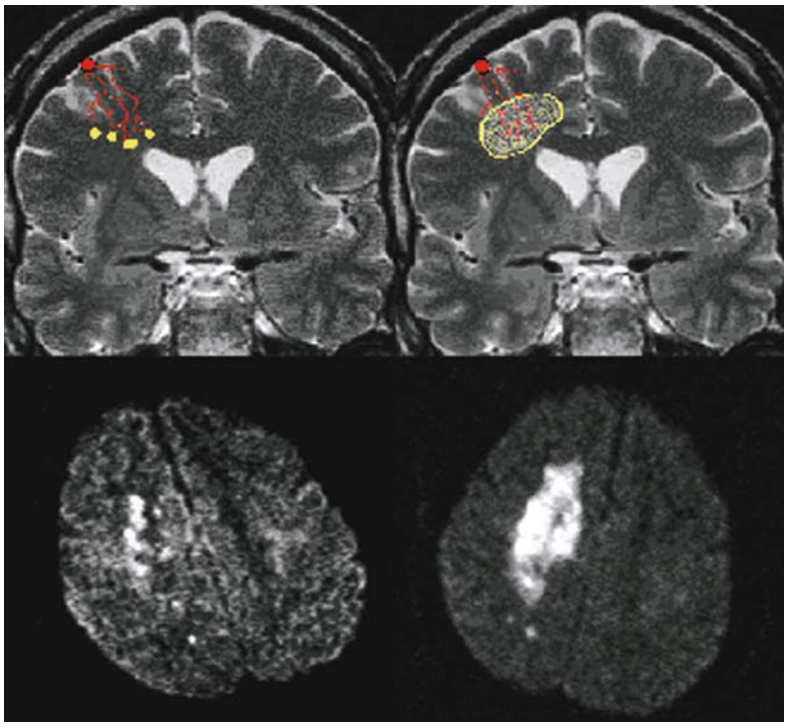

Fig. 15.7. The theoretical concepts of stroke in hemodynamic risk zones – "dot-like" microembolic lesions in the most distal arterial branches resulting from more proximal vessel pathology and impaired emboli washout (*left*) and the complete infarction of the compromised tissue in the borderzone territory (*right*). The *bottom row* gives DWI examples of these lesion patterns

15.4 Evaluation of Vessel Pathology in Occlusive Carotid Disease

MRA is an emerging technique in carotid artery disease taking advantage of the differences of spin signals of flowing blood and static tissue, with the stationary tissue signal effectively suppressed relative to the blood flow signal (see Chap. 5). The ability of non-invasively imaging blood flow and thereby visualizing extra- and intracranial vasculature offers the clinician valuable information. A single measurement is performed within a few minutes. Two techniques are most widely used to assess narrowing of the extracranial vessels and to visualize the intracranial vasculature: contrast-enhanced MRA (CE-MRA) and time-of-flight (TOF) techniques. MRA source images are frequently postprocessed to provide a 3D visualization with an algorithm also termed maximum intensity projection (Mattle and Edelman 1992; Röther et al. 1993). This allows demonstration of the 3D vessel topography and offers the possibility to review the vessels in every desirable plane even after the investigation is concluded.

15.4.1 Obstruction of the Internal Carotid Artery

CE-MRA is a promising technique particularly for the evaluation of the proximal segments from the aortic arch covering the carotid bifurcation (Cloft

et al. 1996; Gass et al. 1997; Patel et al. 1995). Small intravenous doses of paramagnetic contrast agent strongly enhance the MR signal due to T1 shortening. While CE-MRA appears excellent to visualize the site and length of narrowing, it also shows a tendency to overemphasize arterial narrowing. Turbulent flow in case of a high-grade stenosis might therefore not be detected. Hence, complete signal loss over a short vessel segment can indicate high-grade vessel narrowing, but must not indicate vessel occlusion. From a practical standpoint CE-MRA is a very fast technique and therefore less susceptible to patient motion occuring with long acquisition times. Exact timing of the contrast injection is important to avoid obscuring the arterial vessels from hyperintensity due to early venous return. Although it has only recently become available CE-MRA has already contributed considerably to patient management as many vascular surgeons no longer require preoperative conventional contrast angiography, but may use the combination of duplex ultrasound studies and CE-MRA for visualization of the vascular pathology. Figure 15.8 gives an example for a high-grade stenosis identified with Duplex ultrasound and a signal loss over the proximal part of the affected vessel segment on CE-MRA (Gass et al. 2001).

High-resolution MRI has recently emerged as one of the most promising techniques for the noninvasive study of atherosclerosis of the ICA. This method can be used to characterize plaque composition and to monitor progression and is mainly performed using cross-sectional imaging of the vessel (Fig. 15.9). MR techniques are not dependent on the angle of the imaging plane and are less dependent on the skill of the operator than is ultrasound. For the purposes of vascular imaging, MR is unique in that the modality can provide excellent contrast between the vessel wall and adjacent lumen by using flow-sensitive pulse sequences. Thus, MR can be used to image the vessel lumen (flowing blood) and, at the same time, produce tissue information that describes the vessel wall. By using T1-weighted and chemical-selective techniques (Corti et al. 2001; Yuan et al. 2001) the detection of lipid signals (cholesterol and cholesteryl esters) is possible. With the inclusion of sequences that are T2-weighted and T1- or intermediate-weighted with a very short echo time, the specificity of MR imaging techniques has improved and allowed differentiation of necrotic cores from fibrous regions in ex vivo plaque specimens (Gold et al. 1993). Direct MRI of a thrombus has even been shown to be capable of detecting methemoglobin within intraplaque hemorrhage (Moody et al. 2003).

15.4.2 Role of the Anatomy of the Circle of Willis

MRA has been shown to be well suited to investigate the circle of Willis (CW) since abnormalities can be detected by MRI blood flow techniques (Anzola et al. 1995). 3D TOF sequences, although more time consuming than CE-MRA, are still the

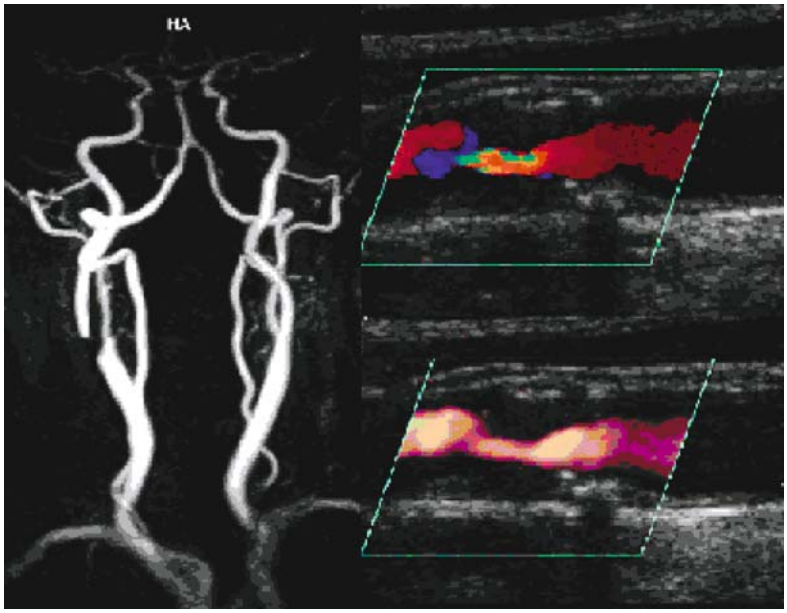

Fig. 15.8. Contrast-enhanced MRA reveals high-grade proximal ICA stenosis with signal void at the level of the right carotid bifurcation (*left*). Color Doppler flow imaging demonstrates high-grade ICA stenosis with turbulent flow (*light blue*, *top right*) and power Doppler shows excellent delineation of the stenosis and increased blood flow velocity (*yellow and red*, *bottom right*)

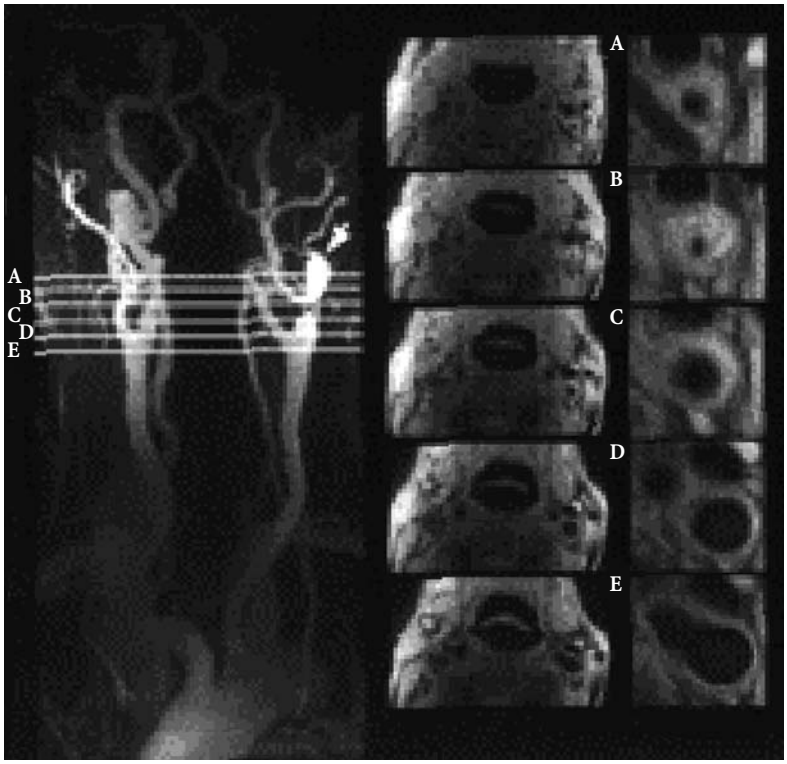

Fig. 15.9. Combined MRA (*left*) and plaque imaging (*right*) in a hypertensive patient with symptomatic left ICA stenosis. Cross-sectional black-blood imaging demonstrates the severely narrowed lumen (*A* and *B*) as well as the extension of the plaque to the carotid bifurcation (*E*), appearing normal on angiography

main method of visualizing the CW. To achieve a high contrast image, the stationary spins of background tissue are usually saturated with magnetization transfer pulses resulting in a low background signal, whereas unsaturated moving spins of blood produce a bright signal. TOF may be used either in a 2D or 3D sequence. In a 2D TOF, a set of thin slices is acquired sequentially, one slice after the other. Data in 3D TOF are acquired as volume (slab) or a set of volumes. The sensitivity of 3D TOF to slowly flowing blood is poor, but it can provide high spatial resolution and is therefore especially useful for the arterial angiography of small vessels with high-flow velocity. TOF sequences are mainly used to image the circle of Willis also covering the distal parts of the extracranial internal carotid and the vertebral arteries.

In patients with obstruction of the internal carotid artery, numerous collateral pathways that redistribute blood to the deprived site can maintain adequate cerebral blood flow. The CW is considered an important primary collateral pathway with its potential believed to be dependent on the presence and size of the component vessels, which vary among normal individuals (Alpers and Berry 1963; Baumgartner et al. 1997; Krabbe-Hartkamp et al. 1998; Macchi et al. 1996; Patrux et al. 1994; Schomer et al. 1994). Using special 2D phase-contrast techniques, hemodynamic information concerning blood flow direction is also achievable. In addition to imaging the extracranial arteries, the CW should also be assessed to detect patent collateral pathways.

Hendrikse and coworkers (2001) investigated whether the presence of borderzone infarcts is related to the collateral ability of the CW in symptomatic and asymptomatic patients with unilateral occlusion of the ICA. They found that in patients with unilateral ICA occlusion, the presence of collateral flow via the posterior communicating artery in the circle of Willis is associated with a low prevalence of borderzone infarcts and that asymptomatic patients with an ICA occlusion do not have an increased collateral function of the CW. Figure 15.10 shows the four patterns of collateral flow via the CW to the hemisphere ipsilateral to the ICA occlusion.

Another study investigating the CW collateral flow by MRA showed that patients with ICA obstruction with minor neurological deficits demonstrated a higher prevalence of complete CW configurations (Hartkamp et al. 1999). It remains unclear whether these patients represent a special population leading to non-severe strokes or whether favorable CW configurations are acquired through secondary hemodynamic adaptation. There is also data pointing to the possibility that acute stroke patients suffering

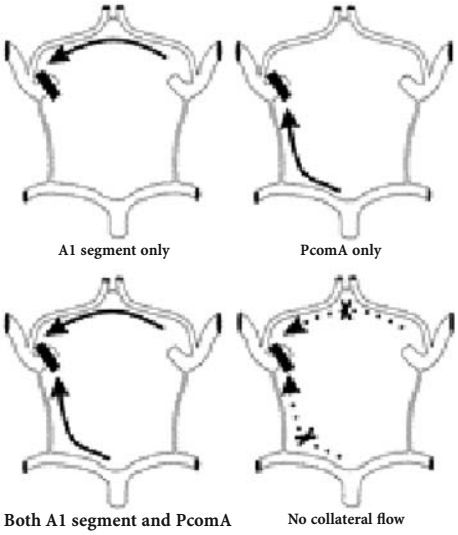

Fig. 15.10. The four patterns of collateral flow via the circle of Willis to the hemisphere ipsilateral to the ICA occlusion. A1 segment indicates A1 segment of ipsilateral ACA, PcomA indicates posterior communicating artery

major stroke in underlying ICA disease may represent a subgroup with a high prevalence of hypo- or aplastic CW, and may, therefore, be unable to adapt in an adequate manner or are destined by genetic factors to suffer stroke in the case of ICA disease (Szabo et al. 2001).

15.5 Use of MRI to Identify Other Causes of Stroke in Patients with Occlusive Carotid Disease

It is well known that in the age groups at risk for high-grade carotid stenosis concomitant myocardial and small vessel disease is often present. A recent analysis of the NASCET data indicated that approximately 20% of strokes in the territory of high-grade symptomatic carotid artery are of cardioembolic and lacunar origin (Barnett et al. 1998). Therefore, it appears important to determine the cause of acute deficits in patients with high-grade carotid stenosis and MRI; particularly DWI and PI seem useful to differentiate different mechanisms of acute ischemia providing a means to differentiate small vessel disease, lacunar stroke, and cardioembolic lesions. All these etiologies may produce multiple discrete lesions with different spatial distributions that may favor one or another stroke mechanism. Even in asymptomatic patients with ICA stenosis PI usually identifies a temporal delay of the contrast bolus arrival to the entire MCA territory, while such asymmetry of the entire MCA territory is usually not seen in patients with small vessel disease or lacunar stroke. Cardiac embolism usually produces a pattern of multiple acute lesions in both hemispheres and both the anterior and posterior circulation, while multiple small lesions in the borderzones of a MCA territory may indicate high-grade carotid stenosis. Conversely in patients with known atrial fibrillation and co-existing high-grade ICA stenosis, PI and DWI may identify acute lesions in hemodynamic risk zones rather more suggestive of ischemia due to high-grade stenosis.

15.6 Treatment of Patients with Occlusive Carotid Disease

Surgical carotid endarterectomy is currently the accepted best standard of treatment for revascularization of extracranial carotid occlusive disease and has been validated by multiple randomized, controlled trials (Barnett et al. 1998; European Carotid Surgery Trialists' Collaborative Group 1991). In the past years, however, carotid artery stenting has been started by different disciplines in an attempt to provide a potential therapeutic alternative to carotid endarterectomy for the treatment of atherosclerotic carotid artery disease. Reliable evaluation of the outcomes of carotid stenting is limited at this time because the outcomes have been reported from case series with few randomized trials and because long-term results are not yet established – randomized clinical studies are in progress (Brown and Hacke 2004; Featherstone et al. 2004; Higashida et al. 2004). A well-known problem of carotid stenting and of carotid surgery is procedure related embolism to the brain and several post-procedure DWI studies have repeatedly shown mainly asymptomatic DWI lesions (van Heesewijk et al. 2002). Different protection devices to prevent embolism are currently under investigation and no single best proceeding has been established to date.

Regardless of the treatment chosen, a dedicated MRI protocol including DWI as well as PI sequences should be performed beforehand in all patients with suspected symptomatic ICA disease. The combination of both methods offers the possibility of identifying patients with potential to benefit from surgery or stenting. In patients with high-grade stenosis, large perfusion deficits and a small acute ischemic

lesion (DWI/PI "mismatch"), recanalization of the ICA should be achieved by all means. Results from a recent study suggested that the recanalizing procedure should ideally be performed within 2 weeks of the patient's last symptoms (Rothwell et al. 2004). Possibly even more importantly, a dedicated MRI protocol may be able to demonstrate, that despite high-grade ICA stenosis intracranial collateralization well compensates for the proximal obstruction, questioning the use and necessity of endarterectomy in these situations.

15.7 Clinical Case Studies

After analyzing initial and final DWI and PI lesion size in stroke patients with > 70% internal carotid artery stenosis, Neumann-Haefelin (1999) found, that most of the mismatch area identified on PI was not at high risk of irreversible tissue damage. In contrast to these findings, patients with initially small DWI lesions and an underlying carotid stenosis can deteriorate and develop considerably larger lesions. Figure 15.11 demonstrates the progressive course of hemodynamic stroke lesions in a 62-year-old patient with symptomatic left ICA occlusion who initially presented with only transient right hemiparesis, but 3 days later showed a progressive hemiparesis of the right side. Fluctuating blood pressure with intermittent systolic values < 140 mmHg were believed to have played a role in further infarct demarcation.

The following two examples show different configurations of the circle of Willis in two patients with occlusive ICA disease. While the 54-year-old patient in Fig. 15.12 suffering from left ICA occlusion shows good collateralization via the posterior communi-

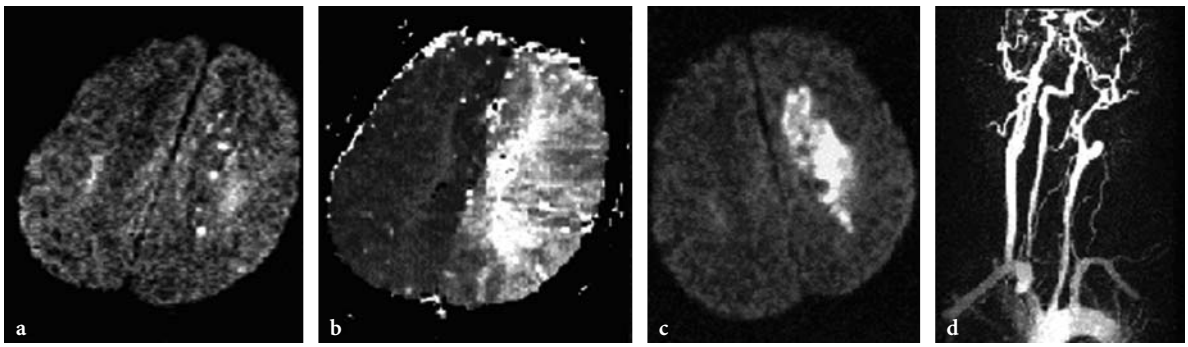

Fig. 15.11a–d. A 62-year-old patient with symptomatic left internal carotid artery occlusion and progressive stroke. Initial DWI shows only punctuate small lesions in the deep borderzone of the left hemisphere (**a**), while the hypoperfused area on the time-to-peak maps affects the complete left middle cerebral artery territory and is most pronounced in the deep borderzone area (**b**). On day 3, the acute lesion has grown considerably larger, paralleling progression of symptoms (**c**). Contrast-enhanced MRA shows proximal occlusion of the left internal carotid artery (**d**)

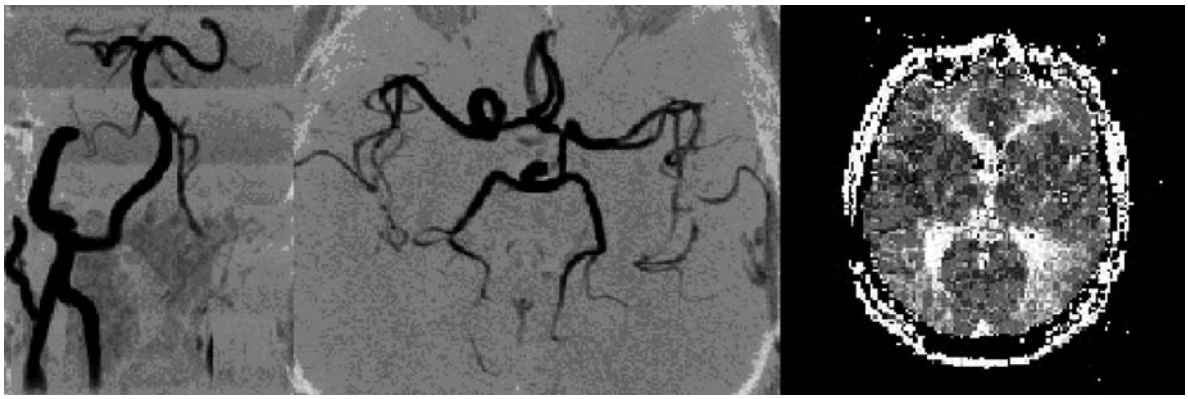

Fig. 15.12. An asymptomatic 54-year-old patient suffering from left internal carotid artery occlusion (left) shows excellent collateralization via the posterior communicating artery and a sufficient filling of the ipsilateral middle cerebral artery (*middle*). As a consequence, perfusion MRI (time-to-peak) detects only a slight asymmetry and delay of contrast agent arrival in the parietal parts of the middle cerebral artery territory (*right*)

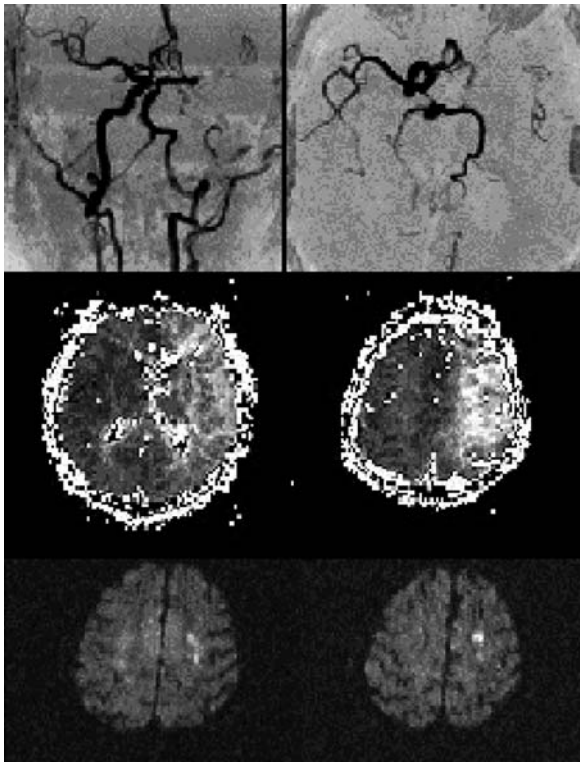

Fig. 15.13. A 76-year-old woman with a subtotal stenosis of the left internal carotid artery shows no sufficient collateral flow and only faint flow signal in the left middle cerebral artery (*upper row*), severe hypoperfusion (time-to-peak maps) of the left middle cerebral artery territory (*middle row*) and small acute hemodynamic stroke lesions on DWI (*bottom row*). The patient was later successfully treated with carotid endarterectomy

cating artery and a sufficient filling of the ipsilateral MCA on MRA, PI shows only a slight delay of contrast agent arrival in the posterior parts of the MCA territory. This patient was clinically asymptomatic. The 76-year-old woman with similar vessel pathology in Fig. 15.13, however, shows no sufficient collateral flow and only faint flow signal in the MCA, severe hypoperfusion of the left MCA territory and small acute hemodynamic stroke lesions on DWI. Duplex ultrasound demonstrated subtotal stenosis of the left ICA and the patient was later successfully treated with endarterectomy.

References

Adams JH, Brierley JB, Connor RCR et al (1966) The effects of systemic hypotension upon the human brain: clinical and neuropathological observations in 11 cases. Brain 89:235–268

Alpers BJ, Berry RG (1963) Circle of Willis in cerebral vascular disorders. Arch Neurol 8:398–402

Anzola GP, Gasparotti R, Magoni M et al (1995) Transcranial Doppler sonography and magnetic resonance angiography in the assessment of collateral hemispheric flow in patients with carotid artery disease. Stroke 26:214–217

Baird AE, Lövblad KO, Schlaug G et al (2000) Multiple acute stroke syndrome: marker of embolic disease? Neurology 54:674–678

Baumgartner RW, Baumgartner I, Mattle HP et al (1997) Transcranial color-coded duplex sonography in the evaluation of collateral flow through the circle of Willis. Am J Neuroradiol 18:127–133

Barnett HJ, Taylor DW, Eliasziw M et al (1998) Benefit of carotid endarterectomy in patients with symptomatic moderate or severe stenosis. North American Symptomatic Carotid Endarterectomy Trial Collaborators. N Engl J Med 339:1415–1425

Bäzner H, Hennerici M (2004) Georg Friedrich Händel's strokes. Cerebrovasc Dis 17:326–331

Bogousslavsky J, Regli F (1986a) Borderzone infarctions distal to internal carotid artery occlusion: prognostic implications. Ann Neurol 20:346–350

Bogousslavsky J, Regli F (1986b) Unilateral watershed cerebral infarcts. Neurology 36:373–377

Brierley JB, Excell BJ (1966) The effects of profound systemic hypotension upon the brain of M. rhesus: physiological and pathological observations. Brain 89:235-268

Brown MM, Hacke W (2004) Carotid artery stenting: the need for randomised trials. Cerebrovasc Dis 18:57–61

Caplan LR, Hennerici M (1998) Impaired clearance of emboli (washout) is an important link between hypoperfusion, embolism, and ischemic stroke. Arch Neurol 55:1475–1482

Chambers BR, Norris JW (1986) Outcome in patients with asymptomatic neck bruits. N Engl J Med 315:860–865

Chaves CJ, Silver B, Schlaug G et al (2000) Diffusion- and perfusion-weighted MRI patterns in borderzone infarcts. Stroke 31:1090–1096

Cloft HJ, Murphy KJ, Prince MR et al (1996) 3D gadolinium-enhanced MR angiography of the carotid arteries. Magn Reson Imaging 14:593–600

Corti R, Fuster V, Badimon JJ et al (2001) New understanding of atherosclerosis (clinically and experimentally) with evolving MRI technology in vivo. Ann NY Acad Sci 947:181–195

Del Sette M, Eliasziw M, Streifler JY et al (2000) Internal borderzone infarction: a marker for severe stenosis in patients with symptomatic internal carotid artery disease. Stroke 31:631–636

Edelman RR, Wielopolski P, Schmitt F (1994) Echo-planar MR imaging. Radiology 192:600–612

European Carotid Surgery Trialists' Collaborative Group (1991) MRC European Carotid Surgery Trial: interim results for symptomatic patients with severe (70–99%) or with mild (0–29%) carotid stenosis. Lancet 337:1235–1243

Featherstone RL, Brown MM, Coward LJ (2004) International carotid stenting study: protocol for a randomised clinical trial comparing carotid stenting with endarterectomy in symptomatic carotid artery stenosis. Cerebrovasc Dis 18:69–74

Gass A, Gaa J, Schwartz A (1997) Cerebral infarction due to internal carotid artery dissection. J Neurol Neurosurg Psychiatry 63:420

Gass A, Gaa J, Sommer A et al (1999) Echo-planar diffusion-weighted MRI in the diagnosis of acute ischemic stroke: characterisation of tissue abnormalities and limitations in the interpretation of imaging findings. Radiologe 39:695–702
Gass A, Meairs S, Neff W et al (2001) Towards visualization of symptomatic carotid stenosis. Arch Neurol 58:658–659
Gold GE, Pauly JM, Glover GH et al (1993) Characterization of atherosclerosis with a 1.5-T imaging system. J Magn Reson Imaging 3:399–407
Guckel FJ, Brix G, Schmiedek P et al (1996) Cerebrovascular reserve capacity in patients with occlusive cerebrovascular disease: assessment with dynamic susceptibility contrast-enhanced MR imaging and the acetazolamide stimulation test. Radiology 201:405–412
Hartkamp MJ, van der GJ, van Everdingen KJ et al (1999) Circle of Willis collateral flow investigated by magnetic resonance angiography. Stroke 30:2671–2678
Heinsius T, Bogousslavsky J, van Melle G (1998) Large infarcts in the middle cerebral artery territory. Etiology and outcome patterns. Neurology 50:341–350
Hendrikse J, Hartkamp MJ, Hillen B et al (2001) Collateral ability of the circle of Willis in patients with unilateral internal carotid artery occlusion: borderzone infarcts and clinical symptoms. Stroke 32:2768–2773
Hennerici M, Hülsbömer HB Hefter H et al (1987) Natural history of asymptomatic extracranial arterial disease. Results of a long-term prospective study. Brain 110:777–791
Hennerici M, Daffertshofer M, Jakobs L (1998) Failure to identify cerebral infarct mechanisms from topography of vascular territory lesions. Am J Neuroradiol 19:1067–1074
Higashida RT, Meyers PM, Phatouros CC et al (2004) Reporting standards for carotid artery angioplasty and stent placement. Technology Assessment Committees of the American Society of Interventional; Therapeutic Neuroradiology and the Society of Interventional Radiology. Stroke 35:e112–e134
Hupperts RM, Warlow CP, Slattery J et al (1997) Severe stenosis of the internal carotid artery is not associated with borderzone infarcts in patients randomized in the European Carotid Surgery Trial. J Neurol 244:45–50
Kang DW, Chu K, Ko SB et al (2002) Lesion patterns and mechanism of ischemia in internal carotid artery disease: a diffusion-weighted imaging study. Arch Neurol 59:1577–1582
Kastrup A, Schulz JB, Mader I et al (2002) Diffusion-weighted MRI in patients with symptomatic internal carotid artery disease. J Neurol 249:1168–1174
Krabbe-Hartkamp MJ, van der GJ, de Leeuw FE et al (1998) Circle of Willis: morphologic variation on three-dimensional time-of-flight MR angiograms. Radiology 207:103–111
Le Bihan D (1991) Molecular diffusion nuclear magnetic resonance imaging. Magn Reson Q 7:1–30
Lee PH, Bang OY, Oh SH et al (2003) Subcortical white matter infarcts. Comparison of superficial perforating artery and internal borderzone infarcts using diffusion-weighted magnetic resonance imaging. Stroke 34:2630–2635
Macchi C, Catini C, Federico C et al (1996) Magnetic resonance angiographic evaluation of circulus arteriosus cerebri (circle of Willis): a morphologic study in 100 human healthy subjects. Ital J Anat Embryol 101:115–123
Maeda M, Yuh WT, Ueda T et al (1999) Severe occlusive carotid artery disease: hemodynamic assessment by MR perfusion imaging in symptomatic patients. Am J Neuroradiol 20:43–51
Mainwaring J (1760) Memoirs of the life of the late Georg Friedrich Händel. Dodsley, London
Mattle HP, Edelman RR (1992) Cerebral magnetic resonance angiography. Neurol Res 14:118–121
Moody AR, Murphy RE, Morgan PS et al (2003) Characterization of complicated carotid plaque with magnetic resonance direct thrombus imaging in patients with cerebral ischemia. Circulation 107:3047–3052
Mull M, Schwarz M, Thron A (1997) Cerebral hemispheric low-flow infarcts in arterial occlusive disease. Lesion patterns and angiomorphological conditions. Stroke 28:118–123
Nakano S, Yokogami K, Ohta H et al (1995) CT-defined large subcortical infarcts: correlation of location with site of cerebrovascular occlusive disease. AJNR 16:1581–1585
Neumann-Haefelin T, Wittsack HJ, Fink GR et al (2000) Diffusion- and perfusion-weighted MRI. Influence of severe carotid artery stenosis on the DWI/PI mismatch in acute stroke. Stroke 31:1311–1317
Ostergaard L, Sorensen AG, Kwong KK et al (1996) High resolution measurement of cerebral blood flow using intravascular tracer bolus passages, part II. Experimental comparison and preliminary results. Magn Reson Med 36:726–736
Patel MR, Kuntz KM, Klufas RA et al (1995) Preoperative assessment of the carotid bifurcation. Can magnetic resonance angiography and duplex ultrasonography replace contrast arteriography? Stroke 26:1753–1758
Patrux B, Laissy JP, Jouini S et al (1994) Magnetic resonance angiography (MRA) of the circle of Willis: a prospective comparison with conventional angiography in 54 subjects. Neuroradiology 36:193–197
Pessin MS, Hinton RC, Davis KR et al (1979) Mechanisms of acute carotid stroke. Ann Neurol 6:245–252
Pollanen MS, Deck JH (1989) Directed embolization is an alternate cause of cererbal watershed infarction. Arch Pathol Lab Med 113:1139–1141
Reith W, Heiland S, Erb G et al (1997) Dynamic contrast-enhanced T2*-weighted MRI in patients with cerebrovascular disease. Neuroradiology 39:250–257
Ries S, Schminke U, Daffertshofer M, Hennerici M (1996) High intensity transient signals (HITS) in patients with carotid artery disease. Eur J Med Res 1:328–330
Rodda RA, Path FRC (1986) The arterial patterns associated with internal carotid infarcts. Stroke 17:69–75
Roh JK, Kang DW, Lee SH et al (2000) Significance of acute multiple brain infarction on diffusion-weighted imaging. Stroke 31:688–694
Rosen BR, Belliveau JW, Vevea JM et al (1990) Perfusion imaging with NMR contrast agents. Magn Reson Med 14:249–265
Röther J, Wentz KU, Rautenberg W et al (1993) Magnetic resonance angiography in vertebrobasilar ischemia. Stroke 24:1310–1315
Röther J, Guckel F, Neff W (1996) Assessment of regional cerebral blood volume in acute human stroke by use of single-slice dynamic susceptibility contrast-enhanced magnetic resonance imaging. Stroke 27:1088–1093
Rothwell PM, Warlow CP (1999) Prediction of benefit from carotid endarterectomy in individual patients: a risk-modelling study. European Carotid Surgery Trialists' Collaborative Group. Lancet 353:2105–2110
Rothwell PM, Eliasziw M, Gutnikov SA et al (2004) Endarterectomy for symptomatic carotid stenosis in relation to clini-

cal subgroups and timing of surgery. Carotid Endarterectomy Trialists Collaboration. Lancet 363:915–924
Sacco RL.(2001) Clinical practice. Extracranial carotid stenosis. N Engl J Med 345:1113–1118
Sakuma H, Nomura Y, Takeda K et al (1991) Adult and neonatal human brain: diffusional anisotropy and myelination with diffusion-weighted MR imaging. Radiology 180:229–233
Schomer DF, Marks MP, Steinberg GK et al (1994) The anatomy of the posterior communicating artery as a risk factor for ischemic cerebral infarction. N Engl J Med 330:1565–1570
Szabo K, Kern R, Gass A et al (2001) Acute stroke patterns in patients with internal carotid artery disease. Stroke 32:1323–1329
Tanner JE (1983) Intracellular diffusion of water. Arch Biochem Biophys 224:416–428
Torvik A (1984) The pathogenesis of watershed infarcts in the brain. Stroke 15:221–223
Yuan C, Mitsumori LM, Beach KW et al (2001) Carotid atherosclerotic plaque: noninvasive MR characterization and identification of vulnerable lesions. Radiology 221:285–299
Van Heesewijk HP, Vos JA, Louwerse ES et al (2002) Carotid PTA and Stenting Collaborative Research Group. New brain lesions at MR imaging after carotid angioplasty and stent placement. Radiology 224:361–365
Van der Zwan A, Hillen B (1991) Review of the variability of the territories of the major cerebral arteries. Stroke 22:1078–1084
Waterston JA, Brown MM, Butler P et al (1990) Small deep cerebral infarcts associated with occlusive internal carotid artery disease. A hemodynamic phenomenon? Arch Neurol 47:953–957
Weiller C, Ringelstein EB, Reiche W et al (1990) The large striatocapsular infarct. A clinical and pathophysiological entity. Arch Neurol 47:1085–1091
Zülch KJ (1963) New concepts concerning the pathogenesis of cerebral ischemia. Ann Radiol 6:7–14

16 Hypoxic–Ischemic Lesions

Karl Olof Lövblad

CONTENTS

16.1 Introduction

As medical technology progresses, more advanced life-support techniques are available. While this is an important benefit to the vast majority of patients, we are also confronted with a small number of patients sustaining lesions to the brain due to hypoxia and ischemia. Since the implications regarding outcome are very serious, it is of utmost importance to recognize these lesions early on, so that the appropriate measures can be taken. The lesions may be localized or diffuse (bilateral, infra- and supra tentorial) depending on duration and acuity of ischemia. Significant acuity may suggest brain death clinically or radiologically (Lövblad and Bassetti 2000). Since these patients often receive various drugs and may be polymorbid (with both cardiac and cerebral pathologies), the physical examination can be difficult and frustrating, even for more experienced clinicians. Electroencephalography can assess central nervous system (CNS) dysfunction, and computed tomography (CT) can exclude hemorrhage and demonstrate diffuse ischemic edema; however, neither method may be sufficiently accurate to exactly delineate the extent of the damage incurred to the CNS. Since magnetic resonance imaging (MRI) appears superior in providing accurate information regarding brain anatomy and pathology, it should be used to assess its value in the diagnosis and management of patients with global cerebral ischemia and hypoxia.

K. O. Lövblad, MD
Neuroradiology Unit, Department of Radiology and Medical Informatics, University Hospitals Geneva, 24 rue Micheli-du-Crest, 1211 Geneva 14, Switzerland

16.2 Global Cerebral Ischemia and Hypoxia

16.2.1 Pathophysiology

At rest, the brain consumes 20% of the total oxygen that the whole body consumes. Global brain ischemia occurs when the arterial blood pressure cannot maintain a sufficient cerebral perfusion pressure. This happens with cardiac dysfunction, shock, and critical increase in intracranial pressure. Cerebral hypoxia is the deprivation of oxygen with a maintained cerebral blood flow. Pure hypoxia will occur in rare instances such as reduced atmospheric oxygen, which is an extremely rare cause of brain hypoxia, or as a result of drowning. Most cases occur in a combination of hypoxia and ischemia since pure hypoxia very often causes cardiac arrest and, thus, interruption of cerebral blood flow. The combination of both hypoxia and ischemia leads to more serious neuronal damage than hypoxia alone.

16.2.2 Causes

The causes of diffuse cerebral ischemia are: circulatory arrest (e.g., cardiac arrest), impaired circulation (strangulation, profound hypotension, extracranial

vascular disease), impaired energy substrate supply (hypoxic hypoxia, hypoglycemia, carbon monoxide poisoning), diffuse small vessel disease (hypertension, eclampsia, types of small vessel arteritis) and micro-embolic disease (fat embolism, disseminated intravascular coagulation, cardiopulmonary bypass procedures) (Toole and Burrow 1990). Strangulation and hanging will lead to hypoxia due to oligemia, airway obstruction, and respiratory arrest in the case of brain stem compression by fractured vertebrae.

16.2.3 Neuropathology

Acute cerebral ischemia affects neurons first and the more resistant glia and blood vessels in later stages. Deep cortical layers such as layer III of the cerebral cortex are especially vulnerable, mainly in the parietal and occipital regions and less in the frontal and temporal areas. The more vulnerable neurons are those of the caudate and putamen, the pyramidal cells of Sommer's area and the Purkinje cells in the cerebellum. The thalamus and brainstem are more resistant to hypoxia and ischemia. White matter is generally considered to be more resistant than grey matter.

The watershed areas (see Chap. 15) are particularly sensitive to ischemia in cardiac arrest, especially in the parietal lobe area in the borderzone between anterior, posterior and middle cerebral artery territories.

Laminar cortical necrosis is the end-stage of cortical ischemia and has been described in many conditions of cellular energy depletion, such as hypoxia and hypoglycemia. It may also be associated with a variety of other diseases affecting the nervous system (Valanne et al. 1996). Laminar cortical necrosis has been studied with nuclear medicine methods (Hawes and Mishkin 1972), but has recently been more extensively studied with CT and MRI.

16.3 Neuroimaging

CT and MRI have been used extensively to show acute cerebral ischemia (stroke) and its sequelae. While CT is mainly used to exclude hemorrhage, it is very specific in detecting changes in the water content of ischemic cerebral tissues.

16.3.1 Computed Tomography

In the early stages of focal brain ischemia, CT can demonstrate areas of hypoattenuation in the brain tissue that correspond to acute severe ischemia (von Kummer et al. 2001). It may be more difficult to detect diffuse pathology (Fig. 16.1). While early changes such as hypoattenuation and sulcal effacement may be detected by experts, the inexperienced interpreter may miss them. The sensitivity of CT

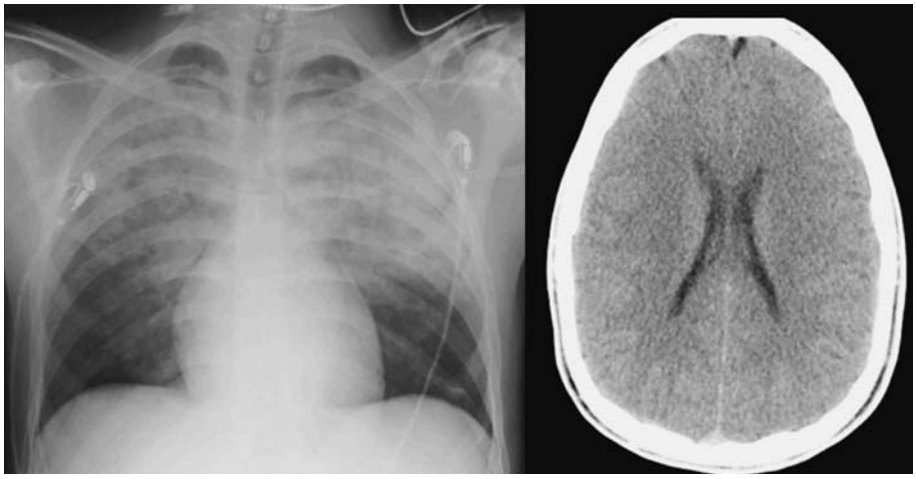

Fig. 16.1. A 20-year-old army recruit, found comatose in the toilets. An AP chest radiograph shows signs of bilateral aspiration pneumonia (*left*). The unenhanced computed tomography image shows no signs of ischemia (*right*)

for hypoxic–ischemic lesions in patients with global brain ischemia or hypoxia has never been directly compared with MRI.

16.3.2 Magnetic Resonance Imaging

Unfortunately, MRI is also insensitive to early ischemia when conventional T1 and T2 sequences are used (Fig. 16.2). Early signs of ischemia can be detected with confidence, mainly as hyperintensities on T2-weighted images (Yuh et al. 1991) not before 8–12 h after symptom onset. With the concurrent development of both faster scanners and sequences that allow echo-planar imaging (Edelman et al. 1994), the implementation of novel imaging techniques like diffusion-weighted MRI (DWI) became available (see Chap. 7) (Figs. 16.3, 16.4).

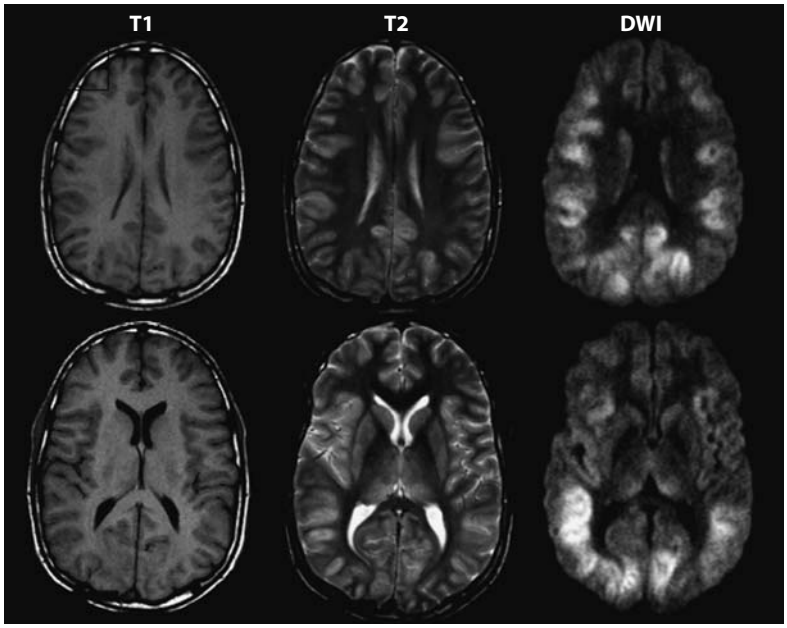

Fig. 16.2. Same patient as in Fig. 16.1. On MRI, the T1-weighted images show no clear pathological findings, the T2-weighted images show slight cortical hyperintensities detectable retrospectively. The diffusion-weighted images (*DWI*) show diffuse cortically located hyperintensities bilaterally

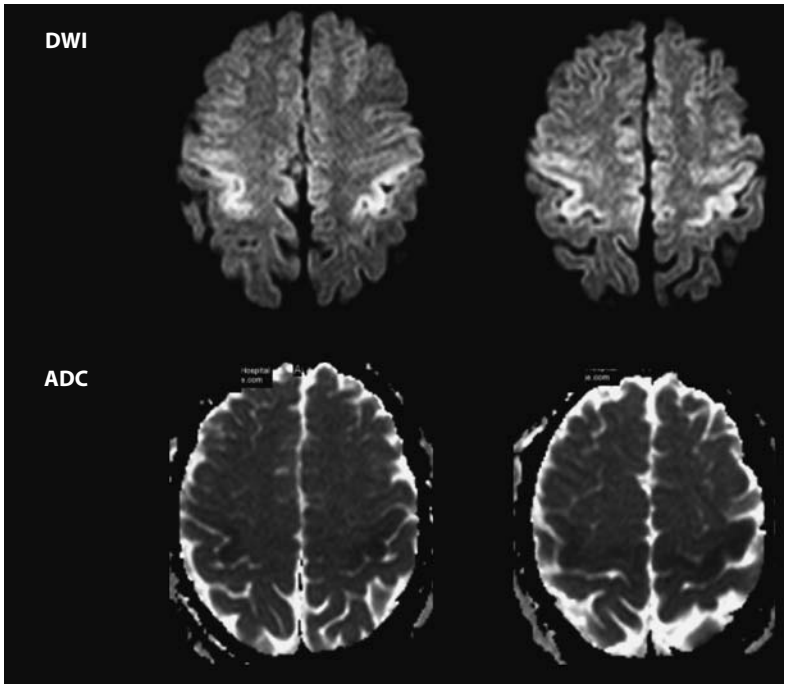

Fig. 16.3. A 42-year-old man, found comatose after cardiac arrest. On the diffusion-weighted images there is hyperintensity in the motor cortex bilaterally (*upper row*). These changes are accompanied by decreased apparent diffusion coefficient (ADC) values (*lower row*)

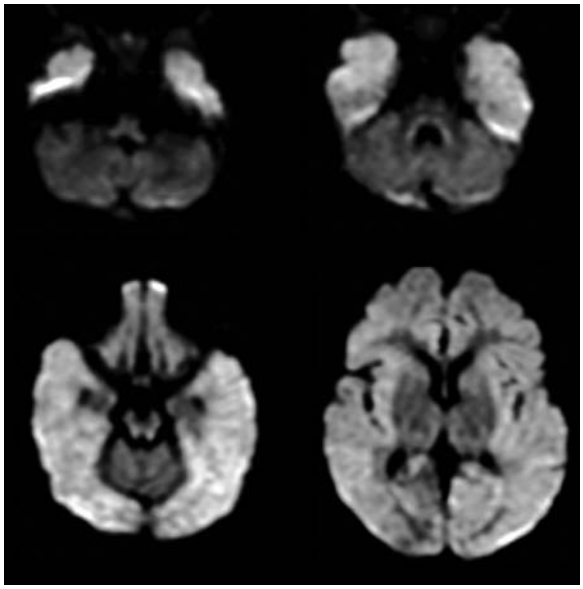

Fig. 16.4. A 6-month-old male with a Fallot tetralogy. The acute diffusion-weighted images show hyperintensities bilaterally, with sparing of the cerebellum and basal ganglia

Cortical ischemia has been studied with conventional MRI protocols (el Quessar et al. 1999; Komiyama et al. 1997, 1998; Takahashi et al. 1993; Sawada et al. 1990) where the involvement of the watershed zones in the parieto-occipito-temporal regions has been more frequently observed than elsewhere. Cerebral edema was also observed in the acute stage (Takahashi et al. 1993).

16.3.2.1 Conventional MRI (T1-, T2-Weighted MRI)

Usually T1-weighted MRI has been proposed to determine the presence of laminar cortical necrosis (Fig. 16.5): Sawada et al. (1990) observed T1 hyperintensities in the affected cortex and interpreted this finding as methemoglobin. Pathology, however, failed to show this. Histopathologically, pannecrosis is found with the death of neurons, glia and blood vessels in the affected tissue. This may result in protein degradation, which could account for the high T1 signal, as well as the possible accumulation of lipids in macrophages. T1 shortening and signal increase occur exclusively in the cortex. This suggests that the cortical necrosis is closely related to the MR signal changes. High protein concentrations or macromolecular concentration accelerate T1 relaxivity by restricting the motion of water, thus causing T1 shortening. Even a small elevation of protein concentration may cause significant T1 shortening.

Sawada et al. (1990) performed serial radiological examinations on a patient with anoxic encephalopathy; they found high T1 signal intensity areas distributed laminarly in the cerebral cortex and diffusely in the putamen in the early term after the anoxic insult, which were thought to reflect tissue necrosis. Correlation with single photon emission CT showed persistent hypoperfusion in the arterial watershed zones. Late T2-weighted MRI revealed diffuse high-intensity lesions in the arterial watershed zones (Sawada et al. 1990). In a study of six patients with cortical necrosis, Takahashi et al. (1993) reported that involvement of the watershed zones in the parieto-occipito-temporal cortex is more frequent and more severe than that in the basal ganglia, thalami, hippocampus, pons and cerebellum. Enhanced T1-weighted images showed cortical laminar enhancement in the early subacute stage; unenhanced T1-weighted images revealed characteristic laminar hyperintense lesions of the cerebral cortex in the late subacute stage. Both of these findings seemed to reflect the progression of cortical laminar necrosis. In the chronic stage, cortical atrophy and delayed but progressive white matter changes were seen (Takahashi et al. 1993).

Komiyama et al. (1997) studied patients with stroke and cortical necrosis by MRI and found that in 13 patients laminar cortical lesions began to appear on T1-weighted images about 2 weeks after the ictus. At 1-2 months they were prominent (Komiyama et al. 1997). They further studied 16 patients with laminar cortical necrosis by conventional MR sequences (T1-weighted, T2-weighted, FLAIR) and confirmed that high intensity cortical lesions were visible on the T1-weighted images from 2 weeks after ictus and became prominent at 1–3 months, then became less apparent, but occasionally remained at high intensity for 2 years. High intensity cortical lesions on FLAIR images became prominent from 1 month, and then became less prominent from 1 year ownward, but occasionally remained at high intensity for 2 years. Subcortical lesions did not display high intensity on T1-weighted images at any stage. On FLAIR images, subcortical lesions initially showed slightly high intensity and then low intensity from 6 months onward due to encephalomalacia (Komiyama et al. 1998).

In a study of six patients with laminar cortical necrosis, MRI showed hyperintense lesions in the cerebral cortex on T1-weighted and T2-weighted images (el Quessar et al. 1999). In four patients,

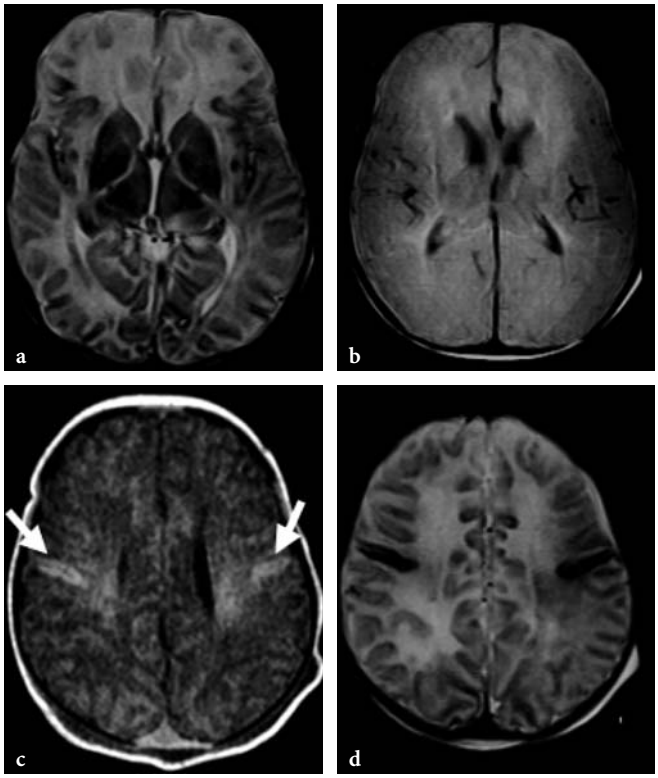

Fig. 16.5a–d. The late imaging shows diffuse cortical necrosis seen as areas of hyperintensity on T2-weighted imaging (**a, d**). Proton density image is shown in (**b**). There are also the typical T1-weighted hyperintensities in the parietal cortex bilaterally (*arrows,* **c**)

cortical laminar necrosis was caused by ischemic stroke, one insult occurred after a cardiac arrest and the last patient had a meningoencephalitis. The time delay from insult to the first MR study varied between 1 week and 3 months. The high intensity signal was still observed a few months after the insult. Cortical laminar necrosis lesions did not demonstrate hemorrhage on CT and MRI studies (el Quessar et al. 1999). Christophe et al. (1994) reported on four patients illustrating the early depiction of multiple types of neuropathologic lesions, which may coexist in the full-term newborn following severe hypoxic–ischemic encephalopathy. They demonstrated the presence of diffuse, postnatal involvement of cerebral cortex and subcortical white matter. They thought that cortical hyperintensity on both proton density- and T1-weighted images are probably related to cellular diffusely or parasagittally distributed necrosis. Hyperintense white matter on proton density-weighted images may result from increased water concentration due to infarct or edema, like low intensity on T1-weighted images and high intensity on T2-weighted images. On follow-up MRI several months later, lesions detected during the postnatal period were converted into cortical atrophy and myelination delay (Christophe et al. 1994). Christophe et al. (2002) also studied 40 children with hypoxic coma and found a strong correlation between first MRI score and neurological outcome (Christophe et al. 2002). The sensitivity of the first MRI score for clinically relevant ischemic lesions was high (96%), even when obtained during the first 3 days, with a specificity of 50% and a positive predictive value of 82%.

16.3.2.2 Diffusion-Weighted MRI

Diffusion-weighted MRI, due to its extreme sensitivity to changes in tissue water and, therefore, to ischemia (Le Bihan et al. 1986; Moseley et al. 1990; van Gelderen et al. 1994; Warach et al. 1992, 1995; Sorensen et al. 1996; Lövblad et al. 1998), makes it possible to demonstrate ischemic changes due to acute hypoperfusion (see Chap. 7). These findings correspond to those found in the early stages of laminar cortical necrosis (Figs. 16.3, 16.6, 16.7).

In a study of 12 patients with postresuscitation encephalopathy, the presence of high signal intensity regions in the bilateral cerebral cortex was the earliest finding (at less than 24 h) on DWI (Goto et al. 2001). Similar abnormality of bright high signal areas in FLAIR and T2 images followed in the early

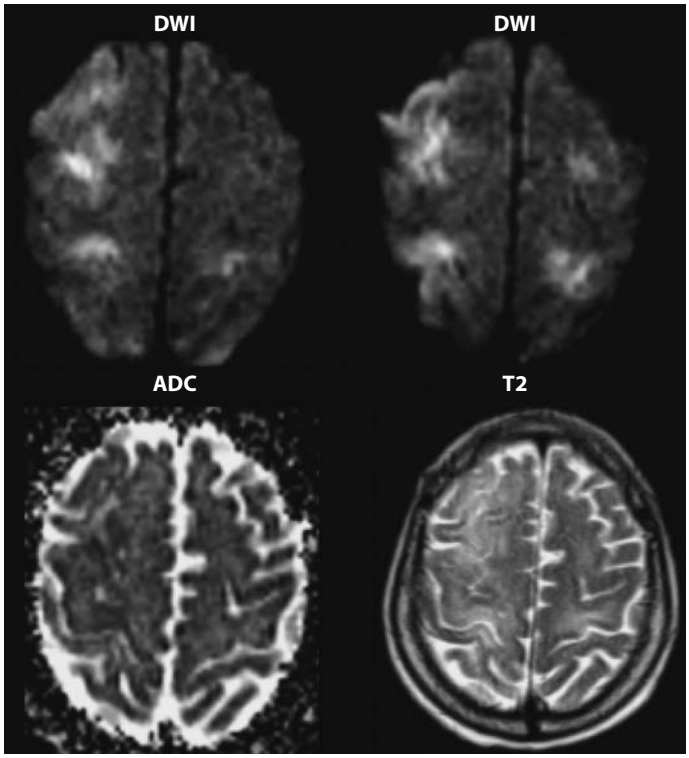

Fig. 16.6. A 55-year-old man with bradycardia. The diffusion-weighted imaging (DWI, *top row*) shows bilateral hyperintensities in the frontal cortex, accompanied by decreased ADC values (*left bottom*). The changes are slightly visible on T2 images (*right bottom*)

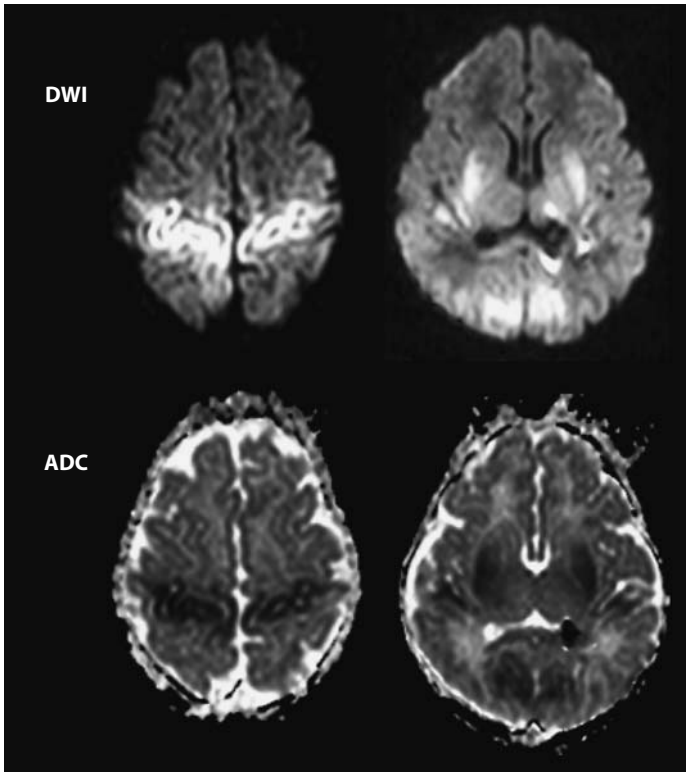

Fig. 16.7. A 15-day-old child with cardiac arrest and coma. The DWI images show bilateral hyperintensities in the cortex and white matter (*top row*), associated with decreased ADC values (*bottom row*)

subacute period (1-13 days). Subsequently, white matter was involved and laminar necrosis in cortical area was observed in the late subacute period (14-20 days). Finally, diffuse brain atrophy and an obscuration of the gray-white matter junction was seen in the chronic stage (after 21 days) (Goto et

al. 2001). The MRI findings closely correlated with poor clinical outcomes. The author saw two patients who had developed cortical necrosis following some form of immunotherapy – in one case it occurred following renal transplant rejection and in the second patient it was intoxitation by FK-506 (Lövblad et al. 2004). These findings confirm those of Bargallo et al. (2000) who reported a patient who developed similar MRI findings after immunosuppressive therapy, suggesting a hypoxic mechanism in these patients. Takeoka et al. (2002), in a series of eight newborns with neonatal hypoxic injury, found that the distribution of DWI abnormalities was consistent with the type of global hypoxic–ischemic injury usually found in full-term neonates with diffuse cortical necrosis, borderzone infarcts, or basal ganglia/thalamic injury. They also found that in each patient, standard MRI sequences substantially underestimated the extent of injury when compared with diffusion-weighted images in neonatal brains (Takeoka et al. 2002). They observed that extensive injury bilateral with basal ganglia, thalamic, and widespread multifocal cortical involvement correlated with poor neurological outcome. They also showed that lesser degrees of injury, limited to smaller sectors of cortical or borderzone involvement, were associated with better neurological outcome.

Using DWI to evaluate patterns of ischemic changes in anoxic brain injury, Singhal et al. (2002) studied clinical and DWI features of three patients with different types of anoxic brain injury: attempted hanging, carbon monoxide poisoning (hypoxic hypoxia), and hanging with cardiac arrest (hypoxic–ischemic encephalopathy). The first two patients, but not the third, recovered substantial neurological function. The distribution of DWI abnormalities was different and correlated well with the distinct neuropathological features of these entities. The prognosis after anoxic encephalopathy depends on the underlying mechanism and its severity, which may be reflected by DWI abnormalities. The two patients with less severe forms of hypoxic injury survived whereas the patient with a combination of hypoxia and ischemia died. They found that hyperintensity throughout the cerebral cortex was in favor of diffuse hypoxia with ischemia, whereas DWI hyperintensities restricted to the thalamus and selected cortical regions suggested primary milder hypoxic injury (Singhai et al. 2002). Hald et al. (2003) reported on a 16-year-old man after a suicide attempt who had normal initial DWI 5-6 h after the event, but pathological findings at 3 days. They were unable to entirely explain the initial normal findings on DWI (Hald et al. 2003).

Table 16.1. Clinical data of 26 patients with global cerebral hypoxia/ischemia

	Age*	Gender	Underlying cause	Time	Outcome	T2	T1
1	20	M	Marijuana abuse	12 h	Death	0	0
2	79	F	Cardiac disease	24 h	Death	0	0
3	2 days	M	Cardiac arrest	20 h	Death	0	0
4	58	F	Cardiac arrest	15 h	Death	0	0
5	8 months	M	Cardiac operation	7 days	Disabled	+	-
6	51	M	Renal transplant	7 days	Death	+	-
7	55	M	Bradycardia	6 days	Disabled	-	0
8	44	M	Cardiac arrest	5 days	Death	-	0
9	4	F	ARDS	8 days	Death	-	0
10	57	M	Barbiturate intoxication	12 h	Death	0	0
11	81	M	Stroke	10 days	Disabled	+	-
12	8	M	Cardiac arrest	5 days	Death	-	0
13	66	M	Tacrolimus intoxication	7 days	Death	-	0
14	51	M	Arrhythmia	12 h	Disabled	0	0
15	9 days	M	Cardiac arrest	5 days	Disabled	-	0
16	12	M	Hanging	2 days	Death	-	0
17	44	M	Cardiac arrest	36 h	Death	-	0
18	70	M	Cardiac arrest	15 h	Disabled	-	0
19	52	M	Cardiac arrest	20 h	Death	-	0
20	57	F	Cardiac arrest	2 days	Death	+	0
21	44	F	Cardiac arrest	24 h	Death	-	0
22	42	M	Cardiac arrest	3 days	Disabled	+	-
23	25 days	M	Cardiac arrest	2 days	Death	+	+
24	53	M	Cardiac arrest	10 h	Disabled	-	-
25	46	M	Cardiac arrest	2 days	Death	+	-
26	35	F	Intracranial hemorrhage	12 days	Death	+	+

ARDS, acute respiratory distress syndrome; *time*, time between onset of symptoms and MRI; *T2,T1*, 0: normal findings; + equivalent to diffusion-weighted MRI; - less extensive changes than suspected on DWI alone * in years if not stated otherwise

The author examined comatose patients with suspected cortical ischemia with DWI who had suffered from cerebral hypoxia often after cardiac arrest (Lövblad et al. 2004). A further evaluation of an expanded series of these patients is presented in Table 16.1 26 patients with lesions attributed to hypoxia that resumes the clinical signs of all patients. This series confirms the initial observation that DWI was superior to T2-weighted MRI regarding the prediction of lesion extent. Table 16.2 presents the patterns and localizationof findings. The DWI lesions were localized in the typical watershed regions in 7 of 26 (27%) (Fig. 16.8). The cortical lesions were unilateral in one patient (4%). Basal ganglia involvement was found in 10 of 26 patients (38%), and there was also white matter involvement in 9 of 26 patients (35%) (Figs. 16.8 and 16.9). Additional infratentorial lesions were found in 3 of 19 patients (35%) (Fig. 16.8).

When comparing the diffusion images to the standard T2-weighted images, the diffusion lesions were more extended in 12 patients (46%), DWI detected lesions not seen in another six patients (T2 negative: 23%; Fig. 16.2) and in only 8 of 26 (31%), patients' T2-weighted imaging confirmed the DWI findings (results equal for DWI and T2-weighted imaging). This finding was also observed by Arbalaez et al. (1999) who found that during the acute period, DWI showed the abnormal basal ganglia, cerebellum, and cortex to a better extent than conventional MR images (Arbelaez et al. 1999).

Table 16.2. Diffusion-weighted imaging findings in 26 cases of cerebral hypoxic–ischemic lesions

Localization		
Supratentorial (bi- and unilateral)	26/26	100%
Bilateral diffuse	22/26	85%
Bilateral focal	3/26	11%
Unilateral	1/26	4%
+Infratentorial	4/26	18%
Watershed type	7/26	27%
Basal ganglia involvement	10/26	38%
White matter involvement	9/26	35%

Of the 26 patients, 19 did not survive; the demised patients had bilateral involvement of the cortex, as well as some degree of involvement of the white matter (9 patients) and basal ganglia (10 patients). Five patients survived with severe disabilities. They did not have white matter or basal ganglia involvement. Based on these MR images obtained in patients with hypoxic-ischemic lesions, it was possible to establish a grading of the DWI findings (Table 16.3), ranging between 1 and 4. All five patients who survived belonged to grades 1 and 2. Patients in grades 3 and 4 all died.

The association of white matter lesions seems to contribute to morbidity. Cortical laminar changes on MRI without concomitant white matter abnormali-

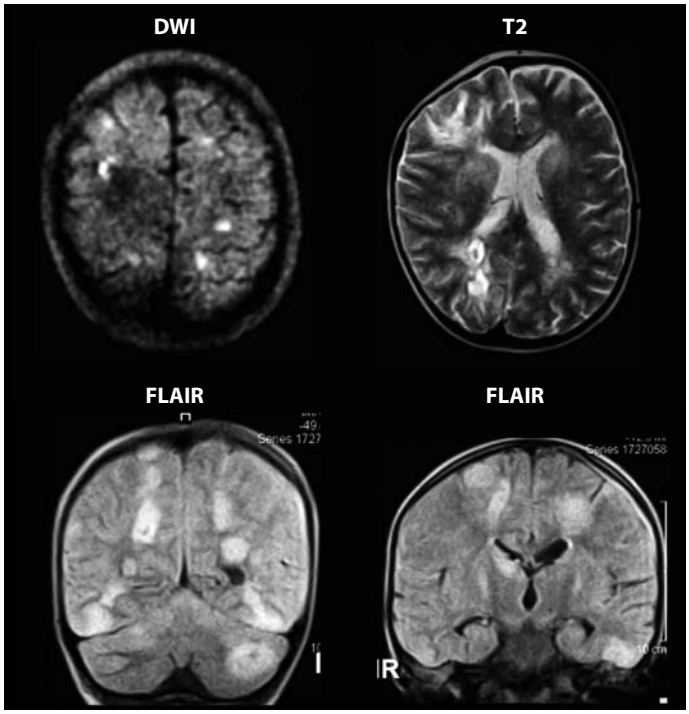

Fig. 16.8. A 4-year-old girl with leukemia suffering from acute respiratory distress syndrome. On DWI there are bilateral hyperintensities partly seen on the T2-weighted and FLAIR images. The lesions affect the cortex, the basal ganglia, the white matter as well as the cerebellum

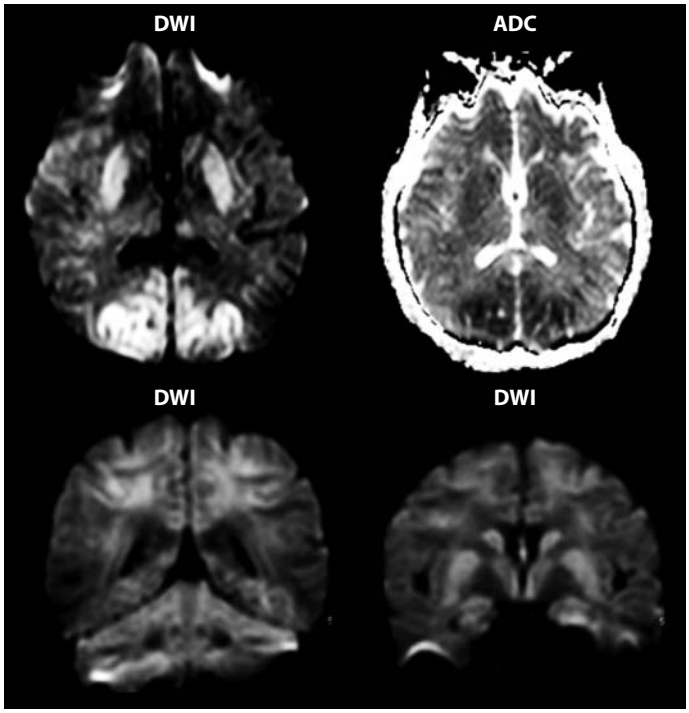

Fig. 16.9. A 44-year-old lady found comatose after cardiac arrest. Bilateral hyperintensities on diffusion-weighted images (DWI) are present in the cortex. There are also hyperintensities in the basal ganglia and subcortical white matter with associated diminished ADC values (*right top*), best seen

Table 16.3. Grading of diffusion-weighted MR imaging (DWI) findings in global cerebral hypoxia/ischemia.

Grade 1: DWI hyperintensities in the fronto-parieto-occipital cortex
Grade 2: DWI hyperintensities in the fronto-parieto-occipital cortex and basal ganglia
Grade 3: DWI hyperintensities in the fronto-parieto-occipital cortex, basal ganglia and supratentorial white matter
Grade 4: DWI hyperintensities in the fronto-parieto-occipital cortex, basal ganglia, white matter and cerebellum

ties was associated with an increased risk of spasticity in children (van der Knaap et al. 1993). In children with white matter lesions, cortical laminar abnormalities did not contribute to the risk of spasticity, which was already highly increased by the presence of white matter damage (van der Knaap et al. 1993).

Laminar necrosis is a rare manifestation of neuronal injury with a very poor prognosis. Laminar necrosis often follows hypotension of relatively slow onset but of long duration. The process thus results from oxygen or glucose depletion caused by anoxia, hypoglycemia, status epilepticus, or ischemic stroke. Most of our patients had some form of circulatory failure.

DWI has the clear advantage that it shows acute changes due to anoxia leading to laminar necrosis. It does not show the subsequent infiltration of lipid-filled macrophages, the imaging correlate of which is potentially seen on T1-weighted images. These findings do, however, appear later on. High-signal cortical lesions began to appear about 2 weeks after the ictus, were prominent at 1-2 months, then became less evident, but occasionally remained for up to 1.5 years (Siskas et al. 2003). T1-weighted changes may correspond to a variety of causes as described by Boyko et al. (1992). The correlation between imaging abnormalities and neuropathological findings could be established in a case presented in Figs. 16.10 and 16.11. In this patient, a severe intoxication had lead to diffuse cortical necrosis both in the neocortex and cerebellar cortex accompanied by widespread neuronal damage (Fig. 16.10).

The findings in all these clinical series are confirmed by those of Kawahara et al. (2000) who found in both animal models and in humans that diffusion-weighted images show hyperintensity with associated drops on the ADC maps. On histopathological correlation, they found microvacuolation in the pyramidal neurons in the CA1 region; at 1 week, the hyperintensity in diffusion-weighted images had disappeared and microvacuolation had also disappeared in the CA1 region, but severely disrupted pyramidal neurons containing pyknotic nuclei had appeared in the CA1 region (Kawahara et al. 2000).

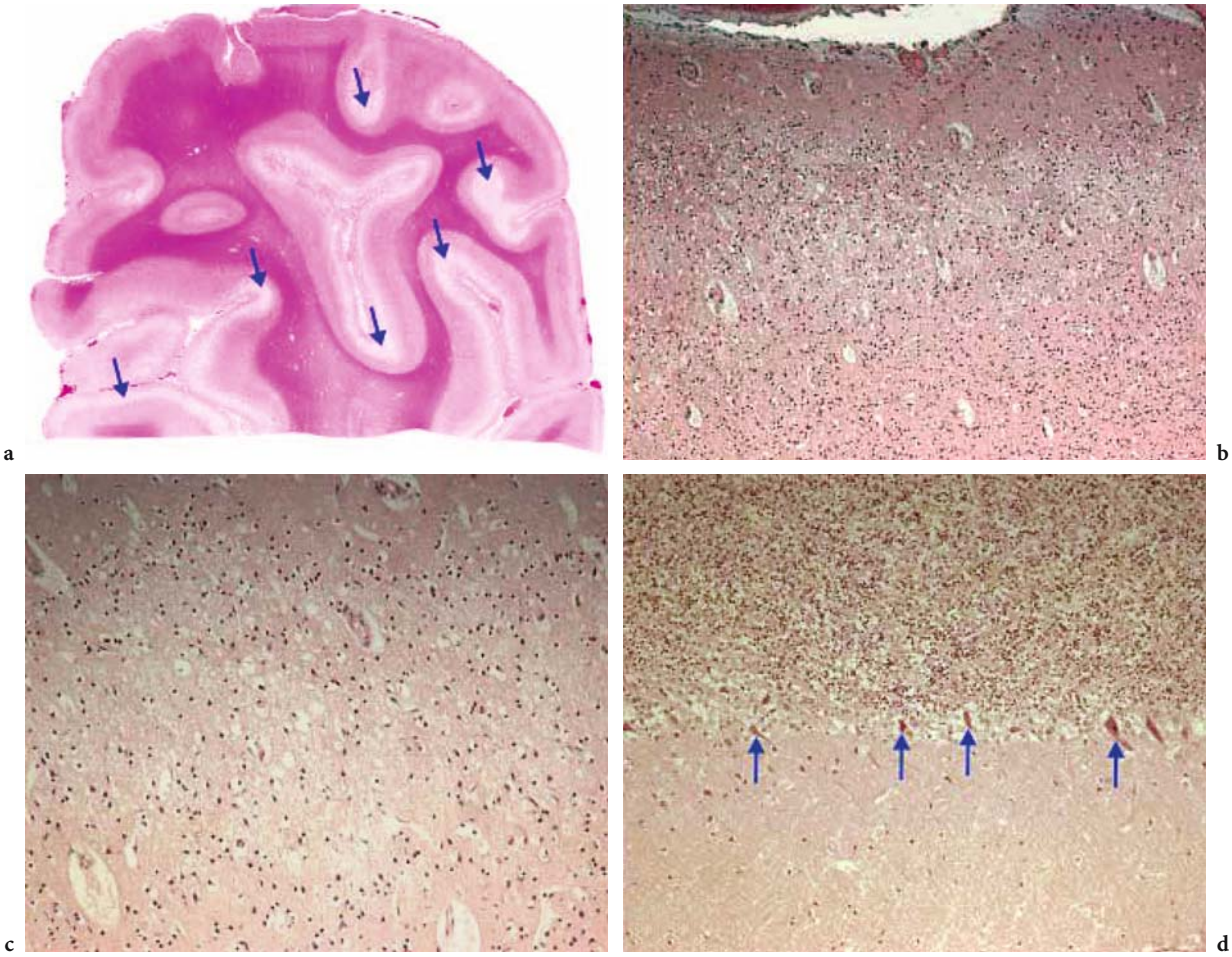

Fig. 16.10a–d. A 66-year-old man found comatose after severe intoxication. The neuropathological findings show: diffuse cortical necrosis (recent, **a**); the *arrows* indicate that edema predominates in the depth of the sulci. There are shrunken neurons with eosinophilic cytoplasm and pyknotic nuclei (**b, c**). The cerebellar cortex shows shrunken necrotic Purkinje cells (**d**)

16.4 Conclusions

In comparison to conventional images provided by MRI and CT, DWI provides an improved sensitivity for the lesion extent in patients with cerebral lesions due to hypoxic and hypoxic–ischemic events. This was also observed by Arbalaez et al. (1999) who found that during the acute period, DWI showed the abnormal basal ganglia, cerebellum, and cortex to a better extent than conventional MR images. Therefore, based on the existing literature, we believe that DWI can help in identifying and classifying the extent of ischemia in patients with global ischemia-hypoxia by giving us an in vivo appraisal of ongoing pathophysiological changes. It is also evident that the earlier the imaging is performed, the more sensitive DWI is for detecting ischemic changes not seen on T2-weighted imaging. The data suggest that more extensive cortical lesions with supplemental lesions in the white matter and/or posterior fossa have a worse prognosis (Lövblad et al. 2004; van der Knaap et al. 1993; Christophe et al. 2002). For the moment, MRI and DWI will remain an indispensable adjunct to the clinical examination and electrophysiology even if its exact role in the forensic management has still to be established with certainty.

Acknowledgements
We thank Dr G.P. Pizzolato for providing us with the neuropathological examinations and figures. We thank Dr J. Delavelle for her invaluable help with the evaluation of the data. Philippe Camarassa provided the invaluable photography. Dr A. Alimenti provided help with evaluation of the DWI data. Dr Lövblad was supported by a grant from the Swiss

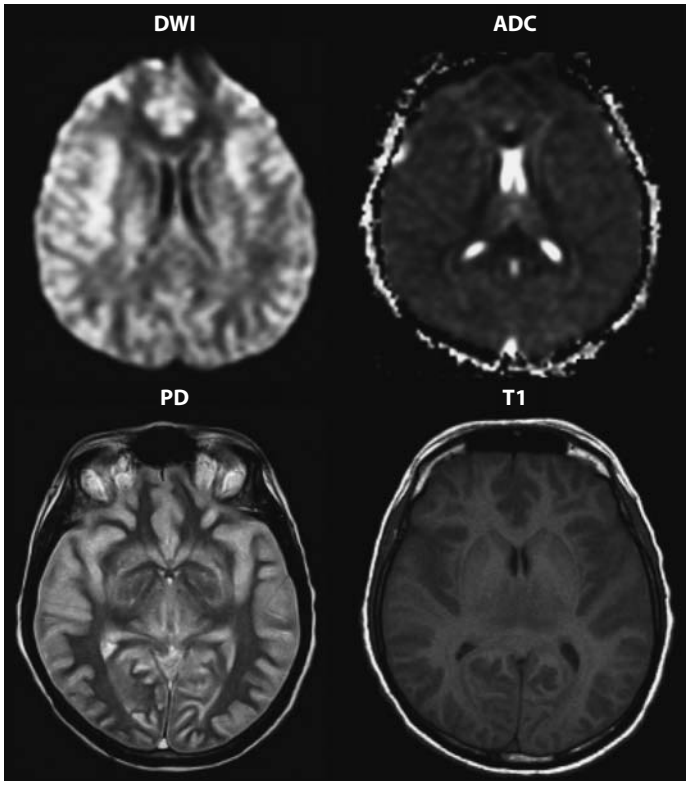

Fig. 16.11. Neuroimaging of the case above (Fig. 16.10) showed diffuse hyperintensity on DWI of both cerebral hemispheres (white brain), affecting all components; cortex, basal ganglia and white matter. There is an associated decrease in the (ADC). The T1 images and (PD) images are also altered with signs of edema

National Foundation, Grant No. 3100-066348.01 "Mapping the ischemic tissue at risk with diffusion and perfusion MRI".

References

Arbelaez A, Castillo M, Mukherji SK (1999) Diffusion-weighted MR imaging of global cerebral anoxia. Am J Neuroradiol 20:999–1007

Bargallo N, Burrel M, Berenguer J, Cofan F, Bunesch L, Mercader JM (2000) Cortical laminar necrosis caused by immunosuppressive therapy and chemotherapy. Am J Neuroradiol 21:479–484

Boyko OB, Burger PC, Shelburne JD, Ingram P (1992) Non-heme mechanisms for T1 shortening: pathologic, CT, and MR elucidation. Am J Neuroradiol 13:1439–1445

Christophe C, Clercx A, Blum D, Hasaerts D, Segebarth C, Perlmutter N (1994) Early MR detection of cortical and subcortical hypoxic-ischemic encephalopathy in full-term-infants. Pediatr Radiol 24:581–584

Christophe C, Fonteyne C, Ziereisen F, Christiaens F, Deltenre P, de Maertelaer V et al (2002) Value of MR imaging of the brain in children with hypoxic coma. Am J Neuroradiol 23:716–723

Edelman RR, Wielopolski P, Schmitt F (1994) Echo-planar MR imaging. Radiology 192:600–612

El Quessar A, Meunier JC, Delmaire C, Soto Ares G, Pruvo JP (1999) MRI imaging in cortical laminar necrosis. J Radiol 80:913–916

Gillard JH, Papadakis NG, Martin K, Price CJ, Warburton EA, Antoun NM et al (2001) MR diffusion tensor imaging of white matter tract disruption in stroke at 3 T. Br J Radiol 74:642–647

Gorelick PB, Kelly MA (1993) Neurological complications of cardiac arrest. In: Vinken PJ, Bruyn GW, Klawans HL (eds) Handbook of clinical neurology, vol 19(63): systemic diseases, part 1. Elsevier, Amsterdam, pp 205–227

Goto Y, Wataya T, Arakawa Y, Hojo M, Chin M, Yamagata S et al (2001) Magnetic resonance imaging findings of postresuscitation encephalopathy: sequential change and correlation with clinical outcome. No To Shinkei 53:535–540

Hald JK, Brunberg JA, Dublin AB, Wootton-Gorges SL (2003) Delayed diffusion-weighted MR abnormality in a patient with an extensive acute cerebral hypoxic injury. Acta Radiol 44:343–346

Hawes DR, Mishkin FS (1972) Brain scans in watershed infarction and laminar cortical necrosis. Radiology 103:131–134

Kawahara H, Takeda Y, Tanaka A, Nagano O, Katayama H, Hirakawa M, Hiraki Y (2000) Does diffusion-weighted magnetic resonance imaging enable detection of early ischemic change following transient cerebral ischemia? J Neurol Sci 181:73–81

Komiyama M, Nishikawa M, Yasui T (1997) Cortical laminar necrosis in brain infarcts: chronological changes on MRI. Neuroradiology 39:474–479

Komiyama M, Nakajima H, Nishikawa M, Yasui T (1998) Serial MR observation of cortical laminar necrosis caused by brain infarction. Neuroradiology 40:771–777

Le Bihan D, Breton E, Lallemand D, Grenier P, Cabanis E, Laval-Jeantet M (1986) MR imaging of intravoxel incoherent motions: application to diffusion and perfusion in neurologic disorders. Radiology 161:401–407

Lövblad KO, Laubach HJ, Baird AE, Curtin F, Schlaug G, Edelman RR et al (1998) Clinical experience with diffusion-weighted MR in patients with acute stroke. Am J Neuroradiol 19:1061–1066

Lövblad KO, Bassetti C (2000) Diffusion-weighted magnetic resonance imaging in brain death. Stroke 31:539–542

Lövblad KO, Wetzel SG, Somon T, Wilhelm K, Mehdizade A, Kelekis A, El-Koussy M et al (2004) Diffusion-weighted MR imaging in cortical ischemia. Neuroradiology 46:175–182

Moseley ME, Cohen Y, Mintorovitch J, Chileuitt L, Shimizu H, Kucharczyk J et al (1990) Early detection of regional cerebral ischemia in cats: comparison of diffusion- and T2-weighted MRI and spectroscopy. Magn Reson Med 14:330–346

Sawada H, Udaka F, Seriu N, Shindou K, Kameyama M, Tsujimura M (1990) MRI demonstration of cortical laminar necrosis and delayed white matter injury in anoxic encephalopathy. Neuroradiology 32:319–321

Schlaug G, Siewert B, Benfield A, Edelman RR, Warach S (1997) Time course of the apparent diffusion coefficient (ADC) abnormality in human stroke. Neurology 49:113–119

Singhal AB, Topcuoglu MA, Koroshetz WJ (2002) Diffusion MRI in three types of anoxic encephalopathy. J Neurol Sci 15:37-40

Siskas N, Lefkopoulos A, Ioannidis I, Charitandi A, Dimitriadis AS (2003) Cortical laminar necrosis in brain infarcts: serial MRI. Neuroradiology 45:283–288

Sorensen AG, Buonano FS, Gonzalez RG, Schwamm LH, Lev MH, Huang-Hellinger FR et al (1996) Hyperacute stroke: evaluation with combined multisection diffusion-weighted and hemodynamically-weighted echo-planar MR imaging. Radiology 199:391–401

Takahashi S, Higano S, Ishii K, Matsumoto K, Sakamoto K, Iwasaki Y et al (1993) Hypoxic brain damage: cortical laminar necrosis and delayed changes in white matter at sequential MR imaging. Radiology 189:449–456

Takeoka M, Soman TB, Yoshii A, Caviness VS Jr, Gonzalez RG, Grant PE et al (2002) Diffusion-weighted images in neonatal cerebral hypoxic-ischemic injury. Pediatr Neurol 26:274–281

Toole JF, Burrow DD (1990) Pathophysiology and clinical evaluation of ischemic vascular disease. In: Youmans JR (ed) Neurological surgery, 3rd edn, vol 3. Saunders, Philadelphia, pp 1463-1515

Valanne L, Paetau A, Suomalainen A, Ketonen L, Pihko H (1996) Laminar cortical necrosis in MELAS syndrome: MR and neuropathological observations. Neuropediatrics 27:154–160

Van der Knaap MS, Smit LS, Nauta JJ, Lafeber HN, Valk J (1993) Cortical laminar abnormalities–occurrence and clinical significance. Neuropediatrics 24:143–148

Van Gelderen P, de Vleeschouwer MHM, DesPres D, Pekar J, van Zijl PCM, Moonen CTW (1994) Water diffusion and acute stroke. Magn Reson Med 31:154–163

Von Kummer R, Bourquain H, Bastianello S, Bozzao L, Manelfe C, Meier D et al (2001) Early prediction of irreversible brain damage after ischemic stroke at CT. Radiology 219:95–100

Warach S, Chien D, Li W, Ronthal M, Edelman RR (1992) Fast magnetic resonance diffusion-weighted imaging of acute stroke. Neurology 42:1717–1723

Warach S, Gaa J, Siewert B, Wielopolski P, Edelman RR (1995) Acute human stroke studies by whole brain echo planar diffusion-weighted magnetic resonance imaging. Ann Neurol 37:231–241

Yuh WT, Crain MR, Loes DJ, Greene GM, Ryals TJ, Sato Y (1991) MR imaging of cerebral ischemia: findings in the first 24 hours. Am J Neuroradiol 12:621–629

17 Spinal Infarcts

Michael Mull and Armin Thron

CONTENTS

17.1 Introduction

The clinical diagnosis of spinal cord ischemia remains difficult and is mainly based on magnetic resonance imaging (MRI). In the last decade MRI has become the imaging modality of first choice in confirming the diagnosis of spinal vascular diseases. Spinal cord ischemia is a rare disease accounting only for 1%–2% of all vascular neurological pathologies. In contrast to the cerebrovascular system, the arteries directly supplying the spinal cord are not significantly affected by atherosclerotic vessel wall changes. Even in the first descriptions of the anterior spinal artery syndrome by Preobraschenski (1904) and Spiller (1909), the central arteries were affected in cases of luetic arteritis. With increasing spatial and contrast resolution, MRI can show circumscribed regions of spinal cord ischemic affection. Moreover, the demonstration of blood vessels in and around the spinal cord based on MRI has substantially improved recently. Nevertheless, the spinal arterial system is seldom examined in detail by spinal digital subtraction angiography (DSA) during life resulting in a limited understanding and fragmentary knowledge of the vascular basis of spinal circulatory disorders. Our knowledge of the spinal cord vascularization remains based on anatomical and microradiographic studies.

The main purpose of this chapter is to define the impact of MRI on the diagnosis of vascular diseases of the spinal cord.

M. Mull, MD
A. Thron, MD
Department of Neuroradiology, Clinic for Diagnostic Radiology, University Hospital of the Technical University, Pauwelsstr. 30, 52074 Aachen, Germany

17.2 Vascular Anatomy of the Spinal Cord

To interpret MR findings in spinal cord ischemia, it is necessary to be aware of the normal arterial supply and venous drainage of the spine and spinal cord. Lesion patterns and concomitant signs such as vertebral body infarction highly depend on the underlying vascular pathology. Anatomical and microangiographic examinations remain the main basis of our understanding in this field (Kadyi 1889; Thron 1988).

17.2.1 Arterial Supply

Segmental arteries supply the spine with blood, including the vertebral bodies, paraspinal muscles, dura, nerve roots, and spinal cord. All these tissues, with the exception of the spinal cord, receive their blood supply from segmental arteries (one on each side) or their equivalents. In particular, the segmental supply of the thoracolumbar region is derived from intercostal and lumbar arteries arising from

the aorta (Fig. 17.1). Sources of blood supply in the cervical and upper thoracic regions are longitudinal arteries following intrauterine vascular rearrangements. In this region the vertebral artery, the deep cervical artery, and the ascending cervical artery give rise to feeders supplying the spinal cord. In the sacral and lower lumbar region, sacral arteries and iliolumbar arteries arise from the internal iliac arteries and supply the caudal spine.

The radicular arteries are the first branches of the dorsal division of the segmental arteries and their regional equivalents. The blood supply of the bony spine consists of arteries, which come directly off the segmental and radicular arteries. Anterior central arteries derive from the segmental artery and supply the anterior and anterolateral portions of the vertebral body. The radicular arteries usually provide the blood supply to the posterior portion of the vertebral body via posterior central arteries and the arch via prelaminar arteries. Thus, the vertebral body is mainly supplied by posterior and anterior central arteries, which derive from the segmental and radicular arteries.

A spinal radicular branch is present at every segmental level. The number of spinal radicular arteries that supply as radiculomedullary arteries the spinal cord, is restricted. They follow the anterior and posterior nerve roots. When they reach the anterior or posterior surface of the spinal cord, they form the anterior or posterior spinal arteries. Thus, the arterial supply of the entire spinal cord depends on a single anterior spinal artery system and paired posterior spinal arteries. The number of anterior radiculomedullary arteries ranges from 2 to 17. The largest ventral radiculomedullary artery which supplies the thoracolumbar cord enlargement is the arteria radicularis magna of Adamkiewicz (Fig. 17.2). In this region large posterior radiculo-pial arteries are also frequently found and form an anastomotic circle around the conus medullaris (arcade of the conus; Kadyi 1889). The highest density of central arteries can be found here in microangiograms

Fig. 17.1a,b. Contrast-enhanced spinal MR angiography, sagittal views. **a** First phase: the segmental arteries are visible (*arrowhead*), note the bright enhancement of the aorta. **b** Second phase: the accompanying veins arise (*arrow*)

a

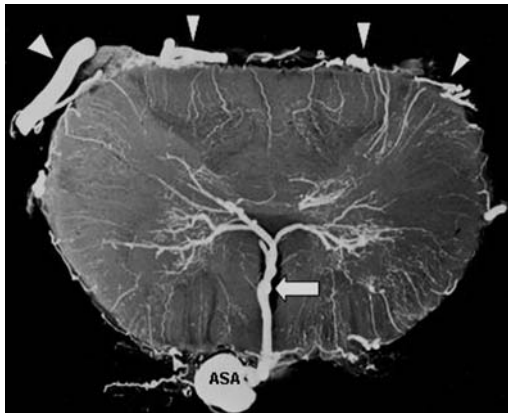

b

Fig. 17.2. a Superficial arteries of the spinal cord. X-ray film of an injected specimen in a.p. view. The anterior spinal artery system is visible on the ventral surface of the cord. **b** Intrinsic spinal cord arteries. X-ray microangiogram of a transverse section (lumbar enlargement). The sulcal or central artery within the anterior fissure (*arrow*) is dominant. Note the posterior and posterolateral spinal arteries at both sides of the posterior root entry zone (*arrowheads*). *ASA*, anterior spinal artery

reflecting the metabolic demand of the thoracolumbar enlargement.

Those spinal radicular arteries that are radiculomedullary arteries, supplying nerve root, pial plexus and medulla, branch in a very typical way to form the anterior spinal artery. The ascending branch continues the direction of the radicular artery in the midline of the anterior surface. The descending branch, being the larger one at thoracolumbar levels, forms a hairpin curve as soon as it reaches the midline at the entrance of the anterior fissure (Fig. 17.3). The artery runs above the vein. The maximum diameter of a spinal radiculomedullary artery or the anterior median anastomotic trunc (anterior spinal artery) is 1 mm. The radicular arteries (< 0.4 mm) that run with the posterior nerve root, supply the posterior and posterolateral longitudinal arteries. Their size totals 0.1–0.2 mm, which is beyond the present spatial resolution of MR scanners. Together with transverse interconnections, these discontinuous trunks supply the network of pial arteries called the "vasocorona" (Lasjaunias et al. 2001; Thron 1988). The normal intrinsic arteries of the spinal cord are also too small (<0.2 mm) to be detected on CT or MR images.

The spinal cord is protected against ischemia by extra- and intradural longitudinal and transverse anastomoses. Extradural longitudinal and transverse interconnections between segmental arteries can compensate for a focal vessel occlusion at the level of the radicular artery (Fig. 17.3). The anterior and posterior spinal arteries represent a system of longitudinal anastomoses that is reinforced from various segmental levels. The intrinsic anastomotic system is supplemented by secondary longitudinal connections between central arteries and by the pial network of the vasocorona. This specific vascular supply explains why spinal infarctions are highly variable, and distinct, predictable vascular territories as present in the brain do not exist (Fig. 17.4). Moreover, the normal arterial vascular system of the spinal cord is not detectable in MRI.

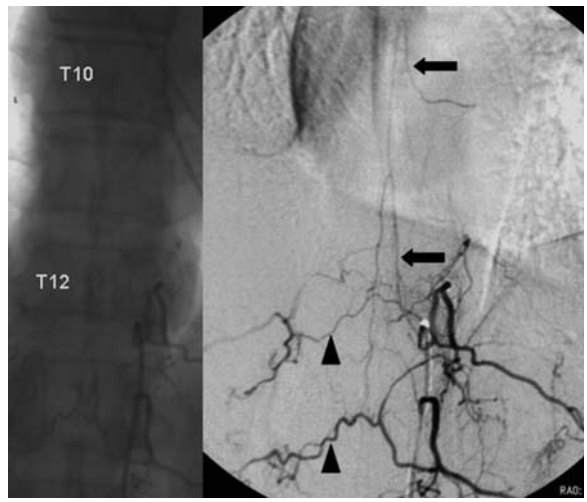

Fig. 17.3. Selective spinal DSA in a 59-year-old woman, p.a. projection. Injection of the 12th left thoracic segmental artery. Filling of the radiculomedullary arteries T12 and T10 on the left side (*arrows*) and the anterior spinal artery system. Collateral filling of the right-sided segmental arteries via retrocorporal anastomoses (*arrowheads*). These extradural anastomoses can compensate for focal vessel occlusions at the level of the radicular artery

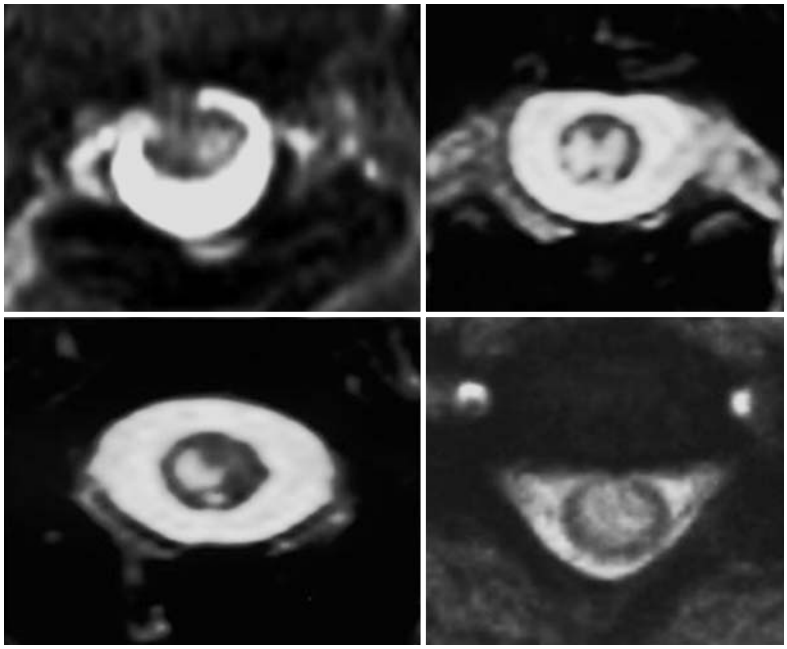

Fig. 17.4. Axial T2-weighted images in four patients with acute ischemic myelomalacia of the spinal cord. The hyperintense infarctions reflect different lesion patterns depending on occlusion site and collateral supply

17.2.2 Venous Drainage

Blood from radial veins of the spinal cord parenchyma and from the small superficial pial veins is collected in two large vessels, the anterior and posterior median spinal veins. The anterior median spinal vein accompanies the artery and can be distinguished by its larger diameter. Posterior, the superficial vein is the only midline vessel, as the arteries run in a more lateral position (Fig. 17.5). The transparenchymal anastomoses take a typical course around the central canal and show up- and downward movements in the sagittal plane. They can be seen on MRI. This is also true for the veins of the thoracolumbar enlargement that are the largest vessels of the spinal cord. The transition of a median vein into a radicular vein shows the same hairpin shape like the artery. The superficial venous trunks drain into the epidural venous plexus via radicular veins. The number of radicular veins draining the spinal cord is only six to eleven for the anterior and five to ten for the posterior systems (Kadyi 1889, Suh and Alexander 1939). The radicular veins reach the inner extradural vertebral venous plexus. Drainage of blood from the spine occurs through the internal and external venous vertebral plexus and extends from the sacrum to the base of the skull. This system is valveless and connected with the azygos and hemiazygos venous systems.

Fig. 17.5. Normal anterior and posterior median spinal veins of the thoracolumbar cord. Sagittal contrast-enhanced T1-weighted MR images (*right side*, subtraction image). The large anterior median vein (*arrows*) continues with the filum terminale

17.3 Causes and Symptoms of Spinal Cord Ischemia

17.3.1 Pathogenetic Principles

Compared with brain ischemia spinal cord strokes are caused by more diverse etiologies. Up-to-now there is no satisfactory and accepted classification of spinal infarcts. Etiologies include circulatory arterial and venous disorders. From a clinical and pathoanatomical point of view it seems reasonable to differentiate between acute ischemic myelomalacia and subacute to chronic vascular myelopathy (Table 17.1). In most cases MRI enables the differentiation of these two main etiologies. A deficient spinal arterial blood flow generally has various causes, ranging from the occlusion of intercostal or lumbar arteries to affection of the intrinsic arteries of the spinal cord .

Many causes of acute spinal cord infarction (of arterial and venous origin) have been reported (Table 17.2). They include diseases of the aorta and aortic surgery, thromboembolic events and cartilaginous disc embolism, vasculitis, coagulopathy, radiation-induced vasculopathy, toxic effects of contrast medium, epidural anesthesia, periradicular nerve root therapy with crystalline corticoids, decompression illness, shock or cardiac arrest, lumbar artery compression and other etiologies (Gravereaux 2001; Mawad et al. 1990; Mikulis et al. 1992; Naiman et al. 1961; Rosenkranz et al. 2004; Toro et al. 1994; Tosi et al. 1996; Weidauer et al. 2002).

Table 17.1. Disorders resulting in primary vascular myelopathy

- Acute vascular myelomalacia
  Acute ischemic myelomalacia of arterial and venous origin
- Subacute/chronic vascular myelopathy
  Dural AV fistula
  AVM of the perimedullary fistula type
  (AVM of the glomerular type)

Table 17.2. Causes of acute spinal cord infarction

- Surgery for aortoiliac occlusive disease
- Dissection of the aorta
- Thrombosis/embolism
- Vasculitis
- Cardiac arrest and systemic hypotension
- Fibrocartilaginous embolism
- Caisson disease
- Lumbar artery compression
- Spinal tumor
- Spinal AVM/SDAVF

Cartilaginous disc embolism, first described by Naiman and colleagues in 1961, is meanwhile a widely accepted cause of acute spinal cord ischemia mainly based on postmortem findings (Mikulis et al. 1992; Toro et al. 1994). Most reported postmortem cases are cervical, but conus medullaris infarctions are also reported. The exact mechanism of disc embolism remains unclear and speculative. An increased intraosseous pressure within the vertebral body, due to acute vertical disc herniations – often after axial trauma – may explain the initial step in a process which ends up in spinal cord ischemia (Tosi et al. 1996). In the clinical course of the histologically established cases of fibrocartilaginous embolism three main characteristics could be identified: (1) the sudden severe pain at onset, (2) the free interval of neurological signs and symptoms ("spinal stroke in progress"), (3) no improvement of the neurological deficit. In our experience, there is a surprisingly high rate of disc herniations in close proximity to the vascular lesions of the cord (Mull et al. 1992). Intravital confirmation of this pathogenetic mechanism is difficult. Nevertheless it may be that the pathogenetic role of disc material has yet not been fully realized.

In contrast to disc embolism, most patients with thrombotic or embolic infarctions show at least partial recovery in the further course of the disease. Nevertheless, depending on the efforts in diagnostic work-up, the cause of spinal cord ischemia often remains undefined or speculative.

Lumbar artery compression by the diaphragmatic crus has been described as a new etiology for spinal cord ischemia (Rogopoulos et al. 2000). A prolonged hyperlordotic position may play a predisposing role in this new syndrome. The 1st right and left and the 2nd right lumbar arteries course through an osteotendinous passage between the vertebral body and the diaphragmatic crus. If spinal cord supplying arteries arise at the level of the first and second lumbar artery, compromise of the spinal cord arterial supply can result in spinal cord ischemia.

Suh and Alexander (1939) and later Zülch (1954, 1976) postulated their traditional hypothesis of a watershed zone of increased ischemic vulnerability near T4. This model was based on the relative hypovascularity of this region.

Cheshire et al. (1996) described 44 patients with spinal cord infarctions. Surprisingly, the mean sen-

sory level of the deficits was observed at T8 and T9 in cases of global ischemia. A review of the clinical literature by Cheshire and colleagues (1996) suggests that the most commonly sensory level found after spinal cord infarction is centered at T12.

Duggal and Lach (2002) analyzed clinical files and neuropathologic specimen in 145 patients with well-documented cardiac arrest or severe hypotension. In this group ischemic myelopathy was found in 46% of patients dying after either cardiac arrest or a severe hypotensive episode. Among the patients with myelopathy, predominant involvement of the lumbosacral level with relative sparing of thoracic levels was observed in 95% of cardiac arrest and hypotensive patients. None of the examined patients developed neuronal necrosis limited to the thoracic level only. These findings indicate a greater vulnerability of neurons in the lumbar or lumbosacral spinal cord to ischemia than other levels of the spinal cord (Duggal and Lach 2002).

Moreover, analysis of data coming from greater MR series and our own observations reveal no predominance of infarcts in the upper and mid-thoracic region (Mawad et al. 1990; Weidauer et al. 2002). Thus, the concept of a vulnerable watershed zone at T4 is no longer valid in acute spinal cord ischemia.

Subacute or chronic vascular myelopathy is the result of disturbances of microcirculation caused by compromised venous outflow or small-vessel disease.

Thus, acute, subacute, or chronic impairment of spinal blood supply can result from a deficient arterial supply and from venous circulatory problems (Mull and Thron 2004). Spinal vascular malformations like spinal dural arteriovenous (AV) fistulas and AV malformations (AVM) of the perimedullary fistula type are the typical disorders associated with venous congestion of the spinal cord. On the other hand, AVM of the glomerular type are seldom combined with a venous outflow disorder.

Spinal dural arteriovenous fistulas (SDAVF) are the most frequent (acquired) AVM of the spinal canal and its meninges. In 1977 Kendall and Logue were the first to recognize that this disease, which had formerly been described as so-called retromedullary angiomas, in fact is an AV fistula situated within the dura mater. This was confirmed by Merland et al. in 1980 who pointed out the angiographic characteristics of the disease in detail (Fig. 17.6).

The AV shunt is located inside the dura mater close to the spinal nerve roots. The arterial blood enters a radicular vein where it passes the dura (Thron et al. 1987; Hassler et al. 1989). Flow in the radicular vein is reversed and directed to the perimedullary veins. The dural shunt is supplied by radiculomeningeal arteries which normally supply the segmental nerve roots and dura. They arise from the segmental vessels that persist as intercostal or lumbar arteries in the thoracolumbar region. Depending on the location of the fistula, the supply may also come from the sacral or hypogastric arteries (Burguet et al. 1985; Heindel et al. 1975; Larsen et al. 1995; Partington et al. 1992; Reinges et al. 2001; Stein et al. 1972). In addition, intracranial dural fistulas have been described to drain to spinal cord veins and evoke the same symptoms as spinal dural fistulas. The cause of the fistulas is unknown so far.

Functional disturbances within the spinal cord are caused by the venous congestion due to arterialization and elevated pressure of the medullary veins (Aminoff et al. 1974). In addition, venous outlets are insufficient and thus reinforcing impairment of the venous circulation and chronic spinal hypoxia. In particular, Merland and coworkers (1980) introduced the concept of blocked venous drainage into the epidural space.

17.3.2 Clinical Aspects

Vascular diseases of the spinal cord are characterized by transverse cord symptoms and can be differentiated by their clinical features and course. Neurologic deficits and imaging findings depend on the level and extent of spinal cord damage. Acute ischemic myelomalacia has an acute onset and pain is a common initial complaint. Symptoms may include nerve root deficits or sphincter weakness (Mull and Thron 1999). But typical clinical syndromes (i.e., anterior spinal artery syndrome) are exceptional presentations in clinical practice. A spinal hemorrhage presents with peracute signs and symptoms and always requires prompt diagnostic investigation, if necessary on an emergency basis.

In most cases congestive myelopathy takes a subacute to chronic course, although acute worsening may be observed. SDAVF is the prototype of a congestive myelopathy. The symptoms in SDAVF are slowly progressive and consist of sensory loss and paraparesis both of which reflect the extent of the cord involvement. They are independent of the location of the fistula (Koenig et al. 1989). An acute onset of the disease (11%) or a progressive development interrupted by intermediate remissions (11%) are the rare forms (Symon et al. 1984). Almost all

Fig. 17.6a–c. Thoracic SDAVF in a 50-year-old man with chronic progressive paraparesis due to congestive myelopathy. **a** Sagittal T2-weighted MRI. The hyperintense lesion (*long arrows*) involves the thoracic cord indicating vascular damage. **b** Dilated perimedullary veins are detectable in the thoracic region (*right image*, *arrows*) after paramagnetic contrast application (T1-weighted MRI). **c** DSA, p.a. projection. Selective contrast injection in the 4th left-sided intercostal artery shows the dural AV fistula (*arrowhead*) draining slowly in the caudal direction

patients have additional sphincter disturbances at the time of diagnosis. The disease affects men more often than women, most of them being in the middle or older age group. In some cases a relapsing and remitting course of the disease can be observed. The symptomatology in SDAVF can cause confusion with other disorders like polyneuropathy, spinal stenosis, transverse myelitis and multiple sclerosis.

17.4 MR Imaging in Spinal Infarcts

17.4.1 Imaging Principles and Differential Diagnoses

The imaging work-up should be guided by a clinical assessment of the lesion level.

MRI is the diagnostic modality of choice, T1- and T2-weighted images are obligatory. Strongly T2-weighted images (e.g., a CISS sequence) may help to detect pathologic vessels within the bright cerebrospinal fluid. Sagittal and transverse images are more important than coronal views. Fat can be suppressed by spectral fat saturation or by using the inversion recovery technique. These sequences are essential in acute spinal cord ischemia to detect associated abnormal bone signals indicating vertebral body infarction. Fluid-attenuated inversion recovery (FLAIR) sequences suppress signals from cerebrospinal fluid and, therefore, help to detect intraspinal hemorrhage. Contrast-enhanced T1-weighted images can reveal abnormal intraspinal vessels. Acute spinal cord ischemia is characterized by a typical time-dependent pattern of contrast enhancement. MRI can directly depict the cause of spinal cord ischemia in dissecting aneurysms of the

aorta. The use of diffusion-weighted MRI (DWI) has been limited in the spine thus far due to very strong susceptibility artefacts. Nevertheless, diffusion imaging has been successfully applied also to spinal cord ischemia (Gass et al. 2000). MRI can directly detect ischemic spinal cord lesions as well as intramedullary, subdural, or epidural hemorrhage. Myelitis and tumor-associated lesions are the most important clinical and imaging differential diagnoses in acute spinal cord ischemia (Table 17.3). CSF examinations are necessary if inflammatory lesions of the spinal cord (transverse myelitis) and multiple sclerosis have to be excluded in the acute phase (de Seze et al. 2001).

Table 17.3. Differential diagnosis in acute non-traumatic transverse lesion

- Hematomyelia
- Multiple sclerosis
- Spinal cord compression
  - Neoplasm
  - Disc herniation
  - Sub-/epidural hematoma
- Abscess/empyema
- Delayed radiation myelopathy
- Acute transverse myelitis
- Spinal AVM
- Ischemic infarction

In the presence of an intraspinal hemorrhage spinal vascular malformation, cavernoma, coagulopathy and tumor have to be differentiated.

In spinal vascular malformations abnormally thick, often tortuous vessels on the surface of the spinal cord can be identified as well as the angioma-like nidus of the AVM. MRI facilitates the differentiation between SDAVF and intramedullary AVM.

Myelography and post-myelographic computed tomography should only follow MRI if there is a high clinical index of suspicion for a SDAVF. Myelography is more sensitive than MRI to detect pathologic perimedullary vessels especially in cases of low-flow fistulas (Gilbertson et al. 1995).

Spinal angiography remains the gold standard in spinal vascular malformations and can help to elucidate the underlying pathology of acute spinal cord ischemia in selected cases (Di Chiro and Wener 1973; Djindjian et al. 1970; Lasjaunias et al. 2001).

17.4.2 MR Correlates of Acute Vascular Myelomalacia

Ischemic infarction of the spinal cord is difficult to establish in the early phase, only 50% of the patients show early demarcation within 24 h. The role of MRI in the acute phase is to exclude hematomyelia, spinal vascular malformation (which requires spinal angiography in special cases) or a compressive lesion.

Common sites of spinal cord infarction are the thoracolumbar enlargement and the conus medullaris in 65%, the cervical region is less commonly affected (only 11% in our own series). The damage of the spinal cord is most accurately demonstrated by MRI in T2-weighted sequences (Brown et al. 1989). Hyperintensity in T2-weighted images may be demonstrated as early as 8 h after onset (Yuh et al. 1992). In most cases pencil-shaped hyperintensive lesions are visible predominantly in the anterior spinal artery system at least in follow-up examinations (Fig. 17.7). Circumscribed infarctions in the posterior spinal artery system are rare (Mascalchi et al. 1998). Moderate swelling is generally present in the acute stage followed by contrast enhancement of the cord and the cauda equina in the subacute stage – usually after 5 days (Amano et al. 1998; Casselman et al. 1991; Friedman and Flanders 1992). Con-

Fig. 17.7. Acute ischemic myelomalacia of the thoracolumbar region in two patients, T2-weighted MR images. The pencil-shaped zone of increased signal represents the acute infarcted cord

trast-enhanced images demonstrate enhancement of the infarct up to 3 weeks after the onset (Berlit et al. 1992; Hirono et al. 1992; Yuh et al. 1992).

In most cases of the thoracolumbar infarction, the swollen cord shows peripheral enhancement of the central gray matter. The concomitant enhancement of the cauda equina was reported first by Friedman and Flanders in 1992 (Fig. 17.8). This phenomenon is a characteristic finding in the course of spinal cord ischemia which might involve the cord itself and the ventral cauda equina as well, which is composed of motor fibre bundles (Amano et al. 1998). It indicates disruption of the blood–cord barrier as well as reactive hyperemia (Friedman and Flanders 1992; Amano et al. 1998). The differential diagnosis of contrast enhancement of the cauda equina includes transverse myelitis, bacterial or viral meningitis, and spinal metastasis.

Abnormal signal or evolution of signal abnormality in a vertebral body associated with a cord lesion is highly suspicious of an acute spinal infarction (Haddad et al. 1996; Yuh et al. 1992). Due to the vascular supply to the vertebral body, the pattern of signal changes is distinct from degenerative disease. The deep medullary portion and the region of the endplates are most vulnerable to ischemia. Yuh et al. (1992) reported early hyperintensity in T2-weighted images due to vertebral body infarction after 8 h. As described before, the radicular arteries supply the vertebral bodies and – inconsistently – the spinal cord, if there is a radiculomedullary artery at the same level. Abnormal bone signals indicate this special vascular condition and can be regarded as a confirmatory sign in spinal infarction (Faig et al. 1998; Yuh et al. 1992). In our patient group, the spinal angiography demonstrated that infarction of the vertebral body indicated the origin of the anterior spinal artery (Fig. 17.9). Bone marrow abnormalities are also detectable in posterior spinal cord syndrome (Suzuki et al. 2003). In the chronic stage the affected cord segment may shrink.

Early detection of the ischemia is desirable with regard to therapeutic implications.

In few studies, DWI is reported to detect spinal cord ischemia in the acute phase (Gass et al. 2000; Bammer et al. 2000; Stepper and Lövblad 2001). Küker and coworkers (2004) recently reported the time course of diffusion abnormality in three patients with acute spinal cord ischemia. They found diffusion abnormality earliest after 8 h. At this time there was only a faint hyperintensity visible in the central part of the conus medullaris. Diffusion abnormality did not last for longer than 1 week. Further stud-

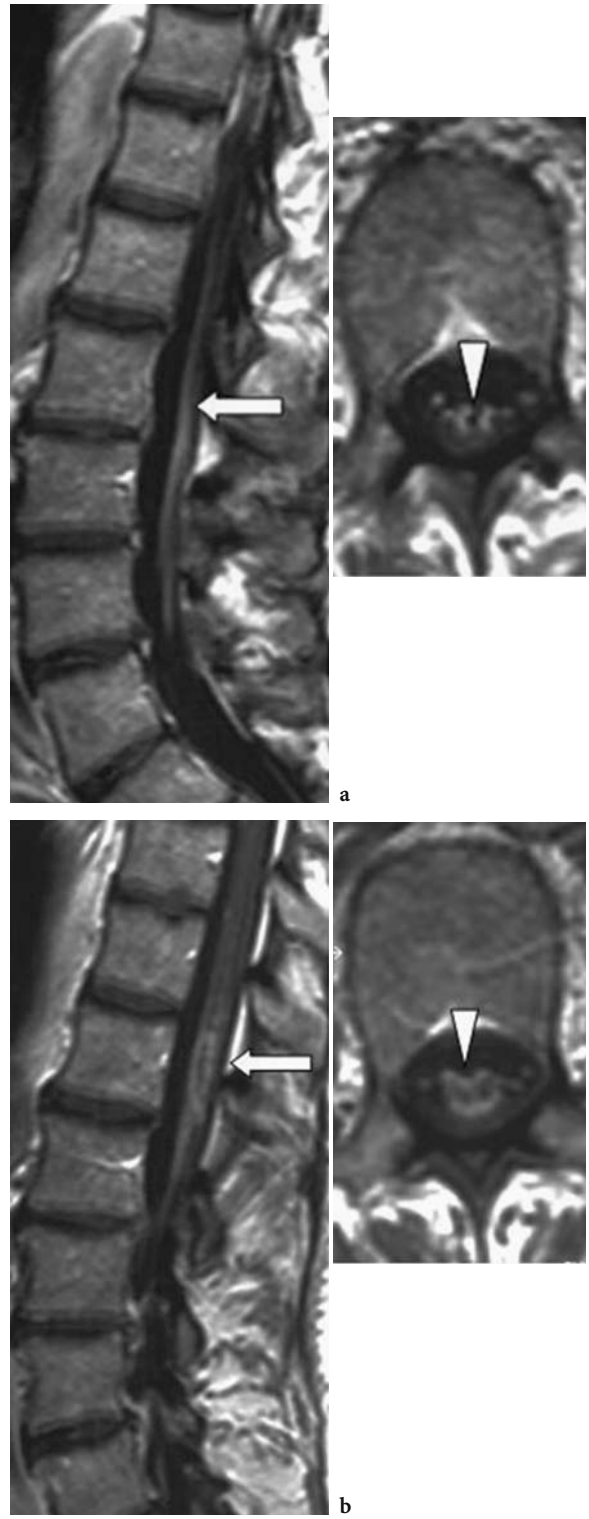

Fig. 17.8a,b. Acute ischemic myelomalacia of the lumbar enlargement 3 weeks after onset of symptoms. Contrast-enhanced T1-weighted images in sagittal and axial orientation at different levels. **a** Enhancement of the ventral cauda equina (*arrow, arrowhead*). **b** Peripheral ring-like enhancement of the affected lumbar enlargement (*arrow, arrowhead*)

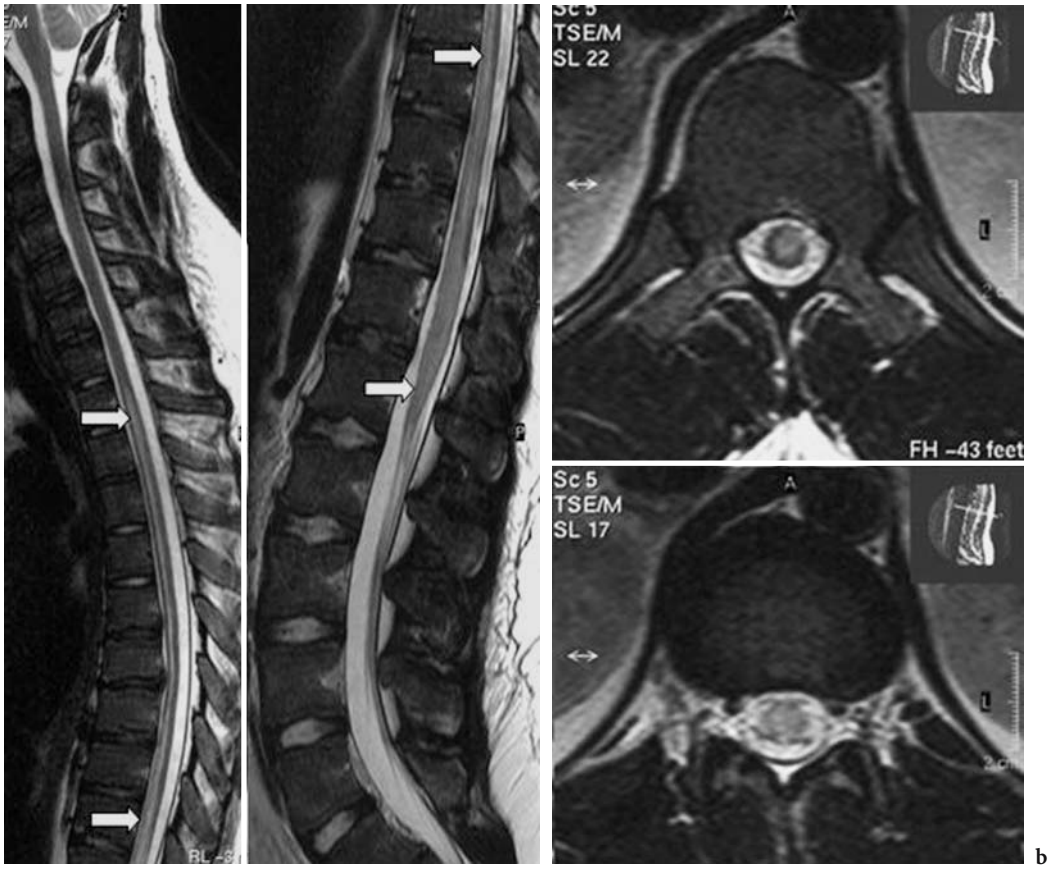

a b

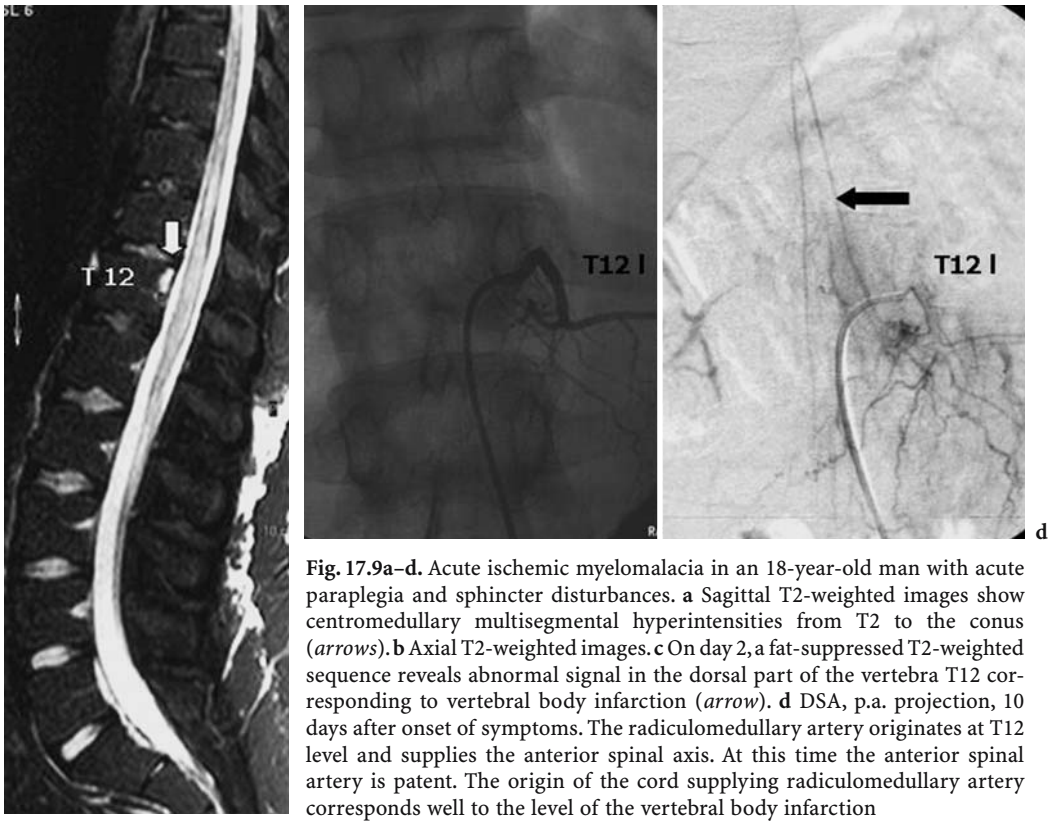

c d

Fig. 17.9a–d. Acute ischemic myelomalacia in an 18-year-old man with acute paraplegia and sphincter disturbances. **a** Sagittal T2-weighted images show centromedullary multisegmental hyperintensities from T2 to the conus (*arrows*). **b** Axial T2-weighted images. **c** On day 2, a fat-suppressed T2-weighted sequence reveals abnormal signal in the dorsal part of the vertebra T12 corresponding to vertebral body infarction (*arrow*). **d** DSA, p.a. projection, 10 days after onset of symptoms. The radiculomedullary artery originates at T12 level and supplies the anterior spinal axis. At this time the anterior spinal artery is patent. The origin of the cord supplying radiculomedullary artery corresponds well to the level of the vertebral body infarction

ies are necessary to determine its sensitivity in the early phase of spinal cord infarction and to establish its specificity in other causes of myelopathy such as myelitis.

17.4.3 MR Correlates of Subacute/Chronic Vascular Myelopathy

17.4.3.1 Spinal Dural Arteriovenous Fistula

In SDAVF the key findings in MRI are the sequelae of the congestive myelopathy and the detection of the arterialized perimedullary veins (Fig. 17.10). MRI shows in almost all cases a long central intramedullary hyperintense lesion in T2-weighted images that spans several cord segments (Koch et al. 1998; Van Dijk et al. 2002). A characteristic finding is a hypointense rim adjacent to the spinal cord lesion.

Fig. 17.10. MRI in thoracic SDAVF, sagittal T2- and contrast-enhanced T1-weighted images. Multisegmental hyperintensive lesion of the thoracic cord with swelling indicating congestive myelopathy. Flow voids in the dorsal CSF compartment represent the arterialized perimedullary veins (*arrow*, T2-weighted image, *left side*), which are clearly visible after intravenous contrast application (*arrow*, T1-weighted image, *right side*).

Fig. 17.11. SDAVF supplied from the left 1st lumbar segmental artery, T2-weighted sagittal and axial MR images. In this case, the perimedullary arterialized veins are not very impressive (arrowhead). Note the peripheral hypointensive rim adjacent to the cord hyperintensity, a typical finding in SDAVF (arrows)

This peripheral spinal cord hypointensity was first described by Hurst and Grossman in 2000 and is probably best explained by slow flow of blood containing deoxyhemoglobin related to the venous hypertension (Fig. 17.11). Abnormally enlarged and tortuous perimedullary veins can show flow voids in spin-echo sequences or enhancement after paramagnetic contrast administration (Terwey et al. 1989). Pathologic perimedullary veins are not always detectable in MRI and in some cases difficult to differentiate from CSF pulsations. If contrast enhancement of the spinal cord lesion is present, the cord lesion may be misdiagnosed as tumor.

Follow-up MRI after treatment shows regression of the hyperintense lesion and may be followed by atrophy. If swelling of the cord and/or the pathologic perimedullary vessels persist after treatment, a residual SDAVF needs to be excluded by DSA.

Spinal DSA is still required to demonstrate the fistula and the supplying segmental artery. Recent developments in MR angiography will help to define non-invasively the level of the fistula (Farb et al.

2002). In most patients the dural fistula is supplied by a thoracic or lumbar artery. Deep located fistulas of the lumbosacral region are rare and beset with particular diagnostic problems mainly due to the unusual anatomic and hemodynamic conditions. In these cases MRI should be focused on the lumbosacral region. The arterialized dilated vein of the filum can be detected in 3-mm slices after paramagnetic contrast administration even if the flow is very slow.

17.4.3.2 Arteriovenous Malformations

Spinal AVMs can be mainly divided into AVM of the perimedullary fistula type and glomerular type. Typically, congestive myelopathy is obvious in AVM of the perimedullary type (Heros et al. 1986; Rosenblum et al. 1987; Thron et al. 2001).

AVMs of the perimedullary fistula type are direct AV shunts that are located on the ventral or dorsal surface of the spinal cord or the conus medullaris, usually in the thoracolumbar area, occasionally thoracic, and rarely cervical. Their location thus is intradural, intra- or extramedullary. They are always supplied by spinal cord vessels, either by the anterior spinal artery (ventrally) or by a posterolateral artery (dorsally), depending on their location. They drain into spinal cord veins (Fig. 17.12). Drainage may even ascend up to the foramen magnum or into the posterior fossa.

AVMs of the glomerular type are more frequent and characterized by a nidus similar to those of most cerebral AVMs. They may be located superficially on the surface of the spinal cord or deep within the cord parenchyma or extend to both compartments. Due to the numerous anastomoses between the spinal cord arteries, the nidus is always supplied by several arteries or branches derived from the anterior

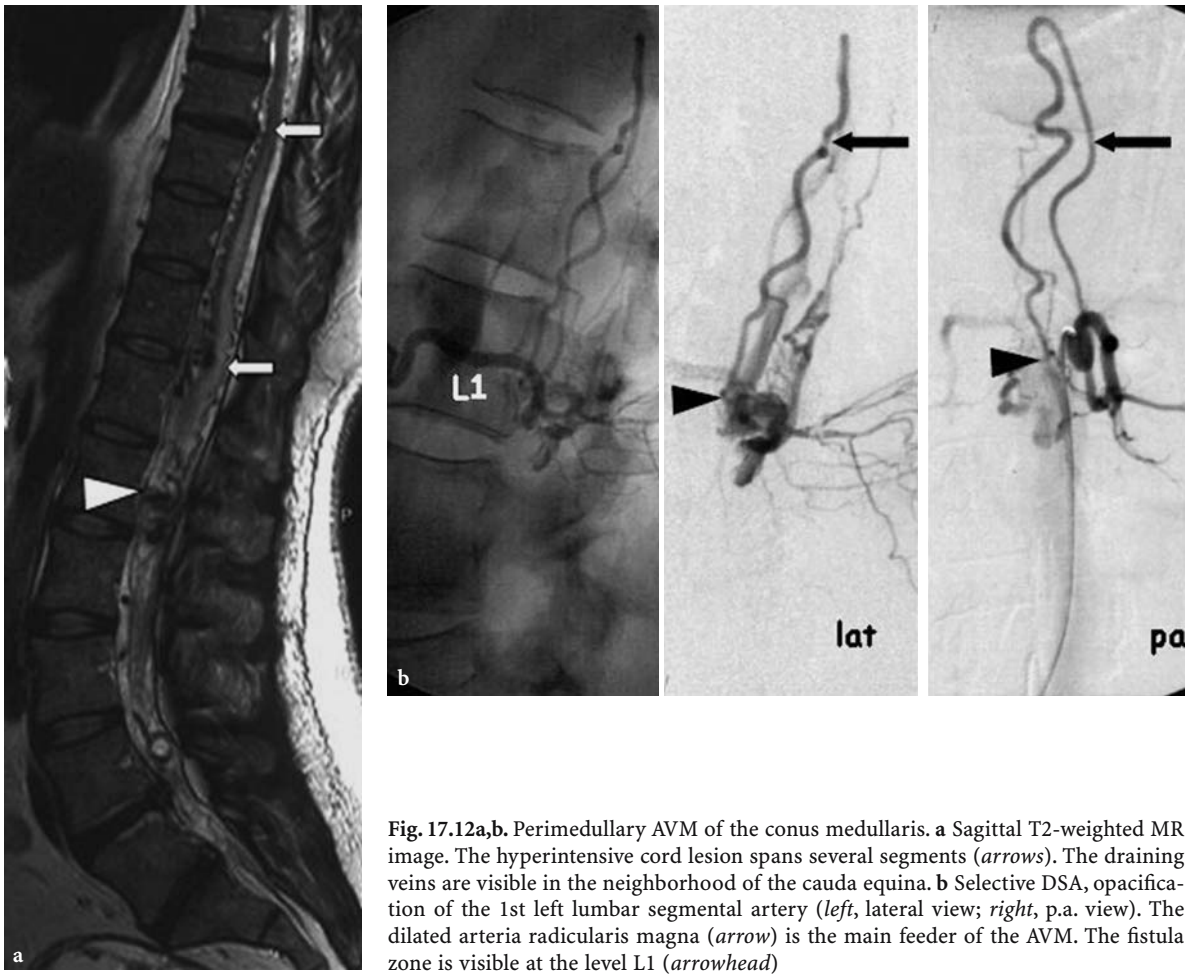

Fig. 17.12a,b. Perimedullary AVM of the conus medullaris. **a** Sagittal T2-weighted MR image. The hyperintensive cord lesion spans several segments (*arrows*). The draining veins are visible in the neighborhood of the cauda equina. **b** Selective DSA, opacification of the 1st left lumbar segmental artery (*left*, lateral view; *right*, p.a. view). The dilated arteria radicularis magna (*arrow*) is the main feeder of the AVM. The fistula zone is visible at the level L1 (*arrowhead*)

or posterior spinal arteries. Spinal AVMs drain into the spinal cord veins and are rarely complicated by congestive myelopathy.

The principal screening method is MRI (Dormont et al. 1988; Thron and Caplan 2003). Abnormally dilated vessels in the spinal cord or the subarachnoid space are the main findings. In AVMs of the glomerular type, the nidus can be differentiated from the draining veins. Intradural AVMs can be associated with hemorrhage in the spinal cord and its surroundings. The hyperintensity in T2-weighted images is not the dominant feature in this type of AVM. The signal characteristics vary over time, comparable with intracerebral hematomas. After endovascular treatment, compromise of the venous outflow may result in a congestive myelopathy.

Perimedullary fistulas type 1 may present with multisegmental hyperintensive cord lesions on T2-weighted images due to congestive myelopathy similar to spinal cord affection in spinal dural AVF.

17.5 Spinal Angiography

17.5.1 MR Angiography and Spinal Cord Vessels

The largest blood vessels of the spinal cord are the veins of the superficial system, the anterior and posterior median vein, the radicular veins, the terminal vein and, furthermore, the transmedullary venous anastomoses. They have an inner vessel diameter of up to 2 mm compared with a maximum diameter of 1 mm on the arterial side. At present, these are the vessels most likely to be seen on MRI. They can either be demonstrated on sagittal T1-weighted images following contrast enhancement as bright structures or, like in myelography, as dark structures within the bright CSF on strongly T2-weighted images. Problems arise in "borderline" cases, especially at the level of the lumbar enlargement, where it is impossible to decide whether the demonstrated blood vessels represent still normal or already path-

Fig. 17.13a–c. First-pass contrast-enhanced MR angiography. **a** Normal finding. **b** Thoracic SDAVF (T7 left, *arrow*). **c** Thoracolumbar spinal AVM (*arrows*)

ological findings due to a SDAVF. This is particularly true for the thoracolumbar enlargement due to a considerable variation of the posterior veins at this location that can show varicosity and elongation (Thron and Mull 2004).

Even if spatial and contrast resolution of these imaging modalities will increase in the future, it might be difficult to differentiate the artery from the vein on the anterior surface of the cord. The anterior spinal artery and vein run very close together. The branching of a radicular artery or vein has a very similar hairpin-configuration, and the level at which a segmental in- or outflow occurs cannot be predicted in a given case.

The only non-invasive way in which a reliable differentiation of superficial spinal cord arteries and veins can be expected, is an MR-based angiographic technique with sufficient spatial resolution and with a time resolution that clearly separates arterial and venous phase. The first MRA techniques used were blood flow-dependent, such as three-dimensional phase contrast angiography and three-dimensional contrast-enhanced time of flight imaging (Bowen et al. 1996). The greatest disadvantages are the long acquisition time (10 min) and the limited visualization of normal intradural arteries. To achieve better visualization without venous overprojection, first-pass MR angiography with a rapid bolus injection of contrast medium and a highly sophisticated acquisition technique, has been proposed (Willinek et al. 2002). This technique makes it possible to distinguish the arterial phase from a later phase in which both arteries and veins are enhanced. Verification of the findings by DSA has rarely been performed. Some authors have shown that the fistula-supplying segmental artery could be located by first-pass contrast-enhanced MR angiography (Binkert et al. 1999; Farb et al. 2002; Shigematsu et al. 2000). By using a first-pass technique with two dynamic phases, the arteria radicularis magna of Adamkiewicz could be separated from the anterior median vein and separately visualized in 69% (Yamada et al. 2000a,b). Recent own investigations comparing MR angiography with DSA findings are encouraging with regard to the identification of the Adamkiewicz artery and the fistula-supplying segmental artery in SDAVF (Backes et al. 2004). Nevertheless, to date, MRI and MR angiography have not been able to precisely detect small-caliber feeding spinal arteries in spinal AVM (Fig. 17.13). Introduction of first-pass contrast-enhanced MR angiography in the routine work-up of spinal vascular pathology will contribute to our understanding of the pathogenetic mechanisms involved.

17.5.2 Spinal Angiography (DSA)

Selective spinal angiography provides the basis for classifying spinal vascular malformations by their location, arterial supply and venous drainage pattern. A profound understanding of the AVM architecture is required for the decision regarding which treatment option(s) should be taken into consideration. In SDAVF, spinal DSA remains the gold standard to identify the fistula-supplying segmental artery. In deep lumbosacral SDAVF, only selective internal iliac arteriography can identify fistulas located in the sacral region supplied by the lateral sacral or iliolumbar arteries.

Selective spinal DSA has a better spatial resolution and plays a main role in the exclusion of spinal vascular malformations. In selected cases affection of the radicular artery and occlusion of the anterior spinal artery system can be demonstrated as well as collateral supply even in the later course of the ischemia (Mull et al. 2002). Thus, spinal DSA helps to identify pathologic vascular conditions in spinal cord ischemia. The main indication remains to exclude a spinal vascular malformation. Angiographic information about the acute phase of spinal cord ischemia is not yet available.

17.6 Treatment

In patients with SDAVF the aim of treatment is to prevent progression of the spinal cord damage. The goal is the permanent occlusion of the dural shunt zone along with the origin of the draining vein. This can be achieved microsurgically or by endovascular treatment using tissue adhesives (Behrens and Thron 1999; Huffmann et al. 1995; Merland et al. 1986; Niimi et al. 1997; Song et al. 2001; Thron and Caplan 2003). Treatment of spinal AVM should be restricted to specialized centers that are experienced in this field.

To identify the location of cord-supplying segmental arteries before aortic surgery can help to reduce the risk of spinal cord ischemia. Monitoring of somatosensory-evoked responses contrib-

utes to identify early signs of spinal cord ischemia during aortic clamping. Before aortic surgery spinal DSA and MR angiography, as described before, can help to identify cord-supplying segmental arteries.

If the diagnosis of a compression of a lumbar artery has been established by dynamic spinal DSA showing complete occlusion of the lumbar artery, surgical section of the diaphragmatic crus may prevent irreversible infarction in this rare condition.

At present there are no recognized effective treatment strategies for spinal cord stroke (Caplan 2003; Mull 2005). Nevertheless, if the cord ischemia is judged to be embolic, effective anticoagulation or antiplatelet drugs should be considered in clinical practice.

17.7 Summary

In the last decade typical signs of spinal cord ischemia have been reported. Confirming and supporting signs of acute ischemic myelomalacia are vertebral body infarction and the pathognomonic contrast enhancement of the cauda equina in the course of the disease. Moreover, bone infarction strongly indicates the proximal occlusion and the level of the affected segmental artery. Cartilaginous disc embolism, embolism following periradicular nerve root therapy and compression of a lumbar artery are underestimated causes of spinal cord ischemia.

In most cases a long, extending cord lesion in the presence of perimedullary veins favors spinal dural AV fistulas as an underlying disorder which has to be confirmed by spinal angiography and separated from perimedullary AV fistulas. Up to now, it is not possible to differentiate local arterial from venous occlusion in the intravital diagnostic work-up. MRI, MR angiography and spinal DSA are complementary diagnostic tools in vascular diseases of the spinal cord which help us to confirm the diagnosis and to come to a better understanding of these rare disorders.

In summary, important advances have been made in our understanding of the underlying pathogenetic mechanism in spinal cord ischemia. This condition remains a diagnostic and therapeutic challenge, but improved diagnosis may result in better treatment in the future.

References

Amano Y, Machida T, Kumazaki T (1998) Spinal cord infarcts with contrast enhancement of the cauda equina: two cases. Neuroradiology 40:669–672

Aminoff MJ, Barnard RO, Logue V (1974) The pathophysiology of spinal vascular malformations. J Neurol Sci 23:255–263

Backes W, Nijenhuis R, Mull M, Thron A, Wilmink J (2004) Contrast-Enhanced MR Angiography of the Spinal Arteries: Current Possibilities and Limitations. Rivista di Neuroradiologia 17 (3):282–291

Bammer R, Fazekas F, Augustin M, Simbrunner J, Strasser-Fuchs S, Seifert T, Stollberger R, and Hartung HP (2000) Diffusion-weighted MR imaging of the spinal cord. AJNR Am J Neuroradiol 21 (3):587–591

Behrens S, Thron A (1999) Long-term follow-up and outcome in patients treated for spinal dural arteriovenous fistula. J Neurol 246:181–185

Berlit P, Klötzsch G, Röther J, Assmus HP, Daffertshofer M, Schwartz A (1992) Spinal cord infarction: MRI and MEP findings in three cases. J Spinal Disord 5:212–216

Binkert CA, Kollias SS, Valavanis A (1999) Spinal cord vascular disease: characterization with fast three-dimensional contrast-enhanced MR Angiography. Am J Neuroradiol 20:1785–1793

Bowen BC, DePrima S, Pattany PM, Marcillo A, Madsen P, Quencer RM (1996) MR angiography of normal intradural vessels of the thoracolumbar spine. AJNR Am J Neuroradiol 17:483–494

Brown E, Virapongse C, and Gregorios JB (1998) MR imaging of cervical spinal cord infarction. J Comput.Assist.Tomogr. 13 (5):920–922

Burguet JL, Dietemann JL, Wackenheim A, Kehr P, Buchheit F (1985) Sacral meningeal arteriovenous fistula fed by branches of the hypogastric arteries and drained through medullary veins. Neuroradiology 27:232–237

Caplan L (2003) Spinal Cord Ischemia. In: Neurological Disorders: Course and Treatment, Second Edition, Elsevier Science: 393–401.

Casselman JW, Jolie E, Dehaene I, Meeus L (1991) Gadolinium-enhanced MR imaging of infarction of the anterior spinal cord. AJNR Am J Neuroradiol 12:561

Cheshire WP, Santos CC, Massey EW, Howard JF (1996) Spinal cord infarction: etiology and outcome. Neurology 47:321–330

de Seze J, Stojkovic T, Breteau G, Lucas C, Michon-Pasturel U, Gauvrit JY, Hachulla E, Mounier-Vehier F, Pruvo JP, Leys D, Destée A, Hatron PY, Vermersch P (2001) Acute myelopathies: Clinical, laboratory and outcome profiles in 79 cases. Brain 124:1509–1521

Di Chiro G, Wener L (1973) Angiography of the spinal cord. A review of contemporary techniques and applications. J Neurosurg 39:1–29

Djindjian R, Hurth M, and Houdart R (1970) L'angiographie de la moelle epiniere. Masson, Paris

Dormont D, Gelbert F, Assouline E, Reizine D, Helias A, Riche MC, Chiras J, Bories J, Merland JJ (1988) MR imaging of spinal cord arteriovenous malformations at 0. 5 T: study of 34 cases. AJNR Am J Neuroradiol 9:833–838

Duggal N, Lach B (2002) Selective vulnerability of the lumbosacral spinal cord after cardiac arrest and hypotension. Stroke 33:116–121

Faig J, Busse O, Salbeck R (1998) Vertebral body infarction as a

confirmatory sign of spinal cord ischemic stroke: report of three cases and review of the literature. Stroke 29:239–243
Farb RI, Kim JK, Willinsky RA, Montanera WJ, terBrugge K, Derbyshire JA, van Dijk JMC, and Wright GA (2002) Spinal dural arteriovenous fistula localization with a technique of first-pass gadolinium-enhanced MR angiography: initial experience. Radiology 222:843–850
Friedman DP, Flanders AE (1992) Enhancement of gray matter in anterior spinal infarction. AJNR Am J Neuroradiol 13:983–985
Gass A, Back T, Behrens S, Maras A (2000) MRI of spinal cord infarction. Neurology 54:2195
Gilbertson JR, Miller GM, Goldman MS, Marsh WR (1995) Spinal dural arteriovenous fistulas: MR and myelographic findings. AJNR Am J Neuroradiol 16:2049–2057
Gravereaux EC, Faries PL, Burks JA, Latessa V, Spielvogel D, Hollier LH, Marin ML (2001) Risk of spinal cord ischemia after endograft repair of thoracic aortic aneurysms. J Vasc Surg 34:997–1003
Haddad MC, Aabed al-Thagafi MY, Djurberg H (1996) MRI of spinal cord and vertebral body infarction in the anterior spinal artery syndrome. Neuroradiology 38:161–162
Hassler W, Thron A, Grote EH (1989) Hemodynamics of spinal dural arteriovenous fistulas. An intraoperative study. J Neurosurg 70:360–370
Heindel CC, G.S. Dugger , F.C. Guinto (1975) Spinal arteriovenous malformation with hypogastric blood supply. J. Neurosurg. 42, 462-464
Heros RC, Debrun GM, Ojemann RG, Lasjaunias PL, Naessens PJ (1986) Direct spinal arteriovenous fistula: a new type of spinal AVM. Case report. J Neurosurg 64:134–139
Hirono H, Yamadori A, Komiyama M, Yakura H, Yasui T (1992) MRI of spontaneous spinal cord infarction: serial changes in gadolinium-DTPA enhancement. Neuroradiology 34:95–97
Huffmann BC, Gilsbach JM, Thron A (1995) Spinal dural arteriovenous fistulas: a plea for neurosurgical treatment. Acta Neurochir (Wien) 135:44–51
Hurst R.W. , and Grossman RI (2000) Peripheral spinal cord hypodensity on T2-weighted MR images: a reliable imaging sign of venous hypertensive myelopathy. AJNR Am J Neuroradiol 21:781–786
Kadyi H (1889) Über die Blutgefäße des menschlichen Rückenmarks. Gubrynowicz u. Schmidt, Lemberg
Kendall BE, Logue V (1977) Spinal epidural angiomatous malformations draining into intrathecal veins. Neuroradiology 13:181–189
Koch C, Hansen HC, Westphal M, Kucinski T, Zeumer H (1998) Die kongestive Myelopathie durch spinale durale arteriovenöse Fisteln. Nervenarzt 69:279–286
Koenig E, Thron A, Schrader V, Dichgans J (1989) Spinal arteriovenous malformations and fistulae: clinical, neuroradiological and neurophysiological findings. J Neurol 236:260–266
Kueker W, Weller M, Klose U, Krapf H, Dichgans J, Naegele T (2004) Diffusion-weighted MRI of spinal cord infarction. High resolution and time course of diffusion abnormality. J Neurol 251:818–824
Larsen DW, Halbach VV, Teitelbaum GP, McDougall CG, Higashida RT, Dowd CF, Hieshima GB (1995) Spinal dural arteriovenous fistulas supplied by branches of the internal iliac arteries. Surg Neurol 43:35-40; discussion 40-1
Lasjaunias P, Berenstein A, ter Brugge KG (2001) Surgical Neuroangiography. Vol. 1. Clinical vascular anatomy and variations. Springer, Berlin
Mascalchi M, Cosottini M, Ferrito G, Salvi F, Nencini P, Quilici N (1998) Posterior spinal artery infarct. AJNR Am J Neuroradiol 19:361–363
Mawad ME, Rivera V, Crawford S, Ramirez A, and Breitbach W (1990) Spinal cord ischemia after resection of thoracoabdominal aortic aneurysms: MR findings in 24 patients. AJNR Am J Neuroradiol 11 (5):987–991
Merland JJ, Riche MC, Chiras J (1980) Les fistules arterioveneuses intra-canalaires, extramedullaires à drainage veineux medullaire. J Neuroradiol 7:271–320
Merland JJ, Assouline E, Rüfenacht D, Guimaraens L, Laurent A (1986) Dural spinal arteriovenous fistulae draining into medullary veins: clinical and radiological results of treatment (embolisation and surgery) in 56 cases. Excerpta Med Int Congr Ser 698:283–289
Mikulis DJ, Ogilvy CS, McKee A, Davis KR, Ojeman RG (1992) Spinal cord infarction and fibrocartilagenous emboli. AJNR Am J Neuroradiol 13:155–160
Mull M (2002) Spinal Diseases. Vascular Diseases. In:Diagnostic and Interventional Neuroradiology. A Multimodality Approach. Hrsg. K. Sartor, Thieme, Stuttgart New York 310-315
Mull M (2005) Der akute Rückenmarkinfarkt: Diagnostik ohne therapeutischen Ansatz ? Klinische Neuroradiologie 15: 79-88.
Mull M, Thron A (1999) Spinale Durchblutungsstörungen. In: Neurologie in Klinik und Praxis. Hrsg: Hopf HC, Deuschl G, Diener HC, Reichmann R; Thieme, Stuttgart New York:402–408
Mull M, Thron A (2004) Imaging of Vscular Diseases of the Spinal Cord. Rivista di Neuroradiologia 17 (3):351–359
Mull M, Thron A, Petersen D, Stoeter P (1992) Acute infarction of the spinal cord: clinical and neuroradiological findings in 20 patients. Neuroradiology 34:43
Mull M, Kosinski C, and Thron A (2002) Acute spinal cord ischemia – contribution of spinal angiography. J. Neuroradiol. 29:1–86
Naiman JL, Donohue WL, Prichards JS (1961) Fatal nucleus pulposus embolism of spinal cord after trauma. Neurology 11:83–87
Niimi Y, Berenstein A, Setton A, Neophytides A (1997) Embolization of spinal dural arteriovenous fistulae: results and follow-up. Neurosurgery 40:675-82; discussion 682-683
Partington MD, D.A. Rüfenacht , W.R. Marsch , D.G. Piepgras (1992) Cranial and sacral dural arteriovenous fistulas as a cause of myelopathy. J. Neurosurg. 76:615–622
Reinges MH, Thron A, Mull M, Huffmann BC, Gilsbach JM (2001) Dural arteriovenous fistulae at the foramen magnum. J Neurol 248:197–203
Rogopoulos A, Benchimol D, Paquis P, Mahagne MH, Bourgeon A (2000) Lumbar artery compression by the diaphragmatic crus: a new etiology for spinal cord ischemia. Ann Neurol 48:261–264
Rosenblum B, Oldfield EH, Doppman JL, Di Chiro G (1987) Spinal arteriovenous malformations: a comparison of dural arteriovenous fistulas and intradural AVM's in 81 patients. J Neurosurg 67:795–802
Rosenkranz M, Grzyska U, Niesen W, Fuchs K, Schummer W, Weiller C, Röther J (2004) Anterior spinal artery syndrome following periradicular cervical nerve root therapy. J Neurol 251:229–231

Shigematsu Y, Korogi Y, Yoshizumi K, et al (2000) Three cases of spinal dural AVF: evaluation with first-pass, gadolinium-enhanced, three-dimensional MR angiography. J Magn Reson Imaging 12:949–952

Song JK, Vinuela F, Gobin YP, Duckwiler GR, Murayama Y, Kureshi I, Frazee JG, Martin NA (2001) Surgical and endovascular treatment of spinal dural arteriovenous fistulas: long-term disability assessment and prognostic factors. J Neurosurg 94:199–204

Spiller W (1909) Thrombosis of the cervical anterior median spinal artery. J Nerv Ment Dis 36:601

Stein SC, Ommaya AK, Doppman JL, Di Chiro G (1972) Arteriovenous malformation of the cauda equina with arterial supply from branches of the internal iliac arteries. Case report. J Neurosurg 36:649–651

Stepper F, Lövblad KO (2001) Anterior spinal artery stroke demonstrated by echo-planar DWI. Eur Radiol 11:2607–2610

Suh T.H. , Alexander L (1939) Vascular system of the human spinal cord. Arch Neurol Psychiat 41:659–677

Suzuki T, Kawaguchi S, Takebayashi T, Yokogushi K, Takada J, Yamashita T (2003) Vertebral body ischemia in the posterior spinal artery syndrome: case report and review of the literature. Spine 28:E260–264

Symon L, Kuyama H, Kendall B (1984) Dural arteriovenous malformations of the spine. Clinical features and surgical results in 55 cases. J Neurosurg 60:238–247

Terwey B, Becker H, Thron AK, Vahldiek G (1989) Gadolinium-DTPA enhanced MR imaging of spinal dural arteriovenous fistulas. J Comput Assist Tomogr 13:30–37

Thron A (1988) Vascular anatomy of the spinal cord. Neuroradiological investigations and clinical syndromes. Springer, Wien New York

Thron A, Mull M (2004) Blood vessels of the Spinal Cord: Anatomical and MR-Imaging Correlation. Rivista di Neuroradiologia 17 (3):277–281

Thron A, Koenig E, Pfeiffer P, Rossberg C (1987) Dural vascular anomalies of the spine – an important cause of progressive radiculomyelopathy. In: Cervos Navarro J, Ferszt R Stroke and microcirculation. Raven Press, New York:159–165

Thron A, Mull M, Reith W (2001) Spinale Gefäßmalformationen. Der Radiologe 41:949–954

Thron AK, Caplan L (2003) Vascular Malformations and Interventional Neuroradiology of the Spinal Cord. In: Neurological Disorders: Course and Treatment, Second Edition, Elsevier Science:517–528

Toro G, Roman GC, Navarro-Roman L, Cantillo J, Serrano B, Vergara I (1994) Natural history of spinal cord infarction caused by nucleus pulposus embolism. Spine 19:360–366

Tosi L, Rigoli G, Beltramello A (1996) Fibrocartilaginous embolism of the spinal cord: a clinical and pathogenetic reconsideration. J Neurol Neurosurg Psychiatry 60:55–60

Van Dijk JM, TerBrugge KG, Willinsky RA, Farb RI, and Wallace MC (2002) Multidisciplinary management of spinal dural arteriovenous fistulas: clinical presentation and long-term follow-up in 49 patients. Stroke 33 (6):1578–1583

Weidauer S, Nichtweiss M, Lanfermann H, Zanella FE (2002) Spinal cord infarction: MR imaging and clinical features in 16 cases. Neuroradiology 44:851–857

Willinek WA, Gieseke J, Conrad R, Strunk H, Hoogeveen R, von Falkenhausen M, Keller E, Urbach H, Kuhl CK, Schild HH (2002) Randomly segmented central k-space ordering in high-spatial-resolution contrast-enhanced MR angiography of the supraaortic arteries: initial experience. Radiology 225:583–588

Yamada N, Okita Y, Minatoya K, Tagusari O, Ando M, Takamiya M, Kitamura S (2000a) Preoperative demonstration of the Adamkiewicz artery by magnetic resonance angiography in patients with descending or thoracoabdominal aortic aneurysms. Eur J Cardiothorac Surg 18:104–111

Yamada N, Takamiya M, Kuribayashi S, Okita Y, Minatoya K, Tanaka R (2000b) MRA of the Adamkiewicz artery: a preoperative study for thoracic aortic aneurysm. J Comput Assist Tomogr 24:362–368

Yuh WT, Marsh EE, Wang AK, Russell JW, Chiang F, Koci TM, Ryals TJ (1992) MR imaging of spinal cord and vertebral body infarction. AJNR Am J Neuroradiol 13:145–154

Zülch KJ (1954) Durchblutung an der Grenzzone zweier Gefäßgebiete als Ursache bisher ungeklärter Rückenmarksschädingungen. Deutsch ZNervenheilk. 172:81–101

Zülch KJ (1976) Pathogenetic and clinical observations in spinovascular insufficiency. Zentralbl Neurochir 37:1–13

18 Veno-Occlusive Disorders

Armin Thron and Michael Mull

CONTENTS

18.1 Introduction

Veno-occlusive disorders of the brain may affect the dural sinuses, the superficial cortical veins and the deep venous system. Occlusion may be due to aseptic or septic thrombosis, to stenoses of the large sinuses at the base of the skull of different origin and to tumors compressing or infiltrating the sinus wall, especially meningiomas. Impaired venous drainage results in venous congestion or congestive infarction which can be accompanied by hemorrhage. Arteriovenous shunting in case of dural arteriovenous fistulas or arteriovenous malformations may have a similar clinical effect. In general practice, cerebral venous and sinus thrombosis (CVST) play the most important role in the group of veno-occlusive diseases.

18.2 Etiology and Risk Factors

Several etiological factors are known to cause CVST, although no specific cause for CVST can be found in about 25% of all cases (Deschiens et al. 1996). One has to differentiate between aseptic CVST as the most common form, septic venous and sinus thrombosis, tumor-induced and trauma-induced CVST. Disease processes that may cause aseptic CVST include hypercoagulopathic states such as those present in polycythemia vera, sickle cell disease, deficiencies of fibrinolytic factors (antithrombin III, protein C, protein S) or disseminated intravascular coagulopathy (Deschiens et al. 1996). Oral contraceptives, pregnancy, and puerperium are also known risk factors for developing an aseptic CVST (Cantu and Barinagarrementeria 1993). In addition, systemic malignancies with paraneoplastic syndromes, lupus erythematodes, drug abuse or low flow situations as present during dehydration or shock may cause CVST. Septic causes are most often encountered in childhood with a chronic or acute mastoiditis involving the neighbouring transverse or sigmoid sinus (Isensee et al. 1992a; Reul et al. 1997). Meningitis, brain abscesses or septicemia are, however, more seldom causes of septic CVST. Concerning tumor induced CVST, meningiomas are prone to obliterate the lumen of the dural sinuses; however, this process evolves slowly over time, therefore, venous collaterals are often present and an acute venous congestion is the exception rather than the rule. Apart from meningiomas other tumor entities only rarely infiltrate the dural sinus walls. CVST caused by trauma is also rather rare; however, fractures that lead to a laceration of the dural wall might cause a venous occlusion.

18.3 Clinical Features and Typical Symptom Combinations

CVST generally shows a subacute onset and course of symptoms. Clinical symptomatology is dependant on the cause, localization, extension and time of development of the venous occlusion. The leading symptom is headache in 70%-90% of all cases

A. Thron, MD; M. Mull, MD
Department of Neuroradiology, Clinic for Diagnostic Radiology, University Hospital of the Technical University, Pauwelsstr. 30, 52074 Aachen, Germany

(Strupp et al. 2003), often associated with nausea and vomiting (Thron et al. 1986). But the spectrum of symptoms and signs varies between an asymptomatic course and rapidly progressive neurological deficits and impaired consciousness.

In asymptomatic cases, the occlusion of an isolated sinus is typically compensated by collaterals or in case of the transverse sinus by a contralateral sinus of adequate size (Thron 2001).

Idiopathic intracranial hypertension (synonyms: benign intracranial hypertension, pseudotumor cerebri syndrome) is characterized by increased CSF pressure (> 250 mm H_2O) in the absence of an intracranial space occupying lesion or inflammation. About 30%-50% of CVST-patients present with this syndrome (Thron et al. 1986). They complain of headache and have papilledema or other symptoms and signs of increased intracranial pressure. In most of these cases a main venous channel is occluded and drainage of the brain depends on smaller sinuses or veins. An example of this situation is the unilateral occlusion of the dominant transverse sinus. The collateral drainage is poor, but sufficient to prevent focal lesions. Recently, advanced MRA techniques have provided evidence that focal stenotic lesions in the transverse sinuses (or comparable venous outflow obstructions of non-thrombotic origin) may be another frequent cause of this syndrome (see Fig. 17.2c-e; Higgins et al. 2002, 2004; Farb et al. 2003) Using more invasive techniques, pressure gradients could be measured in a part of these patients. The relationship between these focal stenoses and the increased intracranial pressure remains to be clarified.

Neurological deficits and seizures occur in the group of patients in whom focal congestive and hemorrhagic lesions occur. The stroke-like symptoms depend on the localization of the brain damage and may be accompanied by seizures (Thron et al. 1986; Strupp et al. 2003). In these cases extension of the thrombus in cortical veins has occurred or the collateral drainage for a distinct area of the brain parenchyma is not sufficient. A typical example of this is the occlusion of a transverse sinus together with the vein of Labbé (see Fig. 18.8; Isensee et al. 1992b). Focal sensorimotor deficits and/or seizures are also the clinical feature of the solitary thrombosis of a superficial cerebral vein which in our experience is rare. This entity may be accompanied by a cortical subarachnoid hemorrhage.

Impaired consciousness and coma may develop with increasing intracranial pressure.

A decrease in mental status, drowsiness, progressive confusion and impaired consciousness may also be the major symptoms of deep cerebral venous thrombosis (Ameri and Bousser 1992; Crawford et al. 1995). Drainage impairment affects mainly the thalamus uni- or bilaterally with venous congestion and/or bleeding (Lafitte et al. 1999) (see Fig. 18.6).

Thrombosis of the cavernous sinus is characterized by proptosis, chemosis, impaired vision and ophthalmoplegia. If it is not septic, prognosis is good because of collateral drainage and spontaneous recanalization. The same symptoms, with the exception of a possible bruit, may result from arteriovenous shunting in carotid-cavernous fistulae. The treatment of choice in this case is endovascular occlusion (thrombosis!) of the cavernous sinus.

The prognosis of extensive CVST is unpredictable and variable. The 5%-30% mortality of CVST still reported in studies between 1991 and 1999 (Strupp et al. 2003) has significantly dropped. In our experience early diagnosis with noninvasive techniques of MRI and MRA has an important influence on prognosis.

Early diagnosis, however, can only be achieved if radiologists contribute to the identification of the subset of patients complaining of headache and who have this potentially life-threatening disease which requires immediate therapy. They need to know the clinical background, be aware of suspect findings in routine MRI and should know the advantages and potential pitfalls and limitations of different MRA techniques and flow-sensitive sequences.

18.3.5 Treatment

Typically, patients with confirmed CVST are treated with intravenous heparin even in the presence of intracerebral hemorrhage. Although there is only one placebo-controlled, double-blind study showing a significant advantage of intravenous dose-adjusted unfractionated heparin therapy in patients with CVST (Einhäupl et al. 1991), heparin as the first-line treatment is recommended because of its efficacy, safety and feasibility (Ameri and Bousser 1992; Bousser 1999). Only in rare cases may fibrinolytic therapy or thrombectomy be considered as alternative treatment options.

18.4 Imaging

To interpret imaging, it is necessary to know the normal anatomy of the cerebral venous system and

to transfer this knowledge to the transversal cuts of the axial cranial CT (CCT) and MRI or to 3D reconstructions of the blood vessels. Moreover, the most important anatomical variants of the dural sinuses must be readily perceived. The normal venous angiogram as detected by digital subtraction angiography (DSA) and MRI is illustrated in Figs. 18.1 and 18.2a,b.

Frequently encountered anatomical variants include (Thron 2001):

- The unilateral hypoplastic transverse and sigmoid sinus with compensation via the contralateral transverse sinus.
- The aplasia of the frontal superior sagittal sinus anterior to the coronary suture with compensation via large bridging veins.
- The high division of the superior sagittal sinus (cranial to the internal occipital protuberance, where the confluens sinuum is normally encountered).
- Pacchioni granulations may be seen as circumscript intraluminal filling defects or gaps.

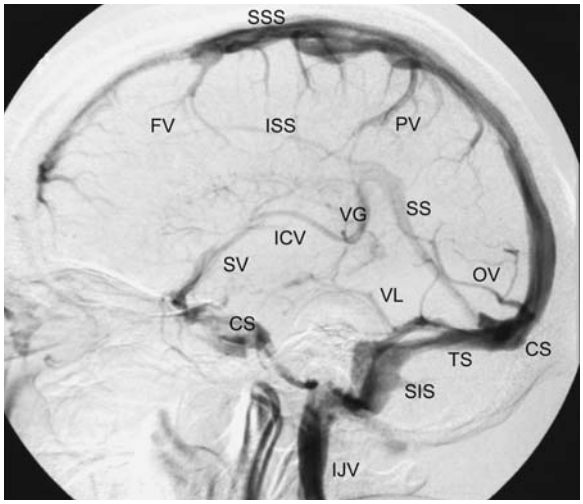

Fig. 18.1. Venous anatomy in digital subtraction angiography (DSA) in lateral projection. *FV*, frontal veins; *PV*, parietal veins; *OV*, occipital veins; *SSS*, superior sagittal sinus; *ISS*, inferior sagittal sinus; *TS*, transverse sinus; *SIS*, sigmoid sinus; *IJV*, internal jugular vein; *SS*, straight sinus; *CS*, confluens sinuum; *VL*, vein of Labbé; *SV*, sylvian vein; *CS*, cavernous sinus; *VG*, vein of Galen; *ICV*, internal cerebral vein; *IJV*, internal jugular vein

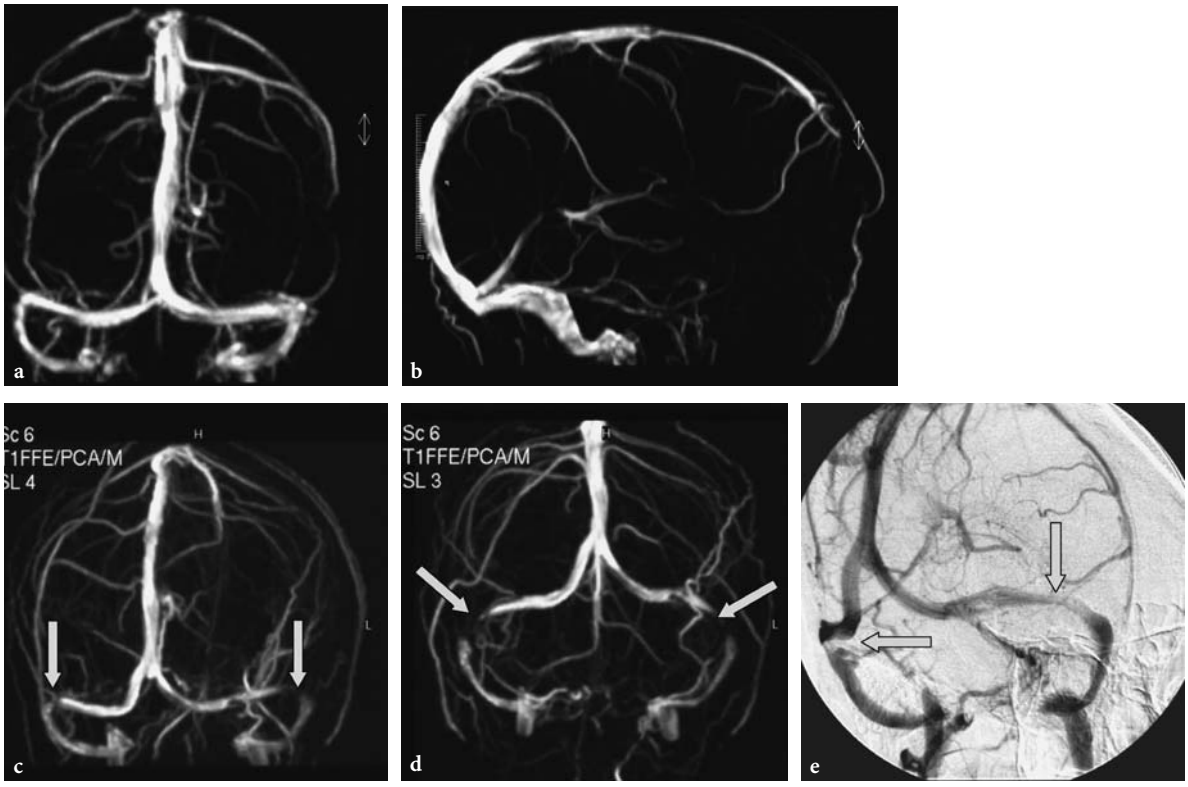

Fig. 18.2. a,b Normal venous anomaly in a 3D phase contrast venous angiogram performed at 1.5 T. **c,d** 3D phase contrast venous angiogram in a patient with idiopathic intracranial hypertension displayed in different projections. The bilateral short stenoses (*arrows*) are well shown by MR venography. **e** digital subtraction angiogram in an oblique projection. Confirmation of the obstructed vessel lumen on both sides (*arrows*), but the finding at this location can only be demonstrated on special projections

Although this book is primarily devoted to magnetic resonance imaging, a brief description of cranial computed tomographic findings in CVST seems to be reasonable since we have learned from CCT that in imaging of brain parenchyma and cerebral veins we have to differentiate between direct and indirect signs of CVST. The direct signs prove the diagnosis by demonstrating thrombus or missing flow within a dural sinus or pial vein, the indirect signs simply raise the suspicion of CVST by demonstrating different forms of venous congestion (Chiras et al. 1985).

In CCT direct signs include the hyperdense sinus in the non-contrast-enhanced scan, the "cord sign" (hyperdense bridging vein) and the "empty triangle sign" in the contrast-enhanced CCT (Virapongse et al. 1987) (see Fig. 18.10). Within the first 2 weeks, thrombosed blood is typically hyperdense on CCT compared to brain parenchyma. Therefore, it is important to start with a non-enhanced CCT scan in patients with suspected CVST (Thron 2001). The density of the thrombus might otherwise be mistaken for a contrast-enhanced vessel lumen. After 2 weeks the thrombus will have become isodense or hypodense to the brain parenchyma. Now the diagnosis can be made following the injection of contrast media which will show the thrombus as a filling defect of the lumen surrounded by either residual contrast-enhanced blood, the contrast enhancing meningeal wall or collateral venous channels outside the dura. This constitutes the empty triangle or empty delta sign on contrast enhanced CCT in a later stage of thrombus evolution.

Indirect signs include global and focal brain edema (see Figs. 18.6, 18.8, 18.9), intraparenchymal hemorrhages that might be solitary or multiple (Fig. 18.3) involving both grey and (preferentially) white matter and intense tentorial enhancement. Concerning the edema that is demonstrated as a hypodense area, the form and localization will typically not correspond to the classical arterial territories (see Fig. 18.8). Hemorrhages will also not suit the typical localization of parenchymal hypertensive bleeds but instead typically also expand to the cortical surface. The tentorium and the falx will appear thickened, engorged and will demonstrate pronounced enhancement that is due to dural venous collaterals.

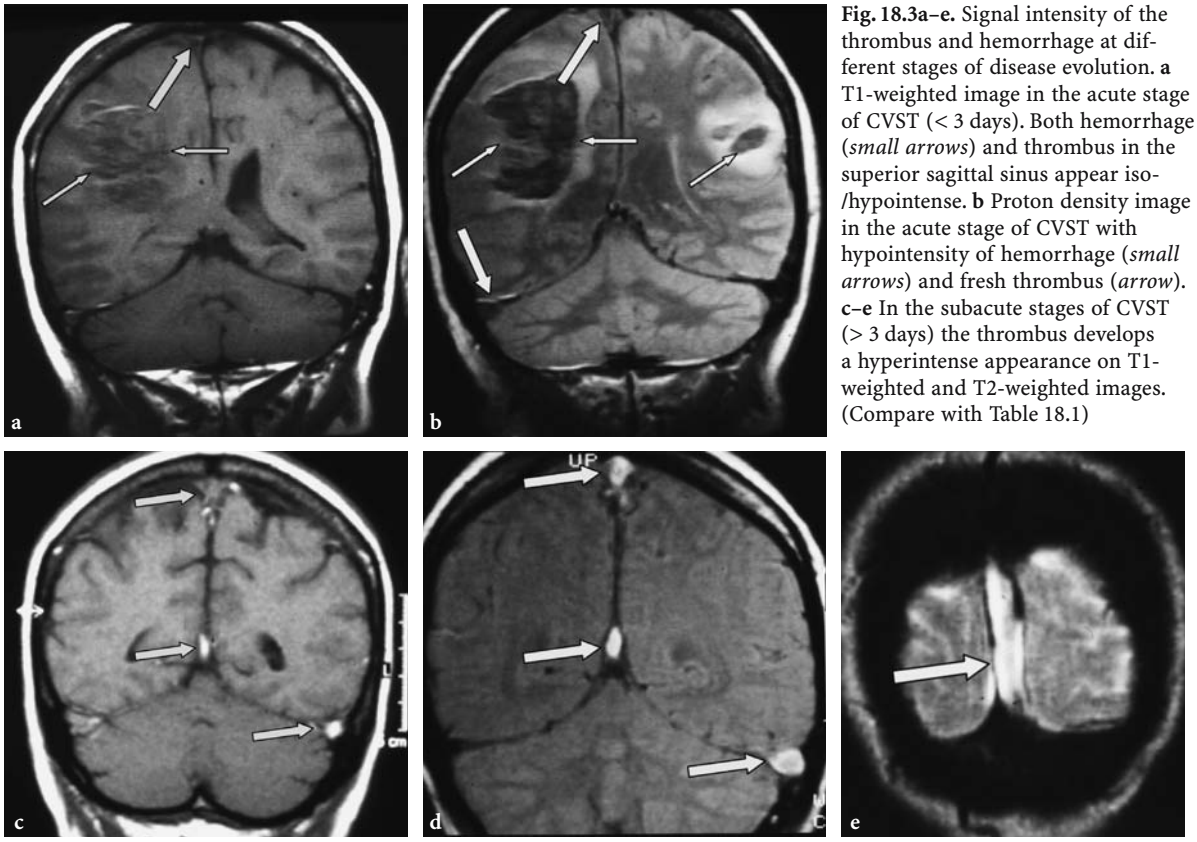

Fig. 18.3a–e. Signal intensity of the thrombus and hemorrhage at different stages of disease evolution. **a** T1-weighted image in the acute stage of CVST (< 3 days). Both hemorrhage (*small arrows*) and thrombus in the superior sagittal sinus appear iso-/hypointense. **b** Proton density image in the acute stage of CVST with hypointensity of hemorrhage (*small arrows*) and fresh thrombus (*arrow*). **c–e** In the subacute stages of CVST (> 3 days) the thrombus develops a hyperintense appearance on T1-weighted and T2-weighted images. (Compare with Table 18.1)

Table 18.1. Time dependant MR signal pattern in intraparenchymal hemorrhage and thrombosed dural sinuses. [Modified from Gomori et al. 1985; Isensee et al. 1994)

Time	Molecule	T1	T2
0-12 h	Oxy Hb	Iso-hypointense	Hyperintense
12-72 h	Deoxy Hb	Iso-hypointense	Hypointense
3-7 Days	MetHb intracellular	Hyperintense	Hypointense
1-4 Weeks	MetHb extracellular	Hyperintense	Hyperintense
> 4 Weeks	Hemosiderin	Iso-hypointense	Hypointense

18.4.1 Magnetic Resonance Imaging and Magnetic Resonance Angiography

The combination of these two MR techniques has become the imaging modality of first choice for the diagnosis and follow-up of CVST (Villringer et al. 1989; Vogel et al. 1994). MRI alone faces the problem that the MR signal of blood and blood products varies with clot age as is shown in Table 18.1 (Gomori et al. 1985). Therefore, a different appearance of a thrombosed vein in T1 and T2 sequences during different stages of thrombus evolution has to be taken into account (Isensee et al. 1994). The very fresh blood clot may be hyperintense in T1- and hypointense in T2-weighted images during the first 12 h. In this very early phase it is very unlikely that patients with CVST are symptomatic and undergo diagnostic procedures. Afterwards the oxyhemoglobin of the acute thrombus has changed to deoxyhemoglobin which is iso- to slightly hypointense to cortex on T1-weighted sequences with a hypointense signal in T2-weighted images (12 h-3 days). Late acute clots (3-7 days) contain intracellular methemoglobin and are hyperintense on T1-weighted sequences and hypointense on T2-weighted images. Subacute thrombi (1-4 weeks after initial thrombosis) are hyperintense on both T1 and T2 scans due to extracellular methemoglobin. Chronically thrombosed sinuses undergo fibrosis with hemosiderin deposition and may develop extensive collaterals. It is clear that the main problem of MRI standard sequences for CVST diagnosis is the iso-hypointense appearance of the acute clot (12-36 h) simulating flow. Problems may also be encountered in chronically thrombosed sinuses (Isensee et al. 1994). During the other phases of clot evolution an abnormal signal within the vessel lumen is evident in at least one of the standard sequences. Bearing this consideration in mind, the sinuses are best visualized using axial and coronal sequences in which the superior and inferior sagittal sinus, as well as the transverse sinuses and the internal veins, are well imaged. Using these standard sequences, it is possible to evaluate normal anatomy or to detect anatomic variations like hypoplasia of one of the transverse sinuses.

Direct signs of CVST in MRI:

- Demonstration of an intraluminal thrombus within a dural sinus or a cerebral vein. This is easy during the time interval between 4 days and 4 weeks of thrombus age due to the high signal of methemoglobin on T1-weighted images (Table 18.1; Fig. 18.3) It may be difficult in cases of a very fresh (< 3 days) or old (> 4 weeks) thrombus which can be organized or partially recanalized (Figs. 18.3, 18.7). Absence of the normal "flow-void" in large veins should raise suspicion of CVST, but this sign is unreliable, as it also appears with slow flow.
- Demonstration of an "empty triangle" or "delta sign" within a sinus, comparable to the finding in CT (see Figs. 18.9, 18.10) following contrast-enhancement.

Indirect signs of CVST in MRI:

- Uni- or bilateral areas of edema that do not correspond to arterial territories (see Figs. 18.6-18.9)
- Uni- or bilateral hemorrhages (see Figs. 18.3, 18.8).
- Pronounced regional enhancement of the leptomeninges (falx, tentorium, convexity) due to the involvement of these structures in collateral drainage (see Fig. 18.9).
- Regional subarachnoid hemorrhage, especially if it is situated on the convexity of the brain. It may be a sign of the rare isolated cerebral vein thrombosis.

Table 18.2 summarizes the sequences and MR techniques which in our experience can be proposed (as mandatory or optional) in the diagnostic management of veno-occlusive disorders of the brain. Venous MRA can either be performed with the time-of-flight (TOF) or with the phase-contrast (PC) technique. In addition to the tomographic images, a flow sensitive gradient-echo sequence should be obtained if CVST is in question. As a fast screening examination we prefer a TOF 2D FLASH sequence (Table 18.2; Fig. 18.4, see 18.6c), oriented 90 degree to the flow direc-

Table 18.2. Diagnostic management of suspected CVST by MRI and MRA

MRI + MRA	Specific Parameters
T1 axial	
T2 coronal	
TOF angiogram (FLASH) 5 mm, coronal, 1:36 min (2D FLASH)	TR/TE/FA: 23/7 ms/40°, 5 slices,
2D-PCA (optional)	TR/TE/FA: 20/5.2/15°,1 slice, 30 mm, sagittal+axial, 1:14 min
3D-PCA (optional)	TR/TE/FA : 16/6.8/10°, 200 slices, 0.8 mm, axial, 9:32 min
DWI (optional)	TR/TE 5100/137 ms, 19 slices, 5 mm, axial
FLAIR (optional)	
3D contrast-enhanced MRA (optional)	
2D dynamic contrast-enhanced subtraction MRA (optional) TR/TE/FA 3.5/1.0/40 coronal+sagittal	

tion (coronal). It provides sufficient anatomical details and gives reliable information whether there is flow (high signal) or no flow (no signal). The only information which is required for correct interpretation is the presence of methemoglobin with a high signal on T1-weighted images. This substance also appears hyperintense on the FLASH image, thus simulating flow. This is one of several reasons why a combination of MR tomographic and angiographic sequences has to be postulated in CVST. 2D or 3D PC MR angiograms, coded for slow flow, are established techniques for the selective demonstration of cerebral veins and should be used as additional standard sequences when evaluating CVST (Fig. 18.2, 18.8--18.11). These sequences create angiographic images and may facilitate image interpretation. However, loss of information on the maximum intensity projection (MIP) images or pitfalls due to artefacts must be taken into account (Fig. 18.10). Therefore, the source images always need to be included in the evaluation. In the case of 3D sequences the examination time is considerably prolonged to about 10 min. Contrast-enhanced venous MRA is an advanced and costly technique (Farb et al. 2003) which, on the other hand, avoids problems created by turbulent flow and improves image quality. Another promising new technique is 2D dynamic (time resolved) contrast-enhanced MR subtraction angiography (Table 18.2; Figs. 18.5, 18.6). It is based on a single-slice T1-weighted gradient-echo sequence and has a temporal resolution of about 0.34 s/image (Krings and Hans 2004). It covers the arterial and venous phase in coronal and sagittal direction and is useful not only in the detection of venous drainage obstruction, but also in the diagnosis of arteriovenous (AV) shunts. This is important because AV fistulae or AV malformations are other important causes for venous drainage impairment. Contrast-enhanced T1-weighted studies can be helpful but are not mandatory. As already mentioned they can demonstrate – similiar to the contrast enhanced CT – an "empty triangle" or delta-sign (Figs. 18.9, 18.10).

An axial fluid-attenuated inversion recovery sequence (FLAIR) is usually acquired additionally to demonstrate parenchymal involvement of CVST. Diffusion-weighted MRI in CVST has gained special attention in recent years because the pathophysiology of diffusion abnormalities is less well understood compared to arterial stroke (Sarma et al. 2004). The more complex pathophysiological process of venous congestion and infarction obviously leads to both vasogenic and cytotoxic edema (Corvol et al. 1998; Keller et al. 1999; Lövblad et al. 2001). Three types of lesions were identified by Mullins et al. (2004). Resolving lesions with elevated diffusion coefficient (vasogenic edema), persisting lesions with low diffusion (cytotoxic edema, patients without seizure activity) and resolving lesions with low diffusion (cytotoxic edema, patients with seizure activity). The observation of the reversibility of restricted diffusion in extensive venous thrombosis was interpreted by Sarma et al. (2004) as the existence of an "intracellular edema" which is reversible for an undefined, variable time.

Our typical MR protocol for suspected CVST includes an axial FLAIR, axial diffusion-weighted MRI, coronal T1 SE and T2 TSE sequences, a coronal gradient echo and a 3D phase contrast venous angiogram with a total imaging time of approximately 20 min.

7.4.1.1 MRA Findings in (Benign and Idiopathic) Intracranial Hypertension

Chronic thrombosis or only partially recanalized dural sinus thrombosis may be diagnosed in these patients (Thron et al. 1986; Wessel et al. 1987). This type is less obvious on the static MRI (Isensee et al. 1994) and requires MR venography, if possible in a contrast-enhanced technique. In children, purulent mastoiditis is an important cause of septic thrombosis (Reul et al. 1997) or

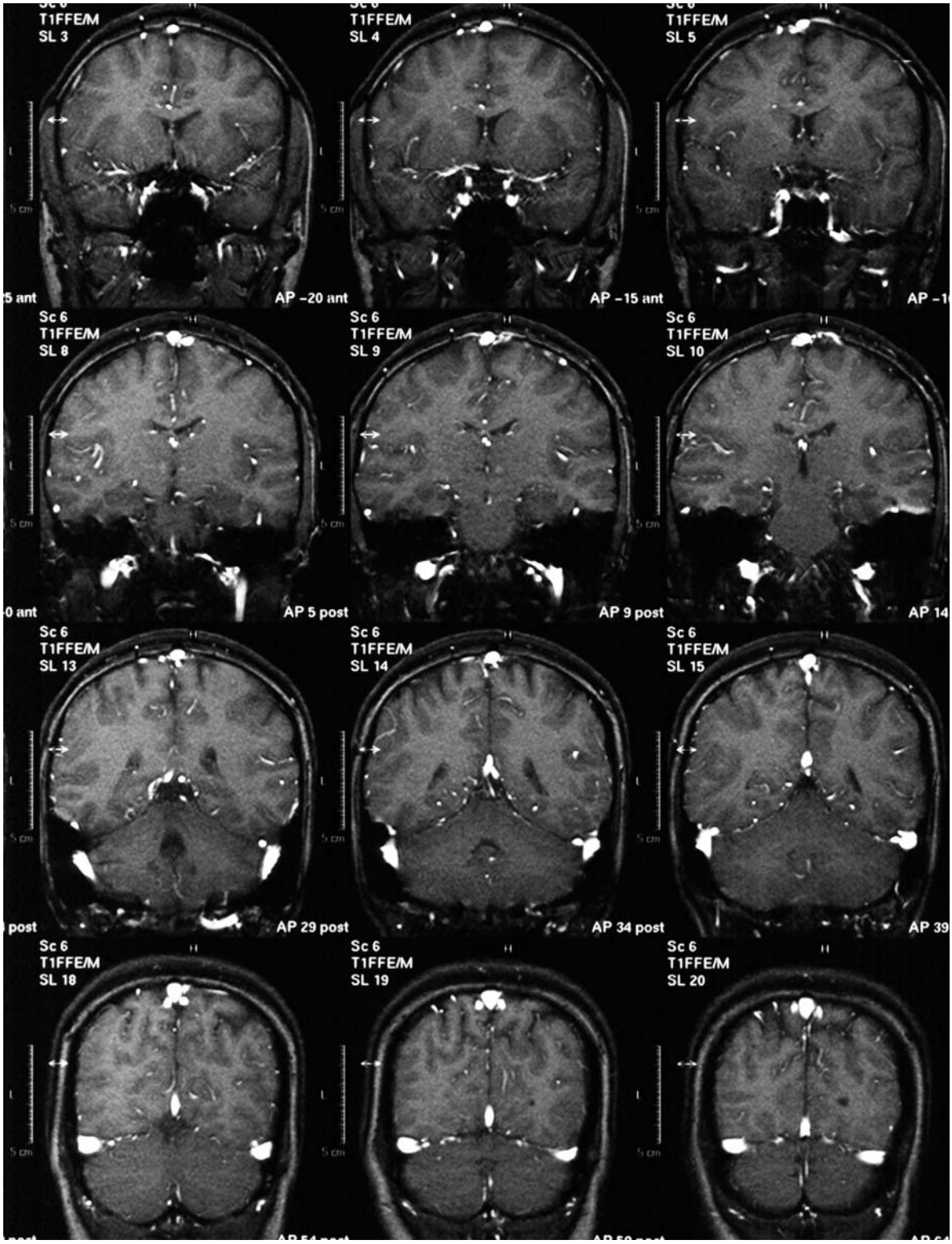

Fig. 18.4. Coronal 2D fast low angle shot (FLASH) (section). This flow-sensitive sequence offers a quick (1:30 min) screening for all major sinuses with additional anatomical information. Important: Comparison with the T1-weighted images is necessary because not only flow, but also methemoglobin appear bright

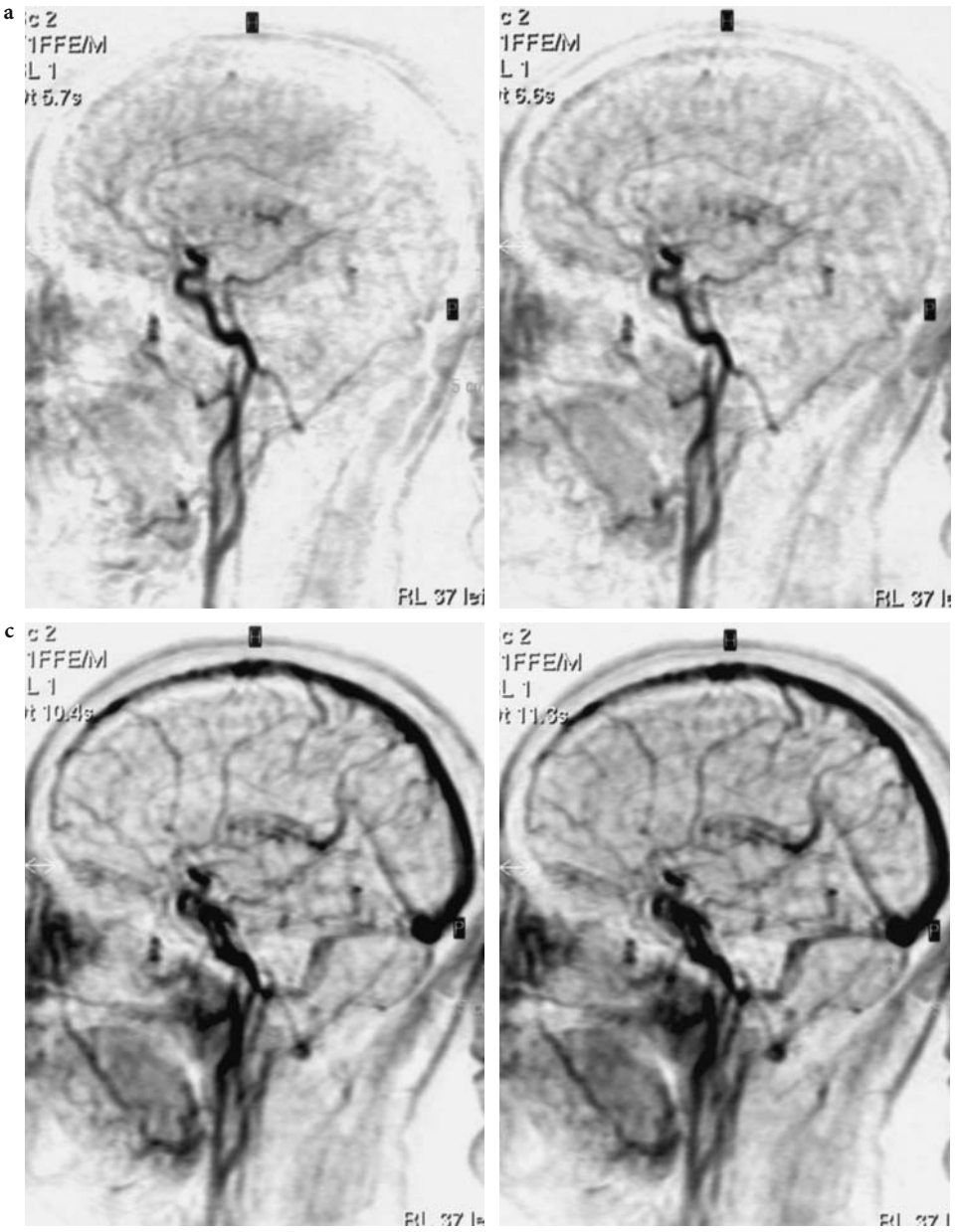

Fig. 18.5a–d. 2D dynamic contrast-enhanced MR subtraction angiography. Normal finding. Selected images from the arterial (**a**,**b**) and venous phase (**c**,**d**) are shown

inflammatory stenosis (Isensee et al. 1992) of the ipsilateral transverse sinus (Reul et al. 1997), followed by raised intracranial pressure. A cystic developmental lesion within a sinus (Küker et al. 1997), or other space-occupying or infiltrating processes, obstructing the lumen of a dural sinus are rare causes.

In patients with idiopathic intracranial hypertension bilaterally narrowed segments in the lateral venous sinuses have been demonstrated compared to normal findings in asymptomatic volunteers using advanced techniques of MR venography (Higgins et al. 2002, 2004; Farb et al. 2003). We have observed similar cases in recent years with unilateral sinus stenosis and contralateral hypoplasia or bilateral stenoses (see Fig. 18.2c-e).

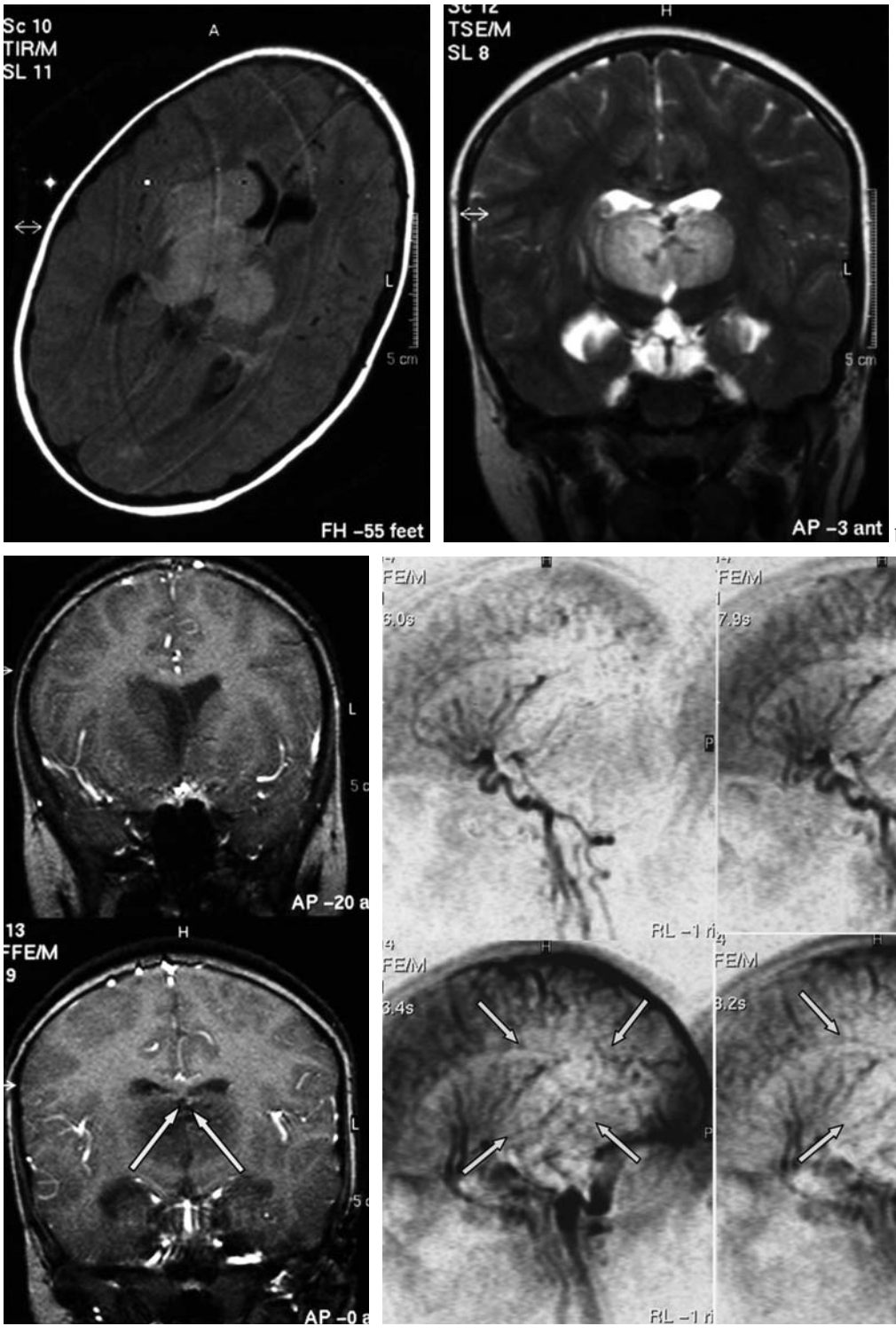

a b c d

Fig. 18.6a–d. Deep cerebral venous thrombosis in an 8-year-old girl presenting with headache, state of confusion and somnolence. **a** Axial FLAIR image with bilateral swelling and hyperintensity of the thalami and right-sided basal ganglia. **b** Coronal T2-weighted image with high signal in both thalami due to edema and/or infarction, suspicious of thrombosis of the deep venous system (internal cerebral veins, straight sinus). **c** On the coronal flow-sensitive Sequence (FLASH) no flow is shown in the internal cerebral veins (*arrows*). **d** 2D dynamic contrast-enhanced MR subtraction angiography. The images from the arterial phase (*upper row*) are normal, in the late venous phase (*lower row*) an area of reduced parenchymal contrast and absence of the internal cerebral veins and straight sinus are shown. (Compare with normal findings in Fig. 18.5)

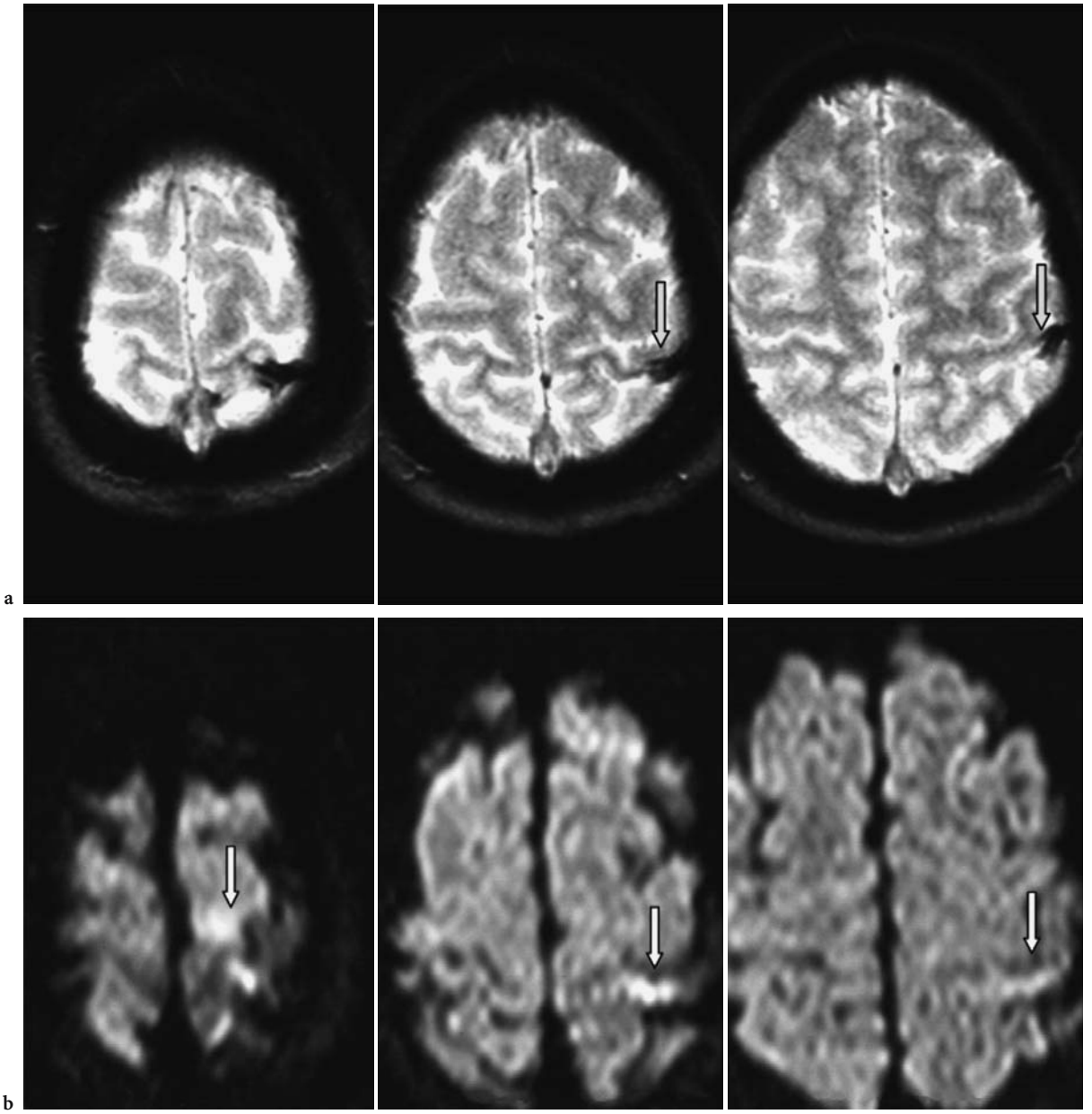

Fig. 18.7a,b. Isolated cortical vein thrombosis in a 16 y old female presenting with focal epileptic seizures. **a** Axial GE (T2*) images show a hypointense signal along the course of a cortical vein (*arrows*) which was also seen as a hyperdense structure on CT (not shown). **b** Axial DWI shows small areas of restricted diffusion in the corresponding brain parenchyma

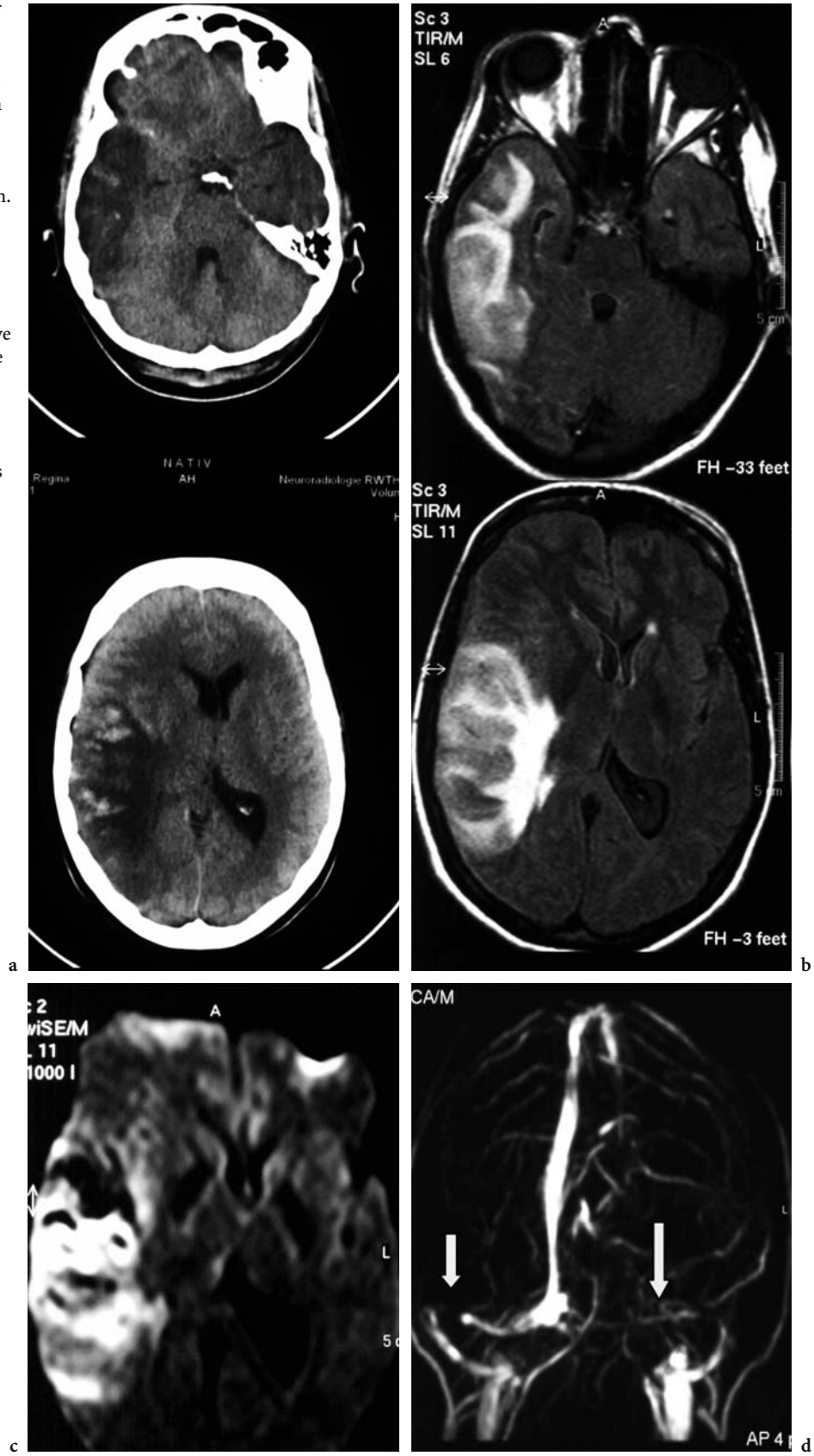

Fig. 18.8a–d. Thrombosis of the transverse sinuses with temporolateral congestive and hemorrhagic infarction on the right side. The lesion corresponds to the drainage territory of the vein of Labbé. **a** CT aspect of the partially hemorrhagic lesion. **b** FLAIR images showing areas of different hyperintensity. **c** DWI with a very inhomogeneous pattern of diffusion abnormalities. **d** 3D PC venography. Extensive thrombosis with incomplete occlusion mainly of the transverse sinuses (*arrows*). On the right side, corresponding to the lesion location, temporal cortical veins (vein of Labbé) are missing (*short arrow*)

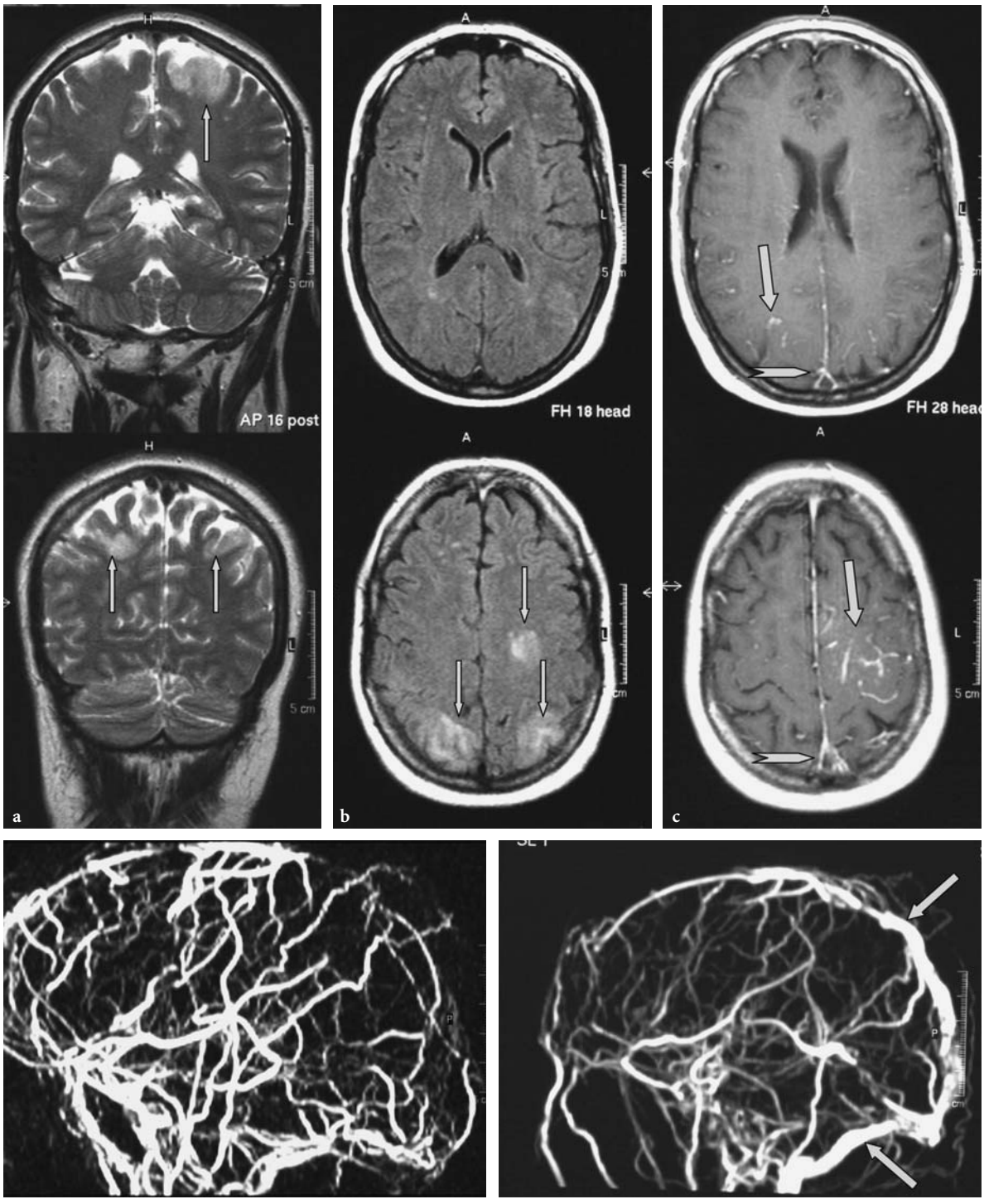

Fig. 18.9a–e. Extensive thrombosis of all main dural sinuses. **a** Coronal T2-weighted images. Only small cortical lesions are present. The signal of the big sinuses is iso-/hypointense and does not indicate thrombotic occlusion. **b** Axial T1-weighted contrast-enhanced images. Intraluminal thrombus is evident in the superior sagittal sinus (*arrowheads*) and increased leptomeningeal enhancement can be demonstrated (*arrows*) indicating collateral drainage through small veins. **c** Axial FLAIR images. Small cortical/subcortical areas of infarction are present (*arrows*). **d** 3D PC MR venogram. Extensive thrombosis of all major dural sinuses. The drainage is restricted to superficial collateral veins. **e** 3D PC MR venogram after 3 months of anticoagulation. Improvement with partial restoration of flow in the superior sagittal and transverse sinuses (*arrows*)

a

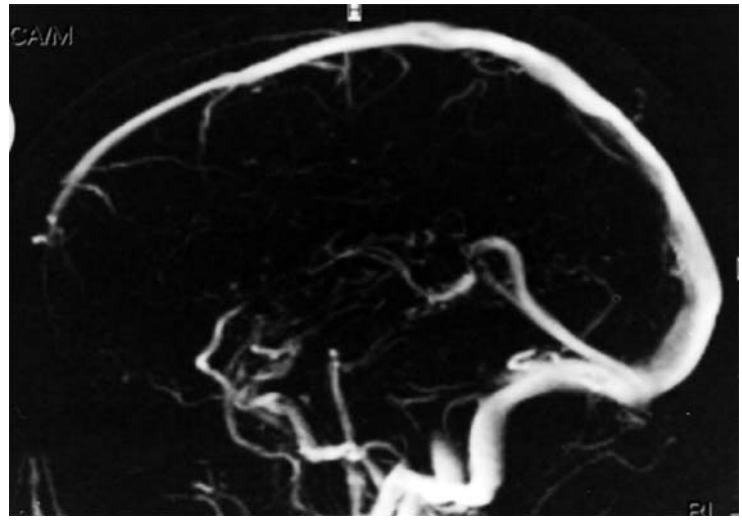

b

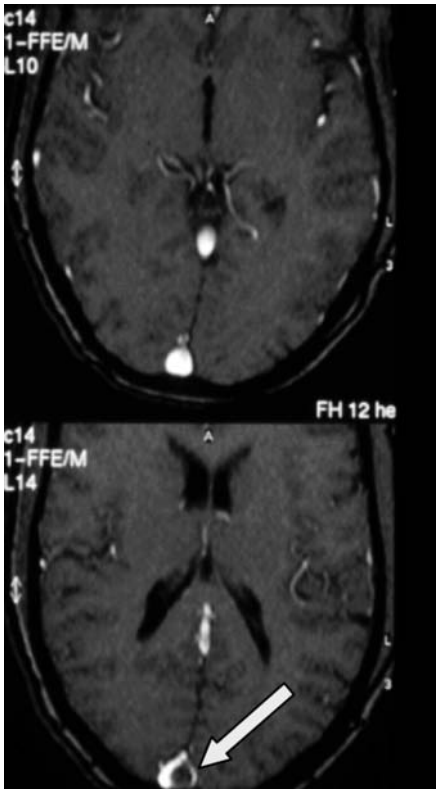

c

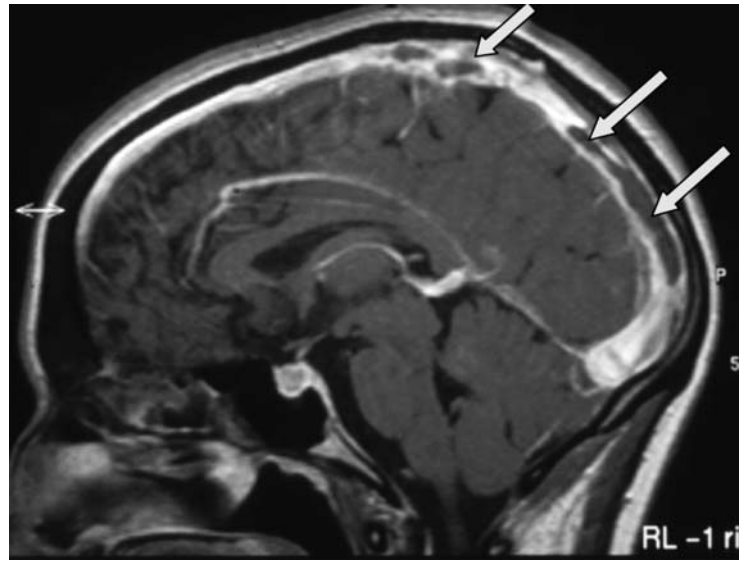

d

Fig. 18.10a–d. Superior sagittal sinus thrombosis in a 29-year-old woman. She was treated with steroids for multiple sclerosis and presented with acute headaches. **a** Contrast-enhanced CT, performed on admission, shows a clear "empty triangle" sign in the superior sagittal sinus as a direct sign of thrombosis. **b** 3D PC MR venography, performed the day after admission in addition to MRI, did not demonstrate a clear pathological finding. **c,d** Contrast-enhanced T1-weighted images in axial (**c**) and sagittal orientation reveal a long thrombus which is not completely occluding the lumen of the sinus

18.4.2 Diagnostic Problems, Potential Artefacts and Pitfalls

- Hypoplasia or even aplasia of a sinus or part of it must be differentiated from thrombus by careful analysis of the standard anatomic sequences (Fig. 18.11). When present, the CCT scan should also be taken into account, since a hypoplastic transverse and sigmoid sinus typically demonstrates a smaller jugular foramen when compared to the normal side.
- Slow or turbulent flow may lead to signal dephasing and false interpretation of impaired or even missing flow within the dural sinuses (Bono et al. 2003). The signal intensities of sigmoid sinuses on PC MR images may be affected by respiration (Kudo et al. 2004). The slow or oscillating flow in transverse sinuses can be demonstrated more reliably with contrast-enhanced studies.
- Non-thrombotic intraluminal notches as present in hypertrophic Pacchioni granulations might also mimick thrombus (Fig. 18.12). On MRI, these intraluminal granulations are hypo- or isointense in T1 and hyperintense in T2-weighted images and well defined (Giraud et al. 2001).
- On the other hand, thrombus characteristics as discussed above might also mask the presence of an acute CVST since the hypointense visualization of acute thrombus (< 3 days) on T2-weighted sequences might be mistaken as a flow void (Fig. 18.3). The same is true for old organized or partially recanalized sinus thrombosis (Fig. 18.9).
- Do not rely on MIP images without looking at the source images. The information loss may be crucial as visualized in Fig. 18.10.
- The diagnosis of isolated cerebral vein thrombosis remains a challenge, because the direct signs as demonstrated in Fig. 18.7 are rarely seen. A "missing" vein or differences in the venous pattern between both hemispheres are unreliable signs, because the distribution and caliber of the cerebral veins is highly variable. The differential diagnosis of an area of T2 hyperintensity which does not correspond to an arterial territory (indirect sign) includes thrombosis of a cerebral vein, vasculitis, infectious disease or posterior leukoencephalopathy. The treatment for each of these diseases is very different. Contrary to most recommendations we do not think that DSA is the right answer to solve this problem, since it encounters the same problem as MR venography.

Fig. 18.11. 3D PC MR venography. There is only minimal flow in the area of the left transverse sinus. As these images do not give any anatomical information the evaluation must include images (CT or MRI) which provide the information whether this dural sinus is present and occluded or whether it is hypo-/aplastic

18.4.2.1 Additional and Competitive Diagnostic Procedures

From a clinical point of view measurement of circulating D-dimer levels might be a very helpful tool to identify the subgroup of headache patients who need immediate further radiological diagnostics (Kosinski et al. 2004). CVST in this group of patients without any focal neurological abnormalities may otherwise be overlooked.

CT venography of cerebral veins is a very reliable technique for the demonstration of intraluminal abnormalities of dural sinuses (Figs. 18.10a, 18.12a; Ozsvath et al. 1997). In particular, multisection CT venography with subtraction of bone is a promising and competitive technique for the evaluation of veno-occlusive disorders of the cerebral veins and sinuses (Majoie et al. 2004). One disadvantage, however, is the radiation exposure. Conventional DSA is typically not needed unless endovascular treatment is necessary, since MRI, MRA and CT are usually sufficient to make a correct diagnosis.

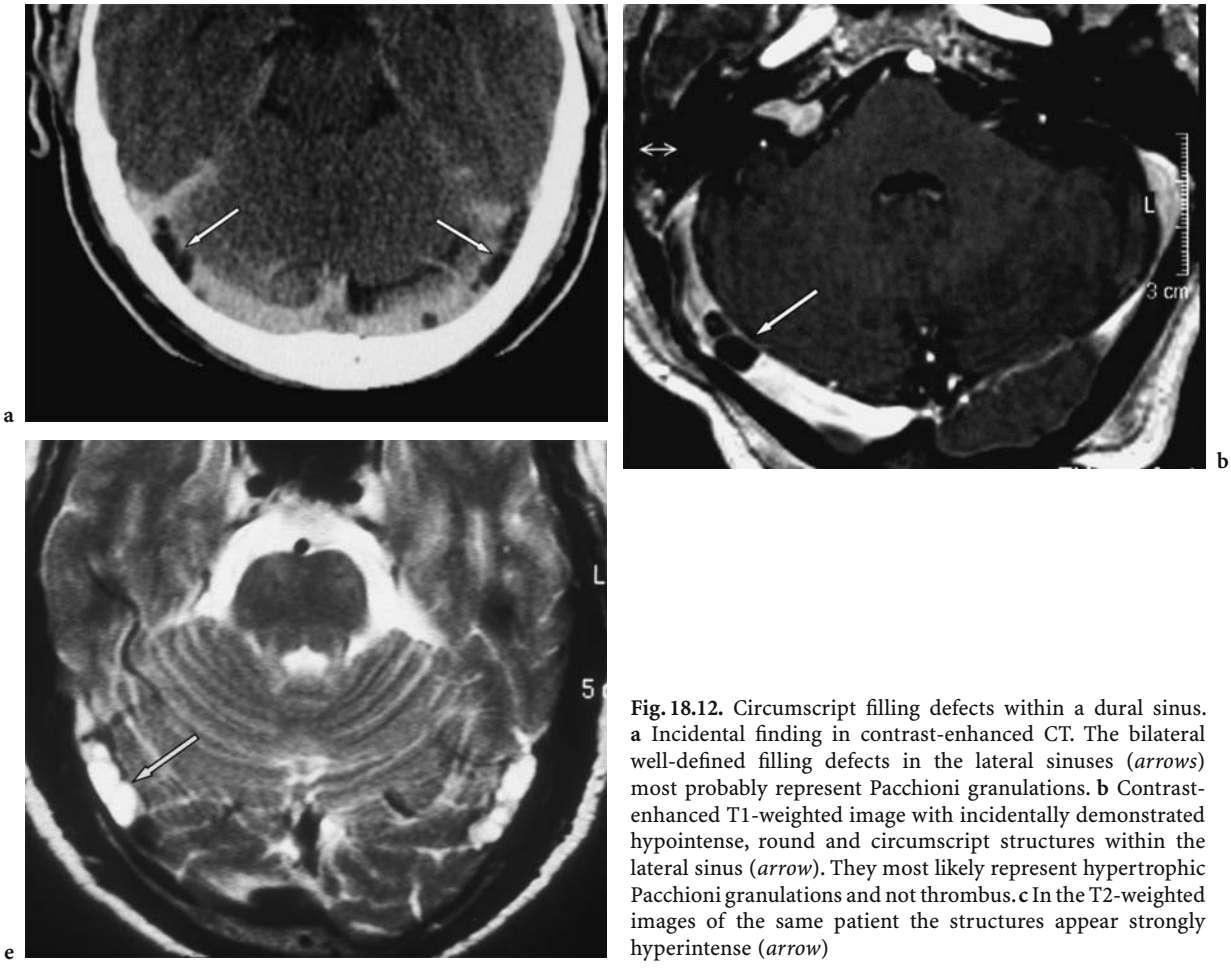

Fig. 18.12. Circumscript filling defects within a dural sinus. **a** Incidental finding in contrast-enhanced CT. The bilateral well-defined filling defects in the lateral sinuses (*arrows*) most probably represent Pacchioni granulations. **b** Contrast-enhanced T1-weighted image with incidentally demonstrated hypointense, round and circumscript structures within the lateral sinus (*arrow*). They most likely represent hypertrophic Pacchioni granulations and not thrombus. **c** In the T2-weighted images of the same patient the structures appear strongly hyperintense (*arrow*)

References

Ameri A, Bousser MG (1992) Cerebral venous thrombosis. Neurol Clin 10:87-111

Bono F, Lupo MR, Lavano A, Mangone L, Fera F, Pardatscher K, Quattrone A (2003) Cerebral MR venography of transverse sinuses in subjects with normal CSF pressure. Neurology 61:1267-1270

Bousser MG (1999) Cerebral venous thrombosis: nothing, heparin, or local thrombolysis? Stroke 30:481-483 (editorial; comment)

Cantu C, Barinagarrementeria F (1993) Cerebral venous thrombosis associated with pregnancy and puerperium. Review of 67 cases. Stroke 24:1880-1884

Chiras J, Bousser MG, Meder JF, Koussa A, Bories J (1985) CT in cerebral thrombophlebitis. Neuroradiology 27:145-154

Corvol JC, Oppenheim C, Manai R, Logak M, Dermont D, Samson Y, Marsault C, Rancurel G (1998) Diffusion-weighted magnetic resonance imaging in case of cerebral venous throbosis. Stroke 29:2649-2652

Crawford SC, Digre KB, Palmer CA, Osborn AG (1995) Thrombosis of deep venous drainage of the brain in adults. Arch Neurol 52:1101--1108

Deschiens MA, Conard J, Horellou MH, Ameri A, Preter M, Chedru F, Samana MM, Bousser MG (1996) Coagulation studies, factor V Leiden, and anticardiolipin antibodies in 40 cases of cerebral venous thrombosis. Stroke 27:1724-1730

Einhäupl KM, Villringer A, Meister W, Mehrain S, Garner C, Pellkofer M, Haberl RM, Pfister HW, Schmiedek P (1991) Heparin treatment in sinus venous thrombosis. Lancet 338:597-600

Farb RI, Vanek I, Scott JN, Mikulis DJ, Willinski RA, Tomlinson G, terBrugge KG (2003) Idiopathic intracranial hypertension. The prevalence and morphology of sinovenous stenosis. Neurology 60:1418-1424

Giraud P, Thobois S, Hermier M, Broussolle E, Chazot G (2001) Intravenous hypertrophic Paccioni granulations: differentiation from venous dural thrombosis. J Neurol Neurosurg Psychiatry 70:700-701

Gomori JM, Grossmann RI, Goldberg HJ, Zimmermann RA, Bilanuk LT (1985) Intracranial hematomas: imaging by high field MR. Radiology 157:87-93

Higgins JN, Owler BK, Cousins C, Pickard JD (2002) Venous sinus stenting for refractory benign intracranial hypertension. Lancet 359:228-230

Higgins JN, Gillard JH, Owler BK, Harkness K, Pickard JD

(2004) MR venography in idiopathic intracranial hypertension: unappreciated and misunderstood. J Neurol Neurosurg Psychiatry 75:621-625

Isensee C, Reul J, Kentrup H, Thron A (1992a) Entzündliche Sinusstenose als Ursache eines Pseudotumor cerebri beim Kind. Angiographie- und MRT-Befunde. Klin Neuroradiol 2:199-202

Isensee Ch, Reul J, Thron A (1992b) Thrombose des Sinus transversus als Ursache temporaler Blutungen. Stellenwert von MRT und Angiographie. Aktuel Neurol 19:78-81

Isensee, Ch, Reul J, Thron A (1994) Magnetic resonance imaging of thrombosed dural sinuses. Stroke 25:29-34

Keller E, Flacke S, Urbach H, Schild HH (1999) Diffusion- and perfusion-weighted magnetic resonance imaging in deep cerebral venous thrombosis. Stroke 30:1144-1146

Kosinski Ch M, Mull M, Schwarz M, Koch B, Biniek R, Schläfer J, Milkereit E, Willmes K, Schiefer J (2004) Do normal D-dimer levels reliably exclude cerebral sinus thrombosis? Stroke 35:2820-2825

Krings T, Hans FJ (2004) New developments in MRA: time-resolved MRA. Neuroradiology 46 [Suppl 2]:214-222

Kudo K, Terae S, Ishii A, Omatsu T, Asano T, Tha KK, Miyasaka K (2004) Physiologic change in flow velocity and direction of dural venous sinuses with respiration: MR venography and flow analysis. AJNR 25:551-557

Küker W, Mull M, Mayfrank L, Weis J, Schiefer J, Thron A (1997) A cystic lesion within the dural sinuses: a rare cause of increased intracranial pressure. Neuroradiology 39:132-135

Lafitte F, Boukobza M, Guichard JP, Reizine D, Woimant F, Merland JJ (1999) Deep cerebral venous thrombosis: imaging in eight cases. Neuroradiology 41:410-418

Lövblad K-O, Bassetti C, Schneider J, Guzman R, El-Koussy M, Remonda L, Schroth G (2001) Diffusion-weighted MR in cerebral venous thrombosis. Cerebrovasc Dis 11:169-176

Majoie CB, van Straten M, Venema HW, den Heeten GJ (2004) Multisection CT venography of the dural sinuses and cerebral veins by using matched mask bone elimination. AJNR 25:787-791

Mullins ME, Grant PE, Wang B, Gonzales RG, Schaefer PW (2004) Parenchymal abnormalities associated with cerebral venous sinus thrombosis: assessment with diffusion-weighted MR imaging. AJNR25:1666-1675

Ozsvath RR, Casey SO, Lustrin ES, Alberico RA, Hassankhani A, Patel M (1997) Cerebral venography: comparison of CT and MR projection venography. AJR 169:1699-1707

Reul J, Weber U, Kotlarek F, Isensee C, Thron A (1997) Cerebral vein and sinus thrombosis-an important cause of benign intracranial pressure increase in childhood. Klin Padiatr 209:116-120

Sarma D, Farb RI, Mikulis DJ, ter Brugge KG (2004) Reversal of restricted diffusion in venous thrombosis: case report. Neuroradiology 46:118-121

Strupp M, Villringer A, Bousser MG (2003) Cerebral venous and sinus thrombosis. In: Brandt T, Caplan LR, Dichgans J, Diener HC, Kennard C (eds) Neurological disorders, course and treatment, 2nd edn. Academic, New York, pp 447-460

Thron A (2001) Diagnostik duraler Sinus- und zerebraler Venenthrombosen. Klin Neurorad 11:185-196

Thron A, Wessel K, Linden D, Schroth G, Dichgans J (1986) Superior sagittal sinus thrombosis: neuroradiological evaluation and clinical findings. J Neurol 233:283-286

Villringer A, Seiderer M, Bauer WM, Laub G, Haberl RL, Einhäupl KM (1989) Diagnosis of superior sagittal sinus thrombosis by three-dimensional magnetic resonance flow imaging (letter). Lancet 1:1086-1087

Virapongse C, Cazenave C, Quisling R, Sarwar M, Hunter S (1987) The empty delta sign: frequency and significance in 76 cases of dural sinus thrombosis. Radiology 162:779-785

Vogel TJ, Bergman C, Villringer A, Einhäupl K, Lissner J, Felix R (1994) Dural sinus thrombosis: value of venous MR angiography for diagnosis and follow-up. Am J Roentgenol 162:1191-1198

Wessel K, Thron A, Linden D, Petersen D, Dichgans J (1987) Pseudotumor cerebri: clinical and neuroradiological findings. Eur Arch Psychiatr Neurol Sci 237:54-60

19 Stroke-Mimicking Conditions

Joachim Röther

CONTENTS

19.1 Introduction

Stroke is a clinical diagnosis and the acute onset of focal neurological symptoms is the major indicator of stroke. Whereas typical stroke symptoms such as hemiparesis, amaurosis or dysarthria are easy to recognize, other stroke syndromes such as vertebrobasilar strokes or predominant neuropsychological manifestations are subject to misdiagnosis especially for non-neurologists. Misdiagnosis may be due to a non-vascular medical condition that simulates a stroke syndrome – a condition coined "stroke mimicry". Or, a stroke may resemble another non-vascular clinical entity – a circumstance termed as "stroke chameleon" (Huff 2002).

19.2 Stroke Mimics

Misdiagnosis of stroke is not uncommon and it is well recognized that nonvascular conditions such as brain tumor, subdural hematoma and cerebral abscess may mimic cerebral ischemia (Groch et al. 1960). Misdiagnosis occurs if details regarding past history are lacking. This may be because the patient is aphasic, comatose or demented. A careful patient history, a skillful examination of the patient, laboratory tests and an imaging study may prevent misdiagnosis. The frequency of misdiagnosis depends on the tests used and the time point chosen when the diagnosis "stroke" is first assigned. Differences of these parameters within previous studies explain the wide range from 5%–33% (Kothari et al. 1995a,b; Ulaki et al. 2000). Misdiagnosis is more frequent if the diagnosis is made by non-neurologists. However, since emergency and intern physicians are often involved in the management of acute stroke patients, the rate of misdiagnosis can be reduced by an acute stroke service with consultation of a neurologist (Norris and Hachinski 1982).

The frequency of misdiagnosis of stroke depends on the intensity of the diagnostic work-up. In previous decades autopsy or cerebral angiography were the only methods to verify false diagnosis (Bull et al. 1960). With the advent of modern neuroimaging techniques the distinction of stroke mimics from true strokes is easier. Since the diagnostic accuracy is higher, the number of stroke misdiagnosis may even rise (Allder et al. 1999).

More than 20 years ago Norris and Hachinski (1982) studied the misdiagnosis of stroke among 821 consecutive patients admitted to a stroke unit. The initial diagnosis was made by a primary care physician and confirmed by a neurology resident in the setting of a general teaching hospital. The diagnosis of stroke proved incorrect in 13% of the patients. Common etiologies for misdiagnosis are summarized in Table 19.1. Post-ictal states after unwitnessed or unrecognized seizures were by far the most common disorders misdiagnosed as stroke. Half of these patients had transient focal neurological signs that seemed to support the diagnosis of stroke.

Clinical skill was important for the correct diagnosis: The likelihood of a correct diagnosis within a subgroup of 50 consecutive cases admitted to the stroke unit without the final diagnosis "stroke" was highest in neurology consultants (76%), followed by neurology residents (32%) and emergency physicians (22%).

J. Röther, MD
Department of Neurology, Klinikum Minden, University of Hannover, Friedrichstr. 17, 32427 Minden, Germany

Table 19.1. Typical conditions that mimic stroke

Non-ischemic CNS disorders
- Todd's paralysis after epileptic seizure
- Migraine aura; hemiplegic migraine
- Psychogenic disorders
- Encephalitis
- Brain abscess
- Brain tumor
- Subdural hemorrhage
- Hypertensive encephalopathy
- Benign paroxysmal postural vertigo
Toxic-metabolic disorders
- Hypoglycemia
- Hyperglycemia
- Hepatic encephalopathy

The study was initiated before cerebral computed tomography (CT) scanners were available and only a subgroup of 244 patients was scanned. Astonishingly, the frequency of the misdiagnosis did not differ whether or not the patients were studied by CT. The authors argue that this is due to the low conspicuity of CT within the first hours after stroke with only 54% positive findings by the second day (Abrams and McNeil 1978). Even though technical advances in CT are enormous, the numbers are similar nowadays with 57% CT-positive strokes in the 6 h time window in the ECASS II trial (Hacke et al. 1998). The incidence of early positive CT findings is higher (73%) in patients with proven arterial occlusions (Furlan et al. 1999).

One might expect that since the early study of Norris and Hachinski in 1982 a lot more knowledge has been accumulated that makes "stroke" a more secure diagnosis. However, Libman et al. (1995) found stroke mimics in as many as 19% (78/411) of a population of consecutive patients referred to an emergency department based on clinical investigation. Unrecognized seizures with postictal neurological deficits (17%), systemic infection (17%), brain tumors (15%) and toxic metabolic disturbances (13%) were the most frequent conditions for misdiagnosis.

A rate of 19% misdiagnosis appears rather high and it is obvious that the frequency of misdiagnosis is not only influenced by the skill of the clinicians but the time point when diagnosis is made. In this study, the assignment to the diagnosis "stroke" was made after the history and physical examination and before laboratory tests and imaging studies were performed. Another explanation for the high number of mimics is that the initial diagnosis was mainly made by emergency physicians (75%) and only 25% of patients were evaluated in conjunction with a neurologist.

Another study shed a more favorable light on the diagnostic skills of emergency physicians supported by neurological telephone consultation. Kothari et al. (1995a) found misdiagnosis of stroke in only 5% of patients seen by emergency physicians after CT and laboratory studies had been performed. Misclassification was due to "paresthesia of unknown cause", seizure, complicated migraine, peripheral neuropathy, cranial nerve neuropathy and psychogenic paralysis. CT and laboratory tests were performed before assignment of the diagnosis and this accounts for the fact that misdiagnosis due to tumors, systemic infections and toxic metabolic disorders was ruled out.

Preventing misdiagnosis of stroke is increasingly important in the acute stage of the disease when thrombolytic or interventional therapies with potential adverse effects are considered. Misdiagnosis may have serious consequences: A misdiagnosed patient may be subject to unjustified thrombolytic therapy and encounter an elevated bleeding risk. Or, another serious nonvascular disorder may be misclassified as stroke and treatment options may be missed.

Scott and Silbergleit (2003) conducted an observational study to evaluate the misdiagnosis of stroke in patients treated with tissue plasminogen activator (tPA) in an emergency department without an acute stroke team, although neurological advice was available on demand. Six of 151 tPA-treated patients (4%) had a final diagnosis other than stroke: conversion disorder (4), complex migraine (1), and Todd's paralysis (1). These mistakenly tPA-treated non-stroke patients luckily did not encounter intracranial hemorrhage and were discharged with little disability. The authors argue that the likelihood to misdiagnose stroke by emergency physicians without the support of a stroke team is low and that complications in the case of misdiagnosis did not occur.

It seems critical to propagate safety of thrombolytic therapy in the case of misdiagnosis on the basis of low numbers as reported by Scott and Silbergleit (2003). Emergency physicians are not always as familiar with acute neurological disorders as in the centers on study in the reports of Kothari et al. (1995a) and Scott and Silbergleit (2003). An acute stroke team should include a neurologist since stroke diagnosis is only the beginning of stroke management. After a stroke has been diagnosed, treatment decisions have to be initiated on the basis of the time window, stroke etiology, neuroimaging and ultrasound findings and this is best done by neurologists.

It was recently reported that the in-hospital mortality rate of tPA-treated patients relates to the frequency of tPA treatments per year (Heuschmann et al. 2003). Departments treating less than five patients per year have a high mortality rate and tPA therapy can not be recommended. Low tPA treatment rates relate to lack of practical experience and this will be worse, if no neurologist is involved. Scott and Silbergleit (2003) found that the consultation of a neurologist improves the accuracy of diagnosis. Although this observation was not significantly related to outcome, it is likely that a larger study population would have shown a significant effect on better outcomes in patients seen by a neurologist.

Neuroimaging is of paramount importance in the work-up of stroke patients. CT distinguishes ischemic from hemorrhagic stroke and helps to exclude less frequent stroke entities such as subarachnoid hemorrhage or venous thrombosis. Since ischemic stroke is often CT-negative in early hours after onset, CT is of limited help to prevent misdiagnosis in the acute stage. In the large thrombolytic trials, early ischemic signs were present in only 31% in the NINDS trial (0–3 h time window) and 57% in the ECASS II trial (3–6 h time window) (Hacke et al. 1998; NINDS Study Group 1995). Conditions such as Todd's paralysis, migraine aura, metabolic or psychogenic disorders that do not show any specific CT abnormalities are not ruled out by CT. However, even a normal CT scan gives important clues and reduces the number of possible differential diagnosis such as symptomatic seizures due to brain tumors, previous territorial infarcts or intracerebral hemorrhage.

Besides conventional CT studies, advanced imaging techniques such as CT angiography, CT perfusion or magnetic resonance imaging (MRI) may be helpful to prevent misdiagnosis. Ischemic lesions are easy to detect with diffusion-weighted imaging (DWI) within a stroke MRI protocol (MR angiography (MRA), DWI and perfusion imaging (PI)) (Röther 2001). Allder et al. (1999) showed that the limited reliability of the clinical diagnosis of stroke is improved by neuroimaging and that misdiagnosis may be decreased to 9% by an intensive work-up using stroke MRI.

It was suggested that the sensitivity of DWI for acute ischemic lesions within the first 12 h of stroke onset is substantially superior as compared to CT (Fiebach et al. 2002; Saur et al. 2003), whereas after 12 h, accuracy is equivalent (Mullins et al. 2002). However, even DWI may be negative in transient ischemic attacks (TIA), brain stem lacunes or mild stroke syndromes (Fig. 19.1). Normal diffusion weighted MRI is found in 30%–80% of TIA patients depending on symptom duration and time point of the DWI study (Crisostomo et al. 2003; Kidwell et al. 1999; Ovbiagele et al. 2003; Rovira et al. 2002).

Ay et al. (1999a) found normal DWI in brain regions clinically implicated in 3.5% (27 of 782) of consecutive patients scanned when stroke-like neurologic deficits were still present. DWI negative stroke mimics were believed to have ischemic stroke because of enduring neurological deficits as observed in approximately 7% (ten of 782 consecutive patients scanned by DWI).

The longer the neurological deficit lasts and the later in the course of the stroke symptoms CT or DWI are performed, the higher the likelihood of a positive finding. Moderate decreases of cerebral perfusion as defined by increased relative mean transit times (rMTT), decreased relative cerebral blood flow (rCBF) but normal relative cerebral blood volume (rCBV) are typically found in DWI negative TIA or stroke patients (Ay et al. 1999b).

We found stroke MRI (FLAIR, MRA, DWI, and PI) helpful in patients with complicated migraine that presented with an aura of aphasia and hemiparesis. A negative DWI in the presence of normal MRA and PI made stroke an unlikely diagnosis and the further course of the disorder with typical migraine headache and complete resolution of the focal neurological signs within a few hours were supportive.

19.3 Of Stroke Mimics and Stroke Chameleons

In the literature, "stroke mimicry" – the misdiagnosis of stroke due to a non-vascular medical condition that simulates a stroke syndrome – refers to cases where the diagnosis of a stroke was made on the basis of a skilled examination but finally turned out to be wrong. Typical examples of stroke mimicry are metabolic and toxic disturbances, complicated migraine, Todd's paralysis, conversion disorders and brain tumors.

Although intracranial mass lesions such as cerebral abscess, subdural hematoma and brain tumors do not usually present with acute stroke-like symptom onset, 6% of brain tumor patients presented with symptoms of less than 24-h duration (Snyder et al. 1993). Misdiagnosis of these cases is easily prevented by CT or MRI and should not play a major role nowadays.

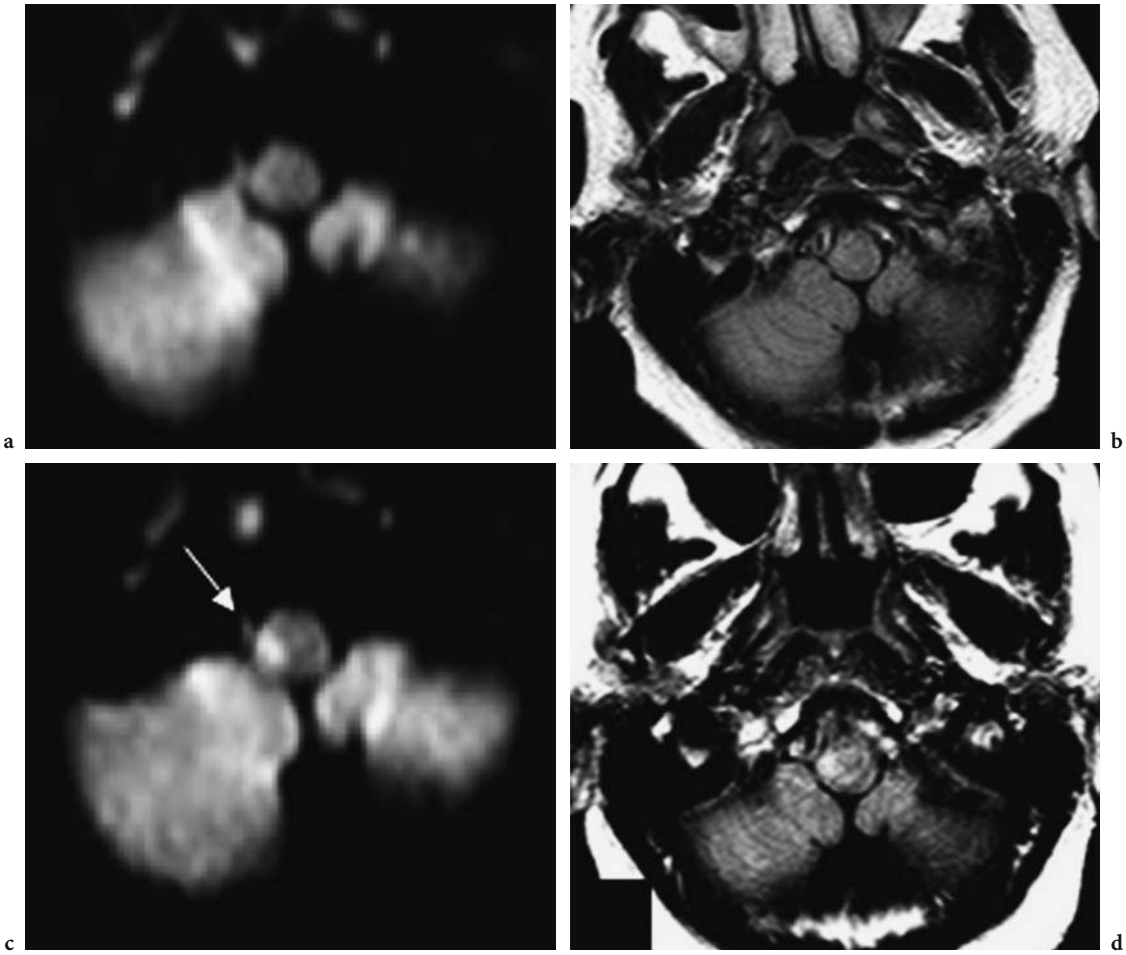

Fig. 19.1a–d. Stroke chameleon – untypical presentation of stroke symptoms leading to the diagnosis of a non-vascular disorder. A 44-year-old female presented with nausea, vertigo and spontaneous rotatory nystagmus without additional symptoms. The initial diagnosis was vestibular neuropathy and normal DWI seemed to support this diagnosis. Additional symptoms such as dissociated sensory disturbance on the left side and facial weakness on the right lead to the final diagnosis of a medullary infarction that was confirmed in an MRI follow-up study. Diffusion-weighted MRI (**a**,**c**) and FLAIR images (**b**,**d**) 12 h (**a**,**b**) and 3 days (**c**,**d**) after symptom onset. An infarction of the dorsolateral medulla is observed on the follow-up MRI that was not visible in the initial study

Seizures are frequent after ischemic stroke and estimates of the rate of postischemic stroke seizures range from 2% to 33%. Cortical location and, possibly, stroke severity are predisposing factors (Bladin et al. 2000; Camilo and Goldstein 2004). The time point of the first seizure varies from months to several years after the stroke. Misdiagnosis of seizures as stroke occurs if the seizure is unwitnessed and followed by focal neurological deficits. This so-called Todd's paralysis is a fascinating and poorly understood condition where transient deficits occur in the absence of a morphological correlate. Neuronal exhaustion and excessive inhibition has been discussed as underlying cause. Commonly, Todd's paralysis is associated with a hemiparesis lasting minutes or hours, rarely as long as 2 days, with subsequent complete remission. Unusual and variable post-epileptic syndromes have been described with ideomotor limb apraxia or a severe hemineglect syndrome lasting up to 70 h after the seizure (Helmchen et al. 1994). Kimura et al. (1998) found prolonged cerebral hyperperfusion in SPECT studies in patients with seizures followed by Todd's paralysis arguing that this may be due to disturbed autoregulation. We have studied a few patients with Todd's paralysis by MRI (conventional MRI, MRA, DWI, and PI) and did not find any specific imaging abnormality (unpublished data). One might speculate that focal epileptic activity results in the depletion of energetic metabolites with consecutive

transient cellular dysfunction. If this hypothesis is correct, ATP depletion is at least not severe enough to cause cell depolarization since DWI was normal in our cases (Binder 2004).

Hypoglycemia may mimic nearly each neurological syndrome including sudden amnesia (Fisher 2002), hemiballismus (Hefter et al. 1993), hemiparesis (Carter and Taylor 2002) and basilar artery occlusion (Röther et al. 1992). It is unclear why hypoglycemia may result in stroke-like pictures with focal neurological deficits instead of producing the more common clinical picture of hypoglycemic coma. Obviously, some kind of *locus minoris resistentiae* results in focal deficits before unconsciousness eventually follows.

Metabolic encephalopathies due to hyperglycemia, hyponatremia and hepatic encephalopathy may go along with focal neurological signs and are rare causes of stroke-like syndromes (Atchison et al. 1992; Berkovic et al. 1984). Wernicke's encephalopathy (Chang 2000), nontraumatic spinal epidural hematoma (Lin 2004), basilar migraine (Meyding-Lamade et al. 1995) and sudden onset of diplopia and ataxia in Miller Fisher syndrome (Cher and Merory 1993) were reported to mimic brainstem stroke. Meniere's disease mimicking drop attacks (Ballester et al. 2002) and conversion disorder masquerading as Dejerine-Roussy syndrome (Ferrante et al. 2004) are other cases of stroke mimicry as are myasthenia gravis (Kleiner-Fisman and Kott 1998) and peripheral nerve lesions (Lampl et al. 1995).

Vague symptoms, a high level of co-morbidity and incomplete patient history seem to contribute to the misdiagnosis of non-vascular disorders as stroke.

Conditions where the untypical presentation of stroke symptoms leads to the misdiagnosis of a non-vascular disorder were termed "stroke chameleons". These are rare instances were ischemic lesions in the subthalamic nucleus may present with movement disorders such as hemiballismus and myoclonus. Bilateral thalamic lesions due to basilar artery embolism may cause confusional states with little additional focal neurological deficits. The misdiagnosis is supported by the difficulty to detect these sometimes rather small paramedian thalamic lesions in CT studies. MRI with its greater conspicuity makes the diagnosis of these small midline ischemic lesions easier and MRI is a great help in the work-up of unusual stroke manifestations. The presentation of ischemic lesions in CT and MRI may sometimes be confusing, especially when the time from symptom onset is unknown and cortical enhancing lesions may be misdiagnosed as metastases (Okamoto et al. 1998).

Sensorimotor deficits imitating peripheral nerve involvement were reported (Back and Mrowka 2001). Ulnar and median nerve-like deficit were due to infarcts located in the thalamus and the corona radiate (Lampl et al. 1995). We have seen two patients with radial nerve-like deficits due to cortical ischemic lesions of the cortical presentation of the hand in the motor cortex. Normal nerve conduction velocity and MRI help to clarify these cases.

In summary, the diagnosis of stroke improves with the clinical skills of the investigator, the use of advanced imaging techniques and the time relapsed since symptom onset. Since "time is brain", it is important to improve the skills of the physicians dealing with acute stroke patients. Various options have been established to improve acute stroke management. In the US, emergency physicians play a crucial role in the management of stroke patients. In other countries, internists are responsible for acute stroke patients in the first place. Acute stroke teams including neurologists reduce the rate of misdiagnosis and the involvement of a neurologist is essential.

Stroke is a heterogeneous disease and acute stroke management includes more than just the initial diagnosis. Acute stroke management should be in the hands of neurologists and neuroradiologists. If such a stroke service is not established, the patient should be referred to the next stroke center. If this is too far away, other options include neurological advice via telemedicine or telephone consultation.

Advanced imaging techniques are warranted more widely to speed up the work-up of stroke patients and to improve the identification of patients who may benefit from reperfusion strategies by specifically displaying the pathology of the individual patient.

References

Abrams HL, McNeil BJ (1978) Medical implication of computed tomography (CAT scanning). N Engl J Med:255-261

Allder SJ, Moody AR, Martel AL, Morgan PS, Delay GS, Gladman JR, Fentem P, Lennox GG (1999) Limitations of clinical diagnosis in acute stroke. Lancet 354:1523

Atchison JW, Pellegrino M, Herbers P, Tipton B, Matkovic V (1992) Hepatic encephalopathy mimicking stroke. A case report. Am J Phys Med Rehabil 71:114-118

Ay H, Buonanno FS, Rordorf G, Schaefer PW, Schwamm LH, Wu O, Gonzalez RG, Yamada K, Sorensen GA, Koroshetz WJ (1999a) Normal diffusion-weighted MRI during stroke-like deficits. Neurology 52:1784-1792

Ay H, Oliveira-Filho J, Buonanno FS, Ezzeddine M, Schaefer PW, Rordorf G, Schwamm LH, Gonzalez RG, Koroshetz WJ (1999b) Diffusion-weighted imaging identifies a subset of lacunar infarction associated with embolic source. Stroke 30:2644-2650

Back T, Mrowka M (2001) Cortical infarction of the 'hand knob' area. Neurology 57:1143

Ballester M, Liard P, Vibert D, Hausler R (2002) Meniere's disease in the elderly. Otol Neurotol 23:73-78

Berkovic SF, Bladin PF, Darby DG (1984) Metabolic disorders presenting as stroke. Med J Aust 140:421-424

Binder DK (2004) A history of Todd and his paralysis. Neurosurgery 54:480-486

Bladin CF, Alexandrov AV, Bellavance A, Bornstein N, Chambers B, Cote R, Lebrun L, Pirisi A, Norris JW (2000) Seizures after stroke: a prospective multicenter study. Arch Neurol 57:1617-1622

Bull JWD, Marshall J, Shaw DA (1960) Cerebral angiography in the diagnosis of acute stroke. Lancet 562-565

Camilo O, Goldstein LB (2004) Seizures and epilepsy after ischemic stroke. Stroke 35:1769-1775

Carter F, Taylor C (2002) Transient hypoglycemic hemiparesis. J Natl Med Assoc 94:999-1001

Chang GY (2000) Acute Wernicke's syndrome mimicking brainstem stroke. Eur Neurol 43:246-247

Cher LM, Merory JM (1993) Miller Fisher syndrome mimicking stroke in immunosuppressed patient with rheumatoid arthritis responding to plasma exchange. J Clin Neuroophthalmol 13:138-140

Crisostomo RA, Garcia MM, Tong DC (2003) Detection of diffusion-weighted MRI abnormalities in patients with transient ischemic attack: correlation with clinical characteristics. Stroke 34:932-937

Ferrante FM, Rana MV, Ferrante MA (2004) Conversion disorder mimicking Dejerine-Roussy syndrome (thalamic stroke) after spinal cord stimulation. Reg Anesth Pain Med 29:164-167

Fiebach JB, Schellinger PD, Jansen O, Meyer M, Wilde P, Bender J, Schramm P, Juttler E, Oehler J, Hartmann M, Hahnel S, Knauth M, Hacke W, Sartor K (2002) CT and diffusion-weighted MR imaging in randomized order: diffusion-weighted imaging results in higher accuracy and lower interrater variability in the diagnosis of hyperacute ischemic stroke. Stroke 33:2206-2210

Fisher CM (2002) Unexplained sudden amnesia. Arch Neurol 59:1310-1313

Furlan A, Higashida R, Wechsler L, Gent M, Rowley H, Kase C, Pessin M, Ahuja A, Callahan F, Clark W, Silver F, Rivera F (1999) Intra-arterial Prourokinase for acute ischemic stroke. JAMA 282:2003-2011

Groch SN, Hurwitz LJ, Wright IS, McDowell F (1960) Intracranial lesions simulating cerebral thrombosis. JAMA 172:1469-1472

Hacke W, Kaste M, Fieschi C, von Kummer R, Davalos A, Meier D, Larrue V, Bluhmki E, Davis S, Donnan G, Schneider D, Diez-Tejedor E, Trouillas P (1998) Randomised double-blind placebo-controlled trial of thrombolytic therapy with intravenous alteplase in acute ischaemic stroke (ECASS II). Second European-Australasian Acute Stroke Study Investigators. Lancet 352:1245-1251

Hefter H, Mayer P, Benecke R (1993) Persistent chorea after recurrent hypoglycemia. A case report. Eur Neurol 33:244-247

Helmchen C, Steinhoff BJ, Dichgans M (1994) Variants of Todd's paralysis: postictal apraxia and prolonged postictal hemineglect. Nervenarzt 65:700-703

Heuschmann PU, Berger K, Misselwitz B, Hermanek P, Leffmann C, Adelmann M, Buecker-Nott HJ, Rother J, Neundoerfer B, Kolominsky-Rabas PL (2003) Frequency of thrombolytic therapy in patients with acute ischemic stroke and the risk of in-hospital mortality. The German Stroke Registers Study Group. Stroke 34:1106-1113

Huff JS (2002) Stroke mimics and chameleons. Emerg Med Clin North Am 20:583-595

Kidwell CS, Alger JR, Di Salle F, Starkman S, Villablanca P, Bentson J, Saver JL (1999) Diffusion MRI in patients with transient ischemic attacks. Stroke 30:1174-1180

Kimura M, Sejima H, Ozasa H, Yamaguchi S (1998) Technetium-99m-HMPAO SPECT in patients with hemiconvulsions followed by Todd's paralysis. Pediatr Radiol 28:92-94

Kleiner-Fisman G, Kott HS (1998) Myasthenia gravis mimicking stroke in elderly patients. Mayo Clin Proc 73:1077-1078

Kothari R, Barsan W, Brott T, Broderick J, Ashbrock S (1995a) Frequency and accuracy of prehospital diagnosis of acute stroke. Stroke 26:937-941

Kothari RU, Brott T, Broderick JP, Hamilton CA (1995b) Emergency physicians. Accuracy in the diagnosis of stroke. Stroke 26:2238-2241

Lampl Y, Gilad R, Eshel Y, Sarova-Pinhas I (1995) Strokes mimicking peripheral nerve lesions. Clin Neurol Neurosurg 97:203-207

Libman RB, Wirkowski E, Alvir J, Rao TH (1995) Conditions that mimic stroke in the emergency department. Implications for acute stroke trials. Arch Neurol 52:1119-1122

Lin IY (2004) Diagnostic pitfall: nontraumatic spinal epidural hematoma mimicking a brainstem stroke. Ann Emerg Med 44:183-184

Meyding-Lamade U, Rieke K, Krieger D, Forsting M, Sartor K, Sommer C, Hacke W (1995) Rare diseases mimicking acute vertebrobasilar artery thrombosis. J Neurol 242:335-343

Mullins ME, Schaefer PW, Sorensen AG, Halpern EF, Ay H, He J, Koroshetz WJ, Gonzalez RG (2002) CT and conventional and diffusion-weighted MR imaging in acute stroke: study in 691 patients at presentation to the emergency department. Radiology 224:353-360

National Institute of Neurological Disorders and Stroke rt-PA Stroke Study Group (1995). Tissue plasminogen activator for acute ischemic stroke. N Engl J Med 333:1581-1587

Norris JW, Hachinski VC (1982) Misdiagnosis of stroke. Lancet 6:328-331

Okamoto K, Ito J, Furusawa T, Sakai K, Watanabe M, Tokiguchi S (1998) Small cortical infarcts mimicking metastatic tumors. Clin Imaging 22:333-338

Ovbiagele B, Kidwell CS, Saver JL (2003) Epidemiological impact in the United States of a tissue-based definition of transient ischemic attack. Stroke 34:919-924

Röther J (2001) CT and MRI in the diagnosis of acute stroke and their role in thrombolysis. Thromb Res 103:S125-S133

Röther J, Schreiner A, Wentz KU, Hennerici M (1992) Hypoglycemia presenting as basilar artery thrombosis. Stroke 23:112-113

Rovira A, Rovira-Gols A, Pedraza S, Grive E, Molina C, Alvarez-Sabin J (2002) Diffusion-weighted MR imaging in the acute phase of transient ischemic attacks. Am J Neuroradiol 23:77-83

Saur D, Kucinski T, Grzyska U, Eckert B, Eggers C, Niesen W, Schoder V, Zeumer H, Weiller C, Rother J (2003) Sensitivity and interrater agreement of CT and diffusion-weighted MR Imaging in hyperacute stroke. Am J Neuroradiol 24:878-885

Scott PA, Silbergleit R (2003) Misdiagnosis of stroke in tissue plasminogen activator-treated patients: characteristics and outcomes. Ann Emerg Med 42:611-618

Snyder H, Robinson K, Shah D, Brennan R, Handrigan M (1993) Signs and symptoms of patients with brain tumors presenting to the emergency department. J Emerg Med 11:253-258

Ulaki SD, Topinka MA, Frasser WR (2000) The accuracy of the emergency physician at diagnosing CVA/TIA in the acute care setting. Acad Emerg Med 7:1165

Subject Index

Q

R

List of Contributors

Hakan Ay, MD
Stroke Service
Massachusetts General Hospital
Harvard Medical School
CNY 149-2301
13th Street
Boston, MA 02129
USA

Tobias Back, MD
Department of Neurology
University Hospital Mannheim
Ruprecht-Karls University Heidelberg
Theodor-Kutzer-Ufer 1–3
68167 Mannheim
Germany

Stephen M. Davis, MBBS, MD, FRACP
Royal Melbourne Hospital
University of Melbourne
Parkville
3050 Melbourne, Vic
Australia

José M. Ferro, MD, PhD
Neurological Service
Department of Neurosciences and Mental Health
Hospital de Santa Maria
University of Lisbon
Av. Prof. Egas Moniz
1649-035 Lisbon
Portugal

Marco Fiorelli, MD, PhD
Department of Neurological Sciences
University La Sapienza
Viale dell'Universitá, 30
00185 Rome
Italy

Georg Gahn, MD
Deptartment of Neurology
University of Technology Dresden
Fetscherstr. 74
01307 Dresden
Germany

Achim Gass, MD
Departments of Neurology/Neuroradiology
University Hospitals Mannheim and Basle
68165 Mannheim
Germany
4031 Basle
Switzerland

Stefan Gottschalk, MD
Department of Neuroradiology
University Hospital Schleswig-Holstein
Campus Lübeck, University of Schleswig-Holstein
Ratzeburger Allee 160
23538 Lübeck
Germany

Sabine Heiland, PhD
Division of Experimental Neuroradiology
Department of Neuroradiology
Ruprecht-Karls University of Heidelberg
Im Neuenheimer Feld 400
69120 Heidelberg
Germany

Johanna Helenius, MD, PhD
Department of Neurology
Helsinki University Central Hospital
Haartmaninkatu 4
00290 Helsinki
Finland

Michael G. Hennerici, MD
Department of Neurology
University Hospital Mannheim
Ruprecht-Karls University Heidelberg
Theodor-Kutzer-Ufer 1–3
68167 Mannheim
Germany

Mathias Hoehn, PhD
In-vivo NMR Laboratory
Max-Planck Institute for Neurological Research
Gleueler Str. 50
50931 Cologne
Germany

Thamburaj Krishnamoorthy, MD
Department of Imaging of Interventional Radiology
Sree Chitra Tirunal Institute for Medical Sciences and Technology
Thrivandrum 695011
Kerala
India

Heinrich Lanfermann, MD
Institute for Neuroradiology
Goethe University of Frankfurt
Scleusenweg 2–16
60590 Frankfurt am Main
Germany

Karl Olof Lövblad, MD
Neuroradiology Unit
Department of Radiology and Medical Informatics
University Hospitals Geneva
24 rue Micheli-du-Crest
1211 Geneva 14
Switzerland

Michael Mull, MD
Department of Neuroradiology
Clinic for Diagnostic Radiology
University Hospital of the Technical University
Pauwelsstr. 30
52074 Aachen
Germany

Tobias Neumann-Haefelin, MD
Department of Neurology
Goethe University of Frankfurt
Schleusenweg 2–16
60528 Frankfurt/Main
Germany

Mark W. Parsons, B.Med.PhD, FRACP
Department of Neurology
John Hunter Hospital
University of Newcastle
New Lambton NSW 2305
Australia

Dirk Petersen, MD
Institute of Neuroradiology
University of Lübeck
Ratzeburger Allee 160
23538 Lübeck
Germany

Ulrich Pilatus, MD
Institute for Neuroradiology
Goethe University of Frankfurt
Schleusenweg 2–16
60528 Frankfurt/Main
Germany

Joachim Röther, MD
Department of Neurology
Klinikum Minden
University of Hannover
Friedrichstr. 17
32427 Minden
Germany

Kristina Szabo, MD
Department of Neurology
University Hospital Mannheim
Ruprecht-Karls University Heidelberg
Theodor-Kutzer-Ufer 1–3
68167 Mannheim
Germany

Turgut Tatlisumak, MD, PhD
Experimental MRI Laboratory
Department of Neurology
Helsinki University Central Hospital
Haartmaninkatu 4
00290 Helsinki
Finland

Armin Thron, MD
Department of Neuroradiology
Clinic for Diagnostic Radiology
University Hospital of the Technical University
Pauwelsstr. 30
52074 Aachen
Germany

Rüdiger von Kummer, MD
Department of Neuroradiology
University of Technology Dresden
Fetscherstr. 74
01307 Dresden
Germany

Susanne Wegener, MD
In-vivo NMR Laboratory
Max-Planck Institute for Neurological Research
Gleueler Str. 50
50931 Cologne
Germany